A Physical Organic Approach Towards Electrophilic Fluorination

NESHAT ROZATIAN

A Physical Organic Approach Towards Electrophilic Fluorination

Neshat Rozatian

A thesis submitted for the degree of Doctor of Philosophy

Department of Chemistry

October 2019

Abstract

Fluorinated compounds have fundamental roles within the pharmaceutical, agrochemical and materials industries. The presence of a fluorine atom can impart beneficial changes to the chemical properties and biological activities of drug molecules, such as improved metabolic stability and enhanced binding interactions. Electrophilic fluorinating reagents of the N−F class, such as Selectfluor™, NFSI and *N*-fluoropyridinium salts, underpin the introduction of fluorine in aliphatic systems in both academic and industrial research. However, the choice of N−F reagent is currently determined through empirical experimentation in the absence of quantitative values for electrophilicities.

Firstly, this thesis will discuss the development of an experimentally-determined kinetic reactivity scale for ten N−F fluorinating reagents. The reactivity scale, which covers eight orders of magnitude, was determined by measurement of relative and absolute rate constants for the fluorination of a range of *para*-substituted 1,3-diaryl-1,3-dicarbonyl derivatives. Similar Hammett parameters across the different fluorinating reagents revealed the mechanisms of fluorination to be similar in each case. The 1,3-diaryl-1,3-dicarbonyl compounds delivered a convenient, sensitive spectrophotometric reporter of reactivity that also led to the discovery of a unique form of tautomeric polymorphism.

Given the pharmaceutical relevance of α,α-difluoroketonic compounds, kinetics studies were performed on keto-enol tautomerism and difluorination of 1,3-dicarbonyl systems to understand the factors that determine selectivity between mono- and di-fluorination. Photoketonization of 1,3-diaryl-1,3-dicarbonyl derivatives and their 2-fluoro analogues was coupled with relaxation kinetics to determine enolization rates, where the presence of additives resulted in significant acceleration of enolization processes in 2-fluoro-1,3-dicarbonyl systems.

Kinetics studies on fluorination were also expanded to other classes of carbon nucleophiles, including indoles and enolates, during attempts to correlate reactivities of the N−F reagents with the Mayr-Patz scale. These experiments provided useful information for determining the reaction monitoring methodology used in other systems and have the potential for further development.

Finally, the studies on fluorination kinetics were expanded to drug-like steroid systems. The kinetics of fluorination of enol ester derivatives of progesterone, testosterone, cholestenone and hydrocortisone by a series of N−F reagents confirmed the applicability of the reactivity scale discussed earlier towards a different class of carbon nucleophiles. Further insight was gained by determination of the epimerisation rates from β- to α-fluoroprogesterone, the more pharmaceutically-relevant isomer.

Memorandum

The work described in this thesis was carried out at Durham University between October 2016 and October 2019. This thesis is the work of the author, except where acknowledged by reference, and has not been submitted for any other degree. The copyright of this thesis rests with the author. No quotation from it should be published without the prior written consent and information derived from it should be acknowledged.

Chapters 2, 3 and 4 have been the subject of the following publications:

1. N. Rozatian, I. W. Ashworth, G. Sandford and D. R. W. Hodgson, *Chem. Sci.*, 2018, **9**, 8692–8702, *A quantitative reactivity scale for electrophilic fluorinating reagents*.
2. N. Rozatian, A. Beeby, I. W. Ashworth, G. Sandford and D. R. W. Hodgson, *Chem. Sci.*, 2019, **10**, 10318-10330, *Enolization rates control mono- versus di-fluorination of 1,3-dicarbonyl derivatives*.

This work has been presented, in part, at symposia including:

1. Postgraduate Gala Symposium, Durham University, UK, June 2019, *oral presentation, awarded 2nd place prize for oral presentation*.
2. SCI's 30th Regional Postgraduate Symposium on Novel Organic Chemistry, University of York, UK, April 2019, *oral presentation, awarded 1st place prize for oral presentation*.
3. AstraZeneca PhD Review Day, AstraZeneca, Macclesfield, UK, April 2019, *poster and oral presentation*.
4. RSC Organic Division Regional Meeting, University of York, UK, March 2019, *poster presentation, awarded 2nd place poster prize*.
5. RSC Organic Division Poster Symposium, London, UK, December 2018, *poster presentation and 1-minute talk*.
6. 22nd International Symposium on Fluorine Chemistry, University of Oxford, UK, July 2018, *poster presentation, awarded runner-up poster prize*.
7. 24th International Conference on Physical Organic Chemistry, University of Algarve, Portugal, July 2018, *poster presentation*.

Acknowledgements

I would like to thank Dr David Hodgson and Prof. Graham Sandford for giving me the opportunity to work on this project, and for their expertise in physical organic chemistry and fluorine chemistry, respectively. I am grateful to AstraZeneca and Durham University Science Faculty for funding this work, as well as my industrial supervisor, Dr Ian Ashworth, for his support.

The advice of Prof. Andrew Beeby is gratefully acknowledged, which greatly helped with parts of the work included in Chapter 3. The work in this thesis would not have been possible without Mr Kelvin Appleby, who expertly and efficiently repaired the UV-vis spectrophotometers. Thanks go to Dr Mark Fox for DFT calculations and Dr Dmitry Yufit for conducting X-ray crystallography. I am grateful to the NMR service, particularly Dr Alan Kenwright and Dr Juan Aguilar-Malavia, for their help with setting up NMR kinetics experiments. Thanks go to Dr Jackie Mosely, Dr Dave Parker and Mr Peter Stokes for running the mass spectrometry service, Mrs Annette Passmoor for running stores, and the Glassblowers. I also thank my students Emily Chin and Alex Cook for carrying out some preliminary experiments regarding Chapter 6 of this thesis.

I am immensely grateful to the Sandford group for their friendship, support and encouragement: Ben “The Yeast”, Alex “Stu”, Josh “J-Dogg” and Marcus “YM”. I will have fond memories of our lunchtime Sporcle quiz challenges, and all the tea and biscuits. My thanks go to our fourth-years: Jonny, Abi, Ellis, Kiera and Ned, as well as former postgrad students: Tony, Etienne, Darren, Bear and Dan. I also thank Kevin, Estelle, Peter, Dr Tucker, Lami, Niamh, Lottie and Chris for their friendship.

I would like to express my gratitude to my parents and grandparents for their endless love and support, and for being both my academic and personal role models. I am proud to be the third generation in my family to receive our doctorates from Durham University.

Abbreviations

Ac	Acetyl
aHF	Anhydrous hydrogen fluoride
Bu	Butyl
$CDCl_3$	Deuterated chloroform
DABCO	1,4-Diazabicyclo[2.2.2]octane
DAST	Diethylaminosulfur trifluoride
DBM	Dibenzoylmethane
DBU	1,8-diazabicyclo[5.4.0]undec-7-ene
DCM	Dichloromethane
Deoxo-Fluor™	Bis(2-methoxyethyl)aminosulfur trifluoride
DFT	Density functional theory
DMF	*N*,*N*-Dimethylformamide
DMSO	Dimethylsulfoxide
ee	Enantiomeric excess
Elec	Electrophile
Equiv	Equivalent
Et	Ethyl
Et_3N	Triethylamine
Et_2O	Diethyl ether
EtOH	Ethanol
EWG	Electron-withdrawing group
GC-MS	Gas chromatography-mass spectrometry
h	Hour

HFIP	1,1,1,3,3,3-Hexafluoroisopropanol
IR	Infra-Red
LC-MS	Liquid chromatography-mass spectrometry
M	mol dm^{-3}
Me	Methyl
MeCN	Acetonitrile
MeCN-d_3	Deuterated acetonitrile
MeOH	Methanol
Min	Minutes
m.p.	Melting point
NaH	Sodium hydride
NaOMe	Sodium methoxide
n.d.	Not determined
NFPy	*N*-fluoropyridinium salts
NFSI	*N*-fluorobenzenesulfonimide
NMR	Nuclear magnetic resonance
Nuc	Nucleophile
Ph	Phenyl
pK_a	Acid dissociation constant
ppm	Parts per million
RT	Room temperature
R_t	Retention time
SET	Single electron transfer
S_N2	Bimolecular nucleophilic substitution

t	Time
$t_{1/2}$	Half-life
Temp	Temperature
Tf	Triflate
THF	Tetrahydrofuran
TLC	Thin Layer Chromatography
UV-vis	Ultra violet-visible
δ	Chemical shift / ppm
ε	Molar extinction coefficient
ε_r	Relative permittivity
λ	Wavelength
ρ	Hammett reaction constant
σ	Hammett substituent constant

Table of Contents

Abstract ..... **i**

Memorandum ..... **iii**

Acknowledgements ..... **v**

Abbreviations ..... **vii**

Chapter 1: Introduction **1**

1.1 Introduction to organofluorine chemistry 1

1.2 Electrophilic fluorinating reagents of the N−F class 5

1.2.1 Selectfluor™ 7

1.2.2 *N*-Fluorobenzenesulfonimide (NFSI) 9

1.2.3 *N*-Fluoropyridinium salts 11

1.3 Quantification of fluorinating power 14

1.3.1 Reduction potentials approach 15

1.3.2 Power variable scale 16

1.3.3 Competitive halogenation approach 17

1.3.4 Kinetics approach 20

1.3.5 Computational approach 23

1.4 Fluorinated 1,3-dicarbonyl compounds 24

1.4.1 Pharmaceutical and industrial relevance of 1,3-dicarbonyl compounds 24

1.4.2 Synthesis of fluorinated 1,3-dicarbonyl compounds 26

1.5 Aims and Objectives 30

Chapter 2: A Quantitative Reactivity Scale for N−F Reagents **32**

2.1 Introduction 32

2.2 Development of the *para*-substituted 1,3-diaryl-1,3-dicarbonyls scaffold 32

2.2.1 Tautomeric polymorphism 36

2.3 Kinetics of fluorination of compounds 107a-m 40

2.4 Product analyses: reaction monitoring by NMR spectroscopy 47

2.5 Product analyses: reaction monitoring by LC-MS 48

2.6 Structure-activity correlations 52

2.7 Reactivity scale for N−F reagents 55

2.8 Determination of activation parameters 59

2.9 Effect of mono- versus di-substitution on rates of fluorination 60

2.10 Comparison with quantitative studies of fluorinating agent reactivities 61

2.11 Comparison with qualitative reactivities of fluorinating reagents in synthetic applications 65

2.11.1 Recent industrial application of the Reactivity Scale 67

2.12 Conclusions 69

Chapter 3: Kinetics of Enolization of 1,3-Dicarbonyl and 2-Fluoro-1,3-Dicarbonyl Derivatives 71
3.1 Introduction 71
3.2 Kinetics of keto-enol tautomerism in compounds 107a and 107c-e 76
3.2.1 Photoketonization-relaxation experiments for 107a and 107c-e 76
3.2.2 Relaxation of 107a in the presence of additives 82
3.3 Kinetics of keto-enol tautomerism in compounds 108a and 108c-e 90
3.3.1 Photoketonization-relaxation experiments for 108a and 108c-e 90
3.3.2 Relaxation of 108a in the presence of additives 98
3.4 Conclusions 101
Chapter 4: Kinetics of Fluorination of 2-Fluoro-1,3-Dicarbonyl Derivatives 103
4.1 Introduction 103
4.2 Initial studies conducted using NMR spectroscopy 105
4.3 Kinetics of fluorination of 108a and 108c-e in MeCN 106
4.4 Structure-activity correlations and determination of activation parameters 110
4.5 Kinetics of fluorination of 108a-enol and 107a-enol in water-MeCN mixtures 113
4.6 Kinetics of fluorination of 108a-enol by Selectfluor™ and NFSI in formic acid-MeCN mixtures 116
4.7 Kinetics of fluorination of 108a-enol by Selectfluor™ with $^{n}Bu_4N^+BF_4^-$ 118
4.8 Synthesis of 2,2-difluoro-1,3-propanedione 109a in a water-MeCN solvent system 119
4.9 Application of kinetic data to synthesis 121
4.10 Comparisons with synthetic reports 126
4.11 Conclusions 128
Chapter 5: Attempts Towards Correlation with the Mayr-Patz Scale 130
5.1 Introduction 130
5.2 Kinetics of fluorination of enamine 133i 133
5.3 Kinetics of fluorination of silyl enol ether 133c 135
5.4 Kinetics of fluorination of 1-methyl indole 133a 137
5.4.1 Kinetics of fluorination of 133a using Selectfluor™ 137
5.4.2 Kinetics of fluorination of 133a using NFSI 143
5.5 Kinetics of chlorination 144
5.5.1 Kinetics of chlorination of 1-methyl indole 133a 144
5.5.2 Chlorination of dimethylamino-substituted enol 107h 146
5.6 Kinetics of fluorination of malonate esters and enolates of 1,3-dicarbonyls 149
5.7 Kinetics studies on the reactions of 1,3-diaryl-1,3-propanedione derivatives with amino-substituted benzhydrilium ions 154
5.8 Conclusions 158
Chapter 6: Kinetics of Fluorination of Steroid Enol Acetates 160

6.1 Introduction 160
6.2 Synthesis of progesterone enol acetate and fluoroprogesterone 166
6.3 Kinetics of fluorination of progesterone enol acetate by N−F reagents 167
6.3.1 Fluorination via Selectfluor™, diCl-NFPy TfO^-/BF_4^- and pentaCl-NFPy TfO^- 167
6.3.2 Fluorination via NFSI, NFPy TfO^- and triMe-NFPy TfO^- 172
6.3.3 Kinetics of fluorination of enol acetate forms of testosterone, cholestenone and hydrocortisone 175
6.3.4 Comparison of reactivities of the N−F reagents 178
6.3.4 Comparison of reactivities of progesterone enol acetate 165 and enols 107a-h 179
6.3.5 Determination of activation parameters 181
6.3.6 Exploration of the effects of additives on rates of fluorination 182
6.3.7 Kinetics of epimerisation 185
6.4 Direct fluorination of progesterone enol acetate using fluorine gas 192
6.5 Conclusions 195
Chapter 7: Conclusions and Future Work 197
Chapter 8: Experimental 204
8.1 General 204
8.1.1 X-ray Crystallography 204
8.2 Kinetics studies conducted by UV-vis spectrophotometry 205
8.3 Experimental to Chapter 2: 205
8.3.1 Computational methods 205
8.3.2 1,3-bis(4'-cyanophenyl)-1,3-propanedione 206
8.3.3 1,3-bis(4'-nitrophenyl)-1,3-propanedione 207
8.3.4 1,3-bis[4'-(dimethylamino)phenyl]-1,3-propanedione 207
8.3.5 2-fluoro-1,3-diphenyl-1,3-propanedione 208
8.3.6 2-fluoro-1,3-bis(4'-fluorophenyl)-1,3-propanedione 209
8.3.7 2-fluoro-1,3-bis(4'-methylphenyl)-1,3-propanedione 210
8.3.8 2-fluoro-1,3-bis(4'-methoxyphenyl)-1,3-propanedione 211
8.3.9 2-fluoro-1,3-bis(4'-chlorophenyl)-1,3-propanedione 212
8.3.10 2-fluoro-1,3-bis(4-cyanophenyl)-1,3-propanedione 213
8.3.11 2,3,4,5,6-pentachloro-*N*-fluoropyridinium trifluoromethanesulfonate 213
8.3.12 Extinction coefficients 214
8.3.13 Summary of all k_{obs} values for 107a-m with 10 N−F reagents 215
8.4 Experimental to Chapter 3: 240
8.4.1 Synthesis of 1-(chloromethyl)-4-aza-1-azoniabicyclo[2.2.2]octane tetrafluoroborate ($ClCH_2$-$DABCO^+$ BF_4^-) 240
8.4.2 Synthesis of bisphenylsulfonylimide sodium salt $(PhSO_2)_2N^-$ Na^+ 240

8.4.3 Photoketonization-relaxation procedure 241
8.4.4 UV-vis spectra for relaxation of 107c-e, 108a and 108c-e in the presence of additives 241
8.4.5 Kinetic data from autocatalytic relaxation of 108a-keto and 108e-keto 246
8.5 Experimental to Chapter 4: 247
8.5.1 Synthesis of 2,2-difluoro-1,3-propanedione 247
8.5.2 T1 values determined for Selectfluor™ and 2-fluoro-1,3-dicarbonyl 108a..... 247
8.5.3 Kinetic parameters used for modelling in NMR-scale reactions 247
8.5.4 Kinetics of fluorination of 108a, 108c-e: spectra and k_{obs} values..... 248
8.5.5 Product analysis by LC-MS on fluorination of 108d-enol with NFSI 254
8.6 Experimental to Chapter 5: 255
8.6.1 Kinetics studies conducted by stopped-flow UV-vis spectrophotometry 255
8.6.2 Synthesis of sodium enolates 144a-d 255
8.6.3 Synthesis of potassium enolates 145a-d..... 256
8.7 Experimental to Chapter 6: 258
8.7.1 Method for direct fluorination of progesterone enol acetate..... 258
8.7.2 Synthesis of progesterone enol acetate 258
8.7.3 Synthesis of 6β-fluoroprogesterone and 6α-fluoroprogesterone..... 259
8.7.4 Synthesis of steroid derivatives 167-172 260
8.7.5 Determination of extinction coefficients..... 265
8.7.6 Kinetics data for fluorination of steroid enol acetates..... 266
Appendices..... 276
Crystal structure data 276
Confirmation of purities of compounds 108a and 108c-e by LC-MS..... 279
References..... 283

Chapter 1: Introduction

1.1 Introduction to organofluorine chemistry

Organofluorine compounds are an important family of molecules that have significant roles in medicinal, agrochemical and material sciences due to the unique properties of the fluorine atom.[1–4] Beneficial changes to the chemical properties and biological activities of compounds can be imparted by the presence of a fluorine atom, such as improved metabolic stability and enhanced binding interactions.[1] Consequently, pharmaceuticals bearing fluoro-aliphatic, -aromatic and -heterocyclic units have become widespread, such as Prozac™, Lipitor®, ciprofloxacin and diclosulam.[5,6] Indeed, 30% of pharmaceuticals introduced to the market in 2018 contained fluorine,[7] and around 50% of the most successful "blockbuster" drugs are fluorine-containing compounds.[8]

In 1862, the first fluoride displacement of halogens was reported by Alexander Borodin, where he achieved the nucleophilic substitution of chloride by fluoride to form benzoyl fluoride. The next major breakthrough came in 1886 when fluorine (F_2) was isolated successfully by Henri Moissan, via the electrolysis of a solution of potassium hydrogen difluoride (KHF_2) in anhydrous hydrogen fluoride (aHF) in a platinum cell at −24 °C.[9,10] To this day, industrial fluorine cells are based on the Moissan cell.

Fluorine is the most electronegative element, with a value of 4.0 according to the Pauling scale.[11] The large difference in electronegativities between carbon and fluorine results in the high polarity of the C−F bond. This polarisation produces a large dipole, hence the favourable interactions between the $C^{\delta+}$ and $F^{\delta-}$ atoms. The C−F bond is thus the strongest covalent bond, with a bond dissociation energy of 440.7 kJ mol^{-1}.[12] The van der Waals radius of the fluorine atom is 1.47 Å, which is smaller than that of the other halogens (chlorine, 1.80 Å; bromine, 1.95 Å; iodine, 2.15 Å). Indeed, in terms of size, fluorine lies between hydrogen and oxygen; thus, the replacement of either of these atoms by fluorine can greatly alter the chemical properties of a compound without significantly affecting the overall sterics of the system. In this context, fluorine-containing motifs have been widely applied as bioisosteres for drug discovery.[13]

Fluorine is the most abundant halogen; it is present in various ores in the earth's crust. The main mineral sources of fluorine are fluorspar (CaF_2), cryolite (Na_3AlF_6) and fluorapatite ($Ca_5(PO_4)_3F$).[14] However, organofluorine compounds are very scarce in

nature,[15] and although over 3700 naturally-occurring organo-halogen compounds are known, relatively few contain fluorine. The most common natural organofluorine species, fluoroacetate **1** (**Figure 1**), was first identified in 1943 in the South African gifblaar plant *Dichapetalum cymosum*.[16] Fluoroacetate is biochemically converted into fluoroacetyl CoA, which enters the tricarboxylic acid (TCA) cycle and condenses with oxaloacetate. This forms 2-fluorocitrate **2**, an inhibitor of aconitase, which shuts down the TCA cycle. 4-Fluorothreonine **3** was isolated from the bacterium *Streptomyces cattleya* in 1986, and is formed by the enzyme-catalysed transfer of fluoroacetaldehyde onto threonine.[17] The metabolic precursor of both fluoroacetate and 4-fluorothreonine in *Streptomyces cattleya* is fluoroacetaldehyde **4**.[18] These metabolites are biosynthesised by pathways initiated by the C−F bond forming enzyme known as fluorinase.[19]

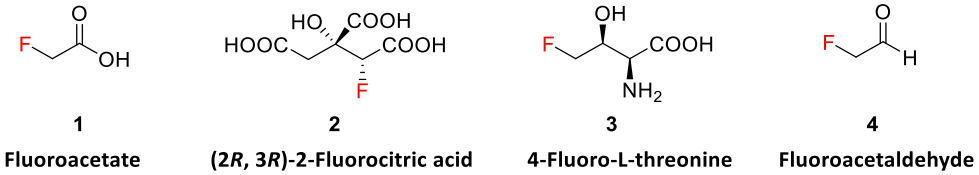

1 Fluoroacetate | **2** (2*R*, 3*R*)-2-Fluorocitric acid | **3** 4-Fluoro-L-threonine | **4** Fluoroacetaldehyde

Figure 1: Examples of naturally occurring organofluorine compounds.

Several properties of organic compounds can be altered by incorporation of a fluorine atom, including pK_a, lipophilicity and protein binding affinity. In 1954, Fried and Sabo discovered that the introduction of a single fluorine atom into the corticosteroid **5** (fludrocortisone, **Figure 2**) increased its potency tenfold.[20] 5-Fluorouracil **6** was developed as an anti-cancer drug,[21] and its analogue, 5-fluorocytosine, was introduced as an anti-fungal agent. The development of 6-fluoroquinolones in the 1980s led to a large class of bactericides, where ciprofloxacin **7** is one of the most widely used antibiotics worldwide. The discovery of pharmaceuticals bearing $-CF_2$, $-CF_3$ and $-CF_2CF_3$ moieties has led to a diversification in the field in more recent years. Pantoprazole **8**, containing the CF_2 moiety, is used to treat stomach ulcers and esophagitis, and in 2016 was the 25th most prescribed medication in the United States.[22]

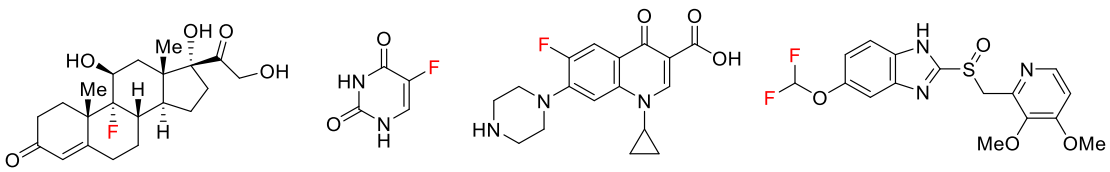

Figure 2: Examples of fluorine-containing drugs.

Currently, all fluorine atoms used for organofluorine chemistry originate from fluorspar, which is converted to aHF using aqueous sulfuric acid. aHF is directly employed in many industrial processes, including Balz-Schiemann and Swarts halogen exchange processes for the manufacture of fluoroaromatic and trifluoromethylaromatic derivatives, respectively.[14] Reactions of aHF with small molecule chloroalkanes are employed to manufacture refrigerants, such as hydrochlorofluorocarbons (HFCs),[23] and fluoropolymers are synthesised via the reactions of aHF with small molecule HFCs.[24]

Secondly, aHF is used for the preparation of the next generation of fluorinating reagents, including F_2, KF and $Et_3N.3HF$ (**Figure 3**). These are reacted further with the appropriate substrates to obtain the fluorinating reagents that are most commonly used in laboratory-scale discovery processes. These reagents are often separated into two main classes: nucleophilic and electrophilic agents. Several commercially-available and shelf-stable reagents of both classes have been developed over the years, thus avoiding the need for specialist equipment or lengthy preparations. Nucleophilic fluorinating reagents include DAST and Deoxo-Fluor™, which are employed for the conversion of C−O bonds to C−F bonds. For the conversion of electron-rich centres, such as the direct conversion of C−H to C−F linkages, nucleophilic fluorinating agents are usually not feasible. In these cases, electrophilic sources of fluorine are employed, such as Selectfluor™ and NFSI (**Figure 3**).

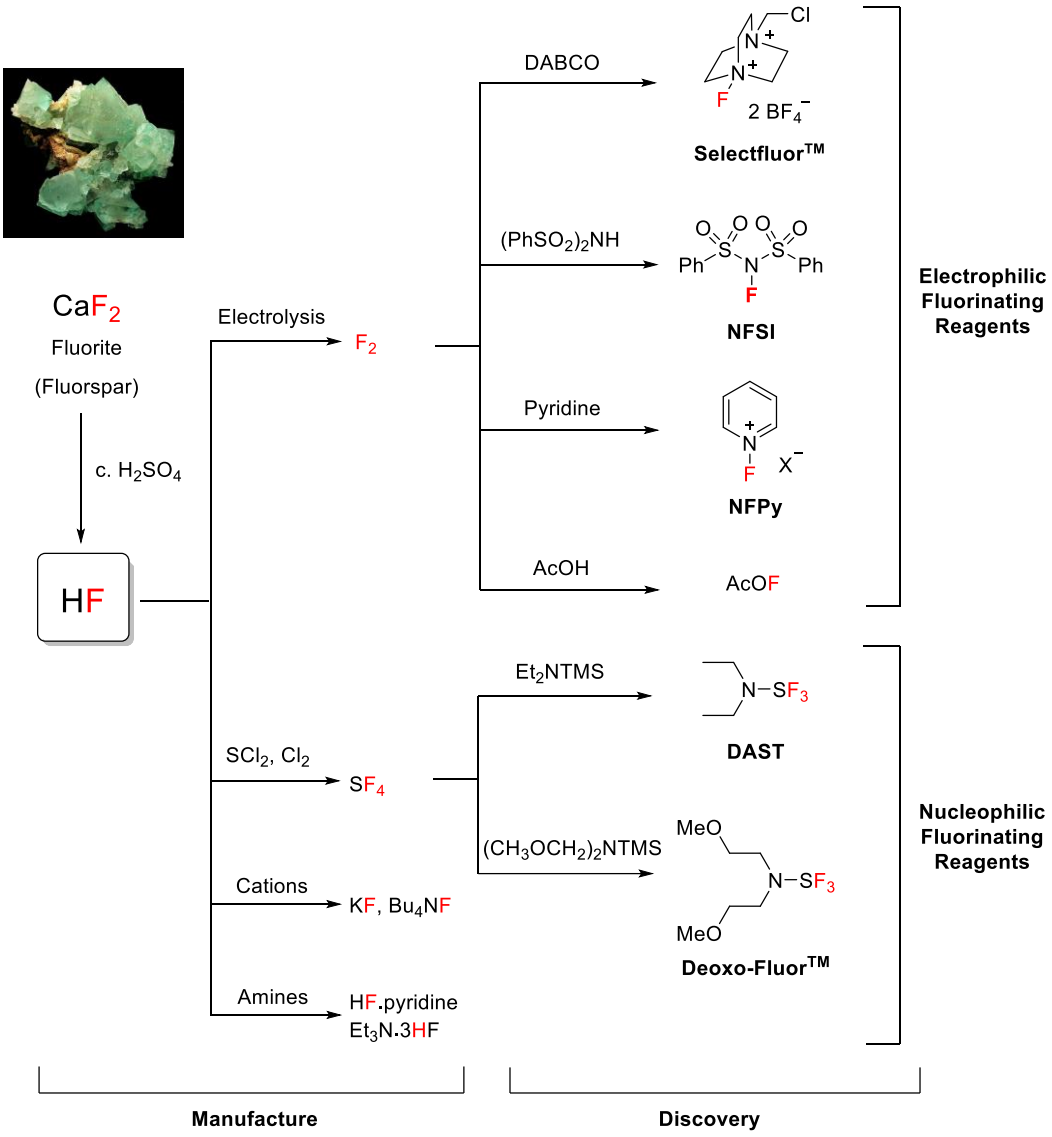

Figure 3: Classes of currently used fluorinating reagents and their sources.[14,25]

The introduction of a fluorine atom into a compound using selective and effective synthetic methods has become an important challenge in organic chemistry.[4] Formation of the carbon-fluorine bond still remains a challenging transformation, mainly due to the high hydration energy of the fluoride anion, high electronegativity of fluorine and highly polarised bonds to fluorine. In the last few decades, nucleophilic and electrophilic fluorinating reagents have revolutionised the field. In particular, bench-stable electrophilic reagents have made a significant impact and are the focus of the present work.

1.2 Electrophilic fluorinating reagents of the N−F class

Electrophilic fluorination represents one of the most direct methods for the selective introduction of fluorine into organic compounds. Early work centred on reagents bearing an O−F bond (e.g. CF_3OF,[26] $FClO_3$,[27] CF_3COOF,[28] CH_3COOF,[29] $CsSO_4F$[30]), or an Xe−F bond (i.e. XeF_2);[31,32] however, these reagents were often too reactive, unselective, difficult to prepare and not available commercially—all of which limited their adoption. Fluorine gas (F_2) requires specialist equipment and training for safe use, which limits its general applicability. A breakthrough came in the 1980s, with the introduction of bench-stable electrophilic fluorinating reagents containing an N−F bond.[33] These reagents have since emerged as effective, selective and easy-to-handle sources of electrophilic fluorine, many of which are now commercially available and do not require specialised handling procedures. N−F reagents can be divided into two classes: (i) neutral N−F reagents and (ii) quaternary ammonium N−F reagents, of which the quaternary salts are believed to be the more powerful. The popularity and broad synthetic application of N−F reagents is partly due to their long shelf life, and they can be handled safely in glassware.

Examples of N−F reagents reported from 1962-2016 are presented in **Figure 4**. The main commercial reagents of this class include NFPy (*N*-fluoropyridinium triflate/tetrafluoroborate, **12**) developed by Umemoto *et al.*,[34–36] NFSI (*N*-fluorobenzenesulfonimide, **17**) developed by Differding,[37] and Selectfluor™ (1-fluoro-4-chloromethyl-1,4-diazoniabicyclo[2.2.2]octane bis[tetrafluoroborate], **19**) developed by Banks *et al*.[38] Stavber and co-workers developed an analogue of Selectfluor™, which was named Accufluor™ (1-fluoro-4-hydroxy-1,4-diazoniabicyclo[2.2.2]octane bis[tetrafluoroborate], **21**).[39] The current widespread interest in the development of novel fluorinating reagents is demonstrated by the fact that several groups, including those of Shibata, Toste and Gouverneur, have reported new reagents in recent years. These contributions include a sterically demanding version of NFSI described by Shibata, *N*-fluoro-(3,5-di-*tert*-butyl-4-methoxy)benzenesulfonimide (NFBSI, **29**).[40] In 2013, Shibata reported chiral analogues of NFSI (**31**).[41] Gouverneur *et al*. reported chiral Selectfluor™ derivatives in 2013 (**32**),[42] followed by a novel N−F reagent derived from the ethano-Tröger's base in 2015 (**33**).[43]

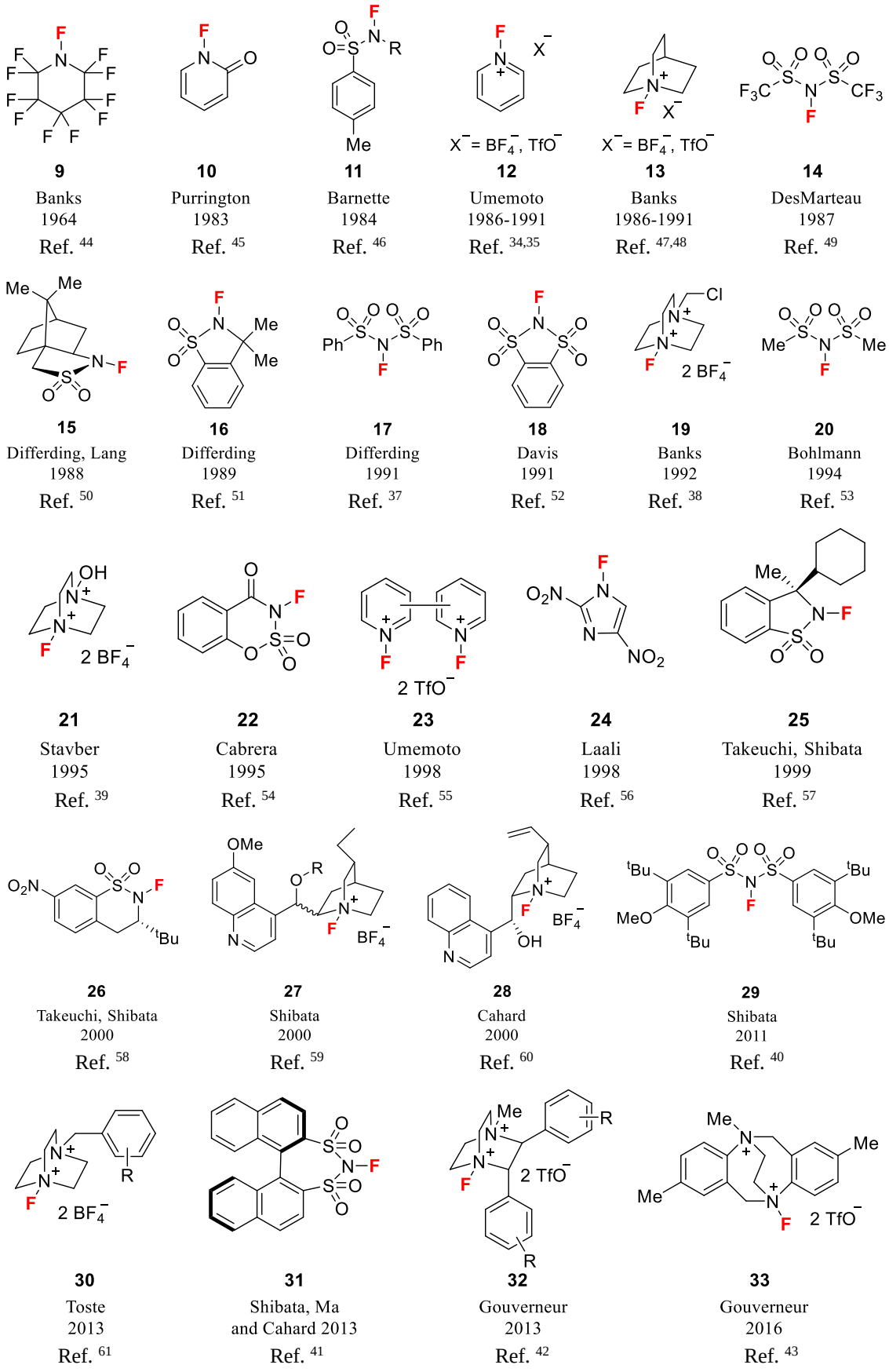

Figure 4: Examples of electrophilic N−F fluorinating reagents.

In electrophilic fluorination, the substrate behaves as the nucleophile, while the electrophile delivers equivalents of "F^+". The mechanism of electrophilic fluorination does not involve the generation of F^+, an unknown species; instead, the fluorine source transfers the fluorine atom to the nucleophile either by single-electron transfer (SET)[62] or through an S_N2 mechanism.[63] Previous reports are generally inconclusive regarding the exact mechanism of fluorination,[64] although, it is widely acknowledged that the mechanism of a specific reaction will depend on the conditions used, the nucleophile and the electrophilic fluorine source. Studies reported while this project was ongoing that provided insight into the mechanism, as well as relevant findings of the present work, will be discussed in later chapters.

1.2.1 Selectfluor™

The chemistry of selectively fluorinated molecules has expanded greatly in the last three decades with the introduction and application of fluorinating agents containing the reactive N−F bond. One of the main classes of electrophilic fluorinating reagents containing this functionality are the *N*-fluoro-1,3-diazoniabicyclo[2.2.2]octane salts, which were first discovered by Eric Banks in 1986.[65] The first compound within this family that was isolated was *N*-fluoroquinuclidinium fluoride (**Figure 5**);[47] however, a significant problem was its hygroscopic nature. Issues regarding the difficult handling of this reagent were easily overcome by varying the counterion; non-nucleophilic ions such as triflate (TfO^-) or tetrafluoroborate (BF_4^-) gave rise to a series of reagents that were easier to handle.[48] These reagents allowed selective fluorination of a range of nucleophiles; however, their synthetic utility was hindered by the low yields of desired products obtained.

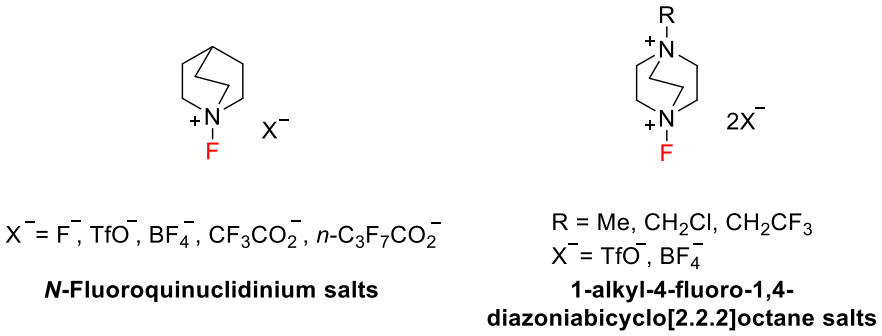

Figure 5: Fluorinating reagents developed by Banks and co-workers.

The next generation of fluorinating reagents consisting of the bicyclooctane structure displayed a DABCO portion instead of quinuclidine.[66] Addition of an electron withdrawing group at the 4-position was found to increase reactivity, with the following order: CF_3CH_2 > CH_2Cl > Me ~ Et ~ C_8H_{17}, determined based on reaction yields.[67] This led to the development of the Selectfluor™ reagent **19** (**Scheme 1**), which is more reactive than the quinuclidine-based reagents, and is a shelf-stable, non-hygroscopic crystalline solid.

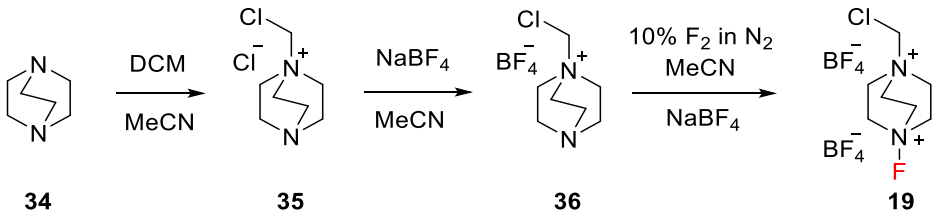

Scheme 1: Synthesis of Selectfluor™ **19**.

Since its discovery, Selectfluor™ has rapidly become a commercial chemical produced on a multi-ton scale, and is now one of the most popular N−F reagents.[68] Every year, 25 tonnes of Selectfluor™ sell for $7.5 million.[69] This reagent is widely used for both small-scale laboratory applications and moderate-scale industrial syntheses, as well as playing an important role in medicinal and drug discovery applications. Selectfluor™ is thermally stable up to 195 °C, has moderate to high solubility and stability in polar solvents (water, MeCN, DMF, MeOH, THF) and has low toxicity. To demonstrate its stability, a self-accelerating decomposition temperature (SADT) test was performed, whereby a 55-gallon drum filled with Selectfluor™ was heated to 56 °C for 7 days; the temperature remained constant within ± 5 °C during this time.[68] Despite its low atom efficiency (only 5.3% by weight is active fluorine), since its first published report, around 135 patents cite Selectfluor™. 80% of all commercially available fluorosteroids are synthesised industrially using Selectfluor™,[69] which replaced highly corrosive reagents such as perchloryl fluoride (ClO_3F).[5,70] Indeed, fluticasone propionate **37** (**Scheme 2**) is one of the most prescribed fluorosteroid products in the pharmaceutical industry. Between 2009 and 2012, global sales of fluticasone propionate-containing therapeutics totalled approximately $17 billion.[69]

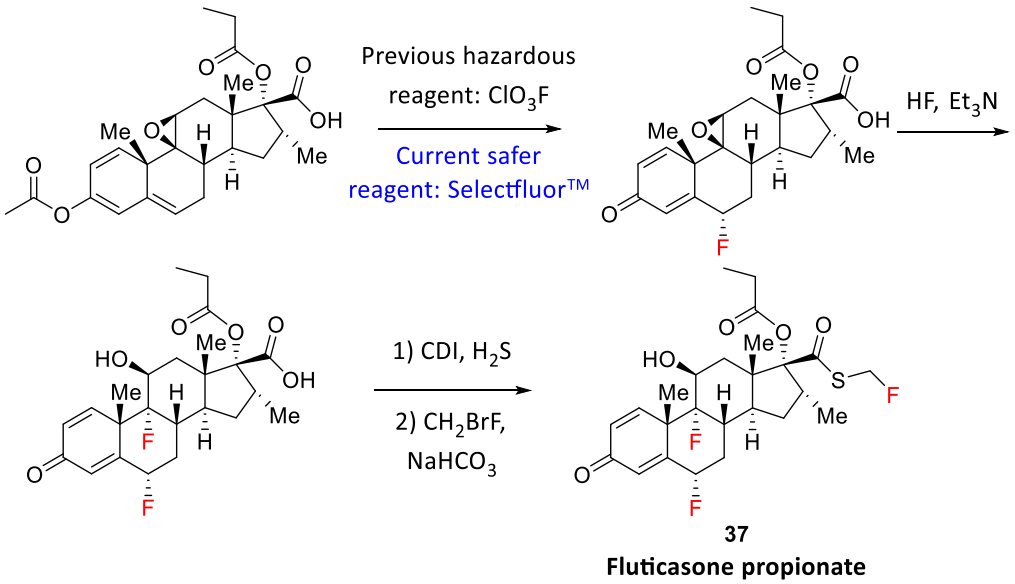

Scheme 2: The use of Selectfluor™ as the fluorinating agent for the preparation of fluticasone propionate **37**, replacing highly corrosive reagents.

1.2.2 *N*-Fluorobenzenesulfonimide (NFSI)

N-Fluorobenzenesulfonimide (NFSI, **17**) was first reported by Differding in 1991.[37] It is a bench-stable, crystalline reagent, which was prepared in one step from the commercially available benzenesulfonimide using 1 equivalent of fluorine gas (F_2/N_2, 10% w/w) in MeCN at −40 °C in the presence of powdered NaF in an ambient pressure reactor. Using an excess of fluorine led to fluorination of the aromatic rings and was thus avoided. After evaporation of the solvent, purification by recrystallisation from Et_2O or column chromatography yielded NFSI in 70% yield. NFSI is soluble in most organic solvents (e.g. THF, methylene chloride, MeCN, toluene). Recent examples of applications of NFSI include several reports by the pharmaceutical industry.

In 2014, NFSI was employed in the difluorination of fluorene to synthesise ledipasvir **38** (**Figure 6**), a therapeutic for the treatment of hepatitis C.[71,72] When used in combination with direct-acting antiviral agents, ledipasvir inhibits non-structural protein 5A (NS5A), which plays a key role in hepatitis C virus RNA replication. Ledipasvir received approval by the FDA in 2014. Following extensive screening with a range of non-fluorinated inhibitors, it was found that lipophilic linkers present in the structures afforded higher potencies, leading to the development of fluorene ring-linked inhibitors (compound **39a**, **Figure 6**). However, the stability of these systems was affected by the propensity for autoxidation to form **39b**, which gave a significant loss of potency.

Blocking the oxidation site with a *gem*-dimethyl group (**39c**) caused a greater reduction in potency, suggesting that a sterically bulky linker was not suitable.

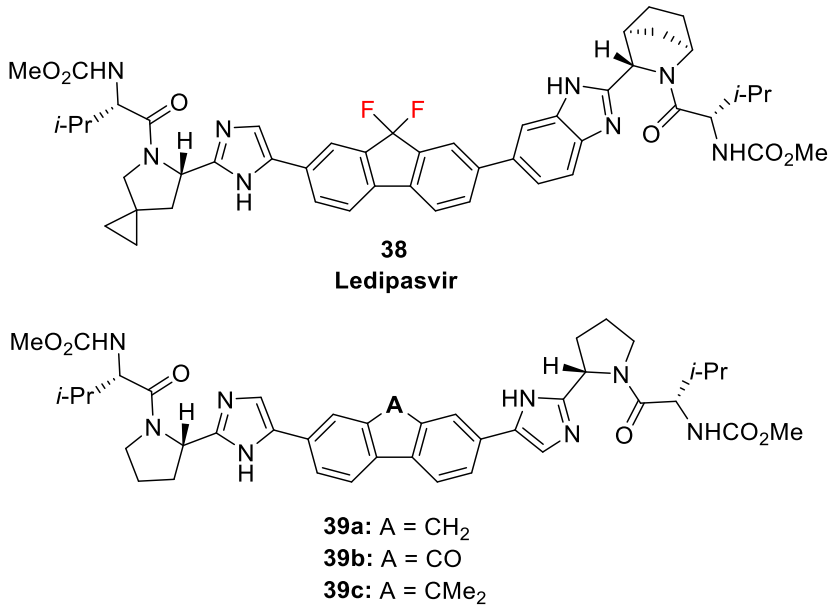

Figure 6: Structure of ledipasvir **38**, and non-fluorinated analogues prepared towards its discovery.

The use of a smaller, lipophilic blocking group, difluoromethylene, gave the difluorofluorene as the most potent inhibitor in the series. Further structural modifications improved the pharmacokinetics, and the oral bioavailability increased 3-fold compared to the non-fluorinated analogue. In the initial synthesis of ledipasvir, the difluorofluorene moiety was formed by treatment of the dibromofluorenone derivative **40** with an excess amount of the nucleophilic fluorinating reagent Deoxo-Fluor™ **41** at high temperatures (**Scheme 3**). However, Deoxo-Fluor™ is thermally unstable,[73] thus, this reaction was unsuitable for industrial scale manufacture.

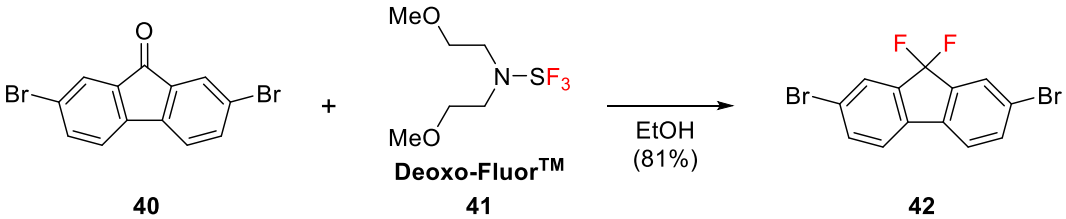

Scheme 3: Synthesis of difluorofluorene **42** using Deoxo-Fluor™ **41**.

An alternative novel process was developed, where fluorene **43** was difluorinated using NFSI **17** in the presence of KHMDS to give **44** (**Scheme 4**). It was essential to premix the substrate and NFSI, with slow addition of the base to the mixture, giving the difluorinated product in excellent yield without isolation of the monofluorofluorene.[71]

Although the reasons for the success of this particular procedure were not given, it exemplifies the sensitivity of fluorinations towards reaction conditions. This process was the first report on the base-promoted difluorination of the 9-position of a fluorene ring system using an electrophilic fluorinating reagent.

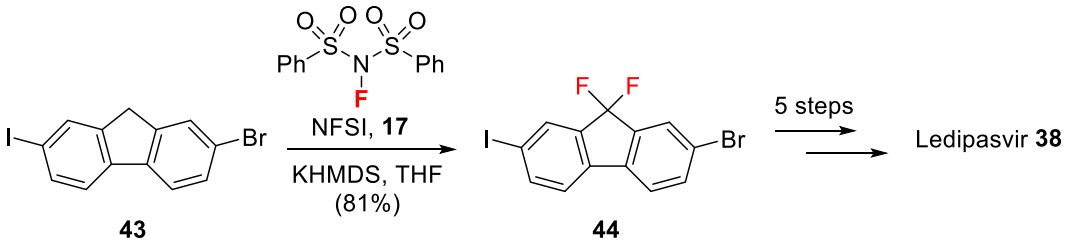

Scheme 4: Improved synthesis of Ledipasvir **38** using NFSI **17** as the fluorinating reagent.

A kilogram-scale enantioselective fluorination using NFSI was reported in 2015 by GlaxoSmithKline[74] for the synthesis of preclinical drug candidate **47**, a tyrosine kinase (Syk) inhibitor (**Scheme 5**). The fluorine atom was introduced into the molecule at the initial stages of the process, via the fluorination of chiral auxiliary **45** in the presence of a chiral catalyst, (*S*)-BINAP-Pd(MeCN)$_2$(TfO)$_2$, and the mild base 2,6-lutidine, in ethanol to yield **46**.

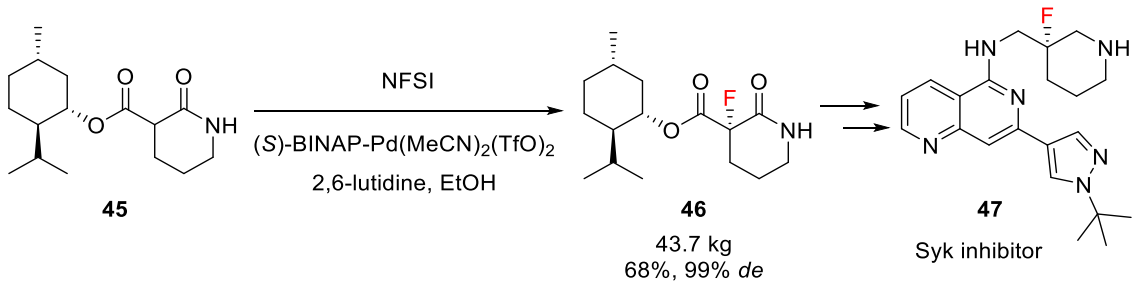

Scheme 5: Synthesis of an Syk inhibitor using NFSI, a chiral auxiliary and a chiral catalyst.

1.2.3 *N*-Fluoropyridinium salts

In 1965, Meinert reported the reaction of F_2 with pyridine in $CFCl_3$ at −70 °C to yield a white precipitate, which upon analysis, revealed a 1:1 ratio of Py:F_2 in the complex.[75] This contrasted with the bis-coordinated complexes of pyridine with other halogens[76] and was assigned a $[PyF]^+F^-$ structure (**Figure 7**). Although the pyridine-F_2 adduct was able to fluorinate uracil and chloroolefins at low temperature, it decomposed at temperatures greater than −2 °C, hence, was not viewed as a viable fluorinating reagent.

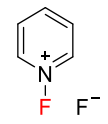

48

[PyF$^+$]F$^-$

Figure 7: Structure of the Py:F_2 complex first isolated.

Umemoto and co-workers successfully converted this intermediate compound to more stable salts, via the *in situ* conversion of the fluoride into the triflate salt by treatment with NaOTf.[34] This led to the development of the *N*-fluoropyridinium (NFPy) salts, which are a range of stable, easy-to-handle crystalline compounds featuring electron withdrawing or electron donating groups on the pyridine ring (**Figure 8**).[31,54]

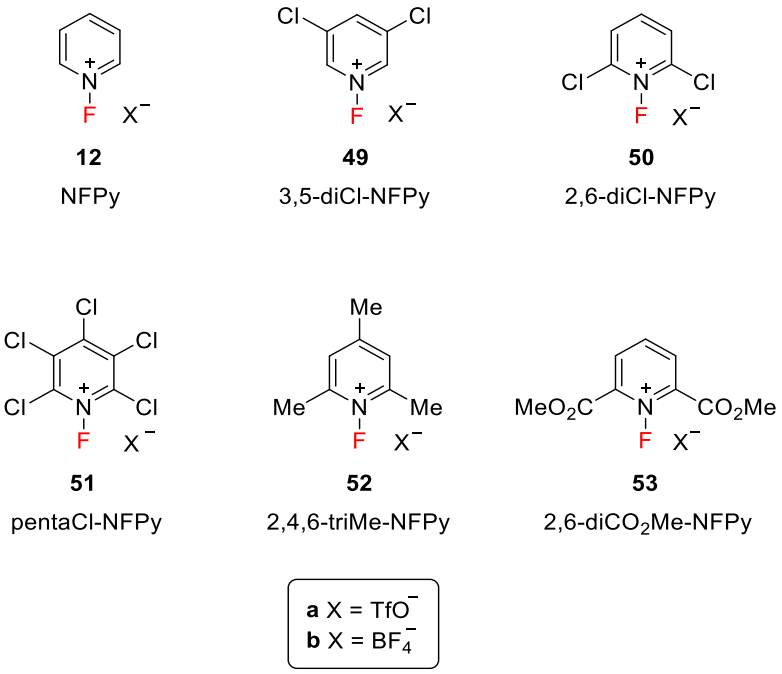

Figure 8: *N*-fluoropyridinium salts developed by Umemoto and co-workers. They will be referred to by the abbreviations shown, in the present work.

Procedures for the preparation of *N*-fluoropyridinium salts involved a one-step reaction from the pyridine with fluorine gas, followed by anion exchange with a Lewis acid, Brønsted acid or the alkali metal salt of the acid to form the BF_4^- or TfO^- salts. Reagents NFPy TfO^-/BF_4^- **12a/b**, 2,6-diCl-NFPy TfO^-/BF_4^- **50a/b** and 2,4,6-triMe-NFPy TfO^-/BF_4^- **52a/b** are commercially available, and several studies have reported their use in laboratory-scale fluorinations. NFPy salts have been used to fluorinate

aromatics, carbanions, active methylene compounds, alkyl- and silyl-enol ethers, vinyl acetates, ketene silyl acetals, olefins and sulfides.[36,77]

Umemoto *et al.* developed two additional series of salts, the *N*-fluoropyridinium-2-sulfonates **54a-e** and the *N*,*N*'-difluorobipyridinium compounds **55a-d** (**Figure 9**).[55,78] In the latter, both fluorine atoms are effective for fluorination. Reagent **55d** was identified as the most reactive and easy-to-handle reagent; indeed, it is commercially available under the name Synfluor™.

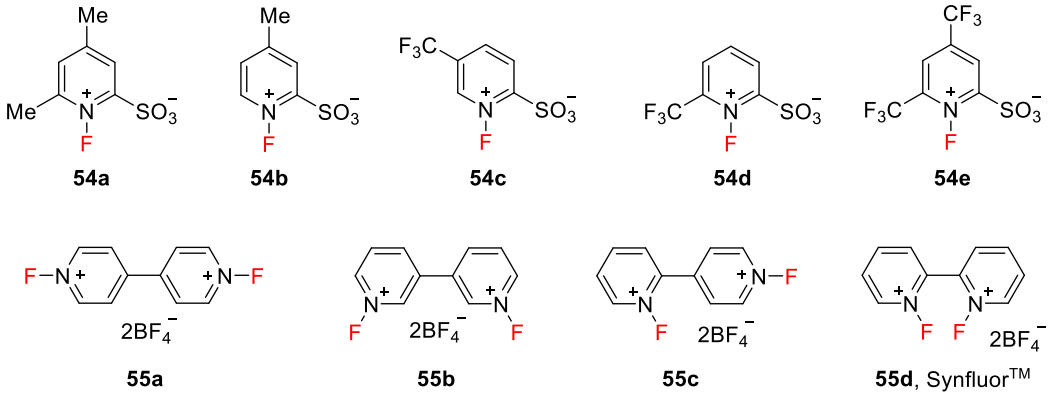

Figure 9: *N*-fluoropyridinium-2-sulfonates (**54a-e**) and *N*,*N*'-difluorobipyridinium salts (**55a-d**) developed by Umemoto and co-workers.

Among the many synthetic applications of the NFPy reagents, in 2006, Sanford *et al.* reported the first palladium-catalysed aromatic fluorinations using NFPy salts.[79] The N–F reagents NFSI **17**, Selectfluor™ **19**, NFPy BF_4^- **12b** and triMe-NFPy BF_4^- **52b** were each screened for the fluorination of 8-methylquinolone **56** in the presence of $Pd(OAc)_2$ (**Scheme 6a**). TriMe-NFPy BF_4^- **52b** was found to give the desired fluorinated product **57a** in 75% yield, while other reagents gave only 9-16% yield. Arylated and acetoxylated side products **57b** and **57c** were obtained due to competing oxidation pathways in varying amounts depending on the N–F reagent used. Secondly, the fluorination of phenylpyridine **58** was successfully achieved using NFPy BF_4^- **12b** to give product **59** in 75% yield, with no formation of side-products analogous to **57b** and **57c**.

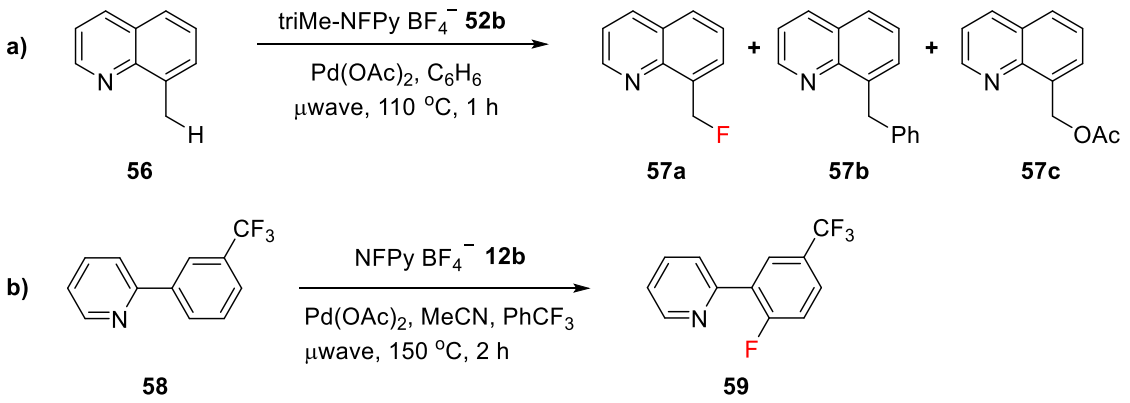

Scheme 6: (a) Pd-catalysed fluorination of 8-methylquinoline **56**. (b) Pd-catalysed fluorination of phenylpyridine **58**.

Finally, the fluorination of more complex structures has been achieved by Shibata *et al.*, where triMe-NFPy TfO⁻ **52a** was employed for the synthesis of fluorobrevianamide E (**Scheme 7**), which is a fluoro-isostere of the corresponding natural product.[80]

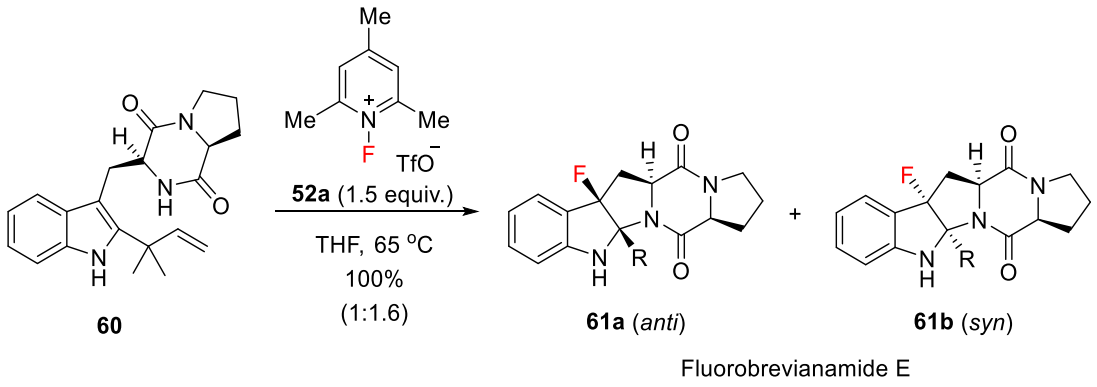

Scheme 7: Synthesis of β-fluoroamine fluorobrevianamide E (**61**) using triMe-NFPy TfO⁻ **52a**.

1.3 Quantification of fluorinating power

Due to the high reactivity of many early fluorinating reagents (CF_3OF, $CsSO_4F$, XeF_2), as well as their high sensitivity to reaction conditions, quantitative analyses of reactions involving these electrophilic fluorinating agents are scarce. Three examples of kinetics studies have been reported: by Appelman and co-workers[81] in 1981 (reactions of fluoroxysulfate with aromatic compounds), oxytrifluoromethylation kinetics studied by Levy and Sterling[82] in 1985 (reactions of CF_3OF with ring-substituted styrenes) and fluorination of alkenes via $CsSO_4F$ and XeF_2 by Stavber *et al.* in 1993.[83]

With the introduction of the N−F reagents, the problems associated with previous types of fluorinating agent were minimised due to the selectivity, stability and optimal

reactivity of the N−F reagents. This enabled more convenient reactivity studies for fluorination and several attempts towards ranking the reactivities of fluorinating reagents have been made over the past 30 years, each employing different experimental approaches.

1.3.1 Reduction potentials approach

In 1992, Lal *et al.* reported electrochemical measurements on ten N−F reagents.[84] Cyclic voltammetry (CV) studies were conducted to determine the peak potential of the first one-electron reduction (E_p^{red}) of the N−F reagents in MeCN or DMF at a Pt electrode. The more negative E_p^{red} values correspond to decreasing oxidising power (selected examples shown in **Figure 10**). The authors found a correlation between the E_p^{red} values and reported synthetic fluorinations of aromatics, hence proposing that the most oxidising reagent (most positive E_p^{red} value) had the greatest fluorinating power. E_p^{red} values measured in DMF for four of the reagents gave slightly different values than those obtained in MeCN, although the relative oxidising powers were the same.

However, there are limitations associated with the reduction potentials approach. Firstly, a fundamental quantity that could provide an indication of the reactivities of N−F reagents is their electrochemical standard potential, E^o, but the reduction of N−F compounds is, in most cases, irreversible. Hence, only the E_p^{red} data are available, which are often precluded by experimental problems leading to uncertainties in the measurements and the interpretation of data. Furthermore, the reported reproducibility of E_p^{red} values obtained by Lal *et al.* was ± 0.05 V,[84] which limits the extent to which reagents of similar E_p^{red} can be differentiated.

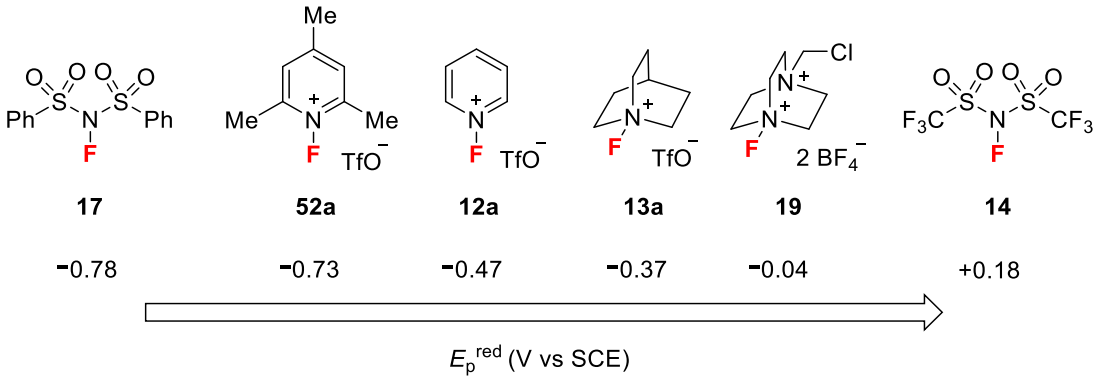

Figure 10: Peak reduction potentials, E_p^{red}, in MeCN for selected N−F reagents obtained by Lal *et al.*[84]

Despite these experimental uncertainties, the electrochemical approach has been continued. In 1999, Evans *et al.*[85] reported E_p^{red} values for six N−F reagents with tetrafluoroborate counterions, and in 2013, He and co-workers[86] reported the values for six NFSI analogues. However, since different experimental conditions were utilised in each report, a detailed comparison of all reduction potentials obtained is not possible.

1.3.2 Power variable scale

Umemoto and co-workers initiated comparative reactivity studies with their power-variable scale for *N*-fluoropyridinium salts, which centred on the electron-donating or electron-withdrawing natures of substituents on the pyridinium rings.[87] The fluorinations of different classes of nucleophiles, including aromatics, carbanions, enol alkyl ethers, vinyl esters, enol silyl ethers, enamines and alkenes were carried out with each *N*-fluoropyridinium salt, and the percentage conversions were compared. The results of fluorination of anisole to give *ortho*- and *para*-fluorinated anisoles are summarised in **Table 1**. Reagents with more electron-withdrawing substituents required less harsh conditions to achieve high conversions. The limitation of this approach is that it reflected reaction yields rather than kinetics parameters, where different temperatures, reaction times and solvents were used for each experiment; hence, reactivities are only comparable in a qualitative manner.

Umemoto *et al.* also attempted to correlate the fluorinating power of *N*-fluoropyridinium salts with their ^{19}F NMR chemical shifts.[88] The pK_a values of the corresponding pyridines were used as an estimate of electron density of the N−F bond. For the 4-substituted and 3,5-substituted salts, the ^{19}F NMR resonances shifted downfield with substitution by increasingly electron-withdrawing groups, hence, some correlation was observed between chemical shift and pK_a. For 2,6-substituted salts, however, no clear trends were observed. Furthermore, there was no dependence of chemical shift upon the counterions.

Table 1: Fluorination of anisole using *N*-fluoropyridinium triflates.

NFPy (1 equiv)	Solvent	Temp / °C	Time / h	Conversion[a] / %	Product yield[b] / %	
					o-fluoro-anisole	*p*-fluoro-anisole
triMe-NFPy **52a**	$(CHCl_2)_2$	147	10	68	42	[c]
NFPy **12a**	$(CHCl_2)_2$	120	18	72	36	[c]
3,5-diCl-NFPy **49a**	$(CHCl_2)_2$	83	18	65	48	50
2,6-diCO_2Me-NFPy **53a**	DCM	40	23	71	44	48
2,6-diCl-NFPy **50a**	DCM	40	7	71	41	41
pentaCl-NFPy **51a**	DCM	RT	0.25	91	36	38

[a] Determined by GC-MS. [b] Determined by GC-MS based on consumed anisole. [c] Yield not determined.

1.3.3 Competitive halogenation approach

In 2004, Togni and co-workers obtained the relative rates of fluorination of a β-keto ester by seven N−F reagents, in the presence of a titanium catalyst, using a competitive halogenations method.[89] The competition reactions (**Scheme 8**) were carried out in the presence of a mixture of *N*-chlorosuccinimide **63** (NCS, 1 equiv.) and the chosen fluorinating agent (1 equiv.). The catalyst [$TiCl_2$(TADDOLato)] **66** (where TADDOL = α,α,α',α'-tetraaryl-2,2-dimethyl-1,3-dioxolan-4,5-dimethanol) was used to give high enantioselectivities. After full consumption of the β-keto ester **62** (1 equiv.) as determined by TLC monitoring, the composition of the resulting mixture **64**/**65** of *α*-halogenated β-keto esters was determined by chiral HPLC. The authors assumed that the chlorination reaction occurred at the same rate (k_{Cl}) independently from the fluorinating agent used for the concomitant fluorination process. The molar ratio of the two halogenated products was considered a relative measure of the rate of fluorination with a given N−F reagent, described by **Equation 1**. The rate constants k_{F} and k_{Cl} are the rates of fluorination and chlorination, respectively. The parameters n_{F} and n_{Cl} represent the molar amounts of fluorination and chlorination products formed, respectively.

$$k_{\mathrm{rel}}(\mathrm{F/Cl}) = \frac{k_{\mathrm{F}}}{k_{\mathrm{Cl}}} = \frac{n_{\mathrm{F}}}{n_{\mathrm{Cl}}} \qquad (\mathbf{1})$$

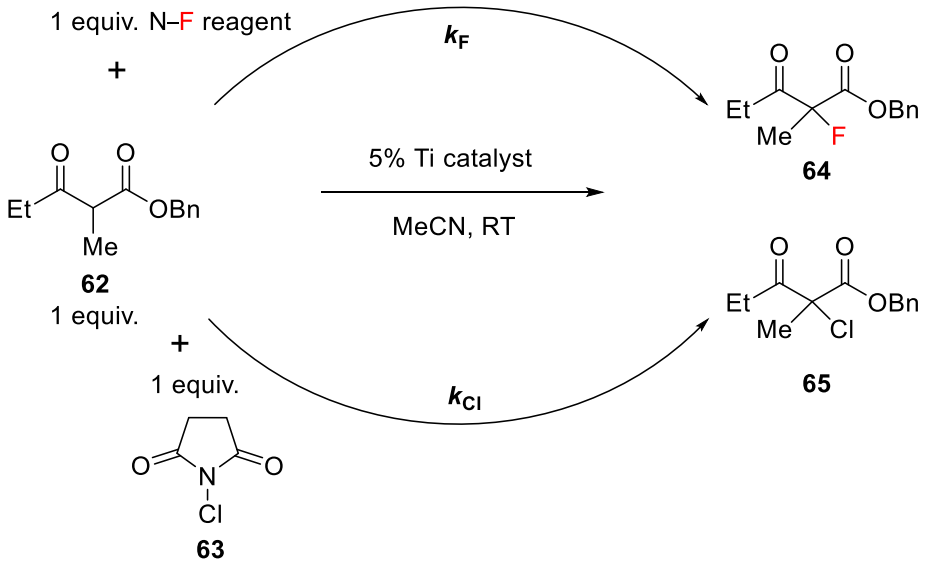

Scheme 8: Competitive halogenation reaction.

The k_{rel}(F/Cl) values were calculated from the ratios of products at the end-point of the reactions as determined by chiral HPLC (**Table 2**). It is not clear from the report whether the yields were calculated based on the amount of both (*R*) and (*S*) enantiomers, or the yield of the major enantiomer only. The yield of fluorinated product in each reaction was divided by that of the chlorinated product to give the k_{rel}(F/Cl) values listed in the table. According to the results, Selectfluor™ **19** and Accufluor™ **21** are the most powerful fluorinating agents. The *N*-fluoropyridinium salts **54d**, **50b** and **55d** showed moderate reactivities. The neutral amine derivatives reacted slowly; for example, NFSI reacted 70 times slower than Selectfluor™, while perfluoropiperidine **9** was the least reactive reagent towards β-ketoester **62**.

However, the limitation of this approach is that the k_{rel}(F/Cl) values captured the whole catalytic cycle rather than individual fluorination rate constants. A computational study on the mechanism of fluorination of β-ketoester **62** in the presence of the Ti catalyst **66** was reported,[90] where it was proposed that binding of the dicarbonyl to the catalyst to form complex **68** precedes the fluorination step (**Scheme 9**). The roles of the Ti catalyst and enolization of the β-ketoester are likely to have a significant effect on the rate constants for the reactions, which were not considered in the competitive halogenation studies.

Table 2: Results of competitive halogenations. Yields were determined by HPLC.

N−F reagent	Product **64**		Product **65**		k_{rel}(F/Cl)
	Yield / %	*ee* / %	Yield / %	*ee* / %	
Selectfluor™ **19**	73	70	27	57	2.72
Accufluor™ **21**	65	60	35	49	1.84
NFPy-2-sulfonate **54d**	45	74	55	38	0.81
diCl-NFPy BF_4^- **50b**	13	53	87	49	0.15
Synfluor™ **55d**	6	45	94	62	0.06
NFSI **17**	4	67	96	63	0.04
N-Fluoro-perfluoropiperidine **9**	3	74	97	64	0.03

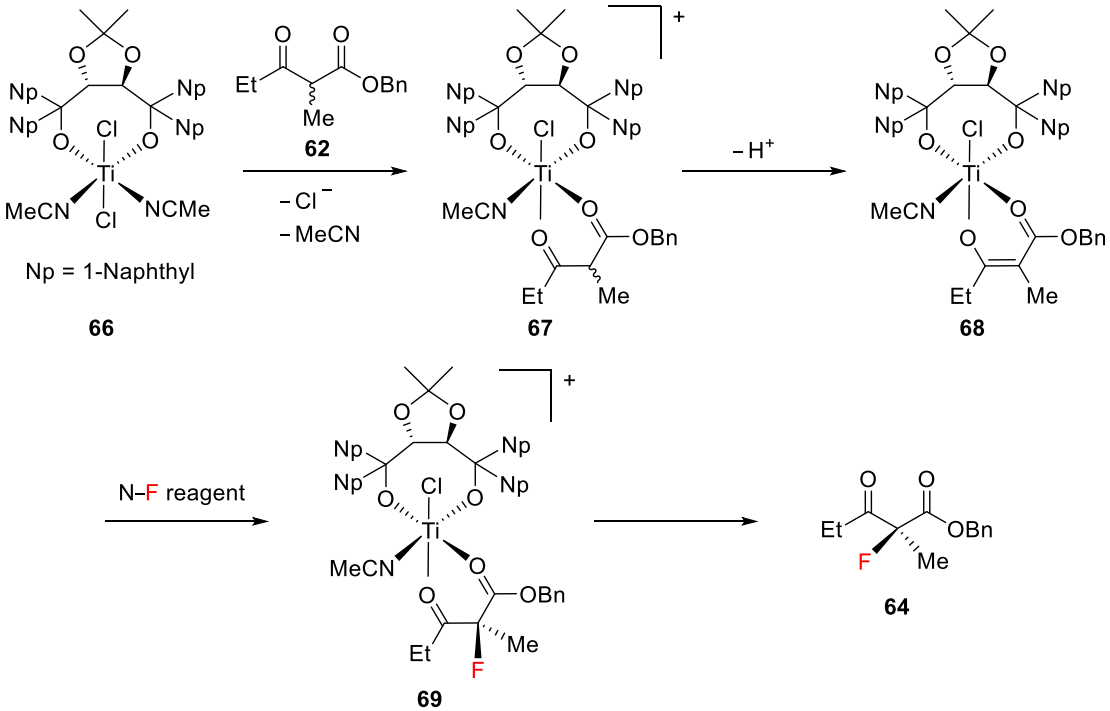

Scheme 9: Proposed mechanism for the Ti-catalysed asymmetric fluorination reaction of a β-ketoester.

1.3.4 Kinetics approach

Kinetics studies are a well-established strategy for determination of predictive reactivity profiles. In this context, Stavber and co-workers reported the kinetics of fluorination of phenols with Selectfluor™ **19** (**Scheme 10**)[91] and alkenes by Accufluor™ **21** (**Scheme 11**).[92] The consumption of these N−F reagents during fluorination reactions was monitored using iodometric titration to obtain kinetic data. Aliquots of thermostatted solutions of the nucleophile were removed at various time intervals and mixed with ice cold KI solution. The liberated iodine was then titrated with $Na_2S_2O_3$. Second-order rate constants were calculated from **Equation 2** below, where c_{A0} and c_{B0} represent initial concentrations of N−F reagent and nucleophile, respectively. The concentrations of N−F reagent and nucleophile after time t are represented by c_A and c_B.

$$\frac{1}{c_{A0} - c_{B0}} \times \frac{\ln(c_{B0} \times c_A)}{\ln(c_{A0} \times c_B)} = k_2 \times t \qquad (2)$$

The substituted phenols **70a-c** were reacted with Selectfluor™ in MeCN at 15 °C (**Scheme 10**), yielding mixtures of 2-fluoro-cyclohexa-3,5-dienones **71a-c** and 4-fluoro-cyclohexa-2,5-dienones **72a-c** in almost equimolar proportions.[91] The rate constants obtained from iodometric titrations are summarised in **Table 3**. The least hindered phenol **70a** was four times more reactive than the most hindered derivative **70c**. The effect on the reaction rate of the presence of an external nucleophile (alcohols, water, trifluoroacetic acid) was also explored. The addition of MeOH resulted in small increases in k_2 values for all three phenols, while ethylene glycol and water decreased the reaction rates considerably.

Additionally, activation parameters ($\Delta G^{‡}$, $\Delta H^{‡}$, $\Delta S^{‡}$) for these reactions were obtained from the linear correlation of k_2 with temperature, as derived from the Eyring equation. The activation free energy $\Delta G^{‡}$ had values of around 80 kJ mol^{-1} at 15 °C for all three phenol substrates, independent of the external nucleophile. The structure of the phenol substrates had little effect on activation enthalpies $\Delta H^{‡}$ (values ~75 kJ mol^{-1}), whereas activation entropies $\Delta S^{‡}$ (values ranging from −5 J K^{-1} mol^{-1} to −40 J K^{-1} mol^{-1}) depended greatly on the substrate structure and the nature of the external nucleophile.

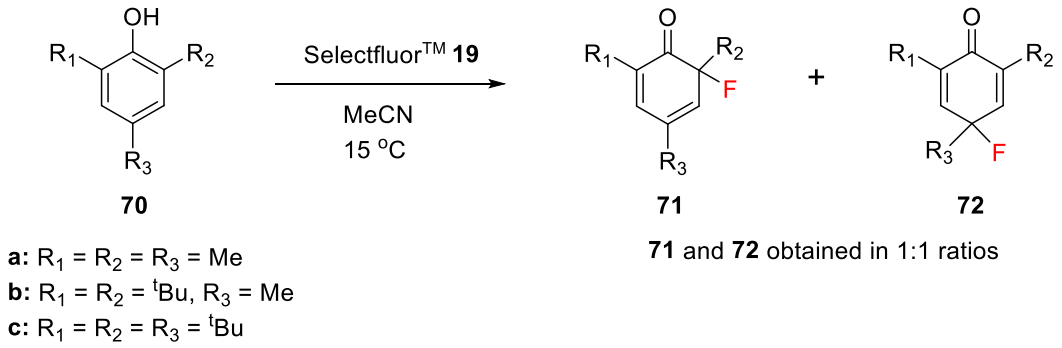

Scheme 10: Fluorination of phenols **70a-c** by Selectfluor™.

In the second study, the fluorination of phenyl-substituted alkenes **73a-c** with Accufluor™ **21** was carried out in MeCN at 24 °C, with MeOH as the secondary nucleophile (**Scheme 11**).[92] Vicinal fluoro-methoxy adducts were obtained, with Markovnikov type regioselectivity. The effect of alkene structure on the rate of fluorination is shown by the rate constants in **Table 3**. The main factor affecting the fluorination rate was the number of phenyl groups around the double bond; introduction of two or three groups into the molecule increased the reactivity of the substrate. However, the rate constant for reaction of tetraphenylethene **73c** was slightly lower than that of triphenylethene **73b**, which was attributed to steric factors. The use of water as the secondary nucleophile gave small reductions in k_2 (1.3- to 2-fold, see **Table 3**). Activation parameters were also determined for the fluorination of alkene **73a**. The $\Delta G^{\ddagger}$ values were 85 kJ mol^{-1} in the presence of each secondary nucleophile. The $\Delta H^{\ddagger}$ parameters were 74 kJ mol^{-1} in the presence of water, and 62 kJ mol^{-1} with MeOH. The $\Delta S^{\ddagger}$ values obtained were −75 J K^{-1} mol^{-1} with MeOH, and −37 J K^{-1} mol^{-1} with water.

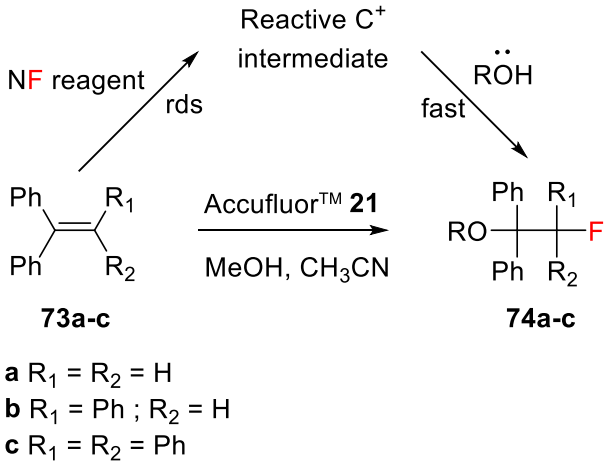

Scheme 11: Fluorination of substituted alkenes **73a-c** by Accufluor™.

Table 3: Summary of second-order rate constants, k_2, for fluorination reactions involving substituted phenols and alkenes.

N−F reagent	Structure	Temp / °C	Solvent	k_2 / M^{-1} s^{-1}
Selectfluor™ **19**	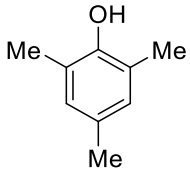 **70a**	15	MeCN	3.5×10^{-2}
	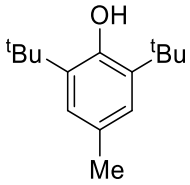 **70b**	15	MeCN	1.5×10^{-2}
	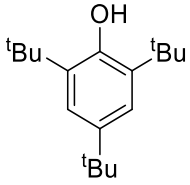 **70c**	15	MeCN	9.0×10^{-3}
Accufluor™ **21**	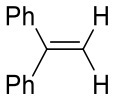 **73a**	24	MeCN/MeOH 11:1 MeCN/H_2O 11:1	9.1×10^{-3} 6.7×10^{-3}
	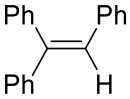 **73b**	24	MeCN/MeOH 11:1	2.7×10^{-2}
	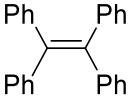 **73c**	24	MeCN/MeOH 11:1	2.0×10^{-2}

1.3.5 Computational approach

One of the earliest attempts towards quantitatively ranking the reactivities of the electrophilic fluorinating reagents was a report by Christe and Dixon in 1992.[93] Based on computational calculations, a scale of F^+ detachment (FPD) energies were developed for a series of so-called oxidative fluorinators with the general formula XF_n^+. These values were (in kcal mol^{-1}): KrF^+ (115.9), N_2F^+ (139.3), XeF^+ (164.8), NF_2O^+ (175.3) and NF_4^+ (180.1), where F^+ itself was set to zero and the value for KrF^+ was calculated from experimental data. The oxidizing power of each species decreased with an increase in FPD energy.

In 1994, Sudlow and Woolf[94] described an approach based on semiempirical molecular orbital calculations for a series of *N*-fluoropyridinium salts and their R_3N precursors. The calculated enthalpy of the "reduction couple" [ΔH_f^o (R_3N) − ΔH_f^o (R_3N^+F)] was correlated with the LUMO energy of the *N*-fluoropyridinium cation, where the calculated enthalpy is related to the FPD energy discussed above. A thermodynamic ordering based on calculated F^+ detachment enthalpies, which correlated with LUMO energies of the *N*-fluoropyridinium ions, was proposed.

In 2016, the FPD approach was extended to 130 electrophilic N−F reagents by Cheng *et al.* for the construction of an energetic scale for fluorination.[95] The fluorinating potentials of the electrophilic N−F reagents in two commonly used solvents, DCM and MeCN, were computed in terms of N−F bond heterolysis energies as expressed by the FPD values (**Equation 3**).

$$Y{-}F \xrightarrow[\Delta H^o]{\text{FPD}} Y^- + F^+ \qquad (\mathbf{3})$$

The FPD scales calculated by Cheng *et al.* cover a range of 112.3 to 290.4 kcal mol^{-1} and 110.9 to 278.4 kcal mol^{-1} in DCM and MeCN, respectively. The scales comprise the *N*-fluorosulfonimides, *N*-fluorosulfonamides, *N*-fluorocarboxamides, *N*-fluoro heterocycles, *N*-fluoropyridiniums and *N*-fluoroammoniums. A scale containing several of the main N−F reagents is shown in **Figure 11**. Lower energies correspond to increasing electrophilic fluorinating power. Selectfluor™ **19**, Accufluor™ **21** and NFSI **17** are found in the mid-region of the series. The *N*-fluoropyridinium salts cover a wider range, with *N*-fluoro-2,3,4,5,6-pentachloropyridinium **51** predicted to have one of the highest fluorinating powers.

However, the positions of Selectfluor™ **19**, NFPy **12** and NFSI **17** are uncertain as, based on the synthetic literature precedent (which will be further discussed in Chapter 2 Section 2.11), these reagents show very different reactivities. Additionally, nucleophiles were not included in their models, so it is challenging to relate the predicted reactivities to specific substrates.

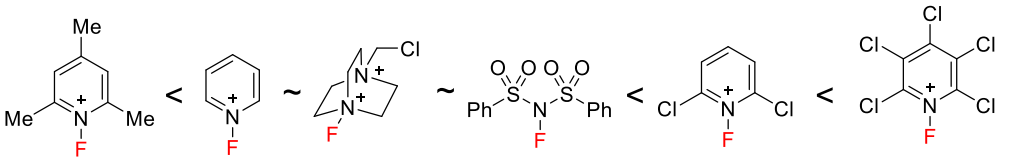

	Trimethyl-NFPy	NFPy	Selectfluor™	NFSI	Dichloro-NFPy	Pentachloro-NFPy
FPD/ kcal mol^{-1} (MeCN)	236.6	230.0	229.8	229.6	204.2	191.8

Figure 11: Selected N−F reagents and their FPD values in MeCN. Counterions were not specified.

1.4 Fluorinated 1,3-dicarbonyl compounds

1.4.1 Pharmaceutical and industrial relevance of 1,3-dicarbonyl compounds

The purpose of the present work was to determine the relative reactivities of N−F reagents using a kinetics approach, underpinned by a class of nucleophiles with industrial and pharmaceutical relevance. Fluorine-containing 1,3-dicarbonyl derivatives are essential building blocks for drug discovery and manufacture.[96] A key example is the antifungal agent voriconazole **81**,[97] a billion-dollar drug marketed by Pfizer. Voriconazole is synthesised from 5-fluoropyrimidine intermediate **77** that is prepared from 2-fluoro-1,3-ketoester **76** (**Scheme 12**). The direct fluorination of heterocycles using F_2 has a number of associated difficulties, including fluorination at multiple sites on the ring and challenging purifications. Therefore, a building block approach is often used in the preparation of complex organofluorine compounds. In this context, finding selective and efficient routes towards the fluorination of 1,3-dicarbonyl derivatives has been the subject of significant interest.

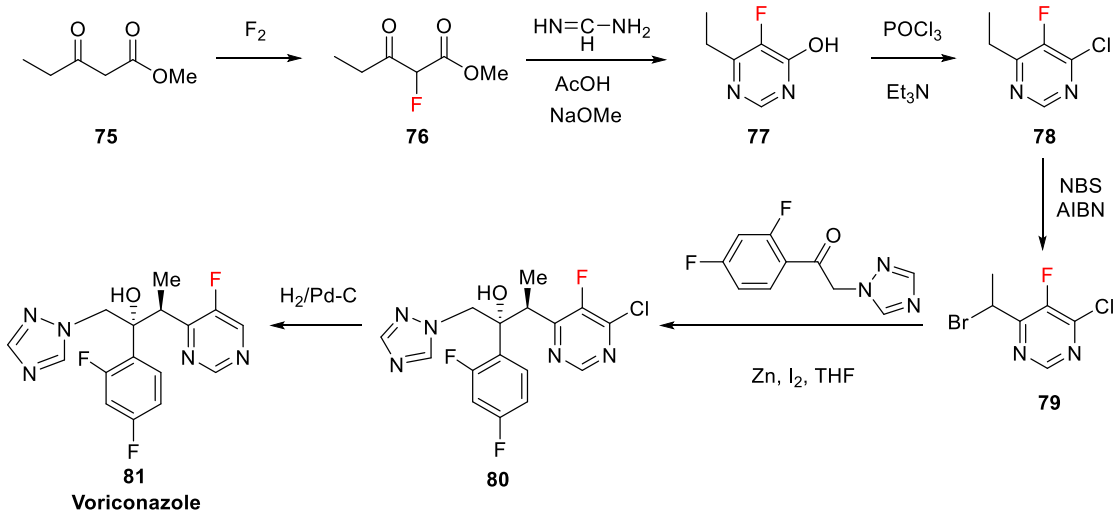

Scheme 12: Synthesis of voriconazole using a building block approach from ketoester **75**.

An important class of fluorinated 1,3-dicarbonyl derivatives are the fluoromalonates, which are versatile synthons utilised in a wide variety of applications. Electrophilic N−F reagents are often utilised for the fluorination of malonate compounds. A team at Merck fluorinated the sodium salt of malonate **82** using Selectfluor™ **19** in THF, towards the synthesis of tyrosine kinase inhibitors for anti-cancer applications (**Scheme 13a**).[98] Selectfluor™ **19** was also used by Merck for the fluorination of diethyl malonate derivatives, such as **85**, towards the preparation of liquid crystal compounds (**Scheme 13b**).[99] NFSI **17** was used in the asymmetric fluorination of prochiral malonate esters (**Scheme 13c**), which were further employed as building blocks for the preparation of pharmaceutically-relevant compounds, including fluorinated β-amino acids, β-lactams and protease inhibitors.[100]

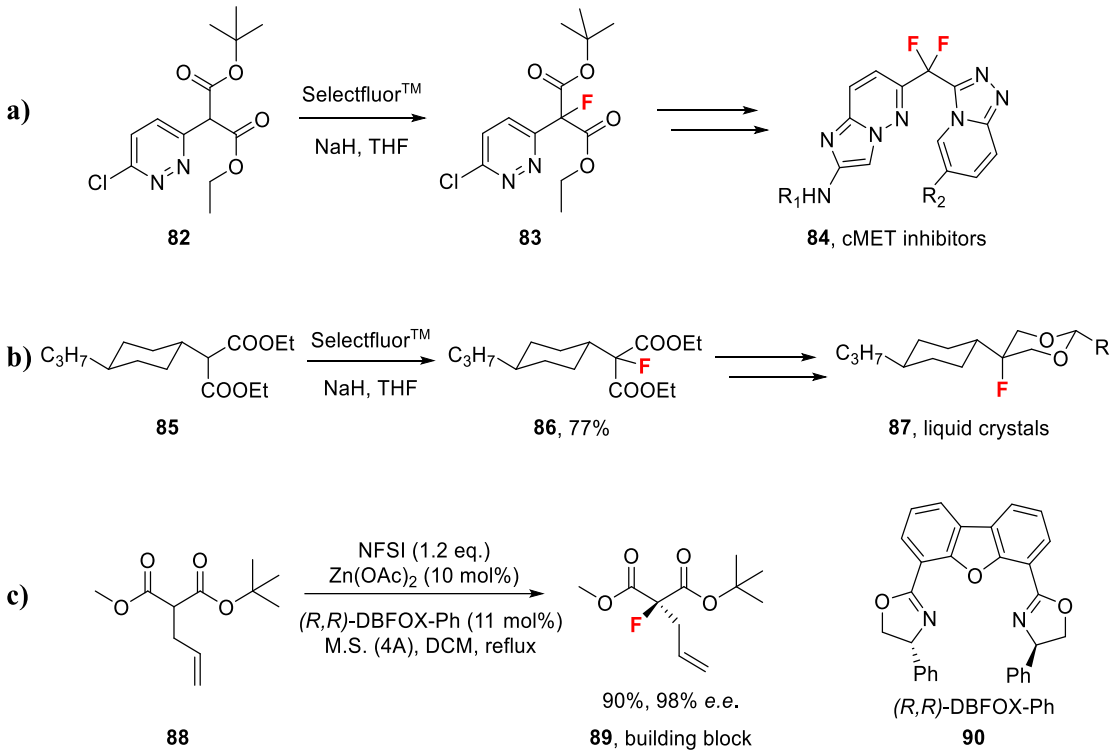

Scheme 13: Synthesis of 2-fluoromalonate derivatives using Selectfluor™ and NFSI for the preparation of industrially-relevant compounds.

1.4.2 Synthesis of fluorinated 1,3-dicarbonyl compounds

Early work regarding the fluorination of 1,3-dicarbonyl derivatives involved fluorinating reagents such as ClO_3F,[101] CF_3OF,[102] XeF_2,[103,104] $(CF_3SO_2)_2NF$[105] and NF_3O,[106] although the low selectivity, difficulties regarding preparation, high reactivity and toxicity of these reagents halted their adoption in discovery and manufacturing processes. Elemental fluorine (F_2) has been successfully used for the fluorination of 1,3-dicarbonyl systems, using both batch and flow techniques on laboratory and manufacturing scales, but this reagent requires specialist handling techniques that are not readily available in most laboratories.[107–112]

With the introduction of electrophilic fluorinating reagents of the N–F class, such as Selectfluor™, NFSI and *N*-fluoropyridinium salts, numerous reports followed concerning the electrophilic fluorination of 1,3-dicarbonyl derivatives. Procedures include catalyst-free reactions,[66] microwave-assisted methods,[113] transition metal (Ti and Ru) catalysed methods,[90,114,115] solvent-free reactions assisted by milling,[116,117] fluorinations in ionic liquids,[118] and reactions conducted in water.[119,120] In many cases, difficulties in controlling mono- versus difluorination were reported, leading to

challenging separations of the product mixtures. Therefore, finding synthetic routes that allow selective fluorination would be of great use.

Eric Banks first reported the selective monofluorination of 1,3-diketones using Selectfluor™.[66] 1,3-diketones **91a-e** were reacted with one equivalent of Selectfluor™ in MeCN at room temperature to give the corresponding α-fluoro derivatives in good yields (**Scheme 14a** and **Table 4**). Diethyl ester **91d** did not react with Selectfluor™ and required the addition of sodium hydride to form the sodium derivative of **91d**, giving the fluorodiester **92d** in 93% yield. Fluorinations occurred more rapidly with compounds that existed, at least in part, in their enolic forms, which suggested that the reactions occurred via the enols or enolates. Difluorination reactions were carried out without base for compounds **91a** and **91e**, although long reaction times were required (**Scheme 14b**). Formation of the sodium enolates of **92b** and **92e** gave the difluorinated products after 1 day.

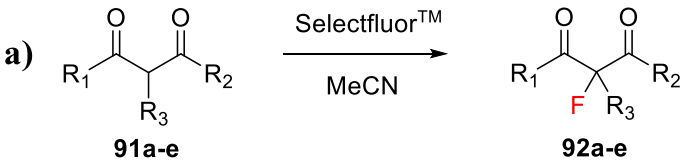

	R_1	R_2	R_3
a	Ph	Ph	H
b	Ph	OEt	H
c	Me	OEt	H
d	OEt	OEt	Ph
e	Ph	NMe_2	H

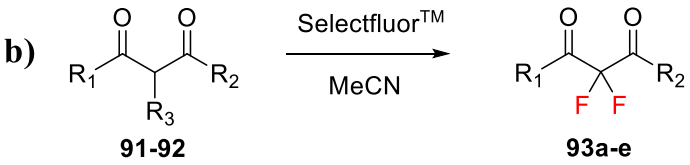

	R_1	R_2	R_3
91a	Ph	Ph	H
92b	Ph	OEt	F
91e	Ph	NMe_2	H
92e	Ph	NMe_2	F

Scheme 14: (a) Monofluorination of 1,3-dicarbonyl compounds **91a-e** via Selectfluor™. (b) Fluorination of **91a**, **92b**, **91e** and **92e** to prepare their difluorinated analogues.

Table 4: Conversion of 1,3-dicarbonyl compounds **91a-e**, **92b** and **92e** to mono- or di-fluorides with Selectfluor™ at RT. Purifications were conducted by recrystallisation or chromatography.

Nuc	R_1	R_2	R_3	Conditions	Selectfluor™ (equiv.)	Time / h	Product (crude yield / %)[a]	Yield / % (pure)
91a	Ph	Ph	H	No base	1.0	5	**92a** (100)	84
91b	Ph	OEt	H	No base	1.0	54	**92b** (88)	22
91c	Me	OEt	H	No base	1.0	120	**92c** (57)	-
91d	OEt	OEt	Ph	NaH	1.0	20	**92d** (96)	93
91e	Ph	NMe_2	H	No base	1.0	3	**92e** (96)	87
91a	Ph	Ph	H	No base	2.1	192	**93a** (96)	78
92b	Ph	OEt	F	NaH	1.1	24	**93b** (95)	95
91e	Ph	NMe_2	H	No base[b]	3.2	647	**93e** (93)	91
92e	Ph	NMe_2	F	NaH	1.2	27	**93e** (84)	73

[a] Crude yields were estimated from percentage conversions via ^{1}H NMR analysis. [b] Heated to 40 °C.

The timescales of these fluorination reactions were significantly reduced using microwave conditions, as reported by Shreeve *et al.* in 2005.[113] Microwave irradiation of 1,3-dicarbonyls **91a-c** for 10 min at 82 °C with 1 equivalent of Selectfluor™ gave the mono-fluorinated products in 70-84% yield. However, traces of α,α-difluorinated products were also isolated. Repeating the reactions with 3 equivalents of Selectfluor™ yielded mixtures of mono- and di-fluorinated products. The addition of 2 equivalents of tetrabutylammonium hydroxide (TBAH) to the reactions gave full conversions to the difluorinated products, which were isolated in 77-88% yield.

Stavber and co-workers have reported the fluorinations of cyclic and acyclic 1,3-dicarbonyls (**Scheme 15**) by Selectfluor™ in aqueous media and by NFSI under solvent-free reaction conditions (SFRC).[120] For reactions conducted in aqueous media, the nucleophile and Selectfluor™ (1.1 equiv., or 2.2 equiv. in the case of **91**) were stirred in H_2O (5 mL) at 70 °C for 4-10 h. For solvent-free reactions, the nucleophile and NFSI were stirred or powdered together until fully mixed, followed by heating at 90 °C to obtain a molten phase system. In all cases, high yields of around 80% were

obtained, except compound **94** which yielded **95** in 40% yield under both reaction conditions.

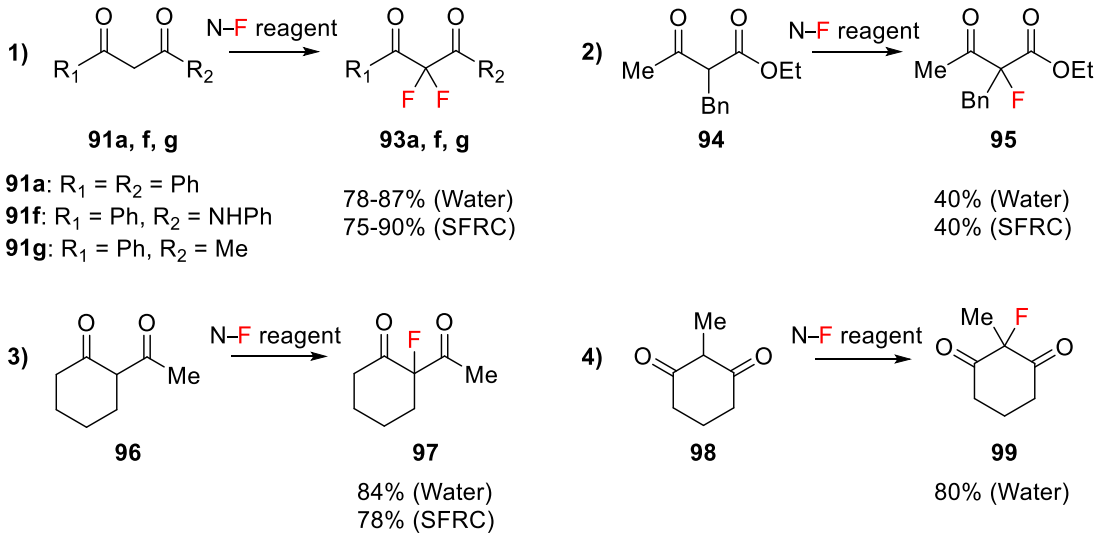

Scheme 15: Fluorination reactions involving 1,3-dicarbonyl compounds in aqueous media with Selectfluor™ and solvent-free reaction conditions (SFRC) with NFSI.

Finally, a study into the preparation of flavanols as potential anti-prostate cancer agents employed NFSI for the α-fluorination of 1,3-dicarbonyl derivative **102** (**Scheme 16**), which was present mainly in the enol form.[121] The 2-fluoro-1,3-dicarbonyl **103** was obtained in the enol form, confirmed by the ^{19}F NMR signal at $\delta = -160.3$ ppm. This was then cyclised under acidic conditions to give flavone **104** for inclusion in cell growth inhibition studies.

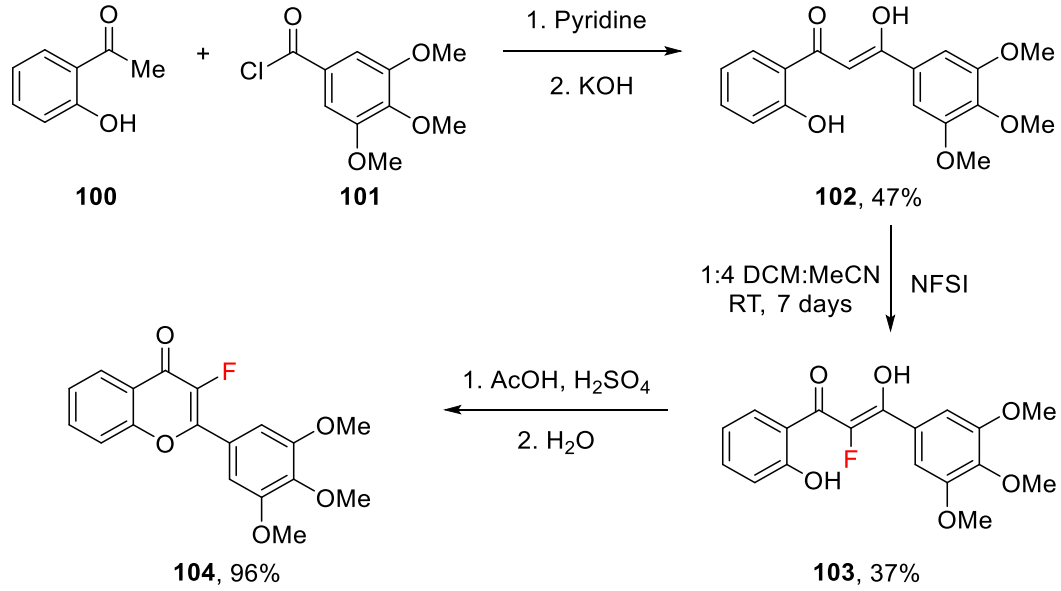

Scheme 16: Synthesis of 3-fluoro-3',4',5'-trimethoxyflavone **104**.

As indicated by the example shown in **Scheme 16**, as well as the early work by Banks *et al.* discussed in this section, enol contents of both fluorinated and non-fluorinated 1,3-dicarbonyls have a key role in dictating the success of a fluorination reaction; this will be the subject of much of the work discussed in Chapters 2, 3 and 4.

1.5 Aims and Objectives

This chapter has given an overview of the commonly-used electrophilic fluorinating reagents of the N−F class, as well as the efforts towards quantification of their reactivities. However, the reduction potentials approach was precluded by experimental uncertainties, and the qualitative Power Variable scale was based mainly on reaction yields. The kinetics studies reported by Stavber were limited to Selectfluor™ and Accufluor™, and those of Togni were conducted in the presence of a titanium catalyst, thus capturing the entire catalytic cycle. Finally, the computational approaches did not consider nucleophilic models. Thus, the choice of N−F reagent is currently determined through empirical experimentation in the absence of quantitative values for electrophilicities. The purpose of the present work is to determine the relative electrophilicities of commonly-used N−F reagents using a physical organic approach. Given the significance of 1,3-dicarbonyl derivatives in a range of applications, as discussed in Section 1.4, these were the main nucleophilic substrates employed in the present work for determination of rates of fluorinations.

The initial aim of this project is to develop convenient methods for studying the kinetics of fluorination reactions. The focus will be on widely-used electrophilic N−F reagents, including Selectfluor™, NFSI and *N*-fluoropyridinium salts. Thus, it is necessary to develop a versatile set of kinetics procedures that can be applied to a range of reaction times and selectivities. Several reaction monitoring methods will be explored, including ^{19}F and ^{1}H NMR spectroscopies ("in magnet" and discontinuous), UV-vis spectrophotometry (conventional and stopped-flow) and mass spectrometry. The techniques employed to study the kinetics of fluorination reactions will depend on the reactivities and half-lives of the reactions. Furthermore, reactions involving changes in chromophores upon fluorination will be amenable to the UV-vis approach; this will be a key focus of this work.

With convenient methods for determining reactivities in hand, the next aim is to develop a quantitative reactivity scale for electrophilic fluorination. This will be done

through the determination of rate constants for fluorination of a range of nucleophilic substrates. This scale will allow users to choose the correct level of reagent reactivity for a given nucleophilic substrate for the synthesis of fluorinated building blocks. Rate constants will provide quantitative indications of reaction times and selectivities, providing a rigorous kinetic scaffold for fluorination.

The nucleophiles employed in the kinetics studies will mainly focus on derivatives of 1,3-dicarbonyls. These will include 1,3-diaryl-1,3-propanediones and malonate esters. Other substrates will also be explored, such as enamines, silyl enol ethers, indoles and enol esters, but the suitability of these compounds for kinetics studies will depend on reaction times.

The next aim is to correlate the reactivities of the N−F reagents with the Mayr-Patz scale, which consists of the most extensive electrophilicity and nucleophilicity scales currently available. The rate constants for suitable nucleophile-electrophile combinations in this study will be plotted using known nucleophilicity parameters, *N*, to afford electrophilicity parameters, *E*, for each fluorinating reagent. These correlations are the key to predictive nucleophile-electrophile pairing.

Chapter 2 will discuss the development of a kinetic toolbox for the determination of rate constants for fluorination reactions, and the construction of a quantitative reactivity scale for electrophilic fluorinating reagents. In addition to the general aims of the project, other relevant avenues will be investigated, including the kinetics of keto-enol tautomerism and enol difluorination, which will be the subjects of Chapters 3 and 4. Although not part of the initial specific aims of this project, these studies provide valuable quantitative information on the factors that affect mono- and di-fluorination of 1,3-dicarbonyl derivatives. Chapter 5 will then discuss the various attempts made towards obtaining the electrophilicity parameters for Selectfluor™ and NFSI. Finally, Chapter 6 will focus on the kinetics of fluorination of progesterone enol acetate, a drug-like system, to test the applicability of the reactivity scale developed in Chapter 2 towards a different class of carbon nucleophiles.

Chapter 2: A Quantitative Reactivity Scale for N−F Reagents

Chapter 1 described how electrophilic fluorinating reagents of the N−F class have revolutionised fluorination chemistry due to their ease of handling, bench-stability and commercial availability. However, the choice of reagents for the fluorination of a new scaffold at the discovery stage has generally been based on a "trial and error" approach rather than an understanding of reactivities of the electrophilic fluorinating reagent and its nucleophilic substrate. Given the importance of fluorination reactions in the chemical, pharmaceutical and materials industries, a source of predictive reactivity data would be highly desirable. This chapter details the development of a firm underpinning for these widely-exploited reagents using a quantitative, kinetics approach.

2.1 Introduction

The previous approaches taken towards the determination of reactivities of electrophilic N−F reagents were discussed in detail in Chapter 1 Section 1.3. These included qualitative, kinetics and computational approaches. Furthermore, as outlined in Section 1.4, fluorine-containing 1,3-dicarbonyl derivatives are essential building blocks for drug discovery and manufacture. In the present work, for the quantification of reactivities of electrophilic fluorinating reagents, the strategy employed involved utilising a common nucleophile scaffold consisting of *para*-substituted 1,3-diaryl-1,3-dicarbonyl derivatives.

2.2 Development of the *para*-substituted 1,3-diaryl-1,3-dicarbonyls scaffold

This project began with the requirement of finding a suitable nucleophile scaffold on which to base kinetics experiments. This scaffold needed to allow tuning of reaction rates to match the technique employed to monitor the reactions. Due to the significant research interests in 1,3-dicarbonyl derivatives, as discussed in Chapter 1, this family of compounds was identified as an appropriate starting point. The 1,3-diaryl-1,3-dicarbonyl derivatives **107a-m** (**Scheme 17**) offered the potential to tune nucleophilicity in a predictable manner through the introduction of substituents that could be amenable to Hammett correlation to give mechanistic insights into the fluorination reaction. Compound **107a** is commercially available and only required purification by

recrystallisation from hexane prior to use in synthetic and kinetics experiments. Compounds **107b-e** and **107i-m** were already available from previous or on-going synthetic studies.[122,123] Compounds **107f-h** were synthesised using modified literature procedures,[124] in good yields (54-77%, see Chapter 8 Section 8.3). The general syntheses of compounds **107a-m** are shown in **Scheme 17**, for completeness. All compounds **107a-m** were purified by recrystallisation for use in the kinetics studies which are discussed in Sections 2.3-2.5 of this chapter.

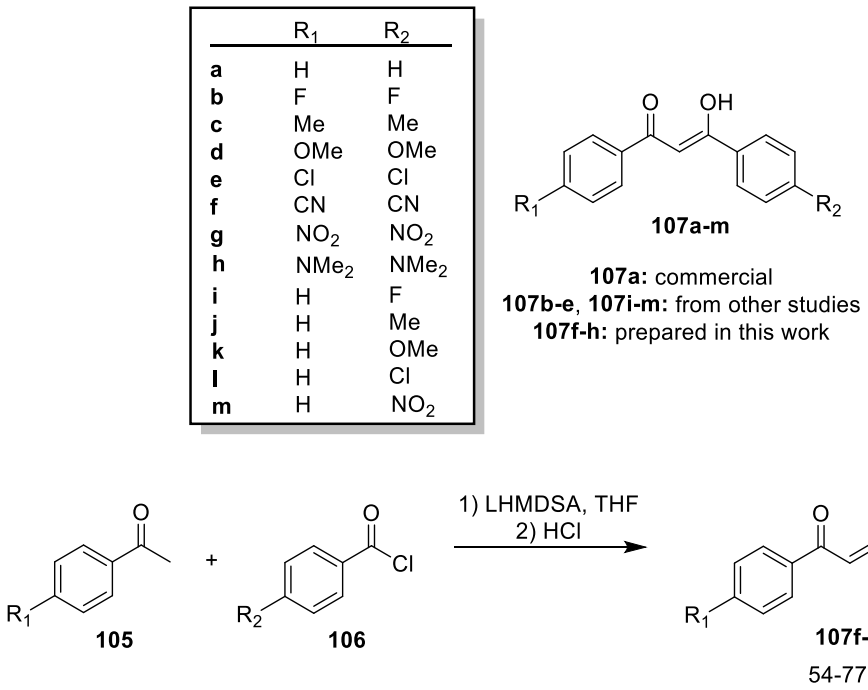

Scheme 17: 1,3-Diaryl-1,3-dicarbonyls **107a-m** and preparation of **107f-h**.

Compounds **107a-h** exist as mixtures of keto and enol tautomers and the ratio for each system was determined by ^{1}H NMR spectroscopy in MeCN-d_3 (**Table 5**). Each tautomer was easily distinguishable, with peaks at ~4.5 ppm and ~7.0 ppm corresponding to the keto and enol forms, respectively, and the OH signal of the enol form at ~16.0 ppm. Compounds **107a-m** exist in 87-95% enol form in MeCN, except **107d** (80% enol) and **107h** (70% enol).

Mono-fluorinated products **108a-f** were prepared as mixtures of keto and enol tautomers using Selectfluor™ in MeCN (**Scheme 18**), with isolated yields of 53-88% following purification by recrystallisation (chloroform, hexane). The lower yields obtained were due to the good solubility of the products in the recrystallisation solvent, and NMR analyses of the supernatant solutions confirmed the presence of product. Where

required, further quantities were recovered by evaporation of solvents from the supernatant and recrystallisation of the solid residues. The ratios of tautomers were determined by ^{19}F NMR spectroscopy in MeCN-d_3 (**Table 5**). Compounds **108a**, **108b**, **108d** and **108e** were present mainly in their ketonic forms (92-98% keto), with **108c** containing slightly more of the enol form (13% enol). The keto-enol contents were also determined in $CDCl_3$, which generally gave similar ratios to those obtained in MeCN-d_3. Compound **108f** was characterised in $CDCl_3$ only and following recrystallisation was obtained mainly in the enol form.

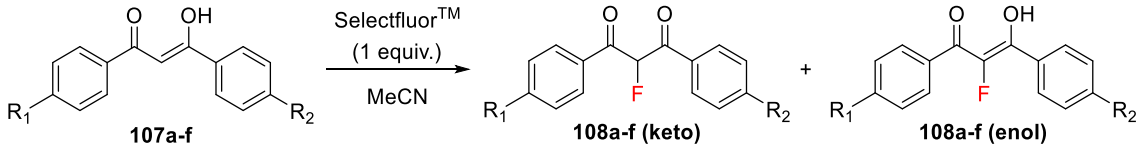

Scheme 18: Fluorination of **107a-f** using Selectfluor™.

UV-vis spectrophotometry formed the basis of the kinetics studies discussed in the next sections. Hence, the UV-vis spectral characteristics of compounds **107a-m** and **108a-e** were explored. Representative examples of spectra obtained for **107a-e** and **108a** are shown in **Figure 12**. In general, two main absorbance bands are present at ~350 nm and ~250 nm, which correspond to the enol and keto tautomers, respectively.

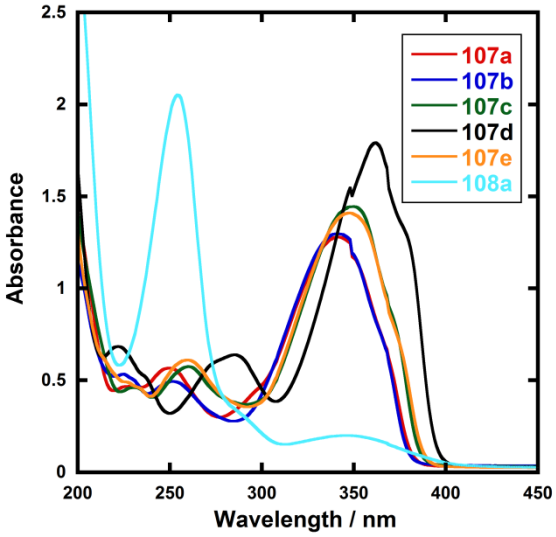

Figure 12: UV-vis spectra of authentic samples of compounds **107a-e** and **108a** (50 μM). Shoulders at 350 nm are artefacts that correspond to the spectrophotometer switching from UV to visible lamps.

The photochemistry of 1,3-dicarbonyl derivatives will be discussed in greater detail in Chapter 3. Extinction coefficients, ε, at each λ_{max} value were determined for **107a** and

108a (see Chapter 8 Section 8.3.12). The λ_{max} (enol) and λ_{max} (keto) values for **107a-m** and **108a-e** are summarised in **Table 5**.

Table 5: Keto:enol ratios for compounds **107a-m** and **108a-e** in MeCN-d_3, determined by relative peak integrals in ^{1}H and ^{19}F NMR spectra. In order to obtain quantitative integral values, relaxation delays of 20 s and 8 s were employed for ^{1}H and ^{19}F NMR experiments, respectively. The solutions were equilibrated for 10 half-lives before NMR spectra were acquired. Keto:enol ratios for **108a-f** in $CDCl_3$ are also summarised. λ_{max}(enol) and λ_{max}(keto) values for **107a-m** and **108a-e** in MeCN, determined by UV-vis spectrophotometry.

Compound	*Para* substituents	Keto:enol ratio	λ_{max}(enol) / nm	λ_{max}(keto) / nm
107a	$R_1 = R_2 = H$	9:91	341	250
107b	$R_1 = R_2 = F$	11:89	341	250
107c	$R_1 = R_2 = Me$	11:89	350	258
107d	$R_1 = R_2 = OMe$	20:80	362	281
107e	$R_1 = R_2 = Cl$	7:93	347	259
107f	$R_1 = R_2 = CN$	5:95	351	256
107g	$R_1 = R_2 = NO_2$	10:90	363	266
107h	$R_1 = R_2 = NMe_2$	27:73	425	345
107i	$R_1 = H$, $R_2 = F$	11:89	341	250
107j	$R_1 = H$, $R_2 = Me$	12:88	347	255
107k	$R_1 = H$, $R_2 = OMe$	13:87	352	240
107l	$R_1 = H$, $R_2 = Cl$	13:87	345	n.d.
107m	$R_1 = H$, $R_2 = NO_2$	9:91	355	261
108a	$R_1 = R_2 = H$	95:5 (95:5)[a]	350	255
108b	$R_1 = R_2 = F$	94:6 (98:2)[a]	341	256
108c	$R_1 = R_2 = Me$	87:13 (97:3)[a]	340	264
108d	$R_1 = R_2 = OMe$	98:2 (98:2)[a]	370	290
108e	$R_1 = R_2 = Cl$	92:8 (82:18)[a]	353	n.d.
108f	$R_1 = R_2 = CN$	n.d. (16:84)[a]	n.d.	n.d.

[a] Determined in $CDCl_3$. (n.d. = not determined)

2.2.1 Tautomeric polymorphism

Following the initial purification of 2-fluoro-1,3-dicarbonyls **108a-e**, further recrystallisations and vapour diffusion crystallisations were carried out from mixtures of hexane and chloroform. It was discovered that the keto and enol forms of **108b** ($R_1 = R_2 = F$) and **108c** ($R_1 = R_2 = Me$) crystallised separately from the same solution. For both compounds, the keto and enol tautomers formed white and yellow crystals, respectively (**Figure 13**). Based on the colour differences, crystals of each tautomer were picked from the supernatant solution and analysed spectroscopically. Both tautomers were stable with respect to tautomerisation in $CDCl_3$ over the course of at least 2-3 days. X-ray crystal structures were obtained for both keto and enol tautomers of **108b** (**Figure 14**) and **108c** (**Figure 15**).

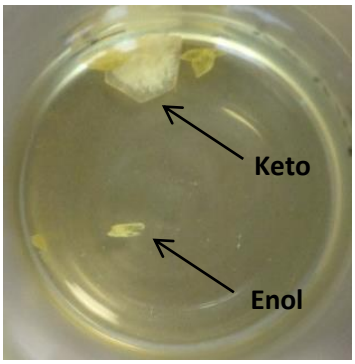

Figure 13: Image of keto (white) and enol (yellow) crystals of **108b** obtained from the same solution (recrystallisation from chloroform and hexane in a glass vial).

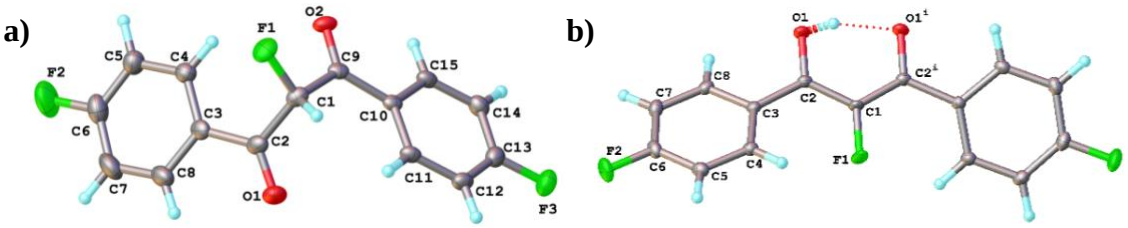

Figure 14: X-ray crystal structures for (a) **108b-keto** and (b) **108b-enol**.

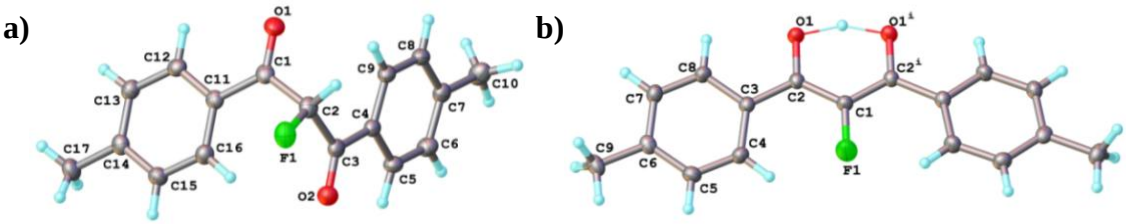

Figure 15: X-ray crystal structures for (a) **108c-keto** and (b) **108c-enol**.

In the case of compound **108a**, an X-ray crystal structure of only the keto form was obtained (**Figure 16**). Conversely, **108d** and **108e** crystallised as the enol tautomers (**Figure 17**).

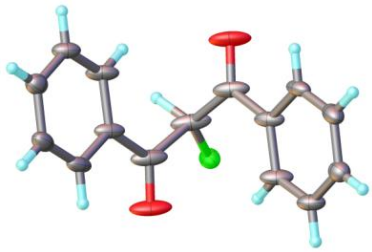

Figure 16: X-ray crystal structure for **108a-keto** ($R_1 = R_2 = H$).

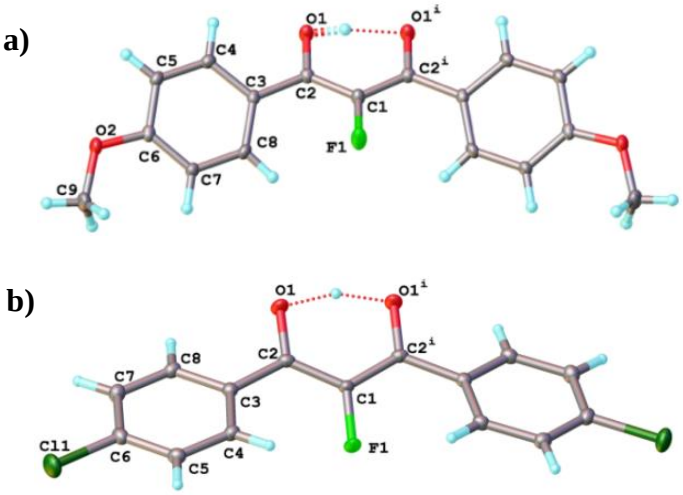

Figure 17: (a) X-ray crystal structure for **108d-enol** ($R_1 = R_2 = OMe$). (b) X-ray crystal structure for **108e-enol** ($R_1 = R_2 = Cl$).

^1H and ^{19}F NMR spectroscopic analyses (in $CDCl_3$) were conducted on the individual crystals of **108b-enol** and **108b-keto**, as well as the supernatant solution containing the keto-enol mixture. The spectra obtained are shown in **Figure 18** and **Figure 19**. The doublet at $\delta = 6.5$ ppm in the ^1H NMR spectrum of **108b-keto** with $^2J_{HF} = 49.3$ Hz is the distinguishing feature of this tautomer. The singlet at $\delta = 14.9$ ppm in the ^1H NMR spectrum of **108b-enol** with $^4J_{HF} = 3.3$ Hz corresponds to the OH peak of this tautomer. The ^{19}F NMR spectrum of **108b-keto** contains a doublet at $\delta = -186$ ppm, while that of **108b-enol** displays a singlet at $\delta = -170$ ppm. Additionally, peaks assigned to the aryl fluorine atoms are shifted upfield by 5 ppm in the ^{19}F NMR spectrum of **108b-enol** compared to **108b-keto**.

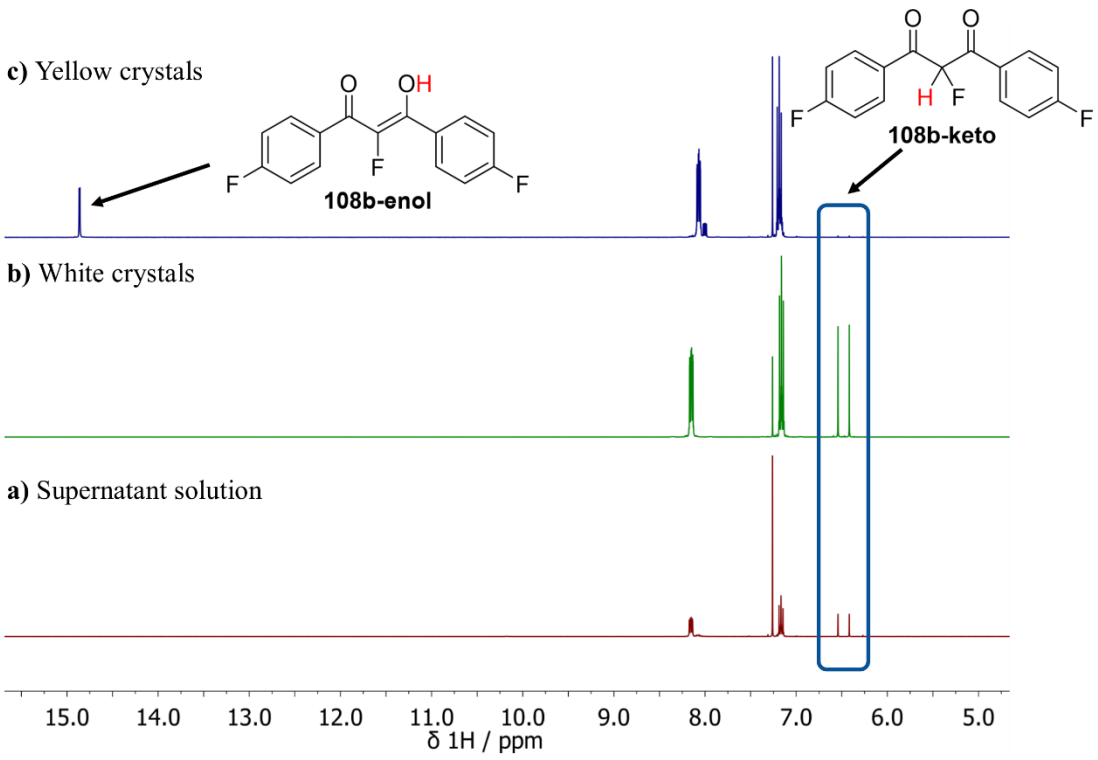

Figure 18: ^{1}H NMR spectra in $CDCl_3$ corresponding to: (a) supernatant solution from recrystallisation of **108b** containing 98:2 keto-enol mixture; (b) white crystals of **108b-keto** after recrystallisation; (c) yellow crystals of **108b-enol** after recrystallisation.

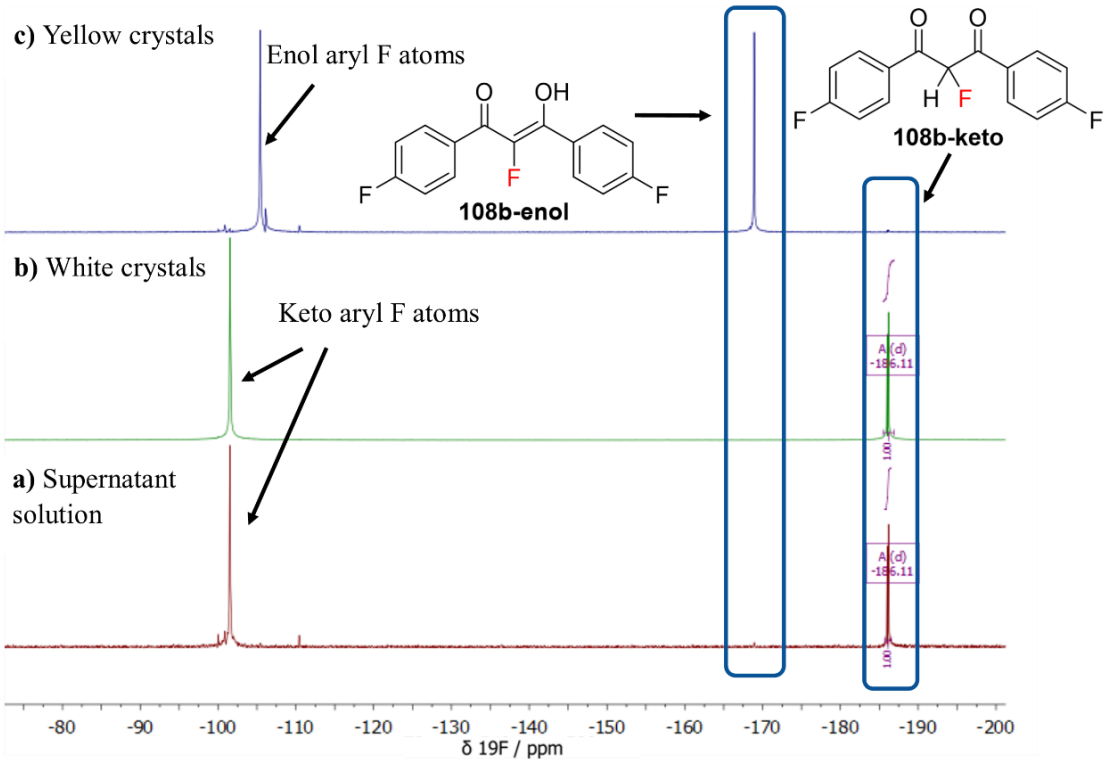

Figure 19: ^{19}F NMR spectra in $CDCl_3$ for **108b**: (a) supernatant solution; (b) **108b-keto**; (c) **108b-enol**.

So-called "tautomeric polymorphs", where tautomers crystallise in different crystal structures, are very rare, with the CSD containing only 16 examples.[125] Compounds **108b** and **108c** are believed to represent the first examples of fluorinated molecules to exhibit this phenomenon. The propensity for systems **108b** and **108c** to produce crystals of both tautomers rests on many kinetic and thermodynamic factors. In order to gauge the influence of the intrinsic stabilities of each tautomer, DFT calculations were conducted by Dr Mark Fox on enol and keto monomers and dimers of **108c** ($R_1 = R_2 =$ Me) (**Figure 20**) using the procedures described by Groom *et al.*[125] (see Chapter 8 Section 8.3 for full description of computational methods). Single point energy calculations were performed on the optimised gas-phase geometries, where the dielectric constant of $\varepsilon_r = 3$ is typical in neutral organic crystals[126] (ε_r represents relative permittivity). The enol form was determined to be more stable as a monomer by 2.0 kJ mol^{-1} but the keto form was more stable as a dimer by 2.0 kJ mol^{-1} when the dielectric constant of $\varepsilon_r = 3$ was applied as the solvent model. The very small relative energies support the possibility that crystals of both forms may be observed experimentally. Dielectric constants of $\varepsilon_r = 0$ and 11 were also applied to further assess the effects of solvent polarities on relative energies (**Table 6**), where $\varepsilon_r = 11$ and $\varepsilon_r = 0$ represent polar and non-polar conditions, respectively. The keto forms became more favourable as the solvent polarity (dielectric constant) was increased.

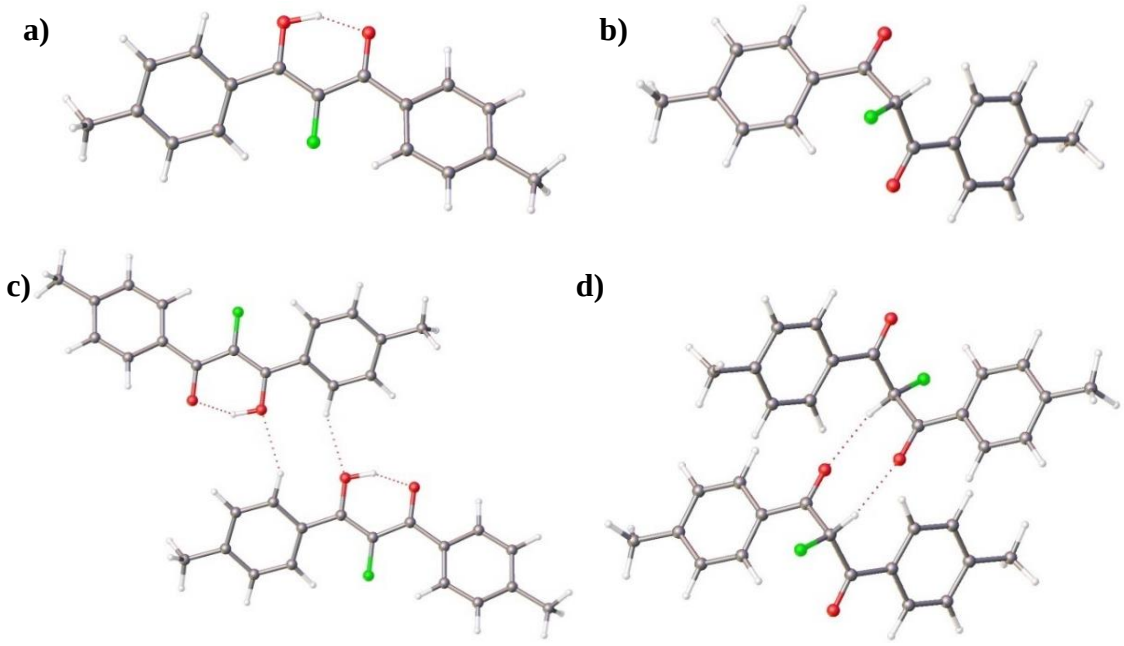

Figure 20: Fully optimised geometries for **108c**. (a) Enol monomer. (b) Keto monomer. (c) Enol dimer, intermolecular H…O distances are 2.623 Å. (d) Keto dimer, intermolecular H…O distances are 2.408 Å.

Table 6: Relative energies in kJ mol^{-1} of tautomers of **108c** at B3LYP/6-311++G**.

Structure of **108c**	Tautomer of **108c**	$\varepsilon_r = 0$	$\varepsilon_r = 3$	$\varepsilon_r = 11$
Monomer	Enol	0	0	0.9
	Keto	7.5	2.0	0
Dimer	Enol	0	2.0	6.4
	Keto	6.6	0	0

2.3 Kinetics of fluorination of compounds 107a-m

The previous section discussed the establishment of the nucleophile scaffold consisting of 1,3-diaryl-1,3-dicarbonyl compounds **107a-m** bearing different electron-donating or electron-withdrawing *para* substituents. The extended conjugation within these systems offered sensitive spectrophotometric output, where keto and enol tautomers displayed markedly different absorption profiles, as shown in **Figure 12** (Section 2.2). Furthermore, in **107a-m**, the tautomeric equilibrium lies towards the enol form, while in **108a-e**, it lies towards the keto form. Hence, the fluorination reactions were suited to monitoring by UV-vis spectrophotometry, due to the distinct difference in spectra of starting materials and products. As well as enhancing or subduing nucleophilicity, compounds **107a-m** were also amenable to Hammett correlation to obtain mechanistic information. With knowledge of the differing keto-enol tautomeric equilibria of starting materials and fluorinated products in hand, the 1,3-diaryl-1,3-dicarbonyls were anticipated to give a convenient nucleophile scaffold on which to base kinetics experiments with a range of commonly-used N−F reagents (**Scheme 19**).

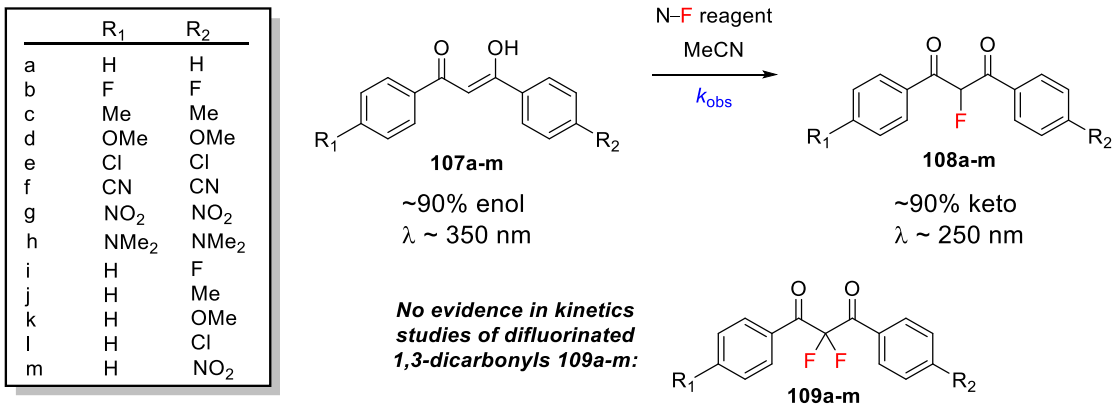

Scheme 19: Kinetics studies for mono-fluorination of **107a-m** by N−F reagents.

In all kinetics studies conducted by UV-vis spectrophotometry and NMR spectroscopy investigated in this chapter, the formation of 2,2-difluoro-1,3-dicarbonyls **109a-m** was not observed on the timescales that were monitored. This was corroborated by NMR studies as well as LC-MS studies (the latter will be discussed in Section 2.5).

Kinetic studies were performed on Selectfluor™ **19**, NFSI **17**, Synfluor™ **55d**, 2,6-dichloro-*N*-fluoropyridinium triflate **50a**, 2,6-dichloro-*N*-fluoropyridinium tetrafluoroborate **50b**, 2,3,4,5,6-pentachloro-*N*-fluoropyridinium triflate **51a**, *N*-fluoropyridinium triflate **12a**, *N*-fluoropyridinium tetrafluoroborate **12b**, 2,4,6-trimethyl-*N*-fluoropyridinium triflate **52a** and 2,4,6-trimethyl-*N*-fluoropyridinium tetrafluoroborate **52b** (**Figure 21**). All reagents were commercially available, except for 2,3,4,5,6-pentachloro-*N*-fluoropyridinium triflate **51a**, which was synthesised from pentachloropyridine **110** and elemental fluorine following the literature procedure[35] (**Scheme 20**).

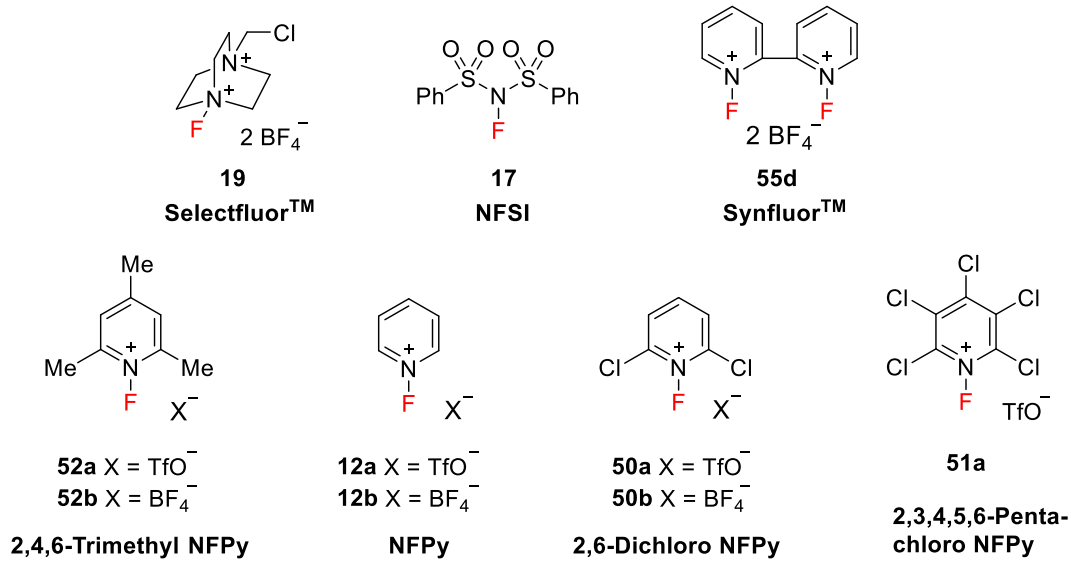

Figure 21: Fluorinating reagents investigated in this work.

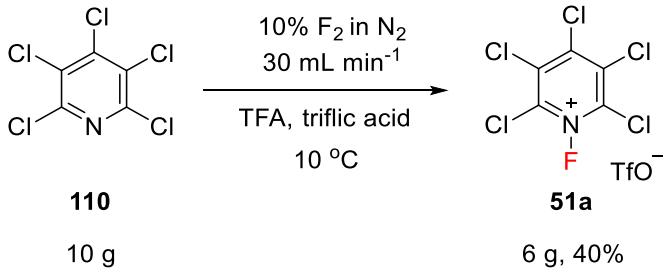

Scheme 20: Synthesis of 2,3,4,5,6-pentachloro-*N*-fluoropyridinium triflate **51a** using **110** and F_2 gas.

The rates of fluorination of nucleophiles **107a-m** with the electrophilic fluorinating reagents shown in **Figure 21** were generally determined by UV-vis spectrophotometry in MeCN. Stock solutions of each reaction partner were prepared, and aliquots were diluted to the required concentration. Following pre-equilibration to the desired temperature, the reactions were performed in cuvettes by mixing the reaction partners (for further experimental methods and instrument details see Chapter 8 Section 8.2).

Time-arrayed multi-wavelength studies of fluorination of **107a-m** by Selectfluor™ **19** showed clean, isosbestic behaviour, suggesting that no intermediate species were built up. A representative example is shown in **Figure 22a** for the fluorination of **107d** (R_1 = R_2 = OMe). As discussed in the previous section, the nucleophiles **107a-m** display absorption bands at λ_{max} = 340-360 nm corresponding to their enol forms, and at λ_{max} = 250-270 nm associated with the diketone form, as well as additional transitions due to the enol tautomer. As each fluorination reaction progressed, the absorption band at ~250 nm increased in intensity, corresponding to the formation of the diketone form of the monofluoro-products **108a-m**, and the starting enol nucleophile signal at λ ~ 350 nm decreased. Plots of absorbance changes at four λ values over time are shown in **Figure 22b** for **107d** and fitting of these data afforded identical first-order rate constants (k_{obs}).

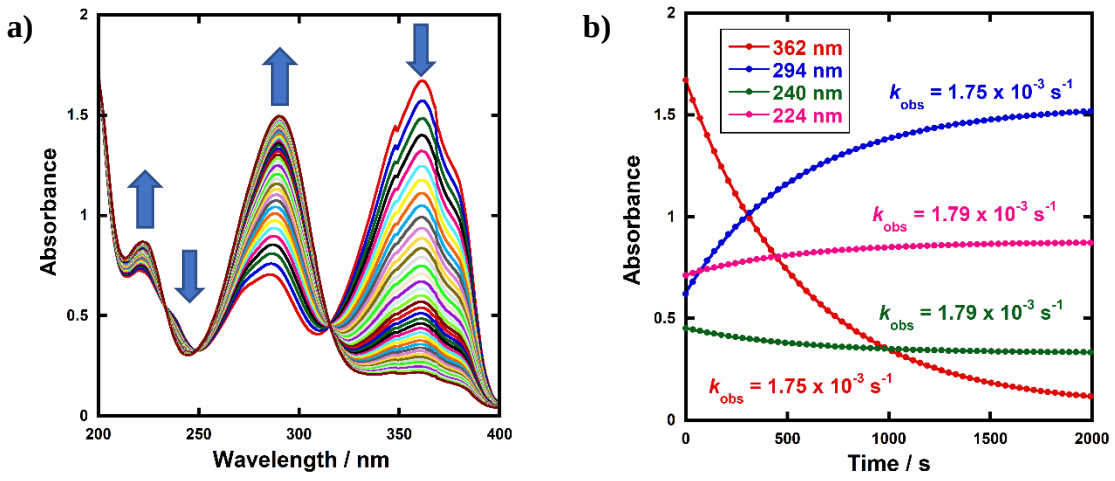

Figure 22: (a) UV-vis spectra during the reaction of **107d** (50 μM) with Selectfluor™ (in MeCN at 25 °C), each spectrum acquired at 30-second intervals. (b) Exponential behaviour at 4 different wavelengths.

Similar behaviours were displayed across the range of 1,3-dicarbonyl derivatives and fluorinating reagents. For example, the fluorination of the mono-substituted 1,3-dicarbonyl **107k** (R_1 = H, R_2 = OMe) by Selectfluor™ also showed isosbestic behaviour

(**Figure 23a**). Plots of absorbance versus time at three λ_{max} values gave identical k_{obs} values (**Figure 23b**). Multi-wavelength UV-vis studies for all other fluorination reactions are included in Chapter 8 Section 8.3.13.

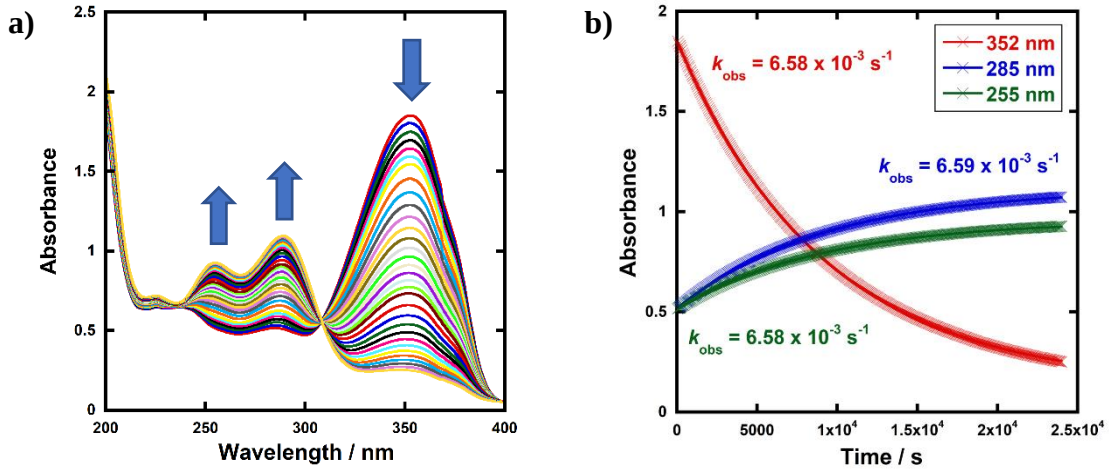

Figure 23: (a) UV-vis spectra during the reaction of **107k** (50 μM) with Selectfluor™ (500 μM) in MeCN at 25 °C, displaying isosbestic behaviour. (b) Exponential behaviour at 3 different wavelengths, with identical rate constants, k_{obs}, determined.

By monitoring the decays in absorbance of the enol tautomer at λ ~ 350 nm, the kinetics of fluorination reactions were conveniently monitored by UV-vis spectrophotometry. All kinetics experiments were carried out with excess electrophile in order to achieve pseudo-first order conditions. Clean exponential decays of absorbance of the UV-active nucleophile were observed in all runs (**Figure 24a**), and the first-order rate constants k_{obs} were obtained from the fitting of plots of absorbance versus time. When k_{obs} values were plotted against Selectfluor™ concentration, a simple linear (i.e. first order) correlation was observed (**Figure 24b**). The direct dependence upon fluorinating reagent concentration demonstrated rate-limiting fluorination and thus the slopes of these graphs gave the second-order rate constants k_2 [M^{-1} s^{-1}] that report on both nucleophilic and electrophilic partners, according to the second-order rate **Equation 4**. The rate constants for the reactions of **107a-m** with each fluorinating reagent are summarised in **Table 7**. All kinetics studies were conducted at 25 °C, although rate constants at additional temperatures were in some cases obtained for the determination of activation parameters (see Section 2.8).

$$\text{Rate} = -\frac{\text{d[Enol]}}{\text{dt}} = k_2[\text{Enol}][\text{NF reagent}] \qquad (\mathbf{4})$$

$$\text{Hence: Rate} = k_{\text{obs}}[\text{Enol}], \text{since [NF reagent]} \approx \text{constant}$$

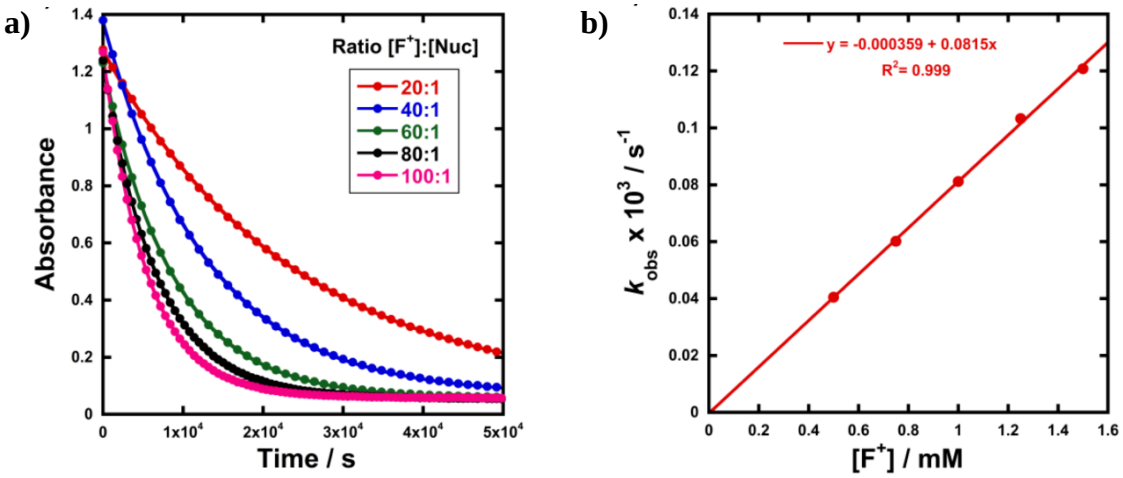

Figure 24: (a) Representative exponential decays of absorbance with different concentrations of N–F reagent. (b) Representative correlation of k_{obs} with [N–F reagent].

Monitoring the kinetics of fluorination reactions involving reagents NFPy TfO^- **12a**, NFPy BF_4^- **12b**, triMe-NFPy TfO^- **52a** and triMe-NFPy BF_4^- **52b** was initially attempted by UV-vis spectrophotometry. However, the reactions were very slow at the low concentrations required by the UV-vis method. These studies were then conducted at higher concentrations of both reaction partners using discontinuous ^1H and ^{19}F NMR spectroscopy reaction monitoring methods, where fluorination reactions proceeded faster and at more measurable rates. Only nucleophile **107d** (R_1 = R_2 = OMe) was used in these kinetics reactions (**Scheme 21**), since it is one of the most reactive nucleophiles in the series. Details of methods and spectra are included in Chapter 8 Section 8.3.

A typical reaction monitoring method by discontinuous ^{19}F NMR spectroscopy involved dissolving enol **107d** and the required fluorinating reagent in MeCN, where the latter was present at a concentration at least 10-fold greater than the concentration of the former, to maintain pseudo-first order conditions. The solution was transferred to an NMR tube containing a D_2O lock tube, and NMR spectra were acquired at ~24-hour intervals for 9-50 days. The NMR tube was kept in a water bath at 25 °C when not acquiring NMR data. Using the MestreNova Data Analysis tool for stacked arrayed NMR data, the signal corresponding to the fluorine atom in **108d** at δ = −188 ppm was integrated in each spectrum (**Figure 25a**). Plots of the integral intensities versus time

showed exponential behaviour (**Figure 25b**). The formation of **108d-enol** was not observed on the timescales of the reactions that were monitored. The difluorinated derivative **109d** was also not observed.

In the case of reagents NFPy TfO^- **12b** and triMe-NFPy BF_4^- **52b**, the reactions were conducted in MeCN-d_3, hence, the ^{19}F NMR data were supplemented by ^1H NMR spectroscopy to determine reaction kinetics. In the ^1H NMR spectra of the reactions, the doublet at δ = 6.80 ppm corresponding to C2-*H* of **108d-keto** was integrated in the stacked arrayed NMR data using the MestreNova Data Analysis tool. Second-order rate constants obtained from these experiments are reported in **Table 7**.

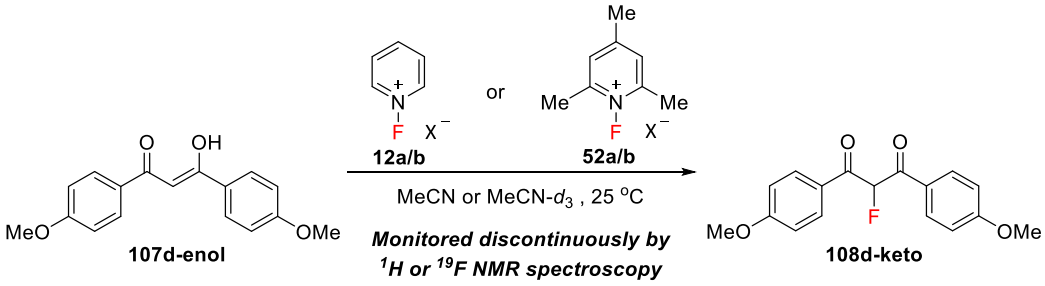

Scheme 21: Fluorination of **107d-enol** by fluorinating reagents **12a**, **12b**, **52a** and **52b** in MeCN at 25 °C, monitored by the discontinuous NMR spectroscopy method.

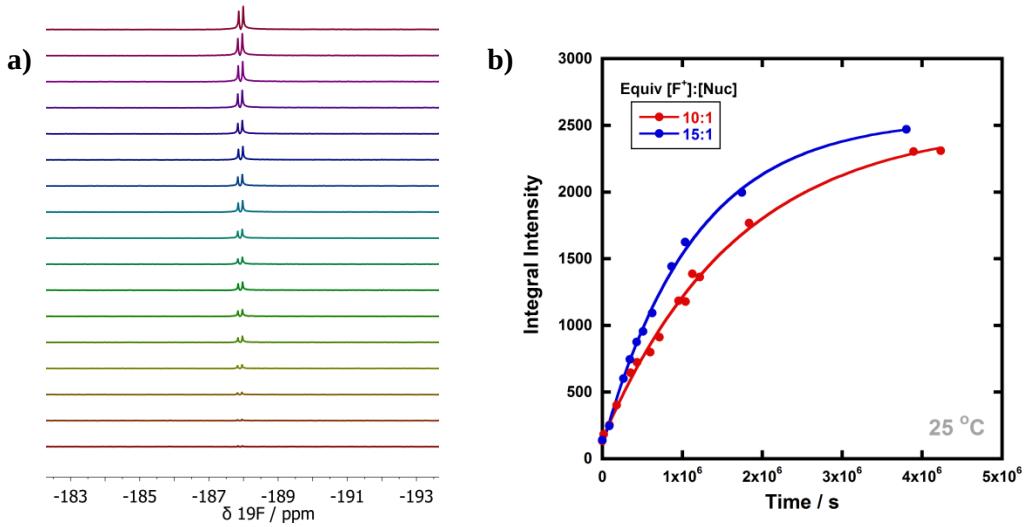

Figure 25: (a) Fluorination of **107d-enol** by triMe-NFPy TfO^- **52a** monitored discontinuously by ^{19}F NMR spectroscopy, showing formation of **108d-keto**, with time intervals of ~1 day between each spectrum. (b) Integral intensities versus time; $[F^+]$ = 439 mM or 659 mM and [Nuc] = 44 mM.

To confirm the clean formation of the expected products for reactions involving Selectfluor™ and *N*-fluoropyridinium salts, product analyses were conducted for reactions involving these reagents, which will be discussed in Sections 2.4 and 2.5.

Table 7: Second-order rate constants (k_2) for the reactions of fluorinating reagents **12a/b**, **17**, **19**, **50a/b**, **51**, **52a/b** and **55d** with nucleophiles **107a-m** in MeCN, at up to four different temperatures (20 °C, 25 °C, 30 °C and 35 °C).

Nucleophile (R groups)	Electrophile	k_2 (20 °C) / M^{-1} s^{-1}	k_2 (25 °C) / M^{-1} s^{-1}	k_2 (30 °C) / M^{-1} s^{-1}	k_2 (35 °C) / M^{-1} s^{-1}
107a-enol (R_1 = R_2 = H)	Selectfluor™ **19**	2.68×10^{-2}	4.20×10^{-2}	6.55×10^{-2}	1.00×10^{-1}
	NFSI **17**		9.87×10^{-6}		
	Cl_2-NFPy TfO^- **50a**	5.26×10^{-3}	9.85×10^{-3}		
	Cl_2-NFPy BF_4^- **50b**	7.98×10^{-3}	1.20×10^{-2}		
	Cl_5-NFPy TfO^- **51a**	2.35	3.53		
107b-enol (R_1 = R_2 = F)	Selectfluor™ **19**	2.05×10^{-2}	3.28×10^{-2}	5.08×10^{-2}	7.14×10^{-2}
	NFSI **17**		8.14×10^{-6}		
	Cl_2-NFPy TfO^- **50a**	2.23×10^{-3}	3.35×10^{-3}		
	Cl_2-NFPy BF_4^- **50b**	8.67×10^{-3}	1.30×10^{-2}		
107c-enol (R_1 = R_2 = Me)	Selectfluor™ **19**	8.32×10^{-2}	1.17×10^{-1}	1.91×10^{-1}	2.86×10^{-1}
	NFSI **17**		3.08×10^{-5}		
	Cl_2-NFPy TfO^- **50a**	1.68×10^{-2}	2.41×10^{-2}		
	Cl_2-NFPy BF_4^- **50b**	2.66×10^{-2}	4.44×10^{-2}		
	Cl_5-NFPy TfO^- **51a**		5.91		
107d-enol (R_1 = R_2 = OMe)	Selectfluor™ **19**	4.31×10^{-1}	6.43×10^{-1}	9.55×10^{-1}	1.40
	NFSI **17**		1.38×10^{-4}		
	Synfluor™ **55d**		6.76×10^{-2}		
	triMe-NFPy TfO^- **52a**		1.34×10^{-6}		
	triMe-NFPy BF_4^- **52b**		2.63×10^{-6}		
	NFPy TfO^- **12a**		6.90×10^{-6}		
	NFPy BF_4^- **12b**		6.29×10^{-6}		
	Cl_2-NFPy TfO^- **50a**	8.12×10^{-2}	1.14×10^{-1}		
	Cl_2-NFPy BF_4^- **50b**	9.33×10^{-2}	1.61×10^{-1}		
	Cl_5-NFPy TfO^- **51a**		2.72×10^{1}		
107e-enol (R_1 = R_2 = Cl)	Selectfluor™ **19**	1.23×10^{-2}	1.82×10^{-2}	3.00×10^{-2}	4.27×10^{-2}
	NFSI **17**		5.75×10^{-6}		
	Cl_2-NFPy TfO^- **50a**	1.96×10^{-3}	2.94×10^{-3}		
	Cl_2-NFPy BF_4^- **50b**	3.65×10^{-3}	5.47×10^{-3}		
	Cl_5-NFPy TfO^- **51a**	1.12	1.42		
107f-enol (R_1 = R_2 = CN)	Selectfluor™ **19**	1.07×10^{-3}	1.60×10^{-3}		
107g-enol (R_1 = R_2 = NO_2)	Selectfluor™ **19**	5.99×10^{-4}	8.99×10^{-4}		
107h-enol (R_1 = R_2 = NMe_2)	Selectfluor™ **19**	7.03×10^{1}	1.05×10^{2}		
	NFSI **17**		1.41×10^{-2}		
107i-enol (R_1 = H, R_2 = F)	Selectfluor™ **19**		3.71×10^{-2}		
107j-enol (R_1 = H, R_2 = Me)	Selectfluor™ **19**		7.70×10^{-2}		
	NFSI **17**		1.82×10^{-5}		
	Cl_2-NFPy BF_4^- **50b**		2.39×10^{-2}		
107k-enol (R_1 = H, R_2 = OMe)	Selectfluor™ **19**		1.89×10^{-1}		
	NFSI **17**		4.18×10^{-5}		
	Synfluor™ **55d**		2.44×10^{-2}		
	Cl_2-NFPy BF_4^- **50b**		4.50×10^{-2}		
107l-enol (R_1 = H, R_2 = Cl)	Selectfluor™ **19**		2.81×10^{-2}		
107m-enol (R_1 = H, R_2 = NO_2)	Selectfluor™ **19**		8.86×10^{-3}		

2.4 Product analyses: reaction monitoring by NMR spectroscopy

In order to corroborate and validate the findings from UV-vis methods, time-arrayed "in-magnet" ^{1}H NMR spectroscopy experiments were employed to confirm the rates of progress of the fluorination reactions and, critically, the identities of the expected mono-fluorination products. Reactions were conducted in NMR tubes under pseudo-first order conditions using excess nucleophile at 25 °C. Here, the nucleophile was used in excess due to the relatively low solubility of Selectfluor™ in MeCN-d_3. A representative example is given in **Figure 26**, where compound **107b** (R_1 = R_2 = F) was reacted with Selectfluor™ in MeCN-d_3 (**Scheme 22**).

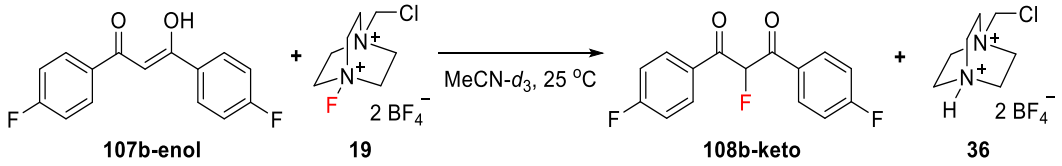

Scheme 22: Fluorination of **107b-enol** by Selectfluor™ to form **108b-keto**, monitored by time-arrayed "in-magnet" ^{1}H NMR spectroscopy.

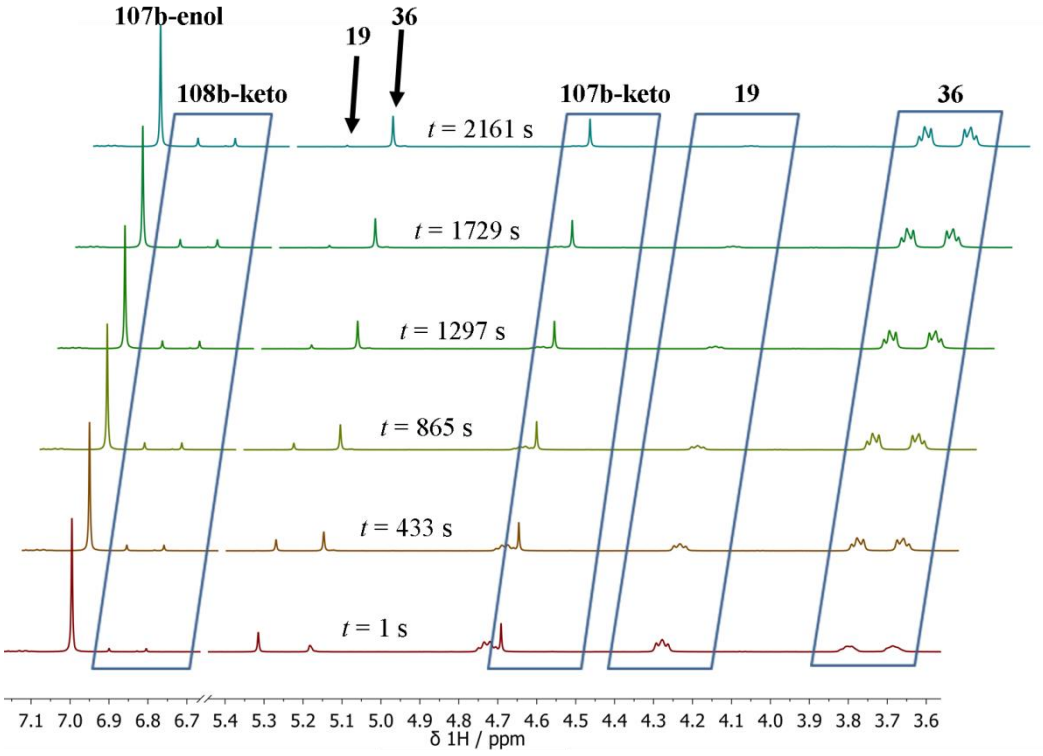

Figure 26: Time-arrayed "in-magnet" ^{1}H NMR experiment with **107b** (50 mM) and Selectfluor™ **19** (5 mM). Spectra were acquired at 3.6 min intervals and illustrative spectra from this time-course are shown above. The enol form of **107b** corresponds to the peak at 7 ppm. Peaks at 5.3 and 5.2 ppm correspond to disappearance of Selectfluor™ **19** and appearance of its defluorinated product, respectively.

The peak integrals from time-arrayed ^{1}H NMR spectroscopy experiments gave exponential behaviours for the fluorination reactions (**Figure 27**), where each curve corresponds to the highlighted ^{1}H signals present in **Figure 26**. The k_{obs} values for each curve are in the range ($1.2 – 1.3 \times 10^{-3}$ s^{-1}), hence, they correspond to the same process. The second-order rate constant obtained was $k_2 = 2.2 \times 10^{-2}$ M^{-1} s^{-1}, which is in very good agreement with that obtained from UV-vis studies (3.3×10^{-2} M^{-1} s^{-1}). The multiplets at 3.7-3.8 ppm correspond to CH_2Cl-DABCO$^+$ BF_4^- **36**, which is the de-fluorinated product of Selectfluor™. Given that the fluorination reaction was rapid, this species was already in evidence in the first NMR spectrum that was acquired.

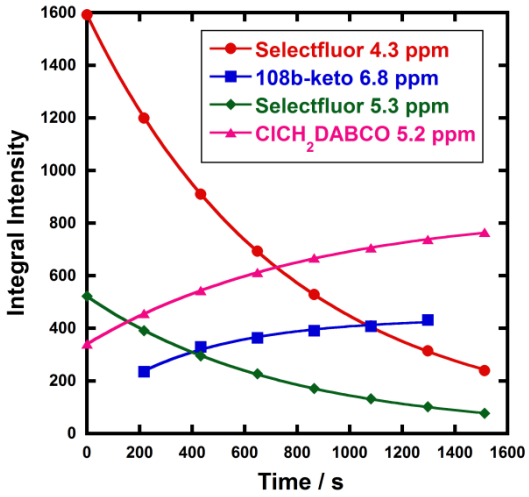

Figure 27: Reaction profile by ^{1}H NMR spectroscopy corresponding to reaction of **107b** with Selectfluor™ **19**.

2.5 Product analyses: reaction monitoring by LC-MS

Further product analyses were conducted using LC-MS experiments. The keto and enol tautomers of both starting materials **107a-m** and products **108a-m** were clearly resolved in LC-MS chromatograms, with their identities being confirmed through diode array analyses and the use of authentic samples. An example is shown for **107a** (**Figure 28**) where viewing the chromatograms at the λ_{max} values of the keto and enol forms (250 nm and 341 nm, respectively) allowed the assignment of the peaks. The peaks corresponding to enol and keto forms of **107a** are labelled. Peaks corresponding to **107a-enol** are present at both 250 nm and 341 nm due to transitions associated with this species at both wavelengths (the photochemical properties of 1,3-diaryl-1,3-dicarbonyls are well understood and will be discussed in detail in Chapter 3 Section 3.1).

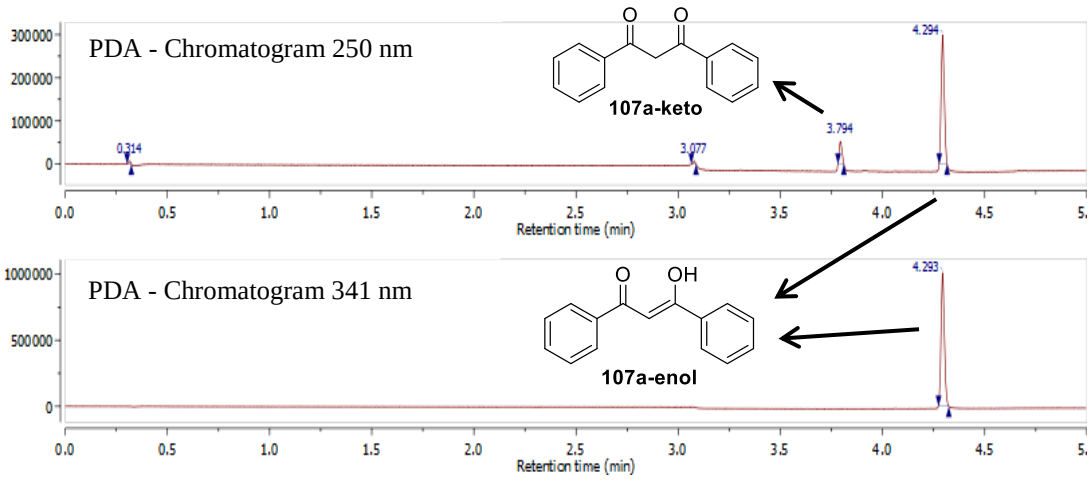

Figure 28: LC-MS trace for **107a** showing separate peaks for keto and enol forms in the chromatogram, verified by viewing the chromatogram at different wavelengths. The peak at 3.077 min is due to the solvent gradient change.

With knowledge of the retention times for each tautomer in hand, a fluorination reaction was conducted under pseudo-first order conditions with a 10-fold excess of Selectfluor™ ([Selectfluor™] = 500 μM, [**107a**] = 50 μM). LC-MS spectra were acquired after 5 h (**Figure 29**) and 24 h (**Figure 30**). Peak integrals of enol and keto starting materials were present in a ratio of 4:1 at both time intervals. While the peak integrals do not represent concentrations, the ratios of both tautomers remained constant throughout the reaction.

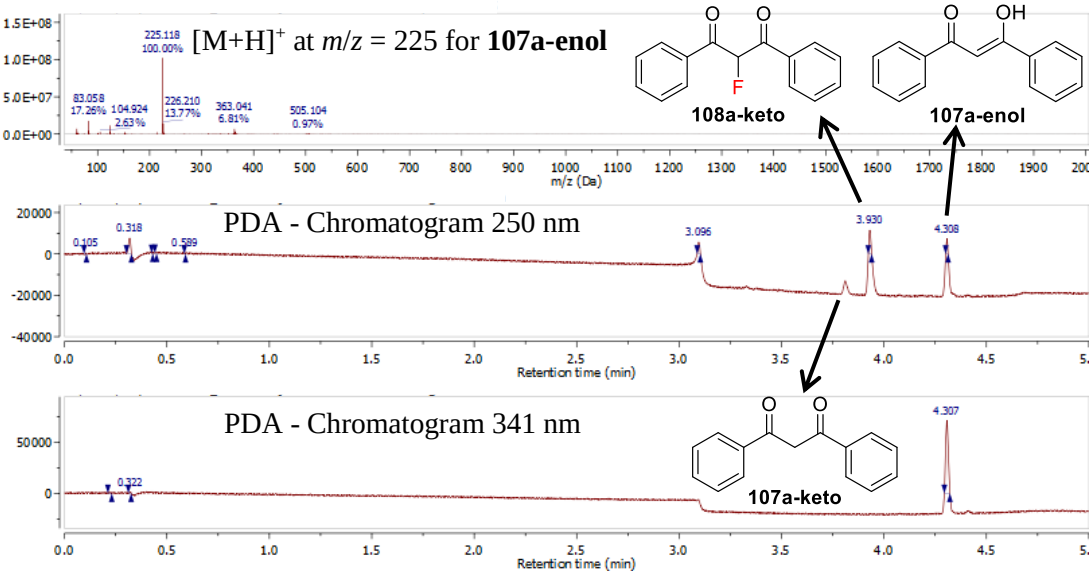

Figure 29: Fluorination of **107a** (50 μM) by Selectfluor™ **19** (500 μM) monitored by LC-MS after 5 hours.

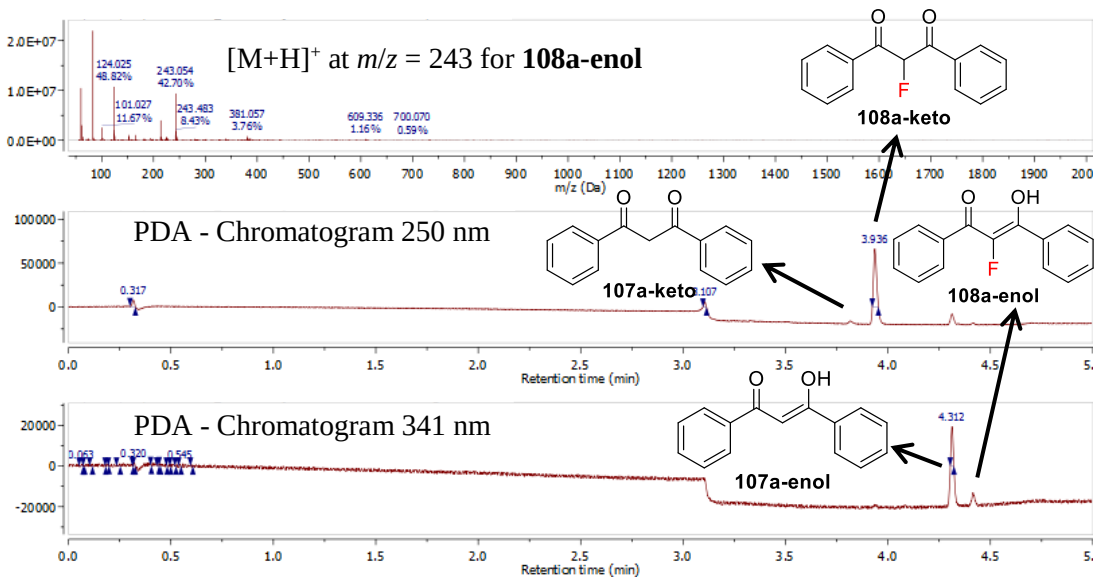

Figure 30: Fluorination of **107a** (50 μM) by Selectfluor™ (500 μM) monitored by LC-MS after 24 hours.

Reaction profiles for fluorination reactions were constructed via integration of peak areas in LC-MS chromatograms. A representative example is shown in **Scheme 23**, where nucleophile **107d** (R_1 = R_2 = OMe) was reacted with diCl-NFPy BF_4^- **50b** under bimolecular conditions (at ~15 °C), where [**107d**] = [**50b**] = 3 mM. The reaction was monitored by LC-MS after 15 min, 1.5 h, 3 h, 21 h and 52 h (**Figure 31**). Peaks corresponding to **107d-keto**, **107d-enol** and **108d-keto** were clearly resolved and identified using diode-array analysis.

The increase in concentration of the fluorinated product **108d** is shown (**Figure 32**), and fitting the data[1] gave k_2 = 3.4 × 10^{-2} M^{-1} s^{-1}, compared to k_2 = 9.3 × 10^{-2} M^{-1} s^{-1} obtained from UV-vis kinetics studies (at 20 °C). The two values are in good agreement considering the temperature differences and the other sources of error that could be introduced between the two experimental platforms.

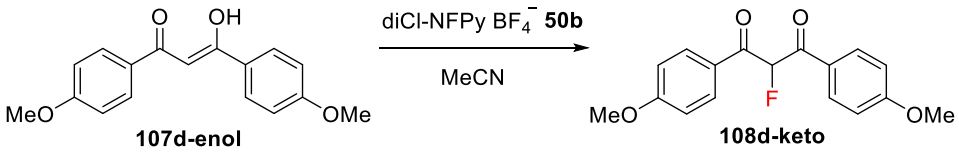

Scheme 23: Fluorination of **107d-enol** (3 mM) by diCl-NFPy TfO^- **50b** (3 mM), directly monitored by LC-MS.

[1] Data fitting in Figure 32 was conducted by Dr David Hodgson.

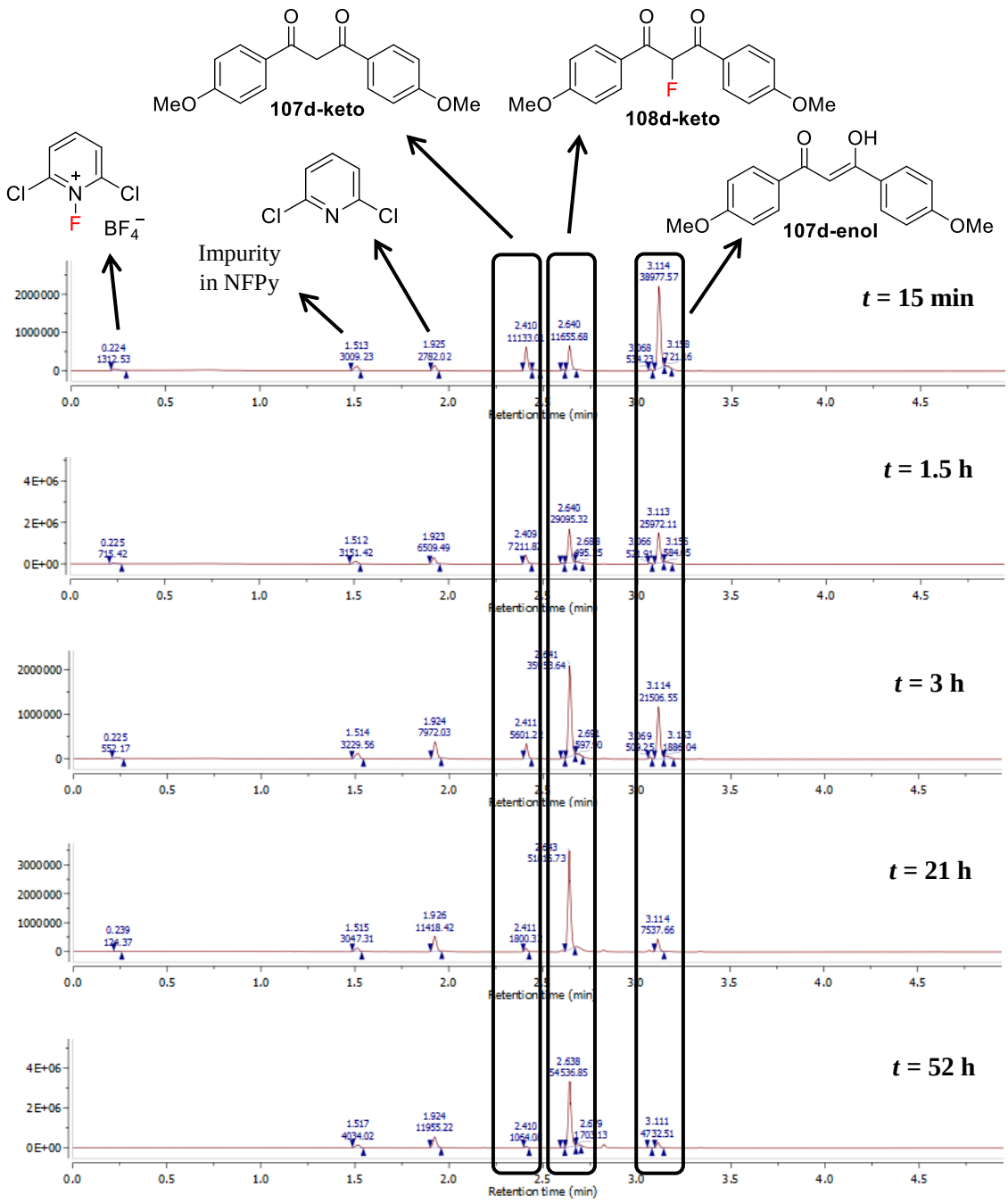

Figure 31: Reaction between **107d** (R_1 = R_2 = OMe) and diCl-NFPy BF_4^- **50b** under bimolecular reaction conditions, monitored by LC-MS analysis ([Nuc] = [F^+] = 3 mM).

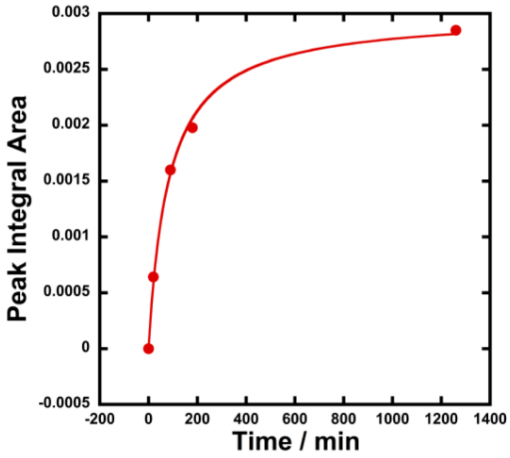

Figure 32: Reaction profile for LC-MS analysis of the reaction between substrate **107d** and Cl_2-NFPy BF_4^- **50b** under bimolecular reaction conditions ([Nuc] = [F^+] = 3 mM).

The LC-MS studies discussed in this section suggested the rapid equilibration of keto and enol tautomers of the starting material during fluorination reactions, although the chromatogram peaks corresponding to the two tautomers were clearly resolved. This suggested that the presence of water in the elution gradient could play an important role in the equilibration processes. These findings formed the basis of the work that will be discussed in Chapter 3.

2.6 Structure-activity correlations

The effects of the *para*-substituents on the rates of fluorination were studied using the Hammett equation[127] (**Equation 5**).

$$\log\left(\frac{k^X}{k^H}\right) = \rho \,.\, \sigma_X \qquad (5)$$

Hammett correlation analyses of the reactions were carried out using σ and σ^+ values taken from the literature.[128,129] The use of σ_p^+ values led to better correlations than with σ_p constants in all cases and representative Hammett plots for Selectfluor™ with di-substituted enols **107a-h** (**Figure 33a, b**) and mono-substituted enols **107i-m** (**Figure 33c, d**) are presented.

The Hammet correlation for **107a-h** using σ_p values gave $\rho = -2.98$ ($R^2 = 0.96$), while that of **107i-m** using σ_p values gave $\rho = -1.12$ ($R^2 = 0.92$), which is a 2.7-fold difference in ρ parameter. Correlations versus σ_p^+ values for **107a-h** gave $\rho^+ = -2.00$ ($R^2 = 0.99$), and for **107i-m** $\rho^+ = -0.83$ ($R^2 = 0.99$) was determined, which is a 2.4-fold difference in ρ^+ parameter. The greater magnitude of the ρ and ρ^+ parameters for di-substituted enols

indicates the greater sensitivity of the rate constant to the presence of two *para*-substituents. The effects of mono- versus di-subtitution on rates of fluorination will be discussed in greater detail in Section 2.9.

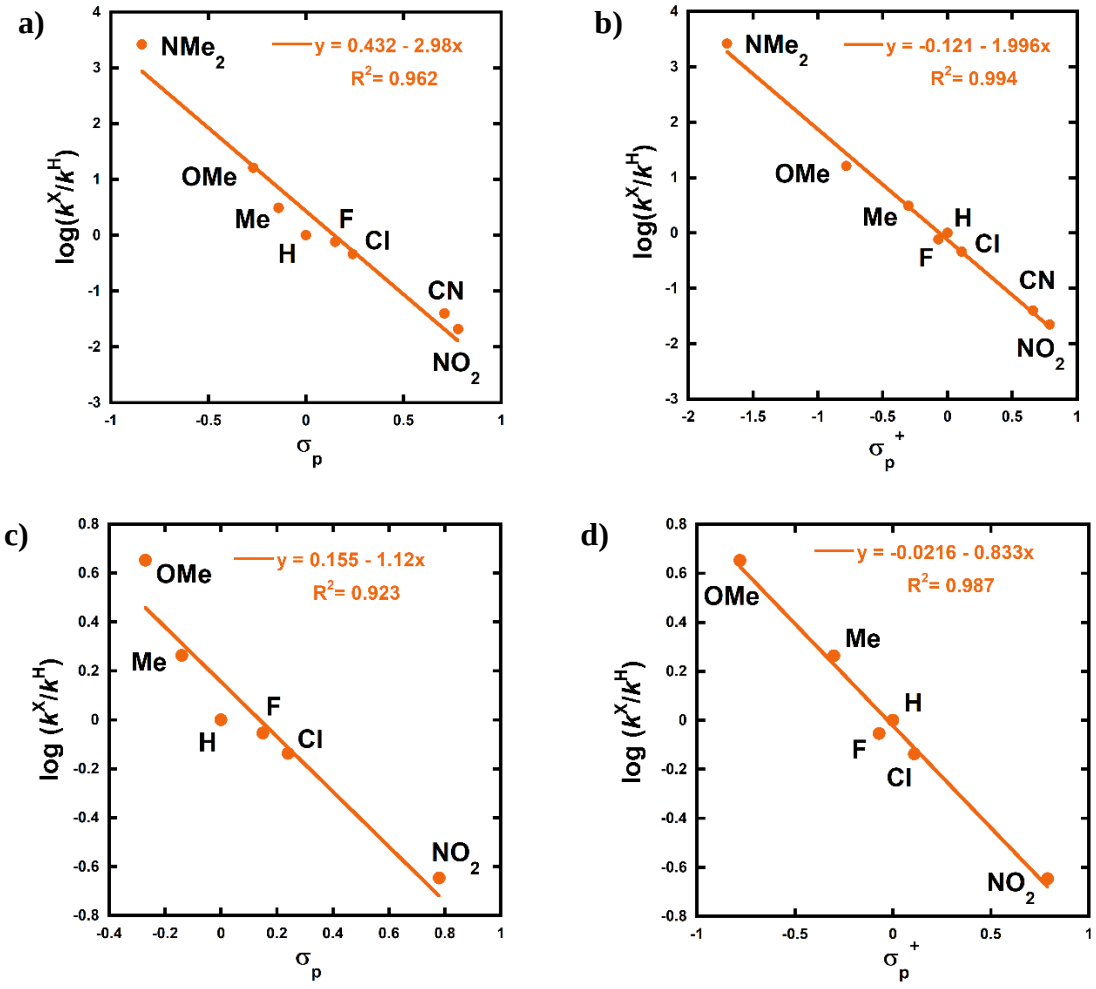

Figure 33: Hammett plots for reactions of Selectfluor™ with **107a-h** correlated against: (a) σ_p values, and (b) σ_p^+ values. Hammett plots for reactions of Selectfluor™ with **107i-m** correlated against: (c) σ_p values, and (d) σ_p^+ values. Rate constants at 20 °C were used to obtain Hammett plots for di-substituted nucleophiles, and for mono-substituted nucleophiles, all rate constants were at 25 °C.

Hammett plots constructed using σ_p^+ constants for the reactions of di-substituted enols **107a-h** with fluorinating reagents **17**, **19**, **50a**, **50b** and **51a** are shown in **Figure 34a**. The ρ^+ values obtained for reactions involving each fluorinating reagent are between −1.4 and −2.0 (**Table 8**), where these negative values indicate moderate reductions in electron density on the substrates during the rate determining fluorination steps. This magnitude of electron deficit at the transition state is consistent with the S_N2-like mechanistic behaviours that are commonly attributed to N−F reagents. For the mono-substituted enols **107i-m**, Hammett plots were constructed using σ_p^+ values for reagents

17, **19** and **50b** (**Figure 34b**). The ρ^+ values obtained were −0.80, −0.83 and −0.72 for reactions of **17**, **19** and **50b**, respectively (**Table 8**). The similarity in each set of ρ^+ values suggests that the fluorination mechanisms are analogous across the range of fluorinating reagents, which is a critical requirement for the construction of a predicitive reactivity scale.

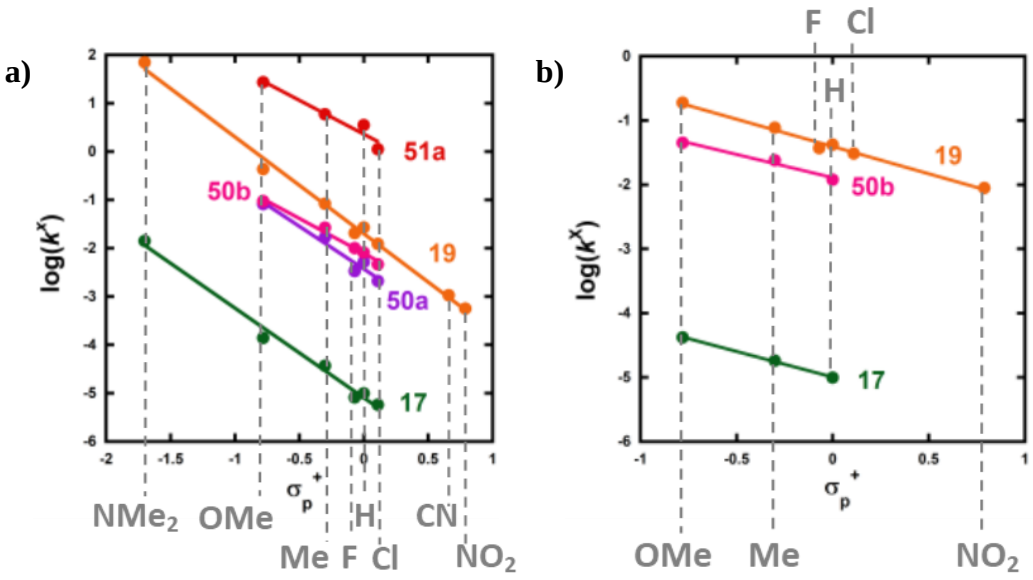

Figure 34: (a) Hammett correlations corresponding to fluorination of di-substituted 1,3-dicarbonyls **107a-h** by fluorinating reagents **17**, **19**, **50a**, **50b** and **51a**. All rate constants used in the correlations were obtained in MeCN at 20 °C for **19**, **50a** and **50b** and at 25 °C for **17** and **51a**. (b) Hammett correlations corresponding to fluorination of mono-substituted 1,3-dicarbonyls **107i-m** by fluorinating reagents **17**, **19** and **50b** in MeCN at 25 °C.

Table 8: The ρ^+ values determined from the Hammett plots shown in **Figure 34**, where σ^+ values were taken from the literature.[128,129]

N−F reagent	Disubstituted derivatives **107a-h**		Monosubstituted derivatives **107i-m**	
	ρ^+ value	R^2 value	ρ^+ value	R^2 value
Pentachloro NFPy TfO^- **51a**	−1.4	0.94	-	-
Selectfluor™ **19**	−2.0	0.99	−0.83	0.99
2,6-Dichloro NFPy BF_4^- **50b**	−1.4	0.98	−0.72	0.98
2,6-Dichloro NFPy TfO^- **50a**	−1.8	0.96	-	-
NFSI **17**	−1.9	0.99	−0.80	0.99

2.7 Reactivity scale for N−F reagents

The key aim of this chapter was to determine a reactivity scale for N−F reagents. Using the absolute rate constants obtained from kinetics studies via UV-vis spectrophotometry and NMR spectroscopy, relative rate constants (k_{rel}) were calculated, using **Equation 6,** with Selectfluor™ as the reference electrophile (**Table 9**).

$$k_{\text{rel}} = \frac{k_2(\text{NF reagent})}{k_2(\text{Selectfluor}^{\text{TM}})} \qquad (6)$$

Across the range of 1,3-dicarbonyl compounds **107a-m**, the k_{rel} values for each fluorinating reagent were in good agreement. For example, the k_{rel} values are all ~2×10^{-4} for NFSI **17**, and ~0.2 for 2,6-dichloro-*N*-fluoropyridinium triflate **50a**. This shows the predictive potential of the scale towards nucleophiles of differing potencies. With the k_{rel} values in hand, a reactivity scale for fluorinating abilities of the N−F reagents in MeCN was constructed (**Figure 35**). The average k_{rel} values for each reagent are reported on this scale.

The most reactive fluorinating reagent on the scale was 2,3,4,5,6-pentachloro-*N*-fluoropyridinium triflate **51a**. Selectfluor™ **19**, 2,6-dichloro-*N*-fluoropyridinium triflate **50a** and 2,6-dichloro-*N*-fluoropyridinium tetrafluoroborate **50b** displayed very similar reactivities, with the counter-ions having small effects on the reactivities of the *N*-fluoropyridinium salts. Synfluor™ **55d** was around 10 times less reactive than Selectfluor™ **19**, although Synfluor™ **55d** was very moisture sensitive and problems arose with competing decomposition reactions when using this reagent in kinetics studies. Therefore, rate constants with this reagent were only obtained with the most reactive nucleophiles (R_1 = R_2 = OMe and R_1 = OMe, R_2 = H), where competitive hydrolysis processes were least significant.

At the other extreme, NFSI **17** and *N*-fluoropyridinium systems **12a**, **12b**, **52a** and **52b** were 4-6 orders of magnitude less reactive than Selectfluor™ **19**. Despite the low reactivity of NFSI **17**, kinetic profiles with nucleophiles **107a-e**, **107h**, **107j** and **107k** could be obtained using UV-vis monitoring within one week, owing to its high level of solubility in MeCN, which allowed large concentrations of NFSI **17** to be used with consequent enhancement of observed rates. Selectfluor™ **19**, on the other hand, showed relatively low solubility in MeCN thus, although it was more reactive, reaction rates were limited because of its poorer solubility.

Although their reactivities were similar to Selectfluor™ **19**, Synfluor™ **55d** and the 2,6-dichloro-*N*-fluoropyridinium salts **50a** and **50b** were very moisture sensitive. Therefore, Selectfluor™ **19** was confirmed to be the most bench-stable and easy-to-handle fluorinating reagent, as water has previously been shown to be a compatible solvent for fluorination reactions involving this reagent.[119] Reagents **12a**, **12b**, **52a** and **52b** were found to be less moisture-sensitive than the dichloro-derivatives, and NMR studies showed that they remained stable in MeCN solution for several weeks. Furthermore, owing to their higher levels of solubility in MeCN, appreciable rates of fluorination could be achieved with these less reactive reagents through the use of higher concentrations.

2,3,4,5,6-Pentachloro-*N*-fluoropyridinium triflate **51a** is highly reactive, even showing reactivity towards glass. This was determined due to the presence of tetrafluoroborate peaks in ^{19}F NMR spectra of this compound, which were present as a result of fluorination of borosilicate glass. It would therefore be advisable to use plastic containers for transportation of this material. This reagent decomposes when heated in MeCN, thus limiting the use of this reagent for reactions in this solvent at temperatures above ~40 °C.

Table 9: Relative rate constants, k_{rel}, for fluorination of **107a-e**, **107h**, **107j** and **107k** by N−F reagents calculated based on the absolute rate constants shown in **Table 7**, with Selectfluor™ **19** as the reference electrophile.

N−F Reagent	k_{rel}							
	107a $R_1 = R_2 = H$	**107b** $R_1 = R_2 = F$	**107c** $R_1 = R_2 =$ Me	**107d** $R_1 = R_2 =$ OMe	**107e** $R_1 = R_2 =$ Cl	**107h** $R_1 = R_2 =$ NMe_2	**107j** $R_1 = H, R_2 =$ Me	**107k** $R_1 = H, R_2 =$ OMe
Selectfluor™ 19	1.0	1.0	1.0	1.0	1.0	1.0	1.0	1.0
NFSI 17	2.4×10^{-4}	2.5×10^{-4}	2.6×10^{-4}	2.2×10^{-4}	3.2×10^{-4}	1.3×10^{-4}	2.4×10^{-4}	2.2×10^{-4}
diCl-NFPy TfO^- 50a	0.2	0.1	0.2	0.2	0.2			
diCl-NFPy BF_4^- 50b	0.3	0.4	0.3	0.2	0.3		0.3	0.2
pentaCl-NFPy TfO^- 51a	87		51	42	91			
Synfluor™ 55d				0.1				0.1
triMe-NFPy TfO^- 52a				2.1×10^{-6}				
triMe-NFPy BF_4^- 52b				4.1×10^{-6}				
NFPy TfO^- 12a				1.1×10^{-5}				
NFPy BF_4^- 12b				1.0×10^{-5}				

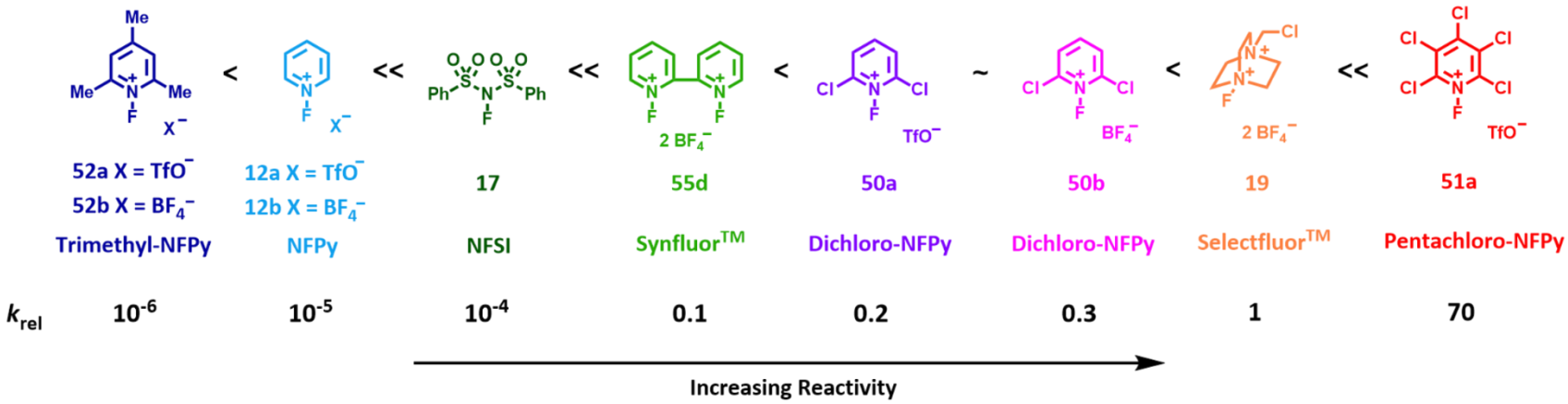

Figure 35: Quantitative reactivity scale of N–F reagents. Relative rate constants were calculated based on the absolute rate constants shown in **Table 7**, with Selectfluor™ as the reference electrophile.

2.8 Determination of activation parameters

Activation parameters ($\Delta G^{\ddagger}$, $\Delta H^{\ddagger}$ and $\Delta S^{\ddagger}$) were obtained from kinetic data for the reactions of Selectfluor™ with **107a-e** (**Figure 36**). The linear form of the Eyring equation (**7**) was used to calculate activation parameters, where the slope of the linear plot of $\ln(k_2/T)$ vs $1/T$ is equal to $-\Delta H^{\ddagger}/R$. The entropy of activation, $\Delta S^{\ddagger}$, was calculated from the intercept of the linear plot, i.e. $\ln(k_B/h) + \Delta S^{\ddagger}/R$. The values for $\Delta G^{\ddagger}$ were calculated from **Equation 8**. The constants k, R, T, k_B and h represent the rate constant k_2, gas constant, absolute temperature, Boltzmann constant and Planck's constant, respectively. The values of $\Delta G^{\ddagger}$, $\Delta H^{\ddagger}$ and $\Delta S^{\ddagger}$ for the fluorinations of **107a-e** are summarised in **Table 10**.

$$ln\frac{k}{T} = \frac{-\Delta H^{\ddagger}}{RT} + \ln\left(\frac{k_B}{h}\right) + \frac{\Delta S^{\ddagger}}{R} \qquad (7)$$

$$\Delta G^{\ddagger} = \Delta H^{\ddagger} - T\Delta S^{\ddagger} \qquad (8)$$

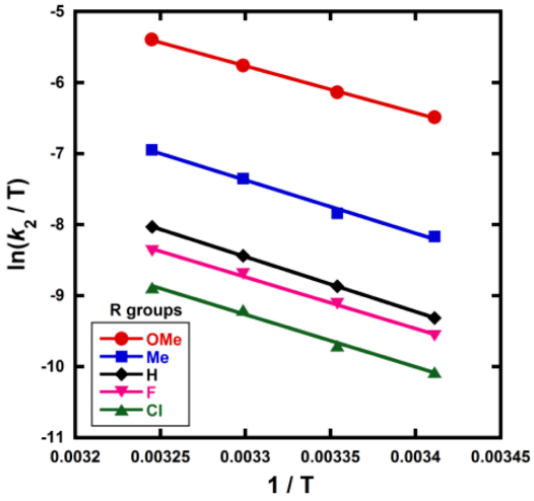

Figure 36: Eyring plots for fluorination of disubstituted 1,3-dicarbonyls **107a-e** by Selectfluor™ **19** in MeCN at 20 °C, 25 °C, 30 °C and 35 °C.

The Eyring plots showed excellent linear correlations, with $R^2 > 0.99$. The moderately negative values of $\Delta S^{\ddagger}$ support a bimolecular rate-determining step for the fluorination reactions. The free energy of activation ($\Delta G^{\ddagger}$) for the fluorination reactions increased from 74.1 kJ mol^{-1} to 82.9 kJ mol^{-1} as the *p*-aryl substituent of the 1,3-dicarbonyl nucleophile changed from OMe to Cl. Enthalpy of activation ($\Delta H^{\ddagger}$) increased from 54.8 kJ mol^{-1} for **107d** (electron-donating substituents) to 61.3 kJ mol^{-1} for **107e** (electron-withdrawing substituents). All three activation parameters are dependent on the

electronic nature of the substituents, and the effect is most marked for the more electron-donating substituent OMe.

Table 10: Activation parameters for fluorination of compounds **107a-e** by Selectfluor™ in MeCN.

Nucleophile	σ_p^+	$\Delta H^‡$ / kJ mol^{-1}	$\Delta S^‡$ / J K^{-1} mol^{-1}	$\Delta G^‡$ / kJ mol^{-1}
107a ($R_1 = R_2 = H$)	0	64.3	−55.8	80.9
107b ($R_1 = R_2 = F$)	−0.07	60.3	−71.1	81.5
107c ($R_1 = R_2 = Me$)	−0.31	62.2	−53.7	78.2
107d ($R_1 = R_2 = OMe$)	−0.78	54.8	−64.6	74.1
107e ($R_1 = R_2 = Cl$)	0.11	61.3	−72.3	82.9

2.9 Effect of mono- versus di-substitution on rates of fluorination

A correlation of k_2 versus the number of *para*-substituents present on each 1,3-dicarbonyl was constructed using the rate constants obtained from kinetics studies with Selectfluor™ **19** and compounds **107a-e**, **107g** and **107i-m** (**Figure 37**)**.** As expected, nucleophiles with two electron-donating substituents (e.g. $R_1 = R_2 = OMe$) showed an increase in reactivity towards fluorination compared with the *mono*-substituted derivatives. Conversely, two electron-withdrawing groups at the *para* positions caused a greater decrease in nucleophilicity at C-2 than only one EWG, and hence the rate of fluorination was slower with the *di*-substituted compounds. The *para*-substituents were thus working in synergy, rather than showing "push-pull" effects.

Furthermore, nucleophiles displaying substituents that have mostly inductive electron-withdrawing or electron-donating effects showed a linear trend in the graphs of k_2 versus number of *para*-substituents. On the other hand, the OMe substituents displayed a non-linear correlation of rate constants versus number of substituents and caused a strong increase in reactivity compared to **107a** due to the strong electron-donating nature of each OMe group. A similar non-linear correlation was obtained with *para*-nitro groups (**Figure 37b**). The non-additive effects between mono- and di-substituted substrates are consistent with the asymmetric nature of enol systems preventing identical conjugation effects by the substituents in the di-substituted systems (**Figure 38**).

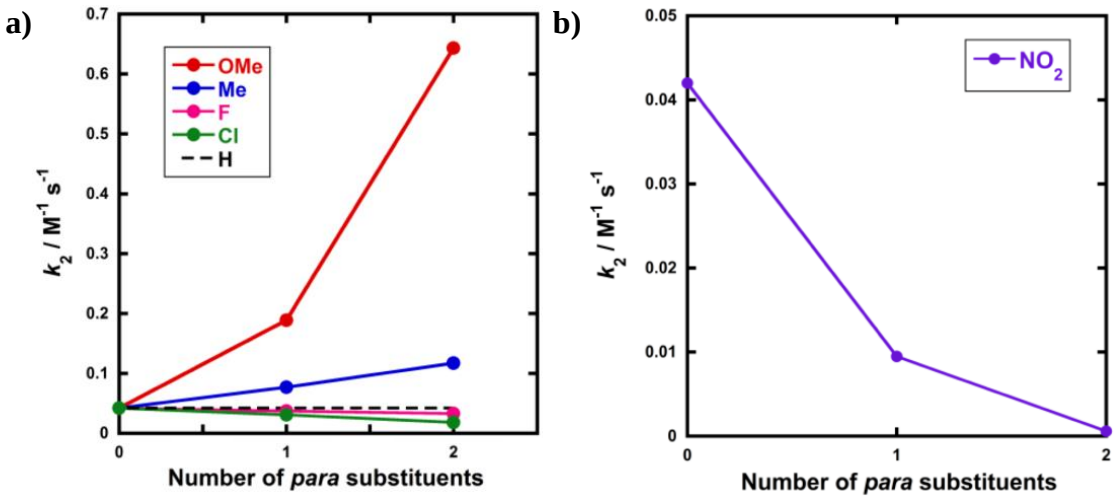

Figure 37: The effect of mono- versus di-substitution on the rate of fluorination; all rate constants for fluorination by Selectfluor™ **19** were obtained in MeCN at 25 °C. (a) Correlations for **107a-e** and **107i-l**. (b) Correlation for **107g** and **107m**.

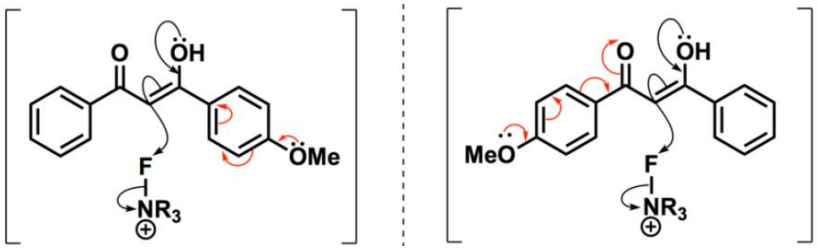

Figure 38: Asymmetry of the enol in the transition state.

The work described in Sections 2.2-2.9 of this chapter were published in *Chemical Science* in September 2018.[130]

2.10 Comparison with quantitative studies of fluorinating agent reactivities

As discussed in Chapter 1, different approaches have previously been undertaken towards quantification of the fluorinating abilities of the N−F reagents. In this section, a comparison of the data discussed in this chapter with such approaches will be made. For each comparison, the measured rate constants, log k_2, for the reactions of N−F fluorinating reagents with **107d-enol** (R_1 = R_2 = OMe) against the corresponding literature parameters will be presented and the trends discussed. **107d-Enol** was selected for these comparisons since it has the most extensive dataset, where second-

order rate constants were determined for the reactions of this compound with all fluorinating reagents studied in the present work.

The use of reduction potentials, E_p^{red}, as a possible measure of fluorinating ability was first proposed by Lal and Syvret in 1992.[84] The rate constants for the reactions of the enol **107d** with the cationic reagents Selectfluor™ **19**, NFPy BF_4^- **12b**, diCl-NFPy BF_4^- **50b** and triMe-NFPy BF_4^- **52b** generally correlate linearly with the corresponding reduction potentials (**Figure 39**). However, NFSI **17** reacts much faster than its reduction potential value suggests. Although the reduction potential for Selectfluor™ **19** is lower than that of diCl-NFPy BF_4^- **50b**, **19** is a more reactive fluorinating reagent than **50b** based on the log k_2 values.

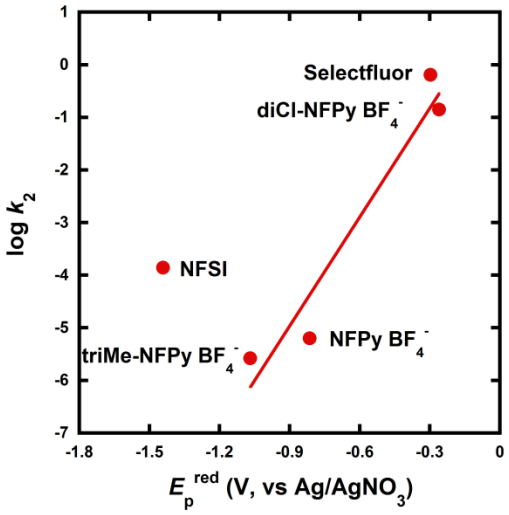

Figure 39: Plot of measured rate constants log k_2 for the reactions of N−F fluorinating reagents with **107d-enol** against the corresponding cathodic peak potentials E_p^{red} (taken from ref [85]). NFSI was not included in the correlation.

As discussed in Chapter 1, Christe and Dixon used enthalpies for the heterolytic cleavage of N−F reagents (fluorine plus detachment energies, FPD) as a measure for the oxidizing strengths of so-called "oxidative fluorinators".[93] Cheng *et al.* extended the work by calculating the FPD values for 130 fluorinating reagents of the N−F class.[95] The reactivities of the *N*-fluoropyridinium salts correlate linearly with their FPD values (**Figure 40**). However, Selectfluor™, which was not included in the line of best fit, deviates significantly from the correlation. This deviation is likely due to the lower intrinsic barrier for reactions occurring at N(sp^3) centres compared with those at N(sp^2) centres. In other words, it is more favourable for Selectfluor™, which is dicationic, to

form a monocation than it is for NFSI, a neutral compound, to form an anion upon loss of the fluorine atom.

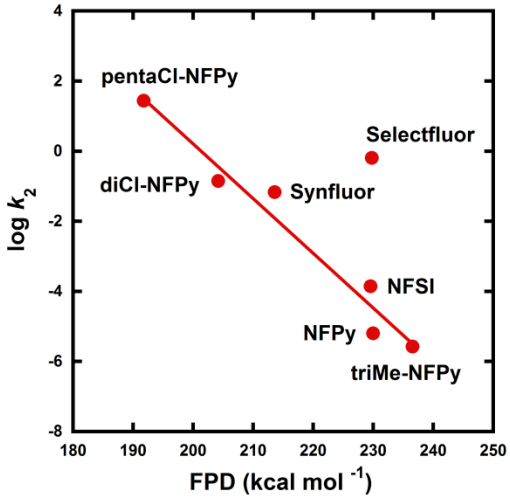

Figure 40: Correlation between rate constants (log k_2) for the reactions of N−F reagents with **107d-enol** against the corresponding FPD values calculated in MeCN (taken from ref [95]).

Figure 41 shows a good correlation between the reactivities of NFPy **12**, NFSI **17**, diCl-NFPy **50** and triMe-NFPy **52** with the basicities of the nucleofugal leaving groups, pK_{aH}. The corresponding N-H compound of diCl-NFPy **50** is the strongest acid; therefore, its conjugate base has the lowest basicity. Weak bases are generally better leaving groups, hence, diCl-NFPy **50** is the strongest fluorinating reagent according to the pK_{aH} values. Therefore, it can be concluded that basicity is a good measure of the fluorinating abilities of these reagents.

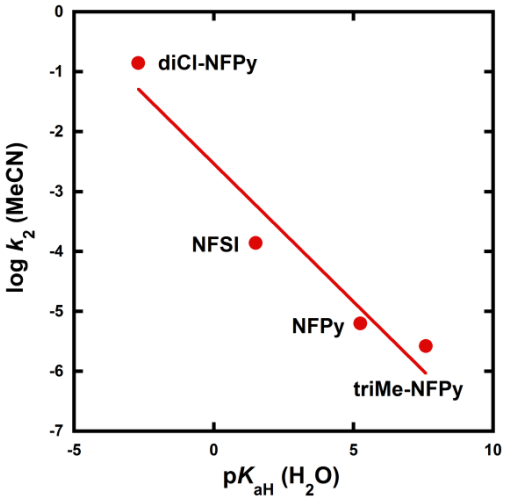

Figure 41: Correlation between the rate constants (log k_2) for the reactions of N−F reagents with **107d-enol** in MeCN against the acidities of the corresponding N−H compounds (conjugate acids) in water (taken from ref [131]).

According to the relative reactivities determined by Togni *et al.*[89] via competitive halogenations, Selectfluor™ reacted 18-fold faster than diCl-NFPy BF_4^- **50b**, 45-fold faster than Synfluor™ and 68-fold faster than NFSI. Therefore, although the overall trend in reactivities is the same as that obtained in the present work, the magnitudes of the relative reactivities are different. The results discussed in Section 2.7 determined that Selectfluor™ is 4-fold more reactive than **50b**, 10-fold more reactive than Synfluor™ and around 4 orders of magnitude more reactive than NFSI. As discussed in Chapter 1, the competition reactions were conducted in the presence of a Ti catalyst and the k_{rel}(F/Cl) values captured the whole catalytic cycle rather than individual fluorination rate constants. Furthermore, the endpoints of reactions were determined by TLC, hence, this competitive halogenation approach was not entirely quantitative.

As discussed in Chapter 1 Section 1.3.4, Stavber *et al.*,[91,92] determined the kinetics of fluorination reactions involving Selectfluor™ and Accufluor™ with phenols and alkenes. Since these studies did not involve the same nucleophiles in each case, it is difficult to quantitatively compare their reactivities. Comparing the most and least reactive phenol and alkene, the k_2 values with Selectfluor™ and Accufluor™ are in the same order. However, the values for Selectfluor™ were obtained at a lower temperature than those of Accufluor™. Accounting for the temperature differences, Selectfluor™ is estimated to be slightly more reactive. Furthermore, the second-order rate constants, k_2, are within an order of magnitude of those for the fluorinations of 1,3-diaryl-1,3-dicarbonyls **107a-e** by Selectfluor™, despite the significant differences in substrate structures.

At the same time as publication of the Reactivity Scale discussed in this chapter, a study conducted by Herbert Mayr *et al.*[132] on reactivities of electrophilic fluorinating reagents was reported. Kinetics studies were carried out on the reactions of enamines with Selectfluor™ **19**, NFSI **17**, NFPy BF_4^- **12b**, diCl-NFPy BF_4^- **50b**, and triMe-NFPy BF_4^- **52b**. Second-order rate constants determined for the fluorination reactions enabled the determination of electrophilicity parameters, *E*, for the N−F reagents, according to a linear free energy relationship known as the Mayr-Patz equation (**9**). This equation will be discussed in detail in Chapter 5. The plot of log k_2 (from the present work) versus *E* parameters (determined by Mayr *et al.*) gave excellent correlation (**Figure 42**). Hence, rate constants derived from reactions of both enols and enamines are in good agreement regarding the fluorinating abilities of the N−F reagents. Furthermore, based on their

kinetic data, Mayr *et al*. concluded that the electrophilic fluorinations of the enamines proceeded via S_N2-type mechanisms, in line with the findings of the present work.

$$\log k = s_N(E + N) \qquad (\mathbf{9})$$

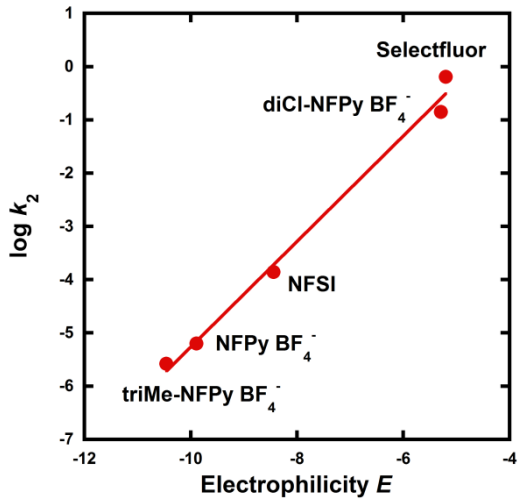

Figure 42: Correlation between rate constants (log k_2) for the reactions of N−F reagents with **107d-enol** against the *E* parameters determined by Mayr *et al.* using enamines (taken from ref [132]).

2.11 Comparison with qualitative reactivities of fluorinating reagents in synthetic applications

There are numerous reports in the literature where trial-and-error approaches were employed to find the most appropriate N−F reagent for the desired transformations. Comparison of our reactivity scale discussed in this chapter with such reports can give a good indication of the applicability of the scale towards synthetic studies.

In 2016, Sato and Sandford *et al.*[122] reported the fluorination of 3,5-diphenylisoxazole **111** using a range of N−F reagents for reaction optimisation (**Table 11**). Under the same conditions, the reaction with Selectfluor™ **19** gave the fluorinated product **112** in 38% yield, while 2,6-diCl-NFPy TfO^- **50a** gave a yield of 33%. With NFSI **17**, trace amounts of fluorination occurred, and when NFPy BF_4^- **12b** and 2,6-diMe-NFPy TfO^- **113** were used, no product was detected. From these studies, Selectfluor™ was identified as the most suitable N−F reagent to carry forward in further optimisations. Since all reactions were conducted under the same conditions, it is possible to make genuine comparisons between yields obtained and reactivities of the N−F reagents. The yields of fluorinated products in these synthetic experiments align excellently with our reactivity scale. Selectfluor™ **19** and 2,6-diCl-NFPy TfO^- **50a** have similar reactivities,

although the reaction with Selectfluor™ **19** gave a slightly higher yield of product **112**; this agrees with our scale, which predicts slightly higher reactivity for Selectfluor™ **19**. NFSI **17** is the next most reactive reagent, while NFPy BF_4^- **12b** and 2,6-diMe-NFPy TfO^- **113** are the least reactive, which is also predicted by our scale.

Table 11: Fluorination of 3,5-diphenyl-4-fluoroisoxazole using different N−F reagents. Yields were determined by ^{19}F NMR spectroscopy with benzotrifluoride as the internal standard.

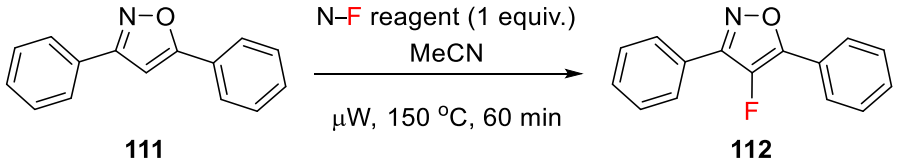

111 **112**

Entry	N−F reagent	Yield of **112** / %
1	Selectfluor™ **19**	38
2	2,6-diCl-NFPy TfO^- **50a**	33
3	NFSI **17**	Trace
4	NFPy BF_4^- **12b**	nd
5	2,6-diMe-NFPy TfO^- **113**	nd

Reaction conditions are, however, a significant factor in fluorination reactions. This was illustrated in a study by Yoshifuji *et al.*[133] Fluorination of azulene **114** was achieved using reagents **12a/b** and **52a/b** to yield 1-fluoroazulene **115a** as the major product, in addition to small quantities of 1,3-difluoroazulene **115b** (**Table 12**). Low yields were explained, firstly, by the sensitivity of fluoroazulenes to heat, generating brown tar. Secondly, competing processes were reported to initiate polymerisation reactions, resulting in deep green precipitates. In a later study by Liu *et al.*, with Selectfluor™ **19** as the fluorinating reagent, 1-fluoroazulene was obtained in 34% yield after 5 minutes at room temperature (**Table 12**, entry 6).[134] The higher yield of **115a** in this case is likely due to a combination of the higher reactivity of Selectfluor™, as well as milder conditions which reduced the amount of decomposition.

Table 12: Fluorination of azulene. Taken from refs.[133,134]

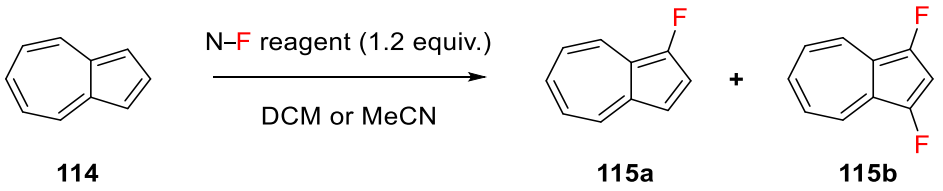

Entry	N−F reagent	Conditions	Yield / %	
			115a	**115b**
1	triMe-NFPy TfO^- **52a**	MeCN, reflux, 30 min	12	5
2	triMe-NFPy TfO^- **52a**	DCM, reflux, 45 min	17	3
3	triMe-NFPy BF_4^- **52b**	MeCN, reflux, 30 min	16	8
4	NFPy TfO^- **12a**	MeCN, 60 °C, 60 min	11	5
5	NFPy BF_4^- **12b**	MeCN, 60 °C, 60 min	9	6
6	Selectfluor™ **19**	MeCN:MeOH 1:5, RT, 5 min	34	3

2.11.1 Recent industrial application of the Reactivity Scale

In a recent study by a team at Takeda Pharmaceutical Company, Japan, the direct regioselective monofluorination of *N*-protected pyridone derivatives using several N−F reagents was reported (**Scheme 24**).[135] It was stated that "The comparison of the reactivity of such fluorinating reagents was investigated by Rozatian *et al.*" which "encouraged us to explore other less reactive electrophilic fluorinating reagents such as Synfluor™, NFSI and [triMe-NFPy TfO^-] to suppress the overreaction observed when using Selectfluor™."[135]

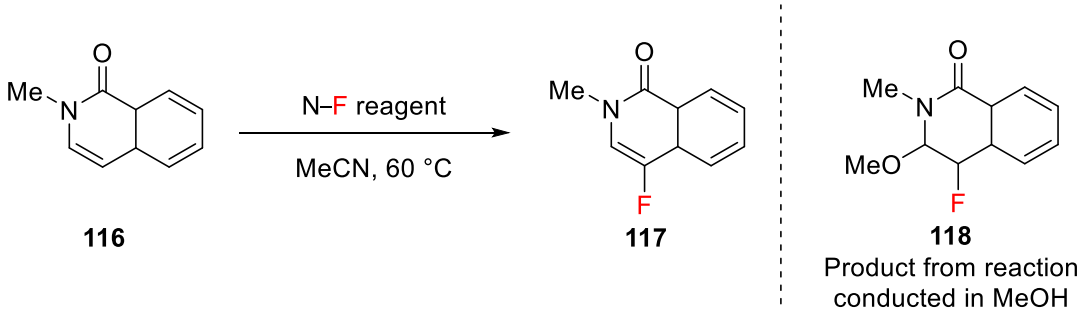

Scheme 24: Monofluorination of pyridone **116** using N−F reagents.

The fluorination of **116** was initially performed in MeCN for 1 h at 60 °C using Selectfluor™, giving a complex mixture of products containing trace amounts of the desired 4-monofluoro-substituted product **117** (**Table 13**, entry 1). The reaction was then performed at room temperature for 16 h, which gave product **117** in 5% yield alongside a mixture of side-products (entry 2). These initial reactions suggested that "Selectfluor™ shows extremely high reactivity toward **116** and that controlling its reactivity is difficult" and thus, as quoted above, the team was encouraged by our reactivity scale discussed in this chapter to use less reactive N−F reagents.

Table 13: Fluorinating reagents used for the monofluorination of **116**.

Entry	N−F reagent (equiv.)	Time / h	Isolated yield / %
1	Selectfluor™ **19** (1.1)	1	[a]
2[b]	Selectfluor™ **19** (1.1)	16	5
3	Synfluor™ **55d** (1.1)	1	[a]
4	NFSI **17** (1.1)	1	33
5	NFSI **17** (2.0)	1	50
6	triMe-NFPy TfO^- **52a** (1.1)	12	No reaction

[a] Mixture of products containing trace amounts of desired product **117**. [b] Reaction was conducted at RT.

The use of Synfluor™ **55d** (entry 3) gave a complex mixture of products, while NFSI **17** (entry 4) regioselectively gave the 4-monofluorinated product **117** in 33% yield. The use of 2.0 equiv. of NFSI **17** (entry 5) increased the yield to 50% without the generation of any side-products. However, triMe-NFPy TfO^- **52a** (entry 6) did not react with pyridone **116** after 12 h, likely due to its lower reactivity compared with the other N−F reagents. Additionally, a nucleophilic fluorinating reagent, 4-*tert*-butyl-2,6-dimethylphenylsulfur trifluoride (Fluolead™) was tested, but no reaction occurred after 12 h. With the identification of NFSI **17** as the best fluorinating reagent, a range of reaction solvents was then screened, including DMF, MeOH and HFIP, although it was found that MeCN gave **117** in the highest yield. The use of MeOH as the solvent resulted in the formation of compound **118** instead of **117** (**Scheme 24**). Elevated temperatures and longer reaction times resulted in the decomposition of **117**. The substrate scope was then increased to a range of other substituted pyridones using the

optimised conditions (NFSI (2.0 equiv.), MeCN, 60 °C, 2-48 h) thus, giving the corresponding 4-monofluorinated products in yields of 22-51%.

Importantly, this report has shown that our reactivity scale is directly relevant to the pharmaceutical industry. Selectfluor™ appears to be too reactive and incompatible with the pyridone system, and the relatively high oxidising strength of this reagent is also likely to have resulted in the formation of side-products from oxidation reactions. As discussed in Section 2.7, Synfluor™ is highly moisture sensitive, and this is a possible explanation for the mixture of side-products observed. NFSI is the weakest known oxidant among the N−F reagents and appears to be well-matched in terms of both reactivity and selectivity with the pyridone systems. Overall, this study shows good correlation with our reactivity scale, as well as its successful synthetic application.

2.12 Conclusions

This chapter has provided a quantitative reactivity scale that spans eight orders of magnitude, for ten commonly-exploited fluorination reagents. The reactivity of each fluorinating reagent was assessed by directly monitoring the kinetics of fluorination reactions with a family of 1,3-diaryl-1,3-dicarbonyl nucleophiles that mirrors the application of the reagents in C−F bond formation. The reactivities of the homologous nucleophiles span 5 orders of magnitude and allowed reactivity determinations to be performed in a genuinely comparative manner using a convenient spectrophotometric readout. Similar Hammett parameters across the range of fluorination reagents revealed the mechanisms of fluorination to be similar. Kinetics studies by UV-vis spectrophotometry were supplemented by those conducted using NMR spectroscopy and LC-MS, thus providing evidence for clean product formation as well as corroborating rate constants.

Our reactivity scale was compared with other parameters (E_p^{red}, FPD, E, pK_a) as well as with synthetic reports. Good correlations of the rate constants discussed in this chapter were found with E parameters and pK_a (H_2O) values, while some discrepancies were found in the correlations with E_p^{red} and FPD values. Generally, the synthetic studies agreed well with the reactivities determined and, in cases where overreaction is observed with more reactive N−F reagents, it is likely due to competition between fluorination and oxidation reactions. There should therefore be a suitable match between

the power of the fluorinating reagent and the substrate's nucleophilicity for a successful fluorination reaction to occur.

Finally, the impact of our scale upon the pharmaceutical industry was highlighted with the discussion of a recent report on fluorination of pyridone substrates by several N−F reagents which, again, was in good agreement with the findings discussed in this chapter.

Chapter 3: Kinetics of Enolization of 1,3-Dicarbonyl and 2-Fluoro-1,3-Dicarbonyl Derivatives

In the previous chapter, a nucleophile scaffold consisting of *para*-substituted 1,3-diaryl-1,3-dicarbonyl derivatives was developed, and kinetics studies with a series of N−F reagents allowed the determination of fluorinating abilities. The keto-enol tautomerism phenomena displayed by the 1,3-dicarbonyls and their monofluorinated analogues posed the opportunity for further exploration of tautomerism within these systems. Furthermore, the product analyses conducted by LC-MS (discussed in Section 2.5) suggested the rapid equilibration of keto and enol tautomers of the starting material during fluorination reactions, although the chromatogram peaks corresponding to the two tautomers were clearly resolved. This suggested that the presence of water in the elution gradient could play an important role in the equilibration processes. This chapter will discuss how the photochemical interconversion properties of both non-fluorinated and fluorinated 1,3-diaryl-1,3-dicarbonyl derivatives were employed to study tautomerism. The effects of reaction additives, including water, formic acid, DABCO and $ClCH_2$-DABCO$^+$ BF_4^- will be discussed. These studies have important implications for fluorination and difluorination reactions, which will directly lead to the experiments that are the subject of Chapter 4.

3.1 Introduction

The chemistry of 1,3-dicarbonyl compounds has been extensively studied.[136] Most 1,3-dicarbonyls can in theory exist as a mixture of isomers, including the hydrogen-bonded enol form, non-hydrogen bonded enols and the diketone tautomer (**Figure 43**). If no hydrogen atoms are present on the α-carbon, the compound cannot enolize and can only exist as the diketone. The s-*cis* and s-*trans* isomers refer to the arrangements of the double bonds in the enol structures, and *E* and *Z* refer to the substituents present on the C=C bond of the enol.

The diketone tautomer can exist as shown in **Figure 43**. The most electrostatically favourable arrangement of the carbonyl groups is in an opposing manner, as in conformer **B**, due to the repulsive interaction of oxygen atoms carrying a δ^- charge.[137] The presence of bulky substituents at R_1 and R_2, such as phenyl groups, can make this arrangement less favourable due to steric hindrance, making the population of

conformer **A** more dominant.[138] An intermediate conformation, conformer **C**, may also occur.[139]

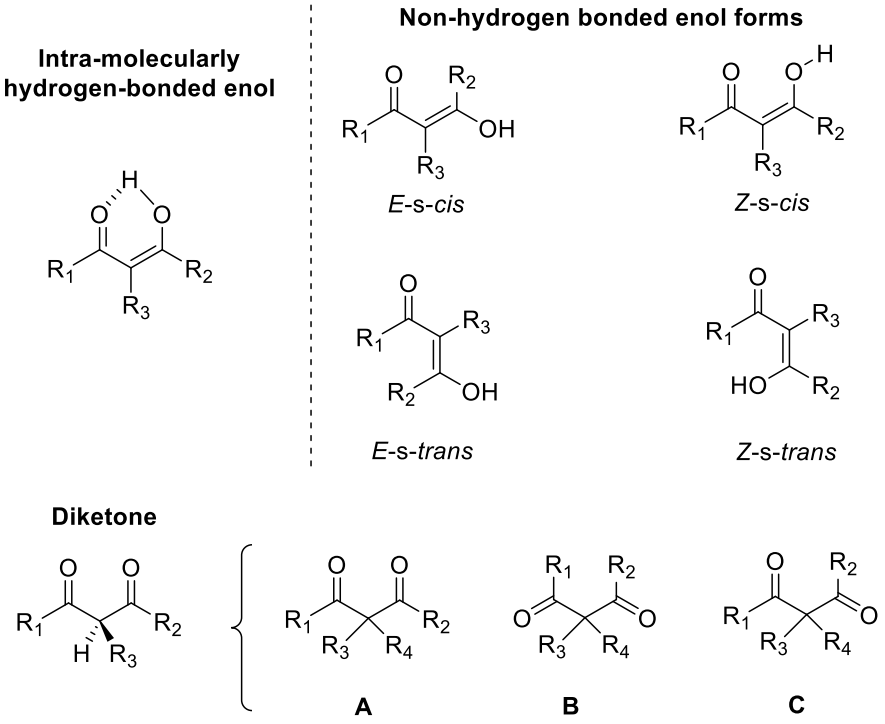

Figure 43: Possible isomers of 1,3-dicarbonyl compounds (R = aryl, allyl or H). Possible conformations of the diketone form **A**, **B** and **C**.[139]

The primary factor in determining the preferred mixture of isomers is the nature of the substituents R_1, R_2 and R_3. Firstly, the intramolecular hydrogen bond stabilises the enol isomer, therefore this is favoured over non-chelated conformers. If present, the non-chelated enols make up less than 3% of the mixture, and the *Z*-s-*cis* non-chelated enol is not usually considered a significantly populated conformer.[139,140] Bulky substituents at R_1 and R_2 tend to favour the chelated enol isomer, as this structure causes the least steric hindrance. Bulky substituents at R_3 can also cause steric hindrance, especially if R_1 and R_2 are also bulky; however, this favours the diketone isomer, which does not need to be planar across the central three carbons and can rotate to relieve strain.[137] Electron-withdrawing substituents at R_3 stabilise the enol tautomer; however, if they are too bulky, steric effects would favour the diketone over the enol. The presence of electron-withdrawing substituents at R_1 and R_2 also favours the enol form.[137]

In solution, the keto-enol equilibrium for 1,3-dicarbonyl compounds is affected by solvent polarity. In the enol isomer, electron density is partially delocalised around the chelate ring, so the enol is less polar than the keto form and is consequently stabilised

by non-polar solvents. Solvents which can form hydrogen bonds to the oxygen atoms or acidic α-hydrogen of the diketone form stabilise this isomer. Intermolecular hydrogen-bonding to the enol form would involve breaking the intramolecular hydrogen bond, which is not favourable. Consequently, the percentage of diketone content is increased by solvents with greater polarity and hydrogen-bonding ability.[141–143]

1,3-dicarbonyl compounds with at least one phenyl group at R_1 and R_2 mainly exist as the chelated enol tautomer, both as a solid and in solution.[139] This is due to the electron-withdrawing ability and bulkiness of the phenyl group, as well as the stabilising force of the intramolecular hydrogen bond. The enol tautomer is usually present in high enough concentrations to allow determination of the enol content by conventional spectroscopic methods e.g. NMR spectroscopy, IR spectroscopy and UV-vis spectrophotometry.[144,145] The enol contents for compound **107a** (R_1 = R_2 = Ph, **Table 14**), also known as dibenzoylmethane, have been determined in different solvents and are summarised in **Table 14**.

Table 14: Reported enol contents for dibenzoylmethane **107a** in various solvents. All enol structures will be represented as shown below, in this work.

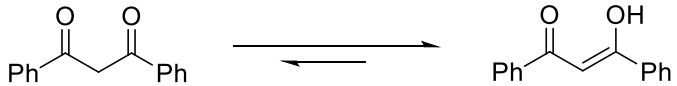

107a-keto **107a-enol**

Solvent	Percentage enol	Reference
Solid	100	[146]
Chloroform	100	[137]
	98	[147]
Hexane, cyclohexane	99	[147]
Acetonitrile	92	[147]
Methanol	89.7	[137]
Water	36.7	[143]

The photochemistry and photo-physics of 1,3-diaryl-1,3-dicarbonyl derivatives have been extensively studied.[139,142] These compounds possess a strong absorption band in the region $\lambda_{max} \approx 340$ nm (**Figure 44**). Extinction coefficients at this wavelength have been reported as $\varepsilon \approx 2 - 2.4 \times 10^4$ mol^{-1} dm^3 cm^{-1}.[148] This band has been assigned to a $\pi^* \leftarrow \pi$ transition in the carbonyl conjugated ethene system of the chelated enol form.[142] This peak is more red-shifted than other aromatic 1,3-dicarbonyl compounds due to strong intramolecular hydrogen bonding. Theoretical studies have shown that there is a strong π-electron interaction between the enol system and the aromatic substituents, which gives greater stability to the excited states. This conjugation accounts for the positions of the π, π* absorption bands.[139] A smaller absorption band is also present at $\lambda_{max} \approx 250$ nm, with an extinction coefficient of $\varepsilon \approx 6 - 10 \times 10^3$ mol^{-1} dm^3 cm^{-1}.[148] This band is due to the aroyl group of the diketone form.

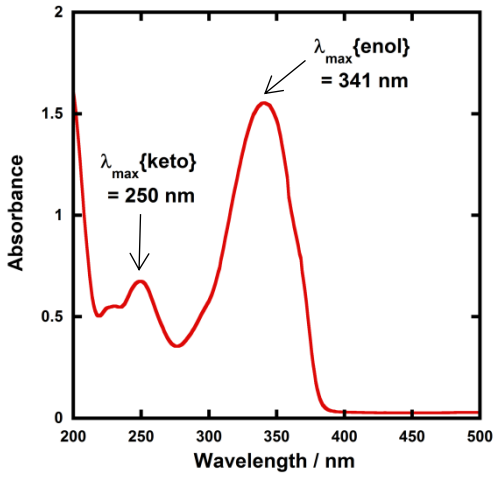

Figure 44: Absorption spectrum of **107a** (50 μM) in MeCN (data obtained in the present work).

Most literature reports suggest that the lowest excited state of dibenzoylmethane **107a** is π, π* in character.[149] The π, π* and n, π* states are likely to be close in energy, and calculations have predicted two $\pi^* \leftarrow$ n transitions in a similar spectral region to the $\pi^* \leftarrow \pi$ transition. Indeed, some 1,3-dicarbonyl compounds, e.g. benzoylacetone and ethyl acetoacetate, are reported to have an n, π* lowest excited singlet state.[150,151] This transition is of low intensity and can be masked by the tail of the higher extinction coefficient π, π* band.

The absorption band at 250 nm is due to the $\pi^* \leftarrow \pi$ transition of the diketone form, although it cannot be due entirely to this since the amount of diketone present is very

small compared to the size of the band.[142] It is therefore likely that another transition due to the enol tautomer is included in this peak.

In the 1970s, the groups of Markov[152,153] and Mazur[154–156] reported photoisomerization of 1,3-dicarbonyl compounds, whereby the keto-enol equilibrium was perturbed towards the keto tautomer upon irradiation. This process reverses to attain the tautomeric equilibrium by a non-photochemical reaction in darkness. The effects of solvents and additives (ethanol, triethylamine) on the rate of photoketonization were studied by Mazur *et al.*;[154] however, relaxation kinetics that provided insights into enolization rates were not performed. In the present work, this photoketonization approach was identified as a means of studying the kinetics of enolization within the 1,3-dicarbonyl nucleophile systems.

The keto-enol equilibrium of carbonyl compounds is an important factor in their reactivity, a subject which has been recognised for over 100 years.[157–159] Given the intriguing keto-enol tautomerism phenomena displayed by the 1,3-diaryl-1,3-dicarbonyl compounds discussed in Chapter 2, as well as their monofluorinated analogues, by taking advantage of their photochemical interconversion properties it was possible to study their tautomerism and fluorination processes in greater detail. The mechanism of fluorination proceeds via reaction of the enol tautomer with an electrophilic fluorinating reagent,[66,108] so a full understanding of the factors that affect keto-enol tautomerism would be beneficial in improving selective mono- and di-fluorinations of 1,3-dicarbonyls.

This chapter will concern the efforts towards the quantification of the factors which affect mono- versus di-fluorination by focussing on the effects of different reaction conditions on the keto-enol tautomerism of the 1,3-diaryl-1,3-dicarbonyl derivatives **107a**, **107c-e, 108a** and **108c-e**. The photoketonization and relaxation experiments on non-fluorinated compounds **107a** and **107c-e** in the absence of additives will be discussed in Section 3.2.1, followed by those in the presence of additives in Section 3.2.2. Experiments related to relaxation of fluorinated compounds **108a** and **108c-e** without additives (Section 3.3.1) and with additives (Section 3.3.2) will also be discussed in detail.

3.2 Kinetics of keto-enol tautomerism in compounds 107a and 107c-e

3.2.1 Photoketonization-relaxation experiments for 107a and 107c-e

The enol tautomers of compounds **107a** and **107c-e** were converted to their keto forms by irradiation of their solutions in MeCN in quartz cuvettes using a 0.5 W UV LED lamp at 365 nm (**Scheme 25**). Spectrophotometric monitoring of the photoketonization of each system showed that, in general, these processes took 2-3 hours. Spectra corresponding to photoketonization of **107a** are shown in **Figure 45**.

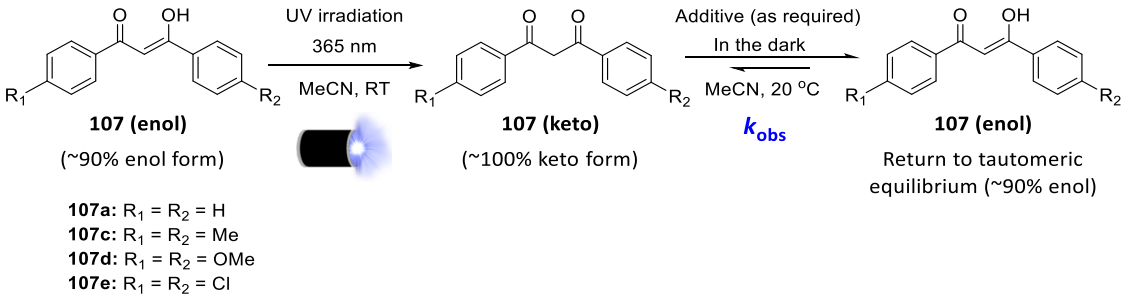

Scheme 25: Photoketonization (step 1) and relaxation (step 2) of compounds **107a** and **107c-e** (50 μM) in MeCN.

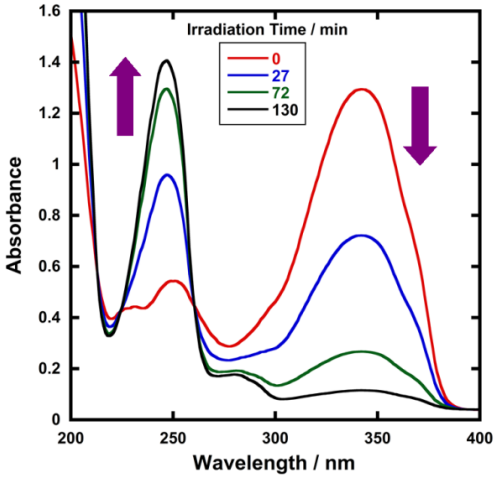

Figure 45: Spectra corresponding to photoketonization of **107a** (50 μM) over time, with decrease at λ_{max} (enol) = 341 nm and increase in absorbance at λ_{max} (keto) = 250 nm.

The re-equilibration (relaxation) kinetics of **107a-keto** in the dark were monitored using time-arrayed multi-wavelength analysis (**Figure 46**). As relaxation occurred, the enol absorbance band at λ_{max} = 341 nm increased while the keto absorbance band at λ_{max} = 250 nm decreased. The tautomeric equilibrium was regained after ~14 hours, and clean isosbestic points were observed during both the photoketonization and the relaxation processes showing that there was no detectable build-up of additional intermediates

during the tautomerization processes on the timescales that were monitored. The re-equilibration of **107a-keto** was studied at four different concentrations and observed first-order rate constants (k_{obs}) were obtained from plots of absorbance at λ_{max} = 341 nm over time (**Figure 47**). When the concentration of **107a** was doubled, there was a small decrease in k_{obs}, which could reflect interaction between substrate molecules at higher concentrations.[160]

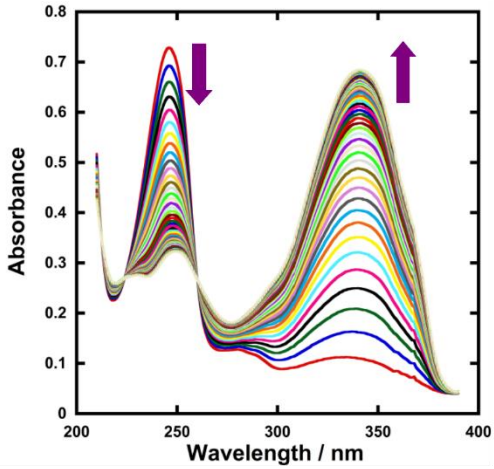

Figure 46: Time-arrayed multi-wavelength analysis for relaxation of **107a** (25 μM) in the dark, each spectrum acquired at 30 min intervals at 20 °C.

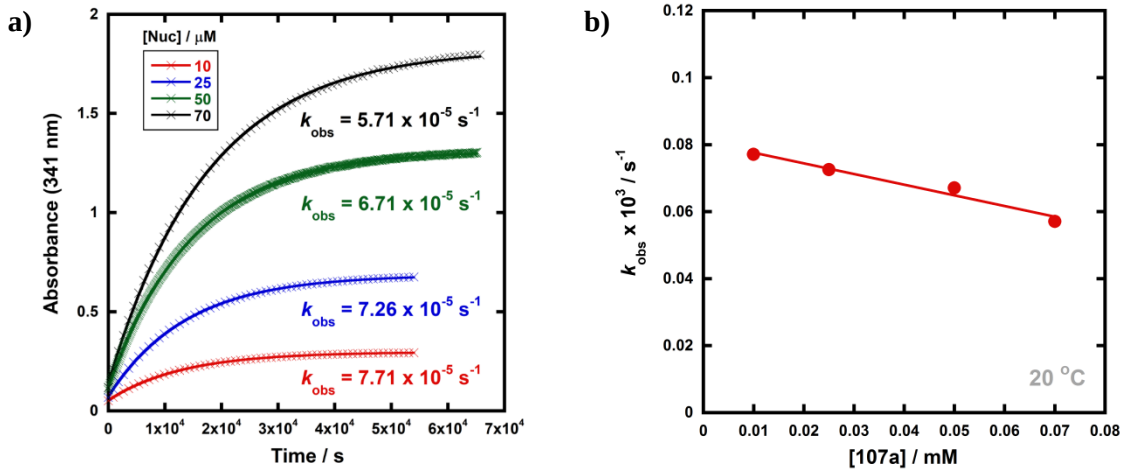

Figure 47: (a) Relaxation of **107a-keto** at different concentrations (10 μM, 25 μM, 50 μM and 70 μM); k_{obs} values obtained at each concentration of **107a** are shown. (b) Trend in k_{obs} values at different concentrations.

The relaxation kinetics of compounds **107c-e** in MeCN were studied using the same procedure (**Figure 48**) and the k_{obs} values obtained are summarised in **Table 17**. The relaxations of **107a** and **107c-e** were conducted in the presence of additives to investigate the effects of species that are commonly present in electrophilic fluorination

protocols upon enolization; these experiments will be discussed in detail in Section 3.2.2.

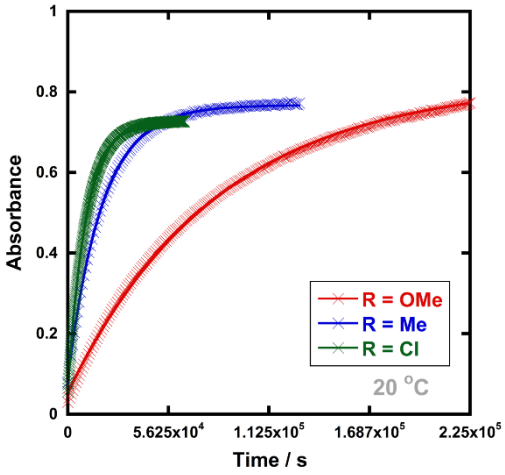

Figure 48: Conversion of keto forms of compounds **107c-e** (25 μM) to the equilibrium keto-enol ratios, monitored by UV-vis spectrophotometry at 20 °C, with data points being acquired every 15 min for **107c** and **107d**, and every 2 min for **107e**.

Keto-enol equilibration is a reversible process with significant proportions of both keto and enol tautomers being present at equilibrium, hence, the equilibrium positions (K_e) for all compounds **107a** and **107c-e** were considered, both in the presence and absence of additives. K_e values were estimated using keto:enol ratios in MeCN-d_3 determined by ^{1}H NMR spectroscopy (**Table 15**). In order to obtain quantitative integral values, relaxation delays of 20 s were employed for ^{1}H NMR experiments. The solutions were equilibrated for 10 half-lives before NMR spectra were acquired. Ratios were determined using keto and enol peak integrals. For example, with **107a**, peaks corresponding to the enol form (δ = 7.08 ppm) and the keto form (δ = 4.72 ppm) were integrated across a 0.05 ppm range.

The observed rate constants, k_{obs}, for re-equilibration of **107a-keto** and the equilibrium constants K_e in the presence of the additives are summarised in **Table 16**. Those of **107c-e** are summarised in **Table 17**. Forward and reverse rate constants k_{for}(H) and k_{rev}(H), respectively, were estimated from k_{obs} values using measured K_e values and **Equations 10** and **11**. Given that the enol forms of **107a** and **107c-e** were dominant at equilibrium, k_{obs} and k_{for}(H) values were in the same order.

$$k_{obs} = k_{for}(H) + k_{rev}(H) \qquad (\mathbf{10})$$

$$K_e = \frac{k_{\text{for}}(\text{H})}{k_{\text{rev}}(\text{H})} \qquad (\mathbf{11})$$

The k_{for}(H) values in the presence of additives were compared with the values obtained without additives and are defined by **Equation 12** in **Table 16**.

$$\text{Ratio} = \frac{k_{\text{for}}(\text{H})\{\text{with additive}\}}{k_{\text{for}}(\text{H})\{\text{MeCN}\}} \qquad (\mathbf{12})$$

Table 15: Keto:enol ratios of **107a** and **107c-e** (25 mM) in MeCN-d_3 determined by ^{1}H NMR spectroscopy. Percentages represent quantities of additive in MeCN-d_3 (*v*/*v*).

Compound	Additive	Quantity of additive in MeCN-d_3	Keto:enol ratio
107a	None	-	9:91
(R_1 = R_2 = H)	H_2O	20% (11 M)	13:87
	H_2O	50% (28 M)	15:85
	Formic acid	1% (0.27 M)	9:91
	Formic acid	2% (0.53 M)	9:91
	Formic acid	3% (0.80 M)	9.5:90.5
	DABCO	25 mM (1 eq)	13:87
	DABCO	50 mM (2 eq)	13:87
	$ClCH_2$-DABCO$^+$ BF_4^-	25 mM (1 eq)	10:90
	Bu_4N^+ BF_4^-	240 mM (10 eq)	10:90
	$(PhSO_2)_2NH$	25 mM (1 eq)	9.5:90.5
107c (R_1 = R_2 = Me)	None	-	11:89
107d	None	-	20:80
(R_1 = R_2 = OMe)	H_2O	10% (5.5 M)	21:79
	Formic acid	2% (0.53 M)	16:84
	DABCO	2.5 mM (0.1 eq)	16:84
	$ClCH_2$-DABCO$^+$ BF_4^-	25 mM (1 eq)	17:83
107e (R_1 = R_2 = Cl)	None	-	7:93

Table 16: Summary of diketone relaxation and equilibrium of **107a**. The k_{obs} values for relaxation of the photo-ketonized form of **107a** (25 μM) were determined in MeCN at 20 °C in the presence of additives.

Percentages represent volumes of additive in MeCN (3 mL total). Equilibrium constants K_e were determined by NMR spectroscopy or by linear interpolation, extrapolation or averaging of the measured data. Forward and reverse rate constants, k_{for}(H) and k_{rev}(H), for enolization and ketonization processes, respectively, were calculated using **Equations 10** and **11**. Ratios were calculated based on **Equation 12**.

Additive	Quantity of additive	k_{obs} / s^{-1}	Approx. $t_{1/2}$	K_e(H)	k_{for}(H) / s^{-1}	k_{rev}(H) / s^{-1}	Ratio
None	-	7.26×10^{-5}	2.7 h	10.5[a]	6.63×10^{-5}	6.31×10^{-6}	1.0
Water	15% (8 M)	8.44×10^{-5}	2.3 h	7.8[c]	7.48×10^{-5}	9.59×10^{-6}	1.1
	20% (11 M)	1.79×10^{-4}	1.1 h	6.9[b]	1.56×10^{-4}	2.27×10^{-5}	2.4
	25% (14 M)	1.84×10^{-4}	1.0 h	6.6[c]	1.60×10^{-4}	2.42×10^{-5}	2.4
	35% (19 M)	3.39×10^{-4}	34 min	6.3[c]	2.93×10^{-4}	4.64×10^{-5}	4.4
	50% (28 M)	7.29×10^{-4}	15 min	5.7[b]	6.20×10^{-4}	1.09×10^{-4}	9.4
Formic acid	0.5% (0.1 M)	1.92×10^{-3}	6 min	10.3[c]	1.75×10^{-3}	1.70×10^{-4}	26
	1% (0.3 M)	4.16×10^{-3}	3 min	10.0[b]	3.78×10^{-3}	3.78×10^{-4}	57
	2% (0.5 M)	4.89×10^{-3}	2 min	10.5[b]	4.46×10^{-3}	4.25×10^{-4}	67
	3% (0.8 M)	6.29×10^{-3}	2 min	9.5[b]	5.69×10^{-3}	5.99×10^{-4}	86
DABCO	2.5 μM	2.92×10^{-3}	4 min	6.7[c]	2.54×10^{-3}	3.80×10^{-4}	39
	12.5 μM	1.34×10^{-2}	1 min	6.7[c]	1.17×10^{-2}	1.74×10^{-3}	176
	25 μM	2.49×10^{-2}	30 s	6.7[b]	2.17×10^{-2}	3.24×10^{-3}	327
	37.5 μM	4.08×10^{-2}	17 s	6.7[c]	3.55×10^{-2}	5.30×10^{-3}	536
	50 μM	5.22×10^{-2}	13 s	6.7[b]	4.54×10^{-2}	6.78×10^{-3}	685
$ClCH_2$–DABCO$^+$ BF_4^-	12.5 μM	1.04×10^{-4}	1.9 h	9.1[c]	9.37×10^{-5}	1.03×10^{-5}	1.4
	25 μM	1.20×10^{-4}	1.6 h	9.1[b]	1.08×10^{-4}	1.19×10^{-5}	1.6
	50 μM	1.32×10^{-4}	1.5 h	9.1[c]	1.19×10^{-4}	1.31×10^{-5}	1.8
	625 μM	1.00×10^{-4}	1.9 h	9.1[c]	9.01×10^{-5}	9.90×10^{-6}	1.4
	1.25 mM	5.12×10^{-5}	3.8 h	9.1[c]	4.61×10^{-5}	5.07×10^{-6}	0.7
	2.5 mM	2.04×10^{-5}	9.4 h	9.1[c]	1.84×10^{-5}	2.02×10^{-6}	0.3
Water and $ClCH_2$–DABCO$^+$ BF_4^- (12.5 μM)	20% (11 M)	2.05×10^{-4}	56 min	6.9[c]	1.79×10^{-4}	2.59×10^{-5}	2.7
	30% (17 M)	2.58×10^{-4}	45 min	6.5[c]	2.24×10^{-4}	3.44×10^{-5}	3.4
	40% (22 M)	4.47×10^{-4}	26 min	6.1[c]	3.84×10^{-4}	6.30×10^{-5}	5.8
^{n}Bu$_4$N$^+$ BF_4^-	240 mM	1.44×10^{-4}	1.3 h	9.1[b]	1.30×10^{-4}	1.43×10^{-5}	2.0
"wet" ^{n}Bu$_4$N$^+$ BF_4^-	150 mM	1.43×10^{-5}	13.5 h	9.1[c]	1.29×10^{-5}	1.42×10^{-6}	0.2
	200 mM	1.55×10^{-5}	12.4 h	9.1[c]	1.40×10^{-5}	1.53×10^{-6}	0.2
$LiBF_4$	50 μM	1.55×10^{-5}	12.4 h	9.1[d]	1.40×10^{-5}	1.53×10^{-6}	0.2
	1.25 mM	1.18×10^{-5}	16.3 h	9.1[d]	1.06×10^{-5}	1.17×10^{-6}	0.2
	2.50 mM	1.08×10^{-5}	17.8 h	9.1[d]	9.73×10^{-6}	1.07×10^{-6}	0.1
$(PhSO_2)_2NH$	125 μM	1.79×10^{-6}	4.5 d	9.5[b]	1.62×10^{-6}	1.70×10^{-7}	0.02
	250 μM	4.41×10^{-6}	1.8 d	9.5[b]	3.99×10^{-6}	4.20×10^{-7}	0.06
$(PhSO_2)_2N^-Na^+$	25 μM	6.39×10^{-7}	13 d	9.1[d]	5.76×10^{-7}	6.33×10^{-8}	0.009
	50 μM	7.96×10^{-7}	10 d	9.1[d]	7.17×10^{-7}	7.88×10^{-8}	0.01
	250 μM	7.04×10^{-6}	27 h	9.1[d]	6.34×10^{-6}	6.97×10^{-7}	0.1
	500 μM	2.50×10^{-5}	7.7 h	9.1[d]	2.25×10^{-5}	2.48×10^{-6}	0.3

[a] Measured by ^{1}H NMR spectroscopy in MeCN-d_3. [b] Measured by ^{1}H NMR spectroscopy in MeCN-d_3 in the presence of additive. [c] Value based on average of measured values or interpolation of measured values. [d] K_e(H) value was assumed to be the same as K_e(H) in $ClCH_2$-DABCO$^+$ BF_4^- and ^{n}Bu$_4$N$^+$ BF_4^-.

Table 17: Summary of diketone relaxation of **107c-e**. The k_{obs} values for relaxation of the photo-ketonized form of **107c-e** (25 μM) were determined in MeCN at 20 °C in the presence of additives. Percentages represent volumes of additive in MeCN (3 mL total). Equilibrium constants K_e were determined by NMR spectroscopy or by linear interpolation, extrapolation or averaging of the measured data. Forward and reverse rate constants, k_{for}(H) and k_{rev}(H), for enolization and ketonization processes, respectively, were calculated using **Equations 10** and **11**. Ratios were calculated based on **Equation 12**.

Nuc	Additive	Quantity of additive	k_{obs} / s^{-1}	Approx. $t_{1/2}$	K_e(H)	k_{for}(H) / s^{-1}	k_{rev}(H) / s^{-1}	Ratio
107c (R=Me)	None	-	5.67×10^{-5}	3.5 h	8.0[a]	5.04×10^{-5}	6.30×10^{-6}	1.0
	Water	50%	3.15×10^{-4}	37 min	8.0[c]	2.80×10^{-4}	3.50×10^{-5}	5.6
	DABCO	2.5 μM	8.03×10^{-4}	14 min	8.0[c]	7.14×10^{-4}	8.92×10^{-5}	14
107d (R=OMe)	None	-	1.29×10^{-5}	15 h	4. 0[a]	1.03×10^{-5}	2.58×10^{-6}	1.0
	Water	50%	1.47×10^{-4}	1.3 h	3.7[b]	1.16×10^{-4}	3.13×10^{-5}	11
	Formic acid	2%	8.27×10^{-3}	1.4 min	5.3[b]	6.96×10^{-3}	1.31×10^{-3}	674
	DABCO	2.5 μM	8.24×10^{-4}	14 min	5.1[b]	6.89×10^{-4}	1.35×10^{-4}	67
	$ClCH_2$–DABCO$^+$ BF_4^-	50 μM	7.11×10^{-6}	27 h	5.0[b]	5.93×10^{-6}	1.19×10^{-6}	0.6
107e (R=Cl)	None	-	1.07×10^{-4}	1.8 h	12.5[a]	9.91×10^{-5}	7.93×10^{-6}	1.0
	Water	50%	2.13×10^{-3}	5 min	12.5[c]	1.97×10^{-3}	1.58×10^{-4}	20
	DABCO	2.5 μM	7.69×10^{-3}	1.5 min	12.5[c]	7.12×10^{-3}	5.70×10^{-4}	72
	$ClCH_2$–DABCO$^+$ BF_4^-	25 μM	7.35×10^{-5}	2.6 h	12.5[c]	6.81×10^{-5}	5.44×10^{-6}	0.7

[a] Measured by ^{1}H NMR spectroscopy in MeCN-d_3. [b] Measured by ^{1}H NMR spectroscopy in MeCN-d_3 in the presence of additive. [c] K_e(H) value was assumed to be the same as K_e(H) in MeCN-d_3 alone.

The effects of the *para*-substituents within **107c-e** on k_{for}(H) in MeCN were studied by Hammett correlation analysis. The rate constants used in these correlations are shown in **Table 18**. Compound **107d** showed deviation from the plot versus σ (**Figure 49b**), although better correlation was obtained for all four species when σ_p^+ values were used (**Figure 49a**). The σ_p^+ scale takes into account the ability of OMe, a strong electron donating substituent, to interact via resonance with the reaction centre. A ρ^+ value of +1.06 was obtained, where this positive value indicates small increases in electron density on the aryl rings of the substrates during the limiting C–H removal step of enolization. Compound **107e** (R = Cl) relaxed most rapidly, whereas compound **107d** (R = OMe) was the slowest, which suggests that rate limiting proton transfer from carbon proceeds towards an anionic intermediate rather than through pre-protonation of the ketone.

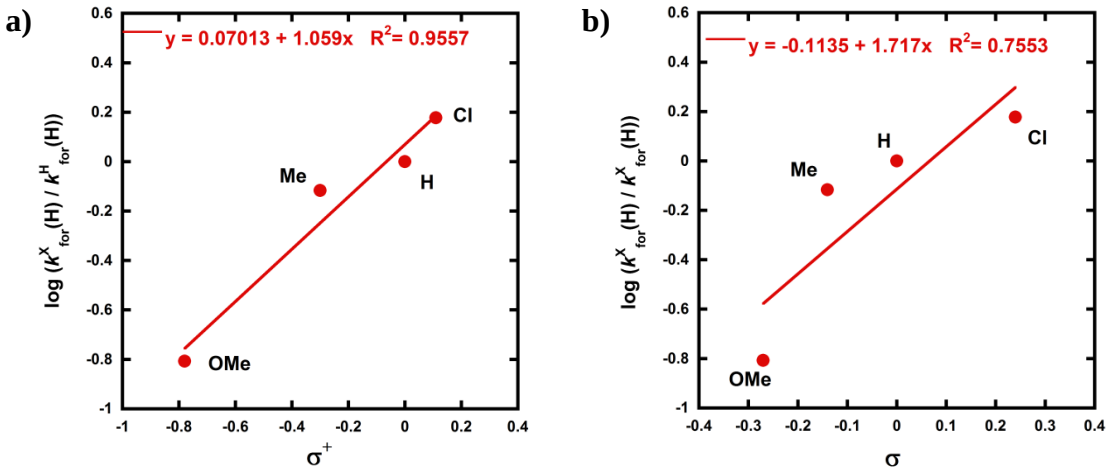

Figure 49: (a) Hammett correlation using σ_p^+ values for conversion of keto forms of **107a** and **107c-e** to the equilibrium keto-enol ratios. (b) Hammett correlation using σ_p values for conversion of keto forms of **107a** and **107c-e** to the equilibrium keto-enol ratios.

Table 18: k_{obs} values obtained for the relaxation of **107a** and **107c-e** (25 μM) at 20 °C in MeCN.

Nucleophile	σ_p^+	k_{obs} / s^{-1}	$k_{for}(H)$ / s^{-1}	$\log\{k^X_{for}(H) / k^H_{for}(H)\}$
107a	0	7.26×10^{-5}	6.63×10^{-5}	0
107c	−0.31	5.67×10^{-5}	5.04×10^{-5}	−0.117
107d	−0.78	1.29×10^{-5}	1.03×10^{-5}	−0.807
107e	0.11	1.07×10^{-4}	9.91×10^{-5}	0.178

3.2.2 Relaxation of 107a in the presence of additives

In order to gain insight into the potential effects of species that are present in widely-employed electrophilic fluorination protocols upon enolization, the effects of water, formic acid, DABCO and $ClCH_2$–$DABCO^+$ BF_4^- upon re-equilibration kinetics were explored. The spectra obtained using **107a** will be discussed individually in this section, while those of **107c-e** are included in Chapter 8 Section 8.4. All rate constants for **107a** are reported in **Table 16** and those of **107c-e** are summarised in **Table 17** in the previous section.

With water as the additive (15−50% of the reaction mixture by volume), increased rates of re-enolization were observed (**Figure 50**), with a 1:1 water:MeCN solvent system giving a 10-fold increase in $k_{for}(H)$ compared to MeCN. The position of the keto-enol equilibrium changed marginally upon moving from MeCN to 1:1 water:MeCN, with K_e values of 10.5 and 5.7 respectively. This is consistent with previous studies upon 1,3-

dicarbonyl systems which show limited variations of K_e values upon changes from single- to mixed-polar solvent systems.[141]

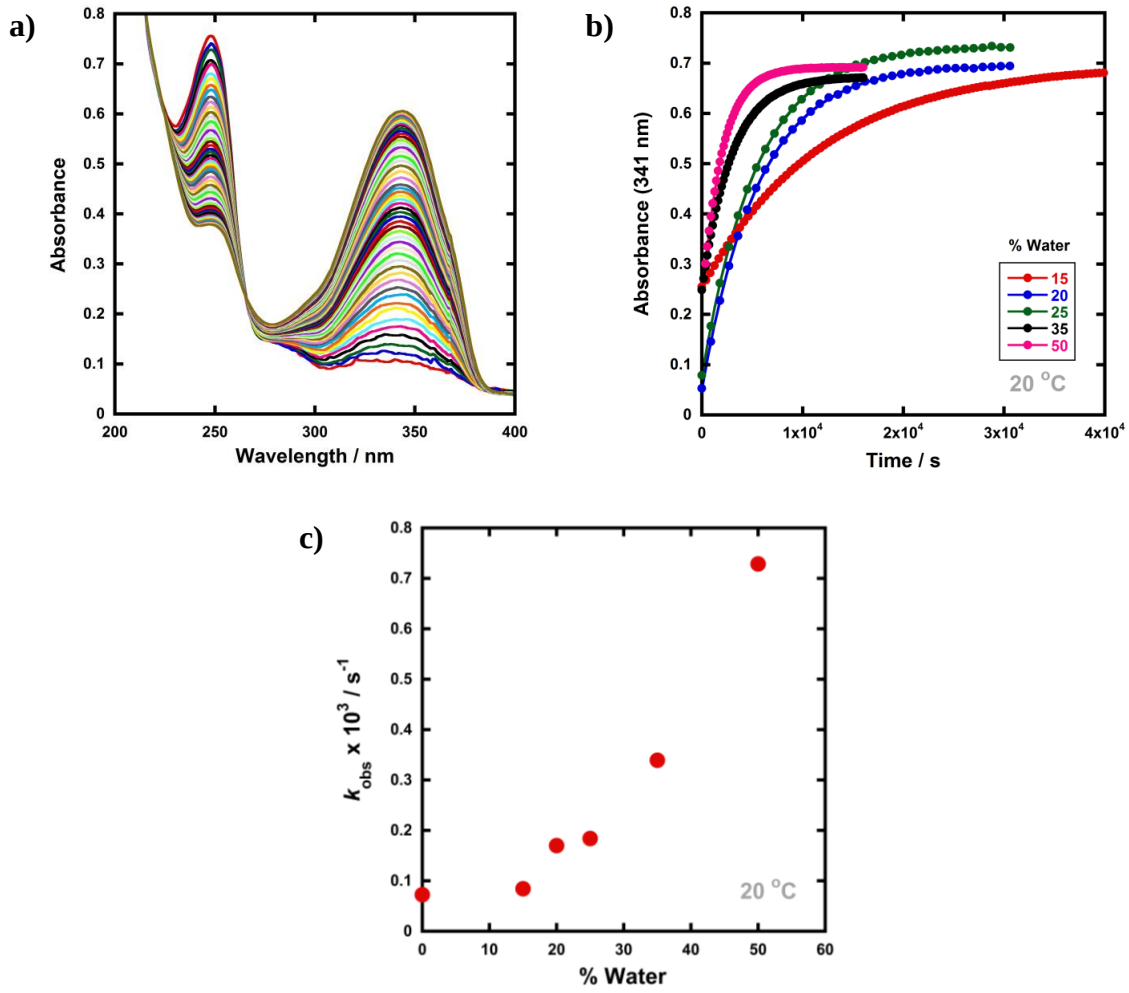

Figure 50: (a) The relaxation of **107a-keto** (25 μM) with 50% *v*/*v* deionised water in MeCN. The scans were acquired every ~40 s for 1 h. (b) The relaxation of **107a-keto** (25 μM) in the presence of deionised water (*v*/*v* 15%, 20%, 25%, 35%, 50% in MeCN), monitored at λ_{max} = 341 nm at 20 °C. (c) Trends observed in the rates of relaxation (k_{obs}) of **107a** (25 μM) upon addition of different quantities of water. The k_{obs} values obtained in each experiment are reported in **Table 16**.

Photophysical studies on di-substituted 1,3-diphenyl-1,3-propanedione compounds have shown that MeCN supports very slow exchange between tautomeric states, whereas protic solvents, including MeCN-water mixtures, enhance rates significantly.[161,162] Water is often used as a solvent or co-solvent in fluorination reactions to aid solubility of Selectfluor™.[120] Studies conducted in the present work show that the solubility limit of Selectfluor™ in water is ~500 mM, compared to ~50 mM in MeCN. Here, it has been shown that the addition of water also increases the rate of enolization, facilitating the conversion of the small amounts of residual diketone to the nucleophilic enol

tautomer, which reacts with the fluorinating reagent. The effects of water on rates of fluorination of 1,3-dicarbonyls and 2-fluoro-1,3-dicarbonyls will be explored in Chapter 4.

The addition of small amounts of formic acid had limited effects on the position of the keto-enol equilibria with all K_e values being ~10, however, greatly enhanced rates of keto-to-enol relaxation were observed (**Figure 51**). Thus, the rate constant for enolization, $k_{for}(H)$, increased 86-fold upon addition of 3% formic acid in comparison to MeCN alone.

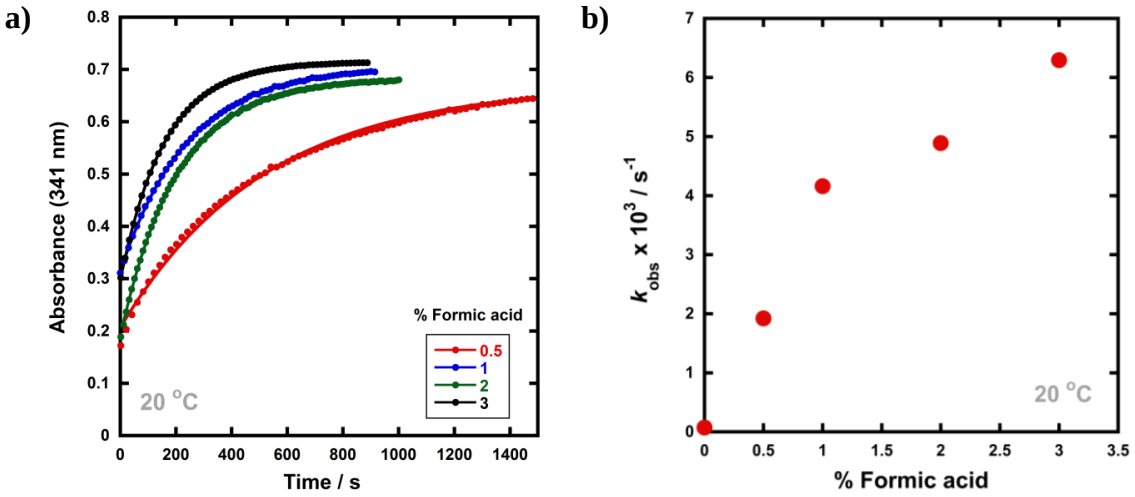

Figure 51: (a) The relaxation of **107a-keto** (25 μM) in the presence of formic acid (*v*/*v* 0.5%, 1%, 2%, 3%), monitored at λ_{max} = 341 nm in MeCN at 20 °C. (b) Trends observed in the rates of relaxation (k_{obs}) of **107a** (25 μM) upon addition of different quantities of formic acid. The k_{obs} values obtained in each experiment are reported in **Table 16**.

The addition of DABCO increased the relaxation rates significantly. For example, with one equivalent (25 μM), a 330-fold acceleration of the enolization process $k_{for}(H)$ was observed. Even with 0.1 equivalents (2.5 μM) of DABCO, the tautomeric equilibrium was regained rapidly. When $k_{for}(H)$ values for relaxation were plotted against DABCO concentration (**Figure 52**), a simple linear (i.e. first order) correlation was observed, giving a second-order rate constant, $k_2 = 9.13 \times 10^2$ M^{-1} s^{-1}. In terms of basicity, DABCO (pK_{aH}(MeCN) = 18.29)[163] is insufficiently basic to quantitatively deprotonate **107a-keto** (for **107a-keto** estimated pK_a(MeCN) = pK_a(DMSO) + 12.9[164] = 13.4[165] + 12.9 = 26.3). Thus, the data suggest that DABCO may operate as a general base catalyst.

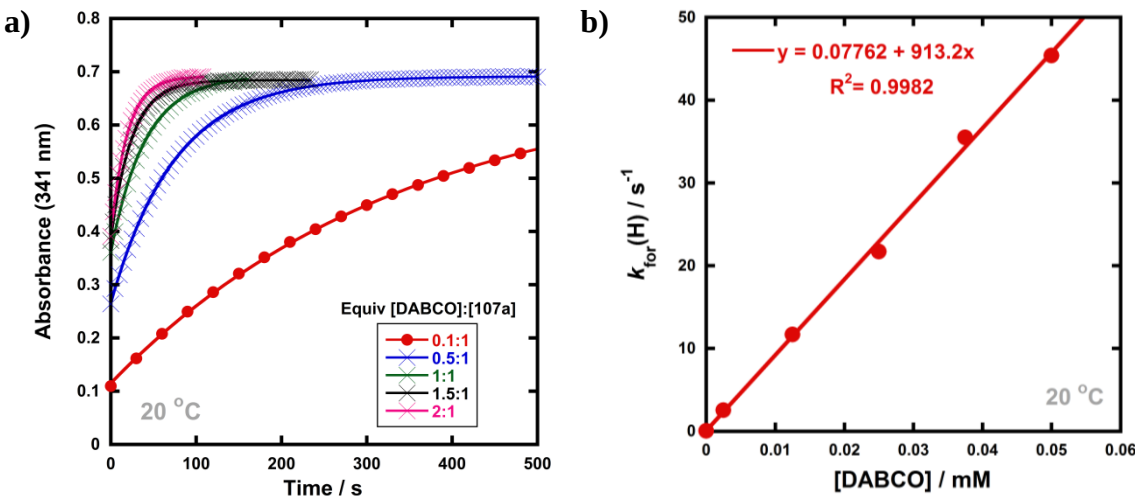

Figure 52: (a) The relaxation of **107a-keto** (25 μM) in the presence of different concentrations of DABCO, monitored at λ_{max} = 341 nm in MeCN at 20 °C. (b) Trends observed in the rates of relaxation (k_{obs}) of **107a** (25 μM) upon addition of different quantities of DABCO. The k_{obs} values obtained in each experiment are reported in **Table 16**.

Upon delivery of electrophilic fluorine, N–F reagents give amines as by-products, which could promote keto-enol tautomerism, and hence the rate of fluorination, if they remain unprotonated. Fluorination reactions using Selectfluor™ result in the formation of $ClCH_2$–$DABCO^+$ BF_4^- **36** (**Scheme 26**). This compound was synthesised via reflux of DABCO in DCM to obtain the chloride salt, followed by a counterion exchange using $NaBF_4$ (see Chapter 8 Section 8.4.1).

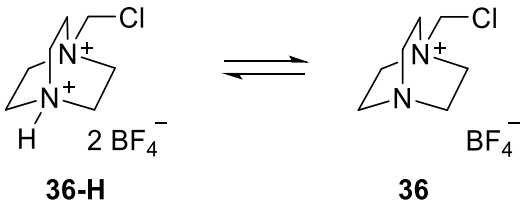

Scheme 26: $ClCH_2$-$DABCO^+$ BF_4^-, the product of loss of fluorine from Selectfluor™.

When 0.5 to 2 equivalents of $ClCH_2$–$DABCO^+$ BF_4^- were added to **107a-keto**, very small (1.4 to 2-fold) increases in k_{obs} and k_{for}(H) were observed (**Figure 53b**). However, the addition of greater quantities of $ClCH_2$–$DABCO^+$ BF_4^- (25–100 equivalents) resulted in reduced k_{for}(H) values (**Figure 53c**). For example, with 100 equivalents of $ClCH_2$–$DABCO^+$ BF_4^-, k_{for}(H) was reduced three-fold. While the $ClCH_2$–$DABCO^+$ cation is unlikely to remain unprotonated and thus will be unable to function as a base, this series of experiments suggested the possibility of salt effects upon the relaxation processes. Rates of reactions, particularly those involving ionic species, can be

influenced by the addition of salts even though the added ions do not themselves participate in the reaction.[166] Electrostatic interactions between ions introduce deviations from ideal behaviour even at low concentrations. Changes in concentrations of non-reacting ions can alter reactivities of reacting ions. Primary salt effects directly influence the rate-determining step, while secondary salt effects modify reaction rates by changing positions of pre-equilbria.[166]

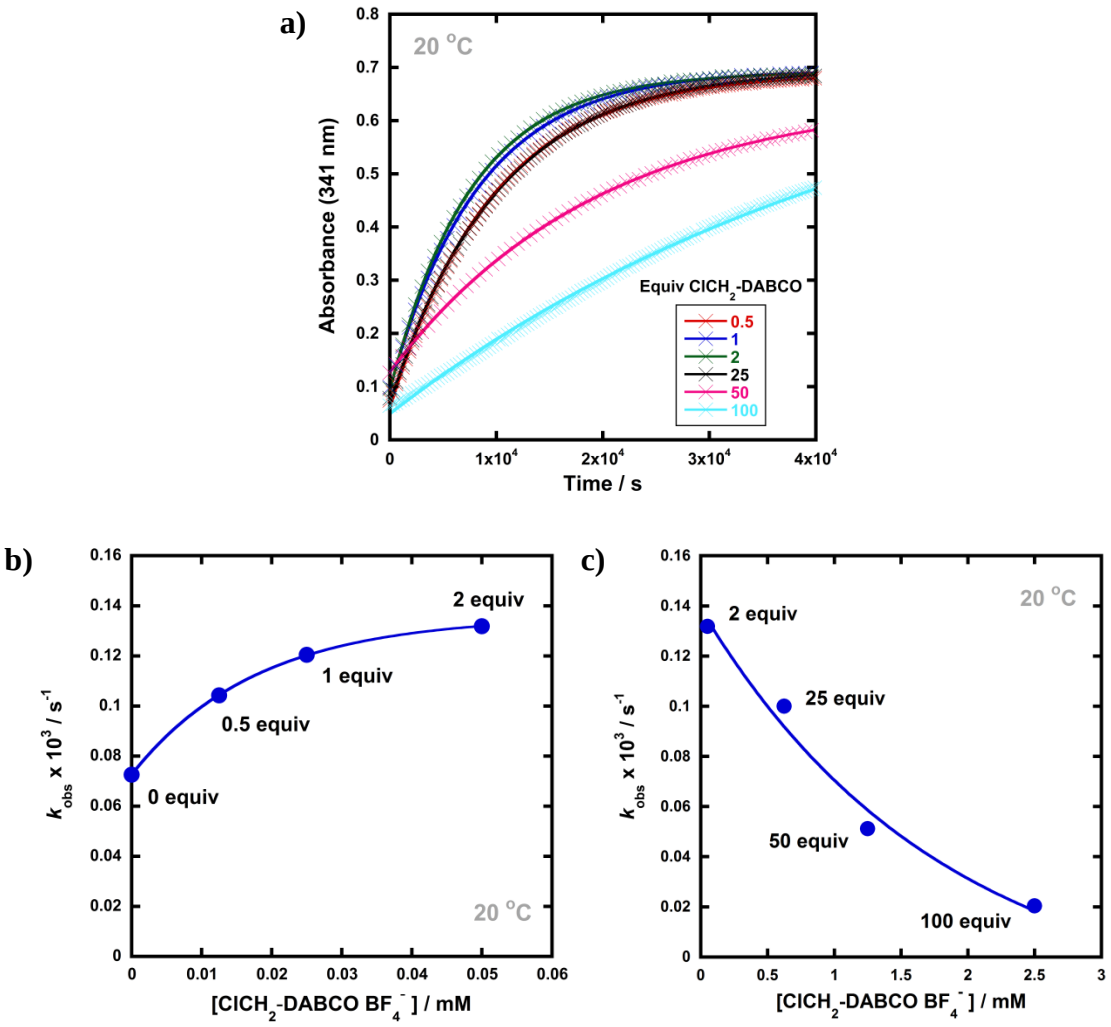

Figure 53: (a) The relaxation of **107a-keto** (25 μM) in the presence of different concentrations of $ClCH_2$−DABCO$^+$ BF_4^-, monitored at λ_{max} = 341 nm in MeCN at 20 °C. (b) Trends observed in the rates of relaxation (k_{obs}) of **107a** (25 μM) upon addition of 0.5−2 equivalents of $ClCH_2$−DABCO$^+$ BF_4^-. (c) Trends observed upon addition of 25−100 equivalents of $ClCH_2$−DABCO BF_4^-. The k_{obs} values obtained in each experiment are reported in **Table 16**.

The relaxation of **107a-keto** in the presence of 20-40% water and $ClCH_2$-DABCO$^+$ BF_4^- (12.5 μM) was monitored to investigate the possibility of combined effects of both additives towards increasing relaxation rates (**Figure 54**). Very small increases in

k_{for}(H) were observed compared to in the presence of water only. For example, with 20% water and $ClCH_2$-DABCO$^+$ BF_4^-, a 2.7-fold increase was obtained while k_{for}(H) increased 2.4-fold in 20% water only.

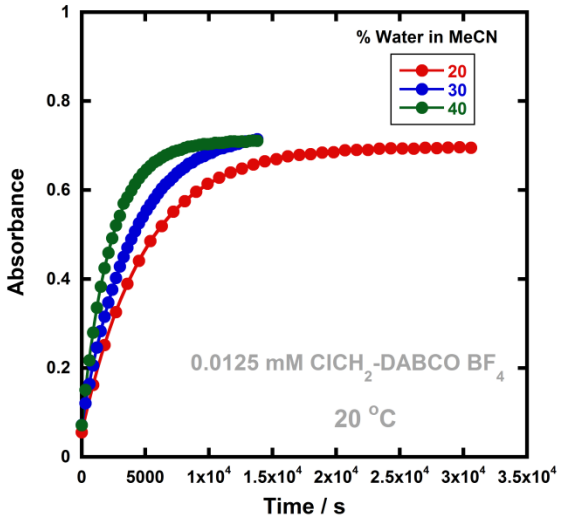

Figure 54: The relaxation of **107a-keto** (25 μM) in the presence of different quantities of water with $ClCH_2$–DABCO$^+$ BF_4^- (12.5 μM) monitored at λ_{max} = 341 nm in MeCN at 20 °C. The k_{obs} values obtained are reported in **Table 16**.

Consequently, relaxation experiments were performed in the presence of 2−100 equivalents of $LiBF_4$ and similar reductions in k_{obs} were observed (**Figure 55**). However, Li salts are known to form chelates with 1,3-diketones, so it is possible that the reductions in k_{obs} resulted from this interaction rather than a salt effect.

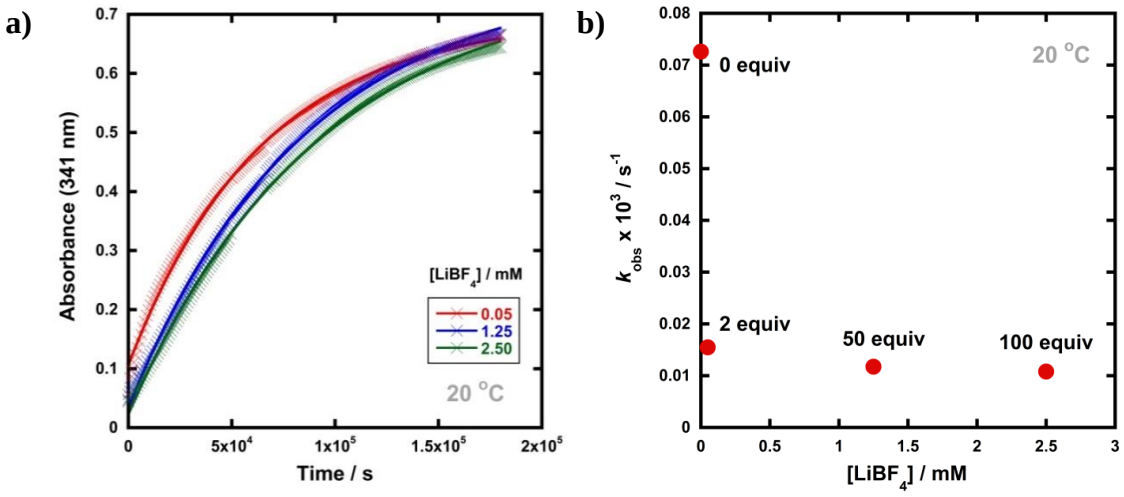

Figure 55: (a) The relaxation of **107a-keto** (25 μM) in the presence of different concentrations of $LiBF_4$, monitored at λ_{max} = 341 nm in MeCN at 20 °C. (b) Trend observed in the rates of relaxation (k_{obs}) of **107a-keto** (25 μM) upon addition of different quantities of $LiBF_4$, in MeCN at 20 °C. The k_{obs} values obtained in each experiment are reported in **Table 16**.

The effects of adding $^{n}Bu_4N^+BF_4^-$, a non-chelating salt, were then explored (**Figure 56**). In order to mimic the salt concentrations in synthetic-scale processes, the effect of adding 240 mM $^{n}Bu_4N^+BF_4^-$ (from a recently acquired sample) to solutions of **107a-keto** was studied. Under these conditions, k_{for}(H) increased 2-fold in comparison to experiments in the absence of salts. Interestingly, the relaxation rates obtained using an older sample of $^{n}Bu_4N^+BF_4^-$ were 10-fold lower than with the recently acquired sample. This difference is likely due to the hygroscopic nature of this reagent, where the combined effects of the salt as well as water resulted in lower relaxation rates, while the recently purchased sample had lower water content.

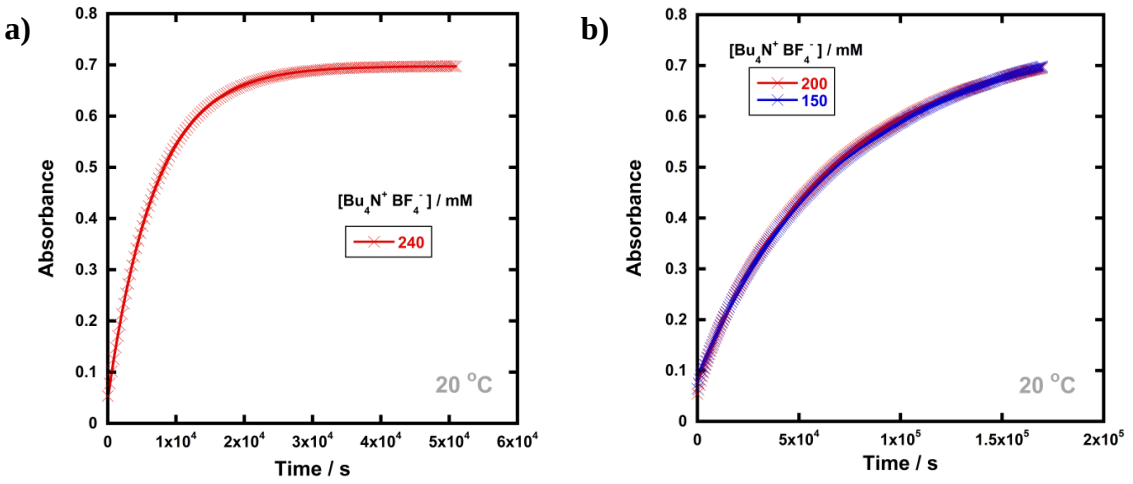

Figure 56: (a) The relaxation of **107a-keto** (25 μM) monitored at λ_{max} = 341 nm in MeCN at 20 °C in the presence of $^{n}Bu_4N^+BF_4^-$ (240 mM) from a recently acquired sample. (b) Relaxation of **107a-keto** (25 μM) in MeCN at 20 °C in the presence of $^{n}Bu_4N^+BF_4^-$ (200 mM and 150 mM) from an older sample. The k_{obs} values obtained are reported in **Table 16**.

The effects of the amine derivative of NFSI, dibenzenesulfonimide ($(PhSO_2)_2NH$, pK_a(MeCN) ~ 11.3)[167] upon the rate of relaxation of **107a-keto** were also explored. Interestingly, the presence of 5 equivalents of $(PhSO_2)_2NH$ resulted in a 40-fold decrease in the relaxation rate constant rate, however, 10 equivalents of $(PhSO_2)_2NH$ gave only a 16-fold decrease (**Figure 57**).

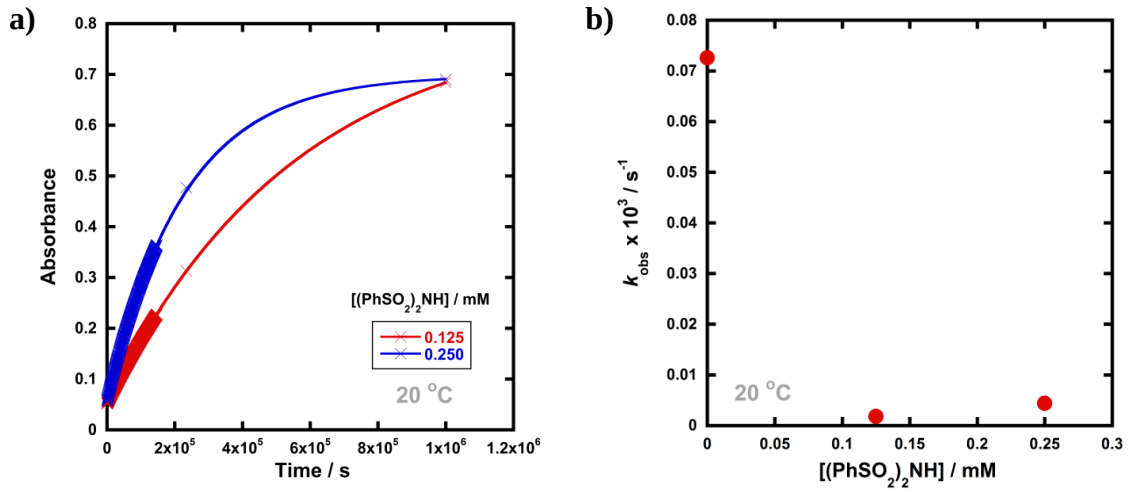

Figure 57: (a) The relaxation of **107a-keto** (25 μM) in the presence of different concentrations of $(PhSO_2)_2NH$, monitored at λ_{max} = 341 nm in MeCN at 20 °C. (b) Trend observed. The k_{obs} values obtained in each experiment are reported in **Table 16**.

The addition of the conjugate base form, $(PhSO_2)_2N^-Na^+$, which was synthesised using NaOMe (see Chapter 8 Section 8.4.2), also showed a similar effect. One equivalent caused a significant reduction in relaxation rate and larger concentrations showed less-pronounced reductions (**Figure 58**). In this case, the reduction in k_{for}(H) is likely due to chelation of the Na^+ ion to diketone **107a**, an interaction previously described by Bordwell.[165]

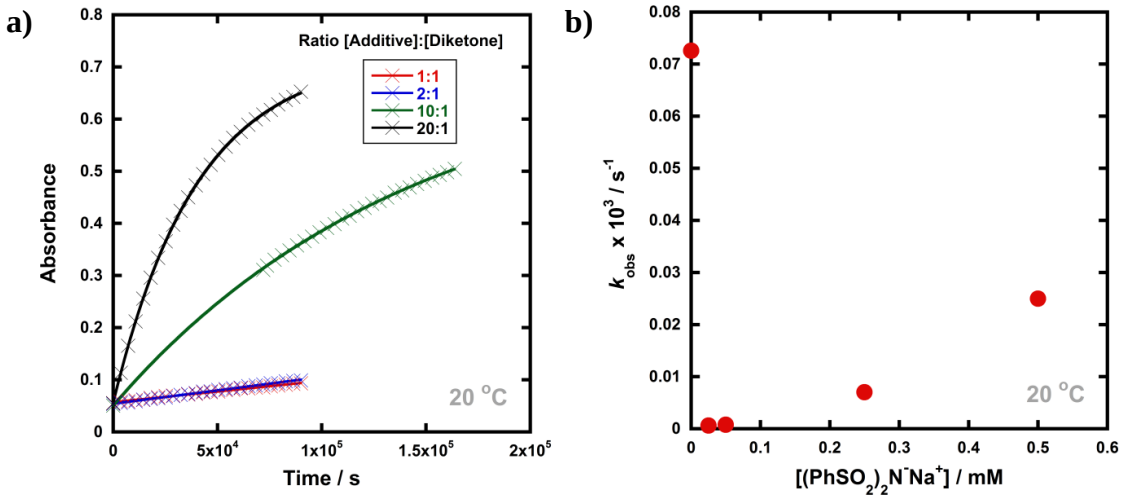

Figure 58: (a) The relaxation of **107a-keto** (25 μM) in the presence of different concentrations of $(PhSO_2)_2N^-Na^+$, monitored at λ_{max} = 341 nm in MeCN at 20 °C. (b) Trend observed. The k_{obs} values obtained in each experiment are reported in **Table 16**.

The relaxation kinetics of keto forms of **107c-e** were explored using the same photoketonization procedure in the presence of additives, and corresponding k_{obs}, K_e,

k_{for}(H) and k_{rev}(H) values are reported in **Table 17**. There were little variations in measured K_e values for **107d** across the range of conditions that were employed. For **107c** and **107e**, it was assumed that the K_e(H) values in the presence of additives would be the same as K_e(H) in MeCN-d_3 alone under conditions where measured values were not obtained. The differences in k_{for}(H) in the presence and absence of additives for **107c-e** were broadly similar to those of **107a**. All spectra obtained for relaxation of **107c-e** in the presence of additives are included in Chapter 8 Section 8.4. In summary, the effects of $ClCH_2$–$DABCO^+$ BF_4^- and other ionic species upon enolization kinetics of **107a** and **107c-e** are measurable, but marginal and potentially complex in nature.

3.3 Kinetics of keto-enol tautomerism in compounds 108a and 108c-e

3.3.1 Photoketonization-relaxation experiments for 108a and 108c-e

The fluoroenol- and fluoroketo-tautomers of **108a** and **108c-e** have distinct absorbance bands at ~350 nm and ~250 nm, respectively. Therefore, in the same way as for compounds **107a** and **107c-e** the tautomerism processes of the fluorinated derivatives were monitored via changes in absorbance of the fluoroenol tautomers. Photoketonization experiments were conducted on 0.50 mM solutions of **108a** and **108c-e** in MeCN in the absence of additives (**Scheme 27**). Spectra corresponding to photoketonization of **108a** are shown in **Figure 59**.

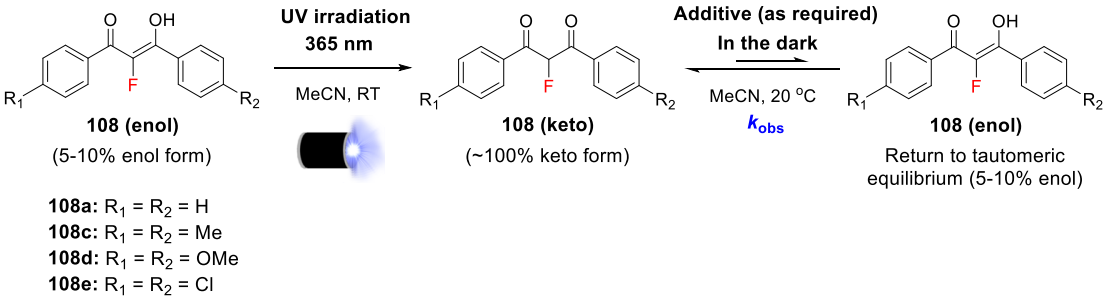

Scheme 27: Photoketonization (step 1) and relaxation (step 2) of compounds **108a** and **108c-e** (0.50 mM) in MeCN.

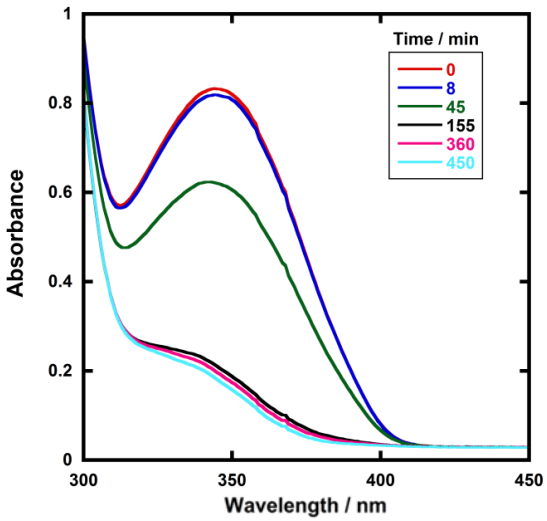

Figure 59: Spectra corresponding to photoketonization of **108a** (0.50 mM) over time, with a decrease at λ_{max}(enol) = 350 nm. Absorbances below 300 nm were saturated due to the high concentration of **108a-keto** and are therefore not shown.

The keto:enol ratios of **108a** and **108c-e** used to determine their K_e values were obtained using ^{19}F NMR spectroscopy by integration of peaks corresponding to the keto (δ ~ −190 ppm) and enol (δ ~ −170 ppm) tautomers. The solutions were allowed to equilibrate for 10 half-lives before NMR spectra were acquired. In order to obtain quantitative integral values, it was necessary to increase the relaxation delays employed for ^{19}F NMR experiments. Hence, inversion recovery experiments were carried out to determine the T1 value for **108a-keto**, which was found to be 4.59 ± 0.06 s for the peak at δ = 190.04 ppm, and 3.90 ± 0.11 s for the peak at δ = 190.30 ppm (within the doublet). This inequivalence in peak T1 value is due to the chemical shift anisotropy associated with some fluorine-containing compounds.[168] Ideally, the relaxation delay should be 5-fold larger than the T1 value, although this was inconvenient as it would have resulted in long acquisition times for each of the NMR spectra. Hence, relaxation delays of 8 s were used as a compromise. The keto:enol ratios are summarised in **Table 19**.

Table 19: Keto:enol ratios of **108a** and **108c-e** (25 mM) in MeCN-d_3, determined by ^{19}F NMR spectroscopy. The ^{19}F NMR spectrum for **108a** with DABCO was acquired after 15 min and showed the loss of the fluorine atom – this will be discussed at the end of Section 3.3.2.

Compound	Additive	Quantity of additive in MeCN-d_3	Keto:enol ratio
108a	None	-	95:5
(R_1 = R_2 = H)	D_2O	50% (28 M)	95:5
	Formic acid	2% (0.53 M)	95:5
	DABCO	25 mM (1 eq)	Loss of F
	H_2O	20% (11 M)	96:4
	Bu_4N^+ BF_4^-	300 mM	96:4
	H_2O, Bu_4N^+ BF_4^-	20%, 250 mM	96:4
108c (R_1 = R_2 = Me)	None	-	87:13
108d	None	-	98:2
(R_1 = R_2 = OMe)	D_2O	50% (28 M)	95:5
	Formic acid	2% (0.53 M)	97:3
	DABCO	25 mM (1 eq)	98:2
108e (R_1 = R_2 = Cl)	None	-	92:8

The K_e values determined for **108a** and **108c-e** are summarised in **Table 20**. Across the range of additives where K_e values were obtained for **108a** and **108d**, these values were broadly constant, in a similar vein to the non-fluorinated systems. Hence, K_e values for **108c** and **108e** were only obtained in MeCN-d_3 and those in the presence of additives were assumed to be the same as the values in MeCN-d_3 only.

Following irradiation of solutions of **108a** and **108c-e**, spectrophotometric kinetic assays for relaxation were conducted, and they showed very slow restoration of the thermodynamic ratio between the two tautomeric forms. In the case of **108a** and **108e**, sigmoidal behaviours were clearly discernible (*vide infra*), which suggested autocatalysis of the processes, and fitting of the data to a model for reversible autocatalysis gave strong support for this hypothesis. **Equations 13** and **14** were solved

numerically using Wolfram Mathematica 11.0.[2] In these equations, k_{for}(uncat) represents the first order rate constant for uncatalysed enolization (s^{-1}) and k_{for}(autocat) represents the second order rate constant for autocatalysed enolization (M^{-1} s^{-1}).

$$\frac{d[\text{ketone}]}{dt} = -k_{for}(\text{uncat})[\text{ketone}] - k_{for}(\text{autocat})[\text{ketone}][\text{enol}] + \frac{k_{for}(\text{uncat})}{K_e}[\text{enol}] + \frac{k_{for}(\text{autocat})}{K_e}[\text{enol}]^2 \qquad (\mathbf{13})$$

$$\frac{d[\text{enol}]}{dt} = k_{for}(\text{uncat})[\text{ketone}] + k_{for}(\text{autocat})[\text{ketone}][\text{enol}] - \frac{k_{for}(\text{uncat})}{K_e}[\text{enol}] - \frac{k_{for}(\text{autocat})}{K_e}[\text{enol}]^2 \qquad (\mathbf{14})$$

For **108a**, absorbance-time data (**Figure 60a**) were transformed to concentration-time data (**Figure 60b**) based on the assumptions that $[\text{ketone}]_{t=0}$ = 0.0005 M and $[\text{ketone}]_{t=\infty}$ = 0.0004748 M, where this latter value was determined from the value of K_e measured by NMR spectroscopy in MeCN-d_3. The fitting delivered k_{for}(uncat) = 3.66 × 10^{-8} s^{-1} and k_{for}(autocat) = 1.58 × 10^{-2} M^{-1} s^{-1}. Reverse rate constants for the processes described by k_{for}(uncat) and k_{for}(autocat) were obtained via K_e using **Equation 15**.

$$K_e = \frac{k_{for}(\text{uncat})}{k_{rev}(\text{uncat})} \quad \text{or} \quad K_e = \frac{k_{for}(\text{autocat})}{k_{rev}(\text{autocat})} \qquad (\mathbf{15})$$

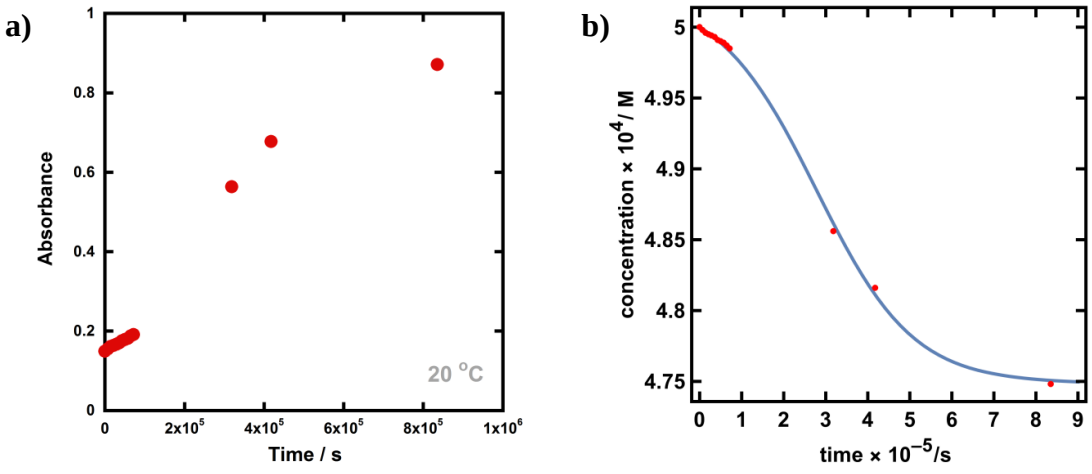

Figure 60: (a) Relaxation of **108a-keto** ([**108a**$_{tot}$] = 0.50 mM) without additives (in MeCN at 20 °C, absorbance monitored at 350 nm), following conversion of the fluoroenol tautomer to the fluoroketo form by irradiation with UV light at 365 nm. (b) Fitted using Wolfram Mathematica.

[2] Fitting of the data for **108a** and **108e** was carried out by Dr David Hodgson using Wolfram Mathematica 11.0.

The relaxation of **108e-keto** reached an endpoint (**Figure 61a**) and using the same method described for **108a-keto**, the absorbance-time data (**Figure 61b**) were first transformed to concentration-time data (**Figure 62**), followed by fitting to a model (using differential **Equations 13** and **14**) in Wolfram Mathematica. The fitting delivered k_{for}(uncat) = 5.38 × 10^{-8} s^{-1} and k_{for}(autocat) = 1.12 × 10^{-2} M^{-1} s^{-1}. Reverse rate constants for the processes described by k_{for}(uncat) and k_{for}(autocat) were obtained via K_e using **Equation 15** (*vide supra*).

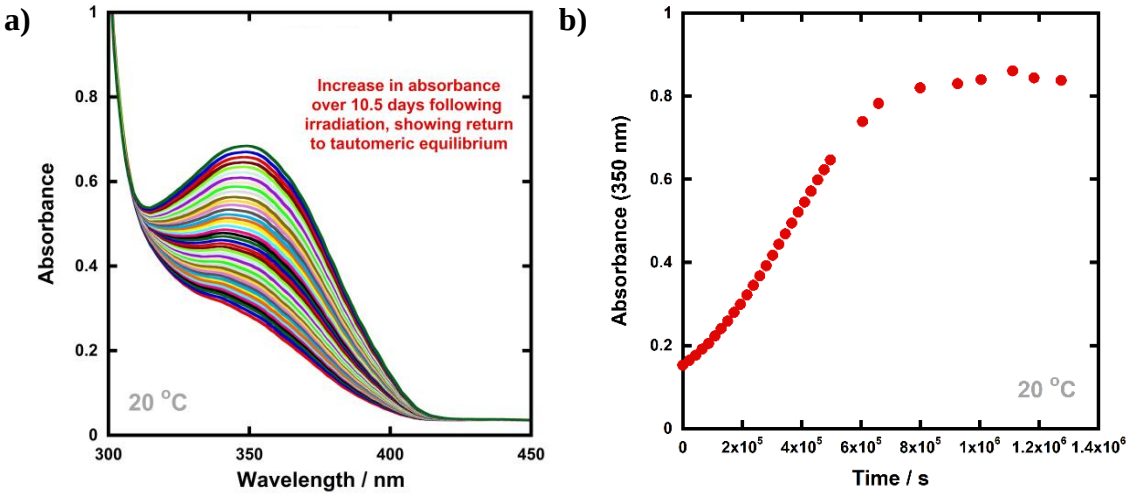

Figure 61: (a) Time-arrayed multi-wavelength analysis for relaxation of **108e-keto** ([**108e**$_{tot}$] = 0.50 mM) at 20 °C, spectra acquired every 6 h over 10.5 days. (b) Absorbance-time data at 350 nm.

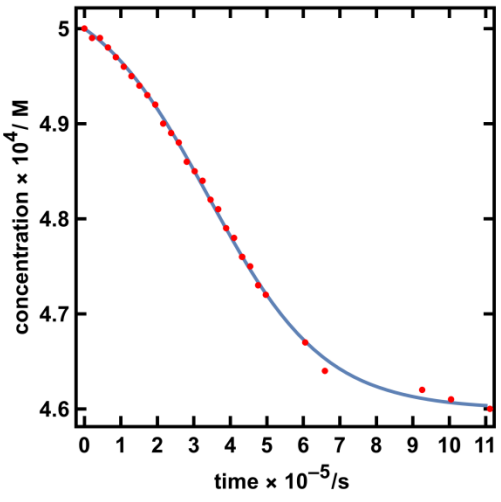

Figure 62: Relaxation of **108e-keto** fitted using Wolfram Mathematica.

In the case of **108d** (R_1 = R_2 = OMe) the multi-wavelength time-arrayed UV-vis spectra for this relaxation showed that reaction progress was extremely slow and did not reach an endpoint even after 11 days (**Figure 63**). Hence, the k_{obs} value for relaxation was

estimated using a zero-order approach (**Figure 64a**), by linear fitting of the first 20% of the reaction, giving the following result:

$$k_{\text{obs}} = \frac{\text{slope}}{\text{total absorbance change}} = \frac{9.69 \times 10^{-8}}{0.78 - 0.070} = 1.37 \times 10^{-7}\ \text{s}^{-1}$$

A second method was employed to confirm the k_{obs} value, which was to use first-order fitting with a fixed endpoint (**Figure 64b**). The rate constant obtained from extrapolation to the endpoint is 1.46×10^{-7} s^{-1}. The two rate constants are within 6% of each other and are thus in good agreement. Thus, the relaxation process has a half-life of 60 days.

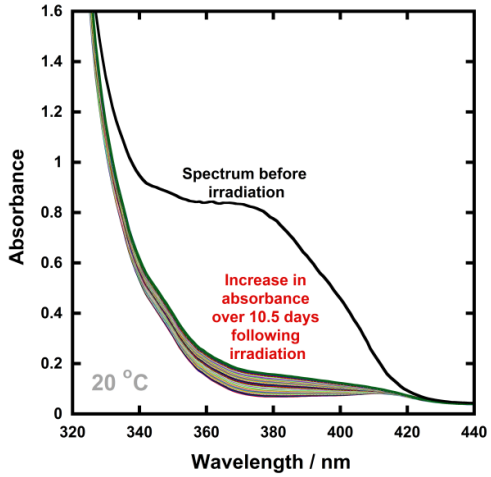

Figure 63: Absorbance spectra for re-enolization of **108d-keto** ([**108d**$_{\text{tot}}$] = 0.50 mM, 20 °C, spectra acquired every 6 h over 10.5 days) following irradiation to the diketone tautomer. The black line corresponds to the spectrum before irradiation, from which the endpoint was obtained.

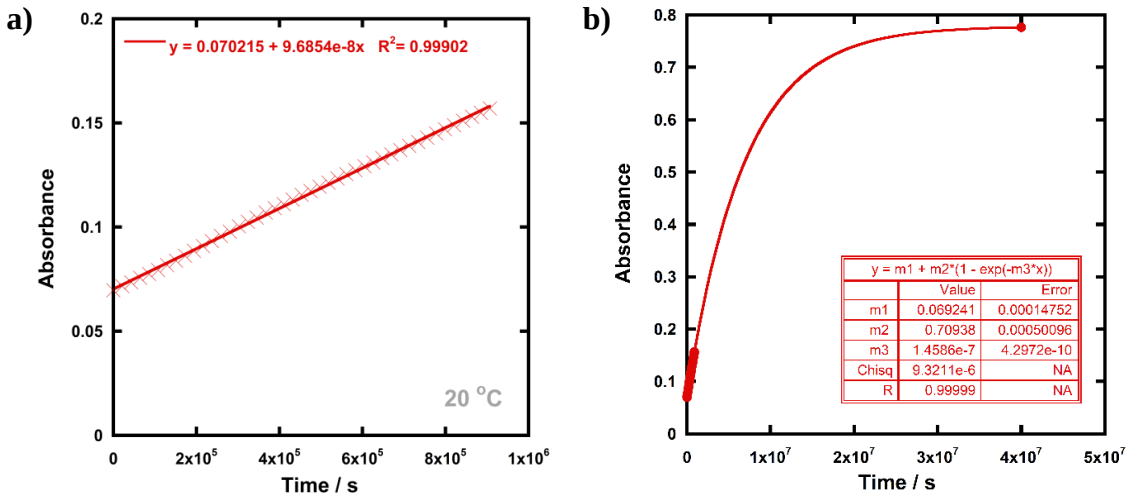

Figure 64: (a) Linear fitting of data points from absorbances of **108d-keto** at 380 nm to obtain the rate constant using a zero-order approach. (b) First-order fitting with a fixed endpoint.

Similarly, the relaxation of **108c-keto** was very slow (**Figure 65a**), hence, the rate constant for relaxation was obtained using the zero-order approach (**Figure 65b**). The rate constant for relaxation was 8.85×10^{-7} s^{-1} and has a half-life of 90 days.

$$k_{\text{obs}} = \frac{\text{slope}}{\text{total absorbance change}} = \frac{3.65 \times 10^{-7}}{0.63 - 0.22} = 8.85 \times 10^{-7}\ \text{s}^{-1}$$

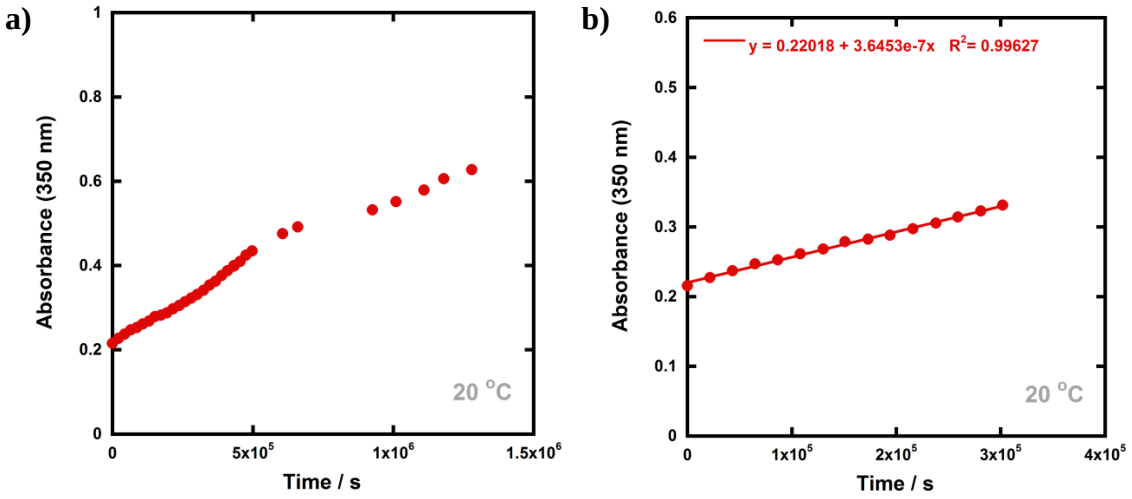

Figure 65: (a) Relaxation of **108c-keto** ([**108c**$_{tot}$] = 0.50 mM) at 20 °C, following conversion of the fluoroenol tautomer to the fluoroketo form by irradiation. (b) Linear fitting to first 20% of relaxation.

For compounds **108c** and **108d**, the $k_{\text{for}}(\text{F})$ and $k_{\text{rev}}(\text{F})$ values were then obtained using **Equations 16** and **17**, and all values are reported in **Table 20**.

$$k_{\text{obs}} = k_{\text{for}}(\text{F}) + k_{\text{rev}}(\text{F}) \qquad (\mathbf{16})$$

$$K_e = \frac{k_{\text{for}}(\text{F})}{k_{\text{rev}}(\text{F})} \qquad (\mathbf{17})$$

For **108a** and **108c-e**, the $k_{\text{for}}(\text{F})$ values in the presence of additives were compared with the values obtained without additives, as in Section 3.2.1, and are defined by **Equation 18**:

$$\text{Ratio} = \frac{k_{\text{for}}(\text{F})\{\text{with additive}\}}{k_{\text{for}}(\text{F})\{\text{MeCN}\}} \qquad (\mathbf{18})$$

Table 20: Summary of diketone relaxation of 2-fluorinated-1,3-dicarbonyl systems. The k_{obs} values for relaxation of photoketonized forms of **108a** and **108c-e** (0.50 mM) were determined in MeCN at 20 °C in the presence of additives. Percentages represent volumes of additive in MeCN (1 mL total volume). Equilibrium constants K_e were determined by NMR spectroscopy or by linear interpolation, extrapolation or averaging of the measured data. Forward and reverse rate constants, k_{for}(F) and k_{rev}(F), for enolization and ketonization processes, of the 2-fluorinated-1,3-dicarbonyl systems, respectively were calculated using **Equations 15**, **16** and **17**. Ratios were calculated based on **Equation 18**.

Nuc	Additive	Quantity of additive	k_{obs} / s^{-1}	Approx. $t_{1/2}$	K_e(F)	k_{for}(F) / s^{-1}	k_{rev}(F) / s^{-1}	Ratio
108a	None	-	-[a]	-	0.053[b]	3.66×10^{-8} (1.58×10^{-2})[c]	6.91×10^{-7} (2.98×10^{-1})[c]	1.0
	Water	10%	4.98×10^{-5}	4 h	0.053[d]	2.49×10^{-6}	4.73×10^{-5}	68
		20%	1.19×10^{-4}	1.6 h	0.053[d,e]	5.95×10^{-6}	1.13×10^{-4}	163
		30%	2.23×10^{-4}	0.9 h	0.053[d]	1.12×10^{-5}	2.12×10^{-4}	305
		40%	3.77×10^{-4}	0.5 h	0.053[d]	1.89×10^{-5}	3.58×10^{-4}	515
		50%	6.78×10^{-4}	0.3 h	0.053[b]	3.39×10^{-5}	6.44×10^{-4}	926
	Formic acid	3%	1.64×10^{-4}	1.2 h	0.053[b]	8.20×10^{-6}	1.56×10^{-4}	224
	DABCO	2.5 μM	1.42×10^{-3}	8 min	-[f]	-[f]	-[f]	-[f]
	$ClCH_2$–	12.5μM	1.01×10^{-6}	8 d	0.053[d]	5.05×10^{-8}	9.60×10^{-7}	1.4
	$DABCO^+$ BF_4^-	25 μM	2.93×10^{-6}	2.7 d	0.053[d]	1.47×10^{-7}	2.78×10^{-6}	4.0
	Water and	20%	1.91×10^{-4}	1 h	0.053[d]	9.55×10^{-6}	1.81×10^{-4}	261
	$ClCH_2$–$DABCO^+$	30%	2.33×10^{-4}	50 min	0.053[d]	1.16×10^{-5}	2.21×10^{-4}	318
	BF_4^-	40%	3.90×10^{-4}	30 min	0.053[d]	1.95×10^{-5}	3.71×10^{-4}	533
	(12.5 μM)	50%	6.94×10^{-4}	17 min	0.053[d]	3.47×10^{-5}	6.59×10^{-4}	948
	$^n Bu_4N^+$ BF_4^-	240 mM	8.38×10^{-5}	2.3 h	0.043[g]	3.42×10^{-6}	8.04×10^{-5}	94
108c	None	-	8.64×10^{-8} [h]	90 d	0.149[b]	1.12×10^{-8} (n.d.)[c]	7.52×10^{-8} (n.d.)[c]	1.0
	Water	50%	9.15×10^{-4}	0.2 h	0.149[i]	1.19×10^{-4}	7.96×10^{-4}	10594
108d	None	-	1.46×10^{-7} [h]	60 d	0.020[b]	2.92×10^{-9} (n.d.)[c]	1.43×10^{-7} (n.d.)[c]	1.0
	Water	20%	3.22×10^{-5}	6 h	0.033[d]	1.04×10^{-6}	3.12×10^{-5}	355
		30%	5.39×10^{-5}	3.6 h	0.040[d]	2.06×10^{-6}	5.18×10^{-5}	706
		40%	9.23×10^{-5}	2.1 h	0.046[d]	4.07×10^{-6}	8.82×10^{-5}	1396
		50%	1.71×10^{-4}	1.1 h	0.053[b]	8.55×10^{-6}	1.62×10^{-4}	2928
	Formic acid	2%	1.73×10^{-5}	11 h	0.031[b]	5.19×10^{-7}	1.68×10^{-5}	178
	DABCO	2.5 μM	1.32×10^{-5}	15 h	0.020[b]	2.64×10^{-7}	1.29×10^{-5}	90
108e	None	-	-[a]	-	0.087[b]	5.37×10^{-8} (1.11×10^{-2})[c]	6.18×10^{-7} (1.28×10^{-1})[c]	1.0
	Water	50%	1.97×10^{-3}	6 min	0.087[i]	1.58×10^{-4}	1.81×10^{-3}	2936

[a] System displayed non-first order autocatalytic behaviour. [b] Measured by ^{19}F NMR spectroscopy in MeCN-d_3 or MeCN-d_3/D_2O. [c] Second order rate constant for autocatalytic process in units of M^{-1} s^{-1}. [d] Value based on average of measured values or interpolation of measured values. [e] A ^{19}F NMR spectroscopy measurement in 20% H_2O/MeCN-d_3 gave K_e(F) = 0.042. [f] Defluorination was observed. [g] Measured in the presence of 300 mM $^n Bu_4N^+$ BF_4^-. [h] Extremely slow process, where rate constant was determined by initial rates method. [i] K_e(F) for 50% H_2O was assumed to be the same as K_e(F) in MeCN-d_3.

The effects of the *para*-substituents within **108a** and **108c-e** on k_{for}(F) in MeCN were studied by Hammett correlation analysis. The use of σ_p^+ values in the construction of the Hammett plot (**Figure 66a**) gave better correlations than with σ_p values (**Figure 66b**). A ρ^+ value of +1.43 was obtained, with an excellent R^2 value of 0.99, where this positive value indicates small increases in electron density on the aryl rings of the substrates during the limiting C–H removal step of enolization. Compared with the ρ^+ value for relaxation of non-fluorinated compounds **107a** and **107c-e**, which was +1.06, the slightly greater magnitude of ρ^+ for fluorine-containing compounds **108a** and **108c-e** indicates a small increase in sensitivity to the nature of the *para*-substituents. The π-donor ability of the fluorine atom coupled with the repulsions between the fluorine lone pairs and the non-bonding electrons on the carbon atom destabilise the sp^2-hybridised enol tautomer. This is likely to be the reason for the significantly longer rates of relaxation in the fluorinated compounds relative to the non-fluorinated systems.

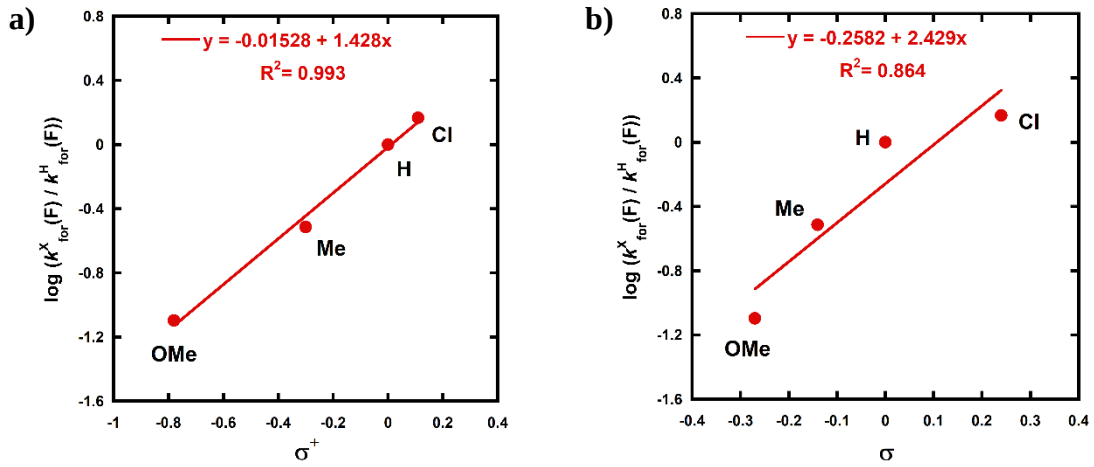

Figure 66: (a) Hammett correlation using σ_p^+ values for conversion of keto forms of **108a** and **108c-e** to the equilibrium keto-enol ratios. (b) Hammett correlation using σ_p values for conversion of keto forms of **108a** and **108c-e** to the equilibrium keto-enol ratios. Rate constants were obtained at 20 °C.

3.3.2 Relaxation of 108a in the presence of additives

The effects of additives on the rates of relaxation of diketone tautomers of **108a** and **108c-e** were then explored, and all data were fitted to first-order exponentials. The corresponding k_{for}(F) and k_{rev}(F) values were obtained via K_e values (**Table 20**). In general, the effects of additives upon k_{for}(F) were significantly greater than for the non-fluorinated series **107a** and **107c-e**. With 20% water in MeCN (**Figure 67**), **108a-keto** k_{for}(F) was 160-fold larger than in the absence of water, whereas for **107a-keto**, only a 2.4-fold enhancement in k_{for}(H) was observed. When the quantity of water in MeCN

was increased to 50%, k_{for}(F) was increased to 930-fold greater than in the absence of water. For compounds **108d** and **108e**, k_{for}(F) increased 3000-fold in 50% water, while **108c** showed a 10000-fold increase.

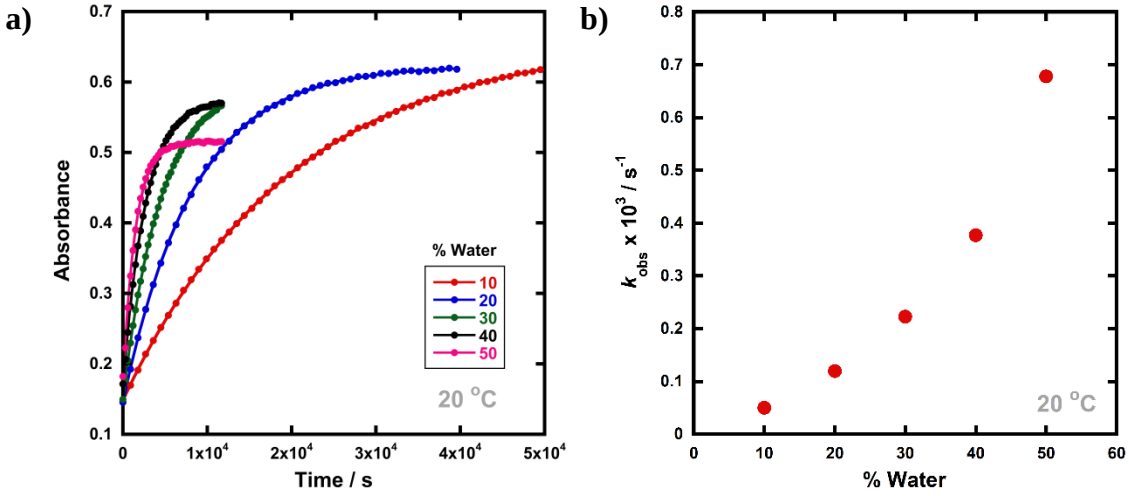

Figure 67: (a) The relaxation of **108a-keto** ([**108a$_{tot}$**] = 0.50 mM) in the presence of different amounts of deionised water in MeCN, monitored at λ_{max} = 350 nm at 20 °C. The k_{obs} values obtained are reported in **Table 20**. (b) The trend observed in the rates of relaxation (k_{obs}) of **108a-keto**.

Addition of formic acid (3% in MeCN) led to an increase in k_{for}(F) of 224-fold (**Figure 68a**), compared with an increase in k_{for}(H) for **107a** with 3% formic acid of 86-fold. 'Spent' Selectfluor™ ($ClCH_2$–DABCO$^+$ BF_4^-, 25 μM) offered a 4-fold increase in k_{for}(F) (**Figure 68b**), whereas the increase in k_{for}(H) for **107a** with this additive was ~2-fold, and only marginally discernible above salt-related medium effects.

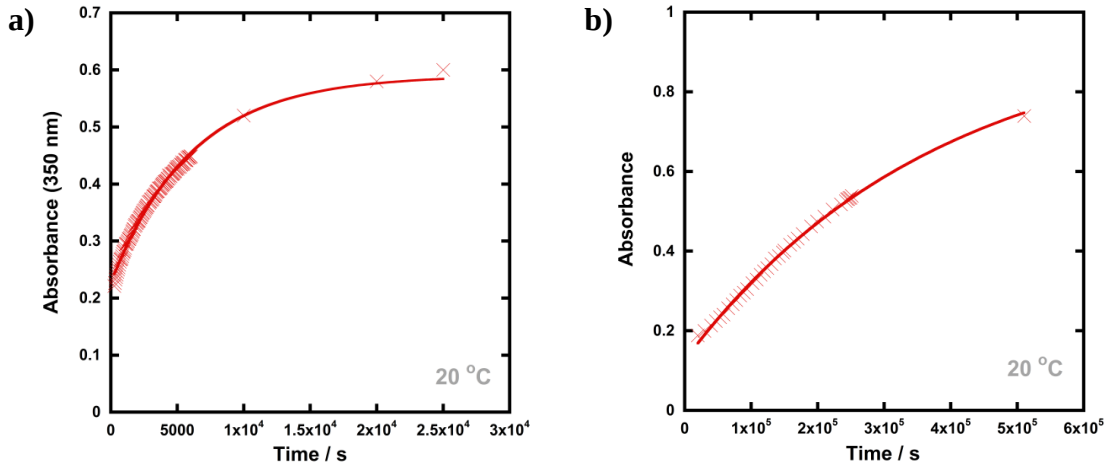

Figure 68: The relaxation of **108a-keto** ([**108a$_{tot}$**] = 0.50 mM) monitored at λ_{max} = 350 nm at 20 °C in the presence of (a) formic acid (3% in MeCN); (b) $ClCH_2$-DABCO$^+$ BF_4^- (25 μM). The k_{obs} values obtained are reported in **Table 20**.

DABCO proved to be an effective agent for de-fluorination of the substrate **108a**. The NMR spectra below (**Figure 69**) correspond to the mixture of **108a** (25 mM) and DABCO (25 mM) after an incubation time of 30 min. In the ^{1}H NMR spectrum, the peak at δ = 6.93 ppm which corresponds to the fluoroketo tautomer had almost disappeared. In the ^{19}F NMR spectrum, peaks at δ = −189.8 ppm (fluoroketo) and δ = −169.5 ppm (fluoroenol) also disappeared and a new peak at δ = +16.5 ppm was present, which may indicate the formation of an N−F species, since N−F signals generally occur in the positive chemical shift region (e.g. Selectfluor™ (N−F) = +47.5 ppm). Additional smaller peaks appeared between −90 ppm and −150 ppm.

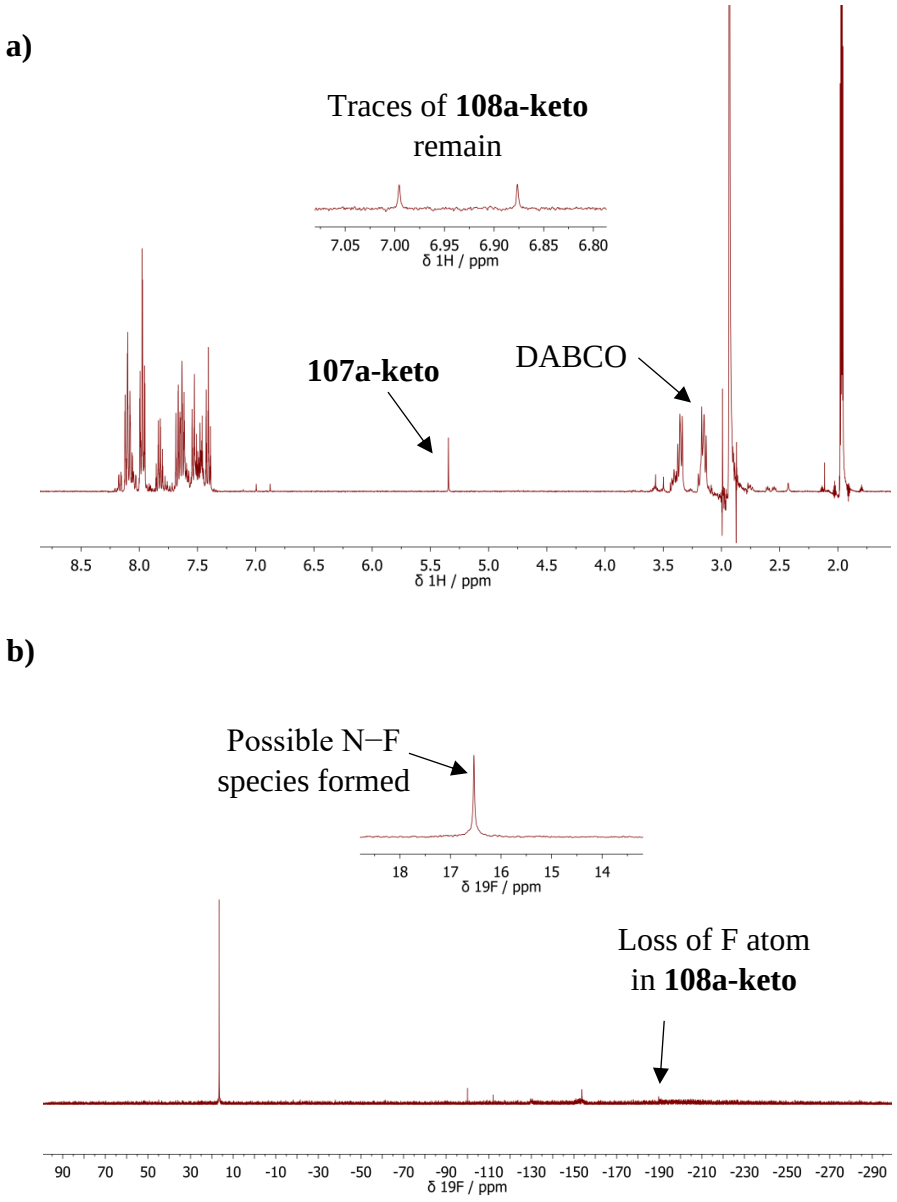

Figure 69: (a) ^{1}H NMR spectrum of the mixture of **108a** and DABCO. (b) ^{19}F NMR spectrum of the same sample.

Previous reports have shown that bromomalonitriles can act as brominating agents,[169,170] which supports the hypothesis that fluorine transfer could have occurred from **108a** to DABCO. The reaction between **108a** and DABCO was monitored by UV-vis spectrophotometry and slightly non-first order behaviour was observed (**Figure 70**). This behaviour is consistent with the NMR studies which showed that more complex reactions than relaxation had occurred.

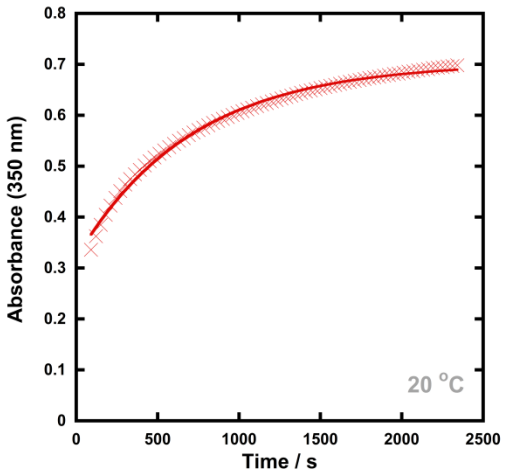

Figure 70: The de-fluorination of **108a-keto** ([**108a**$_{tot}$] = 0.50 mM) in the presence of DABCO (2.50 μM), monitored at λ_{max} = 350 nm in MeCN at 20 °C.

For a mixture of **108d** (R_1 = R_2 = OMe) and DABCO, loss of the 2-fluorine was not observed, which indicates that the propensity for defluorination depends on the *para*-substituent. Further investigation would be required with a larger range of 1,3-dicarbonyl derivatives to greater understand the factors that affect de-fluorination.

3.4 Conclusions

This chapter has discussed the use of a photo-switching method for the determination of the effects of additives on keto-enol tautomerism in the 1,3-diaryl-1,3-dicarbonyls **107a** and **107c-e** and the corresponding fluorinated derivatives **108a** and **108c-e**. Kinetics studies have shown that the addition of water is a simple method for increasing the rate of enolization. Small quantities of formic acid and DABCO were found to greatly increase the enolization rates of **107a** and **107c-e** and formic acid also increased the enolization rate of **108a** and **108c-e**. The presence of DABCO resulted in the de-fluorination of **108a** (R_1 = R_2 = H), as evidenced by NMR studies, whereas **108d** (R_1 = R_2 = OMe) was not de-fluorinated by DABCO.

The non-fluorinated product of Selectfluor™, $ClCH_2{-}DABCO^+\ BF_4^-$, which is rarely considered in synthetic application, had small but detectable effects on keto-enol equilibration kinetics, however, the nature of the effects is not clear. Overall, these data suggest that the tautomerization reactions of the fluoro-systems **108** are accelerated more significantly in the presence of polar additives than those of the non-fluorinated systems **107**. The origin of these rate enhancements could lie in the polarity of the C−F bond, which can interact with the additive via dipole-dipole interactions.

The use of additives in fluorination reactions was anticipated to play a significant role in their reaction kinetics. Thus, the following chapter will concern the application of the data obtained in the present chapter towards fluorination and difluorination reactions.

Chapter 4: Kinetics of Fluorination of 2-Fluoro-1,3-Dicarbonyl Derivatives

In Chapters 2, kinetics studies on fluorination of 1,3-dicarbonyl derivatives **107a-m** were discussed, while Chapter 3 detailed photoketonization and relaxation experiments for the determination of enolization rates. One of the key challenges in the fluorination of 1,3-dicarbonyl derivatives using N−F reagents is the difficulty in controlling mono- versus di-fluorination. This has been widely reported, and often leads to challenging separations of the product mixtures. Therefore, finding synthetic routes that allow selective fluorination by commonly-used N−F reagents would be of great use. In this chapter, kinetics studies on fluorination of 2-fluoro-1,3-dicarbonyl derivatives **108a** and **108c-e** will be discussed in detail. The effects of mixed solvent systems on rates of fluorination will be explored and compared with the non-fluorinated systems.

4.1 Introduction

Bioactive compounds bearing CF_2 groups are found in both the pharmaceutical and agrochemical industries. They are often present as difluoromethyl (CF_2H) and difluoroalkyl (CF_2R) moieties,[171] for example, within the structures of pantoprazole **119**, gemcitabine **120** and sedaxane **126** (**Figure 71**). The chemical properties of these moieties can contribute to altering the biological activities of their compounds. For example, the CF_2H group can often act as a more lipophilic isostere of alcohol, carbinol, thiol, hydroxamic acid and amide groups.[13,172] Additionally, the weakly acidic nature of the CF_2H group can establish hydrogen-bonding interactions to improve binding selectivities.[171–173]

Carbonyl and dicarbonyl species containing α,α-difluoromethylene moieties are highly desirable bioactive compounds. When adjacent to a carbonyl group, the difluoromethylene moiety greatly increases the electrophilicity of the carbonyl group, leading to facile nucleophilic additions. These include the additions of nucleophilic residues of enzyme active sites to α,α-difluoroketonic compounds,[168,174] which have led to the application of α,α-difluoroketones as enzyme inhibitors.[175–177] For example, difluorostatone compounds have been identified as potent inhibitors of HIV-1 protease[178] and of a serine protease in the malaria parasite (**Figure 72**).[179] Difluorostatone **129** inhibits serine proteases through nucleophilic attack by the active site serine at the electrophilic carbonyl group of the difluorostatone moiety, which is

activated by the electron-withdrawing fluorine atoms, to form a hemiketal tetrahedral intermediate.[179]

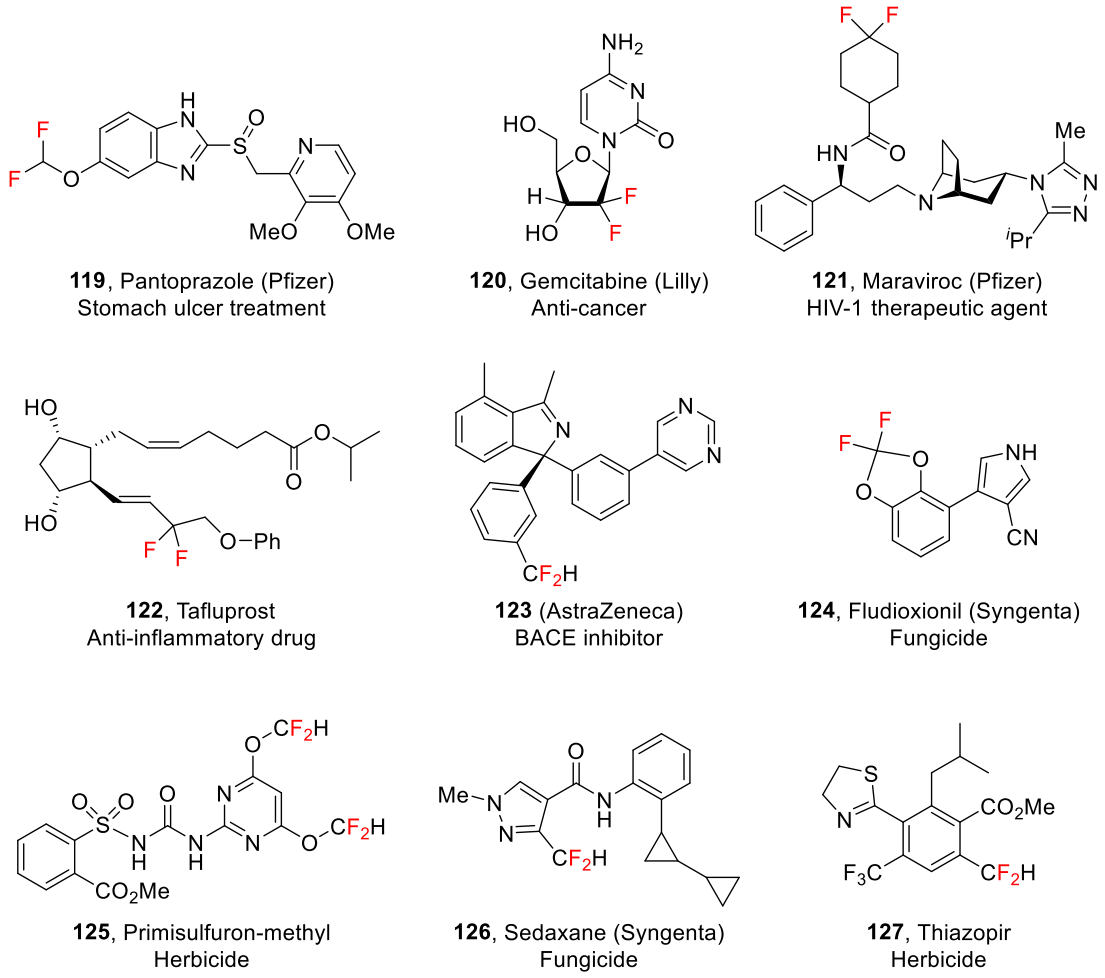

Figure 71: Pharmaceutical and agrochemical compounds bearing the CF_2 moiety.

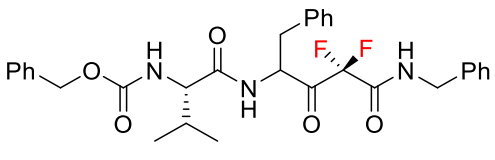

128

Inhibitor of HIV-1 protease

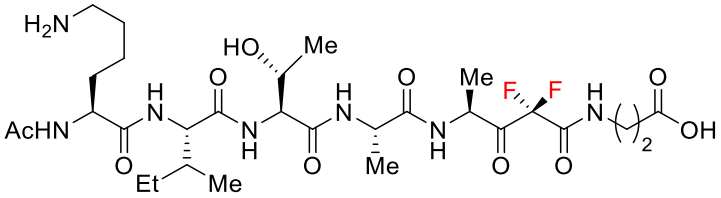

129

Inhibitor of serine protease in malaria parasite

Figure 72: Examples of difluorostatone inhibitors (from refs [178,179]).

Despite the importance of the CF_2 moiety within discovery and manufacture, there have been no quantitative studies on the introduction of two fluorine atoms to form a difluoromethylene unit. Furthermore, although water and formic acid have been used as solvents or co-solvents in electrophilic fluorination reactions,[107,120] their effects upon fluorination reactions are not fully understood. The results discussed in Chapter 3 explored in detail the effects of such additives on keto-enol tautomerism of 1,3-dicarbonyl derivatives, and these findings were of significant relevance towards the work described in the present chapter. In this context, this chapter will firstly discuss preliminary NMR spectroscopy studies employed to gain an initial understanding of the timescale and mechanism of difluorination. Detailed kinetics experiments carried out using UV-vis spectrophotometry will then be discussed under a range of conditions, followed by the application of the kinetic data towards preparation of an authentic sample of 2,2-difluoro-1,3-propanedione **109a** and modelling a synthetic reaction.

4.2 Initial studies conducted using NMR spectroscopy

In preliminary studies, the fluorination of 2-fluoro-1,3-dicarbonyl **108a** by Selectfluor™ was monitored using ^{19}F NMR spectroscopy (**Scheme 28**). The ^{19}F NMR spectrum of **108a** in MeCN-d_3 contained peaks associated with both keto and enol tautomers present in a 95:5 ratio, at $\delta = -190$ ppm and $\delta = -170$ ppm, respectively. Selectfluor™ was added to a solution of **108a** in MeCN-d_3, where [**108a**] = [Selectfluor™] = 29.5 mM. The ^{19}F NMR spectrum acquired after 20 min showed that the peak at $\delta = -170$ ppm corresponding to **108a-enol** had disappeared (**Figure 73**, Spectrum 1). A small singlet at −103 ppm appeared, due to the 2,2-difluoro-1,3-dicarbonyl product **109**.

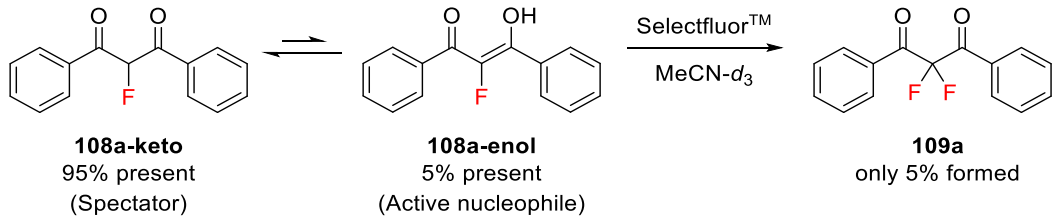

Scheme 28: Preliminary studies on the fluorination of **108a** using Selectfluor™ in MeCN-d_3, monitored by ^{19}F NMR spectroscopy.

The reaction mixture was monitored by ^{19}F NMR spectroscopy for a further 4 days at 20 °C and showed no change in peak intensity of **108a-keto** (**Figure 73**, Spectra 2-5) Thus, this preliminary NMR study confirmed that the tautomerism of **108a-keto** to **108a-enol** did not occur over this timescale. Additionally, **108a-keto** did not react to form the

difluoro-product **109a** over the course of 5 days, hence, fluorination of **108a** occurs only via the enol form. The fluoroketo tautomer acts as a spectator during the addition of the second fluorine atom to **108a-enol**, owing to its slow enolization in MeCN.

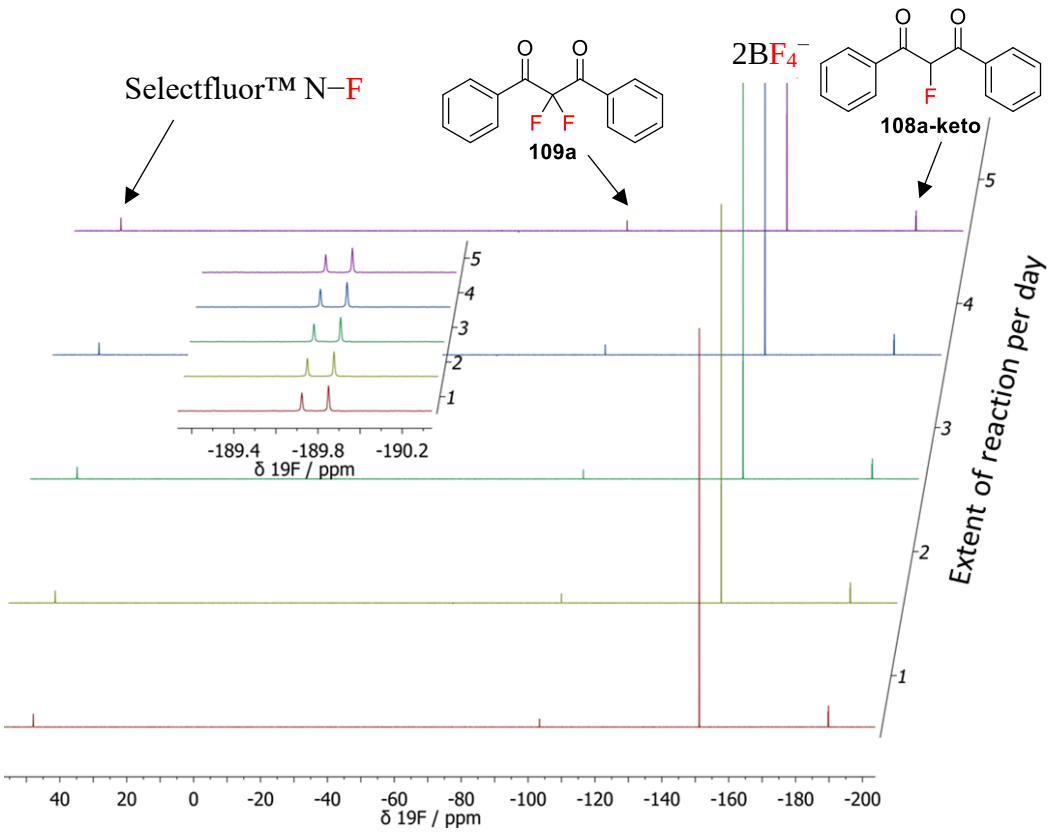

Figure 73: Reaction mixture monitored over 5 days, showing no change in the concentration of **108a-keto**. The doublet at −189.8 ppm corresponding to **108a-keto** is highlighted.

4.3 Kinetics of fluorination of 108a and 108c-e in MeCN

The preliminary studies described in the previous section showed that the fluorination of the fluorine-containing enol **108a** occurred on a timescale that was too rapid to be conveniently monitored by NMR spectroscopy. As discussed in Chapters 2 and 3, compounds **108** exist as mixtures of both keto and enol tautomers, which each have distinct absorbance bands in their UV-vis spectra. Therefore, by capitalising upon this feature, the fluorinations of **108a** and **108c-e** were monitored by UV-vis spectrophotometry. It was necessary to first consider certain practical aspects before conducting kinetic studies.

Firstly, given that compounds **108a** and **108c-e** were prepared from the corresponding non-fluorinated derivatives **107,** it was essential to ensure that even small amounts of residual **107** were not present in the preparations of **108**, as they could interfere with

kinetics studies. In order to confirm the spectrophotometric purities of **108a** and **108c-e**, NMR analyses were supplemented by LC-MS with diode array detection (see Appendices for all spectra). The chromatograms were viewed at or near the λ_{max} values of the enol forms of **107** and **108**. All chromatograms showed only the keto and enol forms of the mono-fluorinated systems **108** and no evidence of un-fluorinated systems **107**. Secondly, since the enol contents of **108a** and **108c-e** are low (~5%), it was necessary to use higher concentrations of these substrates (0.50 mM) for UV-vis kinetic studies, compared with **107a-m** which have high enol contents and were typically employed at concentrations of 50 μM in Chapter 2. The UV-vis spectra of authentic samples of compounds **108a** and **108c-e** are shown in **Figure 74**.

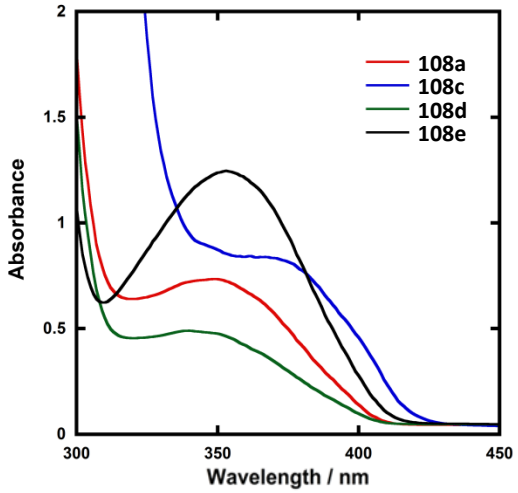

Figure 74: UV-vis spectra of authentic samples of compounds **108a** and **108c-e**. Concentrations of solutions: **108a**, **108d** and **108e** are 0.50 mM; **108c** is 0.40 mM.

By monitoring the decays in absorbance of the fluoroenol tautomers of **108a** and **108c-e** at λ ~ 350 nm, the kinetics of fluorination reactions using Selectfluor™ and NFSI were monitored by UV-vis spectrophotometry (**Scheme 29**). To achieve pseudo-first order conditions, all kinetics experiments were carried out using excess electrophile. Clean exponential decays of absorbance of the nucleophiles (**108a**, **108c-e**) were observed in all runs in MeCN. Representative examples are shown in **Figure 75** for the fluorination of **108a-enol** ($R_1 = R_2 = H$) using Selectfluor™ and in **Figure 76** for the fluorination of **108d-enol** ($R_1 = R_2 = OMe$) using NFSI. The products of the reactions, **109a** and **109c-e**, have been previously characterised in the literature.[116,180]

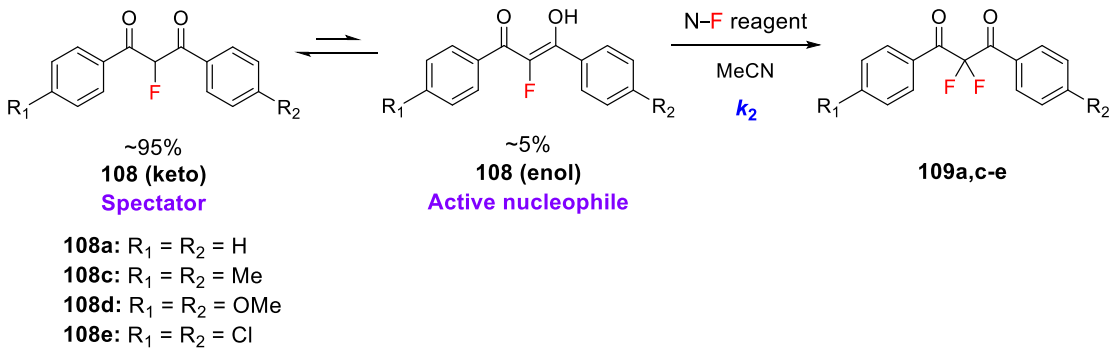

Scheme 29: Reaction scheme for kinetics studies on fluorination reactions of 1,3-dicarbonyls **108a** and **108c-e** with Selectfluor™ and NFSI in MeCN at controlled temperatures.

The first-order rate constants k_{obs} were obtained from the fitting of plots of absorbance versus time (**Figure 75a**, **Figure 76a**). When k_{obs} values were plotted against electrophilic fluorine concentration, linear (i.e. first order) correlations were observed (**Figure 75b**, **Figure 76b**), which projected cleanly through the origin in each case. The direct dependence upon electrophilic fluorine concentration demonstrated rate-limiting fluorination of the fluoroenol that is present in the mixture, and thus the slopes of these graphs gave the second-order rate constant k_2 [M^{-1} s^{-1}] according to **Equation 19**. The rate constants for the reactions of **108a** and **108c-e** with each fluorinating reagent are summarised in **Table 21**. All spectra and kinetic data corresponding to fluorination of **108a** and **108c-e** are included in Chapter 8 Section 8.5.

$$\text{Rate} = \frac{\text{d[Fluoroenol]}}{\text{dt}} = -k_2[\text{Fluoroenol}][\text{NF reagent}] \qquad (\mathbf{19})$$

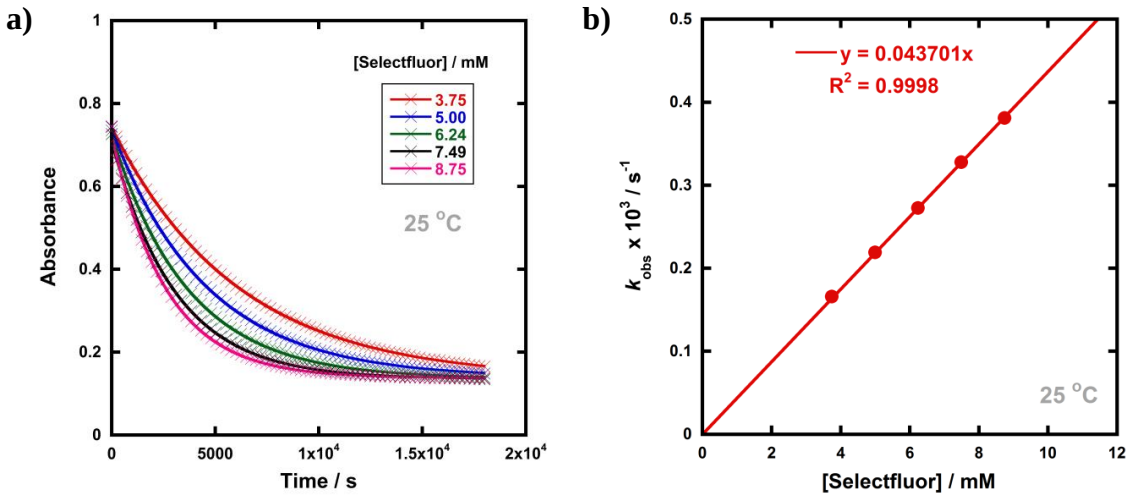

Figure 75: (a) Exponential decays of absorbance of **108a-enol** ([**108a**$_{tot}$] = 0.5 mM, [**108a-enol**] = 25 μM) with different concentrations of Selectfluor™ in MeCN at 25 °C, monitored at λ_{max} = 350 nm. (b) Correlation of k_{obs} values for fluorination of **108a-enol** with [Selectfluor™] in MeCN at 25 °C.

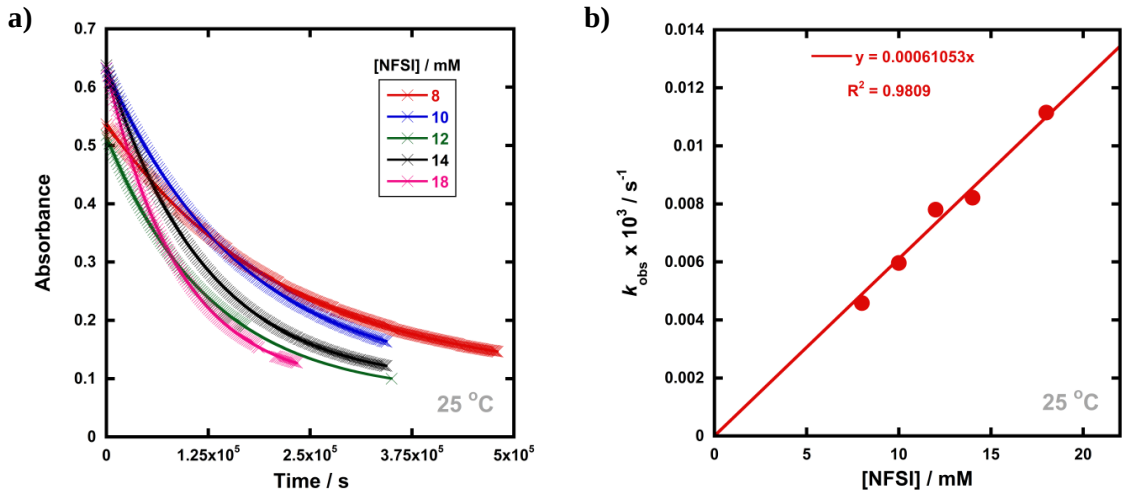

Figure 76: (a) Exponential decays of absorbance of **108d-enol** ([**108d**$_{tot}$] = 0.5 mM, [**108d-enol**] = 10 μM) with different concentrations of NFSI in MeCN at 25 °C, monitored at 380 nm. (b) Correlation of k_{obs} values for fluorination of **108d-enol** with [NFSI] in MeCN at 25 °C.

Table 21: Second-order rate constants (k_2) for the reactions of Selectfluor™ and NFSI with nucleophiles **108a** and **108c-e**, in MeCN at 25 °C, and relative rates, k_{rel}', compared to the reactions of Selectfluor™ and NFSI with nucleophiles **107** and **107c-e.**

Nucleophile	Electrophile	k_2 (25 °C) / M^{-1} s^{-1}	k_{rel}'
108a-enol (R_1 = R_2 = H)	Selectfluor™	4.37×10^{-2}	1.0 (1.1)[a]
	NFSI	4.59×10^{-4}	46
108c-enol (R_1 = R_2 = Me)	Selectfluor™	1.32×10^{-1}	1.1
108d-enol (R_1 = R_2 = OMe)	Selectfluor™	6.77×10^{-1}	1.1 (1.1)[a]
	NFSI	6.11×10^{-4}	4.4
1080e-enol (R_1 = R_2 = Cl)	Selectfluor™	3.07×10^{-2}	1.7
	NFSI	2.47×10^{-4}	43

[a] Using k_2 values for reactions measured at 20 °C

The rates of fluorination of **108a** and **108c-e** by Selectfluor™ and NFSI were compared with the rate constants that were obtained for the fluorinations of **107a** and **107c-e**, using k_{rel}' values, defined in **Equation 20**. The k_{rel}' values are summarised in **Table 21**.

$$k_{rel}' = \frac{k_2 \text{ (addition of second fluorine atom)}}{k_2 \text{ (addition of first fluorine atom)}} \qquad (\mathbf{20})$$

The k_2 values obtained for fluorination of fluoroenols **108** by Selectfluor™ are slightly higher than those for fluorination of enols **107**, with k_{rel}' values of 1.0-1.7 being

observed. With NFSI, the rate enhancement is more pronounced, and the addition of the second fluorine atom to form the CF_2 group is 46-fold faster for **108a-enol**, 4-fold greater for **108d-enol** and 43-fold faster for **108e-enol**.

One might expect that the presence of a highly electronegative fluorine atom would lead to a lowering of the nucleophilicity of the fluoroenol and much lower rates of fluorination. On the other hand, the strong π-donor ability of the fluorine atom could lead to ground-state destabilisation of fluorine atoms at sp^2 centres and thus enhanced nucleophilicity of the fluoroenol. These results suggest that a balance between these opposing effects is observed for fluorinations in MeCN with the more reactive Selectfluor™ system. However, with the less reactive NFSI reagent the fluoroenols **108** are more reactive. The origins of this disparity could lie in the less early transition state structure that is to be expected from the less reactive NFSI system, coupled with the different charge state of the electrophile-nucleophile pair, and thus differing requirements for solvation. Further discussion and comparison with previous reports will be made in Section 4.10.

4.4 Structure-activity correlations and determination of activation parameters

A Hammett plot was constructed for the reactions of fluoroenols **108** with Selectfluor™ using the second-order rate constants reported in **Table 21**. The use of σ_p^+ values (**Figure 77a**) led to a better correlation than with σ_p constants (**Figure 77b**), and $\rho^+ = -1.5$ was obtained, with an excellent R^2 of >0.99. The σ_p^+ scale takes into account the ability of electron donating *para*-substituents to disperse the increase in positive charge, hence, strong resonance interaction occurs between the *para*-methoxy groups and the reaction centre. The value of $\rho^+ = -1.5$ is similar to the ρ^+ values obtained for fluorination of enols **107a-h** by the N−F reagents discussed in Chapter 2, which were between −1.4 to −2.0. Thus, the similarity in ρ^+ values indicates that the mechanisms of addition of a fluorine atom to enols **107** and fluoroenols **108** are closely related. These negative values indicate moderate reductions in electron density on the substrates during the rate determining fluorination steps.

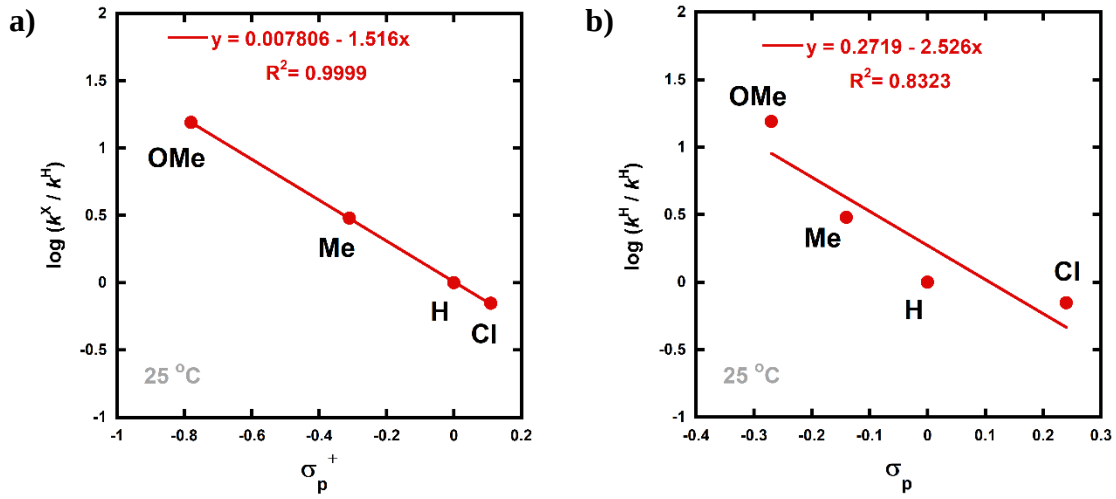

Figure 77: Hammett correlations corresponding to fluorination of **108a**, **108c-e** by Selectfluor™. All rate constants were obtained in MeCN at 25 °C, and are plotted against a) σ_p^+ values, and b) σ_p values.

Activation parameters ($\Delta G^{\ddagger}$, $\Delta H^{\ddagger}$ and $\Delta S^{\ddagger}$) were calculated from kinetic data obtained at four different temperatures (**Table 22**) for the reactions of Selectfluor™ with **108a-enol** and **108d-enol** (**Figure 78**, **Table 23**). As with the results for compounds **107a-e**, the moderately negative values of $\Delta S^{\ddagger}$, alongside the values for ρ^+, support an S_N2-type mechanism for the fluorination reactions.

Table 22: Second-order rate constants, k_2, for fluorination of **108a-enol** ($R_1 = R_2 = H$) and **108d-enol** ($R_1 = R_2 = OMe$) using Selectfluor™ in MeCN at 4 different temperatures.

Nucleophile	k_2 / M^{-1} s^{-1}			
	20 °C	25 °C	30 °C	35 °C
108a-enol	2.95×10^{-2}	4.37×10^{-2}	7.05×10^{-2}	1.02×10^{-1}
108d-enol	4.64×10^{-1}	6.77×10^{-1}	1.03	1.39

Table 23: Activation parameters calculated using the Eyring plots in **Figure 78**.

Nucleophile	$\Delta H^{\ddagger}$ / kJ mol^{-1}	$\Delta S^{\ddagger}$ / J K^{-1} mol^{-1}	$\Delta G^{\ddagger}$ / kJ mol^{-1}
108a-enol	60.7	−66.9	80.6
108d-enol	53.2	−69.7	74.0

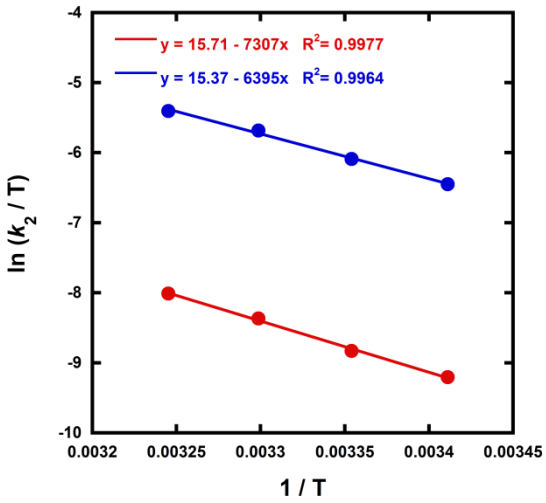

Figure 78: Eyring plots for fluorination of 2-fluoro-1,3-dicarbonyls **108a** (red dataset) and **108d** (blue dataset) by Selectfluor™ in MeCN at 20 °C, 25 °C, 30 °C and 35 °C.

Finally, Hammett plots were constructed for fluorination reactions via NFSI, where the use of σ_p values (**Figure 79a**) gave better correlations than with σ_p^+ values (**Figure 79b**). However, more data points would be required in order to make conclusions from these correlations.

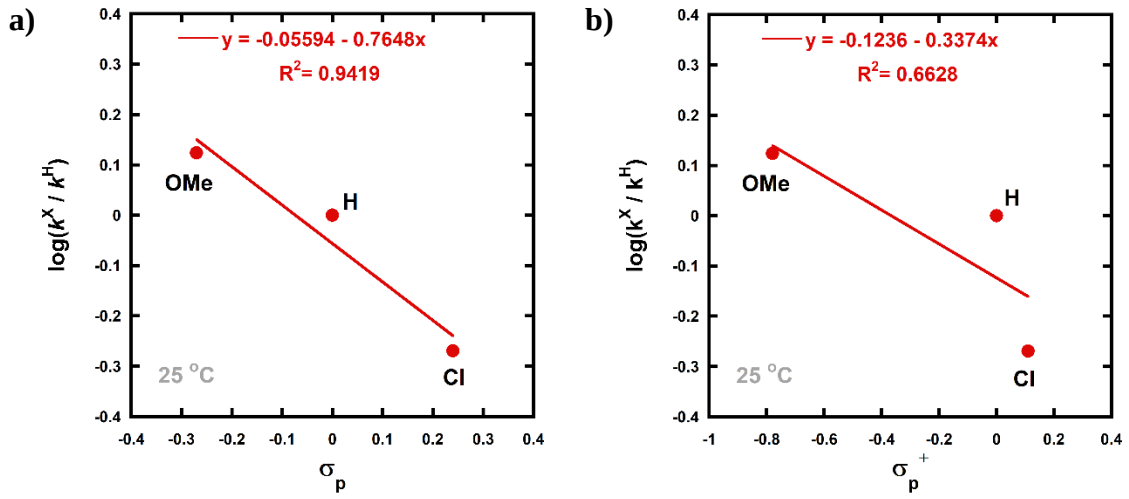

Figure 79: Hammett correlations corresponding to fluorination of **108a**, **108d** and **108e** by NFSI. All rate constants were obtained in MeCN at 25 °C, and are plotted against a) σ_p values, and b) σ_p^+ values.

4.5 Kinetics of fluorination of 108a-enol and 107a-enol in water-MeCN mixtures

The results discussed in Chapter 3 showed that water can significantly enhance the rate of enolization, which suggests that the presence of water during fluorination reactions could enhance the overall rate of fluorination by promoting keto-to-enol tautomerism. To explore this further, the fluorination of **108a-enol** by Selectfluor™ with 20% water in MeCN was studied using UV-vis spectrophotometry (**Scheme 30**).

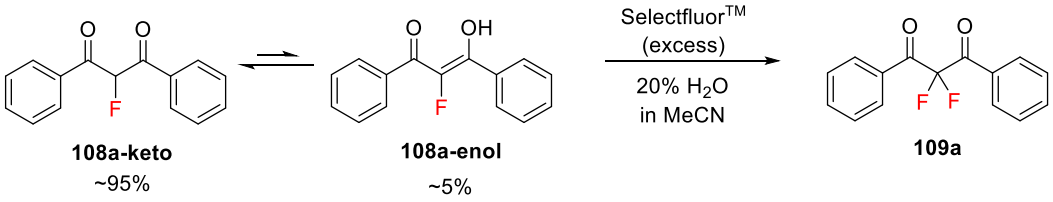

Scheme 30: Fluorination of **108a-enol** using Selectfluor™ with 20% water in MeCN at 20 °C.

To achieve pseudo-first order conditions, all kinetics experiments were carried out using excess Selectfluor™. The decays in absorbance of **108a-enol** at λ_{max} = 350 nm were monitored (**Figure 80a**). However, first-order behaviour was not observed and the plot of the fitted k_{obs} values versus [Selectfluor™] did not intercept the origin (**Figure 80b**). This behaviour is likely due to the complications associated with the presence of substantial keto-enol tautomerism and the formation of the hydrate of **109a** (see Section 4.8) in the presence of water.

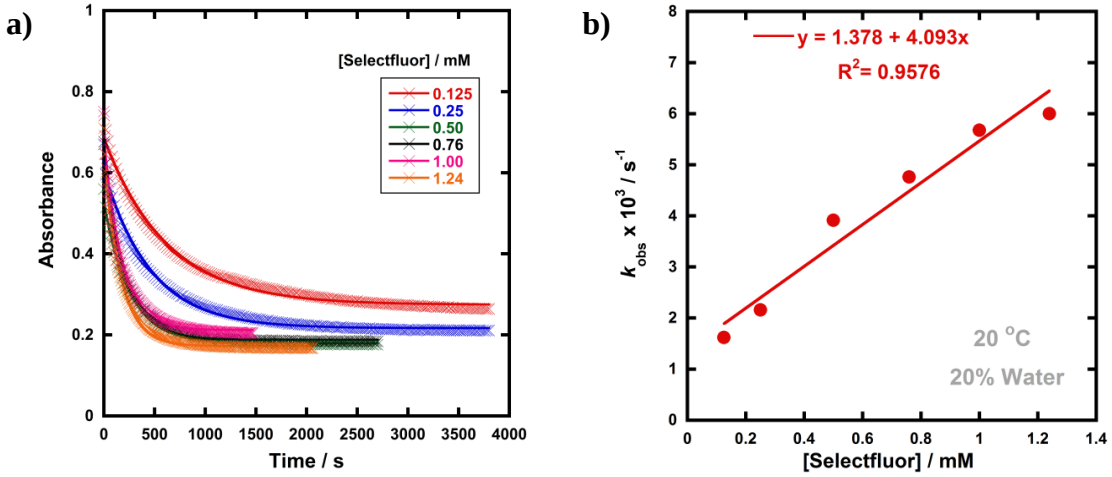

Figure 80: (a) Decays of absorbance of **108a-enol** ([**108a**$_{tot}$] = 0.5 mM, [**108a-enol**] = 25 μM) with different concentrations of Selectfluor™, with 20% water in MeCN at 20 °C. (b) Correlation of k_{obs} with [Selectfluor™].

Hence, the experiments were repeated using an initial rates approach by monitoring only the first 10% of the fluorination reactions. Plots of ln(A-A_{inf}) against time were constructed, where A = absorbance of **108a-enol** and A_{inf} = absorbance of **108a-enol** at the end of the reaction. Gradients of the linear trends at each Selectfluor™ concentration gave the k_{obs} values (**Figure 81a**). The plot of k_{obs} values against [Selectfluor™] gave the second-order rate constant, k_2 = 1.43 M^{-1} s^{-1} (**Figure 81b**).

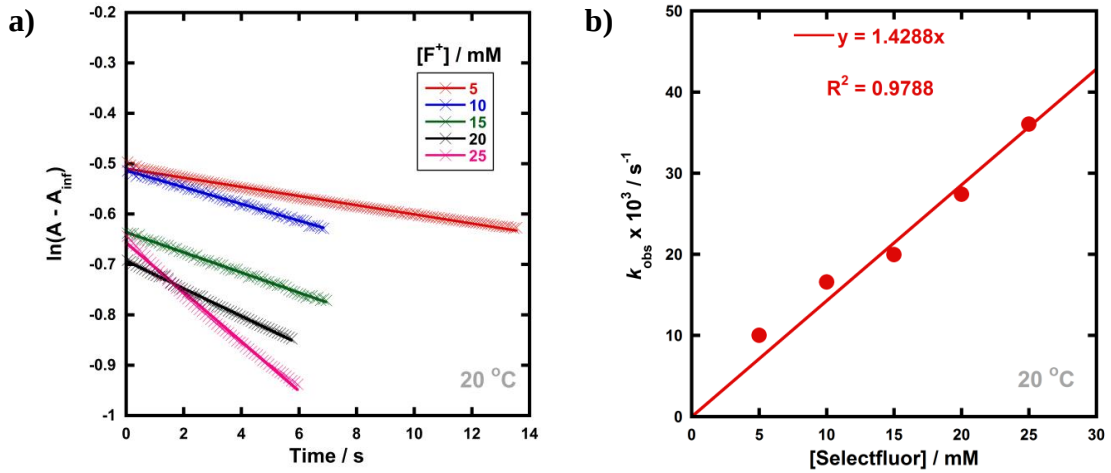

Figure 81: (a) First 10% of fluorination reactions involving **108a-enol** monitored ([**108a**$_{tot}$] = 0.5 mM, [**108a-enol**] = 25 μM). (b) Correlation of k_{obs} from linear fittings with [Selectfluor™].

To enable a comparison of the effects of water upon overall rates of fluorination of fluoroenol versus enol tautomers, studies were conducted on the kinetics of fluorination of **107a-enol** by Selectfluor™ with 20% water in MeCN (**Scheme 31**). The decays in absorbance of **107a-enol** at λ_{max} = 341 nm were monitored, however, non-first order kinetics were observed (**Figure 82a**). Additionally, the plot of k_{obs} values versus [Selectfluor™] did not intercept the origin (**Figure 82b**). LC-MS analysis of the reaction mixtures showed the presence of **109a**, which indicates that the non-first order behaviour is due to multiple enolization and fluorination steps occurring.

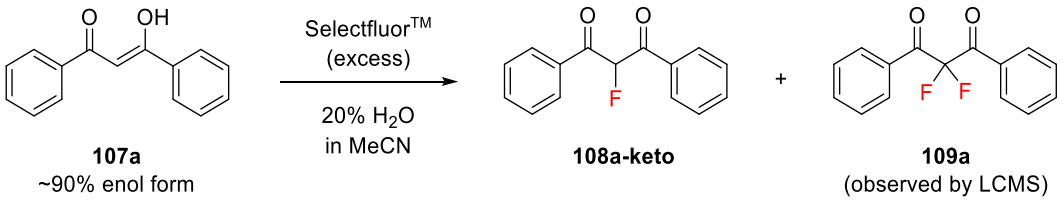

Scheme 31: Fluorination of **107a-enol** using Selectfluor™ with 20% water in MeCN at 20 °C.

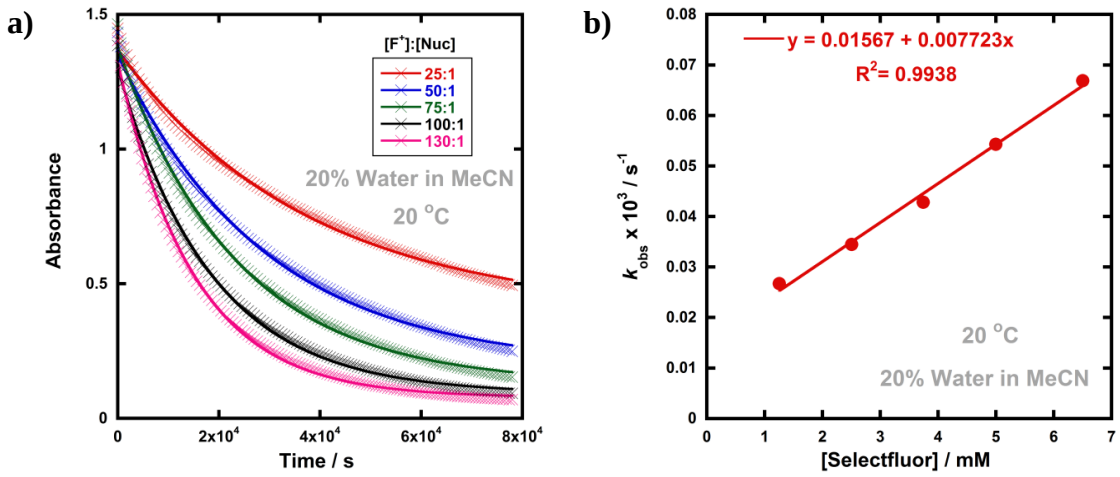

Figure 82: (a) Decays of absorbance of **107a-enol** (50 μM) with different concentrations of Selectfluor™, with 20% water in MeCN at 20 °C. (b) Correlation of k_{obs} with [Selectfluor™].

As with **108a-enol**, the experiments involving **107a-enol** were repeated using an initial rates approach by monitoring only the first 10% of the fluorination reactions by UV-vis spectrophotometry. Plots of $\ln(A-A_{inf})$ versus time were linear and the gradients at each Selectfluor™ concentration gave the k_{obs} values (**Figure 83a**). The plot of k_{obs} values versus [Selectfluor™] gave the second-order rate constant, k_2 = 2.49 × 10^{-2} M^{-1} s^{-1} (**Figure 83b**).

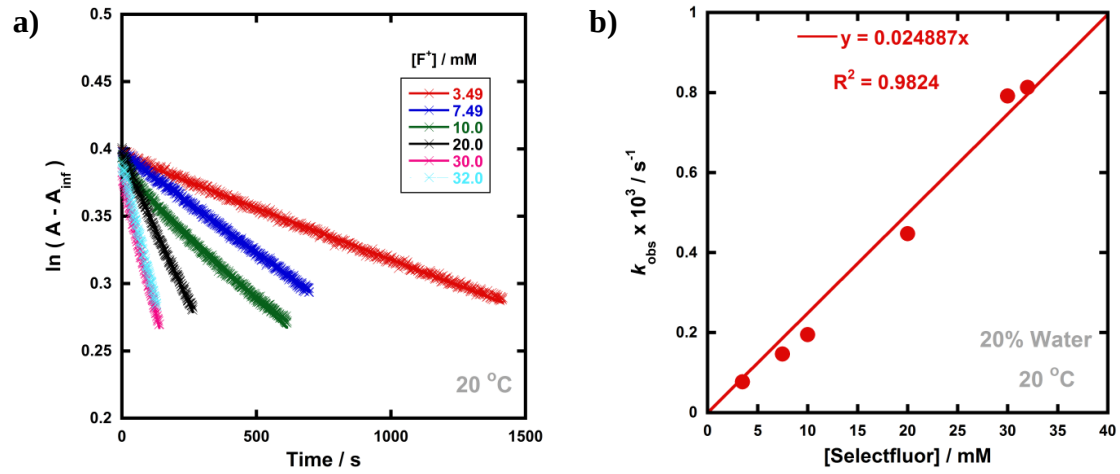

Figure 83: (a) First 10% of fluorination reactions involving **107a-enol** (50 μM) monitored. (b) Correlation of k_{obs} from linear fittings with [Selectfluor™].

The second-order rate constants for fluorination of **107a-enol** and **108a-enol** with 20% water in MeCN, as well as in MeCN only, at 20 °C, are summarised in **Table 24**. The presence of water (20% in MeCN) during the fluorination of **108a-enol** gave a ~50-fold

larger second-order rate constant, k_2, compared to without water, however, the k_2 value for fluorination of **107a-enol** was little changed.

Table 24: Second-order rate constants (k_2) for the reactions of Selectfluor™ with nucleophiles **107a-enol** and **108a-enol** in 20% water in MeCN at 20 °C.

Nucleophile	Solvent system	k_2 (20 °C) / M^{-1} s^{-1}
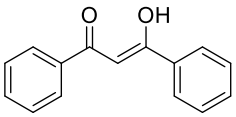 **107a-enol**	MeCN	2.68×10^{-2}
	20% water in MeCN	2.49×10^{-2}
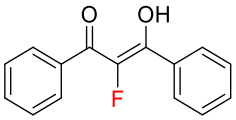 **108a-enol**	MeCN	2.95×10^{-2}
	20% water in MeCN	1.43

4.6 Kinetics of fluorination of 108a-enol by Selectfluor™ and NFSI in formic acid-MeCN mixtures

The effects of formic acid (3-20%) on the rates of fluorination of **108a-enol** by Selectfluor™ and NFSI were explored, and small changes in k_2 values were observed. Rate constants obtained are summarised in **Table 25**. The second-order rate constant for fluorination of **108a-enol** with Selectfluor™ in the presence of 3% formic acid (**Figure 84**) was 1.3-fold higher than in MeCN only. With 5% formic acid, the rate was 1.2-fold higher (for spectra see Chapter 8 Section 8.5). However, the rate was 1.1-fold faster in MeCN than in the presence of 20% formic acid. In all cases, very clean exponential behaviours were observed (**Figure 85**).

Table 25: Second-order rate constants (k_2) for the reactions of Selectfluor™ and NFSI with **108a-enol** in formic acid-MeCN solvent systems. Rate constants obtained in MeCN only are included for comparison.

Electrophile	% Formic acid in MeCN	Temperature / °C	k_2 / M^{-1} s^{-1}
Selectfluor™	0	20	2.95×10^{-2}
	0	25	4.37×10^{-2}
	3	25	5.83×10^{-2}
	5	25	5.35×10^{-2}
	20	20	2.60×10^{-2}
NFSI	0	25	4.59×10^{-4}
	50	25	1.38×10^{-4}

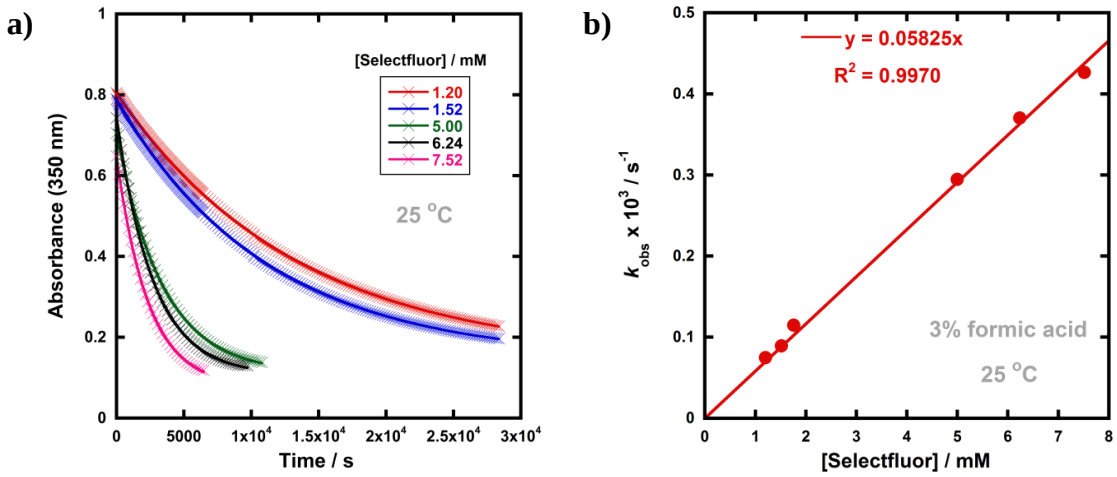

Figure 84: (a) Exponential decays of absorbance of **108a-enol** with different concentrations of Selectfluor™, with 3% formic acid in MeCN at 25 °C. (b) Correlation of k_{obs} with [Selectfluor™].

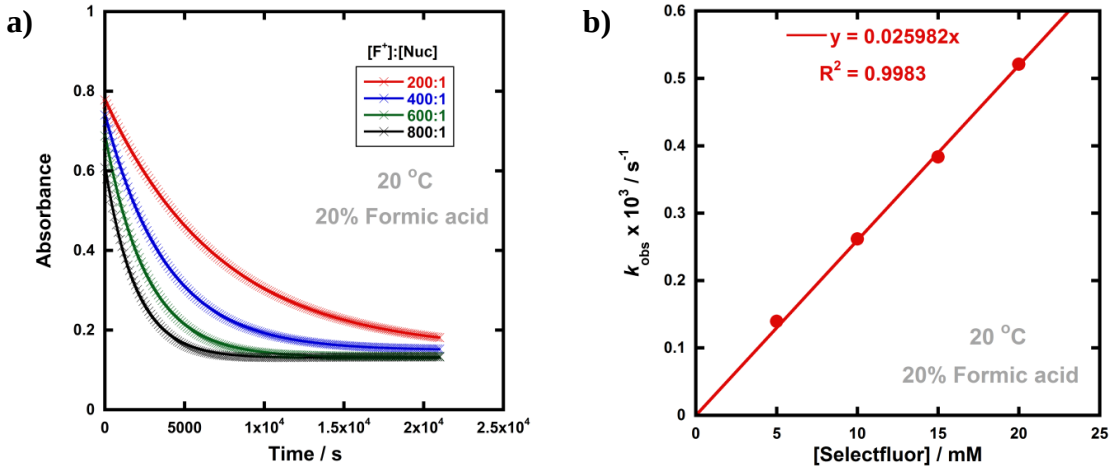

Figure 85: (a) Exponential decays of absorbance of **108a-enol** with different concentrations of Selectfluor™, with 20% formic acid in MeCN at 20 °C. (b) Correlation of k_{obs} with [Selectfluor™].

With NFSI, the rate of fluorination in MeCN only was 3.3-fold faster than in the presence of 50% formic acid. Furthermore, the reaction did not reach completion as indicated from the endpoints in the time-arrayed UV-vis spectra (**Figure 86**). This result may be due to instability of NFSI in formic acid, especially on the long timescales necessary for reactions involving this reagent to reach completion. From these studies, it appears the rate of fluorination is slightly increased by the presence of small quantities of formic acid, although higher concentrations do not have a beneficial effect on the rate.

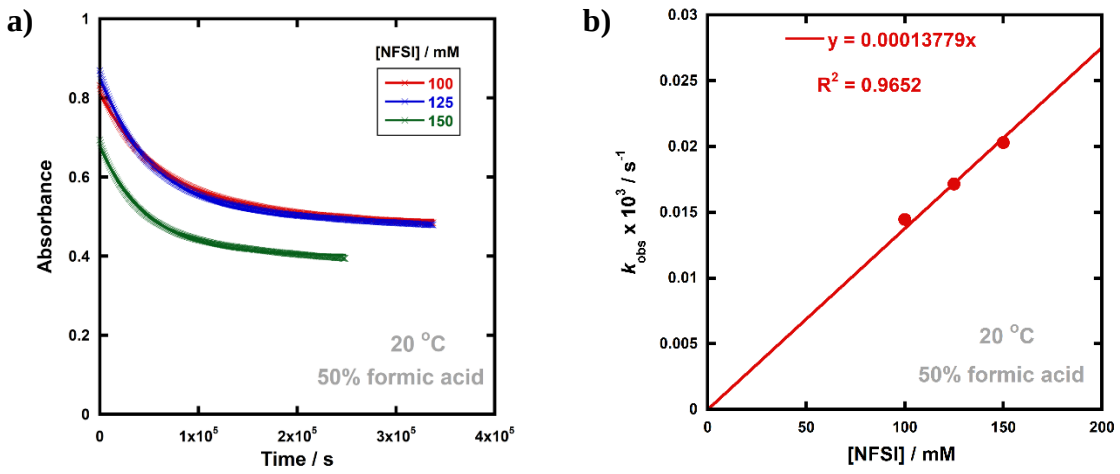

Figure 86: (a) Exponential decays of absorbance of **108a-enol** with different concentrations of NFSI, with 50% formic acid in MeCN at 20 °C. (b) Correlation of k_{obs} with [NFSI].

4.7 Kinetics of fluorination of 108a-enol by Selectfluor™ with $^{n}Bu_4N^+BF_4^-$

Since the presence of certain salts gave enhanced rates of enolization in Chapter 3, the use of $^{n}Bu_4N^+BF_4^-$ as an additive in fluorination reactions was explored. The fluorination of **108a-enol** by Selectfluor™ in the presence of $^{n}Bu_4N^+BF_4^-$ (240 mM) resulted in exponential behaviours (**Figure 87**) and the determined rates of fluorination (k_{obs}) are summarised in **Table 26**. Using an estimated value of $k_{obs} = 7.50 \times 10^{-6}$ s^{-1} for the rate of fluorination with Selectfluor™ (0.25 mM) without additives at 20 °C, the rate in the presence of $^{n}Bu_4N^+BF_4^-$ is 2640-fold higher. This large increase is likely due to the combined effects of the salt itself and inadvertent addition of water owing to the hygroscopic nature of tetraalkylammonium systems.[181]

Table 26: k_{obs} values at different concentrations of Selectfluor™ with $^{n}Bu_4N^+BF_4^-$ (240 mM) in MeCN at 20 °C. Errors are standard error values obtained from data fitting in KaleidaGraph software.

Experiment	Ratio of [F$^+$] : [**108a-enol**]	[F$^+$] / mM	[**108a-enol**] / mM	$k_{obs} \times 10^3$ / s^{-1}
1	5.2:1	0.13	0.025	16.1 ± 0.4
2	10.0:1	0.25	0.025	19.8 ± 0.4

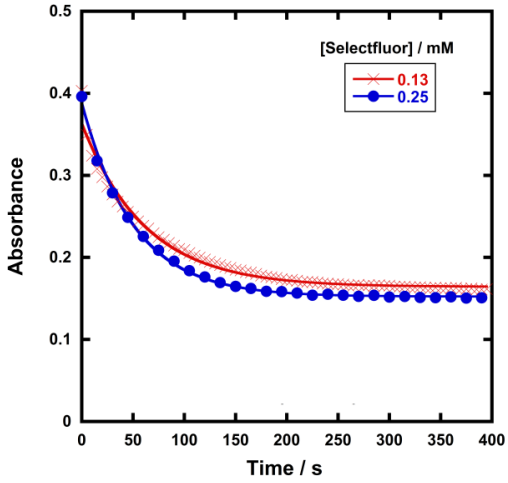

Figure 87: Exponential decays of absorbance of **108a-enol** with different concentrations of Selectfluor™, with $^{n}Bu_4N^{+}BF_4^{-}$ (240 mM) in MeCN at 20 °C.

4.8 Synthesis of 2,2-difluoro-1,3-propanedione 109a in a water-MeCN solvent system

Given the beneficial effect of water as an additive during fluorination reactions, the difluorination of 1,3-diphenyl-1,3-propanedione **107a** was carried out using Selectfluor™ in a 1:5 water:MeCN solvent system to obtain an authentic sample of 2,2-difluoro-1,3-propanedione **109a** in 94% yield after stirring at RT (~ 20 °C) for 3 days (**Scheme 32**). The reaction was monitored by ^{19}F NMR spectroscopy using a non-quantitative wide-sweep method to allow the disappearance of Selectfluor™ to be monitored alongside the evolution of product species (**Figure 88**). An additional peak was present in the ^{19}F NMR spectra at $\delta = -111.9$ ppm which is likely to correspond to a hydrate of **109a**. The formation of a hydrate is expected, as difluoroketones are known to form stable tetrahedral adducts.[175] Upon work-up, the ^{19}F NMR spectrum of the product of this reaction showed the presence of **109a** only (**Figure 89**), and no further purification was necessary.

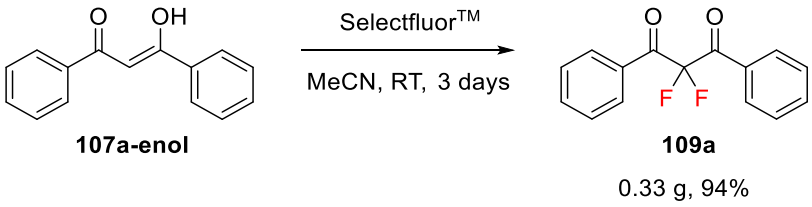

Scheme 32: Synthesis of 2,2-difluoro-1,3-propanedione **109a** using Selectfluor™.

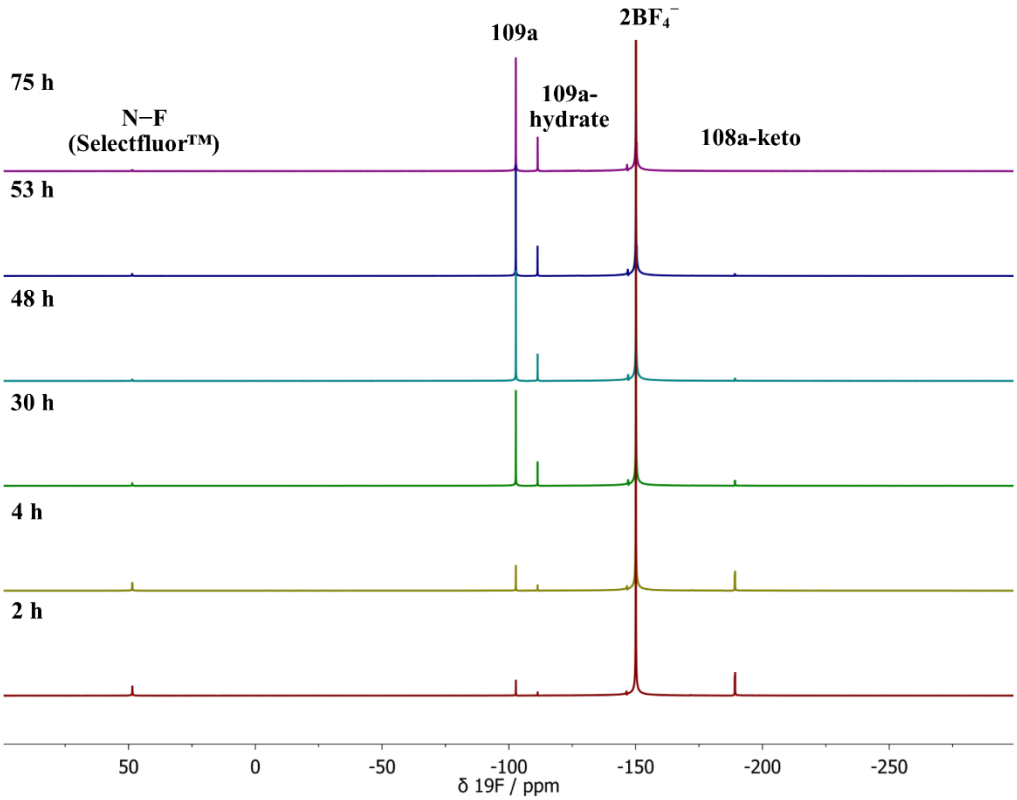

Figure 88: The reaction of **107a** with Selectfluor™ to prepare an authentic sample of **109a** monitored by ^{19}F NMR spectroscopy.

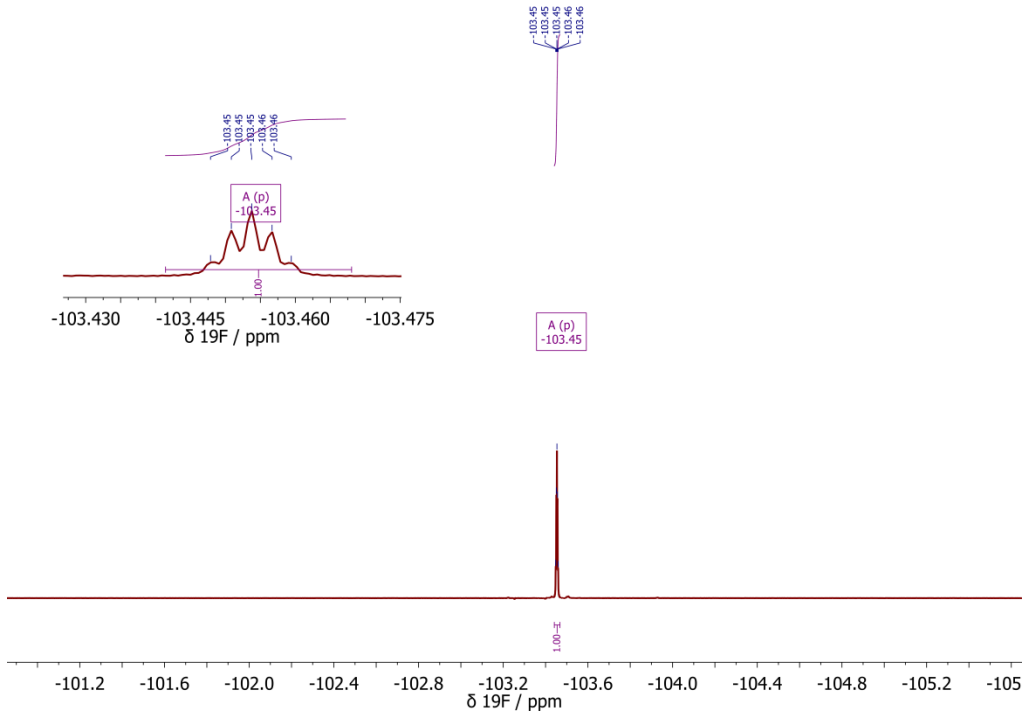

Figure 89: ^{19}F NMR spectrum of 2,2-difluoro-1,3-diphenyl-1,3-propanedione **109a** in MeCN-d_3.

To confirm that the additional peak at δ = −111.9 ppm observed in the ^{19}F NMR spectra for reactions conducted in water/MeCN-d_3 mixtures is a hydrate of **109a**, an NMR spectrum of an authentic sample of **109a** in 20% water in MeCN-d_3 (*v*/*v*) was obtained. The singlet at δ = −111.9 ppm was present (**Figure 90**), hence, this provides supporting evidence for the formation of a hydrate.

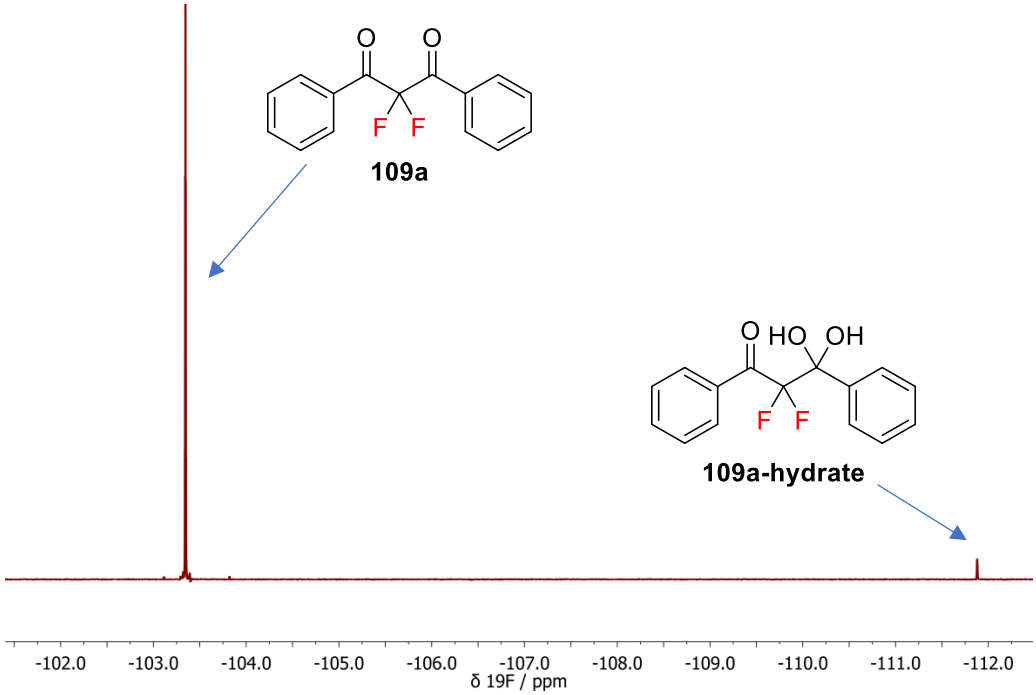

Figure 90: ^{19}F NMR spectrum of 2,2-difluoro-1,3-diphenyl-1,3-propanedione **109a** in 20% H_2O in MeCN-d_3. Signals at δ = −103.4 ppm and δ = −111.9 ppm correspond to **109a** and **109a**-hydrate, respectively.

4.9 Application of kinetic data to synthesis

The kinetic studies discussed in Chapter 3 showed that additives, such as water, facilitate enolization of 1,3-dicarbonyl species **107** and **108**, with especially dramatic effects upon 2-fluoro-1,3-dicarbonyls **108**. As shown in this chapter, the presence of additives has clear effects on the fluorination processes of **107a** and **108a** with Selectfluor™. In order to demonstrate the quantitative applicability of the data to synthetic scenarios, both in the presence and absence of water, NMR experiments were performed to monitor the kinetics of fluorination of **107a** with Selectfluor™ at 20 °C (**Scheme 33**).

In MeCN-d_3 alone, **107a** (30 mM) was reacted with Selectfluor™ **1** (2.1 equivalents) and the evolution of species was monitored by ^{19}F NMR spectroscopy over 6 days

(**Figure 91a**). **108a-Keto** (δ = −190 ppm) was formed rapidly from the large reservoir of **107a-enol** (~90% of total **107a**). Based on the UV-vis kinetic data, the formation of **108a-enol** was expected to be extremely slow, with the formation of **109a** being similarly slow as a result. This was borne out by the very slow appearance of **109a** (δ = −103 ppm), with its formation only being evident at a level of ~4% after 5 days.

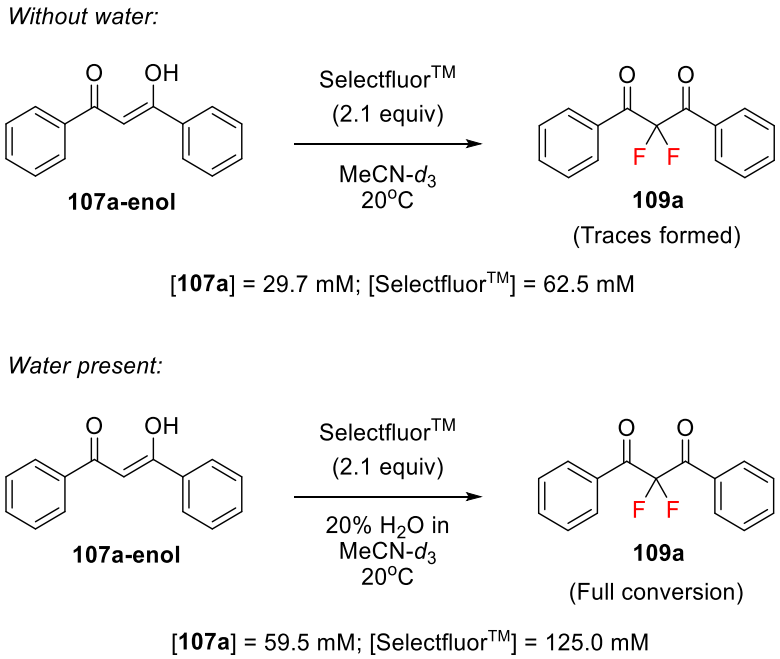

Scheme 33: The conversion of **107a-enol** to **109a** using an excess of Selectfluor™ under two different reaction conditions: 100% MeCN-d_3 and 20% water in MeCN-d_3, monitored by ^{19}F NMR spectroscopy.

The reaction conducted with 20% H_2O in MeCN-d_3 allowed for the use of higher concentrations of Selectfluor™ owing to its enhanced solubility in this medium, thus concentrations of **107a** = 60 mM and Selectfluor™ = 125 mM were used (**Figure 91b**). Plots of peak integral intensities relative to the signal corresponding to the tetrafluoroborate ions were constructed (**Figure 92**). The reaction profile showed rapid build-up of **108a-keto** (δ = −190 ppm) as a result of the large starting concentration of **107a-enol**. Owing to the presence of water, enolization of **108a-keto** was expected to occur more readily, and this was evidenced by the more rapid reduction in the signal for **108a-keto** and the formation of 7.5% **109a** (δ = −103 ppm) after ~3.5 h, with complete conversion to **109a** being achieved over 6 days. Fluorination was expected to be rapid, and this was supported by very low levels of **108a-enol** being detected in the steady state. An additional peak was present at δ = −111.9 ppm which corresponds to a hydrate of **109a**, as confirmed in Section 4.8.

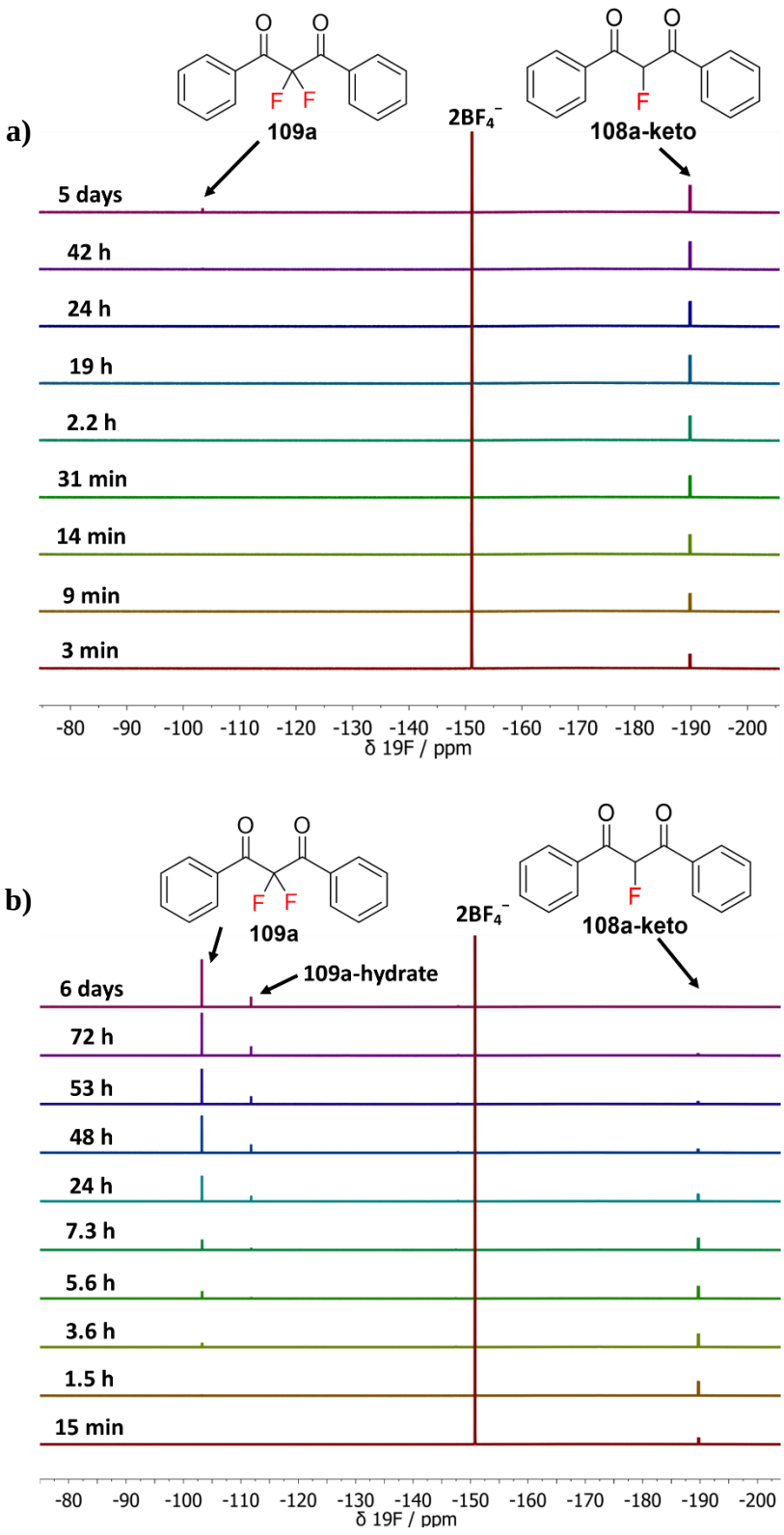

Figure 91: (a) ^{19}F NMR time profile for the reaction between 1,3-dicarbonyl **107a** (30 mM) and Selectfluor™ (62.5 mM) in MeCN-d_3 at 20 °C. (b) ^{19}F NMR time profile for the reaction between 1,3-dicarbonyl **107a** (59.5 mM) and Selectfluor™ (125 mM) in 20% water in MeCN-d_3 at 20 °C.

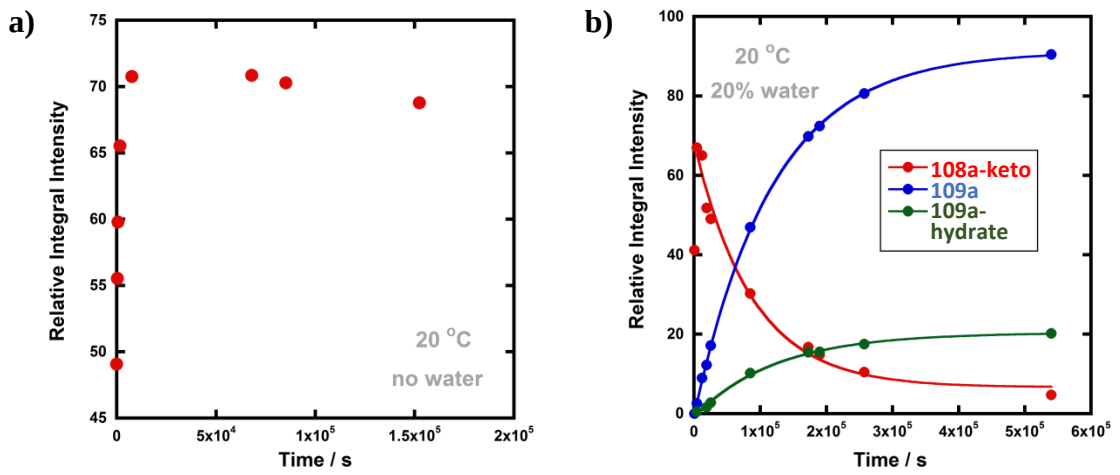

Figure 92: (a) Integral of peak corresponding to **108a-keto** over time for the reaction conducted with 100% MeCN-d_3. (b) Reaction conducted with 20% water in MeCN-d_3, showing the integrals of peaks corresponding to **108a-keto** ($\delta = -189.8$ ppm) and **109a** ($\delta = -103.4$ ppm) over time, as well as the peak at $\delta = -111.9$ ppm which corresponds to the hydrate of **109a**.

The integral intensities were then converted to concentrations and were compared with a numerically-solved differential model[3] of the overall processes (**Scheme 34**) based upon the microscopic rate constants that were measured by UV-vis spectrophotometry in previous sections. The microscopic rate constants (see Chapter 8 Section 8.5.3 for values used) were inserted into the model and numerical methods were employed to solve the differential equations **21-26** listed below.

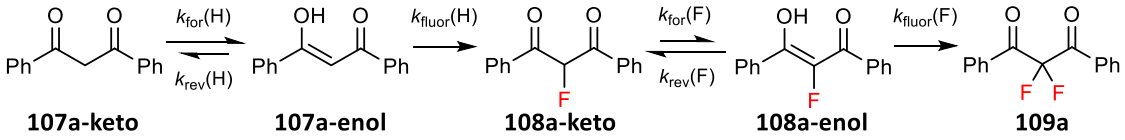

Scheme 34: Overall kinetic model for the difluorination of compound **107a** with Selectfluor™.

$$\frac{d[\mathbf{107a\ keto}]}{dt} = -k_{\text{for}}(\text{H})[\mathbf{107a\ keto}] + k_{\text{rev}}(\text{H})[\mathbf{107a\ enol}] \qquad (\mathbf{21})$$

$$\frac{d[\mathbf{107a\ enol}]}{dt} = k_{\text{for}}(\text{H})[\mathbf{107a\ keto}] - k_{\text{rev}}(\text{H})[\mathbf{107a\ enol}] - k_{\text{fluor}}(\text{H})[\mathbf{107a\ enol}][\text{F}^+] \qquad (\mathbf{22})$$

[3] The differential model was carried out using Wolfram Mathematica by Dr David Hodgson.

$$\frac{d[\mathbf{108a\ keto}]}{dt} = k_{\text{fluor}}(\text{H})[\mathbf{107a\ enol}][\text{F}^+] - k_{\text{for}}(\text{F})[\mathbf{108a\ keto}] + k_{\text{rev}}(\text{F})[\mathbf{108a\ enol}] - k_{\text{auto-for}}(\text{F})[\mathbf{108a\ keto}][\mathbf{108a\ enol}] + k_{\text{auto-rev}}(\text{F})[\mathbf{108a\ enol}]^2 \qquad (\mathbf{23})$$

$$\frac{d[\mathbf{108a\ enol}]}{dt} = k_{\text{for}}(\text{F})[\mathbf{108a\ keto}] - k_{\text{rev}}(\text{F})[\mathbf{108a\ enol}] - k_{\text{fluor}}(\text{F})[\mathbf{108a\ enol}][\text{F}^+] + k_{\text{auto-for}}(\text{F})[\mathbf{108a\ keto}][\mathbf{108a\ enol}] - k_{\text{auto-rev}}(\text{F})[\mathbf{108a\ enol}]^2 \qquad (\mathbf{24})$$

$$\frac{d[\text{F}^+]}{dt} = -k_{\text{fluor}}(\text{H})[\mathbf{107a\ enol}][\text{F}^+] - k_{\text{fluor}}(\text{F})[\mathbf{108a\ enol}][\text{F}^+] \qquad (\mathbf{25})$$

$$\frac{d[\mathbf{109a}]}{dt} = k_{\text{fluor}}(\text{F})[\mathbf{108a\ enol}][\text{F}^+] \qquad (\mathbf{26})$$

The resulting predicted concentration-time profiles of all species were plotted (lines in **Figure 93a, b**) to allow comparison with experimental data (dots in **Figure 93a, b**). For the experiment performed in the absence of added water (**Figure 93a**), the rapid evolution of **108a-keto** was modelled well by using ketonization and enolization rate constants for **107a** in MeCN (determined in Chapter 3). The addition of kinetic terms related to the auto-catalytic keto-enol tautomerism of **108a** were critical to the quantitative agreement between model and experiment for the formation of **109a**, with the formation of **109a** being predicted to reach only 1.7% after ~5 days in the absence of this contribution, but 2.9% (versus ~4% by experiment) when these terms were taken into account.

In the presence of 20% water, the build-up and break-down of **108a-keto** was modelled well alongside the profile for the formation of **109a**, although some over-estimation of the concentration of **108a-keto** was evident in the NMR experiment. Due to the wide range of chemical shift of the species present in these NMR experiments (−100 ppm to −200 ppm), peaks towards the edge of the spectra are generally less quantitative with respect to peaks in the centre. This was minimised by increasing the range of the NMR experiments by 30 ppm at both high and low chemical shifts, i.e. acquiring spectra between −70 ppm and −230 ppm. The relaxation delay was also increased to 8 s (based on the measured T1 values of the species present – see Chapter 8 Section 8.5.2). An error of ± 10% is associated with NMR integrals, which explains the slightly higher concentration of **108a-keto** produced (65 mM) in the reaction with 20% water than

would be expected given the starting concentration of **107a** (59.5 mM). The presence of autocatalysis of the keto-enol equilibration of **108a** was not detected in UV-vis kinetic studies, and thus was not included in the model. However, at the higher concentrations employed in this NMR study, any such terms could become more sizeable and could contribute to improving the model.

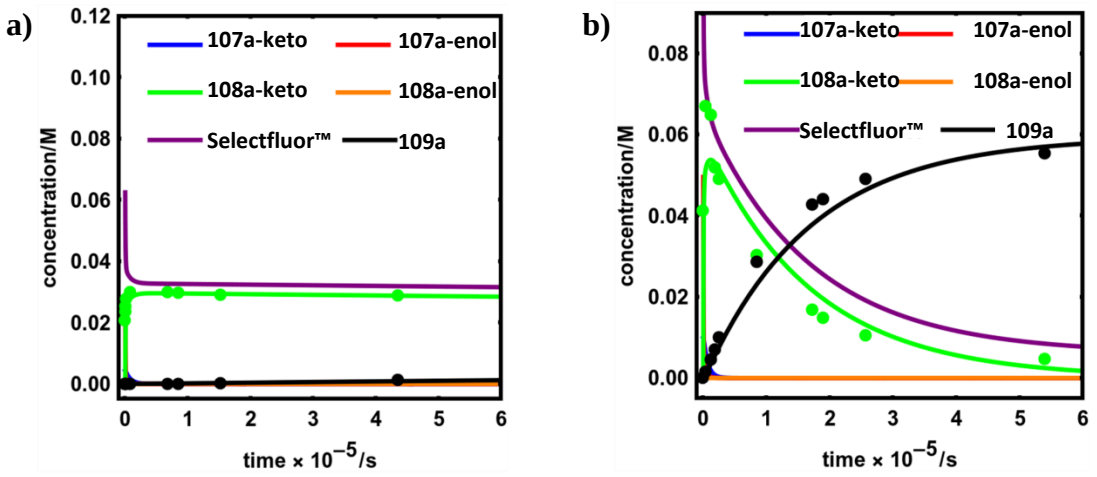

Figure 93: (a) Integrated ^{19}F NMR-time data for the reaction between **107a** (30 mM) and Selectfluor™ (62.5 mM) in MeCN-d_3. (b) Integrated ^{19}F NMR-time data for the reaction between **107a** (59.5 mM) and Selectfluor™ (125 mM) in 20% water in MeCN-d_3.

4.10 Comparisons with synthetic reports

The kinetic studies discussed in Chapters 3 and 4 correlate very well with previous synthetic studies. Firstly, the findings of enhanced nucleophilicity for fluoroenols **108a, 108c-e** over enols **107a**, **107c-e** (discussed in Section 4.3) align with studies conducted by Dolbier *et al.*[182–184] on the kinetic impact of vinylic fluorine substituents upon cyclisation reactions. They reported that the presence of a fluorine atom at an sp^2 centre was disfavoured relative to the sp^3 hybridised analogue, therefore, cyclization reactions occurred readily to form butadiene compounds.

Furthermore, in related carbanion systems, the reactivity was found to be enhanced by the presence of an α-fluorine atom compared to the non-fluorinated carbanion.[185,186] Indeed, the effect of the α-fluorine was even greater in these studies, probably due to the increased repulsion between the oxyanionic charge and fluorine lone pairs in comparison to the enol systems in the present work.

Chambers *et al.*[107,108] reported that during electrophilic fluorination of 1,3-dicarbonyl derivatives by elemental fluorine, the second fluorination step was slower than the first.

However, the results in the present work show that addition of the second fluorine atom proceeds at a rate that is similar to or even greater than the first fluorination step. The previously reported slow rate of difluorination is due to rate-limiting enolization of the mono-fluoro-diketone compound rather than the fluorination process itself. As demonstrated in Chapter 3, the rate of enolization can be enhanced by the addition of water, salt, acid or base, which in turn contributes to an increase in the overall rate of the difluorination mechanism.

As mentioned in Chapter 1 Section 1.4.2, Banks *et al.*[66] first reported the selective monofluorination of **107a** (and other 1,3-dicarbonyl derivatives) using Selectfluor™ in MeCN, which gave 100% crude and 84% pure yields. Complete conversion of **107a** to **108a** was indeed observed in the present work by both spectrophotometric and NMR methods, due to the high enol content of **107a**. Banks found that difluorination reactions required long reaction times of 8-27 days to reach completion, although reaction times were significantly enhanced by using NaH to form sodium enolates of the corresponding 1,3-dicarbonyl compounds. Kinetics studies to explore the reactivities of enolates will be discussed in Chapter 5.

Yi and co-workers[180,187] reacted a series of aromatic 1,3-dicarbonyl compounds with 2.1 equivalents of Selectfluor™ in 10:1 MeCN/H_2O at 25 °C for 1-2 days, to obtain a range of 2,2-difluoro-1,3-diketones in approximately 90% yield. This matches the conclusions from Chapters 3 and 4 that water must be present to facilitate the enolization of **108a-keto** and thus allow difluorination to occur within reasonable timescales.

Pattison *et al.*[188] attempted the difluorination of an aromatic β-ketoester with Selectfluor™ (2.5 equivalents) under reflux conditions in MeCN, which gave an 8:1 ratio of mono- and difluorinated products. This was attributed to the lower enol content of β-ketoesters compared to **107a**.[188] Since water was not used in the reaction, the enolization of the β-ketoester was presumably slow, which explains the low conversion to the difluorinated product.

As mentioned in Chapter 1 Section 1.4.2, Stavber *et al.*[120] reported monofluorinations of cyclic 1,3-diketones and β-ketoesters in water using Selectfluor™ (1.1 equivalents), obtaining yields of 74−91%. The difluorinations of acyclic 1,3-diketones and β-ketoesters via Selectfluor™ (2.2 equivalents) in water gave yields of 78−89%. All reactions were conducted at 70 °C for 4−10 h. Fluorination of the acyclic 1,3-

dicarbonyls could not be selectively stopped at the monofluorination stage, but by using 2.2 equivalents of Selectfluor™ the 2,2-difluoro-1,3-dicarbonyls were obtained without additional activation of the starting material.

Finally, syntheses of α,α-difluoro-β-ketoamides have been achieved using H_2O:PEG-400 solvent mixtures in the presence of K_2CO_3,[189] as well as very recently reported H_2O:MeCN systems[190] in green chemistry research programs, for which the experiments discussed in Chapters 3 and 4 provide supporting mechanistic evidence of the crucial roles of water and base.

4.11 Conclusions

In this chapter, the kinetic data on the fluorination of mono-fluoroenols **108a** and **108c-e** with Selectfluor™ and NFSI under a variety of conditions were discussed in detail. It was determined that the addition of a second fluorine atom occurs at a rate greater than or similar to that of the addition of the first fluorine atom. The rate-limiting step in the overall difluorination mechanism is therefore the enolization of the mono-fluoroketo tautomer, represented by k_{for}(F).

The use of water and $^{n}Bu_4N^+BF_4^-$ as additives during fluorination reactions resulted in greatly enhanced rates of fluorination of **108a-enol** by Selectfluor™ (50-fold with water and 2000-fold with $^{n}Bu_4N^+BF_4^-$). Small quantities of formic acid gave small increases in rates, although higher quantities of acid resulted in slightly decreased rates for both Selectfluor™ and NFSI. Stability studies involving each reagent in acidic solutions would be required to determine the origin of these observations. Overall, the effects of additives upon k_2 support the concept of differential solvation and medium effects along the reaction coordinates of the fluorination and tautomerization processes of the enol and fluoroenol systems, however, their underlying origins are not clear at this stage.

The results discussed in Chapters 3 and 4 are closely interlinked. They give direct evidence that water plays an essential role in accelerating the enolization of mono-fluorodiketone derivatives to allow the formation of difluorodiketones. These findings have important implications for synthetic fluorination procedures: the addition of small quantities of water to partially enolic 1,3-dicarbonyl derivatives increases rates of keto to enol tautomerism, supporting the formation of the key enol intermediates required for both the first and second fluorination steps. Furthermore, water also enhances the rate of

fluorination of fluoroenols, again supporting the expedited formation of pharmaceutically relevant α,α-difluoroketonic compounds.

Chapter 5: Attempts Towards Correlation with the Mayr-Patz Scale

Chapter 2 discussed the successful development of a reactivity scale for widely-used N−F reagents, underpinned by 1,3-diaryl-1,3-dicarbonyl derivatives as nucleophiles. One of the initial aims of this project was to ultimately correlate the reactivities of the N−F reagents with the Mayr-Patz scale, that is, to determine their electrophilicity parameters, *E*, using a kinetics approach. However, as mentioned in Section 2.10, Herbert Mayr and co-workers reported their work on this field in late August 2018. Nevertheless, the steps taken in the present work towards this correlation revealed interesting mechanistic insights. This chapter will firstly give a brief overview of the Mayr-Patz scale, followed by the detailed discussion of each approach employed during attempts to determine the electrophilicities of Selectfluor™ and NFSI. In the final section, attempts towards the determination of nucleophilicities, *N*, of enolate forms of the 1,3-diaryl-1,3-dicarbonyl derivatives **107a-h** will be described.

5.1 Introduction

The development of quantitative scales of nucleophilicity began in the 1950s with the Swain Scott equation[191] (**Equation 27**), where n = nucleophilicity constant ($n_{H_2O} = 0$) and s'_E = sensitivity of electrophile ($s'_{CH_3Br} = 1$).

$$\log\left(\frac{k}{k_{H_2O}}\right) = s'_E n \qquad (\mathbf{27})$$

This was followed by the Ritchie equation[192] (**Equation 28**), where relative reactivities of nucleophiles toward carbocations and diazonium ions could be described by the electrophile-independent nucleophilicity parameter N_+.

$$\log\left(\frac{k}{k_o}\right) = N_+ \qquad (\mathbf{28})$$

The most extensive nucleophilicity scale currently available is the Mayr-Patz scale.[193] It was derived from the rate constants of the reactions of benzhydrilium ions with a wide range of nucleophiles including alkenes, arenes, enol ethers, ketene acetals, enamines, carbanions, amines, alcohols and alkoxides.[194] The Mayr-Patz equation[195] is shown below in **Equation 9**, where *k* is the second-order rate constant at 20 °C, *E* is a

nucleophile-independent electrophilicity parameter, and N and s_N are electrophile-independent nucleophile-specific parameters.

$$\log k = s_N(E + N) \qquad (\mathbf{9})$$

The benzhydrilium ions were defined as the electrophile basis set, where variation of the *meta*- and *para*-substituents altered their electrophilicities by 16 orders of magnitude. Benzhydrilium **130** was defined as $E = 0$ and 2-methyl-1-pentene **131** was defined as $s_N = 1$ (**Figure 94**). Using **Equation 9**, Mayr and co-workers have developed comprehensive scales for electrophilicity and nucleophilicity. To date, the nucleophilicity and electrophilicity parameters cover the range $-8.80 \leq N \leq 30.82$ and $-24.69 \leq E \leq 8.02$, respectively. The wider implication of this scale is the possibility to predict polar organic reaction outcomes by matching reaction partners of suitable reactivity to achieve conversion to the desired product within reasonable timescales.

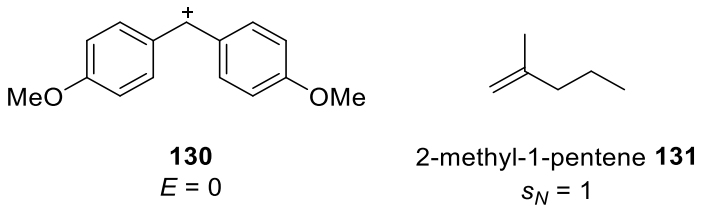

Figure 94: Reference compounds used in the Mayr-Patz scale.

There are three main methods for determination of E, N and s_N parameters. To determine E parameters for new electrophiles, the rate constants for reactions with nucleophiles of known N and s_N parameters must be measured. To determine N and s_N parameters for new nucleophiles, the rate constants must be measured with several electrophiles of known E parameter. Finally, for an approximate determination of N for new nucleophiles, it is possible to assume that s_N is similar to that of a structurally analogous nucleophile, and to measure the rate constant for reaction with a single electrophile of known E parameter, from which it is possible to derive N.[196]

Notably, relatively recent work by the Mayr group investigated the kinetics of chlorination of a range of π-nucleophiles by chlorinating agents **132a-c** in MeCN (**Figure 95**).[197] These polychloroquinone derivatives **132a-c** were suggested to deliver equivalents of "Cl^+" to the substrates, which indicates that the mechanism of chlorination operates in a comparable manner to that of the N–F reagents. Electrophilicity parameters, E, for each chlorinating reagent were derived from kinetics

studies with reference nucleophiles **133a-k** (**Figure 95**), which have known nucleophilicity parameters, *N*. This approach provided an indication of a method by which the *E* parameters of the N−F reagents could be determined in the present work.

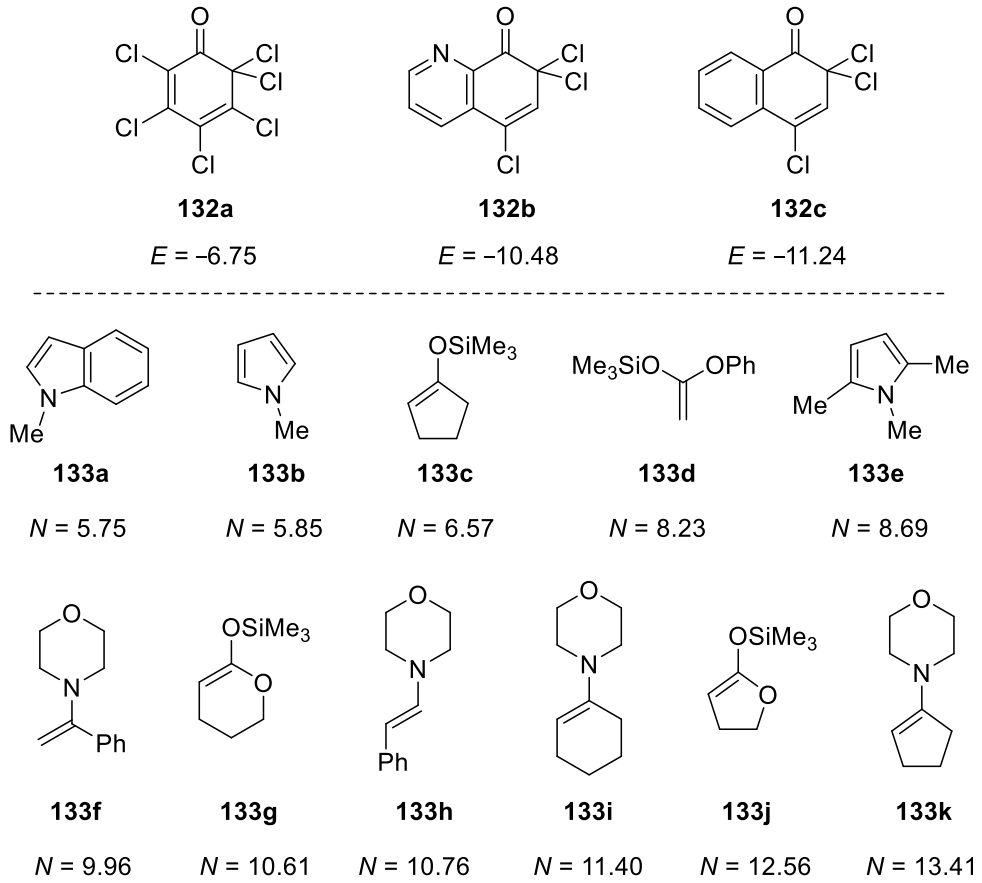

Figure 95: Electrophilicities of polychloroquinones **132a-c** derived from rate constants of reactions with reference nucleophiles **133a-k** at 20 °C in MeCN (from ref [197]).

As discussed in Chapter 2 Section 2.10, Mayr *et al.* recently reported electrophilicity parameters, *E*, for five N−F reagents.[132] Prior to the publication of their report, this had been a broader aim of the present work, and several approaches had been taken towards achieving this correlation. The first method employed was to determine the kinetics of fluorination of several reference nucleophiles from **Figure 95**, which were enamine **133i** (Section 5.2), silyl enol ether **133c** (Section 5.3) and indole **133a** (Section 5.4). The selection of these nucleophiles was based on the range of reactivities offered, allowing tunability of the reaction partners depending on timescales for reactions and the method used to monitor fluorination reactions. Additionally, they are commercially available, thus, did not require lengthy preparations for their use in preliminary investigations. Secondly, the possibility of obtaining an estimate of the nucleophilicity parameters, *N*,

for enols **107a-m** was explored by studying the kinetics of the corresponding reactions with the commercially available chlorinating reagent **132a** (Section 5.5). Although the *N* parameters of enol forms of 1,3-dicarbonyl compounds have not, to date, been measured, the carbanion forms of several 1,3-dicarbonyls have known *N* and s_N parameters (**Figure 96**). In this context, the fluorination of dimethyl malonate **134f** will be discussed in Section 5.6. Finally, in the later stages of this project, the determination of nucleophilicities, *N*, of the 1,3-diaryl-1,3-dicarbonyl derivatives **107a-h** was attempted using benzhydrilium ions as reference electrophiles (Section 5.7).

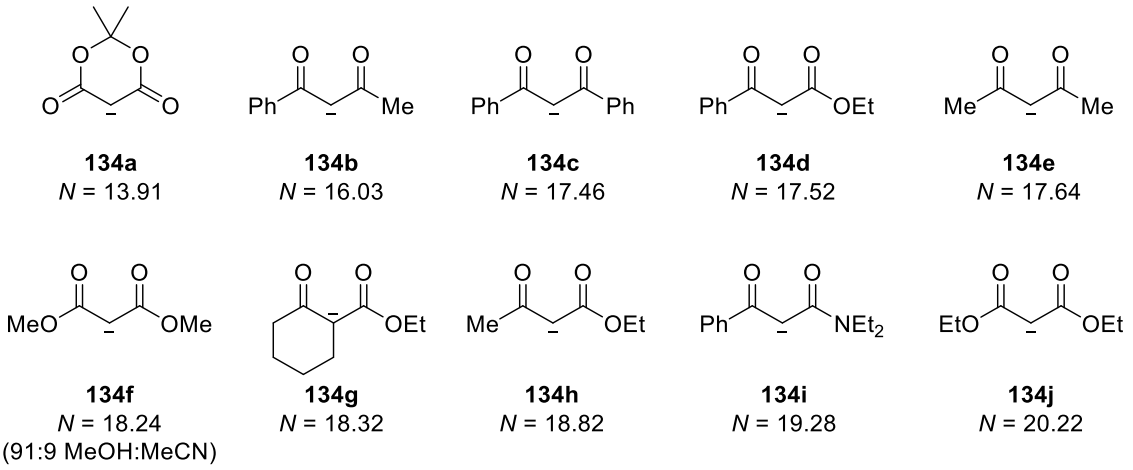

Figure 96: Carbanion forms of several 1,3-dicarbonyl compounds present on the Mayr-Patz scale in order of increasing *N* parameter, with s_N values between 0.64-0.86. Unless otherwise stated, reactivity parameters were determined in DMSO (from ref [194]).

5.2 Kinetics of fluorination of enamine 133i

1-Morpholinocyclohexene **133i** is a reference nucleophile on the Mayr-Patz scale with a nucleophilicity parameter, *N*, of 11.40. The fluorination of **133i** using Selectfluor™ to give 2-fluorocyclohexanone **136i** (**Scheme 35**) was initially monitored by NMR spectroscopy; however, the reaction reached completion within 10 min. Hence, UV-vis spectrophotometry was explored as an alternative. The benefit of this technique over NMR spectroscopy lies in the much shorter delays between mixing of reagents and acquisition of data. Furthermore, the lower concentrations of solutions required by the UV-vis technique leads to lowered rates, thus allowing the kinetics of the reactions to be monitored more conveniently.

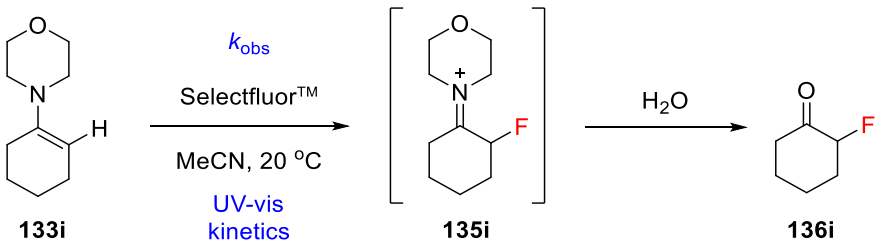

Scheme 35: Fluorination of **133i** by Selectfluor™ in MeCN at 20 °C.

The UV-vis spectrum of 1-morpholinocyclohexanone **133i** contains an absorbance band at λ_{max} = 220 nm, with an extinction coefficient, ε, of 8111 mol^{-1} dm^3 cm^{-1}. Various difficulties were found with regards to this reaction. Firstly, **133i** was found to hydrolyse over time in MeCN. Hence, MeCN was distilled over CaH_2 immediately before preparing the stock solutions. However, hydrolysis was still observed in freshly prepared stock solutions of **133i** in distilled MeCN. A solution of **133i** (0.20 mM) was monitored by time-arrayed multi-wavelength analysis with spectra acquired every 30 min (**Figure 97a**). These studies showed a decrease in the absorbance band at λ_{max} = 220 nm, where the plot of absorbance at λ_{max} = 220 nm versus time gave a linear correlation (**Figure 97b**) and an initial rate constant for hydrolysis of 1.75 × 10^{-5} s^{-1}. A small increase in absorbance at 280-300 nm also occurred (**Figure 97a**), which is likely to correspond to the formation of the cyclohexanone product of hydrolysis. This was confirmed by obtaining the UV-vis spectrum of a standard sample of cyclohexanone, which displayed a band at λ_{max} = 285 nm, with an extinction coefficient, ε, of 22.8 mol^{-1} dm^3 cm^{-1}. This band is due to an π* ← n transition of the C=O bond.[198]

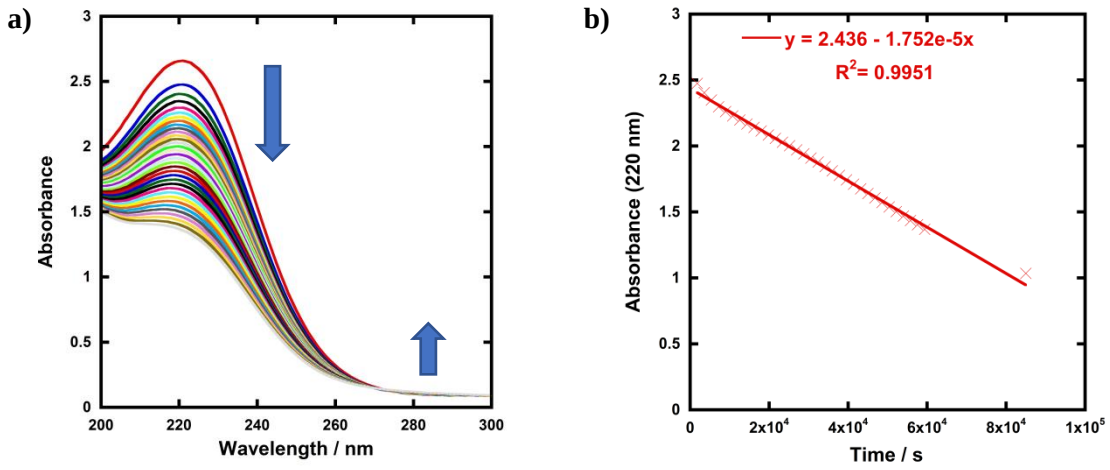

Figure 97: (a) Decrease in absorbance of **133i** (0.20 mM) over 17 h in distilled MeCN, with scans acquired every 30 min. (b) Decrease in absorbance at 220 nm over time to determine the rate of hydrolysis. The final data point was acquired after 24 h.

Nevertheless, the fluorination of **133i** by Selectfluor™ was attempted in distilled MeCN with 10- to 25-fold excesses of the fluorinating reagent. Monitoring the resulting reactions by UV-vis spectrophotometry showed exponential decays of absorbance of the nucleophile **133i** (**Figure 98a**). The plot of k_{obs} values versus [Selectfluor™] gave the second-order rate constant $k_2 = 2.93 \times 10^{-1}$ M^{-1} s^{-1} (**Figure 98b**). However, attempts to repeat these kinetic reactions with the same or different concentrations of Selectfluor™ gave inconsistent results. Often, biphasic behaviour was observed, likely due to the competing hydrolysis of **133i**, or interference from the hydrolysis of the imine intermediate **135i** at the wavelength studied. Furthermore, monitoring the fluorination of **133i** by NFSI was unsuccessful due to the absorbance bands of NFSI that occur between 200-300 nm, which interfered with that of **133i**.

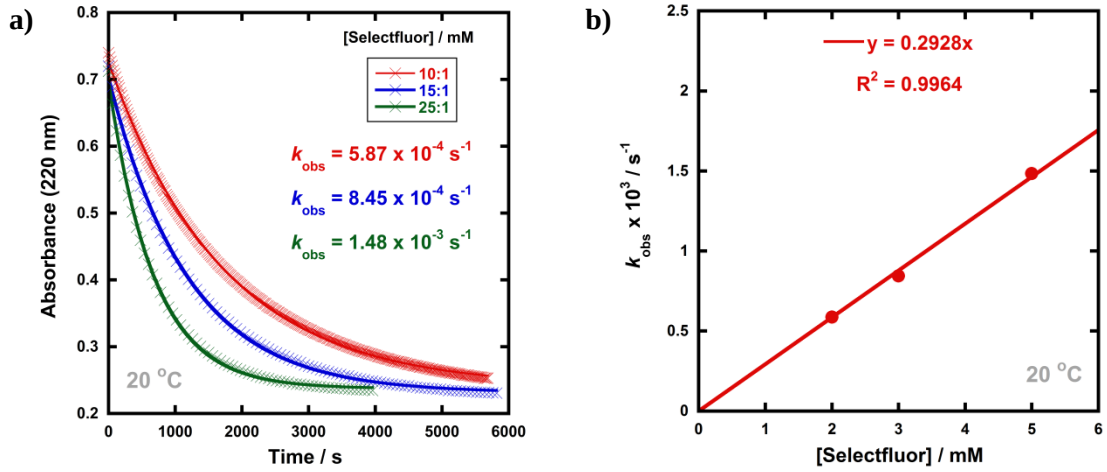

Figure 98: (a) Exponential decays of absorbance of **133i** (0.2 mM) with different concentrations of Selectfluor™ in MeCN at 20 °C, monitored at λ_{max} = 220 nm. The k_{obs} values determined from each curve are shown. (b) Correlation of k_{obs} with [Selectfluor™].

5.3 Kinetics of fluorination of silyl enol ether 133c

The next reference nucleophile studied was silyl enol ether **133c**, which has a nucleophilicity parameter, *N*, of 6.57. The fluorination of **133c** by Selectfluor™ in MeCN-d_3 (**Scheme 36**) was monitored by ^{19}F NMR spectroscopy, which showed that the reaction was complete within 10 min. The ^{19}F NMR spectrum contained three peaks (**Figure 99**). The peak at δ = −197 ppm ($^2J_{HF}$ = 49.9 Hz) corresponds to 2-fluorocyclopentanone, which is in agreement with the literature value[199] (δ = −194 ppm, $^2J_{HF}$ = 50 Hz, solvent not specified). Two further unidentified peaks were present at δ = −162 ppm and −158 ppm, which could correspond to a hydrate or enol form of product **136c**. The Selectfluor™ (N−F) peak at δ = +48 ppm was no longer present; therefore,

this reagent was fully consumed. However, since this reaction was complete within 10 min, it was too fast to be monitored by NMR spectroscopy. Furthermore, since neither reaction partner is chromophoric, this reaction could not be monitored by UV-vis spectrophotometry.

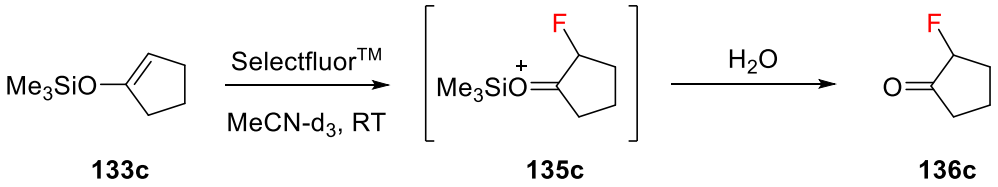

Scheme 36: Fluorination of silyl enol ether **133c** by Selectfluor™ in MeCN-d_3.

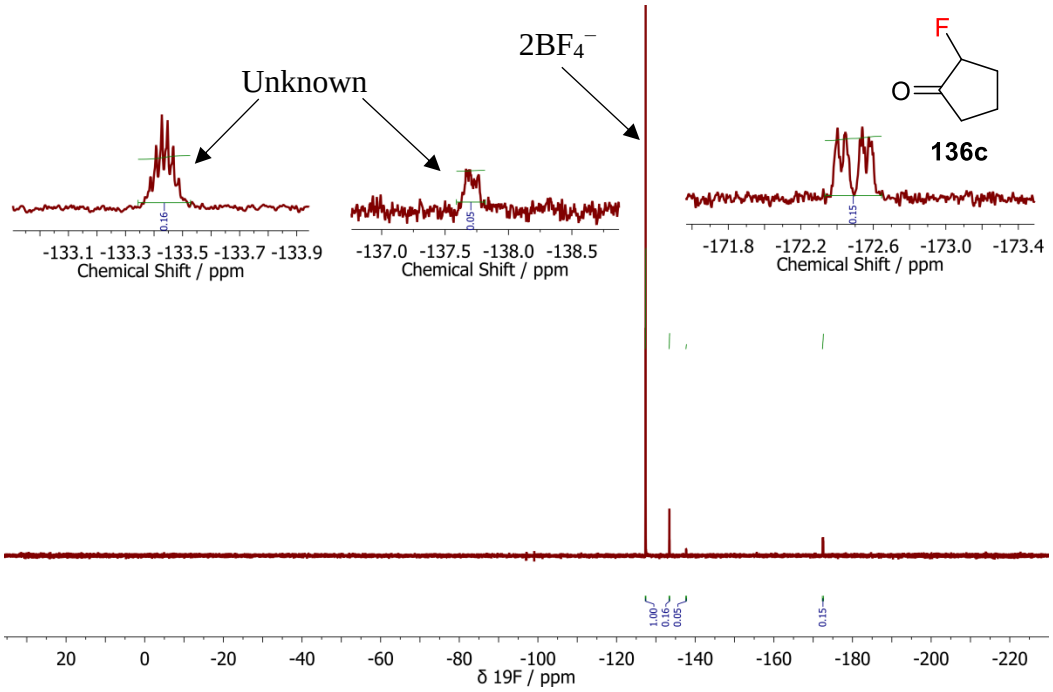

Figure 99: ^{19}F NMR spectrum for fluorination of silyl enol ether **133c** by Selectfluor™.

Finally, the fluorination of **133c** by NFSI was attempted. The reaction with NFSI was monitored over 24 h but showed only a 5% conversion, with no further progression of the reaction. This suggested that the hydrolysis of **133c** due to residual water in the NMR solvent outcompeted fluorination, since NFSI is a much weaker fluorinating reagent compared to Selectfluor™ (around 4000-fold less reactive as determined in Chapter 2). Hence, from these preliminary studies, silyl enol ether **133c** was determined to be an incompatible nucleophile for kinetics studies by UV-vis spectrophotometry and NMR spectroscopy.

5.4 Kinetics of fluorination of 1-methyl indole 133a

5.4.1 Kinetics of fluorination of 133a using Selectfluor™

Due to the problems found with nucleophiles **133c** and **133i**, discussed in the previous sections, it was necessary to choose a less reactive and chromophoric substrate. Thus, 1-methyl indole **133a** was selected as it has the lowest *N* parameter of the nucleophiles shown in **Figure 95**. Compound **133a** was distilled before use, and its UV-vis spectrum contained absorbance bands at λ_{max} = 222 nm and λ_{max} = 282 nm (**Figure 100**).

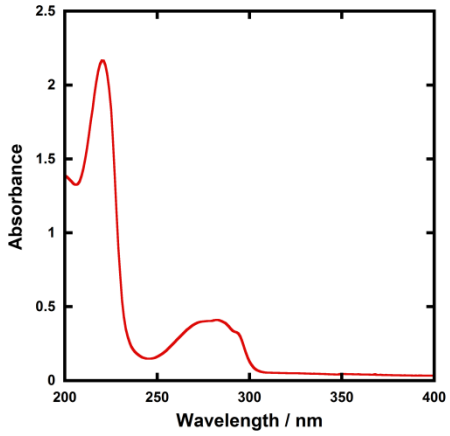

Figure 100: UV-vis spectrum corresponding to 1-methyl indole **133a** (0.05 mM) in MeCN.

Preliminary investigations of the reaction shown in **Scheme 37** began with conducting a multi-wavelength kinetics experiment for the fluorination of **133a** (0.025 mM) by Selectfluor™ (0.25 mM), thus maintaining pseudo-first order conditions (**Figure 101a**). The absorbance bands corresponding to **133a** decreased over time, while the appearance of a band at λ_{max} = 246 nm was observed. The plots of absorbance at λ_{max} values were fitted to first-order exponentials, which gave k_{obs} = 0.89 × 10^{-3} s^{-1} for the process occurring at 222 nm, k_{obs} = 0.93 × 10^{-3} s^{-1} at 282 nm and k_{obs} = 1.12 × 10^{-3} s^{-1} at 246 nm that are likely to correspond to the same process due to the similarity in values obtained (**Figure 101b**).

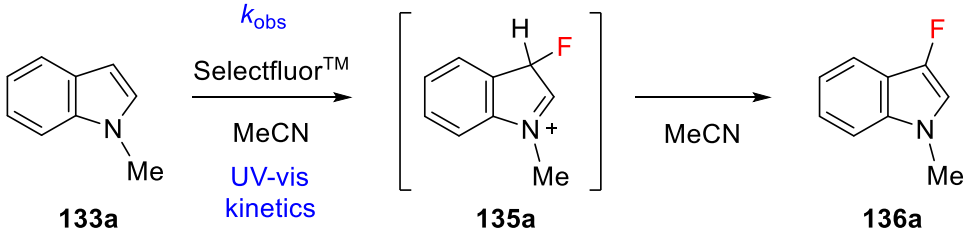

Scheme 37: Fluorination of indole **133a** by Selectfluor™ in MeCN.

Additionally, non-isosbestic behaviour was observed in **Figure 101a**. The plot of absorbances at 232 nm and 298 nm indicated the build-up and decay of an intermediate species (**Figure 102a**). These processes were likely to correspond to the formation and subsequent hydrolysis of intermediate **135a** due to the residual water present in the solvent. The two phases occurring at 232 nm were each fitted to first-order exponentials (**Figure 102b**) and k_{obs} values were determined for each process. The second phase (hydrolysis of the intermediate) was found to be 3-fold slower than the first phase (formation of the intermediate).

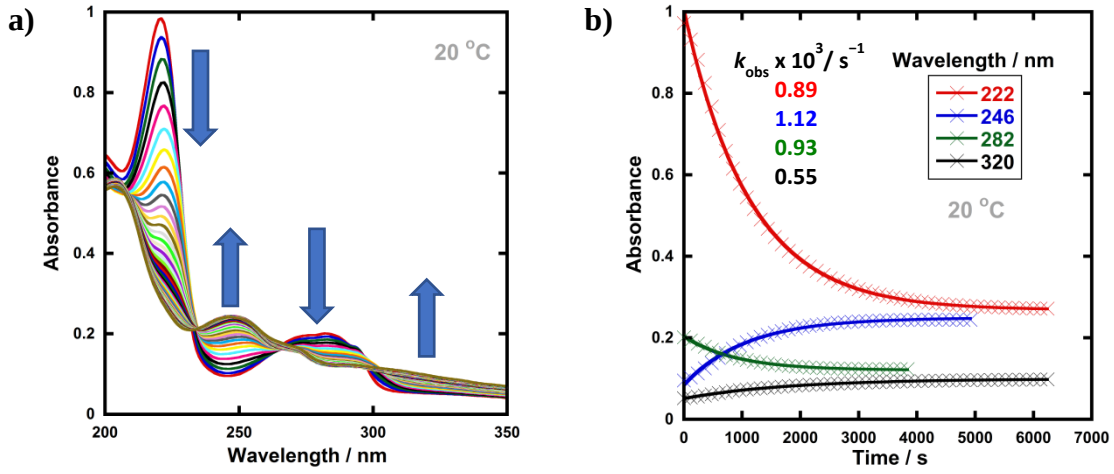

Figure 101: (a) Multi-wavelength kinetics experiment for fluorination of **133a** (0.025 mM) by Selectfluor™ (0.25 mM) in MeCN at 20 °C. Scans were acquired every 2 min for 1.5 h. (b) Changes in absorbance at λ_{max} values over time.

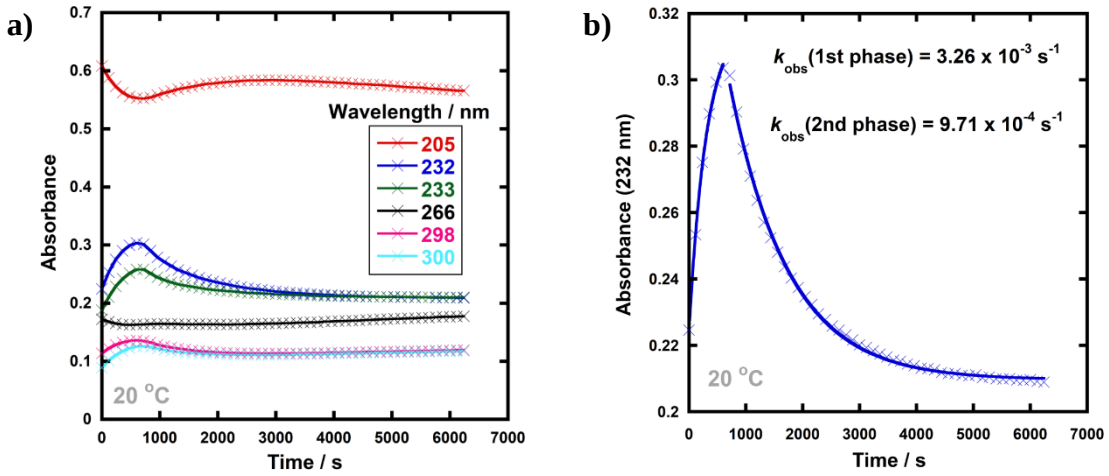

Figure 102: (a) Absorbances at non-isosbestic points indicating formation and decay of an intermediate. (b) Processes occurring at 232 nm in greater detail with k_{obs} values determined for each phase.

Nonetheless, the absorbances at λ_{max} values of indole **133a** had given clean exponential behaviours in **Figure 101b**. Hence, by monitoring the decays in absorbance of indole **133a** at λ_{max} = 222 nm, the kinetics of fluorination reactions were monitored under pseudo-first order conditions using excess Selectfluor™ in MeCN. Clean exponential decays of absorbance of the nucleophile **133a** were observed in all runs (**Figure 103a**). The k_{obs} values were plotted against Selectfluor™ concentration, giving a linear (i.e. first order) correlation (**Figure 103b**), which projected cleanly through the origin and gave the second-order rate constant, k_2 = 3.66 M^{-1} s^{-1}.

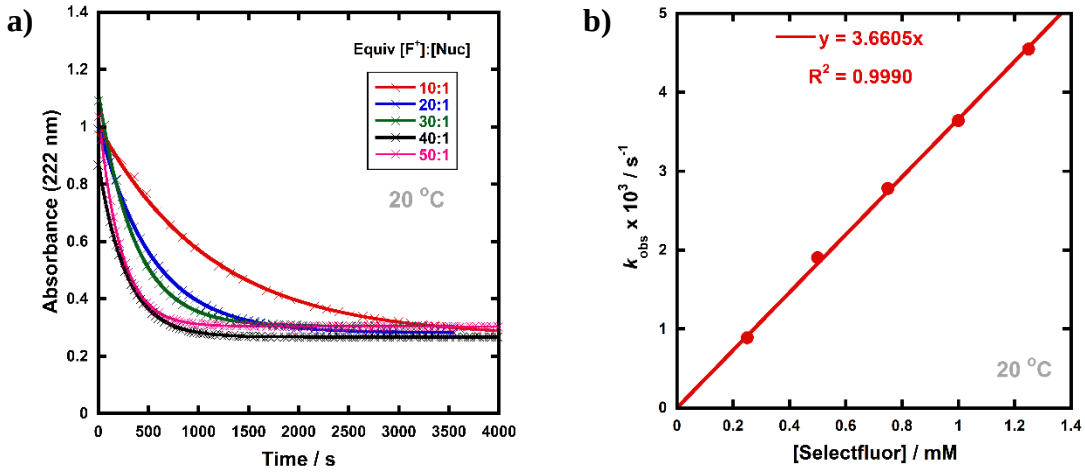

Figure 103: (a) Exponential decays of absorbance of **133a** (0.025 mM) at λ_{max} = 222 nm with different concentrations of Selectfluor™, in MeCN at 20 °C. (b) Correlation of k_{obs} values with [Selectfluor™].

It was hypothesised that the rate of hydrolysis of the intermediate could be increased by using water-MeCN solvent mixtures (**Scheme 38**) and thus give cleaner isosbestic points in the multi-wavelength kinetics arrays. Thus, the fluorination of **133a** by Selectfluor™ in a 1:2 water:MeCN mixture was monitored and the resulting spectra showed clean isosbestic behaviour (**Figure 104**).

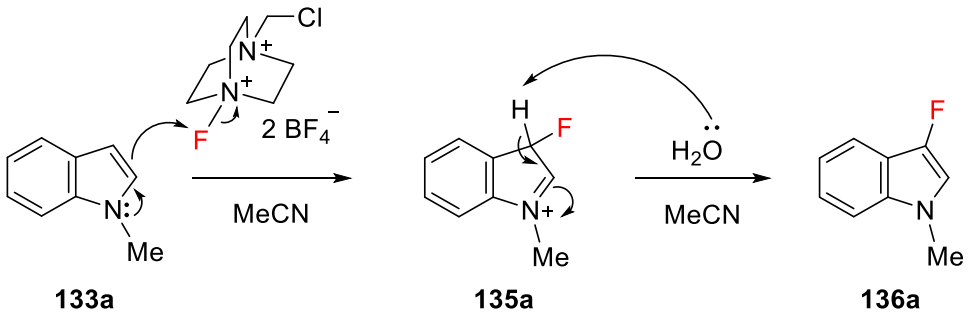

133a 135a 136a

Scheme 38: Mechanism for electrophilic fluorination of indole **133a** and hydrolysis of the intermediate via water.

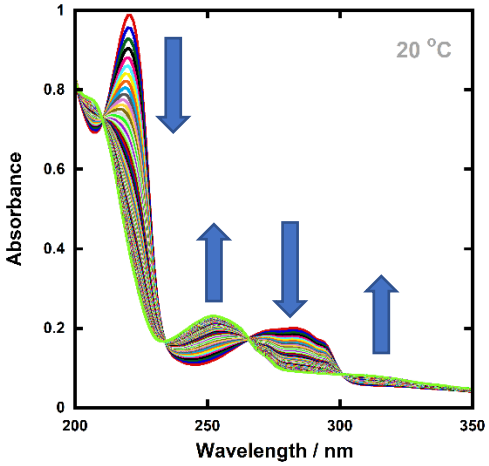

Figure 104: Multi-wavelength kinetics experiment for fluorination of **133a** (0.025 mM) by Selectfluor™ (0.75 mM) in a 1:2 water:MeCN mixture at 20 °C.

The kinetics of fluorination reactions using Selectfluor™ in 1:2 water:MeCN mixtures were then determined by monitoring the decays in absorbance of **133a** at λ_{max} = 222 nm. Reactions were carried out under pseudo-first order conditions using excess electrophile. Clean exponential decays of absorbance of the nucleophile **133a** were observed in all runs (**Figure 105a**). The k_{obs} values were plotted against Selectfluor™ concentration, giving a linear correlation from which the second-order rate constant, k_2 = 2.11 M^{-1} s^{-1}, was determined (**Figure 105b**).

However, this correlation did not project directly through the origin, which suggested that other processes were occurring. This set of experiments involving the addition of water gave contrasting results, where although isosbestic behaviour was obtained, the correlation of k_{obs} values versus [Selectfluor™] was not improved. Product analyses by NMR spectroscopy were therefore required.

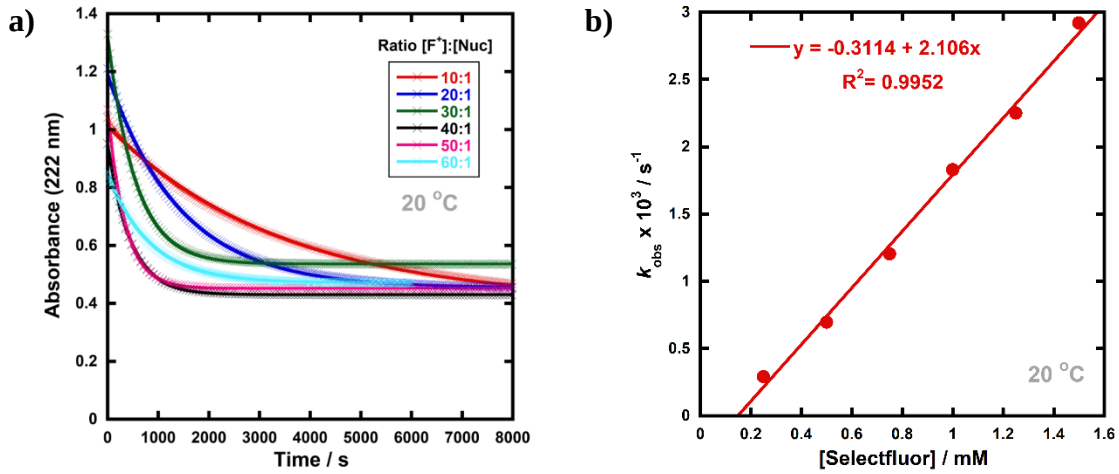

Figure 105: (a) Exponential decays of absorbance of **133a** (0.025 mM) at λ_{max} = 222 nm with different concentrations of Selectfluor™, in 1:2 water:MeCN at 20 °C. (b) Correlation of k_{obs} values with [Selectfluor™].

The fluorination of **133a** (25 mM) by Selectfluor™ (1 equiv.) was carried out in a 2:3 water:MeCN solvent system. Following work-up of the dark brown mixture, a brown residue was obtained. The ^{19}F NMR spectrum of this residue (**Figure 106a**) showed the presence of a small singlet at δ = −176.1 ppm corresponding to 3-fluoro-1-methylindole **136a**, which is in agreement with the literature chemical shift of δ = −176.4 ppm in $CDCl_3$.[200] However, several other unidentified peaks were also present at −85 to −120 ppm. The reaction was then repeated in a 97:3 water:MeCN solvent system, and following work-up of the brown mixture, a much cleaner ^{19}F NMR spectrum was obtained, where the main signal was that of **136a** at δ = −176.1 ppm (**Figure 106b**). The signals at δ = −95, −101 and −119 ppm were not present. In both spectra, tetrafluoroborate was still present even after work-up (δ = −151.8 ppm). Based on relative signal integrals, the approximate percentage of **136a** within the crude reaction mixtures thus increased from 1% to 80%.

Purification of the dark brown oily residues obtained from this fluorination reaction to obtain an authentic sample of 3-fluoro-1-methylindole had limited success. There were difficulties in carrying out column chromatography as polymerisation of the crude products may have occurred on silica. Overall, these reactions showed that other products were formed during the fluorination of indole **133a** with Selectfluor™ in water-MeCN mixtures, which may explain the inconsistencies in kinetics data obtained by UV-vis spectrophotometry. However, the concentration differences between UV-vis monitored reactions (0.025 mM) and synthetic reactions (25 mM) are likely to be

significant, given the propensity for indole polymerisation, which would be encouraged at higher concentrations.

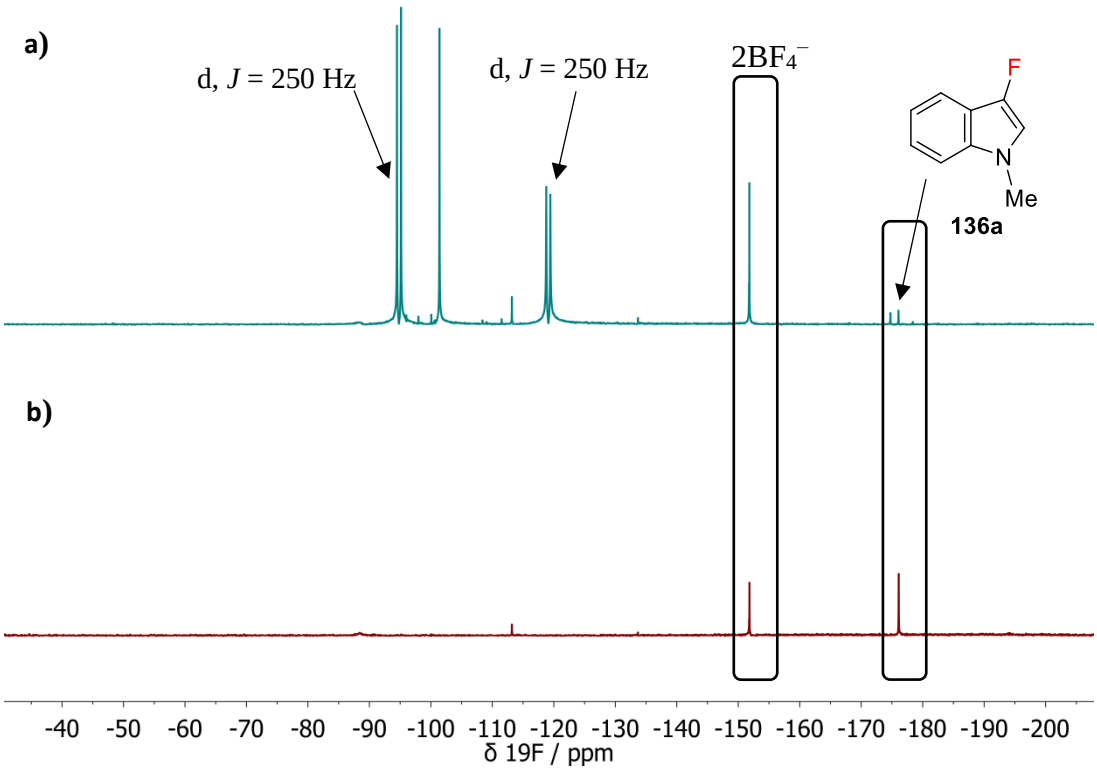

Figure 106: (a) Fluorination of **133a** using Selectfluor™ (1 equiv.) in a 2:3 water:MeCN solvent system; ^{19}F NMR spectrum of brown residue obtained after work-up is shown. (b) Fluorination of **133a** using Selectfluor™ (1 equiv.) in a 97:3 water:MeCN mixture; ^{19}F NMR spectrum of brown residue obtained after work-up is shown.

Finally, assuming the second-order rate constant obtained in MeCN (k_2 = 3.66 M^{-1} s^{-1}, **Figure 103b**) corresponded to the rate of fluorination of **133a**, it was possible to calculate an approximate value for the *E* parameter of Selectfluor™. Given that for **133a**, N = 5.75 and s_N = 1.23, using **Equation 9**, the electrophilicity parameter for Selectfluor™ was estimated to be E = −5.29. Based on this value, Selectfluor™ is predicted to be 1 or 2 orders of magnitude more reactive than chlorinating reagent **132a** (E = −6.75).

It is interesting to compare the reaction discussed in this section with the fluorination of 3-substituted indoles using Selectfluor™ in 1:1 water:MeCN mixtures to synthesise 3-substituted 3-fluorooxindoles (**Scheme 39**), which was reported by Shibata *et al.*[201] The product **138** was characterised using the ^{19}F NMR spectrum which contained a quartet at δ = −153.7 ppm with $^3J_{HF}$ = 22.2 Hz. The corresponding reaction in MeCN gave a

complex mixture of products. It is likely that the substituents on the nitrogen atom play a significant role in dictating the products formed from fluorination reactions involving indoles.

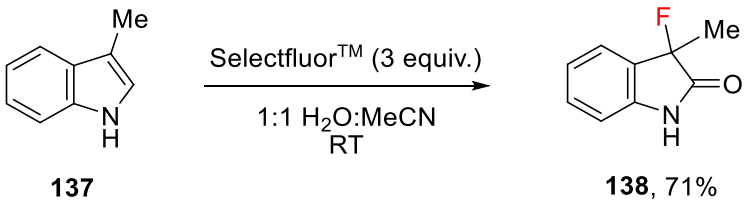

137 **138**, 71%

Scheme 39: Fluorination of 3-methyl indole **137** using Selectfluor™ in a 1:1 water:MeCN solvent system, to form 3-methyl 3-fluorooxindole **138** by Shibata *et al.*[201]

5.4.2 Kinetics of fluorination of 133a using NFSI

It was not possible to monitor the kinetics of fluorination of **133a** by NFSI **17** using UV-vis spectrophotometry due to the absorbance spectra of both species containing overlapping absorbance bands (**Figure 107**).

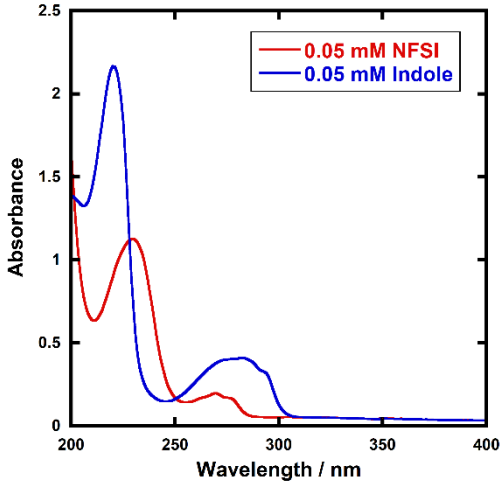

Figure 107: UV-vis spectra for NFSI **17** (0.05 mM, red line) and indole **133a** (0.05 mM, blue line) in MeCN.

Instead, the fluorination of **133a** using NFSI was monitored by ^{19}F NMR spectroscopy. The reaction was carried out in an NMR tube in MeCN-d_3, and the first NMR spectrum was acquired after 15 min (**Figure 108**). A small singlet at $\delta = -182.7$ ppm was present, which may correspond to the fluorinated indole intermediate **135a**. A peak at the same shift was observed for the analogous reaction with Selectfluor™ without water. After a further 25 min, a peak at $\delta = -178.4$ ppm appeared, which could correspond to the product 3-fluoro-1-methylindole **136a**. The singlet at −40 ppm due to NFSI (N−F)

decreased in intensity over 17.5 h and was no longer present in the final spectrum, indicating full transfer of the fluorine atom. On the basis of these unpromising results, no further studies were conducted on this reaction, although it would be interesting to explore the effects of the addition of water.

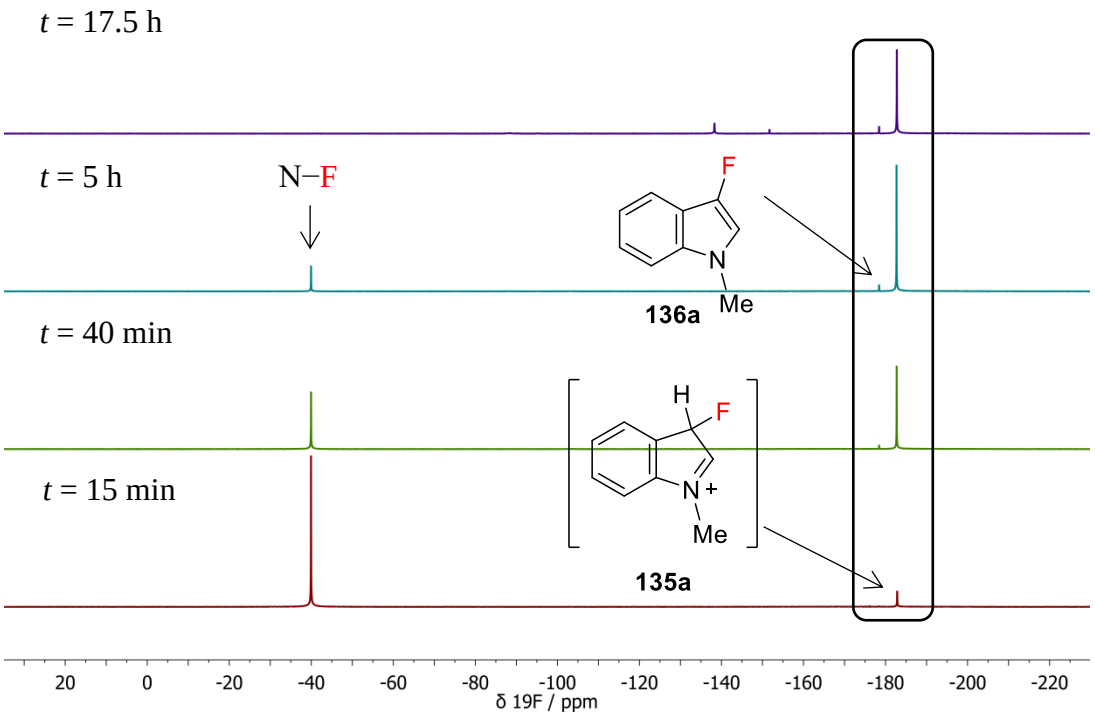

Figure 108: ^{19}F NMR spectra corresponding to the fluorination of **133a** (50 mM) using NFSI (50 mM) in MeCN-d_3, monitored over the course of 17.5 h.

5.5 Kinetics of chlorination

5.5.1 Kinetics of chlorination of 1-methyl indole 133a

The next approach was to use chlorinating reagents of known *E* value for determination of the nucleophilicity parameters, *N*, of the 1,3-diaryl-1,3-dicarbonyl derivatives. The polychloroquinone **132a** is commercially available and was a convenient choice for preliminary studies. Firstly, the chlorination of 1-methyl indole **133a** (**Scheme 40**) was monitored by UV-vis spectrophotometry, to ensure that the kinetics studies were comparable with the same reaction conducted by Mayr *et al.*[197] The correlation of k_{obs} values versus concentrations of **133a** reported in their study is shown in **Figure 109a**, where the second-order rate constant for chlorination was determined to be $k_2 = 4.01 \times 10^{-2}$ M^{-1} s^{-1}. The hydrolysis of intermediate **139** was assumed to be fast and non-rate limiting.

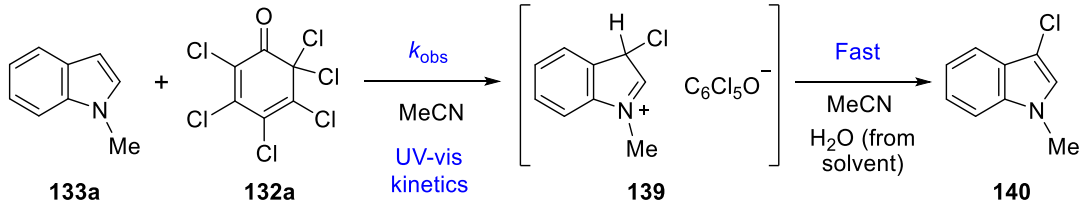

Scheme 40: Chlorination of indole **133a** using chlorinating reagent **132a** in MeCN.

The UV-vis spectrum of **132a** contains an absorbance band at λ_{max} = 368 nm (**Figure 109b**), which upon donation of the chlorine atom to the substrate converts into a pentachlorophenolate ion, which absorbs at a shorter wavelength (λ_{max} = 351 nm).[197] Although both reaction partners are chromophoric, the absorbance band of **132a** is sufficiently distant from that of **133a**, allowing the use of high excesses of the nucleophile to maintain pseudo-first order conditions in kinetics runs.

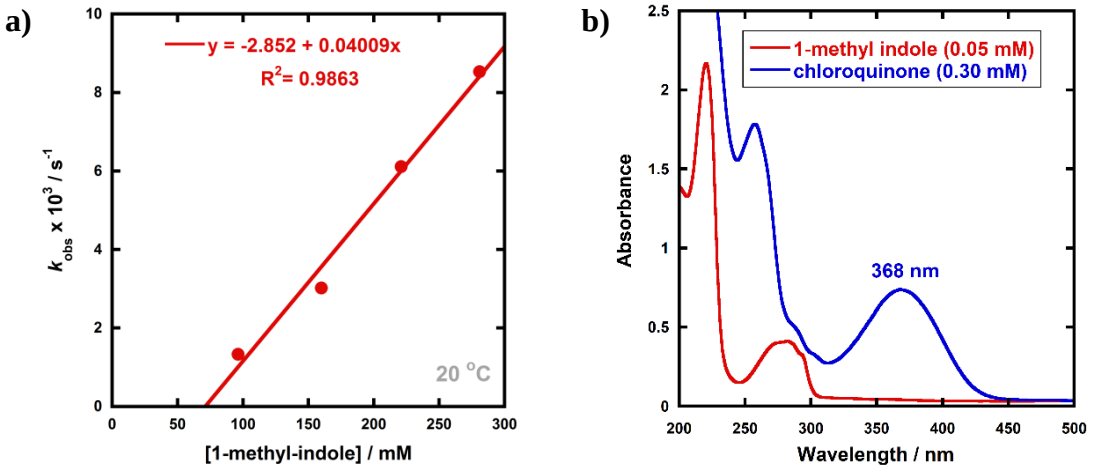

Figure 109: (a) Correlation of k_{obs} values with concentration of 1-methyl indole **133a** (data from ref [197]). (b) Reference spectra corresponding to polychloroquinone **132a** and 1-methyl indole **133a** (data from the present work).

As discussed above, kinetics experiments were conducted with 100- to 500-fold excesses of the nucleophile **133a**, to achieve pseudo-first order conditions. Exponential decays of absorbance of polychloroquinone **132a** at λ_{max} = 368 nm were observed (**Figure 110a**). The k_{obs} values were plotted against the concentrations of **133a**, giving a linear (i.e. first order) correlation (**Figure 110b**) which projected very close to the origin and gave the second-order rate constant, $k_2 = 1.39 \times 10^{-2}$ M^{-1} s^{-1}. Although this value is 2.9-fold lower that the value obtained by Mayr *et al.* (shown in **Figure 109a**), the correlation obtained in **Figure 110b** has a much better R^2 value as well as a closer projection through the origin. The reason for this discrepancy may be the observation in

the present work of the decomposition of the stock solutions of chlorinating reagent **132a** over time, and the need for preparing fresh solutions on the day of the relevant kinetics studies. It is possible that the results obtained by Mayr *et al.* were conducted with a mixture of fresh and old stock solutions, hence giving a poorer correlation. Nevertheless, the second-order rate constant obtained in the present work for chlorination of **133a** is the same order of magnitude as that obtained by Mayr *et al.*, and the difference between the two values is relatively small considering the possibilities of discrepancies in reaction conditions and temperatures.

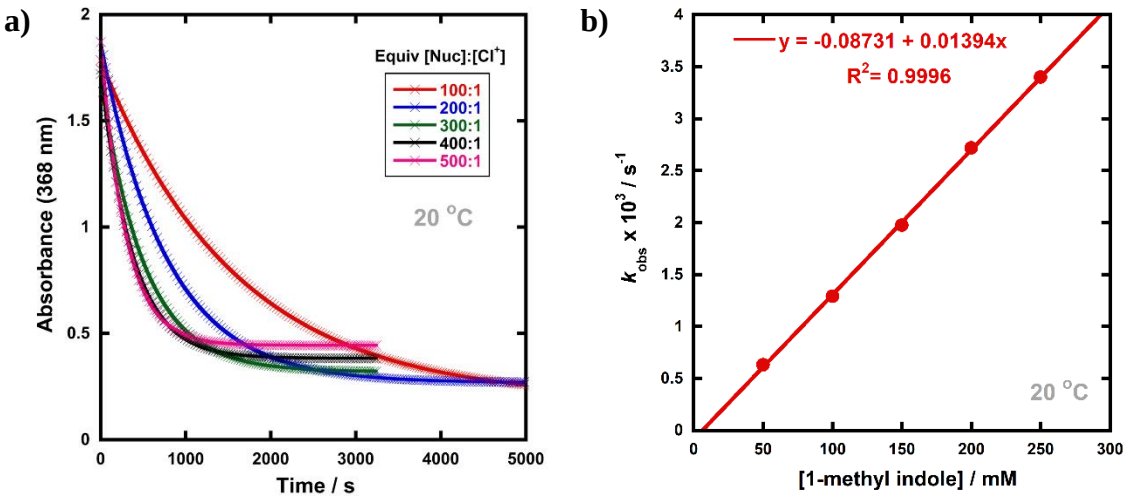

Figure 110: (a) Exponential decays of absorbance of chlorinating reagent **132a** (0.3 mM) at λ_{max} = 368 nm with different concentrations of 1-methyl indole **133a**, in MeCN at 20 °C. (b) Correlation of k_{obs} values with concentration of 1-methyl indole **133a**.

5.5.2 Chlorination of dimethylamino-substituted enol 107h

With knowledge of the UV-vis spectral properties of chlorinating reagent **132a** in hand, the chlorination of enol **107a** (R_1 = R_2 = H) was then considered. However, since the absorbance bands of **107a** (λ_{max}{enol} = 341 nm, λ_{max}{keto} = 250 nm) occur at almost identical wavelengths to **132a**, it was not possible to selectively monitor the λ_{max} value of a single reaction partner. However, the UV-vis spectrum of enol **107h** (R_1 = R_2 = NMe_2) has a band at λ_{max}{enol} = 425 nm, which was sufficiently distant from the absorbances of **132a** to allow the selective monitoring of this band (**Figure 111a**), with an excess of reagent **132a** to maintain pseudo-first order conditions. The chlorination of **107h** by **132a** (**Scheme 41**) was initially monitored using a multi-wavelength kinetics array (**Figure 111b**), which displayed an isosbestic point at 381 nm.

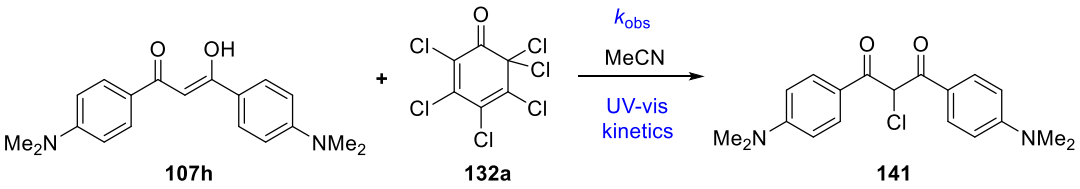

Scheme 41: Chlorination of enol **107h** using reagent **132a** in MeCN.

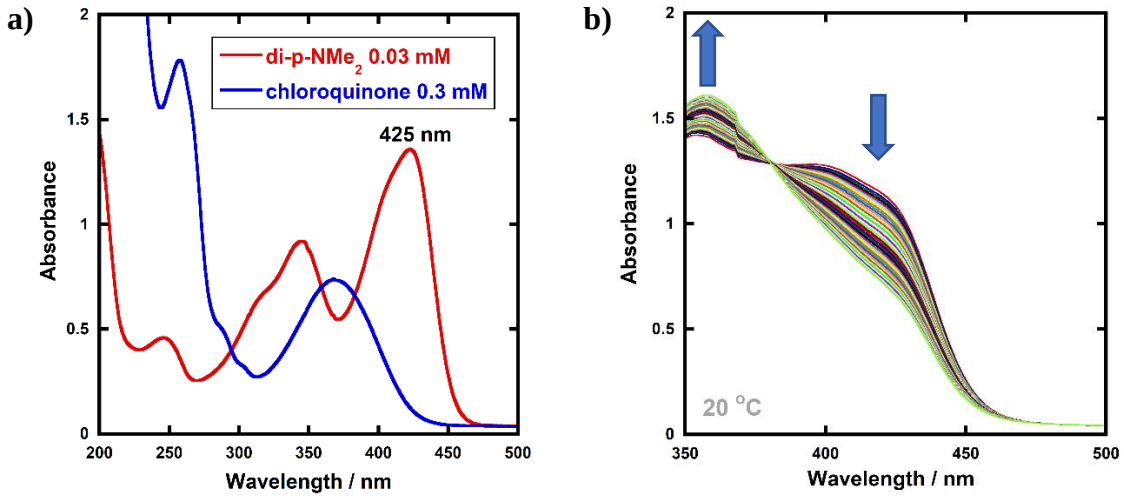

Figure 111: (a) UV-vis spectra corresponding to enol **107h** (0.03 mM) and polychloroquinone **132a** (0.3 mM). (b) Multi-wavelength kinetics array for the chlorination of **107h** (0.03 mM) by **132a** (0.3 mM) in MeCN. The artefact at 370 nm corresponds to the change from UV to visible lamps.

Exponential decays of absorbance of enol **107h** at 425 nm were observed with 10- to 20-fold excesses of **132a** (**Figure 112a**). The k_{obs} values were plotted against the concentration of **132a**, giving a linear correlation, which projected through the origin and gave the second-order rate constant, $k_2 = 3.69 \times 10^{-1}$ M^{-1} s^{-1}.

Additionally, product analysis was conducted using LC-MS to monitor the chlorination of **107h** (3 mM) by **132a** (3 mM) (**Figure 113**). After 15 min, the formation of chlorinated product **141** was clearly visible due to the presence of the corresponding peak at R_t = 2.7 min. Small peaks at R_t = 3.2 min and 2.5 min correspond to the enol and keto tautomers of **107h**. The two adjacent peaks at R_t = 3.0 min were associated with compound **132a**, which was confirmed by obtaining the LC-MS of an authentic sample of **132a**. The peaks at R_t = 3.8 min and 2.4 min were impurities present in the sample of reagent **132a**.

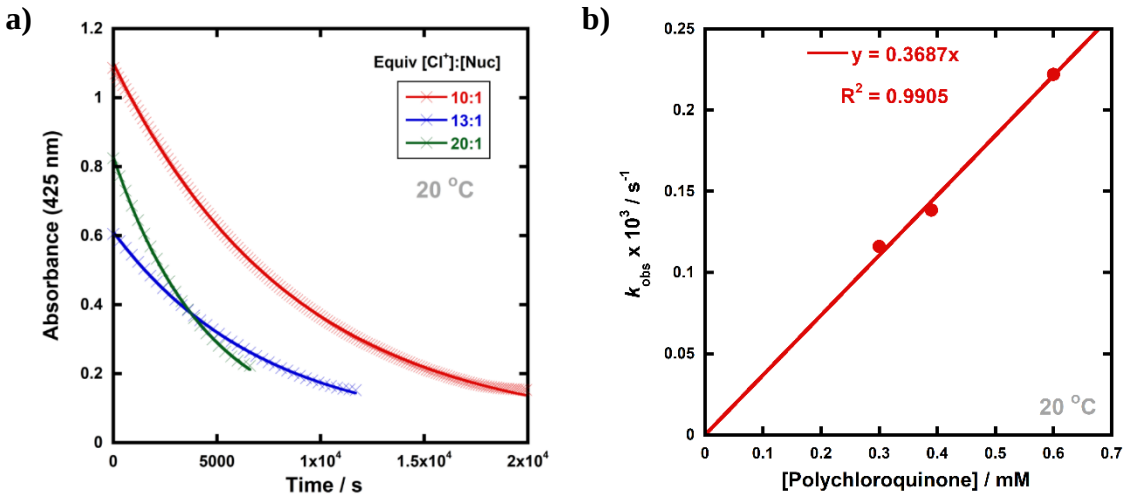

Figure 112: (a) Exponential decays of absorbance of enol **107h** (0.03 mM) at 425 nm with different concentrations of reagent **132a**, in MeCN at 20 °C. (b) Correlation of k_{obs} values with concentration of reagent **132a**.

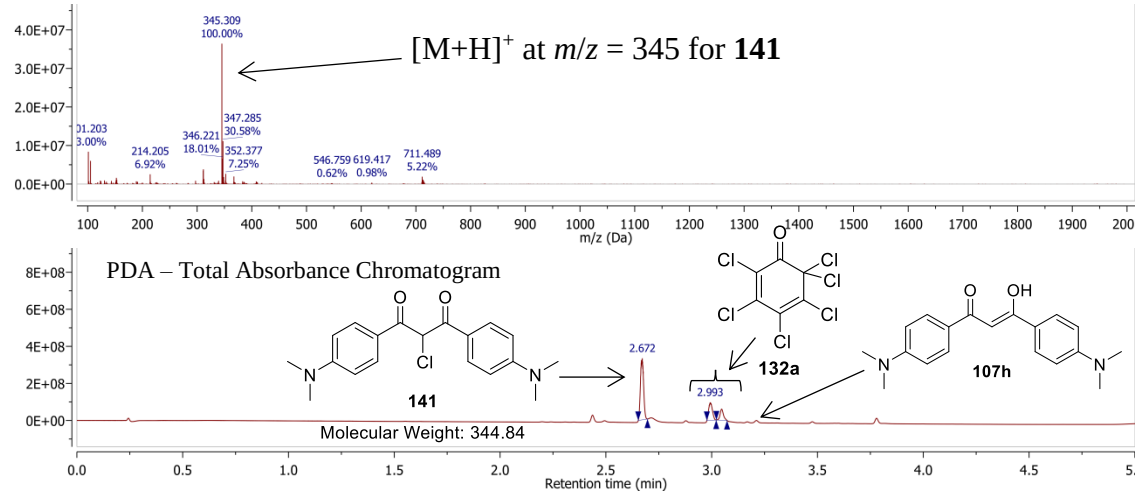

Figure 113: Chlorination of **107h** (3 mM) by polychloroquinone **132a** (3 mM) monitored by LC-MS after 15 min.

The second-order rate constant obtained, $k_2 = 3.69 \times 10^{-1}$ M^{-1} s^{-1}, was used to estimate the *N* parameter for **107h-enol** using **Equation 9**. Assuming an s_N parameter of 0.70 (average of s_N parameters for carbanion forms of 1,3-dicarbonyl derivatives, see **Figure 96**), an *N* parameter of 6.13 was estimated. Enol forms are likely to be far less reactive than enolates. Given that *N* parameters for acyclic 1,3-dicarbonyl derivatives were between 16.03-20.22, the approximate *N* value for **107h-enol** obtained in this section is reasonable. Furthermore, the k_2 value for fluorination of **107h-enol** using Selectfluor™, discussed in Chapter 2, was 7.03×10^{1} M^{-1} s^{-1}. This gives a 191-fold difference with the chlorination rate constant; hence, Selectfluor™ is around 2 orders of magnitude

more reactive than chlorinating reagent **132a** based on kinetics studies with enol **107h**. This is in line with the *E* parameter predicted for Selectfluor™ based on its reactivity with indole **133a** in the previous section.

Unfortunately, it was later learned that it is only possible to derive *N* parameters for new nucleophiles from reactions with reference electrophiles only, that is, the benzhydrilium ions. This will be discussed and explored further in Section 5.7.

5.6 Kinetics of fluorination of malonate esters and enolates of 1,3-dicarbonyls

The carbanion form of diethyl malonate is a nucleophile that has been characterised on the Mayr-Patz scale, with a nucleophilicity parameter, *N*, of 18.24. Based on the synthetic utility of malonate esters as fluorinated building blocks, as discussed in Chapter 1, dimethyl malonate was selected as a nucleophile for investigation in kinetics studies. Dimethyl malonate exists entirely in the dicarbonyl tautomeric form in MeCN (confirmed by ^{1}H NMR spectroscopy in MeCN-d_3). The ^{19}F NMR spectrum of this compound contains a doublet at $\delta = -197$ ppm corresponding to the fluorine atom. The reaction of dimethyl malonate with Selectfluor™ was attempted by varying the conditions including temperature, concentrations, equivalents and reaction time. However, no product peaks corresponding to fluoromalonate **142** were observed in the ^{19}F NMR spectra for each condition tested. **Table 27** lists the different reaction conditions attempted.

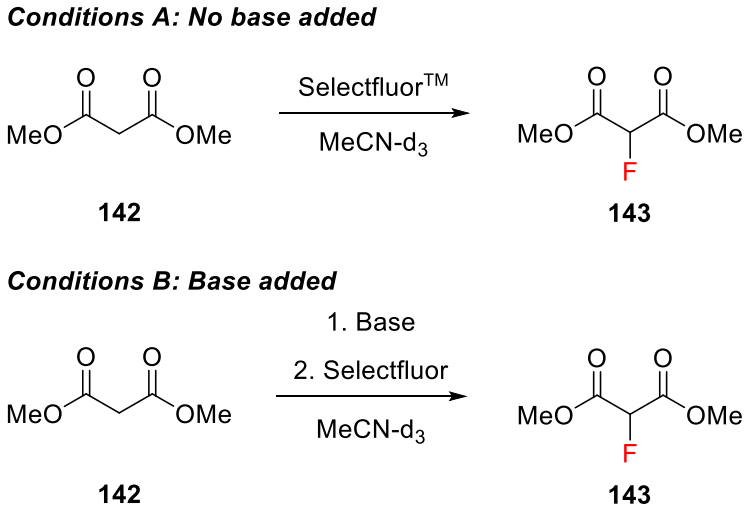

Scheme 42: Conditions A and Conditions B for the fluorination of dimethyl malonate **142** by Selectfluor™.

Since no product peaks were observed in the ^{19}F NMR spectra of the reaction mixtures using relatively mild conditions, harsher conditions were then attempted. The use of microwave conditions has been reported for fluorination of 1,3-dicarbonyl derivatives using Selectfluor™ in MeCN.[113] Microwave heating for 10 min using 10 and 5 equivalents of Selectfluor did not result in any fluoromalonate peaks in the ^{19}F NMR spectra for each reaction. However, after microwave heating for 12 h at 82 °C, a small amount (3%) of dimethyl fluoromalonate **143** was observed by integration of the peaks in the ^{19}F NMR spectrum.

Table 27: Reactions of dimethyl malonate **142** with Selectfluor™, under neutral conditions.

Entry	Reaction conditions	Ratio of [Nuc]:[Elec]	Amount of nucleophile / mmol	Outcome
1	RT for 16 h, then heat at 50 °C for 16 h	10:1	0.4	No reaction
2	RT for 16 h, then heat at 50 °C for 4 h	10:1	0.8	No reaction
3	Microwave, 10 mins, 82 °C	10:1	0.4	No reaction
4	Microwave, 10 mins, 82 °C	5:1	0.4	No reaction
5	Microwave, 12 h, 82 °C	10:1	0.4	3% dimethyl fluoromalonate **143**

The reaction was then attempted under basic conditions (Conditions B, **Scheme 42**). A base was first reacted with dimethyl malonate to form the corresponding enolate. The base and nucleophile were in a 1:1 ratio and were stirred in MeCN-d_3 at room temperature for 30 mins, followed by addition of 0.1 equivalents of Selectfluor™.

The first base to be tested was sodium methoxide, to convert dimethyl malonate into its sodium enolate derivative (**Table 28**, Entry 1). However, sodium methoxide was found to be insoluble in MeCN-d_3. Next, triethylamine was chosen as it is soluble in MeCN-d_3, but there was no observable fluorination by ^{19}F NMR spectroscopy even after heating at 50 °C overnight (Entry 2). The ^{1}H NMR spectrum of a 1:1 mixture of

dimethyl malonate and triethylamine in MeCN-d_3 was obtained, which showed that the dimethyl malonate was still in the dicarbonyl form. The pK_a of dimethyl malonate in DMSO is 15.9,[202] and is predicted to be 28.8 in acetonitrile.[164] The pK_{aH} of triethylamine is 18.5 in MeCN,[203] so it is not basic enough to deprotonate dimethyl malonate to any significant extent.

Next, a stronger base, 1,8-diazabicyclo[5.4.0]undec-7-ene (DBU), was used to deprotonate dimethyl malonate; DBU has a pK_{aH} of 24.3 in MeCN.[203] The reaction gave around 20% fluoromalonate product after 2 h, which was determined by integration of the peaks in the ^{19}F NMR spectrum (Entry 3).

The conditions most commonly reported in the literature for synthesis of fluoromalonates involve the use of NaH in THF. Banks *et al*.[66] reported that diethyl malonate was not attacked by Selectfluor™ under neutral conditions, but its sodium enolate derivative gave the corresponding fluorodiester in 93% yield. This method was then attempted, by stirring dimethyl malonate with NaH in THF for 30 mins before addition of Selectfluor™, pre-dissolved in MeCN-d_3 (Entry 4), where THF and MeCN-d_3 were in a 1:1 ratio. The ^{19}F NMR spectrum of the reaction mixture showed that the reaction was almost complete within 15 min.

Next, the concentrations were reduced 3-fold in order to slow down the reaction; however, after 15 mins, 50% fluoromalonate was formed (Entry 5). Transportation of the NMR tube to the machine, locking and shimming required around 15 mins, therefore, much of this reaction occurred during the dead-time of this NMR method. Thus, the progress of the reaction could not be followed by ^{19}F NMR spectroscopy as the reaction was too rapid. Furthermore, with lower concentrations of the reaction partners, the signals in the ^{19}F NMR spectrum corresponding to the Selectfluor™ N–F peak and the fluorine atom of the fluoromalonate product **143** were very weak and difficult to integrate consistently.

Overall, a range of conditions were tested in order to monitor the reaction of Selectfluor™ with dimethyl malonate by ^{19}F NMR spectroscopy. Milder conditions were ineffective for fluorination of dimethyl malonate. Microwave heating gave small traces of fluoromalonate; however, these conditions were not convenient for monitoring the kinetics of the reaction. The formation of dimethyl fluoromalonate **143** was achieved most efficiently under basic conditions by using NaH in THF. However, this

reaction was too quick to be monitored by NMR and the kinetics of the reaction could not be determined.

Table 28: Reactions of dimethyl malonate **142** with Selectfluor™ in MeCN-d_3, under basic conditions.

Entry	Reaction conditions	Ratio of [Nuc]:[Elec]	Amount of nucleophile / mmol	Outcome
1	NaOMe, MeCN-d_3	10:1	0.5	NaOMe insoluble in MeCN-d_3
2	Et_3N, MeCN-d_3, 50 °C, 16 h	10:1	0.4	No reaction after heating overnight
3	DBU, MeCN-d_3, RT, 2 h	10:1	0.4	20% fluoromalonate **143**
4	NaH, THF, MeCN-d_3, RT, 15 min	10:1	0.4	~80% fluoromalonate **143**
5	NaH, THF, MeCN-d_3, RT, 15 min	10:1	0.13	~50% fluoromalonate **143**

Finally, the fluorination of enolate forms of 1,3-dicarbonyl derivatives using less reactive electrophiles, including NFSI **17** and NFPy TfO^- **12a**, was attempted. The sodium enolate of **107a** was prepared using NaOMe in MeOH-MeCN (**Scheme 43**), before evaporation of the solvent, to give the enolate as a white solid. The structure was confirmed by ^1H NMR spectroscopy and is shown in **Figure 114** (Spectrum 2). Upon dissolution in MeCN-d_3 followed by addition of NFPy TfO^- **12a** (1 equivalent), fluorination of the substrate was not observed by NMR spectroscopy; instead, a return to the keto-enol equilibrium mixture occurred (Spectrum 1). The reaction mixture was monitored by NMR spectroscopy for a further 2 days, but no further changes were observed.

The return to the keto-enol equilibrium was also detected when the nucleophile used was the sodium enolate of dimethyl malonate, as well as with NFSI **17** as the electrophile. This unusual observation is worth noting but further investigations would be required to understand the origin of this effect. The entry of water or residual alcohol

alone are unlikely to have resulted in reprotonation of the enolate, since the enolates themselves were stable for 1 day in MeCN-d_3, which contains residual water.

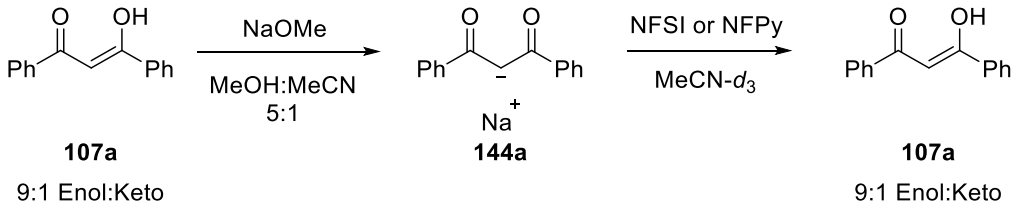

Scheme 43: Synthesis of sodium enolate of **107a** (Step 1) and re-equilibration to the 9:1 enol:keto mixture upon addition of fluorinating reagent (Step 2).

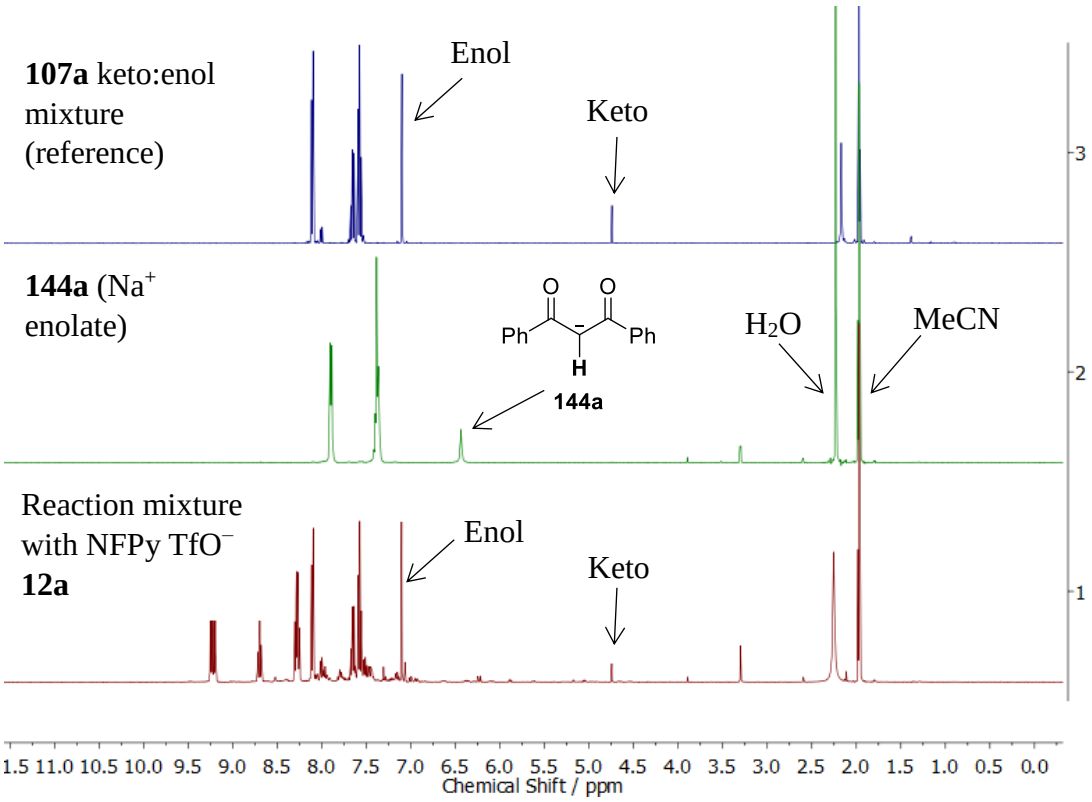

Figure 114: ^{1}H NMR Spectrum 1: reaction mixture containing the products of the reaction between **144a** enolate and NFPy TfO$^-$ **12a**. ^{1}H NMR Spectrum 2: authentic sample of **144a** enolate. ^{1}H NMR Spectrum 3: **107a** 9:1 keto:enol equilibrium mixture as a reference.

5.7 Kinetics studies on the reactions of 1,3-diaryl-1,3-propanedione derivatives with amino-substituted benzhydrilium ions

A collaboration was conducted with Prof. Herbert Mayr to obtain nucleophilicity parameters for sodium and potassium enolates of 1,3-diaryl-1,3-propanedione derivatives (**144a-d** and **145a-d**, **Scheme 44**). This involved using benzhydrilium reference compounds[4] (with known *E* parameters) as the electrophilic reaction partners. The electrophiles used were $(jul)_2CH^+$ **146** and $(dma)_2CH^+$ **147** (**Scheme 44**). The spectrophotometric characteristics of these electrophiles have been previously reported, and their λ_{max} values are known.[204] Additionally, the determination of nucleophilicities of several carbanions, including ketones, β-diketones and β-ketoesters, has previously been conducted in DMSO, where the effects of different counterions (K^+, Na^+, Li^+) on nucleophilic reactivities were investigated.[205] Among the carbanions studied, the *N* parameter for the potassium enolate **145a** was determined (N = 17.46, s_N = 0.65) and product studies were carried out to confirm the structures of the expected products.

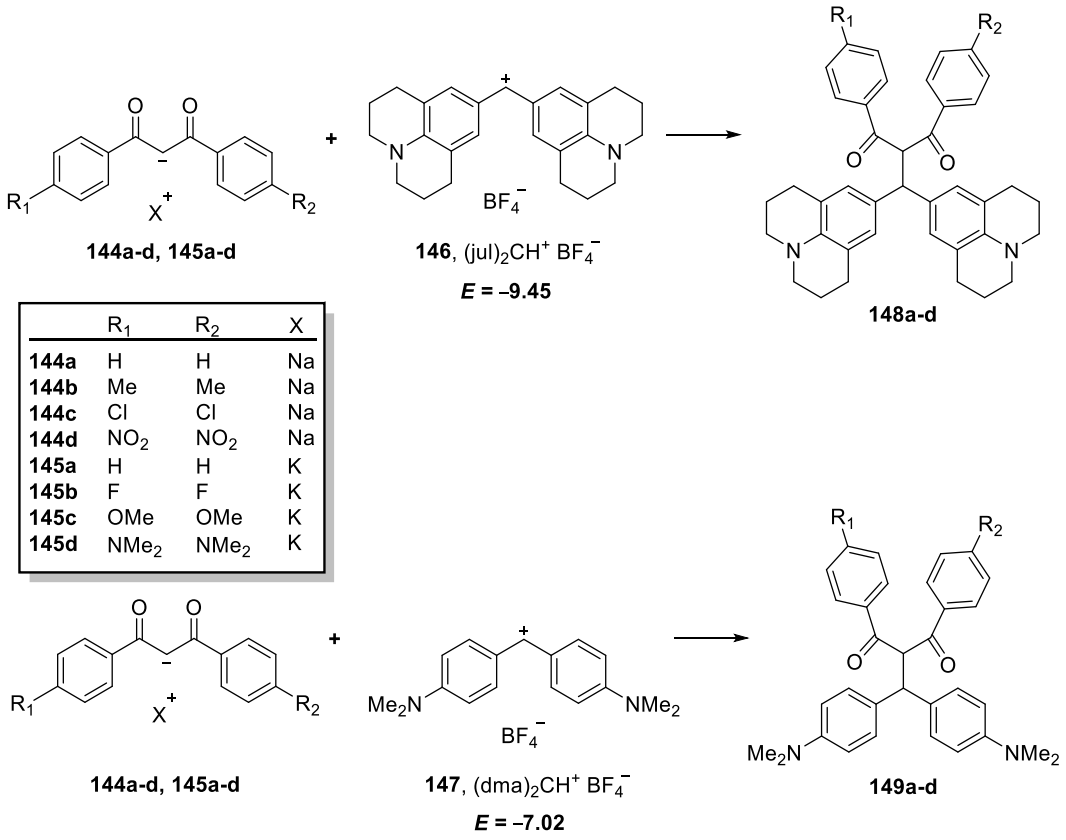

	R_1	R_2	X
144a	H	H	Na
144b	Me	Me	Na
144c	Cl	Cl	Na
144d	NO_2	NO_2	Na
145a	H	H	K
145b	F	F	K
145c	OMe	OMe	K
145d	NMe_2	NMe_2	K

Scheme 44: Nucleophiles (**144a-d**, **145a-d**) and electrophiles (**146**, **147**) used in kinetics experiments in the present work.

[4] Benzhydrilium ions $(jul)_2CH^+$ and $(dma)_2CH^+$ were kindly provided by the Mayr group.

The Na^+ enolates **144a-d** (**Scheme 44**) were synthesised by stirring mixtures of NaOMe and the corresponding 1,3-diaryl-1,3-propanedione **107** at RT for 1 h in MeOH/MeCN (1:1), before evaporation of solvents, to obtain the enolates as yellow solids. The K^+ enolates **145a-d** (**Scheme 44**) were prepared by stirring mixtures of KO^{t}Bu with the corresponding enol **107** for 10 min in EtOH, before evaporation of the solvent. The residues were triturated with Et_2O and dried under vacuum to give the corresponding K^+ enolates as yellow or colourless solids (methods and characterisations are included in the Chapter 8 Section 8.6). Kinetics studies were conducted using stopped-flow UV-vis spectrophotometry, and stock solutions of each reagent were pre-equilibrated to 20 °C in an external water bath. All reactions were carried out in DMSO under pseudo-first-order conditions in the presence of excess enolate. The decrease in absorbance of the benzhydrilium ion was followed: $(jul)_2CH^+$ **146** was monitored at 644 nm, and $(dma)_2CH^+$ **147** was monitored at 616 nm. The choice of DMSO as the solvent was largely due to the low solubilities of the enolates in MeCN, as well as to be consistent with the carbanion study mentioned above.

Some representative examples of spectra obtained are shown below, and all second-order rate constants are summarised in **Table 29**. In many cases, plots of k_{obs} values versus [enolate] displayed large deviations from the origin. This was particularly problematic for reactions involving the more reactive electrophile, $(dma)_2CH^+$ **147** (**Figure 116**). Unfortunately, these preliminary studies indicated that the stopped-flow UV-vis spectrophotometer was not sensitive enough to monitor such rapid reactions, since there were dead-times at the start of reactions where only noise was observed.

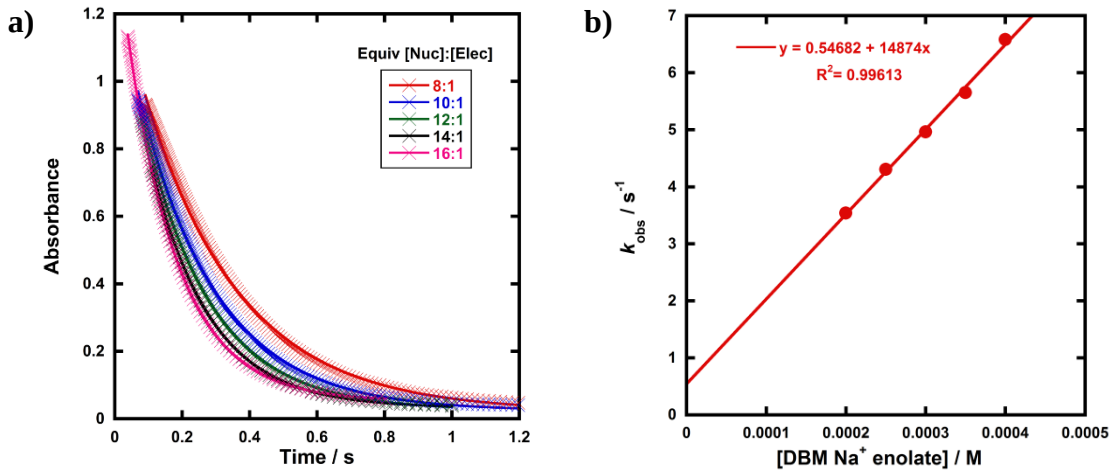

Figure 115: (a) Exponential decays of absorbance of $(jul)_2CH^+$ **146** (0.025 mM) with **144a** (X = Na, R_1 = R_2 = H, 0.2-0.4 mM) in DMSO at 20 °C, at λ_{max} = 644 nm. (b) Correlation of k_{obs} with [**144a**].

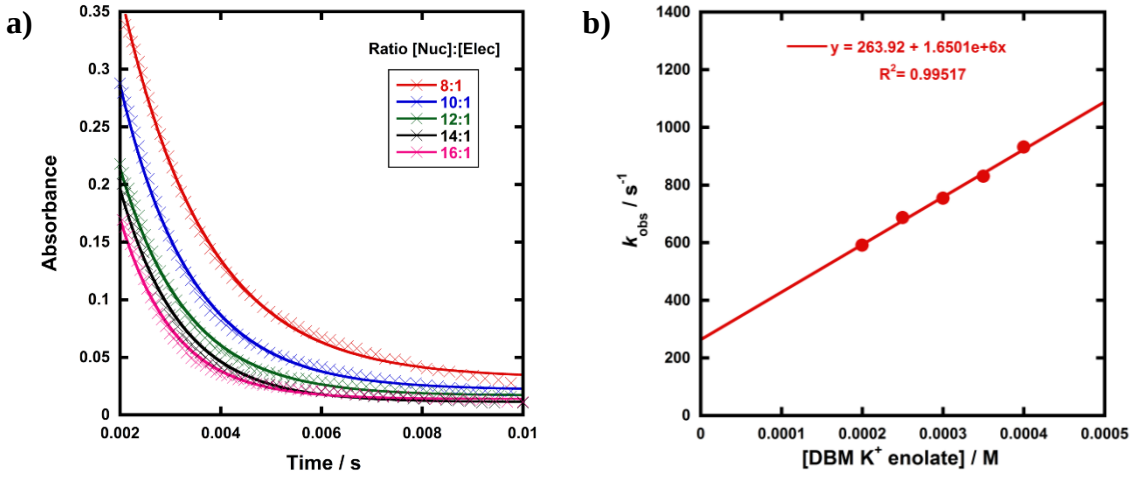

Figure 116: (a) Exponential decays of absorbance of $(dma)_2CH^+$ **147** (0.025 mM) with **145a** (X = K, R_1 = R_2 = H, 0.2-0.4 mM) in DMSO at 20 °C, at λ_{max} = 616 nm. (b) Correlation of k_{obs} with [**145a**].

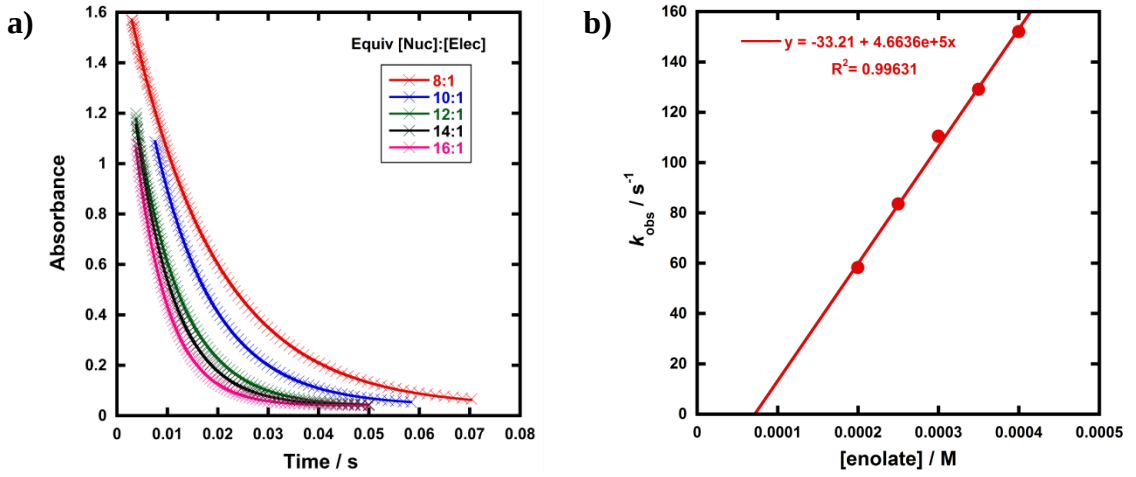

Figure 117: (a) Exponential decays of absorbance of $(jul)_2CH^+$ **146** (0.025 mM) with **145c** (X = K, R_1 = R_2 = OMe, 0.2-0.4 mM) in DMSO at 20 °C, monitored at λ_{max} = 644 nm. (b) Correlation of k_{obs} with [**145c**].

For the reaction involving **145a** (X = K, R_1 = R_2 = H) and $(jul)_2CH^+$ **146**, the second-order rate constant obtained in this work (k_2 = 1.03 × 10^5 M^{-1} s^{-1}) is almost 2-fold lower than that obtained by Mayr *et al.*[205] (k_2 = 1.95 × 10^5 M^{-1} s^{-1}). This is likely due to the lack of temperature control on the stopped-flow apparatus used in the present work, which could have resulted in the discrepancies in rate constants due to temperature differences. Furthermore, the Hammett plots constructed for reactions of **144a-d** and **145a-d** with **146** and **147** show large differences in ρ values, which range from −0.2 to −1.7 (**Figure 118**). Poor correlations are generally observed across the Hammett plots, although for the reactions of **145a-d** with **146** (**Figure 118b**, red), a better correlation was obtained (R^2 = 0.90).

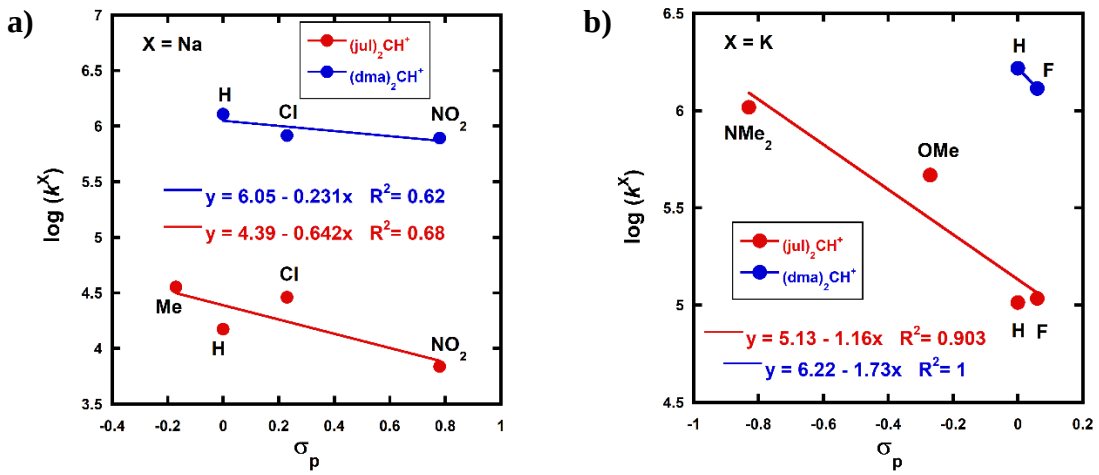

Figure 118: (a) Hammett plots versus σ_p values for reactions of **144a-d** (X = Na) with **146** (red) and **147** (blue)**.** (b) Hammett plots versus σ_p for reactions of **145a-d** (X = K) with **146** (red) and **147** (blue).

Table 29: Summary of second-order rate constants, k_2, for the reactions between enolates **144a-d** and **145a-d** with $(jul)_2CH^+$ **146** and $(dma)_2CH^+$ **147**, in DMSO at 20 °C.

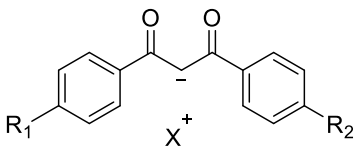

144a-d, 145a-d

Nucleophile	k_2 {$(jul)_2CH^+$} / $M^{-1}\ s^{-1}$	k_2 {$(dma)_2CH^+$} / $M^{-1}\ s^{-1}$	k_2 {$(dma)_2CH^+$} / k_2 {$(jul)_2CH^+$}
144a (Na^+, $R_1 = R_2 = H$)	1.49×10^4	1.28×10^6	86
144b (Na^+, $R_1 = R_2 = Me$)	3.57×10^4	-	-
144c (Na^+, $R_1 = R_2 = Cl$)	2.88×10^4	8.22×10^5	29
144d (Na^+, $R_1 = R_2 = NO_2$)	6.88×10^3	7.82×10^5	114
145a (K^+, $R_1 = R_2 = H$)	1.03×10^5	1.65×10^6	16
145b (K^+, $R_1 = R_2 = F$)	1.08×10^5	1.30×10^6	12
145c (K^+, $R_1 = R_2 = OMe$)	4.66×10^5	-	-
145d (K^+, $R_1 = R_2 = NMe_2$)	1.04×10^6	-	-

Comparing reactions involving nucleophiles with similar reactivities (with H, F, Me and Cl substituents) those with K^+ counterions are approximately one order of magnitude more reactive than those with Na^+ counterions. Finally, the ratios of second-order rate constants for reactions involving $(jul)_2CH^+$ **146** and $(dma)_2CH^+$ **147** vary significantly by 12- to 114-fold (**Table 29**, column 4). Hence, the preliminary data obtained in this section were not of sufficient accuracy or consistency to enable the determination of nucleophilicity parameters.

5.8 Conclusions

This chapter has discussed the different approaches employed to attempt to determine the electrophilicity parameters, *E*, of Selectfluor™ and NFSI using the Mayr-Patz equation. The nucleophiles were chosen based on their reported compatibilities with chlorinating reagent "Cl^+" systems. Unfortunately, 1-morpholinocyclohexene **133i** and silyl enol ether **133c** were unsuitable due to the presence of competing hydrolysis processes, which made monitoring of the fluorination reactions immensely difficult.

By capitalising upon the chromophoric nature of 1-methyl indole **133a**, the kinetics of its fluorination by Selectfluor™ were studied using UV-vis spectrophotometry. Contrasting results were obtained when using single-solvent (MeCN) and dual-solvent (water-MeCN) systems. NMR spectroscopy confirmed the formation of several fluorinated side-products in 2:3 water:MeCN mixtures, although the analogous reaction conducted in 97:3 water:MeCN indicated the formation of 3-fluoro-1-methylindole **136a** with lower quantities of side-products. Using the second-order rate constant obtained from kinetics studies in MeCN via UV-vis spectrophotometry, an estimated value for the electrophilicity parameter of Selectfluor™ was determined to be $E = -5.29$. This value was supported by studies on the chlorination of enol **107h** ($R_1 = R_2 = NMe_2$) by chlorinating reagent **132a**, which found that Selectfluor™ is 1 to 2 orders of magnitude more reactive than **132a** ($E = -6.75$ for **132a** hence $E \sim 5$ for Selectfluor™). The *E* parameter for Selectfluor™ recently determined by Mayr *et al.*[132] from kinetics studies in MeCN with a series of enamines was −5.20. Therefore, the *E* parameter estimated in the present work is in excellent agreement with the value determined by Mayr.

Kinetics studies were conducted on the enolate form of dimethyl malonate **142**, however, reactions with Selectfluor™ were too fast to be monitored by NMR

spectroscopy. Interestingly, no fluorination occurred when NFSI **17** and NFPy TfO^- **12a** were added to the enolate forms of both dimethyl malonate **142** and **107a**. Instead, the return to the keto-enol equilibrium was observed.

Finally, preliminary kinetics experiments were carried out using stopped-flow UV-vis spectrophotometry to study the reactions of benzhydrilium ions with sodium and potassium enolates of 1,3-diaryl-1,3-dicarbonyl derivatives. Due to inconsistencies in measurements, lack of accurate temperature control and extremely high rates of reactions, the completion of kinetics studies was not possible within the timescale of this project. Upon resolution of the aforementioned experimental problems, future work could be conducted on this subject, which will be discussed further in Chapter 7.

Chapter 6: Kinetics of Fluorination of Steroid Enol Acetates

In the previous chapters, it was demonstrated that a quantitative approach towards electrophilic fluorination enables a greater understanding of the reactivities of nucleophilic and electrophilic partners, and the factors that are important for such reactions. Methods were developed using UV-vis spectrophotometry and NMR spectroscopy to directly monitor the kinetics of fluorination reactions. This chapter will discuss the application of these methods to steroid compounds, which are more structurally complex and pharmaceutically-relevant drug-like systems. The primary aim was to determine the applicability of our reactivity scale, discussed in Chapter 2, towards a different class of carbon nucleophiles. Kinetics studies enabled activation parameters, effects of additives and rates of epimerisation to be determined. The final section will discuss the use of fluorine gas for fluorination of the steroid system.

6.1 Introduction

In 1954, Emily Sabo and Josef Fried discovered for the first time that the introduction of a fluorine atom into a medicinally useful compound led to a significant enhancement in its biological activity.[20] They reported syntheses of analogues of hydrocortisone acetate **150a**, a steroid hormone with anti-inflammatory and thymolytic activity, with substitution of the 9-αH atom for an iodine, bromine, chlorine or fluorine atom (**Table 30**). The activity was found to be inversely proportional to the size of the halogen atom, with increases in activity observed only for the chlorinated and fluorinated derivatives relative to the parent compound. The fluorinated derivative **150b** possessed 10.7 times the activity of hydrocortisone acetate **150a**, whereas the chloro-steroid **150c** was only 4 times more active, and the bromo- and iodo-steroids **150d** and **150e** gave decreases in activities.

FDA approval of fludrocortisone **150b** came in 1955 and, to this day, it is prescribed for the treatment of adrenogenital syndrome and postural hypotension. Numerous fluorinated steroids have subsequently been introduced to the marketplace for the treatment of various disease classes.[206] In particular, fluorosteroids bearing a fluorine atom at the 6-position, such as flurandrenolide **151** and fluticasone **152**, continue to be commercially significant (**Figure 119**).

Table 30: Activities of halogenated hydrocortisone derivatives, determined from assays of glycogen from rat liver.[20,207]

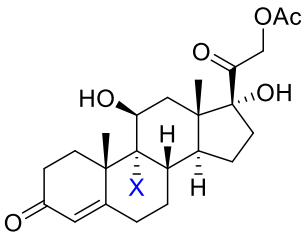

150a-e

Compound	X	Activity
150a	H	1
150b (fludrocortisone)	F	10.7
150c	Cl	4
150d	Br	0.28
150e	I	0.1

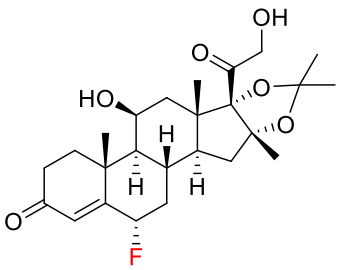

Flurandrenolide, **151**
skin irritation, dermatosis

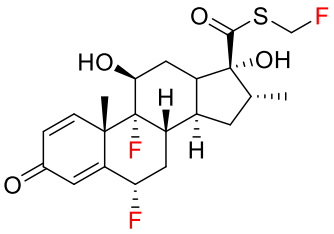

Fluticasone, **152**
nasal inflammation

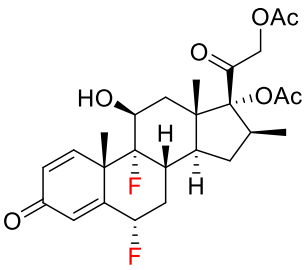

Diflorasone Diacetate, **153**
psoriasis, dermatitis

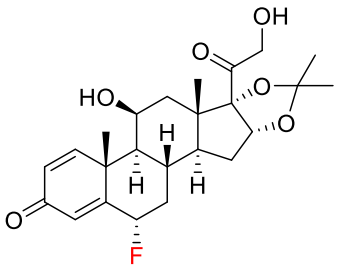

Flunisolide, **154**
nasal inflammation

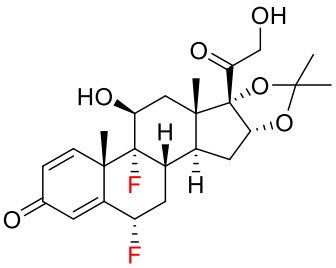

Fluocinolone Acetonide, **155**
skin inflammation

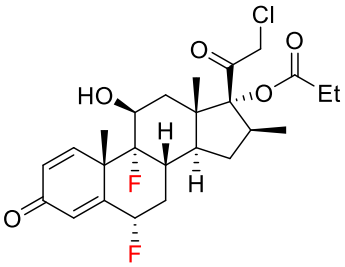

Halobetasol Propionate, **156**
skin inflammation, dermatitis

Figure 119: 6-Fluorocorticosteroid drugs currently on the market.

In early syntheses of fluorinated steroids, the incorporation of a fluorine atom at the 6-position was achieved by oxidation of a double bond to form the 5,6-epoxide, which was opened by a fluoride source, such as $BF_3{\cdot}Et_2O$ (**Scheme 45**).[208–211] The 5-hydroxy group was eliminated to give the 6α-fluorinated 4,5-unsaturated product. This multi-step procedure was inefficient and resource intensive, hence, alternative methods were sought.

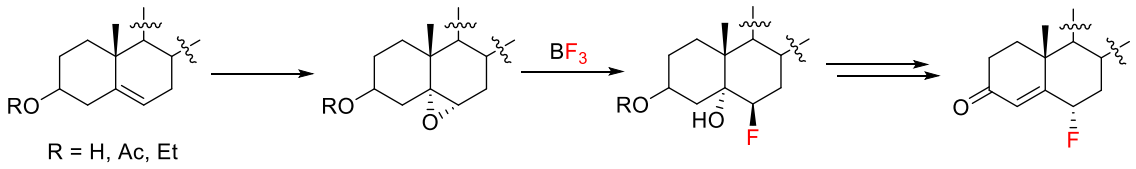

Scheme 45: Preparation of 6α-fluorosteroids via epoxide ring opening with BF_3.

More recent approaches towards the introduction of a fluorine atom at the 6-position involve the reaction of a steroid enolate derivative with an electrophilic fluorinating agent. Early examples of this transformation involved the use of O–F reagents such as perchloryl fluoride (ClO_3F)[212,213] and trifluoroacetyl hypofluorite (CF_3COOF),[214] but due to the toxicities and explosive natures of these reagents, they were not suitable for large scale use.

In the 1990s, electrophilic fluorinating reagents of the N–F class, including *N*-fluoropyridinium salts,[87] NFSI **17**,[215] Selectfluor™ **19**[38] and Accufluor™ **21**,[216] were used for the fluorination of steroid enolate derivatives (**Table 31**). Of these reagents, Selectfluor™ is a bench-stable, non-toxic and selective fluorinating agent that is often used in larger scale applications, for example, in the manufacture of fluticasone **152**, as discussed in Chapter 1. Indeed, 80% of commercially available fluorosteroids are synthesised industrially using Selectfluor™,[69] which is supported by the patent literature.[217–219]

Table 31: Synthesis of 6-fluorosteroids using N−F reagents: NFPy TfO⁻ **12a**, Selectfluor™ **19** and Accufluor™ **21**, as well as the O−F reagent trifluoroacetyl hypofluorite for comparison.

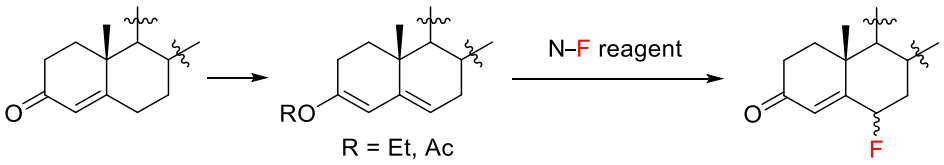

Enol ester	N–F reagent	Yield / % (α : β ratio)
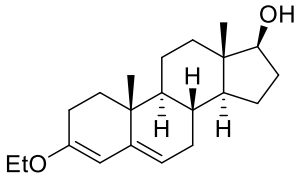	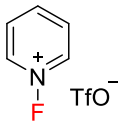 **12a**	72 (1 : 2) (Ref. 87)
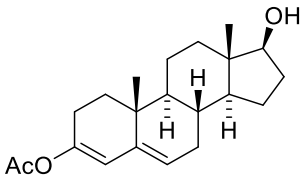	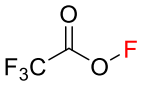	70 (2 : 3) (Ref. 214)
	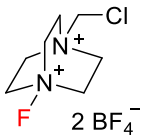 **19**	95 (2 : 3) (Ref. 38)
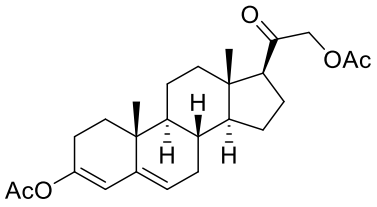	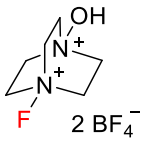 **21**	89 (1 : 2.2) (Ref. 216)

The 6-fluorosteroids are formed as a mixture of α- and β-isomers, where the former is usually the desired isomer due to optimal biological activity. The ratio depends upon the fluorinating reagent employed, steroid structure, temperature and timescale of the reaction. These factors were explored by Herrinton *et al.*[220] who found that Selectfluor™ was the best reagent for fluorination of 3,4-dienol acetates **157-159** (**Table 32**). Fluorination of **157** by NFSI at 40 °C in THF gave the complete consumption of the enol ester, resulting in a mixture of the corresponding α- and β-fluorosteroids in a 5:95 ratio, hence, exhibiting selectivity for the β-fluoro isomer. This contrasted with the other N−F reagents which gave no selectivity, however, the origin of this observation was unknown.

Table 32: Fluorination of enol acetates **157-159** by Selectfluor™ **19**, NFSI **17** and *N*-fluoropyridinium pyridine heptafluorodiborate **160**.

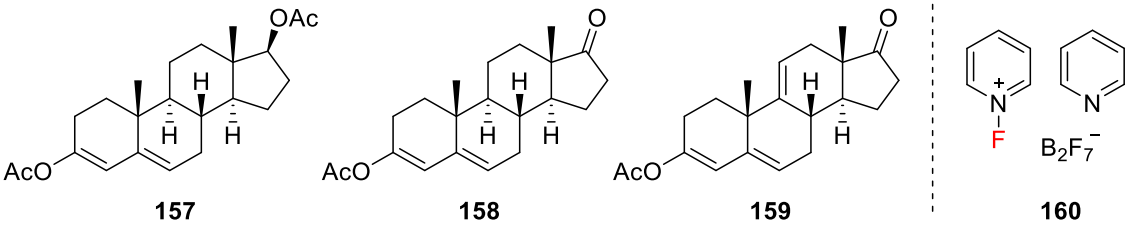

157 **158** **159** **160**

Nucleophile	N−F reagent[a]	Temp / °C	Time / h	α:β[b]	3-keto-4,6-dienone[b]
157	NFPy py $B_2F_7^-$ **160**	40	120	54:15	24
	NFPy py $B_2F_7^-$ **160**	80	3	39:46	8
	NFSI **17**	40	24	5:95	0
	Selectfluor™ **19**	0	3	50:43	0
	Selectfluor™ **19**	80	3	50:32	5
158	NFPy py $B_2F_7^-$ **160**	40	120	54:0	41
	NFPy py $B_2F_7^-$ **160**	80	3	45:5	35
	Selectfluor™ **19**	0	3	44:51	0
	Selectfluor™ **19**	80	3	73:0	24
159	NFPy py $B_2F_7^-$ **160**	40	120	38:37	24
	NFPy py $B_2F_7^-$ **160**	80	3	45:34	11
	Selectfluor™ **19**	0	3	56:43	0
	Selectfluor™ **19**	80	3	45:21	0

[a] Reactions involving NFPy and Selectfluor™ were conducted in MeCN with 1.2 equiv. of N−F reagent. The reaction involving NFSI was conducted in THF with 1.5 equiv. of this reagent. [b] The ratios and amounts of by-products were determined using HPLC and NMR spectroscopy.

The apparent increase in α-fluoro selectivity at different temperatures with *N*-fluoropyridinium pyridine heptafluorodiborate **160** was attributed to the selective dehydrohalogenation of the β-fluoro isomer to form the 3-keto-4,6-dienone product

(**Figure 120**). Both isomers were initially formed in 1:1 ratio but, as reactions progressed, the β-fluoro isomer decreased in concentration while the α-fluoro isomer did not change and the amount of 3-keto-4,6-dienone increased. It was suggested that the elimination of HF from the β-isomer was favoured due to the axial orientation of the fluorine atom. This elimination pathway could have also been promoted by pyridine, which is part of the structure of NFPy py $B_2F_7^-$ **160**, acting as a base.

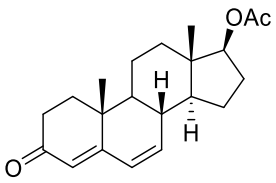

161

Figure 120: 3-Keto-4,6-dienone side-product. The side-product formed during the fluorination of steroid **157** is shown as an example.

The kinetics and process development for the deoxofluorination of a steroid using the nucleophilic fluorinating reagent Deoxo-Fluor™ **41** have been reported for a kilogram-scale reaction, where kinetic models were proposed based on concentration-time profiles obtained from HPLC and online IR analysis for both batch and continuous processes.[221] However, there have been no kinetics studies on the electrophilic fluorination of steroidal enolate systems, although a very recent paper by Nelson *et al.*[222] reported the kinetics of fluorination of enol ester systems based on a tetralone core by Selectfluor™ (**Scheme 46**). The focus of these studies was to establish the mechanistic pathway by which fluorination occurs using Hammett correlations. From their kinetics experiments, it was reported that an S_N2 reaction occurred rather than SET.

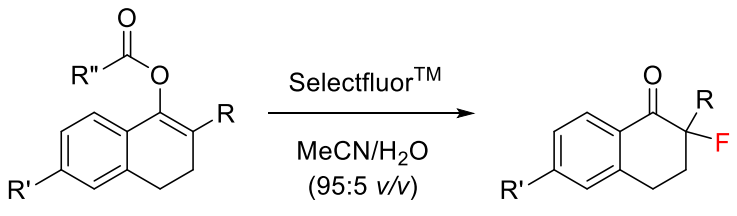

162 **163**

R = H, Br, Ph

R' = H, OMe, OAc, Cl, CO_2Me

R" = Me, Ph

Scheme 46: Fluorination of tetralone derivatives using Selectfluor™ by Nelson *et al.*[222]

In the present work, there appeared to be scope for conducting kinetics experiments on the fluorination of steroids by a range of N−F reagents in order to gain more quantitative information on such reactions. This first required the choice of a suitable steroidal nucleophile. Progesterone enol acetate was thus chosen for kinetics studies since it contains the enolizable α,β-unsaturated ketone system that directs fluorination to the 6-position. This steroid is synthesised in a simple one-step procedure from commercially-available progesterone. Initial experiments were conducted by Dr Antal Harsanyi[223] on the fluorination of progesterone enol acetate using fluorine gas in formic acid, which was qualitatively compared with the analogous fluorination using Selectfluor™ in MeCN-acetone mixtures.

The following sections will discuss the present work on steroid synthesis, kinetics of fluorination by N−F reagents under different conditions, and the relative reactivities of the N−F reagents. Following the establishment of methods for monitoring the kinetics of fluorination of progesterone enol acetate, the studies were extended to three other steroid enol acetate systems, which were prepared from their commercially available starting materials: testosterone, cholestenone and hydrocortisone. The final sections will outline the kinetics of epimerisation of 6β-fluoroprogesterone to the pharmaceutically relevant 6α-fluoroprogesterone, as well as synthetic studies for improving the fluorination of progesterone enol acetate using fluorine gas.

6.2 Synthesis of progesterone enol acetate and fluoroprogesterone

Progesterone enol acetate **165** was synthesised in 65% yield following a modified literature procedure,[224] by heating progesterone **164**, acetyl chloride and acetic anhydride at 100 °C for 1 hour (**Scheme 47**). The structure was confirmed using ^{1}H and ^{13}C NMR spectroscopy, where all peaks were in agreement with previously reported values,[225] and the X-ray crystal structure (**Figure 121**) was also determined. The fluorination of **165** was conducted using Selectfluor™ to obtain authentic samples of both isomers of 6-fluoroprogesterone **166**, adopting a previously described method (**Scheme 47**).[38] A mixed solvent system of MeCN and acetone was required due to the low solubility of **165** in MeCN, the commonly used solvent for fluorination reactions, and the low solubility of Selectfluor™ in acetone. Following aqueous work-up, the ratio of **166-α** to **166-β** was 1:2, as identified by integration of peaks in the ^{19}F NMR spectrum (−184 ppm and −165 ppm, respectively, in MeCN-d_3, quantitative NMR parameters were used). The reaction proceeded very cleanly with no side-products

observed. The isolation of pure samples of 6α-fluoroprogesterone (**166-α**) and 6β-fluoroprogesterone (**166-β**) was achieved using column chromatography.

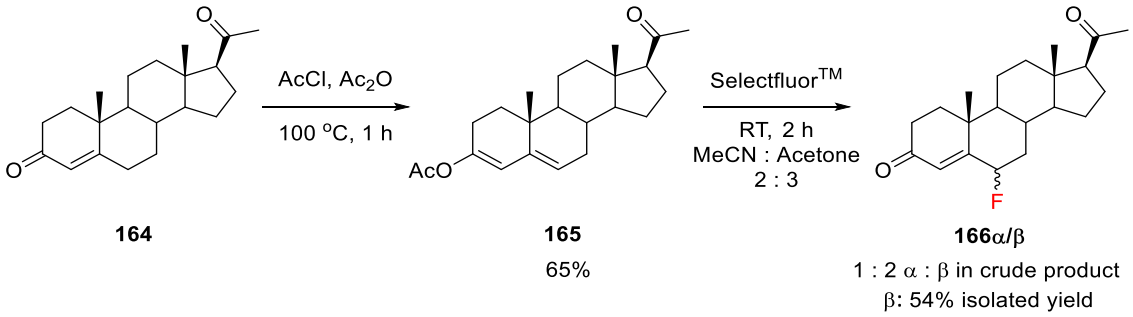

Scheme 47: Synthesis of progesterone enol acetate **165** from progesterone **164**, followed by fluorination of **165** using Selectfluor™ to afford 6-fluoroprogesterone **166** as a mixture of α and β isomers in a 1:2 ratio.

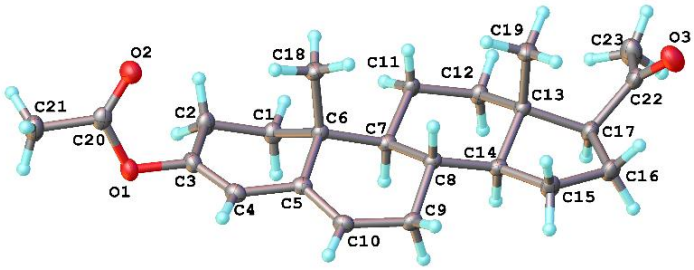

Figure 121: X-ray crystal structure for progesterone enol acetate **165**.

6.3 Kinetics of fluorination of progesterone enol acetate by N−F reagents

6.3.1 Fluorination via Selectfluor™, diCl-NFPy TfO^-/BF_4^- and pentaCl-NFPy TfO^-

Kinetics studies were conducted on the fluorination of progesterone enol acetate **165** by Selectfluor™ in MeCN using UV-vis spectrophotometry. Although the fluorination of **165** discussed in Section 6.2 was carried out in MeCN-acetone mixtures to maximise the solubilities of the reaction partners, solubility was not an issue at the low concentrations used in UV-vis studies. Hence, kinetics studies discussed in this section were conducted in MeCN only, to be consistent with those reported in previous chapters. Additionally, the UV-vis spectrum of HPLC grade acetone contained broad absorbance bands at 200-250 nm, likely due to the stabilisers present and transitions associated with the C=O bond that occur in this region, so was not suitable for kinetics

studies conducted by UV-vis spectrophotometry as the absorbance bands of **165** were masked.

Selectfluor™ is non-chromophoric whereas the UV-vis spectrum of **165** has an absorbance band at λ_{max} = 235 nm (**Figure 122**). The absorbance bands of α- and β-fluoroprogesterone occur at λ_{max} = 233 nm and λ_{max} = 232 nm, respectively. Extinction coefficients for each species were determined using the Beer-Lambert law and are summarised in **Table 33** (for all UV-vis spectra see Chapter 8 Section 8.7.5).

Table 33: Extinction coefficients for progesterone enol acetate **165**, α-fluoroprogesterone **166-α** and β-fluoroprogesterone **166-β** in MeCN.

Steroid	λ_{max} / nm	ε / mol^{-1} dm^3 cm^{-1}
Progesterone enol acetate **165**	235	19466
α-Fluoroprogesterone **166-α**	233	16022
β-Fluoroprogesterone **166-β**	232	12764

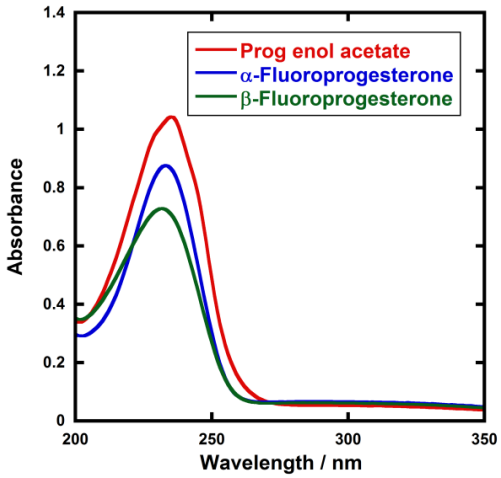

Figure 122: UV-vis spectra corresponding to progesterone enol acetate **165** (red line), **166-α** (blue line) and **166-β** (green line) in MeCN.

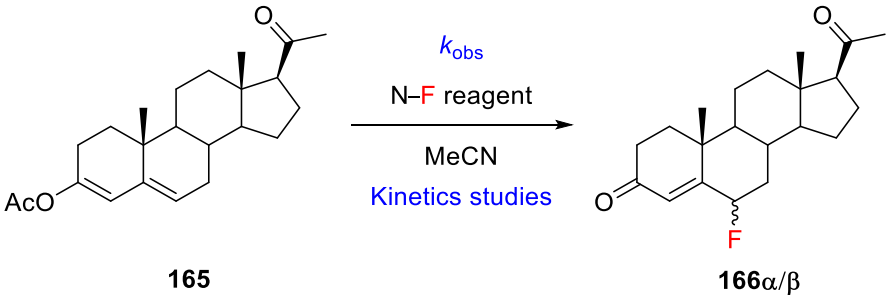

165 **166α/β**

Scheme 48: Kinetics studies on fluorination of progesterone enol acetate **165** by N−F reagents in MeCN at controlled temperatures.

The absorbance of progesterone enol acetate **165** was monitored during the fluorination reactions (**Scheme 48**). All kinetics experiments were carried out with excess Selectfluor™ to achieve pseudo-first order conditions. Clean exponential decays of absorbance of the nucleophile were observed in all runs (**Figure 123a**), and the first-order rate constants k_{obs} were obtained from the fitting of plots of absorbance versus time (for individual k_{obs} values see Chapter 8 Section 8.7.6). When k_{obs} values were plotted against Selectfluor™ concentration, a first order correlation was observed (**Figure 123b**). The direct dependence upon the concentration of Selectfluor™ demonstrates rate-limiting fluorination, thus, the slope of this graph gave the second-order rate constant k_2 [M^{-1} s^{-1}] according to the second-order rate **Equation 29**.

$$\text{Rate} = -\frac{\mathrm{d}[\mathbf{165}]}{\mathrm{dt}} = k_2[\mathbf{165}][\text{NF reagent}] \qquad (\mathbf{29})$$

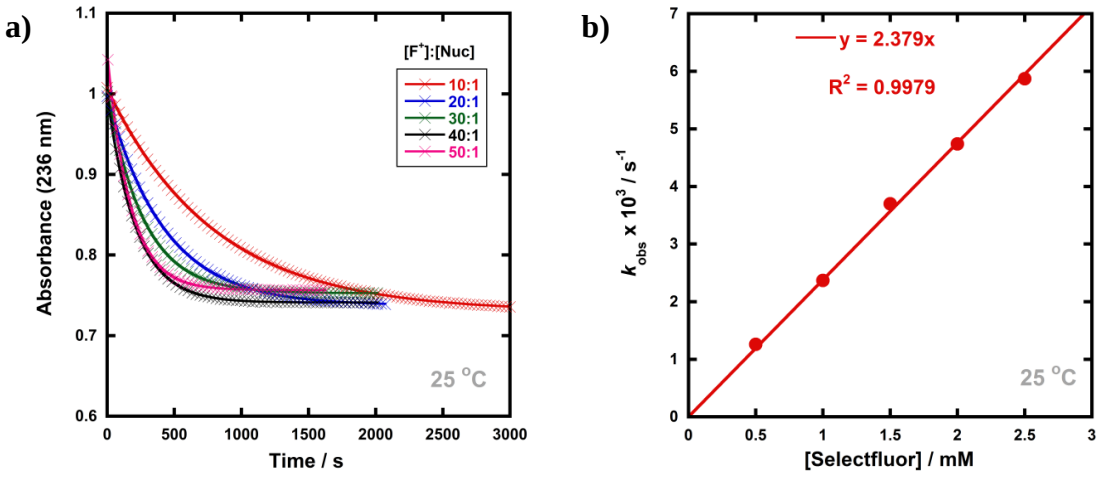

Figure 123: (a) Exponential decays of absorbance of **165** (0.05 mM) with different concentrations of Selectfluor™ in MeCN at 25 °C. (b) Correlation of k_{obs} with [Selectfluor™].

Following the establishment of the UV-vis method with Selectfluor™, the kinetics of fluorination of **165** using other N−F reagents were studied. Since *N*-fluoropyridinium salts are chromophoric, in contrast to Selectfluor™, some alterations of the method were necessary. Due to the presence of broad absorbance bands between 200-240 nm in the UV-vis spectra of diCl-NFPy TfO^- **50a** and diCl-NFPy BF_4^- **50b**, the absorbance of **165** was masked when using large concentrations of the fluorinating reagent. Therefore, the absorbance band of diCl-NFPy TfO^-/BF_4^- (**50a/b**) at λ_{max} = 288 nm was monitored instead, with an excess of **165**, which did not mask the absorbance band at 288 nm, (**Figure 124a**). Similarly, the UV-vis spectrum for pentalCl-NFPy TfO^- **51a** has an absorbance band at λ_{max} = 320 nm (**Figure 124b**), which was monitored in kinetics experiments.

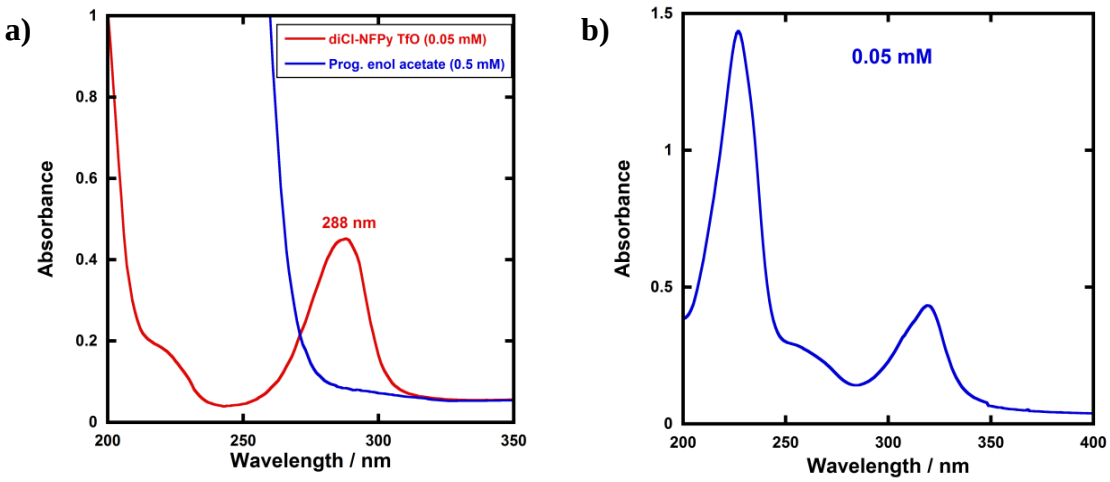

Figure 124: (a) UV-vis spectrum for diCl-NFPy TfO^- **50a** (0.05 mM, red line) and progesterone enol acetate **165** (0.50 mM, blue line) in MeCN, replicating the typical concentrations used in kinetics runs. (b) UV-vis spectrum for a solution of pentaCl-NFPy TfO^- **51a** (0.05 mM) in MeCN.

Kinetics experiments were conducted using excess **165** giving clean exponential decays of absorbance of N−F reagent in all runs (**Figures 125-127**). When k_{obs} values were plotted against the concentration of **165**, first order correlations were, again, observed and the second-order rate constants k_2 were determined from the slopes. All k_2 values are summarised in Section 6.3.3 (**Table 34**), and all k_{obs} values are included in Chapter 8 Section 8.7.6. Product analyses of selected runs were carried out for the reactions of each N−F reagent by LC-MS, as well as by ^{19}F and ^{1}H NMR spectroscopic analysis, to confirm the clean formation of the expected products.

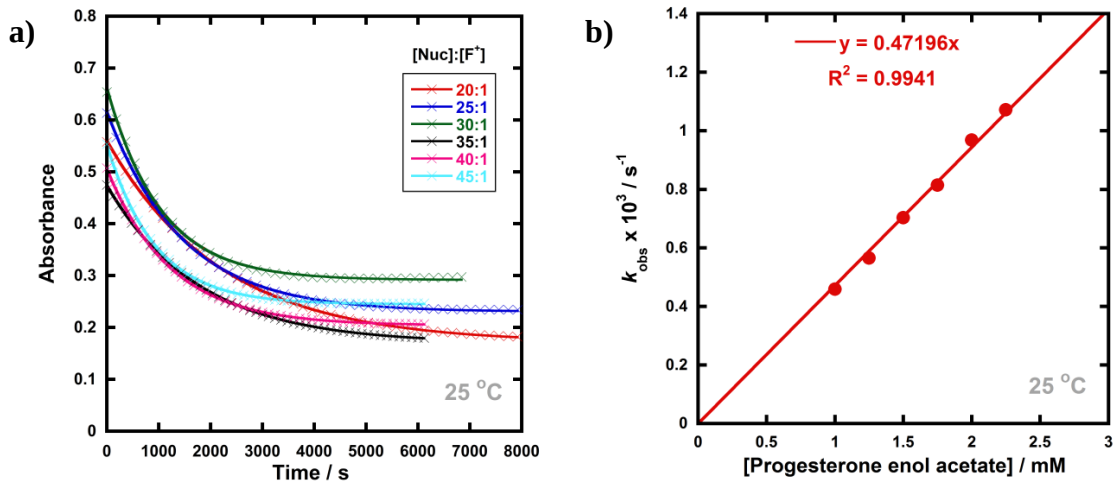

Figure 125: (a) Exponential decays of absorbance of diCl-NFPy TfO^- **50a** (0.05 mM) with different concentrations of **165** in MeCN at 25 °C. (b) Correlation of k_{obs} with [**165**].

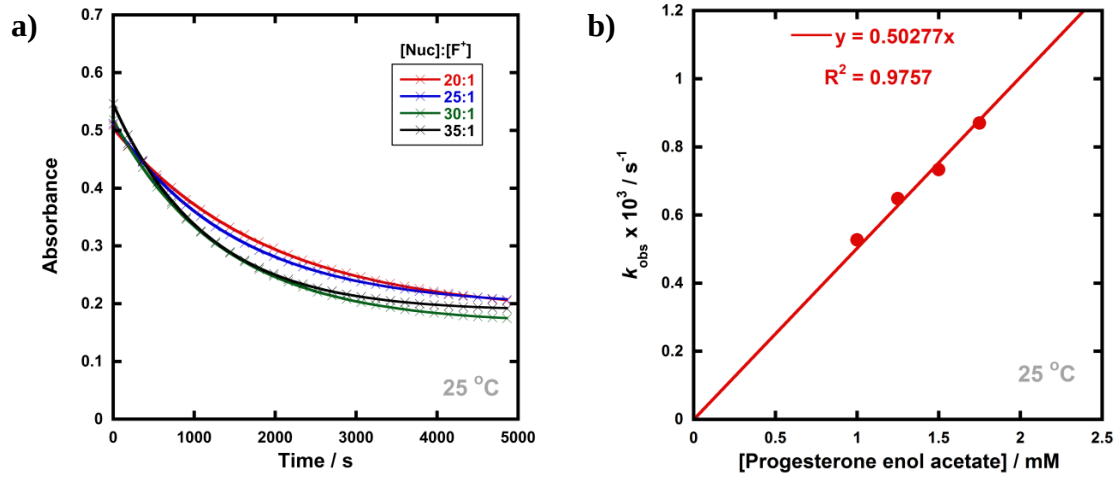

Figure 126: (a) Exponential decays of absorbance of diCl-NFPy BF_4^- **50b** (0.05 mM) with different concentrations of **165** in MeCN at 25 °C. (b) Correlation of k_{obs} with [**165**].

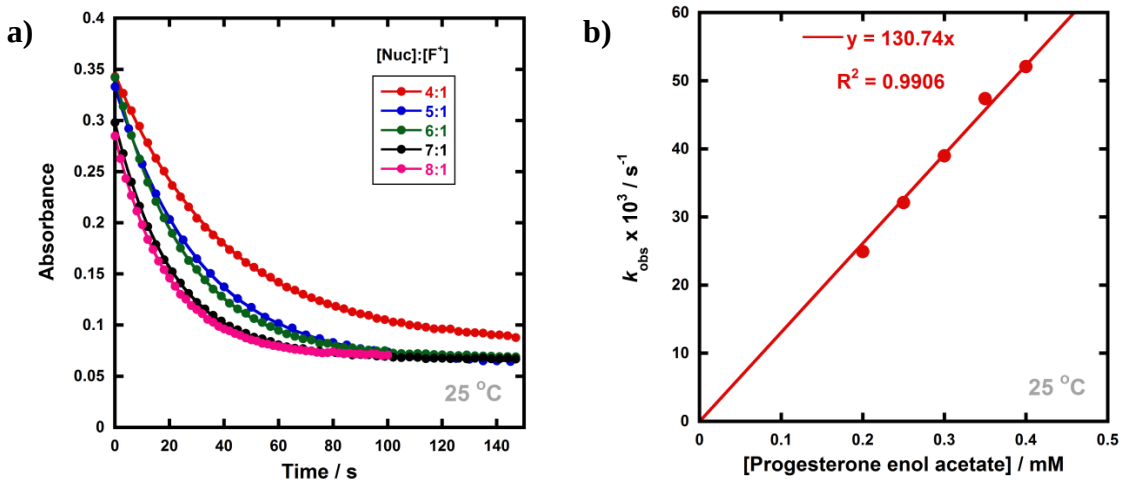

Figure 127: (a) Exponential decays of absorbance of pentaCl-NFPy TfO$^-$ **51a** (0.05 mM) with different concentrations of **165** in MeCN at 25 °C. (b) Correlation of k_{obs} with [**165**].

6.3.2 Fluorination via NFSI, NFPy TfO$^-$ and triMe-NFPy TfO$^-$

The fluorination of progesterone enol acetate **165** by NFSI **17**, *N*-fluoropyridinium triflate **12a** and 2,4,6-trimethyl-*N*-fluoropyridinium triflate **52a** were too slow to be monitored using the UV-vis method. Hence, they were studied by quantitative ^{1}H NMR spectroscopy, where the use of higher concentrations of reaction partners was expected to afford higher observed rates that could be monitored on a more reasonable timescale. All kinetics experiments were carried out with excess N−F reagent in MeCN-d_3 at 25 °C to achieve pseudo-first order conditions (steroid **165** was not used in excess due to its relatively low solubility in MeCN-d_3 compared to the N−F reagents). In the case of NFSI, reactions were monitored discontinuously over the course of 1 day (**Figure 128**). The peaks at δ = 5.67 ppm and δ = 5.41 ppm correspond to C**6**H and C**4**H, respectively, of **165**. The doublet of triplets at δ = 5.05 ppm and the doublet at δ = 5.87 ppm are associated with C**6**H and C**4**H, respectively, of **166-β**. The doublet of doublet of doublets at δ = 5.20 ppm and the peak at δ = 5.92 ppm correspond to C**6**H and C**4**H, respectively, of **166-α**.

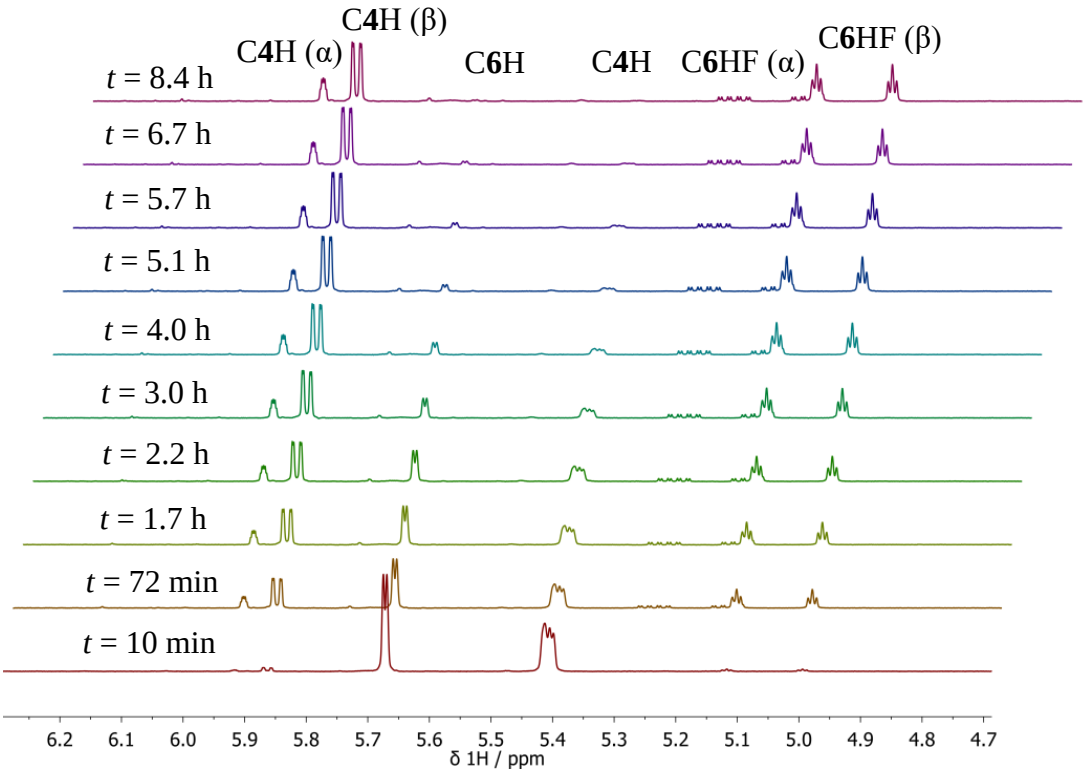

Figure 128: Fluorination of **165** by NFSI in MeCN-d_3 at 25 °C, monitored by ^{1}H NMR spectroscopy. Quantities used were [**165**] = 17.5 mM, [NFSI] = 526.0 mM. Peaks corresponding to **165** are labelled as C**6**H and C**4**H. Peaks associated with **166-α** and **166-β** are also labelled.

The signals corresponding to C**6**H of **165**, **166-α** and **166-β** were each integrated over the course of the reactions and the relative peak integrals gave exponential behaviours. **Figure 129a** shows the decreases in integrals of C**6**H of **165** over the course of 1 day. The k_{obs} values were obtained from the fitting of plots of integral intensities versus time and second-order rate constants, k_2, were obtained from plots of k_{obs} against concentration of the N−F reagent. The k_2 values for consumption of **165** (**Figure 129b**) and appearance of **166-β** (**Figure 130a**) and **166-α** (**Figure 130b**) gave similar values of 3.33×10^{-4} M^{-1} s^{-1}, 3.31×10^{-4} M^{-1} s^{-1} and 3.42×10^{-4} M^{-1} s^{-1}, respectively.

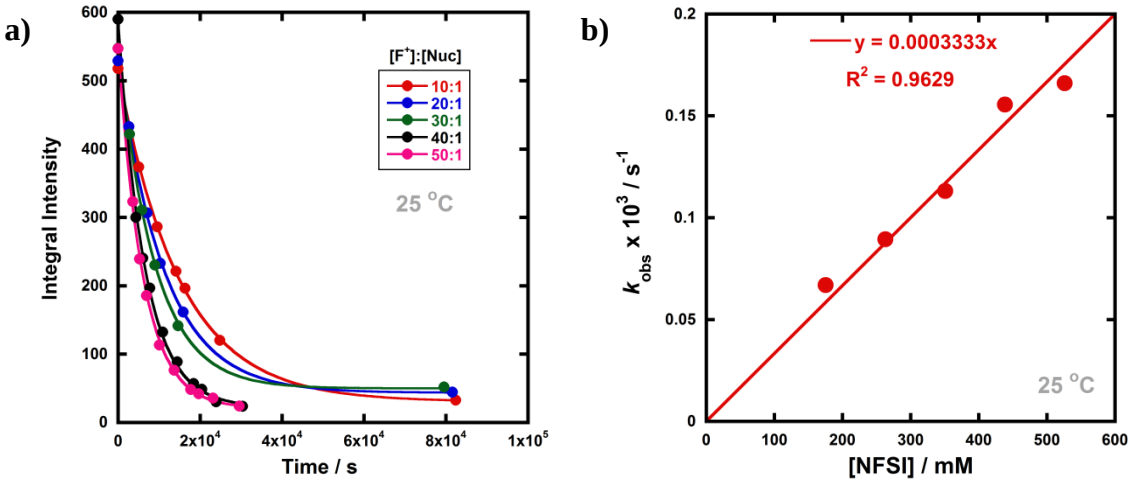

Figure 129: (a) Exponential decays of integral intensity of **165** with different concentrations of NFSI in MeCN-d_3 at 25 °C. (b) Correlation of k_{obs} with [NFSI].

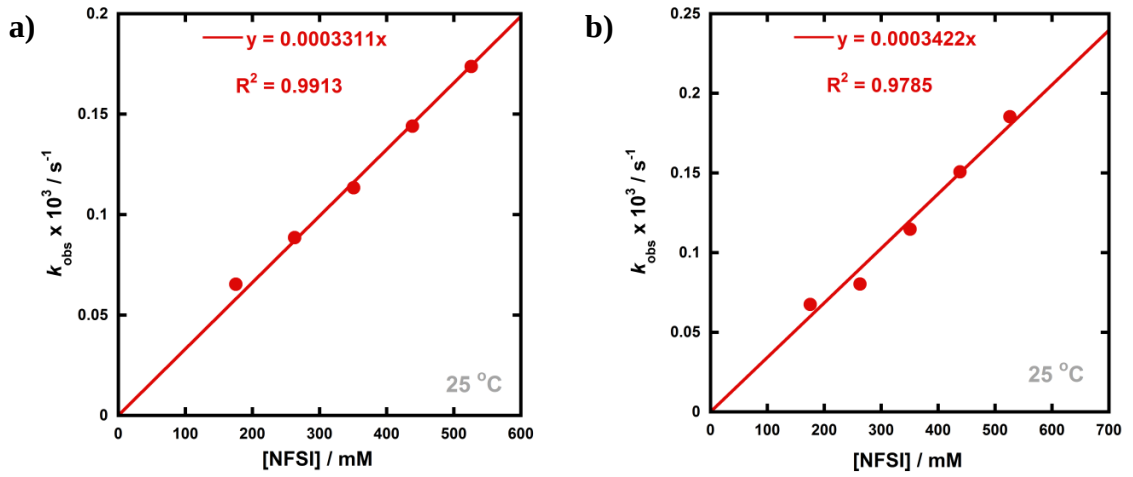

Figure 130: Plots of k_{obs} versus [NFSI], where the k_{obs} values were obtained from integrals of peaks corresponding to (a) 6-β-fluoroprogesterone **166-β** and (b) 6-α-fluoroprogesterone **166-α**.

The kinetics of fluorination of **165** by NFPy TfO$^-$ **12a** (**Figure 131**) and triMe-NFPy TfO$^-$ **52a** (**Figure 132**) were determined via the same method. Reactions were monitored discontinuously by ^{1}H NMR spectroscopy until the end-points were reached: up to 9 days for NFPy TfO$^-$ **12a** and up to 3 weeks for triMe-NFPy TfO$^-$ **52a**. The second-order rate constants, k_2, obtained for each reagent are summarised in the next section, and individual k_{obs} values are reported in Chapter 8 Section 8.7.6.

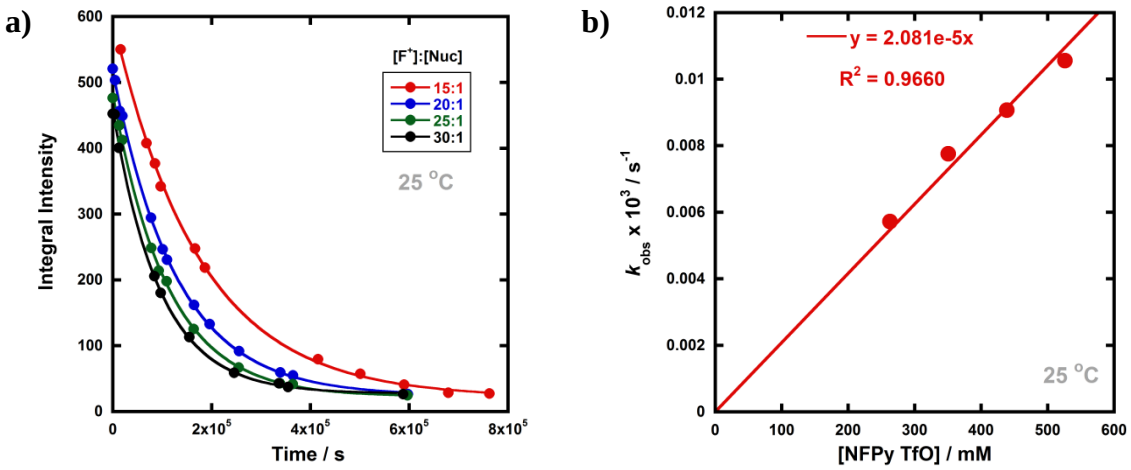

Figure 131: (a) Exponential decays of integral intensity of **165** with different concentrations of NFPy TfO$^-$ **12a** in MeCN-d_3 at 25 °C. (b) Correlation of k_{obs} with [NFPy TfO$^-$].

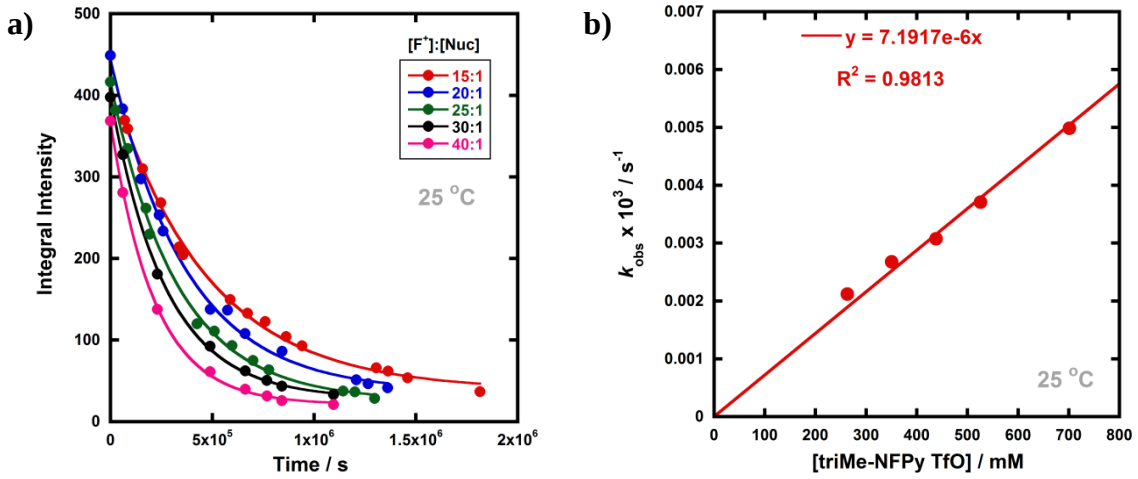

Figure 132: (a) Exponential decays of integral intensity of **165** with different concentrations of triMe-NFPy TfO$^-$ **52a** in MeCN-d_3 at 25 °C. (b) Correlation of k_{obs} with [triMe-NFPy TfO$^-$].

6.3.3 Kinetics of fluorination of enol acetate forms of testosterone, cholestenone and hydrocortisone

Following the establishment of methods for monitoring the kinetics of fluorination of progesterone enol acetate **165** in the previous sections, other steroid enol acetate systems were then studied (**Scheme 49**). Testosterone enol diacetate **167**, cholestenone enol acetate **168**, hydrocortisone enol tetraacetate **169** and their fluorinated derivatives were synthesised by Ben J. Murray using the same procedures as progesterone (see Chapter 8 Section 8.7.4). The UV-vis spectra for compounds **167-169** each contain an absorbance band at λ_{max} = 235 nm (**Figure 133**).

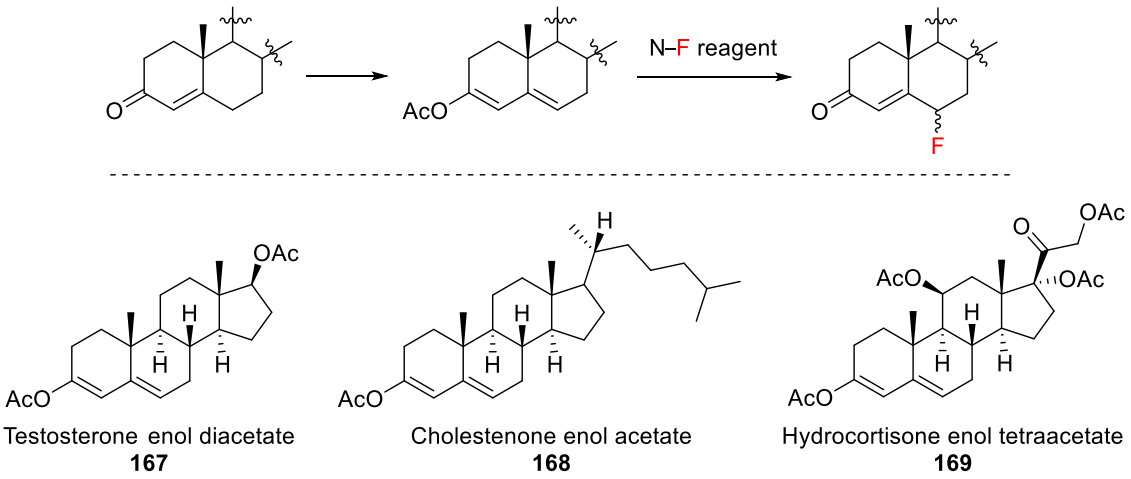

Scheme 49: Synthesis of enol acetates **167**-**169** from testosterone, cholestenone and hydrocortisone, respectively. Kinetics of fluorination of enol acetates **167**-**169** using N−F reagents to obtain the corresponding 6-fluorosteroids as mixtures of α and β isomers.

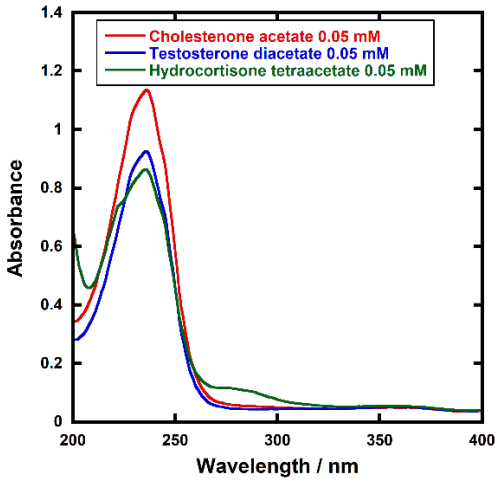

Figure 133: Reference UV-vis spectra for steroids **167**-**169** in MeCN.

Kinetics studies were conducted on the fluorination of steroid enol acetates **167**-**169** using similar procedures as those discussed in Section 6.3.1. The k_2 values are reported in **Table 34**, as well as those of **165**. All spectra relating to kinetics studies on fluorination of **167**-**169** are included in Chapter 8 Section 8.7.6. Relative rate constants (k_{rel}) were determined using **Equation 6** (from Chapter 2)**,** with Selectfluor™ as the reference electrophile, thus enabling a comparison of reactivities (**Table 34**). The reactivity differences match those discussed in Chapter 2 for fluorination of enolic 1,3-dicarbonyl systems **107** by the N−F reagents. Detailed comparisons of the reactivity differences will be made in Section 6.3.4.

$$k_{\text{rel}} = \frac{k_2(\text{NF reagent})}{k_2(\text{Selectfluor}^{\text{TM}})} \qquad (\mathbf{6})$$

Table 34: Summary of rate constants (k_2) for the fluorination of enol acetates **165** and **167-169** by N−F reagents in MeCN or MeCN-d_3 at 25 °C, and k_{rel} values calculated using **Equation 6**.

Nucleophile	Electrophile	k_2 / M^{-1} s^{-1}	k_{rel}
Progesterone enol acetate **165**	Selectfluor™ **19**	2.38	1.0
	NFPy TfO^- **12a**	2.08×10^{-5}	1.1×10^{-5}
	NFSI **17**	3.33×10^{-4}	2.2×10^{-4}
	diCl-NFPy TfO^- **50a**	4.72×10^{-1}	2.5×10^{-1}
	diCl-NFPy BF_4^- **50b**	5.03×10^{-1}	1.8×10^{-1}
	pentaCl-NFPy TfO^- **51a**	1.31×10^{2}	4.2×10^{1}
	triMe-NFPy TfO^- **52a**	7.19×10^{-6}	2.1×10^{-6}
Testosterone enol diacetate **167**	Selectfluor™ **19**	2.11	1.0
	diCl-NFPy TfO^- **50a**	4.41×10^{-1}	2.1×10^{-1}
	pentaCl-NFPy TfO^- **51a**	1.42×10^{2}	6.7×10^{1}
Cholestenone enol acetate **168**	Selectfluor™ **19**	3.18	1.0
	pentaCl-NFPy TfO^- **51a**	1.94×10^{2}	6.1×10^{1}
Hydrocortisone enol tetraacetate **169**	Selectfluor™ **19**	1.06	1.0
	pentaCl-NFPy TfO^- **51a**	5.54×10^{1}	5.2×10^{1}

The nucleophilic reactivities of enol acetates **165** and **167**-**169** were assessed using the k_{rel}'' values defined by **Equation 30**, which were determined using the second-order rate constants, k_2, summarised in **Table 34**. The k_{rel}'' values are reported in **Table 35**. Unsurprisingly, the reactivity differences across the four compounds are small. Progesterone enol acetate **165** and testosterone enol diacetate **167** have, on average, very similar reactivities. Cholestenone enol acetate **168** is, on average, 1.4-fold more reactive than **165**, and hydrocortisone enol tetraacetate **169** is 2.3-fold less reactive than

165. Since the major structural change across this range of steroids is the substituent at the C-17 position, this appears to have a small effect on the nucleophilicities. The electron-withdrawing acetate groups in **169** are likely to result in reduced nucleophilicity of this compound, whereas the inductive electron-donating alkyl chain at the C-17 position of **168** increases its nucleophilicity.

$$k_{\mathrm{rel}}'' = \frac{k_2(\text{steroid enol acetate})}{k_2(\text{progesterone enol acetate } \mathbf{165})} \qquad (\mathbf{30})$$

Table 35: Comparison of reactivities of steroid enol acetates **165** and **167**-**169** using k_{rel}'' values defined by **Equation 30** determined using the k_2 values summarised in **Table 34**.

Nucleophile	k_{rel}''		
	Selectfluor™ **19**	diCl-NFPy TfO^- **50a**	pentaCl-NFPy TfO^- **51a**
Progesterone enol acetate **165**	1.0	1.0	1.0
Testosterone enol diacetate **167**	0.89	0.93	1.08
Cholestenone enol acetate **168**	1.34	-	1.48
Hydrocortisone enol tetraacetate **169**	0.45	-	0.42

6.3.4 Comparison of reactivities of the N−F reagents

Using the absolute rate constants (k_2) obtained from kinetics studies described in Sections 6.3.1 and 6.3.2 for the fluorination of progesterone enol acetate **165**, summarised in **Table 34**, relative rate constants (k_{rel}) were calculated using **Equation 6** with Selectfluor™ as the reference electrophile.

The reactivities match those determined in Chapter 2 for fluorinations of 1,3-dicarbonyl derivatives **107a-m** by N−F reagents. The k_{rel} values for **107d-enol** (R_1 = R_2 = OMe), which has the most extensive dataset for each fluorinating reagent, are listed in **Table 36** to enable direct comparisons. The k_{rel} values of **165** and **107d** for each N−F reagent are in excellent agreement, with differences of only 0.6 to 1.4-fold (**Table 36**, column 4). This reinforces the predictive nature of the reactivity scale.

Table 36: Summary of k_{rel} values determined with **Equation 6** using rate constants (k_2) for the fluorination of progesterone enol acetate **165** by N−F reagents in MeCN or MeCN-d_3 at 25 °C. The k_{rel} values for 1,3-dicarbonyl **107d** obtained in Chapter 2 are included for comparison. Comparisons of the k_{rel} values for the substrates with each fluorinating reagent are shown.

Electrophile	k_{rel} (**165**)	k_{rel} (**107d**)	k_{rel} (**165**) / k_{rel} (**107d**)
Selectfluor™ **19**	1.0	1.0	1.0
NFPy TfO$^-$ **12a**	8.7×10^{-6}	1.1×10^{-5}	0.8
NFSI **17**	1.4×10^{-4}	2.2×10^{-4}	0.6
diCl-NFPy TfO$^-$ **50a**	2.0×10^{-1}	2.5×10^{-1}	0.8
diCl-NFPy BF_4^- **50b**	2.1×10^{-1}	1.8×10^{-1}	1.2
pentaCl-NFPy TfO$^-$ **51a**	5.5×10^{1}	4.2×10^{1}	1.3
triMe-NFPy TfO$^-$ **52a**	3.0×10^{-6}	2.1×10^{-6}	1.4

6.3.4 Comparison of reactivities of progesterone enol acetate 165 and enols 107a-h

The nucleophilic reactivity of progesterone enol acetate **165** was compared with those of the 1,3-dicarbonyl derivatives **107a-h** discussed in Chapter 2, using the second-order rate constants, k_2, for fluorination of these substrates by Selectfluor™ and NFSI. These two N−F reagents were selected for this comparison since they show markedly different reactivities, as well as having the most extensive datasets for fluorination kinetics. Using **Equation 31**, k_{rel}''' is defined as the k_2 value for fluorination of a nucleophile divided by the k_2 value for fluorination of **107a-enol** (R_1 = R_2 = H).

$$k_{rel}''' = \frac{k_2(\text{nucleophile})}{k_2(\mathbf{107a}\ \text{enol})} \qquad (\mathbf{31})$$

The k_{rel}''' values are summarised in **Table 37**. Comparing k_{rel}'''(Selectfluor™) and k_{rel}'''(NFSI) values for each nucleophile, the values are in excellent agreement. When k_{rel}''' values with a single N−F reagent are compared across the range of nucleophiles, the reactivities of the nucleophiles span 5 orders of magnitude (**Figure 134**), and compound **165** is one order of magnitude more reactive than **107a-enol**.

Table 37: The k_{rel}''' values obtained using **Equation 31** and second-order rate constants (k_2, obtained in MeCN at 25 °C) which were used to calculate k_{rel}'''.

Nucleophile	k_2(Selectfluor™) / M^{-1} s^{-1}	k_2(NFSI) / M^{-1} s^{-1}	k_{rel}''' (Selectfluor™)	k_{rel}''' (NFSI)
107a, R = H	4.20×10^{-2}	9.87×10^{-6}	1.0	1.0
107b, R = F	3.28×10^{-2}	8.14×10^{-6}	7.8×10^{-1}	8.2×10^{-1}
107c, R = Me	1.17×10^{-1}	3.08×10^{-5}	2.8	3.1
107d, R = OMe	6.43×10^{-1}	1.38×10^{-4}	1.5×10^{1}	1.4×10^{1}
107e, R = Cl	1.82×10^{-2}	5.75×10^{-6}	4.3×10^{-1}	5.8×10^{-1}
107f, R = CN	1.60×10^{-3}	-	3.8×10^{-2}	-
107g, R = NO_2	8.99×10^{-4}	-	2.1×10^{-2}	-
107h, R = NMe_2	1.05×10^{2}	1.41×10^{-2}	2.5×10^{3}	1.4×10^{3}
165	2.38	3.33×10^{-4}	5.7×10^{1}	3.4×10^{1}

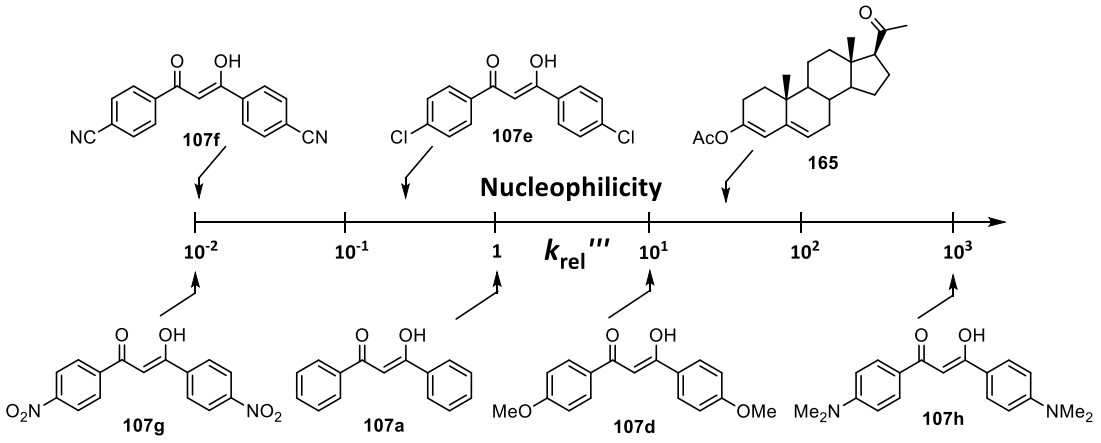

Figure 134: Reactivity scale for some nucleophiles used in this work, with 1,3-dicarbonyl **107a** (R_1 = R_2 = H) as the reference.

The nucleophilicities of enols and enol acetates have not yet been characterised on the Mayr-Patz scale. Silyl enol ethers have nucleophilicities $N \sim 3 – 8$ in MeCN and ethyl vinyl ether has N = 3.92 in DCM.[194] N is a logarithmic scale, hence, a one-unit difference in N translates to a ten-fold difference in reaction rate.[226] Given that the N

parameter for **107h-enol** estimated in Chapter 5 was 6.13, and that **107h-enol** is 40-fold more reactive than **165**, an *N* parameter of ~5 could be predicted for progesterone enol acetate **165**. The full range of nucleophilicity parameters for the substrates included in **Table 37** would therefore be $N \sim 1 - 6$. Although these values for *N* are only estimates, they are plausible since the predicted values fall within the range of measured (silyl) enol ethers.

6.3.5 Determination of activation parameters

Activation parameters ($\Delta G^{\ddagger}$, $\Delta H^{\ddagger}$, $\Delta S^{\ddagger}$) were obtained from kinetic data for the reactions of progesterone enol acetate **165** with Selectfluor™ **19** and diCl-NFPy TfO^- **50a** at four different temperatures (**Table 38**). The linear form of the Eyring equation was used to calculate activation parameters using the procedure described in Chapter 2 Section 2.8 (**Figure 135**).

Table 38: Second-order rate constants (k_2) for the fluorination of progesterone enol acetate **165** by Selectfluor™ **19** and diCl-NFPy TfO^- **50a** in MeCN at 4 temperatures.

N–F reagent	k_2 (25 °C) / M^{-1} s^{-1}	k_2 (30 °C) / M^{-1} s^{-1}	k_2 (35 °C) / M^{-1} s^{-1}	k_2 (40 °C) / M^{-1} s^{-1}
Selectfluor™ **19**	2.38	3.61	4.96	6.77
diCl-NFPy TfO^- **50a**	4.72×10^{-1}	7.03×10^{-1}	9.62×10^{-1}	1.38

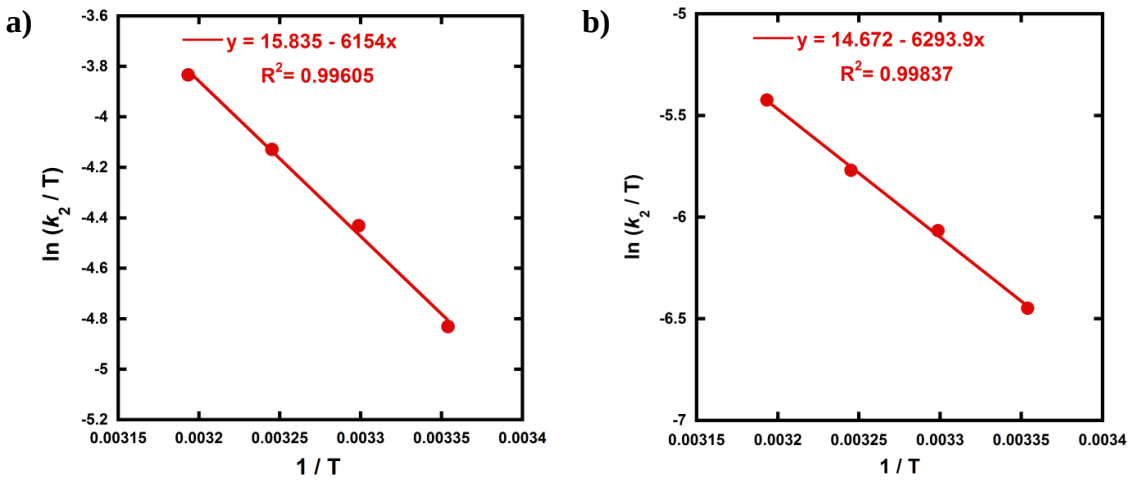

Figure 135: Eyring plots for fluorination of progesterone enol acetate **165** at 4 different temperatures by (a) Selectfluor™ **19** and (b) diCl-NFPy TfO^- **50a**.

As with the activation parameters obtained for fluorination of 1,3-dicarbonyl derivatives **107a-e**, the moderately negative values of $\Delta S^{\ddagger}$ (**Table 39**) support bimolecular, S_N2-type fluorinations with similar mechanisms. For enols **107a-e**, $\Delta H^{\ddagger}$ values were between +55 to +64 kJ mol^{-1}, $\Delta S^{\ddagger}$ were between −54 to −72 J K^{-1} mol^{-1}, and $\Delta G^{\ddagger}$ ranged from +74 to +83 kJ mol^{-1}. Hence, the similarity in activation parameters for the enols **107a-e** and enol ester **165** are consistent with a common mechanism for fluorination of these substrates.

Table 39: Activation parameters obtained from Eyring correlations.

N−F reagent	$\Delta H^{\ddagger}$ / kJ mol^{-1}	$\Delta S^{\ddagger}$ / J K^{-1} mol^{-1}	$\Delta G^{\ddagger}$ / kJ mol^{-1}
Selectfluor™ **19**	+51.2	−65.9	+70.8
diCl-NFPy TfO^{-} **50a**	+52.3	−75.6	+74.8

6.3.6 Exploration of the effects of additives on rates of fluorination

As previously mentioned, Selectfluor™ **19** shows excellent solubility and good stability in water; additionally, the use of green solvents such as water is attractive due to the potential for reducing the environmental impact of the process. Chapter 4 discussed the increases in rates of fluorination of **107a-enol** in MeCN with water as an additive. Hence, to explore the suitability of water as a co-solvent for fluorination of progesterone enol acetate **165**, kinetics studies were carried out on the fluorination of **165** in water-MeCN mixtures. Furthermore, experiments in the presence of additives were conducted to explore whether the ester hydrolysis step (**Scheme 50**, *vide infra*) is rate-determining, whereby the use of secondary nucleophiles would result in significant rate enhancements. Hence, the use of MeOH as a secondary nucleophile during fluorination reactions with Selectfluor™ was also explored.

Reactions were conducted in the presence of different quantities of water, and rate constants were determined using UV-vis spectrophotometry. Representative examples are shown in **Figure 136** for 20% water in MeCN (*v*/*v*), and rate constants (k_2) are summarised in **Table 40**. The trend observed was a decrease in fluorination rates as the amount of water was increased (**Figure 138**). Although Selectfluor™ is highly soluble in water, **165** has low solubility in this solvent. However, precipitation of **165** was not observed as its concentration in UV-vis monitored reactions was low (0.05 mM).

Therefore, the results show that water is not a suitable additive or co-solvent for increasing the rate of fluorination of **165**.

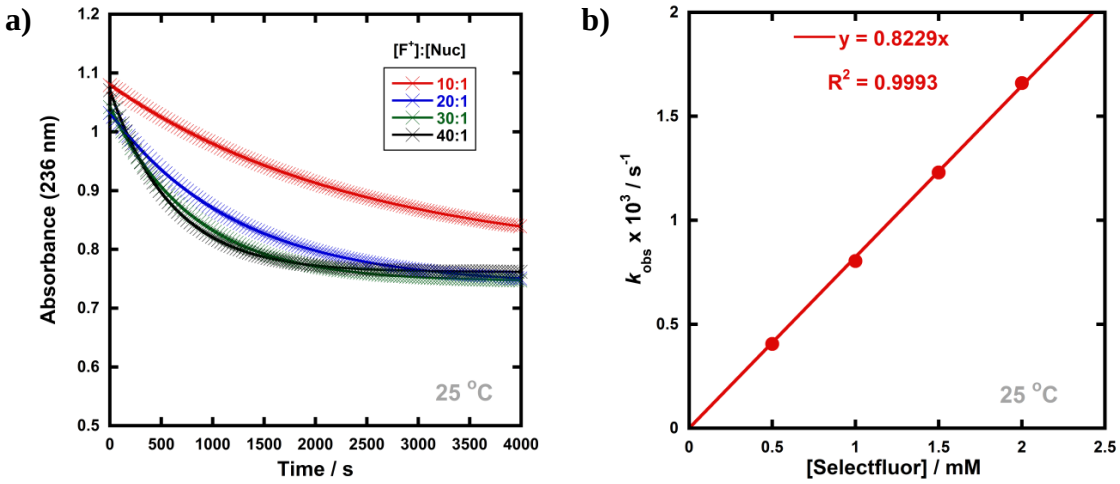

Figure 136: (a) Exponential decays of absorbance of **165** with different concentrations of Selectfluor™ at 25 °C, with 20% water in MeCN (*v*/*v*). (b) Correlation of k_{obs} with [Selectfluor™].

Representative examples with MeOH as the additive are presented in **Figure 137** for 20% MeOH in MeCN (*v*/*v*), and all rate constants are included in **Table 40**. The trends observed in k_2 values are shown in **Figure 138**. The values for k_2 increased 1.2-fold to 2.87 M^{-1} s^{-1} with 30% MeOH compared to the value in the absence of additives, however, the rate was only 1.1-fold higher with 50% MeOH. Hence, given that there was little variation in rate upon addition of MeOH, the ester hydrolysis step is not likely to be rate-determining.

Furthermore, the nucleophilicities of water and MeOH have been previously determined.[227] A 10:90 MeOH:MeCN mixture has N = 5.55, 20:80 has N = 6.04, and 50:50 has N = 6.67. For water:MeCN mixtures: 10:90 has N = 4.56, 20:80 has N = 5.02 and 50:50 has N = 5.05. Hence, MeOH is more nucleophilic than water in MeCN, and the increase in nucleophilicity upon use of larger volumes of MeOH is more significant than for water. If the ester hydrolysis step was rate-limiting, the second-order rate constants for reactions involving MeOH would have been significantly larger.

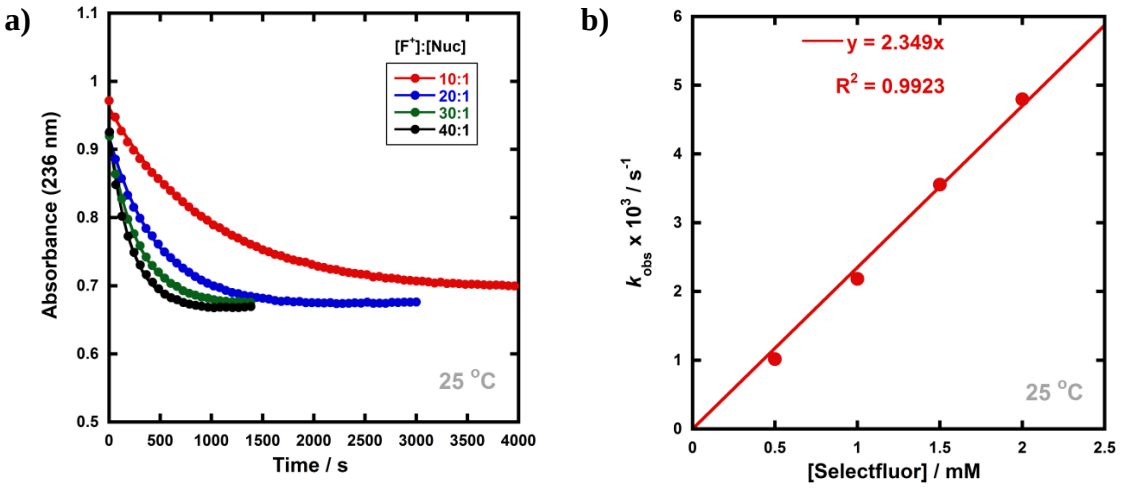

Figure 137: (a) Exponential decays of absorbance of **165** with different concentrations of Selectfluor™ at 25 °C, with 20% MeOH in MeCN (*v*/*v*). (b) Correlation of k_{obs} with [Selectfluor™].

Table 40: Rate constants (k_2) for the fluorination of progesterone enol acetate **165** by Selectfluor™ in the presence of additives (water and MeOH) in MeCN at 25 °C.

Additive	% Additive in MeCN (*v*/*v*)	k_2 / M^{-1} s^{-1}
None	-	2.38
Water	5	1.47
	10	1.22
	20	8.23×10^{-1}
	30	6.14×10^{-1}
MeOH	10	2.39
	20	2.35
	30	2.87
	40	2.78
	50	2.71

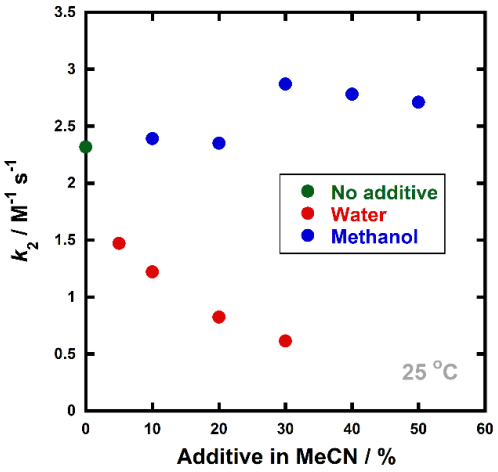

Figure 138: Effects of additives, water and MeOH, on the rates of fluorination of **165** by Selectfluor™.

Following fluorination, the hydrolysis of the ester group can occur by the mechanism shown in **Scheme 50**. Based upon the kinetic data obtained in the presence of secondary nucleophiles, the hydrolysis step is fast, and the fluorination step is rate-determining.

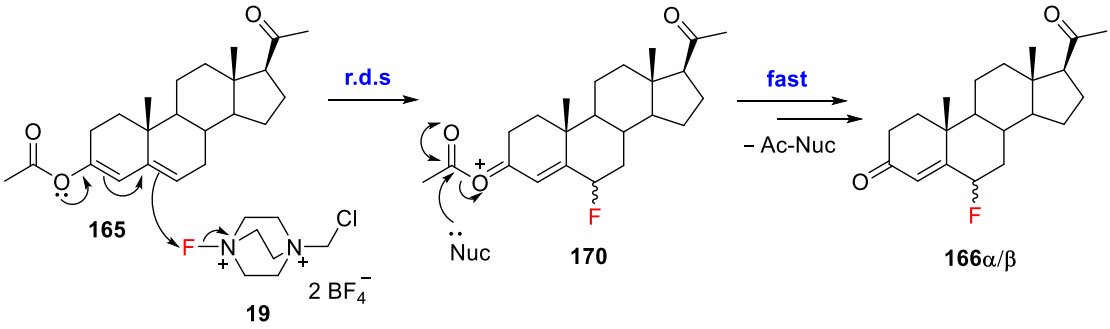

Scheme 50: Proposed mechanism for the hydrolysis of the acetate group of **170** in the presence of a secondary nucleophile.

6.3.7 Kinetics of epimerisation

The 6α-fluorosteroids are generally desired due to optimal biological activity of this isomer.[228,229] However, the low stereoselectivities of the fluorination reactions studied in this chapter result in the formation of the 6β-isomer as the major product (**Table 41**). Selectfluor™ **19** gave the highest proportion of the desired 6α-isomer, while the least reactive N–F reagents (NFSI **17**, NFPy TfO^- **12a** and triMe-NFPy TfO^- **52a**) yielded the next highest proportion of this isomer. The most reactive N–F reagent, pentaCl-NFPy TfO^- **51a**, gave a slightly lower amount of the 6α-isomer than the least reactive reagents. Interestingly, the reagents with reactivities that are the most comparable with Selectfluor™ (diCl-NFPy TfO^-/BF_4^- **50a/b**) resulted in the lowest selectivities for the

6α-isomer. The counter-ion appears to have little effect on the β:α ratios, since the triflate and tetrafluoroborate salts of diCl-NFPy **50** gave identical selectivities.

Table 41: Ratios of 6α- to 6β-fluoroprogesterone (**166-α**:**166-β**) formed upon fluorination by N−F reagents, as determined by ^{19}F NMR spectroscopy in MeCN-d_3.

Steroidal nucleophile	N−F reagent	Ratio of 6α:6β fluoroprogesterone
Progesterone enol acetate **165**	Selectfluor™ **19**	34:66
	NFPy TfO^- **12a**	22:78
	NFSI **17**	23:77
	diCl-NFPy TfO^- **50a**	13:87
	diCl-NFPy BF_4^- **50b**	13:87
	pentaCl-NFPy TfO^- **51a**	20:80
	triMe-NFPy TfO^- **52a**	23:77
Testosterone enol diacetate **167**	Selectfluor™ **19**	43:57
Cholestenone enol acetate **168**	Selectfluor™ **19**	38:62
Hydrocortisone enol tetraacetate **169**	Selectfluor™ **19**	35:65

Herrinton *et al.*[220] have shown that crystallisation-driven equilibration in the presence of strong acids allowed the mixture of isomers to be equilibrated to the 6α-isomer. Following solvent and acid screening, the optimal conditions found for this equilibration were EtOAc in anhydrous HCl. The method used by Harsanyi[223] was to dissolve **166-β** in glacial acetic acid and dry HCl gas was bubbled through the solution for 1.5 h, which was based on the procedure reported by Ringold.[208] The solvents were evaporated and recrystallisation from MeOH gave **166-α** in 74% yield.

To enable a study of the rates of epimerisation, the reactions were conducted by adding **166-β** (60 mM) to a solution of pre-dissolved HCl in acetic acid (0.25-1.00 M) in NMR tubes equipped with D_2O lock tubes, allowing the reactions to be monitored directly by ^{19}F NMR spectroscopy. Relaxation delays of 10 s were used to achieve quantitative

integrals and spectra were acquired every 15 min for several hours until end-points were reached. **Figure 139** shows the NMR data obtained for the epimerisation of **166-β** with 0.50 M HCl in AcOH. The triplet of doublets at δ = −165.6 to −165.9 ppm corresponds to **166-β**, which decreased in intensity over time. The doublet of doublet of doublets at δ = −183.0 to −183.1 ppm is associated with **166-α** and increased in intensity. Additional peaks were present at δ = −165.56 ppm, which overlapped with part of the adjacent **166-β** peaks. Similarly, small peaks appeared over time adjacent to the **166-α** peaks.

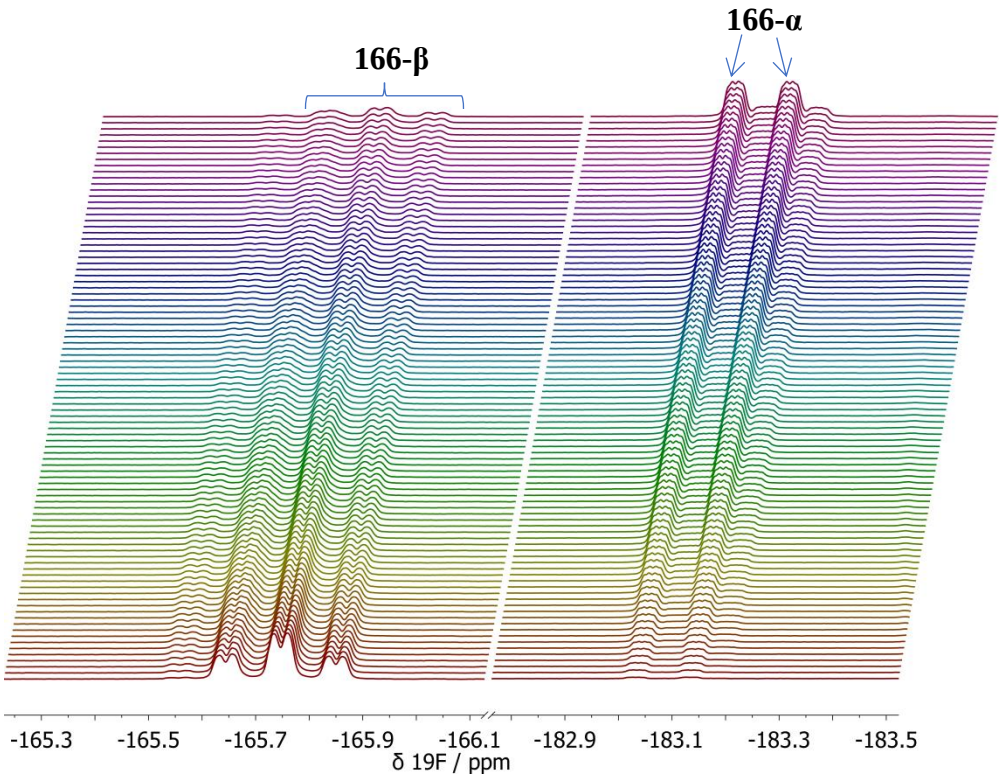

Figure 139: Time-arrayed ^{19}F NMR spectroscopic monitoring of the epimerisation of **166-β** to **166-α** with 0.50 M HCl in AcOH. Spectra were acquired every 15 min for 17 h with relaxation delays of 10 s.

The reaction profiles for each species in the epimerisation mixture are shown in **Figure 140**. Due to significant overlap between the peaks present, partial signal integration was employed to accurately integrate a portion of the signals corresponding to each species. To confirm that the experiment was quantitative, the integrals at each timepoint were summed and were found to vary by only ~5% throughout the reaction, where this variation is also likely to be due to the drift in NMR shims at later timepoints, as well as the intrinsic signal-to-noise of the integrated signals. The integrals corresponding to **166-α** (black data points) were fitted to a first-order exponential, whereas those of **166-β** (red data points) showed deviations from the first-order fitting (**Figure 140**). The

integrals of the small signals at δ = −165.56 ppm (blue data points) clearly showed the formation and decay of an intermediate.

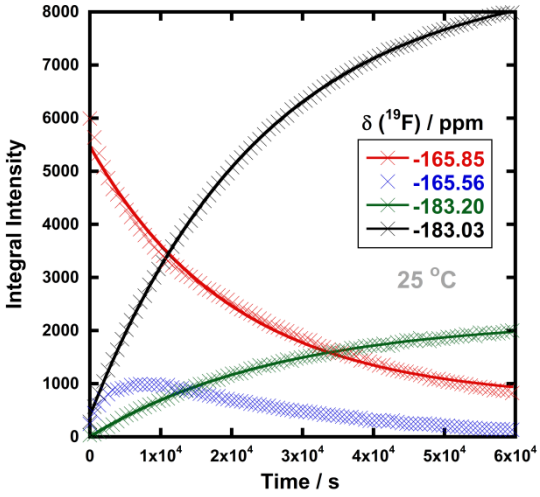

Figure 140: Reaction profiles for the species present in the epimerisation of **166-β** to **166-α** with 0.50 M HCl in AcOH.

The epimerisation studies were repeated using additional concentrations of HCl in AcOH (0.25 M, 0.75 M and 1.00 M). Similar reactions profiles to those shown in **Figure 140** were obtained for the species present. The signals at −183.03 ppm were integrated, and plots of relative integral intensities versus time are shown in **Figure 141a**. The second-order rate constant, k_2, for epimerisation was obtained from a plot of k_{obs} versus [HCl] (**Figure 141b**) and determined to be 9.12×10^{-5} M^{-1} s^{-1}.

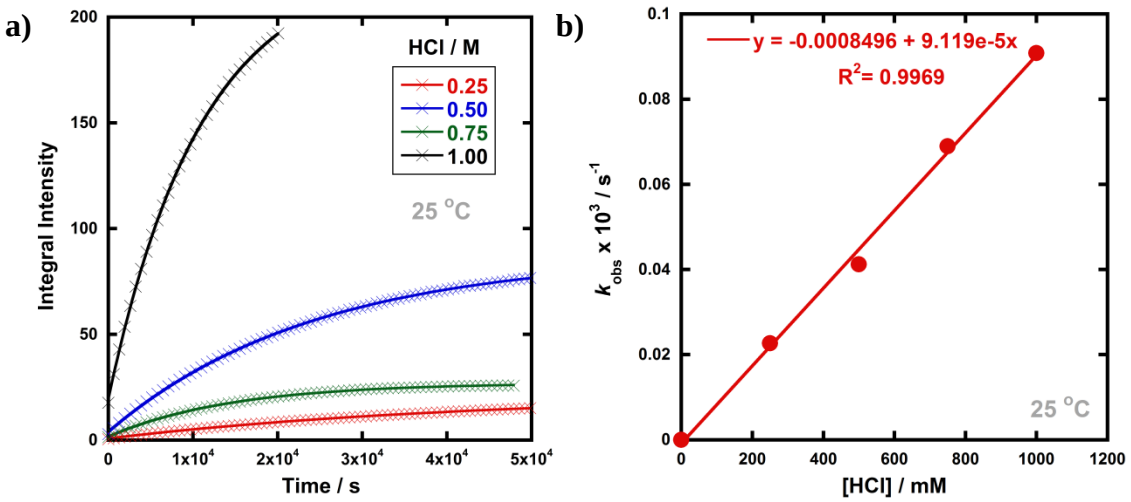

Figure 141: (a) Epimerisation of **166-β** to **166-α** in a solution of HCl in AcOH, with different concentrations of HCl, showing integrals of **166-α** at δ = −183.03 ppm over time. (d) Correlation of k_{obs} values versus [HCl].

All k_{obs} values are summarised in **Table 42**, in addition to those obtained for the rate of formation of the smaller signal at δ = −183.20 ppm. The ratios of the larger peak at −183.03 ppm to the smaller one at −183.20 ppm at the end-points of all reactions was approximately 5:1.

Table 42: The k_{obs} values for epimerisation of **166-β** to **166-α** with different concentrations of HCl in AcOH.

[HCl] / M	k_{obs} (−183.03) × 10^5 / s^{-1}	k_{obs} (−183.20) × 10^5 / s^{-1}
0.25	2.27	-[a]
0.50	4.12	3.75
0.75	6.90	-[a]
1.00	9.08	8.08

[a] Due to overlapping signals and drift in NMR shims as reactions progressed, it was not possible to determine accurate k_{obs} values.

Figure 142a displays the proton-decoupled ^{19}F NMR spectrum of the epimerisation mixture (with 0.50 M HCl in AcOH) at the end-point of the reaction. Following work-up of the epimerisation mixtures, the crude products were obtained as a yellow oil, where NMR analysis showed that the α and β fluoro-isomers were present in a 4:1 ratio (**Figure 142b**). The LC-MS chromatogram trace for the crude products is shown in **Figure 143**. The largest peak at R_t = 2.66 min corresponds to **166-α** (as confirmed by comparison with the LC-MS chromatogram of an authentic sample). The adjacent peak at R_t = 2.71 min is due to **166-β**. For the smaller peak at R_t = 2.79 min, the molecular ion signal had the same mass as the fluoroprogesterone isomers. This peak is likely to be associated with the small signal at δ = −165.90 ppm observed in the ^{19}F NMR spectrum of the crude product after work-up (**Figure 142b**). Finally, the peak at R_t = 2.83 min corresponds to progesterone **165**, which could have formed due to loss of the fluorine atom from species **171-β** or **171-α** (**Scheme 51**, *vide infra*).

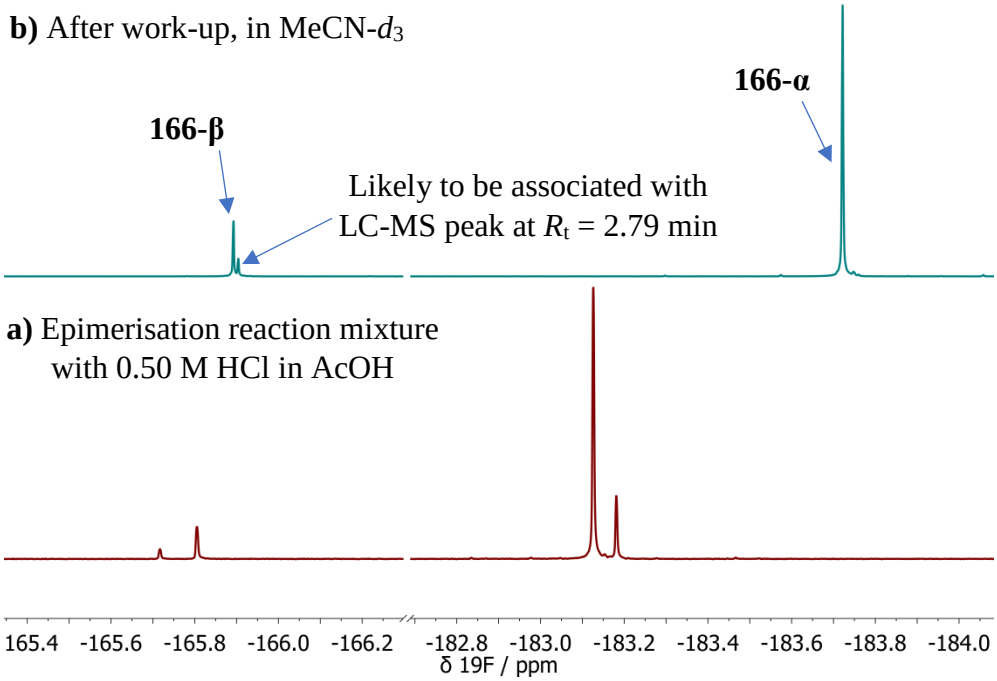

Figure 142: (a) Proton-decoupled ^{19}F NMR spectrum of the reaction mixture at the end of an epimerisation reaction (0.50 M HCl in AcOH). (b) Proton-decoupled ^{19}F NMR spectrum of crude product after work-up, in MeCN-d_3.

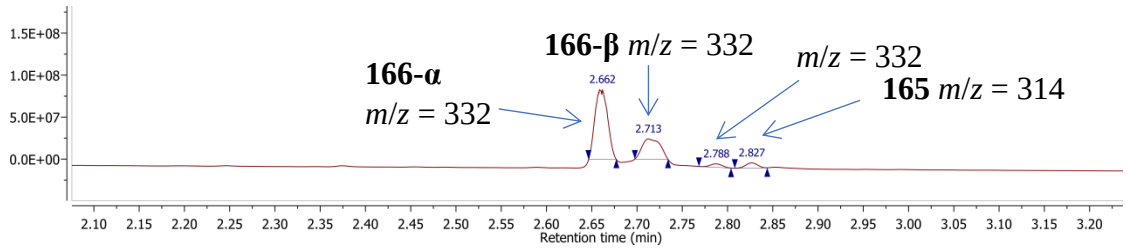

Figure 143: LC-MS chromatogram trace for crude product obtained upon work-up of epimerisation reactions.

The small signals at δ = −165.56 and −183.20 ppm in **Figure 139** are likely to be product-related species, due to their similarity in chemical shift and coupling patterns. It was hypothesised that these small signals could be associated with the protonated forms, **171-β** and **171-α**, of the fluorosteroids (**Scheme 51**). An alternative hypothesis is that the signals correspond to hemiacetals **173-β** and **173-α**, formed via reactions of **171-β** and **171-α** with AcOH (**Scheme 51**, blue pathways). To test these hypotheses, an authentic sample of **166-α** was incubated in solutions of AcOH, 0.50 M HCl in AcOH, and 1.00 M HCl in AcOH for 45 min and ^{19}F NMR spectra were acquired. In the proton-coupled spectra for HCl-AcOH solutions, the smaller peaks at δ = −183.10 and −183.20 ppm adjacent to the major peaks at δ = −183.03 and −183.15 ppm were present

(**Figure 144a**), and this was also observed in proton-decoupled spectra (**Figure 144b**). However, signals corresponding to only one species were observed in AcOH. This confirms that the additional peaks are indeed either due to protonation of the fluorosteroid isomers, or the formation of hemiacetals.

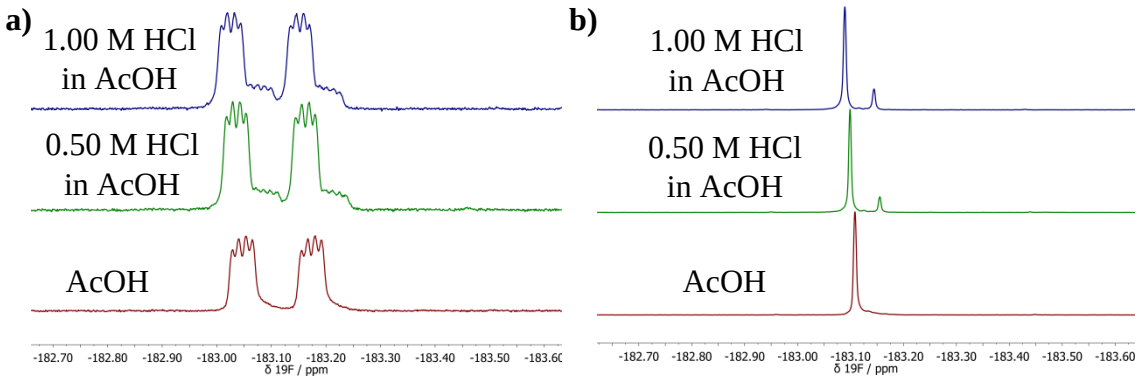

Figure 144: ^{19}F NMR spectra for **166-α** in AcOH, 0.50 M HCl in AcOH and 1.00 M HCl in AcOH, where (a) are proton-coupled; (b) are proton-decoupled.

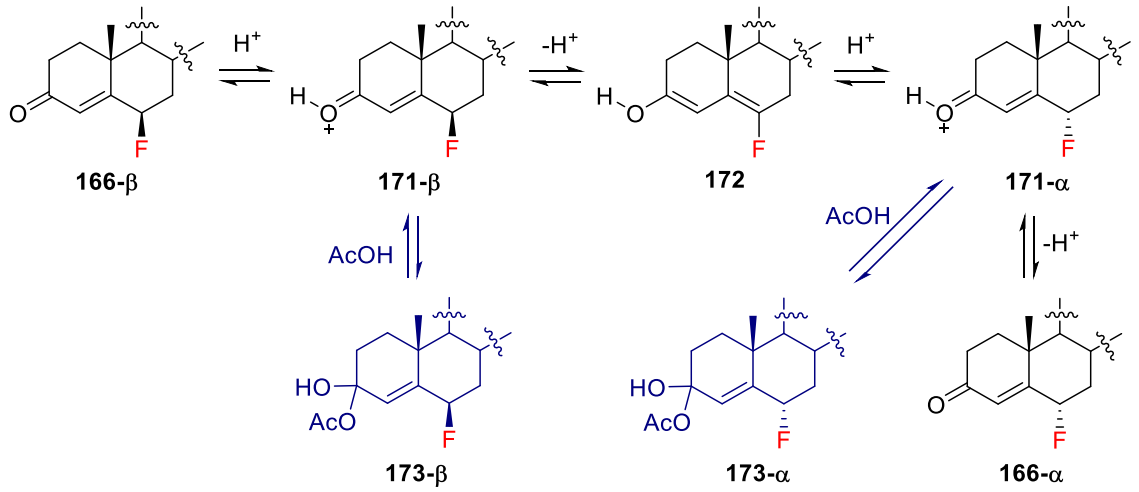

Scheme 51: Proposed mechanism for epimerisation of **166-β** to **166-α**. Another pathway, hemiacetal formation via AcOH, is proposed.

Finally, the possibility of DABCO and $ClCH_2$-$DABCO^+$ BF_4^- influencing rates of β-to-α epimerisation was explored by incubating 1 equivalent of each compound with an authentic sample of **166-β** for 1 week in MeCN-d_3. However, no formation of **166-α** was observed. It was thought that, since fluorination reactions using Selectfluor™ resulted in the formation of $ClCH_2$-$DABCO^+$ BF_4^-, this salt could have some effect upon epimerisation (*cf.* small increases in enolization rates in Chapter 3), although the $ClCH_2$−$DABCO^+$ cation is unlikely to remain unprotonated and thus will be unable to function as a base.

6.4 Direct fluorination of progesterone enol acetate using fluorine gas

As discussed in Chapter 1, Selectfluor™ is used for the fluorination of approximately 80% of fluorosteroids produced industrially. However, Selectfluor™ has low atom efficiency (only 5.3% by weight is active fluorine) and, although its commercial price is reasonable for small-scale discovery use, it is less cost-effective for production applications. Most electrophilic fluorinating reagents are prepared using fluorine gas (F_2), therefore, this precursor has gained attention as a greener and less wasteful alternative.[230] There have been no reports of the fluorination of steroidal enolate systems at the 6-position using F_2, although there have been reports of fluorination of tertiary C-H positions.[231,232] Since selective direct fluorination of steroids by F_2 could provide a less expensive and less resource-intensive route to commercially important 6-fluorosteroid derivatives, progesterone enol acetate **165** was a convenient substrate for direct fluorination using F_2.

Direct fluorination of **165** using F_2 (**Scheme 52**) was carried out in formic acid solution by Harsanyi,[223] since it is one of the preferred solvents for fluorination of enolate systems.[233] Progesterone enol acetate **165** was dissolved in formic acid and reacted with 1.4 equivalents of fluorine gas for 50 min (**Table 43**, entry 1); after evaporation of the solvent, a yellow oily material was obtained. Analysis of the crude product mixture showed the presence of progesterone **164**, **166-α** and **166-β** (in an approx. 1:1:1 ratio) as well as other impurities due to unidentified fluorinated and non-fluorinated species. Progesterone **164** was the product of enol-acetate hydrolysis due to the acidic nature of the reaction medium. Further optimisations of the process were not attempted.

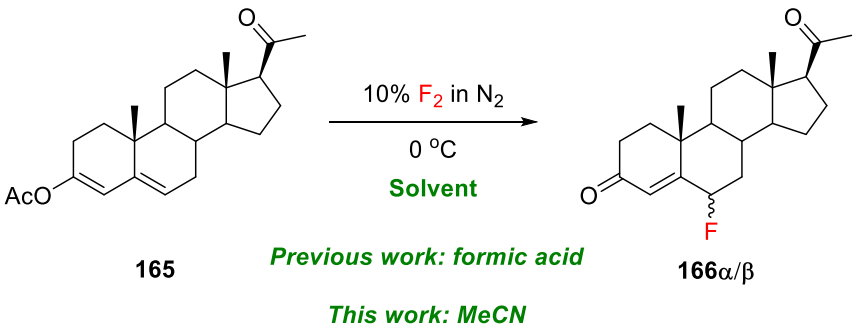

Scheme 52: Fluorination of **165** using F_2 (10% in N_2) at 0 °C to synthesise **166α/β**.

In the present work, it was hypothesised that conducting the direct fluorination in non-acidic media could reduce the hydrolysis of **165** to **164**. Secondly, using less harsh conditions, such as shorter reaction times and lower number of equivalents of F_2, could

lead to fewer side-products. Polar solvents can encourage polarisation of the fluorine molecule, thus making it more susceptible to nucleophilic attack. Therefore, appropriate reaction media for selective fluorination reactions using fluorine gas are often high dielectric aprotic solvents (such as MeCN) or strong protonic acids (such as formic or sulfuric acids). MeCN was thus selected as a potentially suitable solvent for fluorination of **165** using F_2.

Direct fluorination reactions were conducted in MeCN by altering the flow rates, number of equivalents of F_2 and reaction times. Each experiment was initially evaluated qualitatively based on whether the crude product mixture yielded oils or crystals upon evaporation of solvents. The use of greater than 1.1 equivalents of F_2 and long reaction times (**Table 43**, entries 3 and 4) gave yellow oils. Conditions that yielded crystalline crude products were 1.1 equivalents with 5 mL min^{-1} flow rate for 27 min (entry 2) and 1.1 equivalents with 10 mL min^{-1} flow rate for 13 min (entry 6). Shorter reaction times are preferable, so the latter are the best set of conditions from these preliminary studies.

Table 43: Reaction conditions for the fluorination of **165** using F_2 (10% in N_2) and the nature of the crude products as determined from visible inspection. Entry 1 was from Harsanyi PhD Thesis[223]; entries 2-6 are experiments conducted in the present work.

Entry	Solvent	Flow rate / mL min^{-1}	Equiv. of F_2	Reaction time / min	Nature of crude products
1	Formic acid	20	1.4	50	Yellow oil
2	MeCN	5	1.1	27	Pale yellow crystals
3	MeCN	5	2.0	48	Orange oil
4	MeCN	5	1.5	36	Yellow oil
5	MeCN	10	1.5	18	Yellow oil/crystals
6	MeCN	10	1.1	13	Pale yellow crystals

Upon evaporation of solvents, analysis of the crude product mixtures by ^{1}H and ^{19}F NMR spectroscopy showed that the selectivity of the direct fluorination reactions for

166-α and **166-β** were 1:2, which is the same as that of fluorination using Selectfluor™. Although progesterone **164** was not detected, unreacted progesterone enol acetate **165** was present in all entries. For entry 2, the ratio of **165** to **166α/β** was around 1:1, as determined by ^{1}H NMR spectroscopy. The ^{19}F NMR spectra for entries 2-6 are shown in **Figure 145**. The signal at δ = −150 ppm present in all spectra is due to fluorinated borosilicate glass, which is likely to have formed from the presence of HF in the crude reaction mixtures. The conditions described by entry 3 yielded the highest amounts of fluorinated side products, which are evident in the NMR spectrum. The spectra for entries 2 and 4-6 display similar proportions of fluorinated side-products. Upon standing for 1-2 days, the crude samples containing crystalline products gradually showed the appearance of oily material, hence, the presence of small quantities of HF (formed as a side-product in reactions involving F_2) could have caused decomposition of **166α/β** to other fluorinated steroid derivatives.

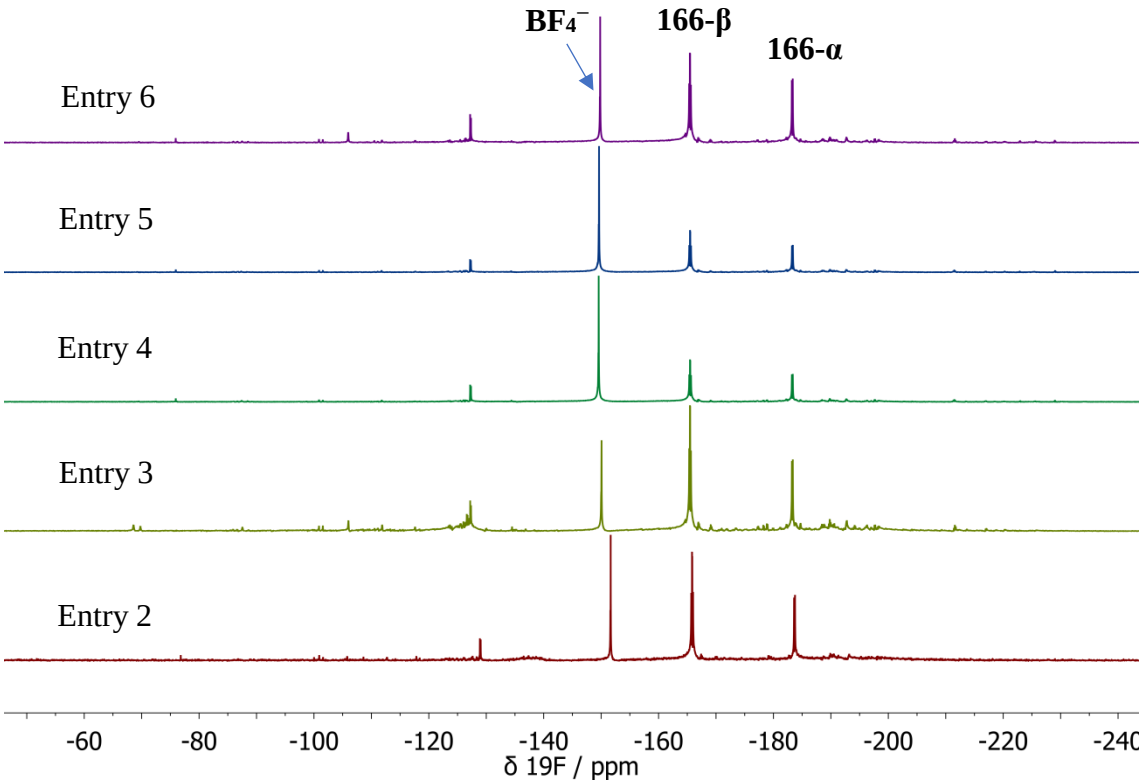

Figure 145: ^{19}F NMR spectra for crude products from fluorination of **165** by F_2 in MeCN under a range of reaction conditions.

Future experiments should involve the use of chromatographic analyses to obtain more quantitative information of product distributions, as well as analysis of crude products immediately after evaporation of solvents, to avoid the formation of additional side-

products from standing in HF. Overall, from these qualitative initial studies, the best conditions consisted of a small excess of F_2 with high flow rate. Furthermore, it is likely that conducting the reaction using a flow reactor would further increase the conversions and reduce the quantities of side products.

6.5 Conclusions

In this chapter, the kinetics of fluorination of progesterone enol acetate using seven N−F reagents were discussed. The method of analysis was tuned to the reactivity of the system: less powerful electrophiles were studied via ^{1}H NMR spectroscopy while more reactive ones were studied using UV-vis spectrophotometry. Relative rate constants were calculated from absolute rate constants, which correlated well with the reactivity scale detailed in Chapter 2. This highlights the predictive nature of the scale towards a different class of carbon nucleophiles. Activation parameters were determined for the fluorination of progesterone enol acetate by Selectfluor™ **19** and diCl-NFPy TfO^- **50a**. The moderately negative values of $\Delta S^‡$ are consistent with an S_N2 mechanism.

To expand the steroidal substrate family, kinetics studies were conducted on the fluorination of testosterone enol diacetate **167**, cholestenone enol acetate **168** and hydrocortisone enol tetraacetate **169** using Selectfluor™, diCl-NFPy TfO^- **50a** and pentaCl-NFPy TfO^- **51a**. The substituent at the C-17 position has a small but measurable effect upon the rate of fluorination.

The presence of different quantities of water during the fluorination of progesterone enol acetate by Selectfluor™ **19** led to small reductions in the k_2 values, hence, water is not a suitable additive for this reaction. MeOH had little effect on fluorination rates, with very small increases (up to 1.2-fold) observed. Hence, the ester hydrolysis step is not likely to be rate-determining, as significant rate enhancements would have been observed if this was the case, given the nucleophilicity of MeOH in MeCN. A similar conclusion was given by Nelson *et al.*[222] in their work on tetralone derivatives, where fluorination via Selectfluor™ in water-MeCN and MeOH-MeCN mixtures proceeded by similar rates.

The kinetics of epimerisation of 6-β-fluoroprogesterone to 6-α-fluoroprogesterone using different concentrations of HCl in acetic acid were studied by quantitative ^{19}F NMR spectroscopy. Analysis of the species present in epimerisation mixtures gave evidence for the formation of hemiacetals or protonated forms of the fluorosteroid isomers.

Finally, some improvements were made for the fluorination of progesterone enol acetate via F_2 by conducting reactions in MeCN, using high flow rates and a small excess of F_2. The conversion to 6-fluoroprogesterone was around 50% under these conditions. Larger excesses of F_2 resulted in the formation of greater quantities of fluorinated side-products. Further improvements may be possible by conducting the reaction in a continuous flow reactor rather than a batch system. Comparing the batch processes performed in this study for fluorination of progesterone enol acetate using Selectfluor™ and F_2, the former results in the cleanest formation of desired products with minimal to no side-products formed.

Chapter 7: Conclusions and Future Work

Chapter 2 of this thesis delivered extensive kinetics studies on fluorination reactions of 1,3-dicarbonyl derivatives using a range of experimental techniques, including UV-vis spectrophotometry, NMR spectroscopy and LC-MS. This led to the construction of a quantitative reactivity scale for ten widely-used electrophilic N−F reagents (**Figure 146**). Similar Hammett parameters across the range of fluorinating reagents revealed the mechanisms of fluorination to be similar. These results highlighted the achievement of the primary aims of this project.

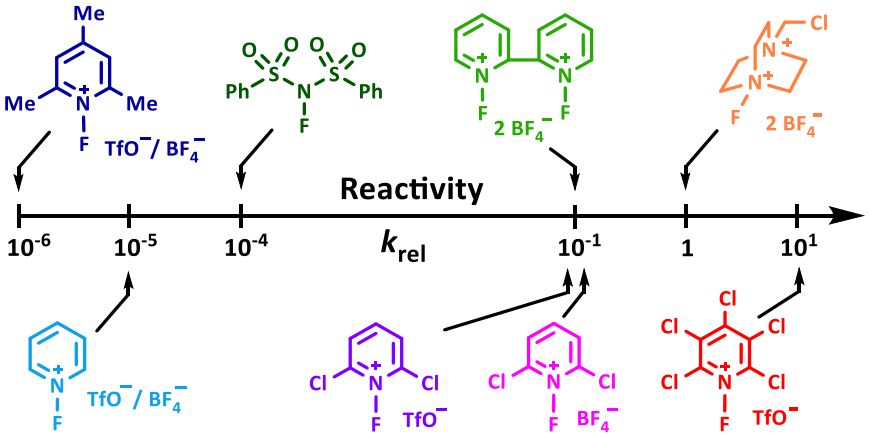

Figure 146: Quantitative reactivity scale for electrophilic fluorinating reagents of the N−F class, constructed using absolute and relative rate constants determined from kinetics studies.

The significance of keto-enol tautomerism was identified in the early stages of this project, during the development of the nucleophile scaffold consisting of 1,3-diaryl-1,3-dicarbonyl derivatives. Additionally, the serendipitous and unprecedented crystallisation of both fluoroketo and fluoroenol tautomers of 2-fluoro-1,3-dicarbonyls highlighted the importance of tautomerism within fluorine-containing systems. Chapters 3 and 4 delivered the determination of all rate constants for fluorination and enolization towards the preparation of 2,2-difluoro-1,3-dicarbonyl compounds (**Figure 147**). Importantly, enolization rates were found to control mono- versus di-fluorination, which can also be tuned via reaction additives such as water, acid, base and salt.

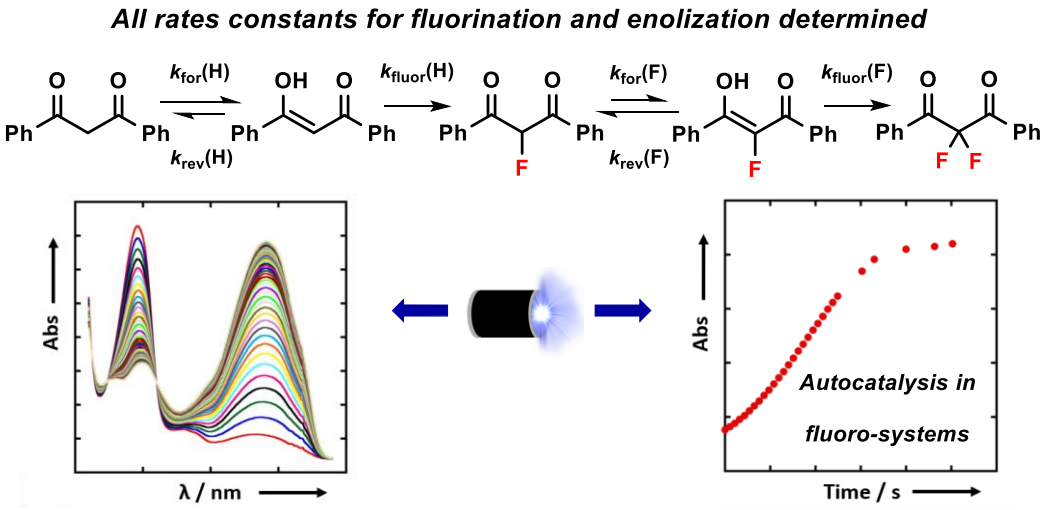

Figure 147: Photoketonization and relaxation studies enabled the determination of all rate constants for enolization, supplemented by kinetics studies on mono- and di-fluorination.

The kinetics of fluorination of a variety of nucleophile systems, including enamines, silyl enol ethers, indoles and enolates were explored in Chapter 5, during attempts to determine the electrophilicity parameters, *E*, of the N−F reagents. Although these systems delivered limited success, they were important for the development of suitable reaction monitoring techniques to match the reactivities of the substrates. Furthermore, the *E* parameter for Selectfluor™ estimated based on kinetics studies with 1-methyl indole, and corroborated by chlorination studies, was in excellent agreement with that reported by Mayr *et al*. in their recent report.[132]

Finally, Chapter 6 explored the kinetics of fluorination of steroid enol acetates, which are more structurally complex and pharmaceutically-relevant drug-like systems. Thus, the applicability of the reactivity scale (**Figure 146**) towards a different class of carbon nucleophiles was confirmed. Kinetics studies were also conducted on the epimerisation of 6-β-fluoroprogesterone to 6-α-fluoroprogesterone in HCl-AcOH solutions, where signals corresponding to hemiacetal or protonated forms of both fluoro-isomers were observed by ^{19}F NMR spectroscopy during reactions.

In the years 2018-2019, there have been several studies on the reactivities of various fluorinating reagents. Reports by Mayr *et al.*[132] on electrophilicities of five N−F reagents correlated to enamines and carbanions, as well as by Nelson *et al.*[222] on the fluorination of tetralone derivatives with Selectfluor™, provided kinetic and mechanistic data that support the present work. Kinetics studies on the

trifluoromethylating reagent trifluoromethyltrimethylsilane ($TMSCF_3$, known as the Ruppert-Prakash reagent),[234] as well as on electrophilic trifluoromethylthiolating and difluoromethylthiolating reagents,[235] highlight the growing interest in a more quantitative approach towards the introduction of fluorine-containing moieties to organic compounds. Additionally, there has been continued interest in the development of new fluorinating reagents, for example, a new generation of radical fluorinating reagents based on *N*-fluoro-*N*-arylsulfonamides.[236]

Future work on the areas developed in this thesis could involve additional studies on tautomeric polymorphism. As mentioned in Chapter 2, the crystallisation of both keto and enol forms of the 2-fluoro-1,3-dicarbonyl derivatives appeared to depend upon the nature of the substituents. Therefore, the synthesis and crystallisation of 2-fluorinated 1,3-dicarbonyl derivatives bearing different *para*-substituents to those that have already been synthesised and investigated in the present work could be carried out (**Figure 148**). Both mono- and di-substituted compounds could be tested. This could then be extended to *meta*- and *ortho*-substituents as well as expanding the scope to 2-fluorinated β-ketoesters, β-ketoamides and malonate esters. In addition to X-ray crystallography, computational studies could also provide further insight into the tautomeric polymorphism phenomenon.

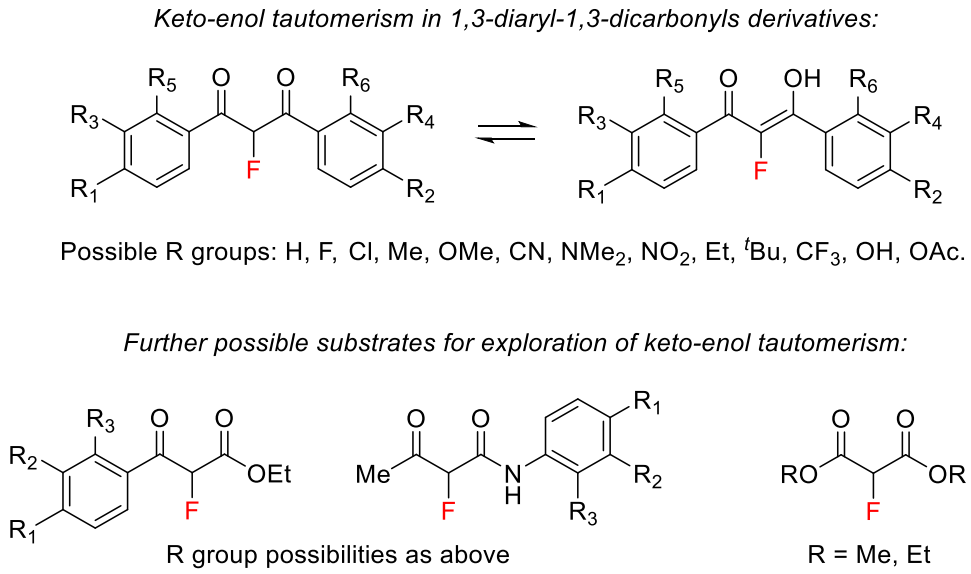

Figure 148: Possibilities for further work on synthesis and crystallisation of 2-fluoro-1,3-dicarbonyl derivatives, including ketoesters, ketoamides and malonate esters.

Kinetics studies with additional fluorinating reagents could be carried out, including analogues of *N*-fluoropyridinium salts and NFSI that were not studied in this thesis (**Figure 149**). The reactivity scale developed in the present work shows that there is an interval in reactivity of 3 orders of magnitude between Synfluor™ and NFSI. Analogues of NFSI could be prepared by design, where the aryl substituents can be altered in order to tune the reactivity of the reagent. Increasing the number of fluorine substituents on the *N*-fluoropyridinium ring is likely to result in increased fluorinating ability and these derivatives are expected to be more reactive than pentaCl-NFPy TfO^- **51a**. Since the stability of **51a** above 40 °C was low and required storage below 0 °C, this limits its suitability as a commercial reagent. Therefore, the use of fluorinating reagents more reactive than **51a** would be limited by their low persistence. The balance between reactivity and bench-stable nature is a key challenge for the development of new fluorinating reagents.

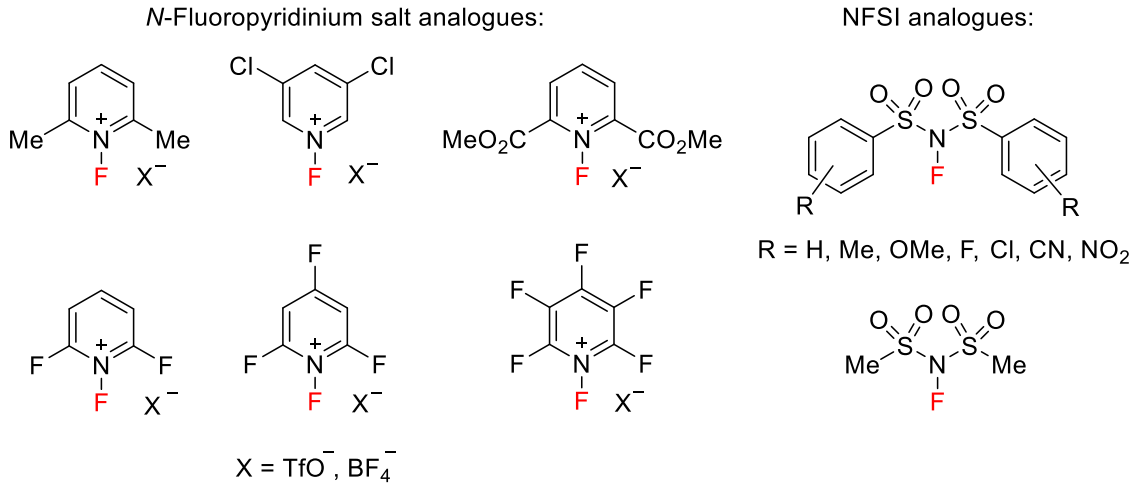

Figure 149: Derivatives of *N*-fluoropyridinium salts and NFSI that were not included in kinetics studies in this thesis.

The fluorination of substrates with halogen and alkyl substituents at the 2-position could be explored (**Figure 150**). Steric effects are likely to affect the rates of fluorination of substrates with bulky substituents such as ^{t}Bu. Larger halogens such as Cl and Br are likely to affect fluorination rates by both electronic and steric effects. The chloro- and bromo- substituents would be particularly useful in further investigating the origin of the increased sensitivity of 2-fluoro-1,3-dicarbonyl compounds during keto-to-enol relaxation processes.

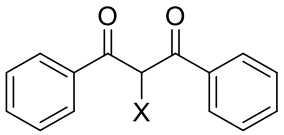

This work: X = H, F.
Future work: X = Br, Cl, Me, Et, ^{t}Bu.

Figure 150: Possible substrates that could be studied in future work, with different substituents at the 2-position.

Kinetics studies could be expanded to the fluorination of 2-fluorinated β-ketoesters, β-ketoamides and malonate esters such as those shown in **Figure 148**. Metal-catalysed fluorination reactions of 1,3-dicarbonyl derivatives, involving Ti and Ru catalysts previously described in the literature, could also be studied using a kinetics approach.

In Chapter 3, the de-fluorination of 2-fluoro-1,3-diphenyl-1,3-propanedione by DABCO was discovered. This reaction could be investigated in greater detail since the *para*-substituent appears to affect the outcome. Reactions with other bases, such as DBU, pyridine and quinuclidine, could be carried out, as well as exploring if de-fluorination is possible using 2,2-difluoro-1,3-dicarbonyl derivatives. The photoketonization-relaxation experiments could be expanded to additional 1,3-dicarbonyl derivatives such as those shown in **Figure 148**. Conducting further studies on the autocatalytic nature of relaxation of monofluoro-diketone derivatives could provide further insight into the origin of this effect. In Chapter 4, the greater reactivites of mono-fluoroenols relative to non-fluorinated enols was associated with the relatively lower stability of fluorine atoms at sp^2-centres. The origin of these findings could be explored using DFT calculations.

To further develop the work discussed in Chapter 5, the kinetics of fluorination of aromatic systems such as indoles, pyrroles and anisoles can be carried out, since fluoroaromatic compounds are widespread in pharmaceuticals. Further exploration of the use of water as a co-solvent for the fluorination of indoles could be conducted and applied to pyrrole systems. The determination of nucleophilicity parameters, *N*, for enols and enolates could be continued using benzhydrilium ions displaying lower electrophilicities than the ions already investigated in the present work (**Figure 151**), since reactions involving $(dma)_2CH^+$ were extremely fast and difficult to monitor accurately using stopped flow UV-vis spectrophotometry. The enol forms of the 1,3-diaryl-1,3-propanediones are estimated to be several orders of magnitude less reactive

than their enolate forms, hence, nucleophilicities could be determined using more reactive benzhydrilium ions ($E \sim 0$).

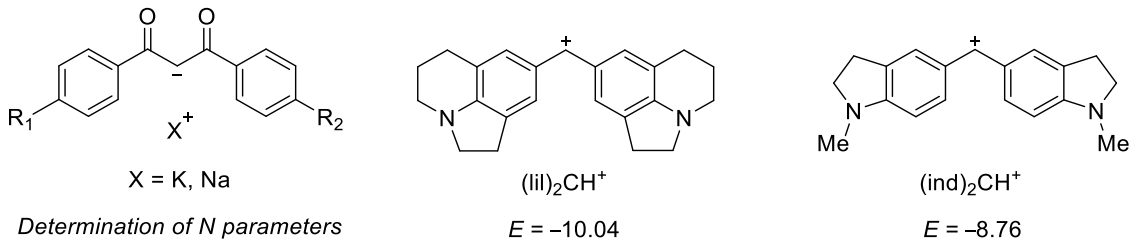

Figure 151: Benzhydrilium ions predicted to have correct levels of reactivity for determination of reaction kinetics with enolates of 1,3-diaryl-1,3-propanedione derivatives.

Finally, further work could be carried out on the topics covered in Chapter 6, given the significance of fluorosteroids within the pharmaceutical industry. Due to the highly corrosive nature of F_2, determining reaction kinetics is challenging. Thus, monitoring the fluorination of progesterone enol acetate with F_2 via *in situ* IR spectroscopy using a Mettler-Toledo ReactIR probe could provide information on the relative rates of formation of the desired product and side products. For the preparative reaction with F_2, conducting the reaction in a continuous flow reactor rather than a batch system could reduce the formation of side products. The substrate scope could be expanded to enolizable steroids of different classes, such as nestorone (a progestogen), prednisone (a glucocorticoid), and fludrocortisone (a corticosteroid) for further kinetics studies on fluorination reactions involving the N−F reagents (**Scheme 53**). This would enable both a detailed comparison of nucleophilic reactivities of the steroid enol esters, and a more quantitative understanding of the preferences for α- and β-fluoroisomers.

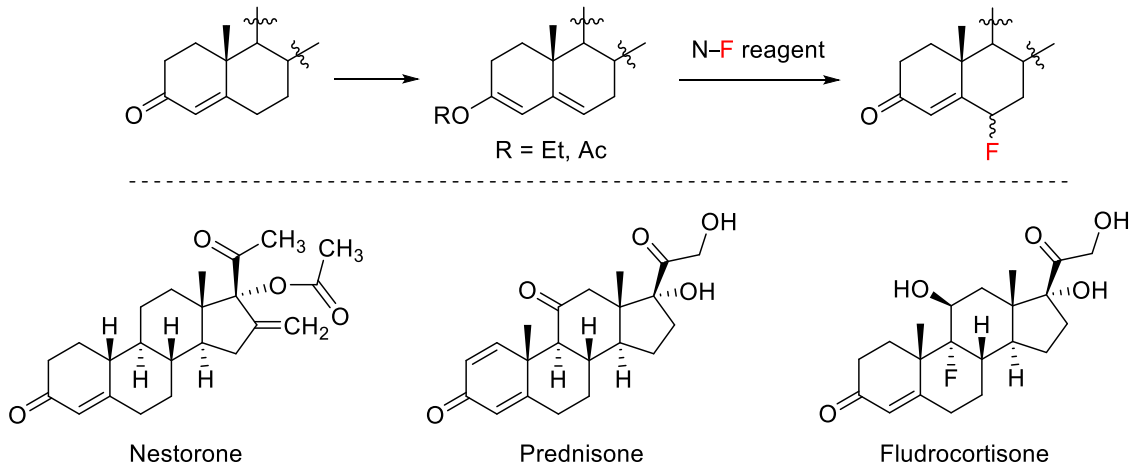

Scheme 53: Enolizable steroids as possible substrates for future kinetics studies on fluorination reactions.

The physical organic approaches taken in this project towards electrophilic fluorination and keto-enol tautomerism have revealed valuable quantitative information for the design of fluorination reactions. The wider impact of our reactivity scale, discussed in Chapter 2, has already been reported by other groups in aiding the process of N−F reagent selection.[135,237] Certainly, the continuation of quantitative studies using a wider range of both fluorinating reagents and substrates would be of great benefit for both discovery and manufacture.

Chapter 8: Experimental

8.1 General

^{1}H NMR (400 MHz), ^{13}C NMR (101 MHz) and ^{19}F NMR (376 MHz) were measured on a Bruker-Avance 400 MHz spectrometer. Kinetic NMR data in Chapters 2 and 6 were acquired on a Varian Inova-500 MHz spectrometer. Stopped-flow kinetics data was acquired using an Applied Photophysics stopped-flow UV-vis spectrophotometer. LC-MS data were obtained using a triple quadrupole mass spectrometer equipped with an Acquity UPLC (Waters Ltd, UK), EH C18 column (1.7μm, 2.1mm × 50mm) and a photodiode array detector. Conditions for LC resolution were as follows: buffer A = water, 0.1% formic acid; buffer B = MeCN. Elution conditions: Flow rate = 0.6 mL/min; 0-0.2 min isocratic 95% A, 5% B; 0.2-4 min linear gradient to 5% A, 95% B; 4-4.5 min isocratic 5% A, 95% B; 4.5-5 min linear gradient to 95% A, 5% B. Chemicals were purchased from Fluorochem, TCI or Sigma Aldrich and, unless otherwise stated, used without purification. NMR solvents were purchased from Cambridge Isotopes Inc., supplied by Goss Scientific and Sigma-Aldrich. These chemicals were used without further purification and stored under appropriate conditions, as detailed in the manufacturer's instructions. Organic solvents were used without further purification. Selectfluor™ and NFSI were purchased from Fluorochem; fluorinating reagent **50a** was purchased from Sigma-Aldrich; fluorinating reagents **12a**, **12b**, **50b**, **52a**, **52b** and **55d** were purchased from TCI and used without further purification. HPLC grade MeCN supplied by Fisher Scientific was used throughout for kinetics studies. Formic acid (Romil SpR Super Purity Reagent) was used in Chapters 3 and 4.

8.1.1 X-ray Crystallography

The X-ray single crystal data were collected using λMoKα radiation (λ =0.71073Å) at 120.0(2)K on a Bruker SMART CCD 6000 (graphite monochromator, fine-focus tube, Monocap optics) (compounds **108c-keto, 108c-enol**) and a Bruker D8Venture (Photon100 CMOS detector, IμS-microsource, focusing mirrors) (all other compounds) diffractometers equipped with a Cryostream (Oxford Cryosystems) open-flow nitrogen cryostats. All structures were solved by the direct method and refined by full-matrix least squares on F2 for all data using Olex2[238] and SHELXTL[239] software. All non-disordered non-hydrogen atoms were refined anisotropically, hydrogen atoms were refined isotropically, however, the hydrogen atoms in structures **108c-enol** and **108a-**

keto were placed in the calculated positions and refined in riding mode. Molecule **108a-keto** showed whole molecule disorder and all atoms were refined with fixed SOF=0.5. Crystal data and parameters of refinement are listed in the Appendices. Crystallographic data for the structure were deposited with the Cambridge Crystallographic Data Centre as a supplementary publication CCDC-1857922-1857928.

8.2 Kinetics studies conducted by UV-vis spectrophotometry

Kinetics studies were carried out using a Varian Cary-100 Bio UV-vis Spectrophotometer equipped with a Cary Temperature Controller unit, or a Varian Cary-50 Bio UV-vis Spectrophotometer connected to a Varian Cary PCB-150 Water Peltier system. Samples were contained in quartz absorption cuvettes with a path length of 1 cm. All spectra were zeroed against air. Reactions were followed by monitoring the disappearance of the nucleophile or electrophile at a fixed wavelength corresponding to the maximum absorbance (λ_{max}) of the reaction partner. All reactions were carried out under pseudo-first-order conditions in the presence of excess nucleophile or electrophile, as stated. Standard error values are reported for k_{obs} values and were obtained from data fitting in KaleidaGraph software. Stock solutions of purified nucleophiles **107a-m** (5-10 mM) and N−F reagents **12a/b**, **17**, **19**, **50a/b**, **52a/b**, **51** and **55d** (5-180 mM) in MeCN (HPLC grade) were prepared in volumetric flasks. For kinetics studies involving water-sensitive N−F reagents (**55d**, **50a** and **50b**), MeCN was distilled from CaH_2 immediately before use. Aliquots of each stock solution were removed and diluted accordingly to the desired concentration. In a typical experiment, an aliquot of the stock solution of the nucleophile was diluted to the desired concentration in a cuvette, which was placed in the spectrophotometer for 10 mins to equilibrate to the required temperature. The required fluorinating reagent was then added, and the cuvette was inverted 3 times to mix the reagents. The cuvette was immediately returned to the spectrophotometer and kinetics studies were carried out using the "Scanning Kinetics" or "Single Wavelength Kinetics" programs.

8.3 Experimental to Chapter 2:

8.3.1 Computational methods

Geometry optimisations were carried out on the keto and enol monomers and dimers of **107c** in the gas phase with the B3LYP[240,241] functional and the 6-311++G** basis set[242,243] using the software package Gaussian09. These optimised geometries were

confirmed as true minima by frequency calculations. Single point energy calculations with the Gaussian09 default polarisation continuum solvent model (IEF-PCM) at B3LYP/6-311++G** were performed on the optimised gas-phase geometries with a dielectric constant of ε = 3 as the average dielectric constant for neutral organic crystals.[126]

8.3.2 1,3-bis(4'-cyanophenyl)-1,3-propanedione

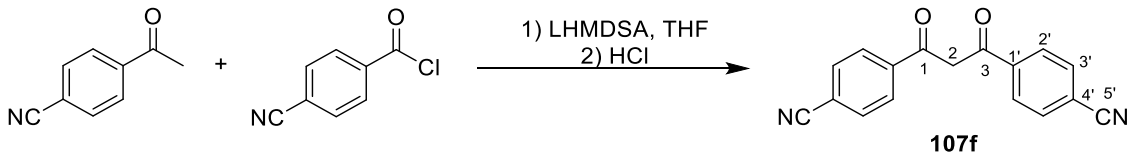

107f

A mixture comprising of 4'-acetylbenzonitrile (0.50 g, 3.44 mmol) and $LiN(SiMe_3)_2$ (1 M in THF, 6.89 mmol, 6.9 mL) in anhydrous THF (7 mL) were stirred at −78 ºC for 30 min. 4'-Cyanobenzoyl chloride (0.57 g, 3.44 mmol) was added and the mixture was stirred at RT overnight. Upon quenching the reaction with 37% HCl (1 mL), the product was precipitated as a yellow solid and was recovered by filtration and washed with water. The filtrate was extracted with ethyl acetate (3 x 10 mL), and the combined organic phases were washed with sodium bicarbonate (10 mL) and water (10 mL). Drying ($MgSO_4$) and evaporation of solvent *in vacuo* yielded further product. Both batches of solid were recrystallised from EtOH to give pure 1,3-bis(4'-cyanophenyl)-1,3-propanedione (0.51 g, 54%) as a yellow solid. **IR** (ATR) υ_{max}/ cm^{-1} 3070 (C-H arom), 2230 (CN), 1582 (enol), 1522, 1447, 1290, 1222, 1020, 860, 784, 694, 542. **^{1}H NMR** (400 MHz, $CDCl_3$) δ = 8.08 (4H, d, $^3J_{HH}$ = 8.2 Hz, 2'-*H*), 7.81 (4H, d, $^3J_{HH}$ = 8.3 Hz, 3'-*H*), 6.86 (1H, s, 2-*H* of enol). **^{13}C NMR** (101 MHz, $CDCl_3$) δ = 184.2 (C-1, C-3), 138.8 (C-4'), 132.6 (C-1'), 127.8 (C-2'), 117.9 (C-5'), 116.1 (C-3'), 94.5 (C-2). **ESI-MS** (ES^-, R_t 2.892 min) *m*/*z* 273.091 $[M-H]^-$. **M.p.** (EtOH) = 220 °C (lit. m.p. 220– 222 °C).

These assignments are in agreement with the literature.[244]

8.3.3 1,3-bis(4'-nitrophenyl)-1,3-propanedione

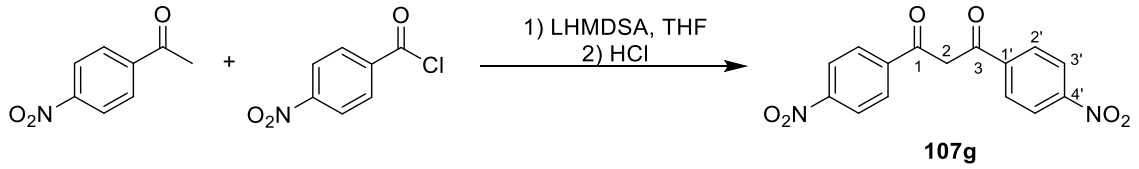

107g

A mixture comprising of 4'-nitroacetophenone (0.52 g, 3.16 mmol) and $LiN(SiMe_3)_2$ (1 M in THF, 6.06 mmol, 6.1 mL) in anhydrous THF (7 mL) was stirred at −78 °C for 30 min. 4'-Nitrobenzoyl chloride (0.59 g, 3.16 mmol) was added and the mixture was stirred at RT overnight. The crude product was quenched with 37% HCl (1 mL), and the product precipitated as a brown solid which was filtered and washed with water. The filtrate was extracted with ethyl acetate (3 x 10 mL), washed with sodium bicarbonate (10 mL) and water (10 mL) and dried ($MgSO_4$). The solvent was evaporated to yield the crude as a red solid. Both batches of crude product were recrystallised from ethyl acetate to give pure 1,3-bis(4'-nitrophenyl)-1,3-propanedione (0.76 g, 77%) as a brown solid (98% enol tautomer in $CDCl_3$). **IR** (ATR) υ_{max}/ cm^{-1} 3126 (C-H arom), 1580 (conj. enol), 1510 (s, NO_2), 1340 (s, NO_2), 1320, 1224, 1109, 1048, 1010, 857, 786, 744, 709; **^{1}H NMR** (400 MHz,$CDCl_3$) δ = 15.99 (1H, s, RC=C-O*H*), 8.40-8.32 (4H, m, 2'-*H*), 8.20-8.13 (4H, dq, J_{HH} = 9.2, 2.2 Hz, 3'-*H*), 6.93 (1H, s, 2-*H* of enol). **^{13}C NMR** (101 MHz, $CDCl_3$) δ = 184.3 (C-1, C-3), 150.6 (C-4'), 140.7 (C-1'), 128.7 (C-2'), 124.4 (C-3'), 95.4 (C-2). **ESI-MS** (ES^-, R_t 3.159) *m/z* 313.273 $[M-H]^-$. **HRMS (ES^-/Q-TOF) *m/z*:** $[M-H]^-$ Calcd for $C_{15}H_9N_2O_6$ 313.0469; found 313.0453. **M.p.** (EtOAc) = 237-238 °C (lit. m.p. 238 – 243 °C).

These assignments are in agreement with the literature.[245]

8.3.4 1,3-bis[4'-(dimethylamino)phenyl]-1,3-propanedione

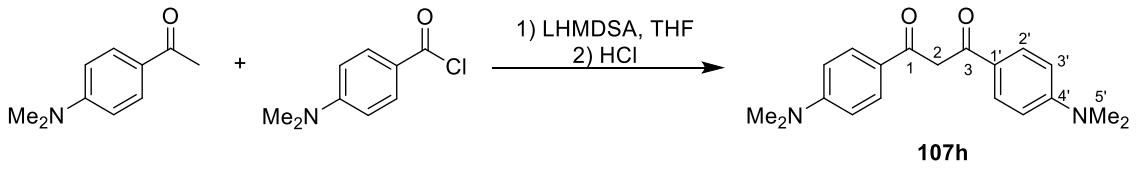

107h

A mixture comprising of 1-[4'-(dimethylamino)phenyl]ethanone (1.0 g, 6.13 mmol) and $LiN(SiMe_3)_2$ (1 M in THF, 12.3 mmol, 12 mL) in anhydrous THF (14 mL) were stirred at −78 °C for 30 min. 4'-(Dimethylamino)benzoyl chloride (1.13 g, 6.13 mmol) was added and the mixture was stirred at RT overnight. The crude product was quenched with KH_2PO_4 (3 g), extracted with ethyl acetate (3 x 30 mL), washed with sodium

bicarbonate (30 mL) and water (30 mL) and dried ($MgSO_4$). The solvent was evaporated to yield the crude as a yellow solid. This was recrystallised from ethanol to yield 1,3-bis[4'-(dimethylamino)phenyl]-1,3-propanedione (1.18 g, 62%) as brown crystals (70% enol in MeCN-d_3). **IR** (ATR) υ_{max}/ cm^{-1} 2894, 1602, 1561, 1476, 1432 1370, 1235, 1164, 1063, 948, 923, 783, 710. **^{1}H NMR** (400 MHz, MeCN-d_3): enol signals: δ = 7.92 (4H, d, $^3J_{HH}$ 9.2, 2'-*H*), 6.80 (1H, s, 2-*H*), 6.77 (4H, d, $^3J_{HH}$ 9.1, 3'-*H*), 3.05 (12H, s, 5'-*H*); keto signals: δ = 7.83 (4H, d, $^3J_{HH}$ 9.2, 2'-H), 6.71 (4H, d, $^3J_{HH}$ 9.1, 3'-*H*), 4.42 (2H, s, 2-*H*), 3.03 (12H, s, 5'-*H*). **ESI-MS** (ES^+, R_t 3.244) *m*/*z* 311.753 $[M+H]^+$ enol, (ES^+, R_t 2.510) *m*/*z* 312.589 $[M+2H]^+$ keto.

These assignments are in agreement with the literature.[246]

8.3.5 2-fluoro-1,3-diphenyl-1,3-propanedione

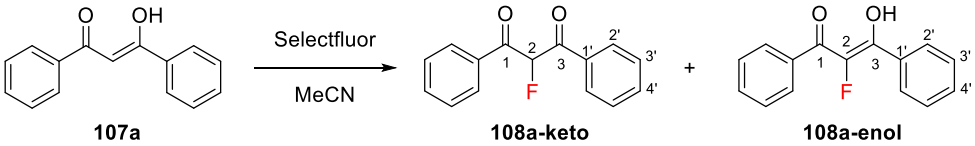

1,3-diphenyl-1,3-propanedione (227 mg, 1 mmol) was dissolved in dry MeCN (10 mL) and Selectfluor™ (354 mg, 1 mmol) was added. The reaction mixture was stirred at room temperature for 2.5 h and monitored by TLC. The solvent was evaporated *in vacuo*, and the white residue was dissolved in CH_2Cl_2 (20 mL) and washed with water (5 × 20 mL). The organic phase was separated, dried ($MgSO_4$), solvent evaporated *in vacuo* and the crude product was obtained as an off-white solid. Recrystallisation was done from hexane to obtain white crystals of 2-fluoro-1,3-diphenyl-1,3-propanedione (170 mg, 70%) as a 98:2 mixture of keto:enol forms in $CDCl_3$. **IR** (ATR) υ_{max}/ cm^{-1} 3071 (C-H arom), 1698 (C=O), 1670 (C=O), 1593 (arom C=C), 1576, 1448, 1284, 1229, 1181, 1098, 967, 868, 778, 708. **^{1}H NMR** (400 MHz, $CDCl_3$) δ = 10.18 (1H, s, RC=C-O*H*), 8.15-8.05 (4H, dq, J_{HH} = 7.7, 1.2 Hz, 2'-*H* keto), 7.65-7.59 (2H, m, 4'-*H* keto), 7.52-7.46 (4H, m, 3'-*H* keto), 6.54 (1H, d, $^2J_{HF}$ = 49.2 Hz, 2-*H* keto). **^{13}C NMR** (101 MHz, $CDCl_3$) δ = 191.5 (d, $^2J_{CF}$ = 20.2 Hz, C-1, C-3), 134.9 (s, C-4'), 133.9 (d, $^4J_{CF}$ = 1.9 Hz, C-2'), 130.2 (d, $^3J_{CF}$ = 3.5 Hz, C-1'), 129.1 (s, C-3'), 97.0 (d, $^1J_{CF}$ = 199.0 Hz, C-2). **^{19}F NMR** (376 MHz, $CDCl_3$) δ = −186.9 (d, J_{FH} = 49.8 Hz, keto), −166.5 (s, enol). **ESI-MS** (ES^+, R_t 3.988) *m*/*z* 243 $[M+H]^+$ enol; (ES^+, R_t 3.390) *m*/*z* 265 $[M+Na]^+$ keto. **M.p.** (hexane) = 65-66 °C (lit. m.p. 66.5-66.7 °C).

These assignments are in agreement with the literature.[118]

Crystal structure: keto tautomer

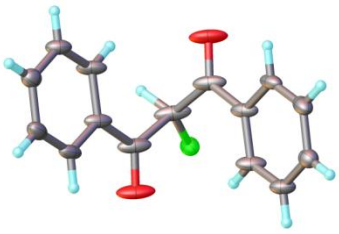

8.3.6 2-fluoro-1,3-bis(4'-fluorophenyl)-1,3-propanedione

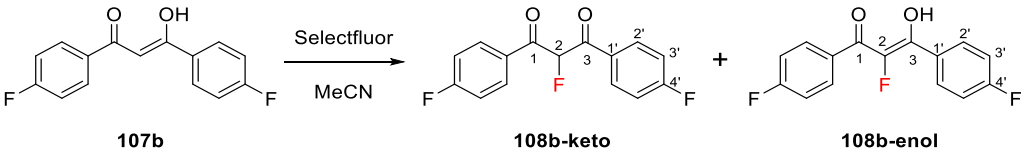

107b **108b-keto** **108b-enol**

1,3-bis(4'-fluorophenyl)-1,3-propanedione (131 mg, 0.50 mmol) was dissolved in MeCN (10 mL) and Selectfluor™ (178 mg, 0.50 mmol) was added. The reaction mixture was stirred at room temperature for 96 h. The solvent was evaporated *in vacuo*, and the yellow residue was dissolved in CH_2Cl_2 (20 mL) and washed with water (5 × 20 mL). The organic phase was separated, dried ($MgSO_4$), solvent evaporated *in vacuo* and the crude product was obtained as a yellow solid. The crude material was purified by recrystallisation from a mixture of chloroform and hexane, to yield the pure product as a yellow solid (100 mg, 71%, 98:2 keto:enol). An additional recrystallisation step was carried out (chloroform, hexane), and on visual inspection, two different types of crystals were seen to be present. Crystals of **108b-keto** were white whereas crystals of **108b-enol** were yellow. Individual crystals were analysed by NMR spectroscopy and X-ray crystallography to confirm the constitutions of these tautomers.

Keto tautomer: **^{1}H NMR** (400 MHz, $CDCl_3$) δ = 8.19-8.12 (4H, m, 2'-*H*), 7.20-7.12 (4H, m, 3'-*H*), 6.48 (1H, d, $^{2}J_{HF}$ = 49.3, 2-*H*). **^{13}C NMR** (101 MHz, $CDCl_3$) δ = 189.8 (d, $^{2}J_{CF}$ = 20.4 Hz, C-1, C-3), 166.9 (d, $^{1}J_{CF}$ = 258.2 Hz, C-4'), 133.2 (dd, J_{CF} = 9.7, 3.8 Hz, C-2'), 130.1 (t, $^{3}J_{CF}$ = 2.6 Hz, C-1'), 116.5 (d, $^{2}J_{CF}$ = 22.0 Hz, C-3'), 97.0 (d, $^{1}J_{CF}$ = 199.7 Hz, C-2). **^{19}F NMR** (376 MHz, $CDCl_3$) δ = −186.1 (d, $^{1}J_{FH}$ = 49.9 Hz, C2-*F*), −101.5 (s, 2 × C4'-*F*).

Enol tautomer: **^{1}H NMR** (400 MHz, $CDCl_3$) δ = 14.86 (1H, d, ^{4}J = 3.3 Hz, RC=C-O*H*), 8.11-8.03 (4H, m, 2'-*H*), 7.23-7.15 (4H, m, 3'-*H*). **^{13}C NMR** (101 MHz, $CDCl_3$) δ = 174.9 (d, $^{2}J_{CF}$ = 21.1 Hz, C-1), 165.5 (d, $^{1}J_{CF}$ = 254.9, C-4'), 144.3 (d, $^{1}J_{CF}$ = 235.8 Hz, C-2), 132.0 (t, $^{3}J_{CF}$ = 9.13 Hz, C-2'), 129.9 (d, $^{3}J_{CF}$ = 9.13 Hz, C-1'), 116.1 (d, $^{2}J_{CF}$ =

21.7 Hz, C-3'). **^{19}F NMR** (376 MHz, $CDCl_3$) δ = −168.9 (s, C2-*F*), −105.4 (s, 2x C4'-*F*).

Crystal structures: keto and enol tautomers

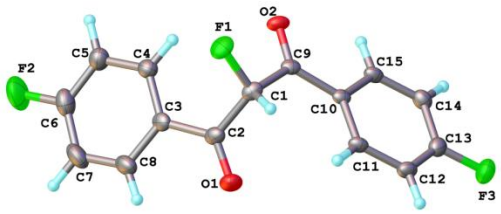

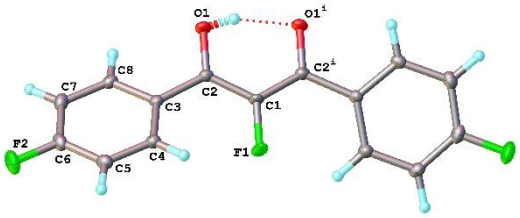

8.3.7 2-fluoro-1,3-bis(4'-methylphenyl)-1,3-propanedione

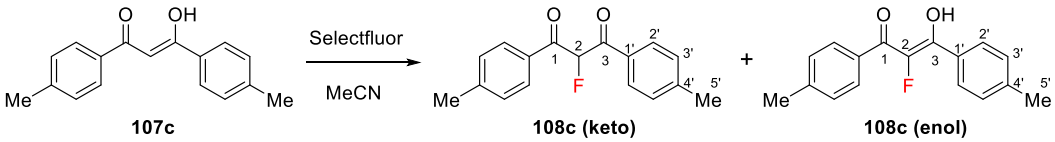

1,3-bis(4'-methylphenyl)-1,3-propanedione (141 mg, 0.56 mmol) was dissolved in MeCN (15 mL) and Selectfluor™ (198 mg, 0.56 mmol) was added. The reaction mixture was stirred at room temperature for 44 h. The solvent was evaporated *in vacuo* to give a residue which was dissolved in CH_2Cl_2 (20 mL) and washed with water (5 × 20 mL). The organic phase was separated and dried ($MgSO_4$). The solvent was evaporated *in vacuo* to give the crude product as a yellow solid. The crude material was purified by recrystallisation from a mixture of chloroform and hexane, to yield the pure product as a yellow solid (80 mg, 53%). Low yield was obtained as the product is very soluble in chloroform, so some product is lost during recrystallisation, but can be recovered from the supernatant. The pure compound contained a 97:3 mixture of keto:enol forms in $CDCl_3$. An additional recrystallisation step was performed (chloroform/hexane) to obtain crystals of **108c-keto** (white) and **108c-enol** (yellow). **IR** (ATR) υ_{max}/ cm^{-1} 1697 (C=O), 1667 (C=O), 1604 (arom C=C), 1288, 1246, 1233, 1186 (C-F), 1091, 1038, 960, 877, 825, 752, 686. **^{1}H NMR** (400 MHz, $CDCl_3$) δ = 15.02 (1H, br, s, RC=C-O*H*), 8.02-7.96 (4H, m, 2'-*H* keto), 7.30-7.23 (4H, m, 3'-*H* keto), 6.49 (1H, d, $^2J_{HF}$ = 49.3 Hz, 2-*H* keto), 2.43 (6H, s, 5'-*H* enol), 2.40 (6H, s, 5'-*H* keto). **^{13}C NMR** (101 MHz, $CDCl_3$) δ = 190.9 (d, $^2J_{CF}$ = 20.1 Hz, C-1, C-3 keto), 175.7 (d, $^2J_{CF}$ = 20.9 Hz, C-1 enol), 145.8 (s, C-4' keto), 143.2 (s, C-4' enol), 131.3 (d, $^4J_{CF}$ = 2.2 Hz, C-2' keto), 130.1 (d, $^3J_{CF}$ = 3.5 Hz, C-1' keto), 129.6 (s, C-3' keto), 96.9 (d, $^1J_{CF}$ = 198.5 Hz, C-2 keto), 21.9 (s, C-5' keto), 21.8 (s, C-5' enol). **^{19}F NMR** (376 MHz, $CDCl_3$) δ =

−186.7 (d, $^{2}J_{FH}$ = 49.8 Hz, keto), −168.8 (s, enol). **ESI-MS**: *m*/*z* 271 (61%) $[M+H]^+$, 288 (100%) $[M+NH_4]^+$. **M.p.** (chloroform/hexane) = 88 – 89 °C.

Crystal structures: keto and enol tautomers

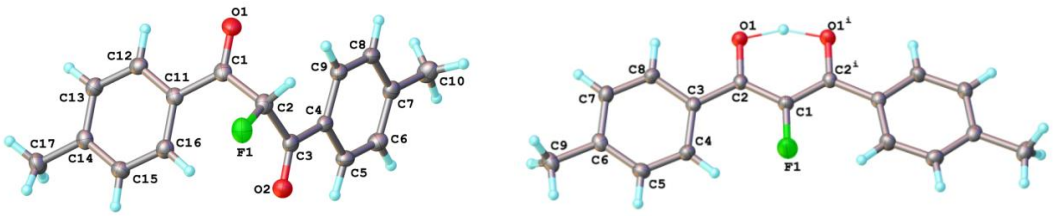

8.3.8 2-fluoro-1,3-bis(4'-methoxyphenyl)-1,3-propanedione

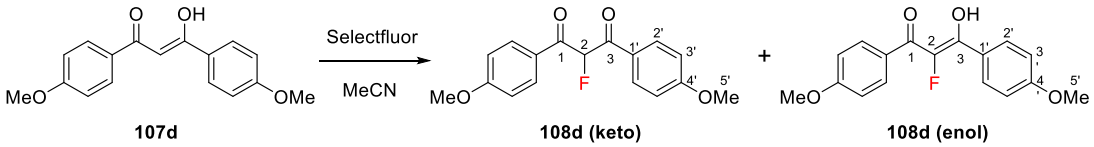

107d **108d (keto)** **108d (enol)**

1,3-bis(4'-methoxyphenyl)-1,3-propanedione (129 mg, 0.45 mmol) was dissolved in MeCN (10 mL) and Selectfluor™ (160 mg, 0.45 mmol) was added. The reaction mixture was stirred at room temperature for 2 h. The solvent was evaporated *in vacuo* and the white residue was dissolved in CH_2Cl_2 (20 mL) and washed with water (5 x 20 mL). The organic phase was separated, dried ($MgSO_4$) and the solvent evaporated *in vacuo*. The crude product was obtained as a yellow oil which partially solidified under vacuum. Recrystallisation was done from a mixture of chloroform and hexane to yield the pure product as a yellow solid (88 g, 64%), as a 98:2 mixture of keto:enol forms. Crystals of **108d-enol** were obtained via vapour diffusion crystallisation. **IR** (ATR) υ_{max}/ cm^{-1} 3014 (C-H arom), 2844 (C-H methyl), 1683 (C=O), 1659 (C=O), 1598 (arom C=C), 1571, 1510, 1312, 1252, 1170 (C-F), 1081, 1012, 961, 828. **^{1}H NMR** (400 MHz, $CDCl_3$) δ = 15.29 (1H, br, s, RC=C-O*H*), 8.14-8.07 (4H, m, 2'-*H*, keto), 8.07-8.02 (4H, m, 2'-*H*, enol), 7.01-6.95 (4H, m, 3'-*H*, enol), 6.96-6.90 (4H, m, 3'-*H*, keto), 6.45 (1H, d, $^{2}J_{HF}$ = 49.4 Hz, 2-*H*, keto), 3.86 (6H, s, 5'-*H*). **^{13}C NMR** (101 MHz, $CDCl_3$) δ = 189.9 (d, $^{2}J_{CF}$ = 20.0 Hz, C-1, C-3), 164.9 (s, C-4'), 132.7 (d, $^{3}J_{CF}$ = 3.6 Hz, C-1'), 126.9 (d, $^{4}J_{CF}$ = 2.1 Hz, C-2'), 114.3 (s, C-3'), 97.3 (d, $^{1}J_{CF}$ = 198.2 Hz, C-2), 55.9 (s, C-5'). **^{19}F NMR** (376 MHz, $CDCl_3$) δ = −186.0 (d, $^{2}J_{FH}$ = 50.0 Hz, keto), −169.4 (s, enol). **ESI-MS** (ES^+, R_t 2.638) *m*/*z* 303 (100%) $[M+H]^+$. **M.p.** (chloroform/hexane) = 65 °C. Lit: from DCM/hexane 87-88 °C.

These assignments are in agreement with the literature.[247]

Crystal structure: enol tautomer

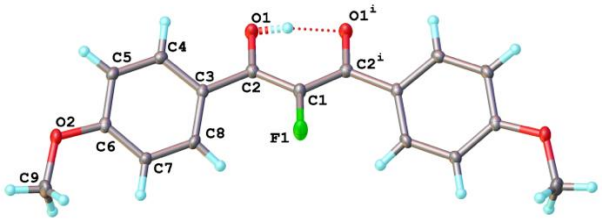

8.3.9 2-fluoro-1,3-bis(4'-chlorophenyl)-1,3-propanedione

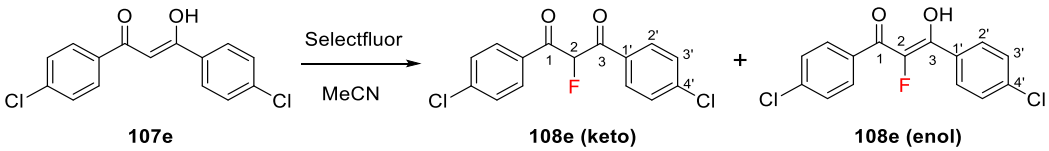

107e 108e (keto) 108e (enol)

1,3-bis(4'-chlorophenyl)-1,3-propanedione (150 mg, 0.51 mmol) was dissolved in MeCN (20 mL) and Selectfluor™ (181 mg, 0.51 mmol) was added. The reaction mixture was stirred at room temperature for 96 h. The solvent was evaporated *in vacuo* and CH_2Cl_2 (20 mL) was added to the yellow residue, which was then washed with water (5 × 20 mL). The organic phase was separated, dried ($MgSO_4$) and the solvent evaporated *in vacuo* to obtain the crude product as a yellow solid. Initial purification was carried out by recrystallisation (chloroform/hexane) to obtain the pure product as yellow crystals (140 mg, 88%, keto:enol 82:18 in $CDCl_3$). Recrystallisation was performed via vapour diffusion to obtain **108e-enol** as yellow crystals. **IR** (ATR) υ_{max}/ cm^{-1} 2560 (C-H arom), 1679 (C=O), 1588 (C=C arom), 1425, 1400, 1295, 1178, 1090, 99, 838, 746. **M.p.** (chloroform/hexane) = 122 – 123 °C. **Elem. Anal.** Calcd for $C_{15}H_9Cl_2FO_2$: C, 57.9; H, 2.92; N, 0. Found: C, 57.62; H, 2.50; N, -0.09.

Keto tautomer: **^{1}H NMR** (400 MHz, $CDCl_3$) δ = 8.06-8.02 (4H, m, 2'-*H*), 7.48-7.44 (4H, m, 3'-*H*), 6.47 (1H, d, $^2J_{HF}$ = 49.2 Hz, 2-*H*). **^{13}C NMR** (101 MHz, $CDCl_3$) δ = 190.2 (d, $^2J_{CF}$ = 20.5 Hz, C-1, C-3), 141.8 (s, C-4'), 132.0 (d, $^4J_{CF}$ = 2.3 Hz, C-2'), 131.6 (d, $^3J_{CF}$ = 3.8 Hz, C-1'), 129.6 (s, C-3'), 96.9 (d, $^1J_{CF}$ = 200.1 Hz, C-2). **^{19}F NMR** (376 MHz, $CDCl_3$) δ = −186.6 (d, $^2J_{FH}$ = 49.8 Hz).

Enol tautomer: **^{1}H NMR** (400 MHz, $CDCl_3$) δ = 14.74 (1H, br, s, RC=C-O*H*), 8.00-7.95 (4H, m, 2'-*H*), 7.50-7.45 (4H, m, 3'-*H*). **^{13}C NMR** (101 MHz, $CDCl_3$) δ = 175.0 (d, $^2J_{CF}$ = 21.2 Hz, C-1), 144.5 (d, $^1J_{CF}$ = 236.9 Hz, C-2), 139.3 (s, C-4'), 131.7 (d, $^4J_{CF}$ = 5.0 Hz, C-2'), 130.8 (d, $^3J_{CF}$ = 9.0 Hz, C-1'), 129.2 (s, C-3'). **^{19}F NMR** (376 MHz, $CDCl_3$) δ = −168.0 (s).

Crystal structure: enol tautomer

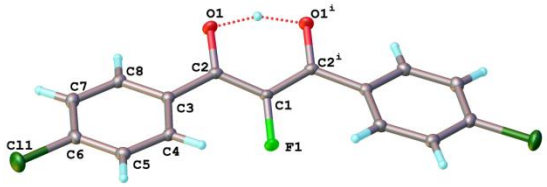

8.3.10 2-fluoro-1,3-bis(4-cyanophenyl)-1,3-propanedione

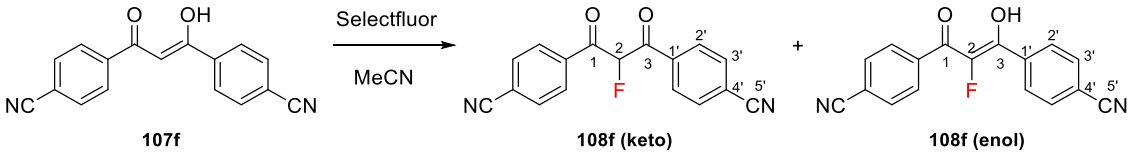

1,3-bis(4'-cyanophenyl)-1,3-propanedione (71 mg, 0.26 mmol) was dissolved in MeCN (15 mL) and Selectfluor™ (92 mg, 0.26 mmol) was added. The reaction mixture was stirred at room temperature for 1 week. The solvent was evaporated *in vacuo*, and the yellow residue was dissolved in CH_2Cl_2 (20 mL) and washed with water (5 × 20 mL). The organic phase was separated, dried ($MgSO_4$) and the solvent was evaporated *in vacuo*. The crude product was obtained as a yellow solid, which was purified by recrystallisation (chloroform/hexane) to give the pure product as an 84:16 mixture of enol:keto forms (47 mg, 62%). **^{1}H NMR** (400 MHz, $CDCl_3$) δ = 15.02 (1H, br, s, RC=C-O*H*), 8.07-8.01 (4H, m, 2'-*H*), 7.82-7.76 (4H, m, 3'-*H*), 6.55 (1H, d, $^2J_{FH}$ = 48.9, 2-*H* keto). **^{19}F NMR** (376 MHz, $CDCl_3$) δ = −187.2 (d, $^2J_{FH}$ = 48.8 Hz, keto), −166.9 (s, enol). **ESI-MS** (ES^-, R_t 2.457 min) *m*/*z* 291.232 $[M-H]^-$.

8.3.11 2,3,4,5,6-pentachloro-*N*-fluoropyridinium trifluoromethanesulfonate

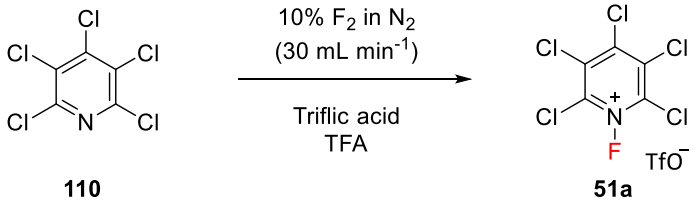

Pentachloropyridine (10.0 g, 39.8 mmol) was dissolved in trifluoroacetic acid (330 mL), and triflic acid (5 mL, 56.5 mmol) was added to the solution. The mixture was purged with nitrogen for 15 min and maintained at 10 °C using a temperature-controlled bath. F_2 (10% v/v in N_2) was passed through the mixture at 30 mL min^{-1} for 21 h. The mixture was purged with nitrogen for 15 min, then the trifluoroacetic acid was evaporated *in vacuo*, and the oily residue treated with ethyl acetate. The resulting white

solid was filtered, washed with ethyl acetate, and dried *in vacuo*. Recrystallisation from cold MeCN gave the product as a white crystalline solid (6.08 g, 36%). **^{19}F NMR** (376 MHz, MeCN-d_3) δ = +47.0 (s, NF), −79.4 (s, TfO^-). The assignments are in agreement with the literature.[35]

8.3.12 Extinction coefficients

Extinction coefficients were calculated using the Beer-Lamber Law (**Equation 32**), where A = absorbance at wavelength in question, ε = molar extinction coefficient at wavelength in question, c = concentration in mol dm^{-3}, and l = path length in cm.

$$A = \varepsilon c l \qquad (\mathbf{32})$$

For each system examined, the absorption spectra of 6 solutions of known concentration, in the range 0.0125 mM to 0.05 mM, were measured. A graph of absorbance versus concentration was constructed, the gradient of which gave the extinction coefficient in mol^{-1} dm^3 cm^{-1}.

Table 44: Extinction coefficients obtained for **107a** and **108a** (from figure below).

Compound	ε (enol) / mol^{-1} dm^3 cm^{-1}	ε (enol) / mol^{-1} dm^3 cm^{-1}
107a	24700	10170
108a	2700	40500

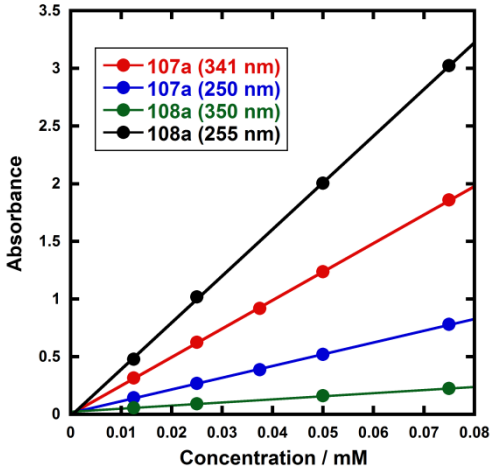

Figure 152: Determination of extinction coefficients for **107a** and **108a** at λ_{max} of absorbance bands.

8.3.13 Summary of all k_{obs} values for 107a-m with 10 N−F reagents

Fluorination of **107a** with Selectfluor™

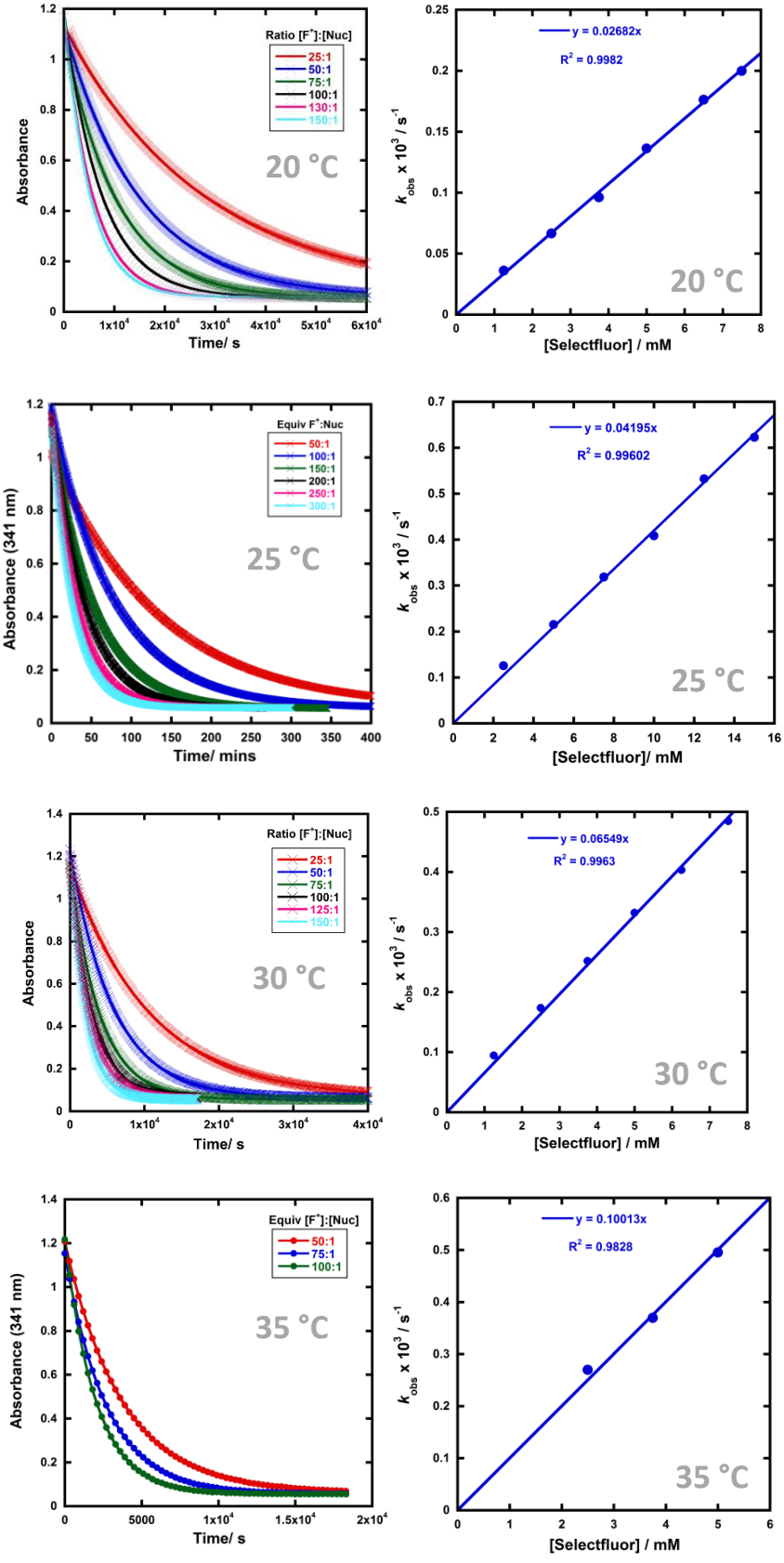

Fluorination of **107b** with Selectfluor™

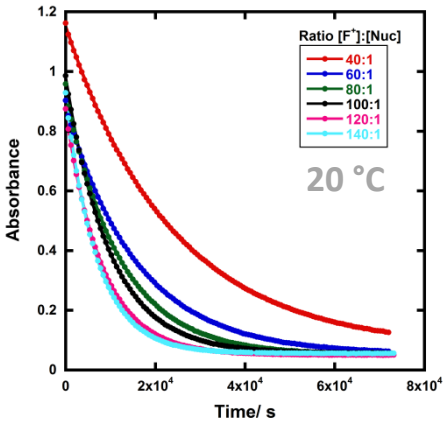

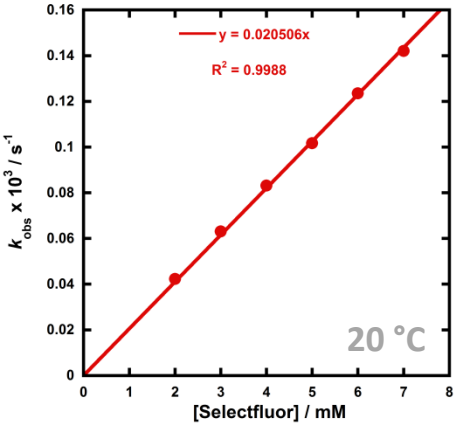

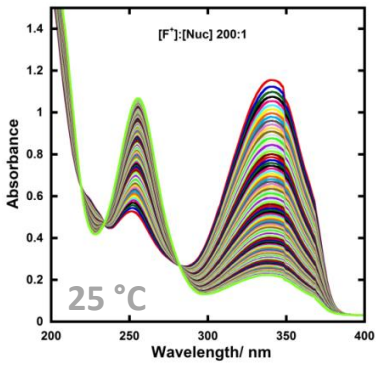

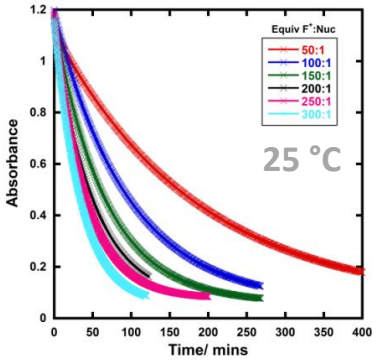

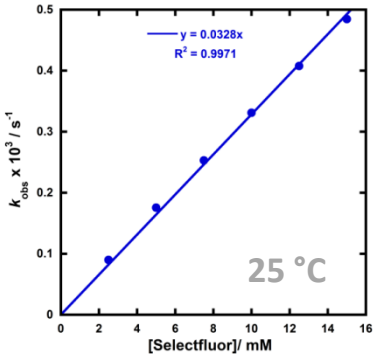

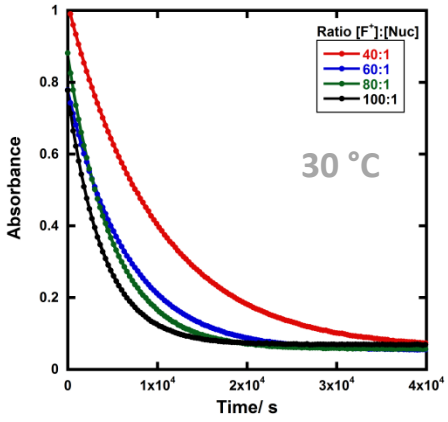

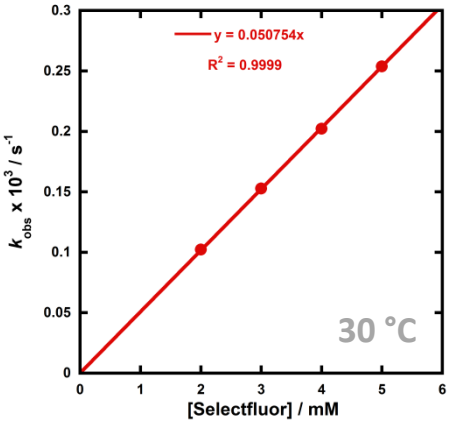

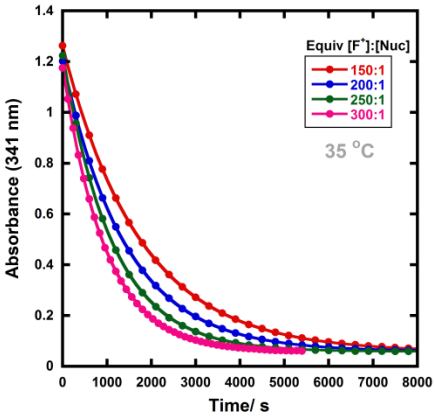

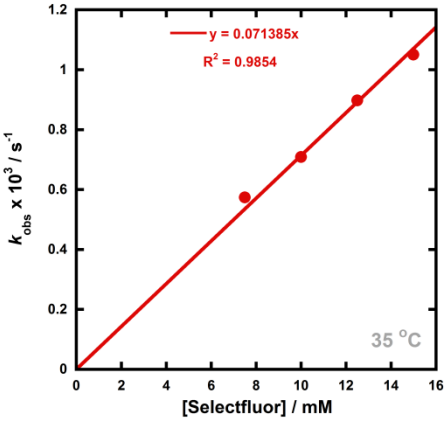

Fluorination of **107c** with Selectfluor™

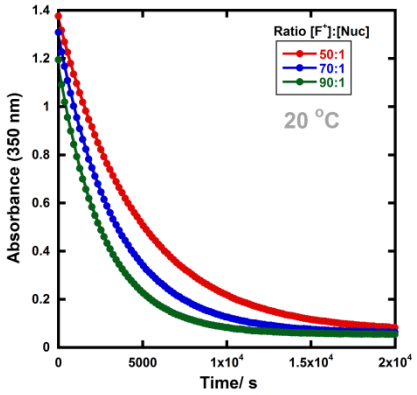

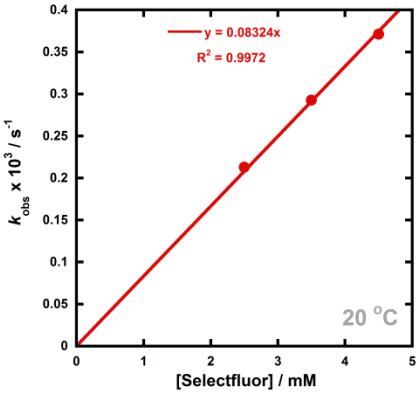

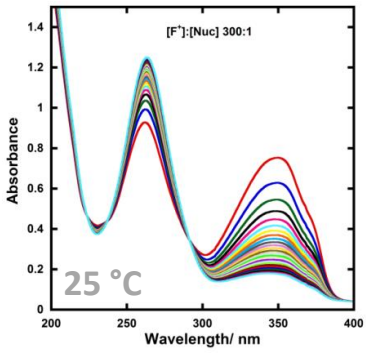

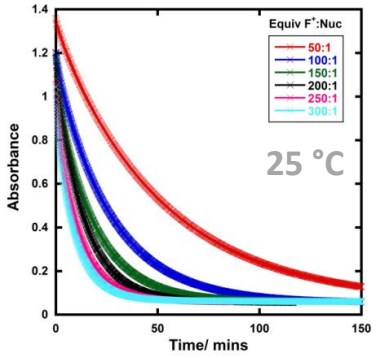

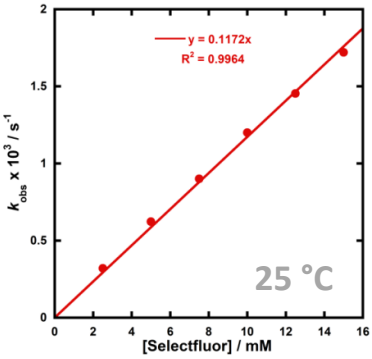

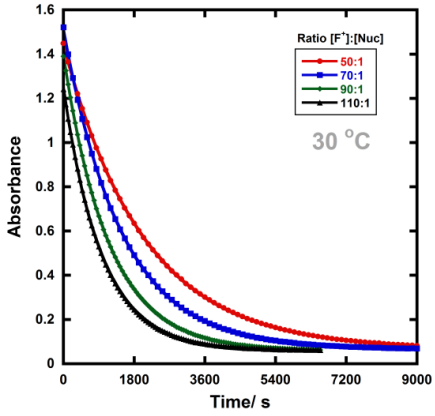

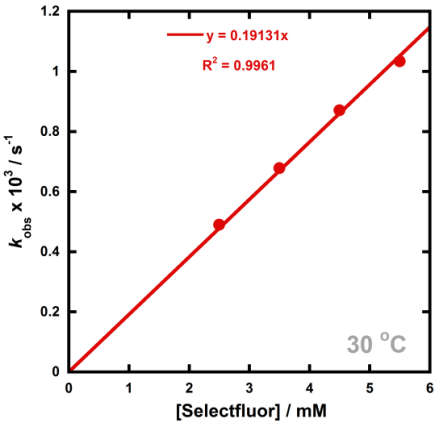

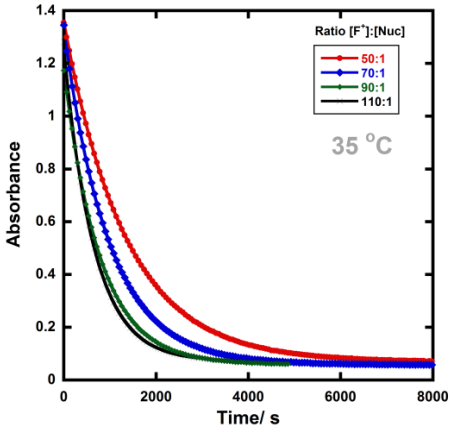

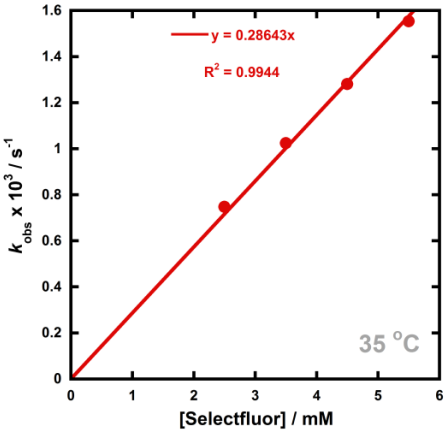

Fluorination of **107d** with Selectfluor™

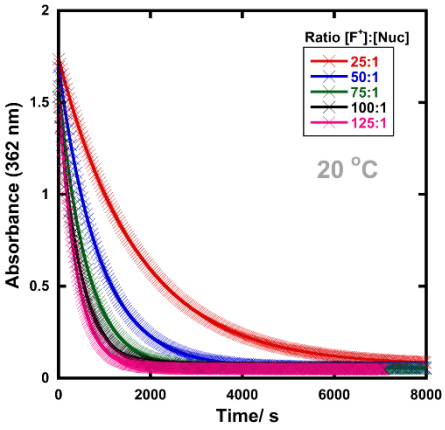

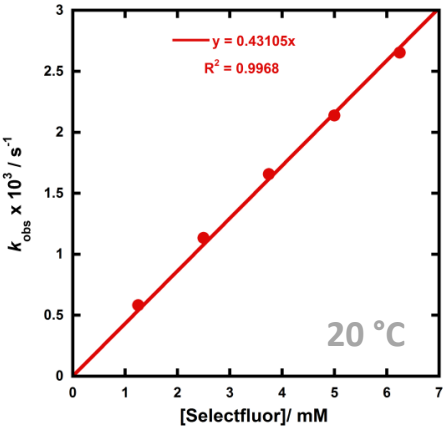

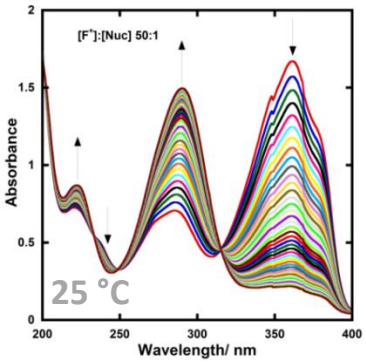

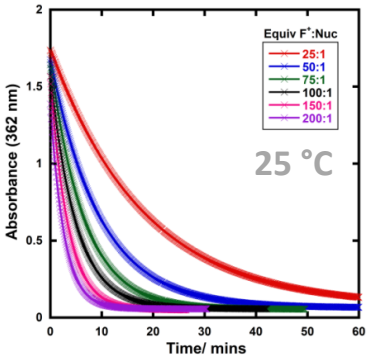

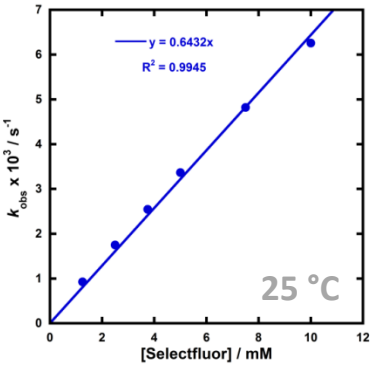

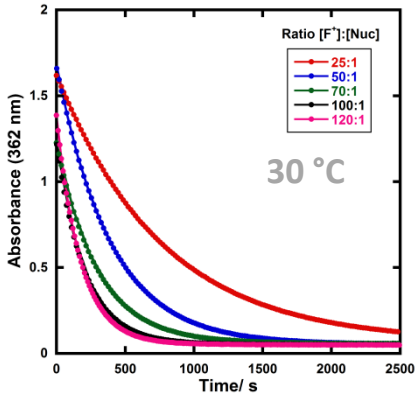

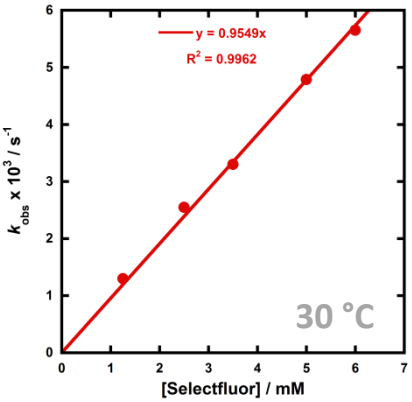

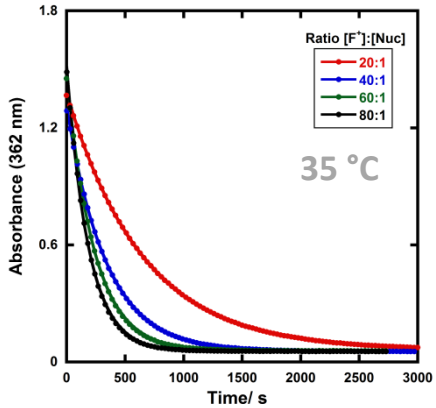

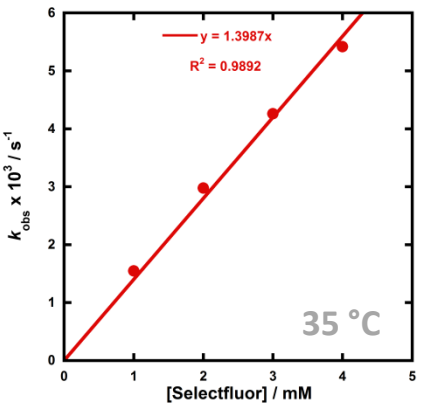

Fluorination of **107e** with Selectfluor™

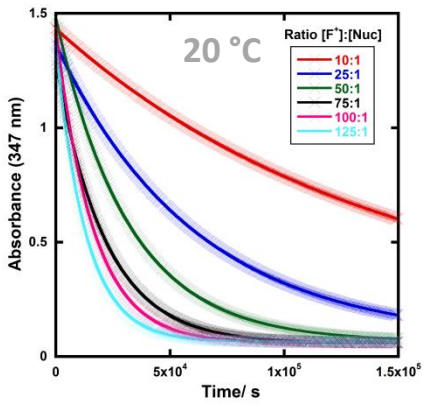

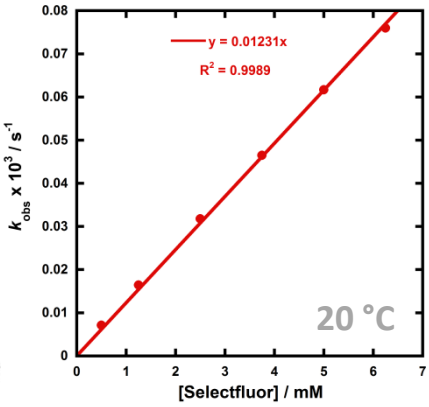

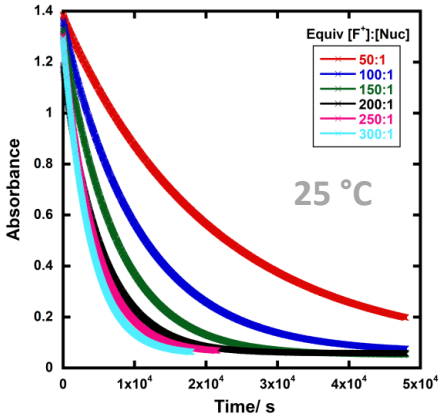

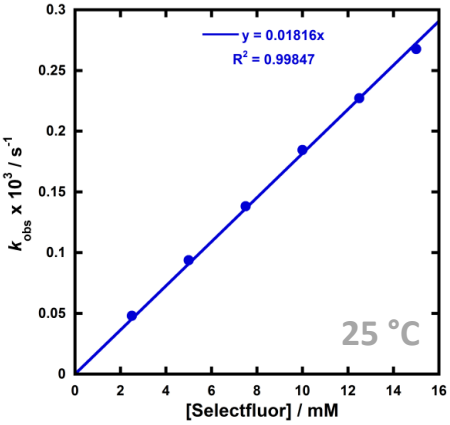

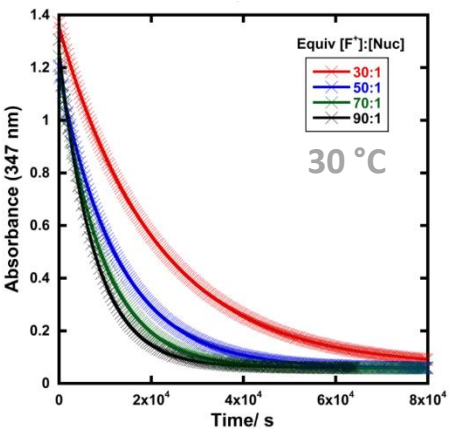

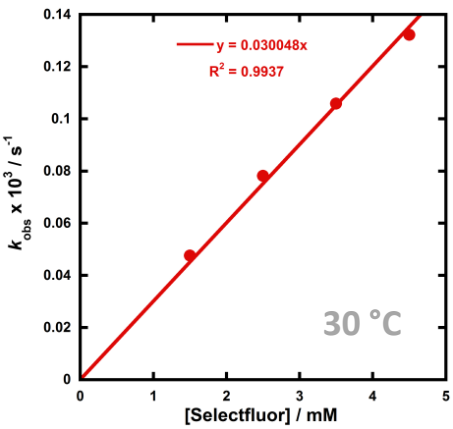

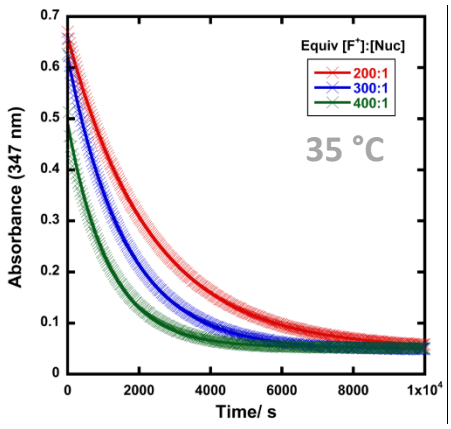

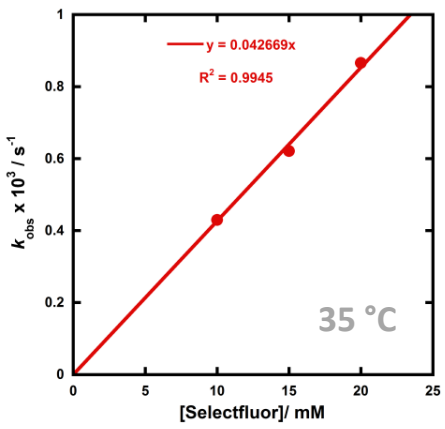

Fluorination of **107f** with Selectfluor™

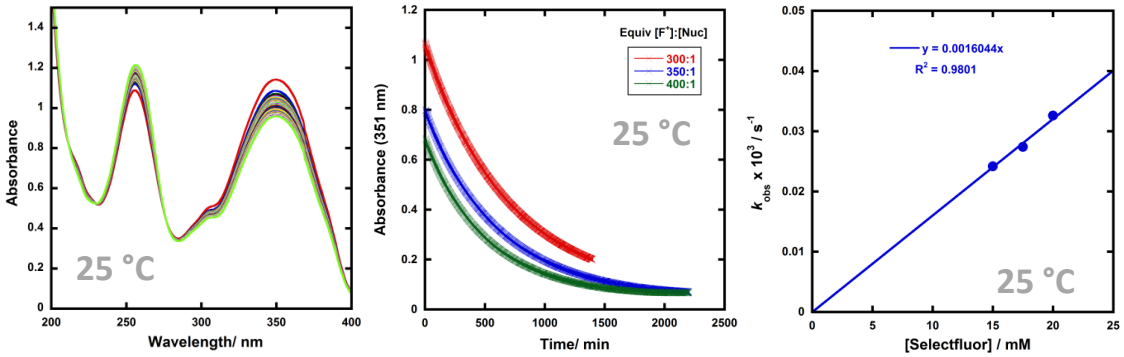

Fluorination of **107g** with Selectfluor™

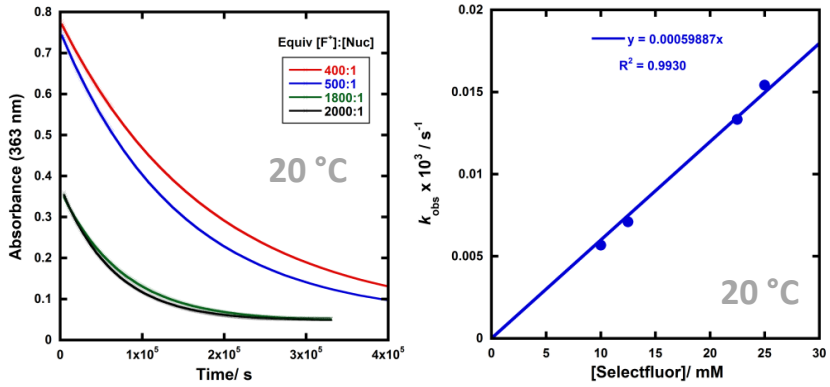

Fluorination of **107h** with Selectfluor™

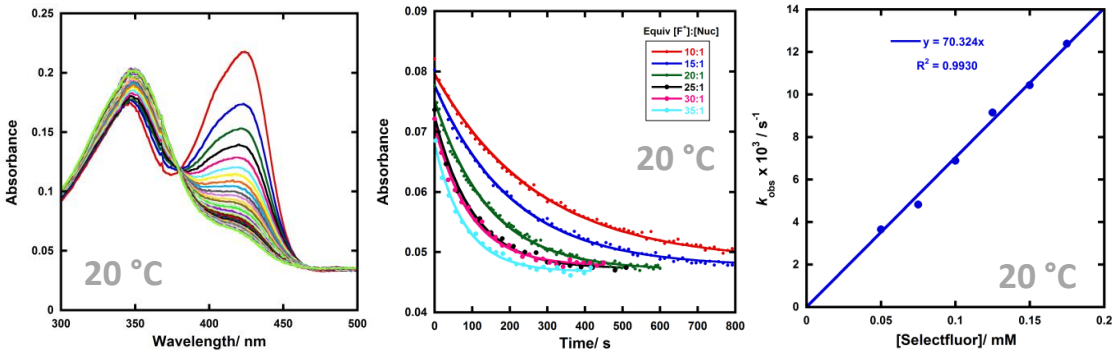

Fluorination of **107i** with Selectfluor™

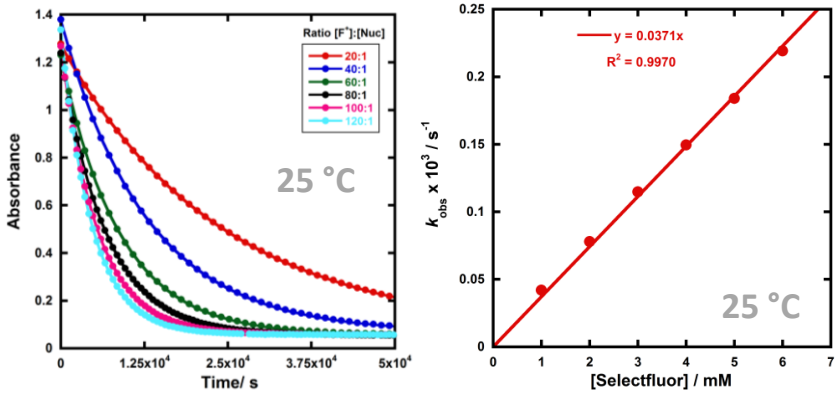

Fluorination of **107j** with Selectfluor™

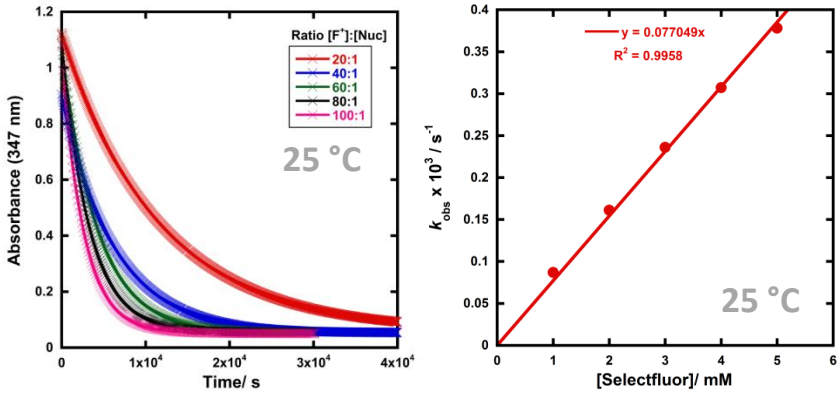

Fluorination of **107k** with Selectfluor™

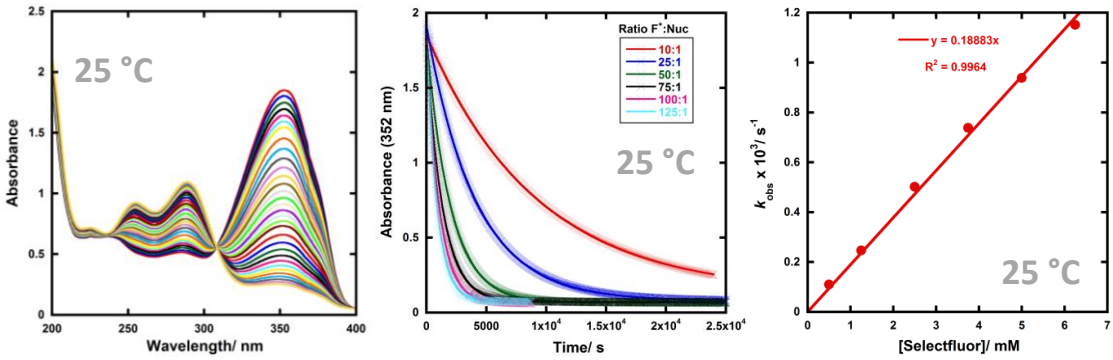

Fluorination of **107l** with Selectfluor™

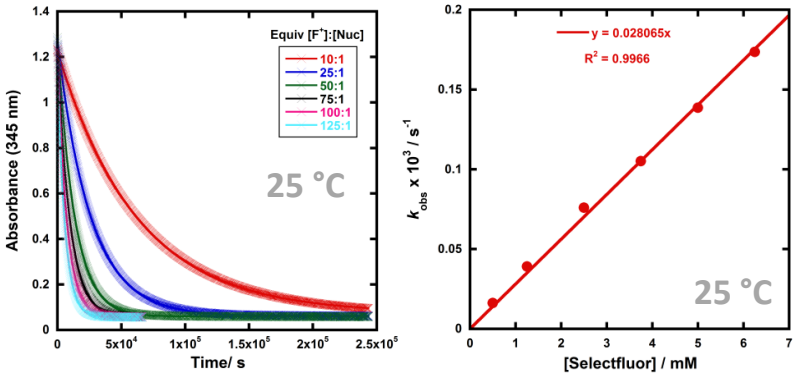

Fluorination of **107m** with Selectfluor™

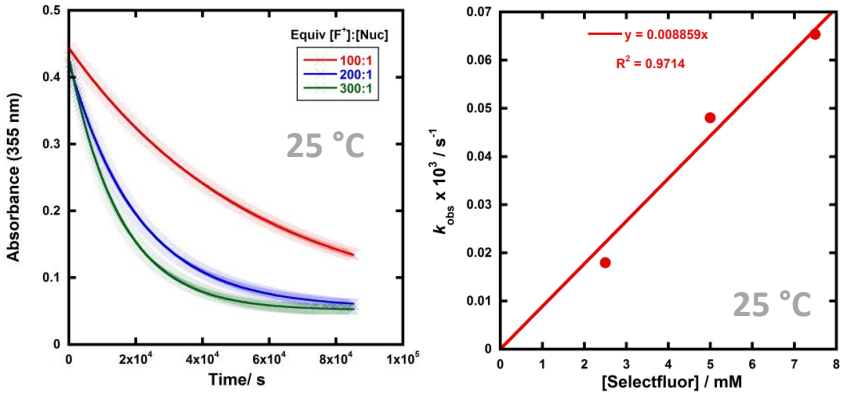

Fluorination of **107a** with NFSI

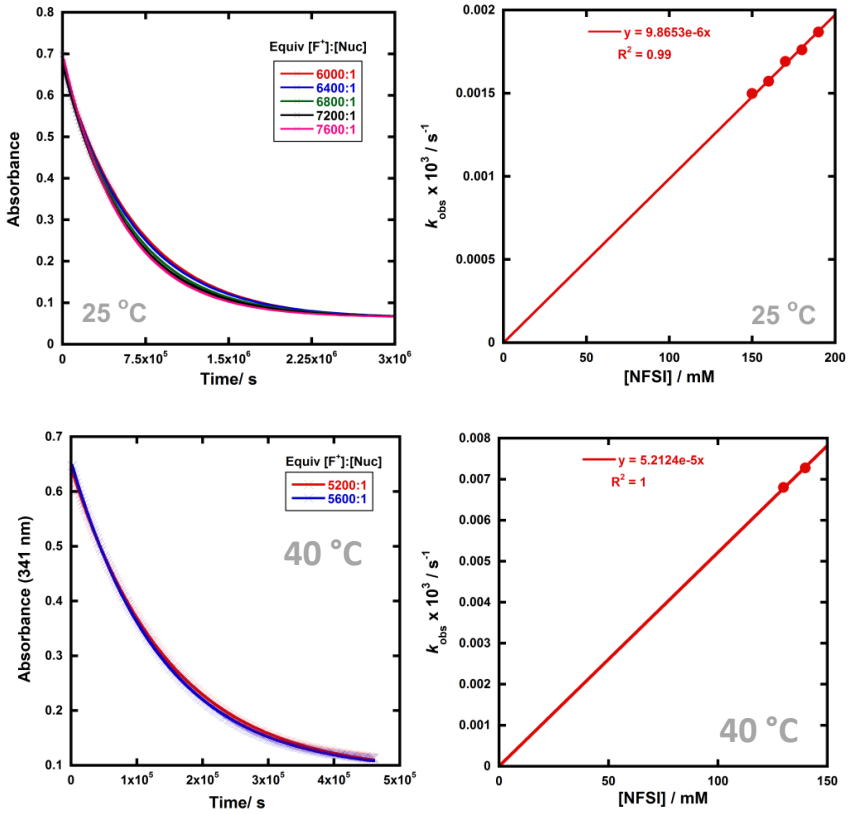

Fluorination of **107b** with NFSI

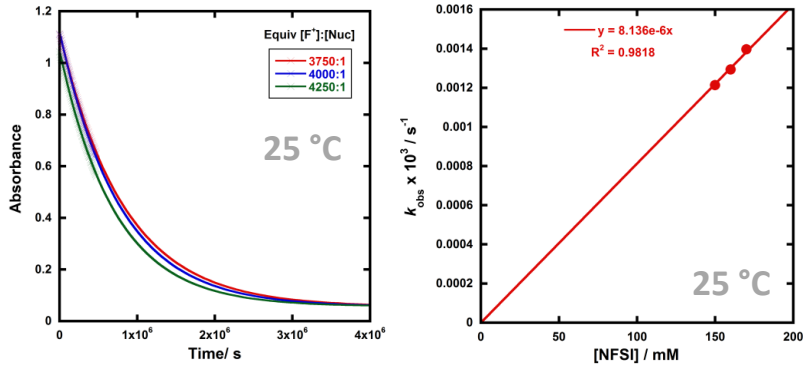

Fluorination of **107c** with NFSI

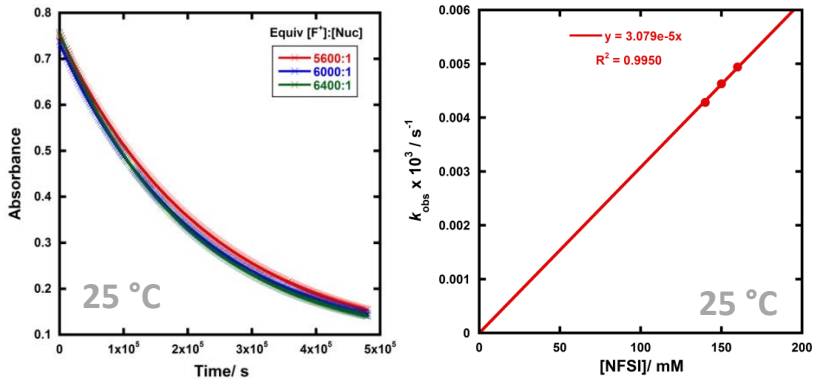

Fluorination of **107d** with NFSI

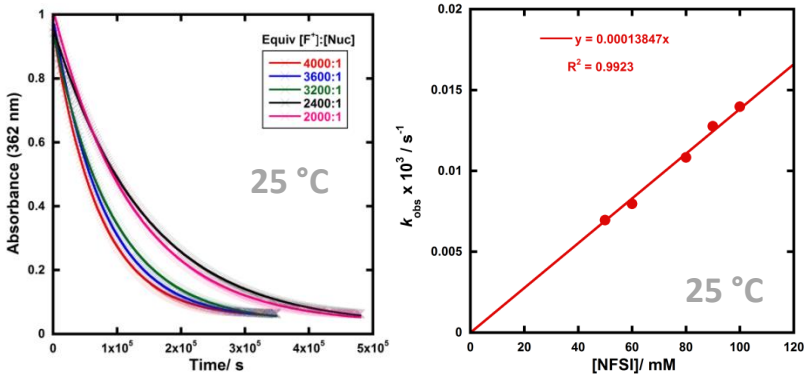

Fluorination of **107e** with NFSI

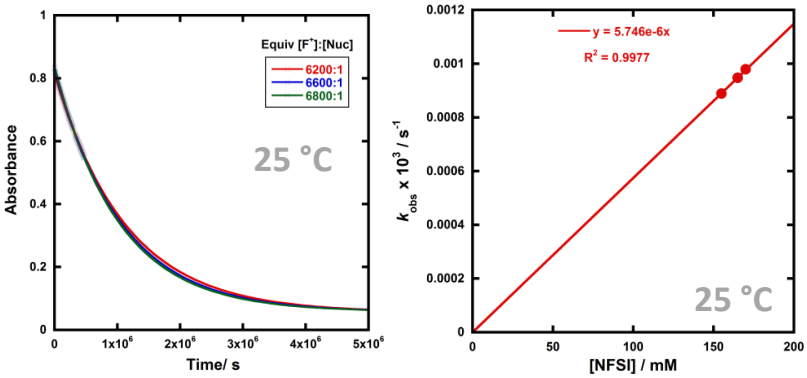

Fluorination of **107h** with NFSI

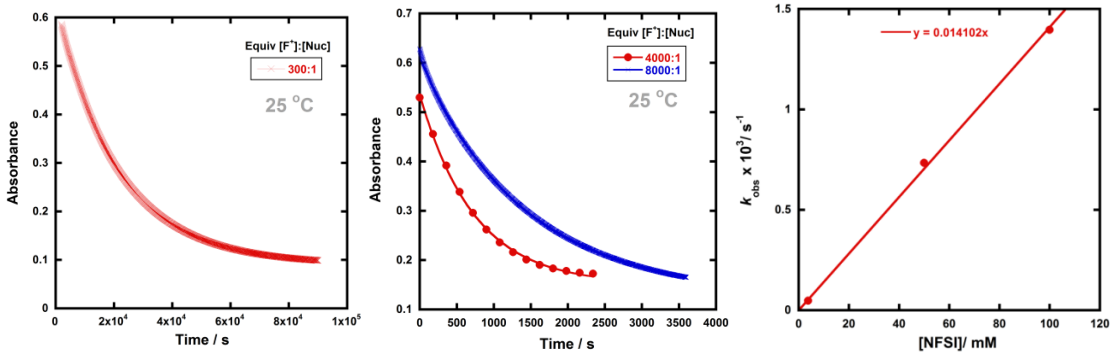

Fluorination of **107j** with NFSI

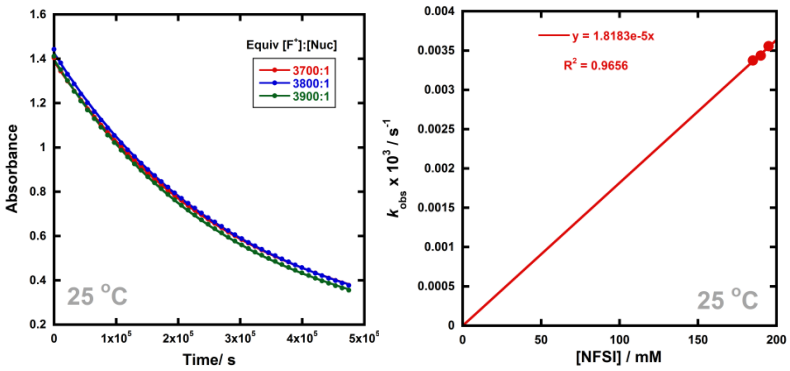

Fluorination of **107k** with NFSI

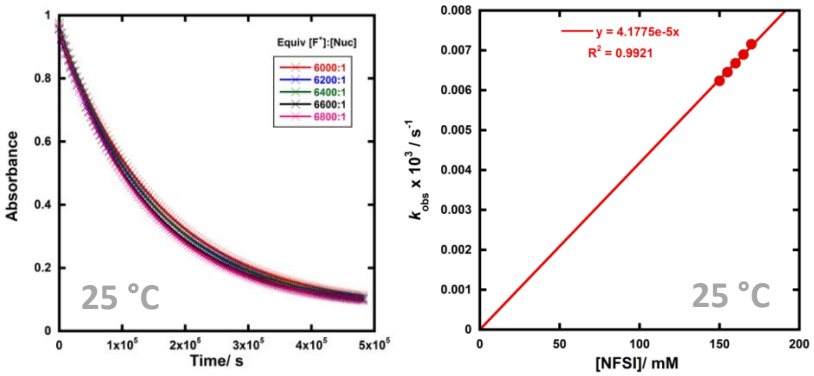

Fluorination of **107d** with Synfluor™

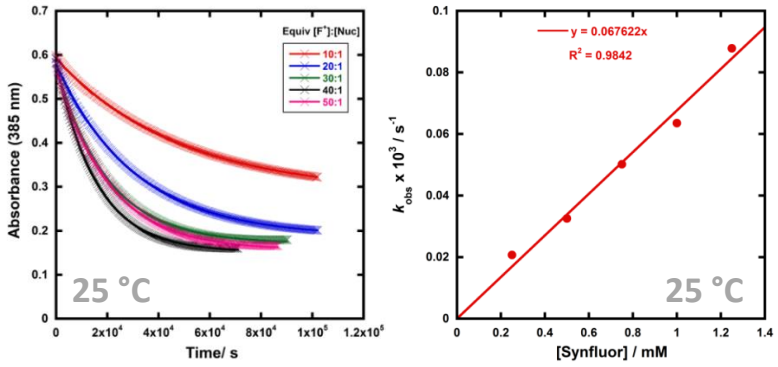

Fluorination of **107k** with Synfluor™

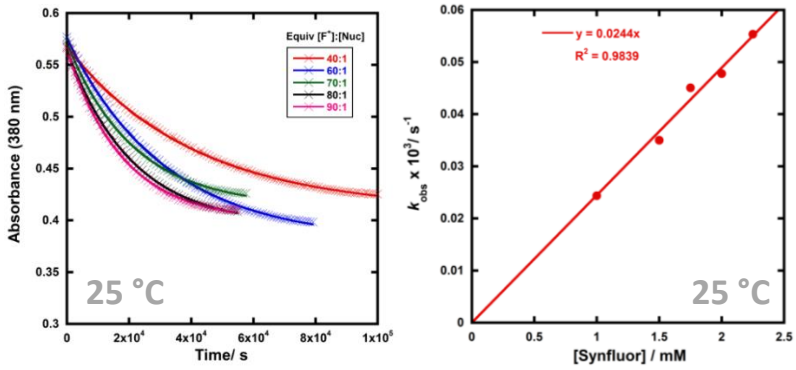

Fluorination of **107a** with diCl-NFPy TfO^{-}

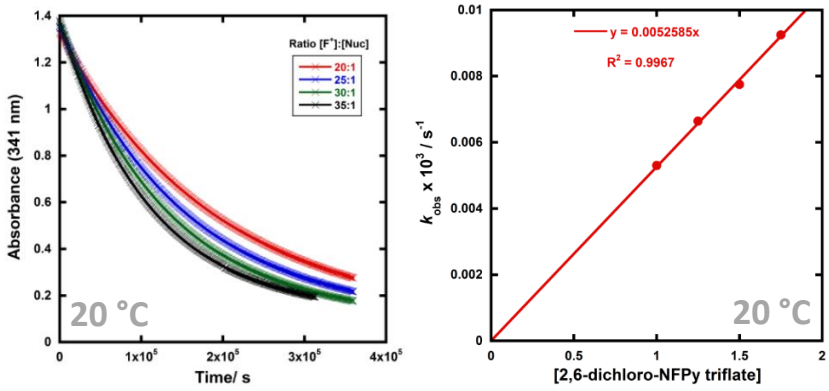

Fluorination of **107b** with diCl-NFPy TfO$^-$

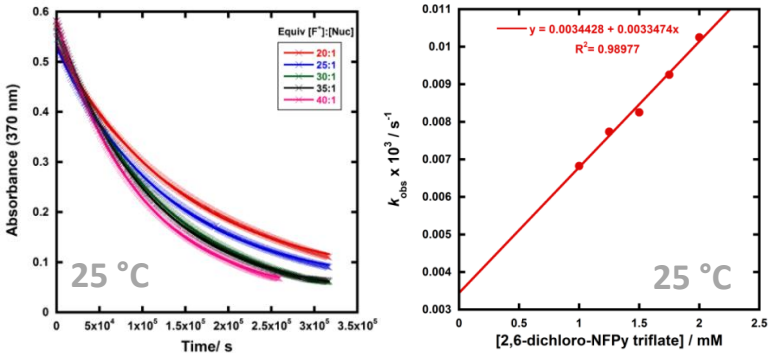

Fluorination of **107c** with diCl-NFPy TfO$^-$

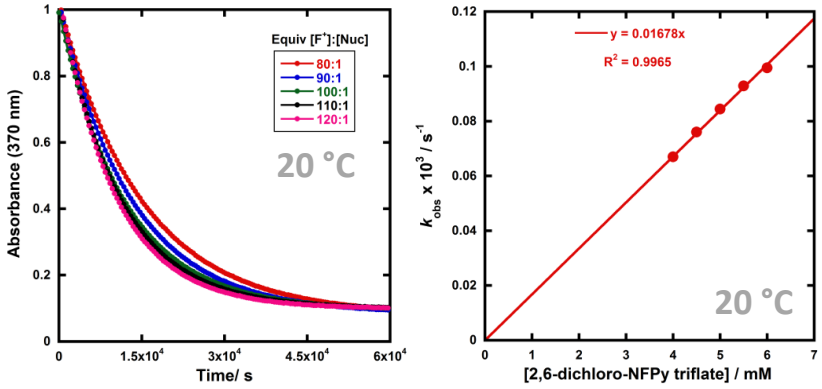

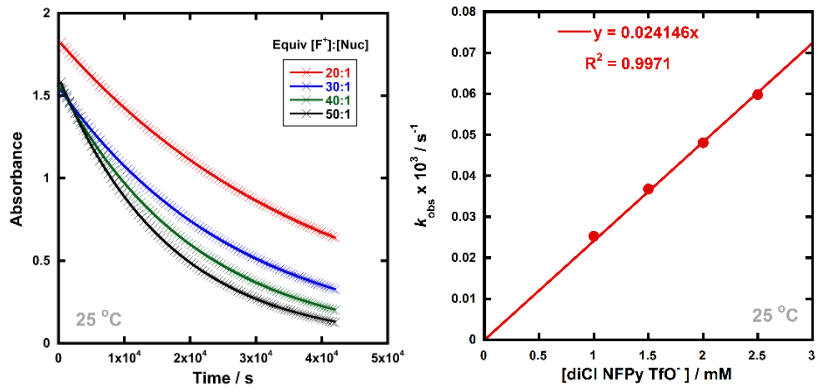

Fluorination of **107d** with diCl-NFPy TfO$^-$

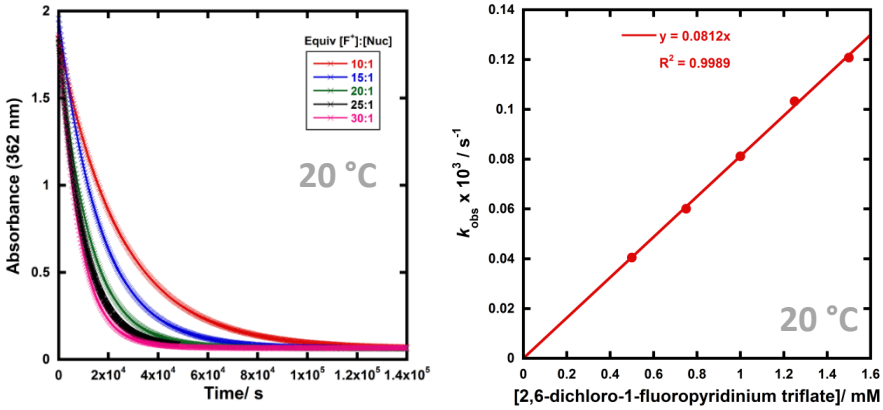

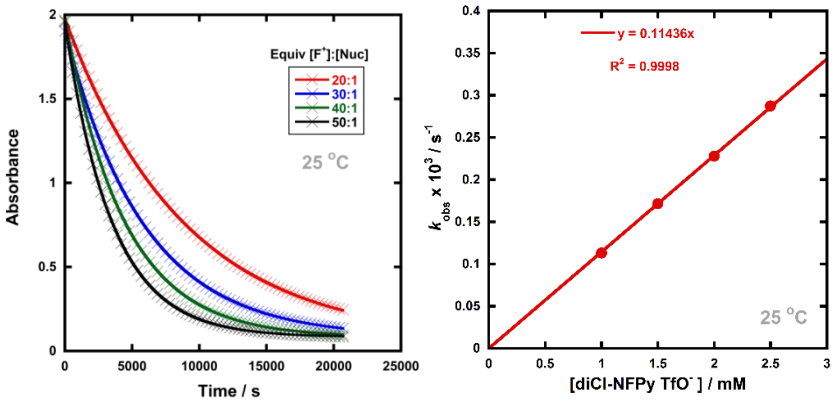

Fluorination of **107e** with diCl-NFPy TfO^-

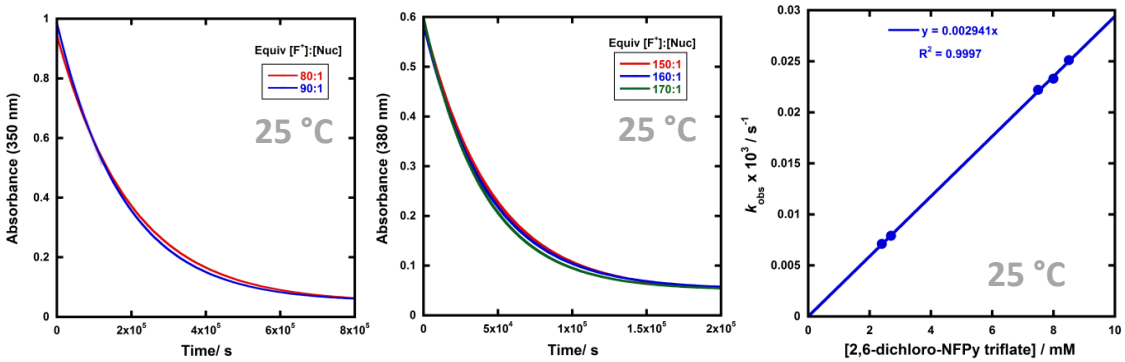

Fluorination of **107a** with diCl-NFPy BF_4^-

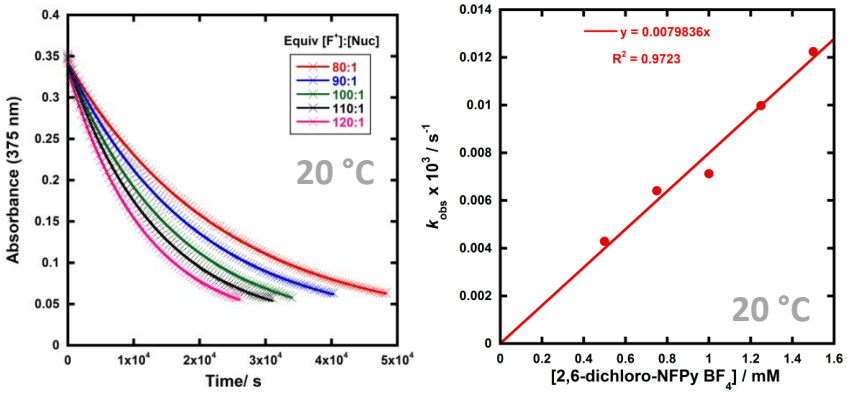

Fluorination of **107b** with diCl-NFPy BF_4^-

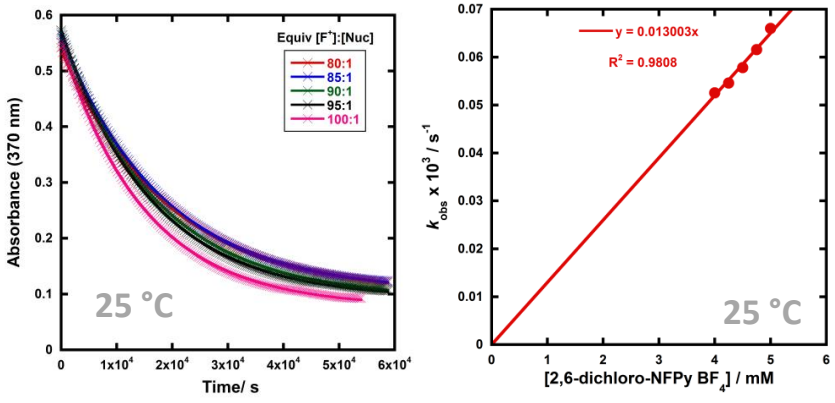

Fluorination of **107c** with diCl-NFPy BF_4^-

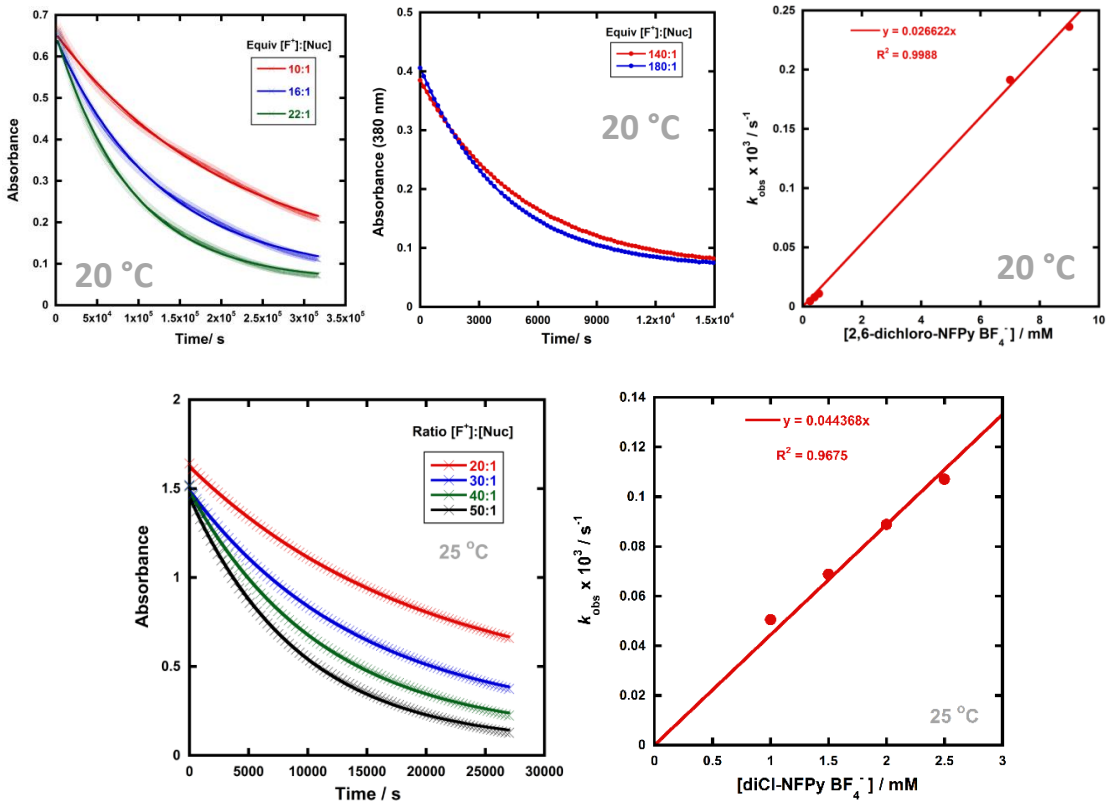

Fluorination of **107d** with diCl-NFPy BF_4^-

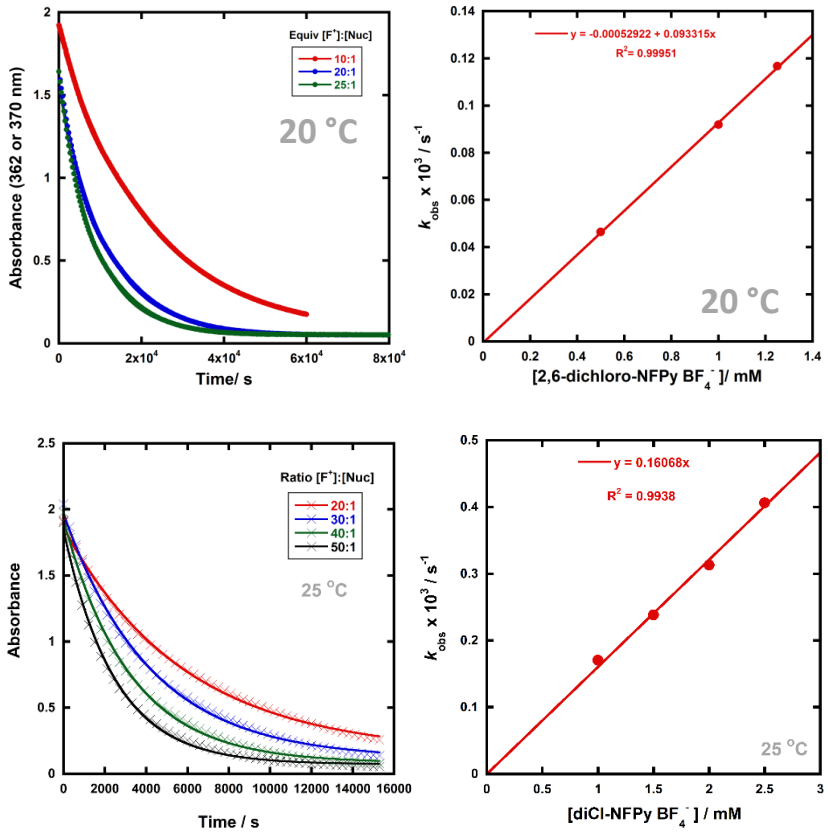

Fluorination of **107e** with diCl-NFPy BF_4^-

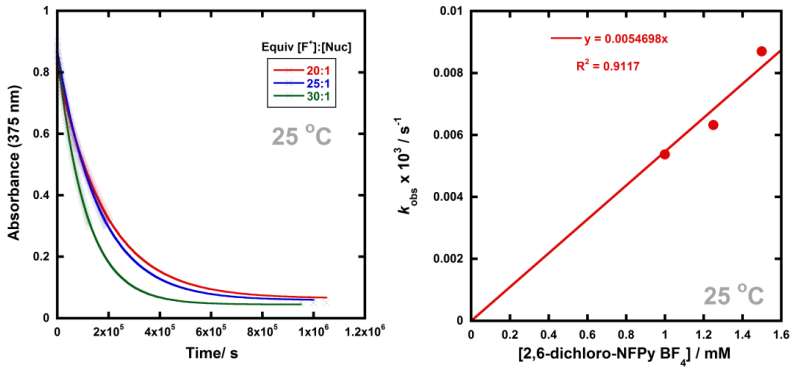

Fluorination of **107j** with diCl-NFPy BF_4^-

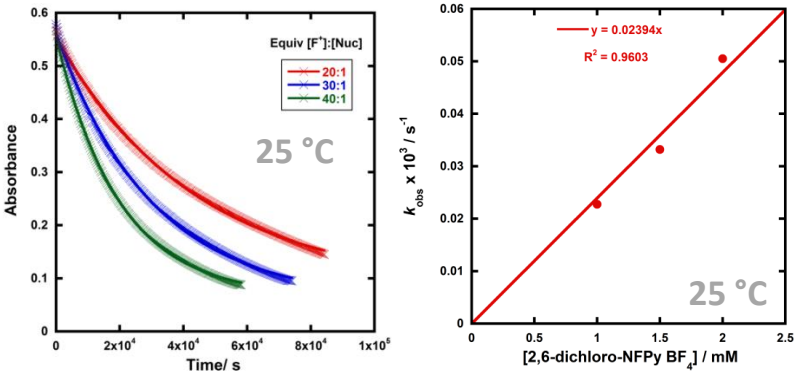

Fluorination of **107k** with diCl-NFPy BF_4^-

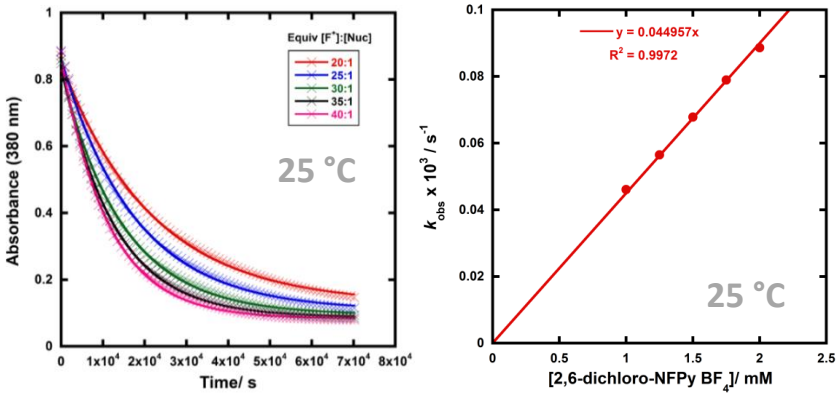

Fluorination of **107a** with pentaCl-NFPy TfO^-

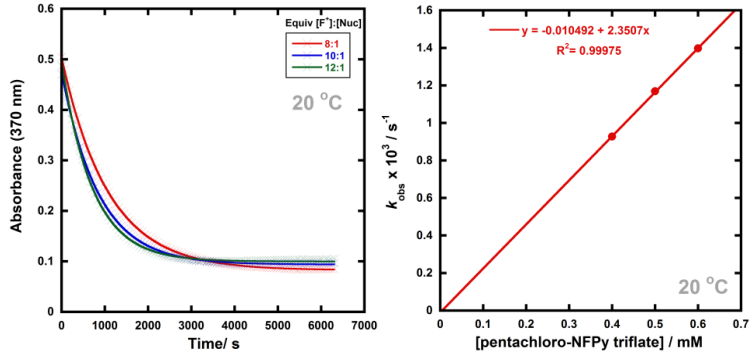

Fluorination of **107c** with pentaCl-NFPy TfO$^-$

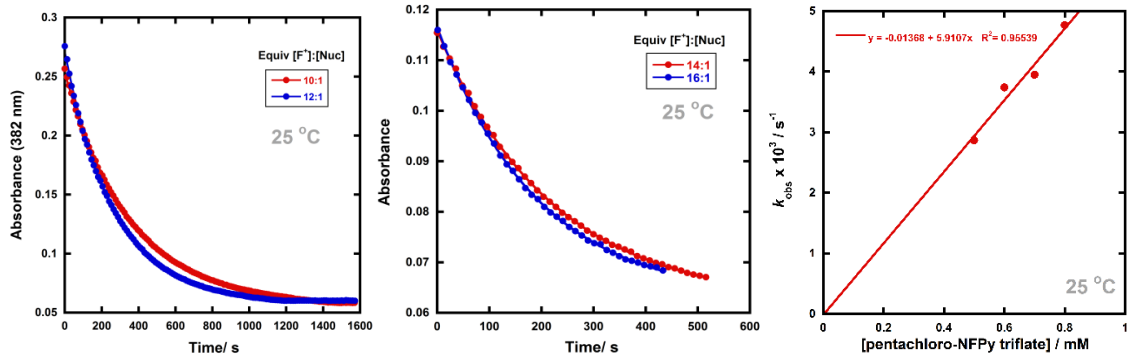

Fluorination of **107d** with pentaCl-NFPy TfO$^-$

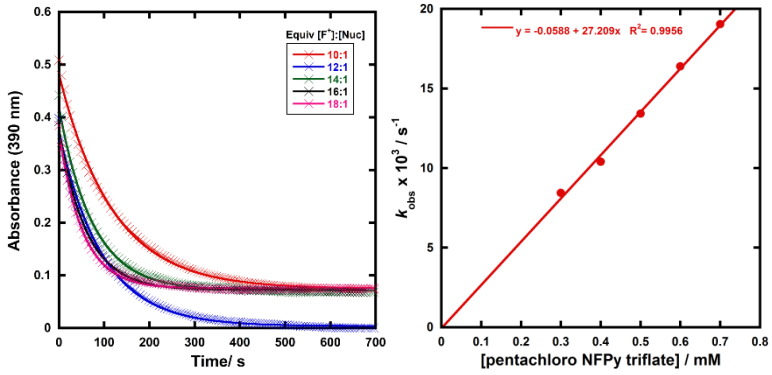

Fluorination of **107e** with pentaCl-NFPy TfO$^-$

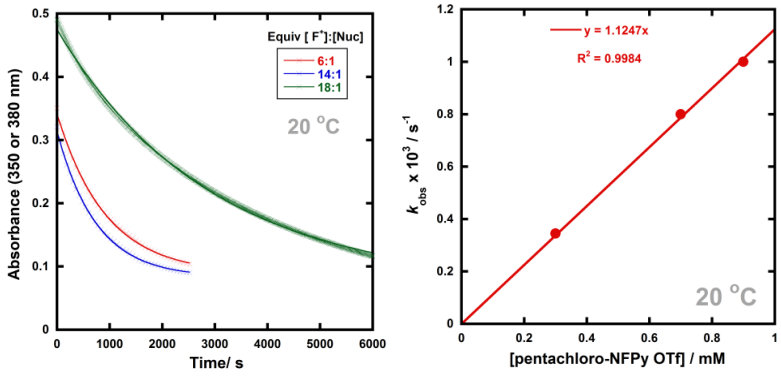

Fluorination of **107d** with NFPy TfO$^-$ (monitored by NMR spectroscopy)

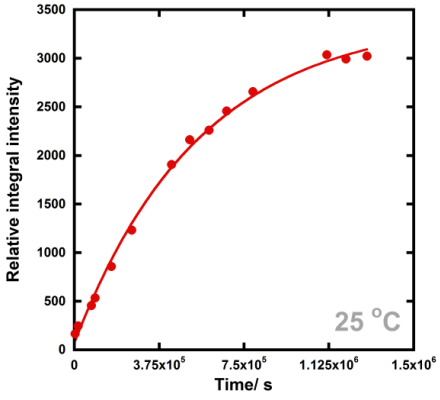

Fluorination of **107d** with NFPy BF_4^- (monitored by NMR spectroscopy)

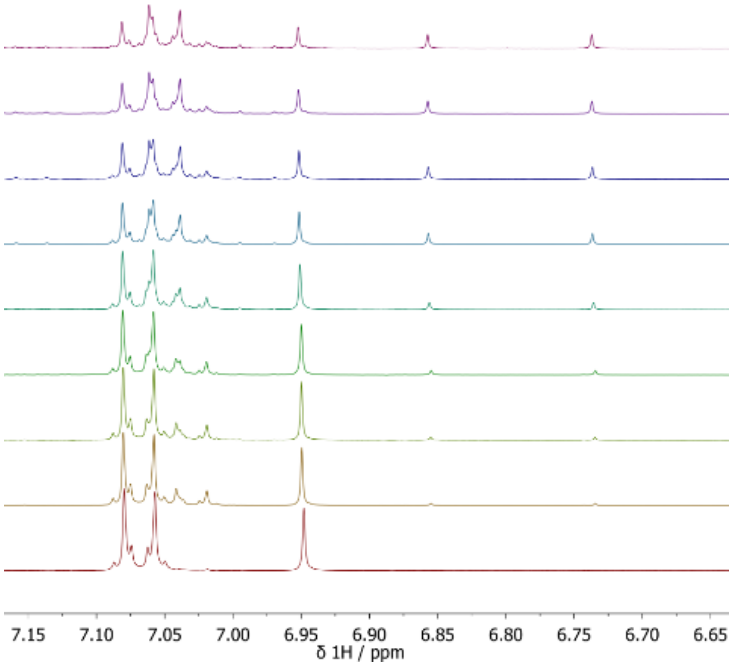

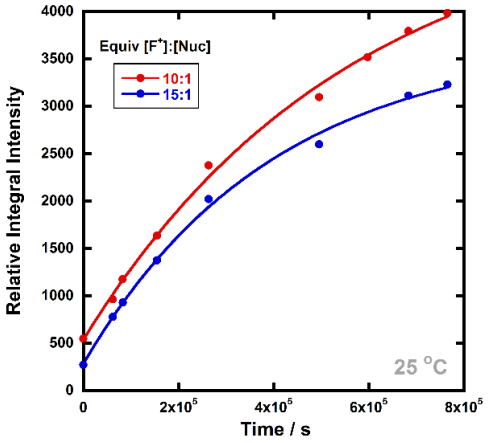

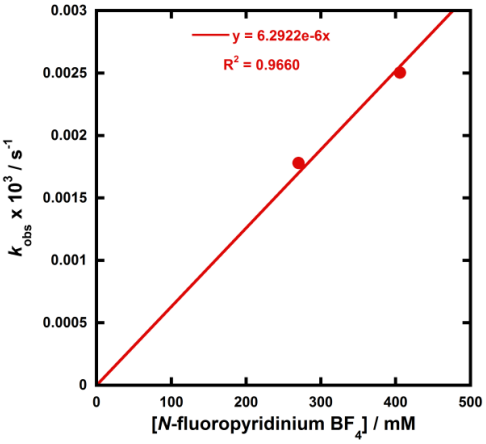

Fluorination of **107d** with triMe-NFPy TfO^- (monitored by NMR spectroscopy)

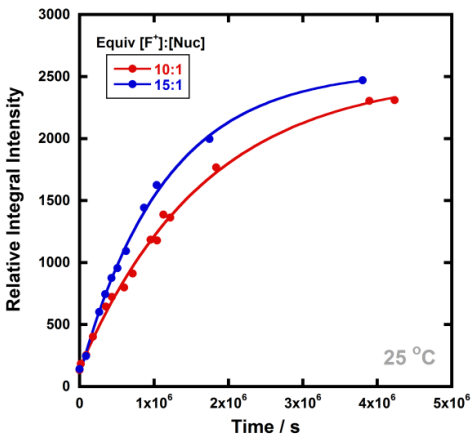

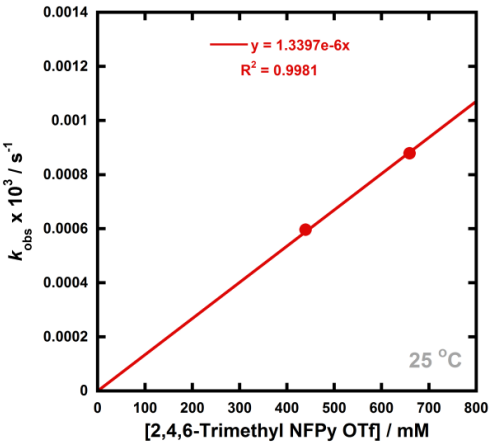

Fluorination of **107d** with triMe-NFPy BF_4^- (monitored by NMR spectroscopy)

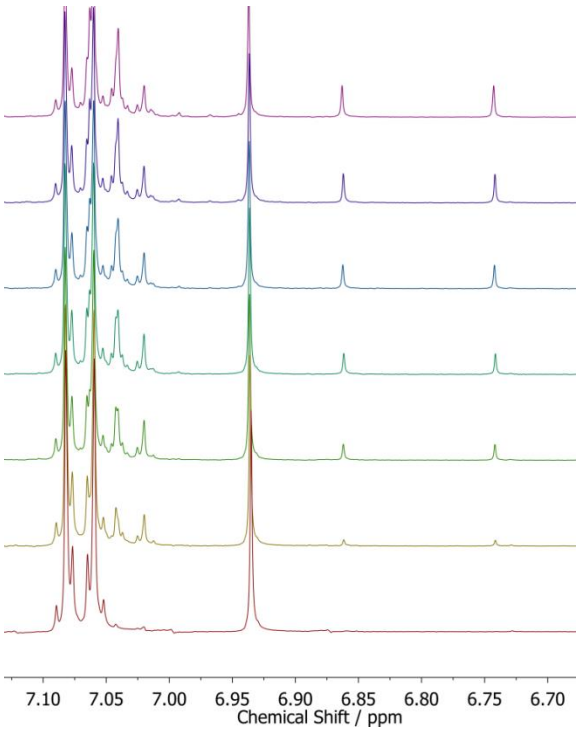

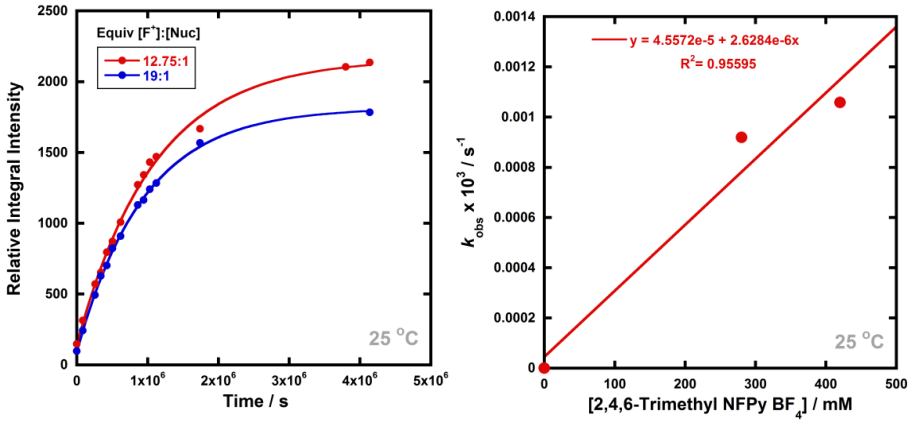

Table 45: All k_{obs} values for fluorination of **107a-m**.

Electrophile	Nucleophile	Temp / °C	Ratio of F^+ : Nuc	$[F^+]$: [Nuc] / mM	$k_{obs} \times 10^4$ / s^{-1}
Selectfluor™	**107a-enol**	20	25:1	1.25 : 0.05	0.3611 ± 0.0004
			50:1	2.5 : 0.05	0.6657 ± 0.0003
			75:1	3.75 : 0.05	0.9624 ± 0.0003
			100:1	5.0 : 0.05	1.3626 ± 0.0009
			130:1	6.5 : 0.05	1.763 ± 0.001
			150:1	7.5 : 0.05	1.998 ± 0.002
		25	50:1	2.5 : 0.05	1.2574 ± 0.0003
			100:1	5.0 : 0.05	2.1523 ± 0.0003
			150:1	7.5 : 0.05	3.1863 ± 0.0003
			200:1	10.0 : 0.05	4.0851 ± 0.0008
			250:1	12.5 : 0.05	5.3238 ± 0.0008
			300:1	15.0 : 0.05	6.2273 ± 0.0009
		30	25:1	1.25 : 0.05	0.9438 ± 0.0003
			50:1	2.5 : 0.05	1.7361 ± 0.0006
			75:1	3.75 : 0.05	2.5188 ± 0.0009
			100:1	5.0 : 0.05	3.322 ± 0.001
			125:1	6.25 : 0.05	4.032 ± 0.001
			150:1	7.5 : 0.05	4.847 ± 0.001
		35	50:1	2.5 : 0.05	2.698 ± 0.002
			75:1	3.75 : 0.05	3.697 ± 0.003
			100:1	5.0 : 0.05	4.953 ± 0.004
	107b-enol	20	40:1	2.0 : 0.05	0.4228 ± 0.0006
			60:1	3.0 : 0.05	0.631 ± 0.001
			80:1	4.0 : 0.05	0.832 ± 0.002
			100:1	5.0 : 0.05	1.0166 ± 0.0007
			120:1	6.0 : 0.05	1.236 ± 0.001
			140:1	7.0 : 0.05	1.420 ± 0.002
		25	50:1	2.50 : 0.05	0.8993 ± 0.0004
			100:1	5.00 : 0.05	1.7559 ± 0.0008
			150:1	7.50 : 0.05	2.5305 ± 0.0008
			200:1	10.0 : 0.05	3.310 ± 0.001
			250:1	12.5 : 0.05	4.076 ± 0.002
			300:1	15.0 : 0.05	4.846 ± 0.002

Electrophile	Nucleophile	Temp / °C	Ratio of F^+ : Nuc	$[F^+]$: [Nuc] / mM	$k_{obs} \times 10^4$ / s^{-1}
Selectfluor™	**107b-enol**	30	40:1	2.0 : 0.05	1.022 ± 0.005
			60:1	3.0 : 0.05	1.527 ± 0.008
			80:1	4.0 : 0.05	2.02 ± 0.01
			100:1	5.0 : 0.05	2.54 ± 0.03
		35	150:1	7.5 : 0.05	5.737 ± 0.003
			200:1	10.0 : 0.05	7.088 ± 0.007
			250:1	12.5 : 0.05	8.97 ± 0.02
			300:1	15.0 : 0.05	10.51 ± 0.03
	107c-enol	20	50:1	2.5 : 0.05	2.127 ± 0.002
			70:1	3.5 : 0.05	2.925 ± 0.003
			90:1	4.5 : 0.05	3.711 ± 0.006
		25	50:1	2.50 : 0.05	3.210 ± 0.001
			100:1	5.00 : 0.05	6.235 ± 0.001
			150:1	7.50 : 0.05	9.005 ± 0.003
			200:1	10.0 : 0.05	12.000 ± 0.006
			250:1	12.5 : 0.05	14.538 ± 0.007
			300:1	15.0 : 0.05	17.21 ± 0.01
		30	50:1	2.50 : 0.05	4.900 ± 0.004
			100:1	5.00 : 0.05	6.783 ± 0.008
			150:1	7.50 : 0.05	8.704 ± 0.005
			200:1	10.0 : 0.05	10.335 ± 0.009
		35	50:1	2.50 : 0.05	7.477 ± 0.004
			100:1	5.00 : 0.05	10.24 ± 0.01
			150:1	7.50 : 0.05	12.81 ± 0.02
			200:1	10.0 : 0.05	15.54 ± 0.04
	107d-enol	20	25:1	1.25 : 0.05	5.822 ± 0.002
			50:1	2.50 : 0.05	11.333 ± 0.005
			75:1	3.75 : 0.05	16.554 ± 0.007
			100:1	5.00 : 0.05	21.383 ± 0.008
			125:1	6.25 : 0.05	26.53 ± 0.02
		25	25:1	1.25 : 0.05	9.266 ± 0.002
			50:1	2.50 : 0.05	17.505 ± 0.004
			75:1	3.75 : 0.05	25.46 ± 0.01
			100:1	5.00 : 0.05	33.674 ± 0.009
			150:1	7.50 : 0.05	48.21 ± 0.04
			200:1	10.0 : 0.05	62.563 ± 0.03

Electrophile	Nucleophile	Temp / °C	Ratio of F^+ : Nuc	$[F^+]$: [Nuc] / mM	$k_{obs} \times 10^4$ / s^{-1}
Selectfluor™	**107d-enol**	30	25:1	1.25 : 0.05	12.999 ± 0.007
			50:1	2.5 : 0.05	25.50 ± 0.02
			70:1	3.5 : 0.05	33.01 ± 0.04
			100:1	5.0 : 0.05	47.87 ± 0.06
			120:1	6.0 : 0.05	56.53 ± 0.05
		35	20:1	1.0 : 0.05	15.47 ± 0.01
			40:1	2.0 : 0.05	29.77 ± 0.04
			60:1	3.0 : 0.05	42.6 ± 0.1
			80:1	4.0 : 0.05	54.2 ± 0.2
	107e-enol	20	10:1	0.5 : 0.05	0.0710 ± 0.0001
			25:1	1.25 : 0.05	0.1642 ± 0.0001
			50:1	2.5 : 0.05	0.3177 ± 0.0001
			75:1	3.75 : 0.05	0.4647 ± 0.0001
			100:1	5.0 : 0.05	0.6169 ± 0.0002
			125:1	6.25 : 0.05	0.7600 ± 0.0003
		25	50:1	2.50 : 0.05	0.48142 ± 0.00005
			100:1	5.00 : 0.05	0.93811 ± 0.00007
			150:1	7.50 : 0.05	1.3824 ± 0.0001
			200:1	10.0 : 0.05	1.8462 ± 0.0002
			250:1	12.5 : 0.05	2.2726 ± 0.0002
			300:1	15.0 : 0.05	2.6767 ± 0.0007
		30	30:1	1.5 : 0.05	0.4755 ± 0.0007
			50:1	2.5 : 0.05	0.781 ± 0.001
			70:1	3.5 : 0.05	1.058 ± 0.002
			90:1	4.5 : 0.05	1.322 ± 0.003
		35	200:1	10 : 0.05	4.297 ± 0.004
			300:1	15 : 0.05	6.21 ± 0.01
			400:1	20 : 0.05	8.66 ± 0.09
	107f-enol	25	300:1	15.0 : 0.05	0.2417 ± 0.0001
			350:1	17.5 : 0.05	0.2741 ± 0.0001
			400:1	20.0 : 0.05	0.3260 ± 0.0002
	107g-enol	20	400:1	10.0 : 0.025	0.0568 ± 0.0004
			500:1	12.5 : 0.025	0.0710 ± 0.0006
			1800:1	22.5 : 0.0125	0.1333 ± 0.0002
			2000:1	25.0 : 0.0125	0.1542 ± 0.0003

Electrophile	Nucleophile	Temp / °C	Ratio of F^+ : Nuc	$[F^+]$: [Nuc] / mM	$k_{obs} \times 10^4$ / s^{-1}
Selectfluor™	**107h-enol**	20	10:1	0.05 : 0.005	36.5 ± 0.5
			15:1	0.075 : 0.005	48.2 ± 0.7
			20:1	0.10 : 0.005	69 ± 1
			25:1	0.125 : 0.005	98 ± 6
			30:1	0.15 : 0.005	104 ± 5
			35:1	0.175 : 0.005	124 ± 6
	107i-enol	25	20:1	1.0 : 0.05	0.4197 ± 0.0004
			40:1	2.0 : 0.05	0.780 ± 0.001
			60:1	3.0 : 0.05	1.148 ± 0.001
			80:1	4.0 : 0.05	1.495 ± 0.001
			100:1	5.0 : 0.05	1.840 ± 0.001
			120:1	6.0 : 0.05	2.193 ± 0.002
	107j-enol	25	20:1	1.0 : 0.05	0.8692 ± 0.0004
			40:1	2.0 : 0.05	1.6115 ± 0.0008
			60:1	3.0 : 0.05	2.361 ± 0.002
			80:1	4.0 : 0.05	3.073 ± 0.004
			100:1	5.0 : 0.05	3.783 ± 0.009
	107k-enol	25	10:1	0.50 : 0.05	1.096 ± 0.001
			25:1	1.25 : 0.05	2.463 ± 0.001
			50:1	2.50 : 0.05	5.017 ± 0.002
			75:1	3.75 : 0.05	7.380 ± 0.003
			100:1	5.00 : 0.05	9.386 ± 0.003
			125:1	6.25 : 0.05	11.515 ± 0.004
	107l-enol	25	10:1	0.50 : 0.05	0.16224 ± 0.00007
			25:1	1.25 : 0.05	0.39121 ± 0.00009
			50:1	2.50 : 0.05	0.7594 ± 0.0002
			75:1	3.75 : 0.05	1.0515 ± 0.0003
			100:1	5.00 : 0.05	1.3858 ± 0.0005
			125:1	6.25 : 0.05	1.7356 ± 0.0006
	107m-enol	25	100:1	2.5 : 0.025	0.1793 ± 0.0002
			200:1	5.0 : 0.025	0.4803 ± 0.0006
			300:1	7.5 : 0.025	0.654 ± 0.001
NFSI	**107a-enol**	25	6000:1	150 : 0.025	0.01498 ± 0.00007
			6400:1	160 : 0.025	0.0157 ± 0.0002
			6800:1	170 : 0.025	0.0169 ± 0.0003
			7200:1	180 : 0.025	0.0176 ± 0.0003
			7600:1	190 : 0.025	0.0187 ± 0.0002

Electrophile	Nucleophile	Temp / °C	Ratio of F^+ : Nuc	$[F^+]$: [Nuc] / mM	$k_{obs} \times 10^4$ / s^{-1}
NFSI	**107a-enol**	40	5200:1	130 : 0.025	0.0680 ± 0.0002
			5600:1	140 : 0.025	0.0728 ± 0.0002
	107b-enol	25	3750:1	150 : 0.04	0.01214 ± 0.00004
			4000:1	160 : 0.04	0.01293 ± 0.00005
			4250:1	170 : 0.05	0.01397 ± 0.00006
	107c-enol	25	5600:1	140 : 0.025	0.04283 ± 0.00004
			6000:1	150 : 0.025	0.04629 ± 0.00004
			6400:1	160 : 0.025	0.04941 ± 0.00004
	107d-enol	25	2000:1	50 : 0.025	0.0695 ± 0.0001
			2400:1	60 : 0.025	0.0797 ± 0.0002
			3200:1	80 : 0.025	0.1083 ± 0.0002
			3600:1	90 : 0.025	0.1276 ± 0.0003
			4000:1	100 : 0.025	0.1397 ± 0.0004
	107e-enol	25	6200:1	155 : 0.025	0.00889 ± 0.00001
			6600:1	165 : 0.025	0.00947 ± 0.00001
			6800:1	170 : 0.025	0.00979 ± 0.00001
	107h-enol	25	300:1	3.75 : 0.025	0.4757 ± 0.0001
			4000:1	50 : 0.0125	7.339 ± 0.009
			8000:1	100 : 0.0125	13.6 ± 0.4
	107j-enol	25	3700:1	185 : 0.05	0.0337 ± 0.0003
			3800:1	190 : 0.05	0.0344 ± 0.0003
			3900:1	195 : 0.05	0.0356 ± 0.0003
	107k-enol	25	6000:1	150 : 0.025	0.0624 ± 0.0001
			6200:1	155 : 0.025	0.0645 ± 0.0002
			6400:1	160 : 0.025	0.0668 ± 0.0001
			6600:1	165 : 0.025	0.0689 ± 0.0002
			6800:1	170 : 0.025	0.0715 ± 0.0002
Synfluor™	**107d-enol**	25	10:1	0.5 : 0.05	0.2070 ± 0.0009
			20:1	1.0 : 0.05	0.3256 ± 0.0009
			30:1	1.5 : 0.05	0.502 ± 0.002
			40:1	2.0 : 0.05	0.636 ± 0.002
			50:1	2.5 : 0.05	0.878 ± 0.002
	107k-enol	25	40:1	2.0 : 0.05	0.0244 ± 0.0002
			60:1	3.0 : 0.05	0.0350 ± 0.0002
			70:1	3.5 : 0.05	0.0451 ± 0.0006
			80:1	4.0 : 0.05	0.0478 ± 0.0005
			90:1	4.5 : 0.05	0.0553 ± 0.0007

Electrophile	Nucleophile	Temp / °C	Ratio of F^+ : Nuc	$[F^+]$: [Nuc] / mM	$k_{obs} \times 10^4$ / s^{-1}
diCl-NFPy TfO^-	**107a-enol**	20	20:1	1.0 : 0.05	0.05301 ± 0.00005
			25:1	1.25 : 0.05	0.06640 ± 0.00005
			30:1	1.5 : 0.05	0.07748 ± 0.00006
			35:1	1.75 : 0.05	0.09116 ± 0.00007
	107b-enol	25	20:1	1.0 : 0.05	0.06826 ± 0.00006
			25:1	1.25 : 0.05	0.07736 ± 0.00005
			30:1	1.5 : 0.05	0.08253 ± 0.00002
			35:1	1.75 : 0.05	0.09255 ± 0.00002
			40:1	2.0 : 0.05	0.10250 ± 0.00003
	107c-enol	20	80:1	4.0 : 0.05	0.6696 ± 0.0005
			90:1	4.5 : 0.05	0.7601 ± 0.0005
			100:1	5.0 : 0.05	0.8444 ± 0.0006
			110:1	5.5 : 0.05	0.9287 ± 0.0007
			120:1	6.0 : 0.05	0.9948 ± 0.0009
		25	20:1	1.0 : 0.05	0.2527 ± 0.0008
			30:1	1.5 : 0.05	0.3675 ± 0.0007
			40:1	2.0 : 0.05	0.481 ± 0.001
			50:1	2.5 : 0.05	0.598 ± 0.001
	107d-enol	20	10:1	0.50 : 0.05	0.4046 ± 0.0002
			15:1	0.75 : 0.05	0.6013 ± 0.0004
			20:1	1.00 : 0.05	0.8115 ± 0.0005
			25:1	1.25 : 0.05	1.0326 ± 0.0004
			30:1	1.50 : 0.05	1.2070 ± 0.0007
		25	20:1	1.0 : 0.05	1.132 ± 0.004
			30:1	1.5 : 0.05	1.714 ± 0.004
			40:1	2.0 : 0.05	2.279 ± 0.005
			50:1	2.5 : 0.05	2.871 ± 0.004
	107e-enol	25	80:1	2.4 : 0.03	0.0711 ± 0.0006
			90:1	2.7 : 0.03	0.0791 ± 0.0005
			150:1	7.5 : 0.05	0.222 ± 0.002
			160:1	8.0 : 0.05	0.233 ± 0.001
			170:1	8.5 : 0.05	0.251 ± 0.002
diCl-NFPy BF_4^-	**107a-enol**	20	80:1	4.0 : 0.05	0.04291 ± 0.00005
			90:1	4.5 : 0.05	0.06408 ± 0.00005
			100:1	5.0 : 0.05	0.07122 ± 0.00006
			110:1	5.5 : 0.05	0.09979 ± 0.00007
			120:1	6.0 : 0.05	0.12241 ± 0.00007

Electrophile	Nucleophile	Temp / °C	Ratio of F^+ : Nuc	$[F^+]$: [Nuc] / mM	$k_{obs} \times 10^4$ / s^{-1}
diCl-NFPy BF_4^-	**107b-enol**	25	80:1	4.00 : 0.05	0.5254 ± 0.0007
			85:1	4.25 : 0.05	0.5459 ± 0.0008
			90:1	4.50 : 0.05	0.578 ± 0.001
			95:1	4.75 : 0.05	0.616 ± 0.001
			100:1	5.00 : 0.05	0.660 ± 0.002
	107c-enol	20	10:1	0.25 : 0.025	0.0471 ± 0.0006
			16:1	0.40 : 0.025	0.0785 ± 0.0006
			22:1	0.55 : 0.025	0.1093 ± 0.0005
			140:1	7.00 : 0.05	1.913 ± 0.003
			180:1	9.00 : 0.05	2.362 ± 0.003
		25	20:1	1.0 : 0.05	0.5055 ± 0.004
			30:1	1.5 : 0.05	0.688 ± 0.006
			40:1	2.0 : 0.05	0.888 ± 0.007
			50:1	2.5 : 0.05	1.07 ± 0.01
	107d-enol	20	10:1	0.5 : 0.05	0.464 ± 0.001
			20:1	1.0 : 0.05	0.919 ± 0.004
			25:1	1.25 : 0.05	1.167 ± 0.006
		25	20:1	1.0 : 0.05	1.70 ± 0.03
			30:1	1.5 : 0.05	2.38 ± 0.04
			40:1	2.0 : 0.05	3.13 ± 0.05
			50:1	2.5 : 0.05	4.06 ± 0.06
	107e-enol	25	20:1	1.0 : 0.05	0.05370 ± 0.00009
			25:1	1.25 : 0.05	0.06323 ± 0.00008
			30:1	1.5 : 0.05	0.8700 ± 0.0001
	107j-enol	25	20:1	1.0 : 0.05	0.228 ± 0.001
			30:1	1.5 : 0.05	0.332 ± 0.003
			40:1	2.0 : 0.05	0.505 ± 0.003
	107k-enol	25	20:1	1.0 : 0.05	0.461 ± 0.005
			25:1	1.25 : 0.05	0.565 ± 0.006
			30:1	1.5 : 0.05	0.678 ± 0.007
			35:1	1.75 : 0.05	0.790 ± 0.007
			40:1	2.0 : 0.05	0.886 ± 0.009
pentaCl-NFPy TfO^-	**107a-enol**	20	8:1	0.4 : 0.05	9.28 ± 0.01
			10:1	0.5 : 0.05	11.69 ± 0.04
			12:1	0.6 : 0.05	13.98 ± 0.08

Electrophile	Nucleophile	Temp / °C	Ratio of F^+ : Nuc	$[F^+]$: [Nuc] / mM	$k_{obs} \times 10^4$ / s^{-1}
pentaCl-NFPy TfO^-	**107c-enol**	25	10:1	0.5 : 0.05	28.65 ± 0.01
			12:1	0.6 : 0.05	37.36 ± 0.04
			14:1	0.7 : 0.05	39.46 ± 0.02
			16:1	0.8 : 0.05	47.65 ± 0.02
	107d-enol	25	6:1	0.3 : 0.05	84.4 ± 0.9
			8:1	0.4 : 0.05	104 ± 1
			10:1	0.5 : 0.05	134 ± 2
			12:1	0.6 : 0.05	164 ± 2
			14:1	0.7 : 0.05	190 ± 2
	107e-enol	20	6:1	0.3 : 0.05	3.45 ± 0.02
			14:1	0.7 : 0.05	8.01 ± 0.01
			18:1	0.9 : 0.05	10.02 ± 0.01
NFPy BF_4^-	**107d-enol**	25	10:1	270 : 27	0.0018 ± 0.0003
			15:1	406 : 27	0.0025 ± 0.0003
triMe NFPy TfO^-	**107d-enol**	25	10:1	439 : 44	0.00059 ± 0.00003
			15:1	659 : 44	0.00088 ± 0.00004
triMe NFPy BF_4^-	**107d-enol**	25	12.75:1	280 : 22	0.00092 ± 0.00004
			19:1	420 : 22	0.0011 ± 0.0002

8.4 Experimental to Chapter 3:

8.4.1 Synthesis of 1-(chloromethyl)-4-aza-1-azoniabicyclo[2.2.2]octane tetrafluoroborate ($ClCH_2$-DABCO$^+$ BF_4^-)

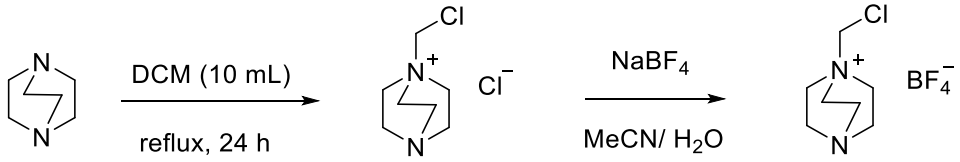

1,3-Diazabicyclo[2.2.2]octane (DABCO) (1.02 g, 9.19 mmol) was dissolved in DCM (10 mL) and stirred at reflux for 24 h. A white solid formed which was filtered, washed with DCM (10 mL) and dried under vacuum to give 1-(chloromethyl)-4-aza-1-azoniabicyclo[2.2.2]octane chloride (1.05 g, 60%). **^{1}H NMR** (400 MHz, D_2O) δ = 5.15 (s, 2H, C*H*$_2$Cl), 3.58 (t, $^3J_{HH}$ = 7.6 Hz, 6H), 3.28 (t, $^3J_{HH}$ = 7.7 Hz, 6H). **^{13}C NMR** (101 MHz, D_2O) δ = 68.3 (*C*H_2Cl), 51.2, 44.0. These assignments are in agreement with the literature.[248]

1-(Chloromethyl)-4-aza-1-azoniabicyclo[2.2.2]octane chloride (1.05 g, 5.33 mmol) was dissolved in MeCN (15 mL) and deionised water (5 mL). $NaBF_4$ (0.59 g, 5.35 mmol) was added and the mixture was stirred at RT for 17 h. The solvents were removed *in vacuo*, and the solid residue was re-dissolved in MeCN. The insoluble NaCl was filtered off. The solvent was removed *in vacuo* to give 1-(chloromethyl)-4-aza-1-azoniabicyclo[2.2.2]octane tetrafluoroborate as a white solid (1.29 g, 97%). **^{1}H NMR** (400 MHz, D_2O) δ = 5.12 (s, 2H, C*H*$_2$Cl), 3.56 (t, $^3J_{HH}$ = 7.6 Hz, 6H), 3.26 (t, $^3J_{HH}$ = 7.7 Hz, 6H). **^{13}C NMR** (101 MHz, D_2O) δ = 68.3 (*C*H_2Cl), 51.2, 43.9. **^{19}F NMR** (376 MHz, MeCN-*d*$_3$) δ = −151 (B*F*$_4$). These assignments are in agreement with the literature.[248]

8.4.2 Synthesis of bisphenylsulfonylimide sodium salt $(PhSO_2)_2N^-$ Na^+

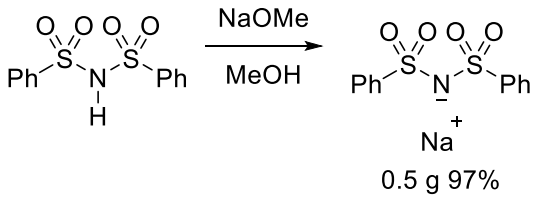

$(PhSO_2)_2NH$ (0.50 g, 1.7 mmol) was dissolved in MeOH (5 mL). NaOMe (0.09 g, 1.7 mmol) was added and the mixture was stirred at RT for 2 h. Evaporation of the solvent gave the product as a white solid (0.52g, 97%). **^{1}H NMR** (400 MHz, DMSO-d_6) δ =

7.70-7.64 (m, 4H), 7.46-7.34 (m, 6H). **^{13}C NMR** (101 MHz, DMSO-d_6) δ = 145.8, 130.4, 128.0, 126.2. These assignments are in agreement with the literature.[249]

8.4.3 Photoketonization-relaxation procedure

From stock solutions of **107a**, **107c-e**, **108a** and **108c-e**, aliquots were removed and prepared at the required concentration in quartz cuvettes, equipped with stirrer bars. The stirred solutions were irradiated with a 365 nm UV lamp for 3 h, at room temperature. The UV lamp was then removed and, if required, the additive was transferred to the cuvette. Time arrayed multi-wavelength scans were acquired every 15 min, to avoid continuous irradiation of the cuvette at smaller time intervals, which would slow down the rate of relaxation. Time-arrayed single-wavelength scans were conducted, as required.

8.4.4 UV-vis spectra for relaxation of 107c-e, 108a and 108c-e in the presence of additives

Relaxation of **107c-keto**:

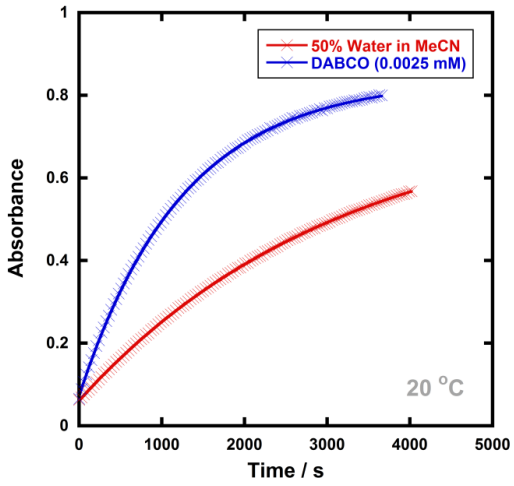

Figure 153: Relaxation of **107c-keto** (25 µM) in the presence of water (50% in MeCN, red) and DABCO (2.5 µM in MeCN, blue) at 20 °C.

Relaxation of **107d-keto**:

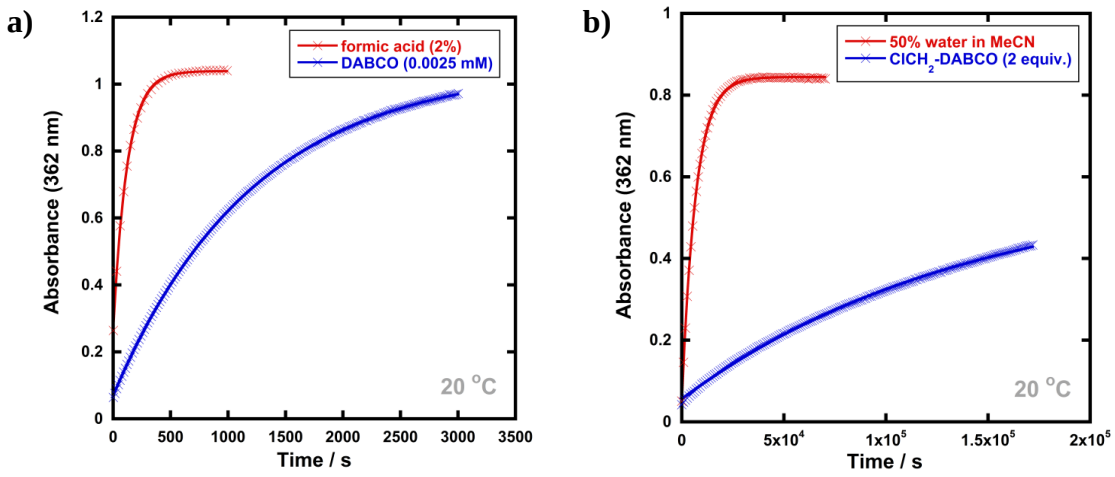

Figure 154: Relaxation of **107d-keto** (25 µM) at 20 °C in the presence of (a) formic acid (2% in MeCN, red) and DABCO (2.5 µM in MeCN, blue); (b) water (50% in MeCN, red) and $ClCH_2$-$DABCO^+$ BF_4^- (50 µM in MeCN, blue).

Relaxation of **107e-keto**:

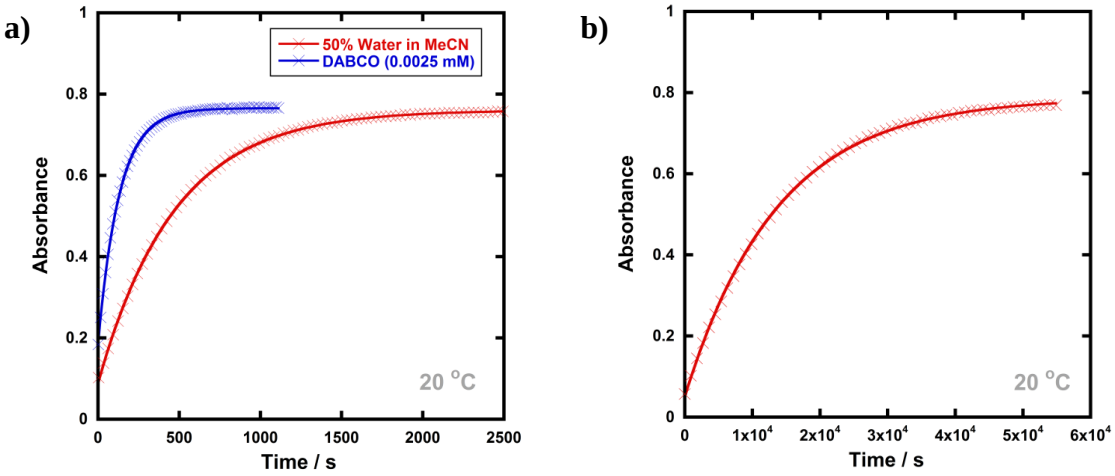

Figure 155: Relaxation of **107e-keto** (25 µM) at 20 °C in the presence of (a) water (50% in MeCN, red) and DABCO (2.5 µM in MeCN, blue); (b) $ClCH_2$-$DABCO^+$ BF_4^- (25 µM).

Relaxation of **108a-keto**:

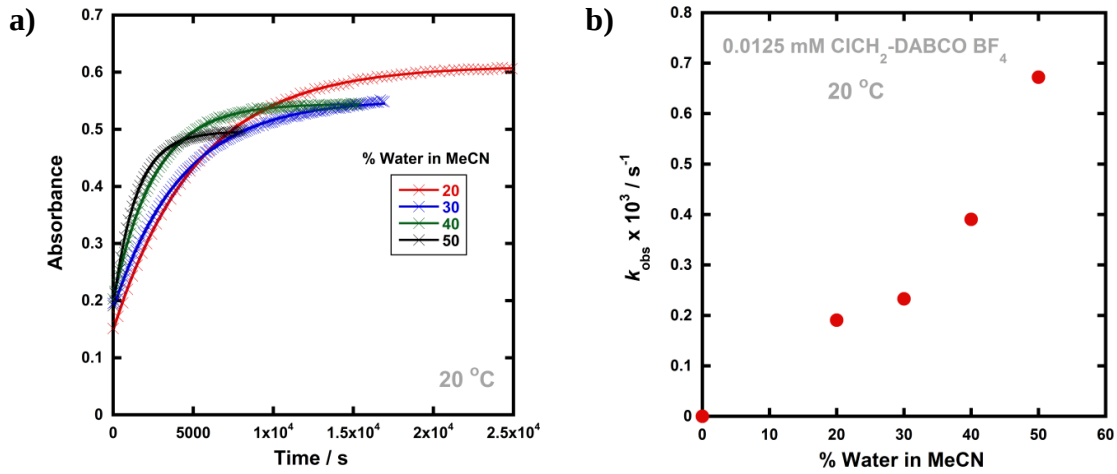

Figure 156: The relaxation of **108a-keto** ([**108a**$_{tot}$] = 0.50 mM) in the presence of 20-50% water and $ClCH_2$-DABCO$^+$ BF_4^- (12.5 μM), monitored at λ_{max} = 350 nm in MeCN at 20 °C.

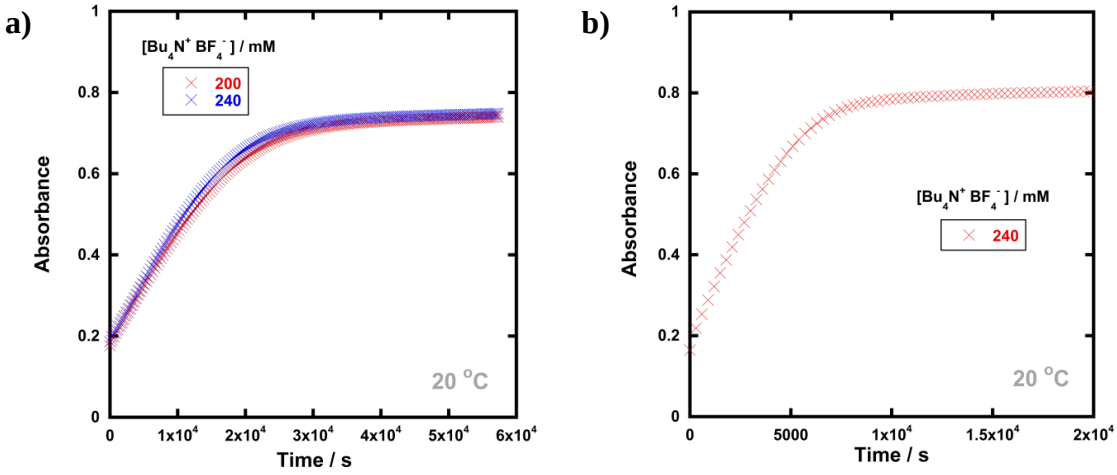

Figure 157: The relaxation of **108a-keto** ([**108a**$_{tot}$] = 0.50 mM) monitored at λ_{max} = 350 nm in MeCN at 20 °C in the presence of (a) different concentrations of Bu_4N^+ BF_4^- from an old bottle and (b) Bu_4N^+ BF_4^- from a new bottle.

Relaxation of **108d-keto**:

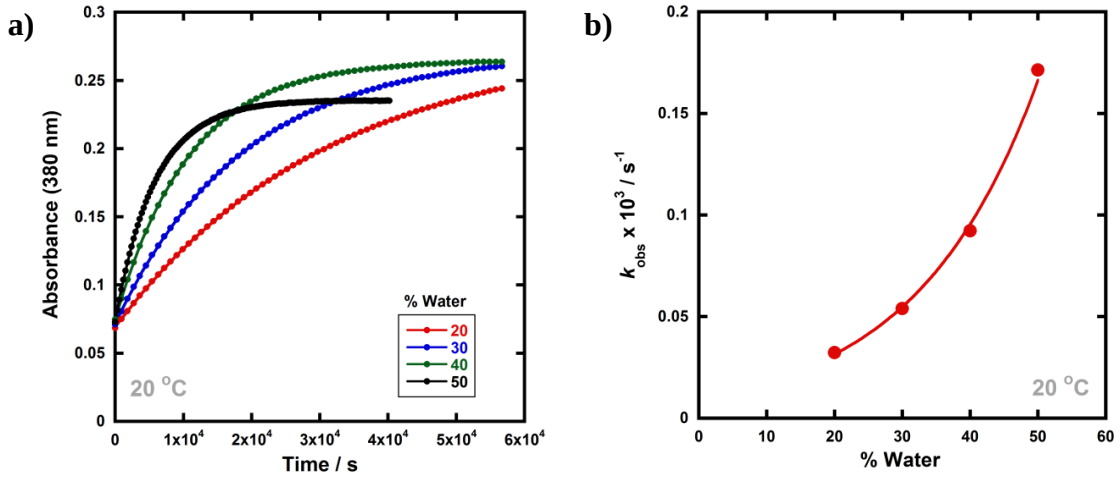

Figure 158: (a) Relaxation of **108d-keto** ([$108d_{tot}$] = 0.50 mM) following conversion of the fluoroenol tautomer to the fluoroketo form by irradiation with UV light at 365 nm. (b) Correlation of k_{obs} values for relaxation, obtained with different quantities of water at 20 °C.

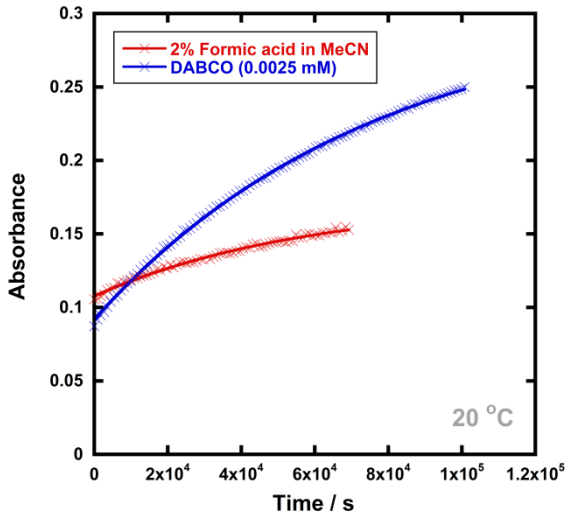

Figure 159: Relaxation of **108d-keto** ([**$108d_{tot}$**] = 0.50 mM) in the presence of additives: formic acid (2% in MeCN, red), DABCO (2.5 µM in MeCN, blue) at 20 °C.

Relaxation of **108c-keto** and **108e-keto**:

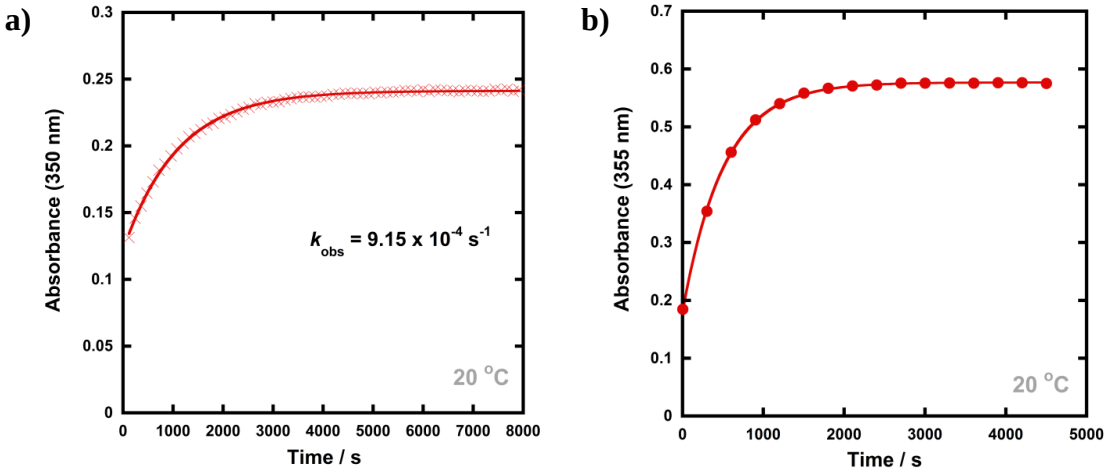

Figure 160: (a) Relaxation of **108c-keto** ([**108c**$_{tot}$] = 0.25 mM) with 50% water in MeCN at 20 °C. (b) Relaxation of **108e-keto** ([**108e**$_{tot}$] = 0.50 mM) with 50% water in MeCN at 20 °C.

8.4.5 Kinetic data from autocatalytic relaxation of 108a-keto and 108e-keto

Table 46: Absorbance-time data and diketone concentrations for relaxation of **108a-keto** and **108e-keto** obtained using UV-vis spectrophotometry.

108a			**108e**		
Time / s	Absorbance	Concentration / mM	Time / s	Absorbance	Concentration / mM
2.35	0.14959	0.5	4.65	0.15261	0.5
7201.8	0.15534	0.4998	21604	0.16427	0.499
14402	0.16135	0.4996	43204	0.17649	0.499
21602	0.16411	0.4995	64803	0.19117	0.498
28802	0.16691	0.4994	86404	0.20484	0.497
36002	0.17052	0.4993	108000	0.22265	0.496
43202	0.17589	0.4991	129600	0.24092	0.495
50402	0.17866	0.4990	151200	0.25903	0.494
57602	0.18179	0.4989	172800	0.27965	0.493
64801	0.18803	0.4987	194400	0.2993	0.492
72002	0.19158	0.4985	21600	0.32194	0.490
318600	0.56351	0.4856	23700	0.3448	0.489
417600	0.67768	0.4816	259200	0.36762	0.488
835200	0.87131	0.4748	280800	0.3924	0.486
			302400	0.41736	0.485
			324000	0.4437	0.484
			345600	0.46889	0.482
			367200	0.4945	0.481
			388800	0.52114	0.479
			410400	0.54526	0.478
			432000	0.57172	0.476
			432900	0.57132	0.476
			454500	0.59862	0.475
			476100	0.623	0.473
			497700	0.64661	0.472
			605700	0.73878	0.467
			659700	0.78255	0.464
			926100	0.83	0.462
			1005300	0.84	0.461
			1111500	0.861	0.460

8.5 Experimental to Chapter 4:

8.5.1 Synthesis of 2,2-difluoro-1,3-propanedione

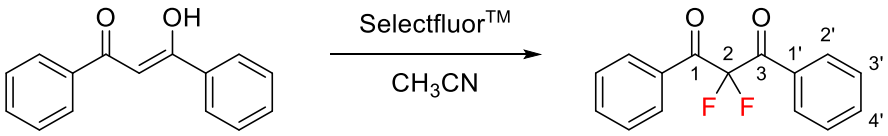

107a-enol **109a**

1,3-diphenyl-1,3-propanedione **107a** (300 mg, 1.34 mmol) was dissolved in MeCN (8 mL) and deionised H_2O (2 mL), and Selectfluor™ (995 mg, 2.81 mmol) was added. The reaction mixture was stirred at room temperature for 3 days and aliquots from the mixture (0.75 mL) were directly monitored by ^{19}F NMR spectroscopy using a D_2O lock tube (aliquots were returned to the reaction mixture following analysis). The solvent was evaporated *in vacuo*, and the white residue was dissolved in ethyl acetate (20 mL) and washed with water (3 × 20 mL) and brine (20 mL). The organic phase was separated, dried ($MgSO_4$), solvent evaporated *in vacuo* and 2,2-difluoro-1,3-diphenyl-1,3-propanedione **109a** was obtained as colourless crystals (329 mg, 94%). Further purification was not required. **IR** (ATR) υ_{max}/ cm^{-1} 3072, 1695, 1594, 1449, 1251, 1136, 940, 887, 771, 720, 679, 664, 570, 523. **^{1}H NMR** (400 MHz, MeCN-d_3) δ = 8.05 (4H, ddt, J_{HH} = 7.8, 2.3 Hz, $^5J_{HF}$ = 1.1 Hz, 2'-*H*), 7.79-7.71 (2H, m, 4'-*H*), 7.63-7.53 (4H, m, 3'-*H*). **^{13}C NMR** (101 MHz, MeCN-d_3) δ = 187.5 (t, $^2J_{CF}$ = 26.8 Hz, C-1, C-3), 135.5 (s, C-4'), 131.4 (d, $^4J_{CF}$ = 1.6 Hz, C-2'), 129.9 (t, $^3J_{CF}$ = 2.6 Hz, C-1'), 129.2 (s, C-3'), 112.5 (t, $^1J_{CF}$ = 265.4 Hz, C-2). **^{19}F NMR** (376 MHz, MeCN-d_3) δ = −103.4 (p, $^5J_{FH}$ = 1.1 Hz). **ESI-MS** (ES^+, R_t 2.965) *m*/*z* 261.211 $[M+H]^+$. These assignments are in agreement with the literature.[120]

8.5.2 T1 values determined for Selectfluor™ and 2-fluoro-1,3-dicarbonyl 108a

T1 values were determined using inversion recovery experiments. For Selectfluor™: T1(N−F at +48 ppm) = 1.294 ± 0.006 s and T1(BF_4^- at −150 ppm) = 4.92 ± 0.09 s. For the doublet corresponding to **108a-keto**: 4.59 ± 0.06 s for the peak at δ = 190.04 ppm, and 3.90 ± 0.11 s for the peak at δ = 190.30 ppm.

8.5.3 Kinetic parameters used for modelling in NMR-scale reactions

Kinetic parameters used for modelling in NMR-scale reactions in MeCN-d_3 were:

k_{for}(H) = 1.30 × 10^{-4} s^{-1}; k_{fluor}(H) = 4.20 × 10^{-2} s^{-1}; k_{rev}(F) = 6.91 × 10^{-7} s^{-1}; k_{rev}(H) = 1.44 × 10^{-5} s^{-1}; k_{for}(F) = 3.66 × 10^{-8} s^{-1}; k_{fluor}(F) = 2.95 × 10^{-2} s^{-1}; $k_{auto\text{-}for}$(F) = 1.58 × 10^{-2} s^{-1}; $k_{auto\text{-}rev}$(F) = 0.30 M^{-1} s^{-1}.

Kinetic parameters used for modelling in NMR-scale reactions in 20% H_2O/MeCN-d_3 were:

k_{for}(H) = 1.56 × 10^{-4} s^{-1}; k_{fluor}(H) = 1.86 × 10^{-2} M^{-1} s^{-1}; k_{rev}(F) = 1.13 × 10^{-4} s^{-1}; k_{rev}(H) = 2.32 × 10^{-5} s^{-1}; k_{for}(F) = 5.95 × 10^{-6} s^{-1}; k_{fluor}(F) = 1.44 M^{-1} s^{-1}; $k_{auto\text{-}for}$(F) = 0 M^{-1} s^{-1}; $k_{auto\text{-}rev}$(F) = 0 M^{-1} s^{-1}.

8.5.4 Kinetics of fluorination of 108a, 108c-e: spectra and k_{obs} values

Fluorination of **108a-enol** with Selectfluor™:

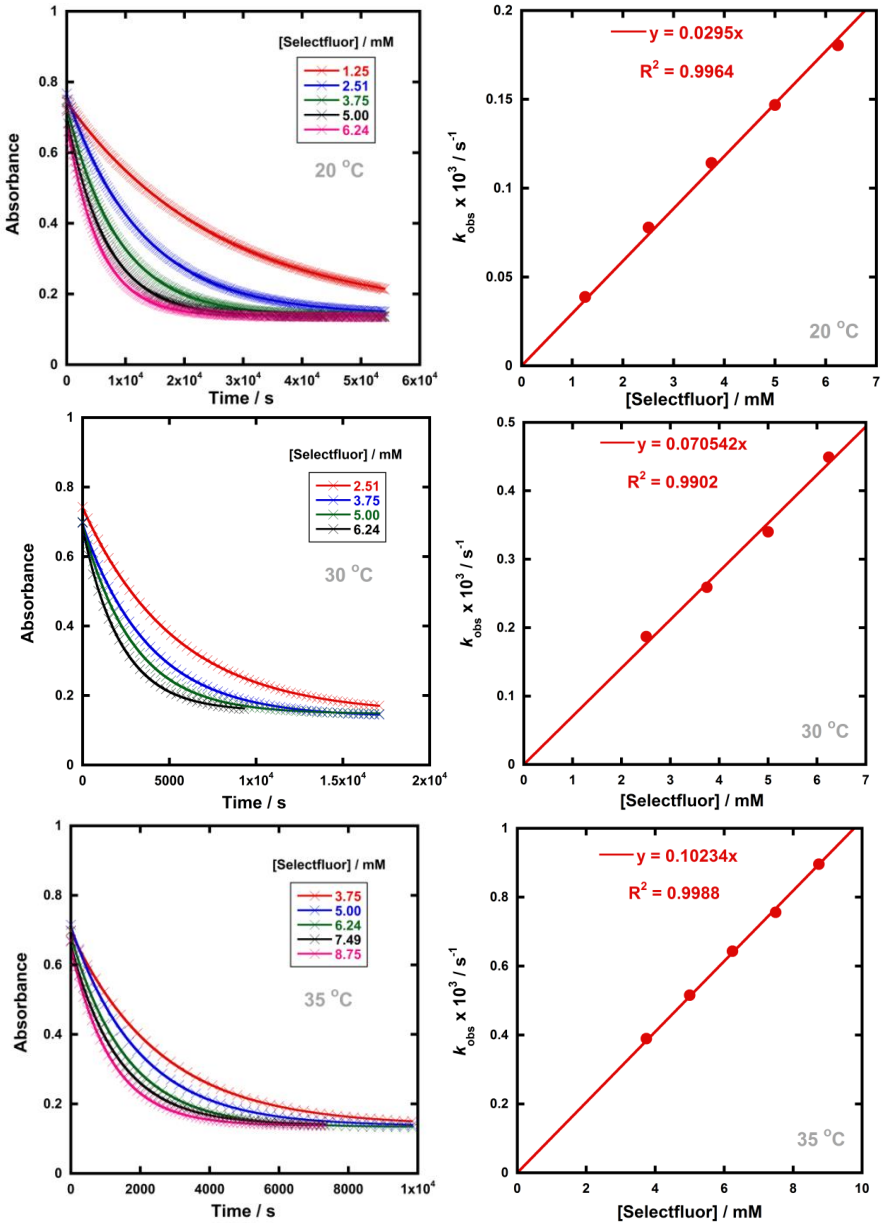

Fluorination of **108d-enol** with Selectfluor™:

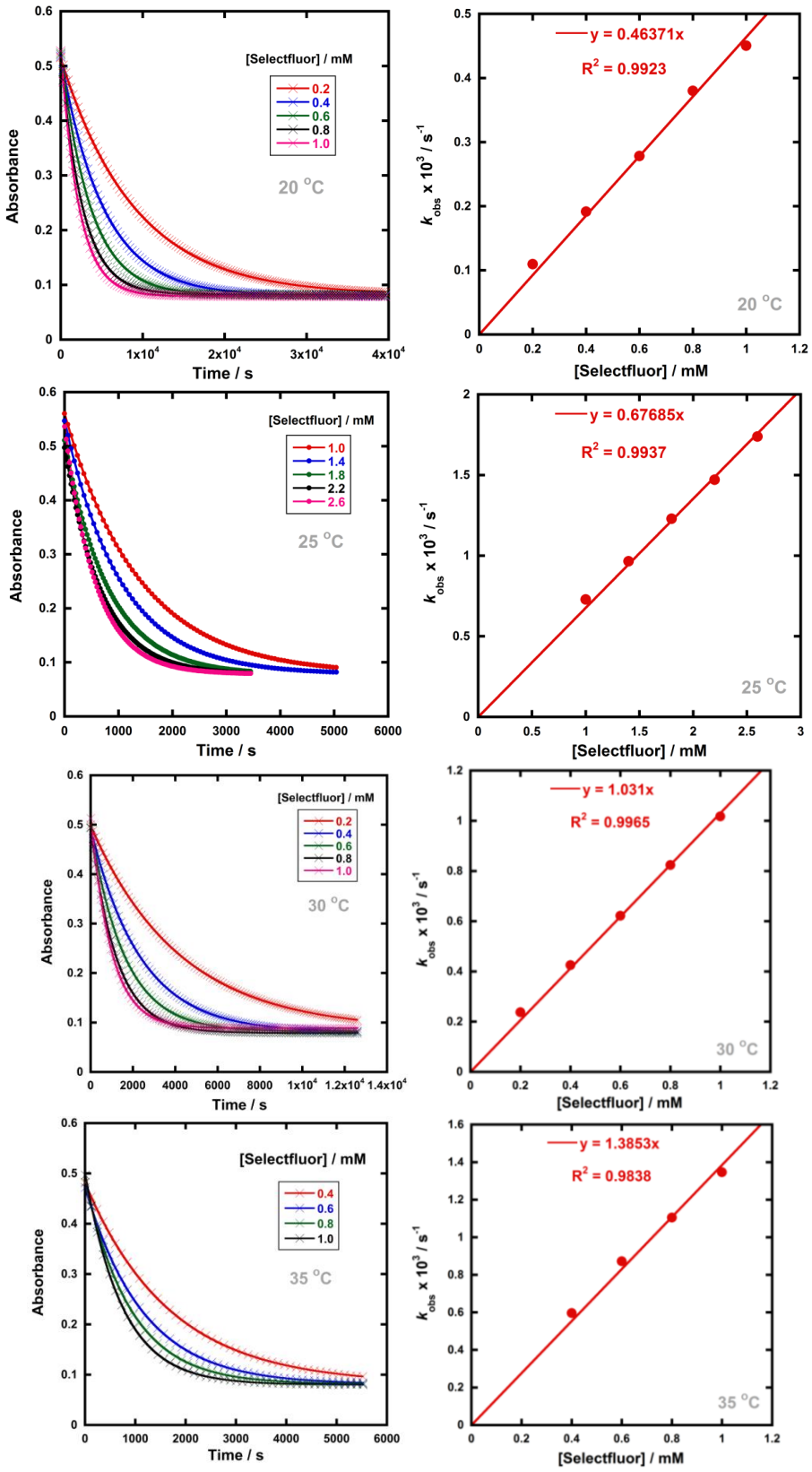

Fluorination of **108c-enol** with Selectfluor™:

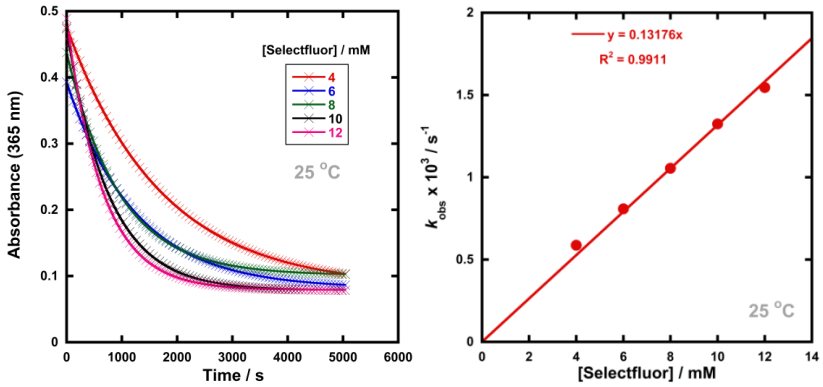

Fluorination of **108e-enol** with Selectfluor™:

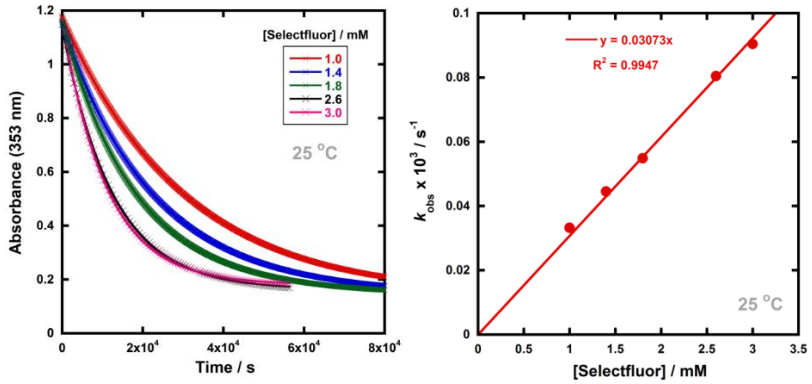

Fluorination of **108a-enol** with NFSI:

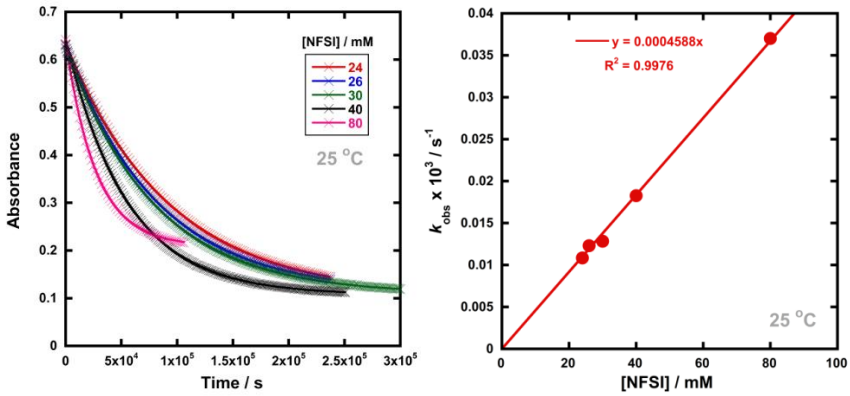

Fluorination of **108e-enol** with NFSI:

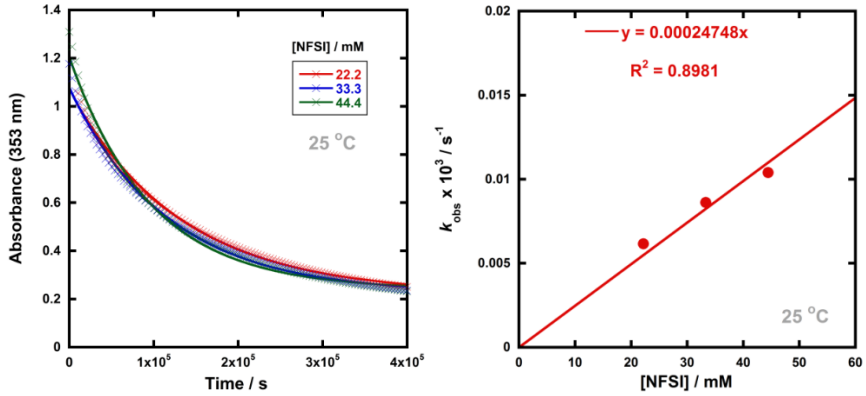

Fluorination of **108a-enol** with Selectfluor™ with 5% formic acid in MeCN:

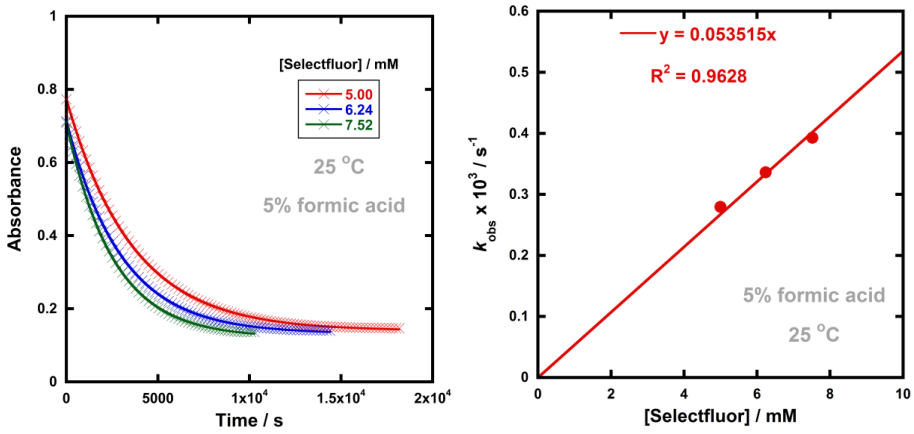

Table 47: All k_{obs} values for fluorination of **108a** and **108c-e**.

Electrophile	Nucleophile	Temp / °C	Ratio of F^+ : Nuc	$[F^+]$: [Nuc] / mM	$k_{obs} \times 10^3$ / s^{-1}
Selectfluor™	**108a-enol**	20	50:1	1.25 : 0.025	0.0388 ± 0.0008
			100:1	2.50 : 0.025	0.0779 ± 0.0009
			150:1	3.75 : 0.025	0.114 ± 0.002
			200:1	5.00 : 0.025	0.147 ± 0.003
			250:1	6.24 : 0.025	0.181 ± 0.006
		25	150:1	3.75 : 0.025	0.1658 ± 0.0004
			200:1	5.00 : 0.025	0.2191 ± 0.0006
			250:1	6.24 : 0.025	0.273 ± 0.001
			300:1	7.49 : 0.025	0.328 ± 0.002
			350:1	8.75 : 0.025	0.381 ± 0.002
		30	100:1	2.51 : 0.025	0.1871 ± 0.0004
			150:1	3.75 : 0.025	0.2592 ± 0.0007
			200:1	5.00 : 0.025	0.340 ± 0.001
			250:1	6.24 : 0.025	0.449 ± 0.006
		35	150:1	3.75 : 0.025	0.3864 ± 0.0009
			200:1	5.00 : 0.025	0.508 ± 0.002
			250:1	6.24 : 0.025	0.631 ± 0.005
			300:1	7.49 : 0.025	0.728 ± 0.003
			350:1	8.75 : 0.025	0.850 ± 0.007
	108d-enol	20	20:1	0.2 : 0.01	0.1109 ± 0.0001
			40:1	0.4 : 0.01	0.1918 ± 0.0001
			60:1	0.6 : 0.01	0.2782 ± 0.0002
			80:1	0.8 : 0.01	0.3801 ± 0.0003
			100:1	1.0 : 0.01	0.4506 ± 0.0004
		25	100:1	1.0 : 0.01	0.7280 ± 0.0003
			140:1	1.4 : 0.01	0.9648 ± 0.0003
			180:1	1.8 : 0.01	1.2288 ± 0.0003
			220:1	2.2 : 0.01	1.4714 ± 0.0003
			260:1	2.6 : 0.01	1.7386 ± 0.0005
		30	20:1	0.2 : 0.01	0.2378 ± 0.0003
			40:1	0.4 : 0.01	0.4253 ± 0.0004
			60:1	0.6 : 0.01	0.6215 ± 0.0004
			80:1	0.8 : 0.01	0.8239 ± 0.0004
			100:1	1.0 : 0.01	1.018 ± 0.001

Electrophile	Nucleophile	Temp / °C	Ratio of F^+ : Nuc	[F^+] : [Nuc] / mM	$k_{obs} \times 10^3$ / s^{-1}
Selectfluor™	**108d-enol**	35	40:1	0.4 : 0.01	0.5965 ± 0.0008
			60:1	0.6 : 0.01	0.8721 ± 0.0009
			80:1	0.8 : 0.01	1.105 ± 0.002
			100:1	1.0 : 0.01	1.346 ± 0.002
	108c-enol	25	77:1	4.0 : 0.052	0.5887 ± 0.0003
			115:1	6.0 : 0.052	0.8075 ± 0.0005
			154:1	8.0 : 0.052	1.051 ± 0.001
			192:1	10.0 : 0.052	1.318 ± 0.001
			231:1	12.0 : 0.052	1.540 ± 0.002
	108e-enol	25	25:1	1.0 : 0.04	0.03325 ± 0.00001
			35:1	1.4 : 0.04	0.04451 ± 0.00001
			45:1	1.8 : 0.04	0.05489 ± 0.00003
			65:1	2.6 : 0.04	0.0805 ± 0.0002
			75:1	3.0 : 0.04	0.0904 ± 0.0003
NFSI	**108a-enol**	25	960:1	24.0 : 0.025	0.01085 ± 0.00003
			1040:1	26.0 : 0.025	0.01231 ± 0.00003
			1200:1	30.0 : 0.025	0.01285 ± 0.00002
			1600:1	40.0 : 0.025	0.01827 ± 0.00004
			3200:1	80.0 : 0.025	0.0370 ± 0.0001
	108d-enol	25	800:1	8.0 : 0.01	0.00458 ± 0.00001
			1000:1	10.0 : 0.01	0.00596 ± 0.00001
			1200:1	12.0 : 0.01	0.00780 ± 0.00002
			1400:1	14.0 : 0.01	0.00822 ± 0.00001
			1800:1	18.0 : 0.01	0.01113 ± 0.00002
	108e-enol	25	555:1	22.2 : 0.04	0.0062 ± 0.0001
			833:1	33.3 : 0.04	0.0086 ± 0.0002
			1110:1	44.4 : 0.04	0.0104 ± 0.0002
Selectfluor™	**108a-enol**	20	5:1	0.125:0.025	1.62 ± 0.02
1:4 H_2O:MeCN			10:1	0.25 : 0.025	2.16 ± 0.01
			20:1	0.50 : 0.025	3.91 ± 0.01
			30.4:1	0.76 : 0.025	4.76 ± 0.01
			40:1	1.00 : 0.025	5.68 ± 0.05
			49.6:1	1.24 : 0.025	6.00 ± 0.06

Electrophile	Nucleophile	Temp / °C	Ratio of F^+ : Nuc	$[F^+]$: [Nuc] / mM	$k_{obs} \times 10^3$ / s^{-1}
Selectfluor™	**108a-enol**	20	200:1	5.0 : 0.025	10.01
1:4 H_2O:MeCN			400:1	10.0 : 0.025	16.59
Initial rates			600:1	15.0 : 0.025	19.96
approach			800:1	20.0 : 0.025	27.40
			1000:1	25.0 : 0.025	36.05
Selectfluor™	**108a-enol**	25	48:1	1.20 : 0.025	0.0752 ± 0.0001
3% formic acid			61:1	1.52 : 0.025	0.0898 ± 0.0001
			70:1	1.76 : 0.025	0.1146 ± 0.0001
			200:1	5.00 : 0.025	0.2946 ± 0.0008
			250:1	6.24 : 0.025	0.370 ± 0.001
			300:1	7.52 : 0.025	0.426 ± 0.002
Selectfluor™	**108a-enol**	25	200:1	5.00 : 0.025	0.2794 ± 0.0006
5% formic acid			250:1	6.24 : 0.025	0.3362 ± 0.0009
			300:1	7.52 : 0.025	0.393 ± 0.001
Selectfluor™	**108a-enol**	20	200:1	5.0 : 0.025	0.1395 ± 0.0002
20% formic acid			400:1	10.0 : 0.025	0.2617 ± 0.0003
			600:1	15.0 : 0.025	0.383 ± 0.001
			800:1	20.0 : 0.025	0.521 ± 0.002
Selectfluor™	**107a-enol**	20	25:1	1.25 : 0.05	0.0267 ± 0.0006
1:4 H_2O:MeCN			50:1	2.50 : 0.05	0.0344 ± 0.0005
			75:1	3.75 : 0.05	0.0428 ± 0.0005
			100:1	5.00 : 0.05	0.0543 ± 0.0006
			130:1	6.50 : 0.05	0.6690 ± 0.0006
Selectfluor™	**107a-enol**	20	70:1	3.49 : 0.05	0.0769
1:4 H_2O:MeCN			150:1	7.49 : 0.05	0.1467
Initial rates			200:1	10.0 : 0.05	0.1947
approach			400:1	20.0 : 0.05	0.4474
			600:1	30.0 : 0.05	0.7916
			640:0	32.0 : 0.05	0.8130

8.5.5 Product analysis by LC-MS on fluorination of 108d-enol with NFSI

In order to confirm that the product of the fluorination of **108d-enol** (R_1 = R_2 = OMe, 0.50 mM) with NFSI (0.20 mM) was indeed **109d**, for selected UV-vis runs, LC-MS analysis was carried out on the reaction mixture in the cuvette at the end of the reaction. The peak at R_t = 2.63 min (figure below) corresponds to **108d-keto**. As expected, this remains unreacted as it comprises ~98% of the keto-enol equilibrium, and as relaxation

is slow it does not occur on the timescale of the fluorination reaction. The peak at R_t = 2.99 min corresponds to **109d** (*m*/*z* = 321.29).

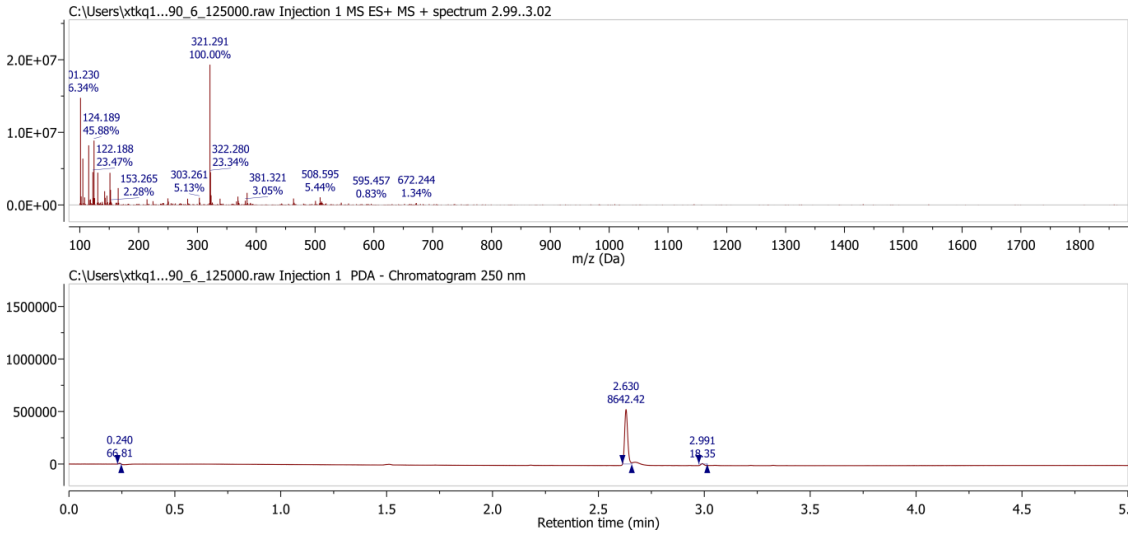

8.6 Experimental to Chapter 5:

8.6.1 Kinetics studies conducted by stopped-flow UV-vis spectrophotometry

Kinetics studies were conducted on an Applied Photophysics stopped-flow instrument equipped with a SpectraKinetic Monochromator. Stock solutions of nucleophiles and electrophiles (5-10 mM) were prepared in dry DMSO and aliquots were removed and diluted accordingly to the required concentrations. Solutions in glass vials were equilibrated to approximately 20 °C in an external water bath prior to being loaded into the driving syringes.

8.6.2 Synthesis of sodium enolates 144a-d

General procedure: The 1,3-diphenylpropane-1,3-dione derivative (0.04-0.2 mmol, 1 equiv.) was dissolved in MeCN (4 mL). NaOMe (1 equiv.) was dissolved in MeOH (4 mL) and added dropwise to the enol, at RT. After 1 h, the solvent was evaporated under reduced pressure to give the enolate.

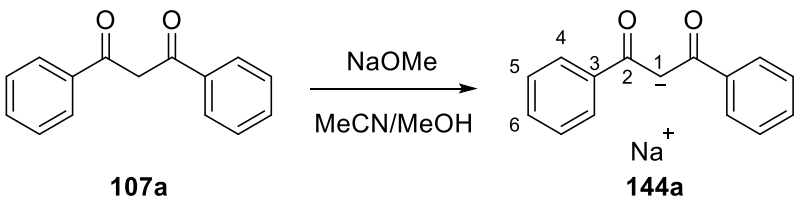

107a **144a**

Sodium 1,3-dioxo-1,3-diphenylpropan-2-ide was obtained from 1,3-diphenylpropane-1,3-dione (50 mg, 0.22 mmol) and NaOMe (25 mg, 0.22 mmol) as a pale yellow solid.

^{1}H NMR (400 MHz, MeCN-d_3) δ = 6.39 (s, 1 H, 1-*H*), 7.32-7.40 (m, 6 H, 5-*H*, 6-*H*), 7.84-7.91 (m, 4 H, 4-*H*).

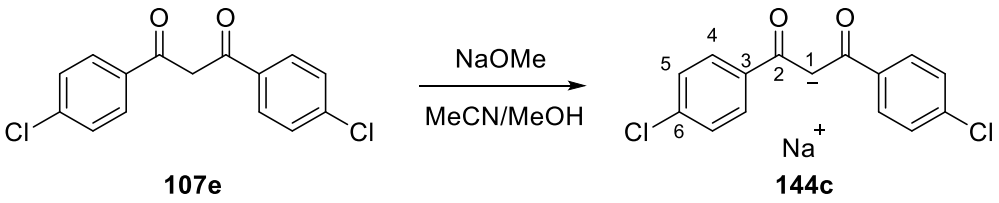

107e **144c**

Sodium 1,3-dioxo-1,3-bis(4'-chlorophenyl)propan-2-ide was obtained from 1,3-bis(4'-chlorophenyl)-1,3-propanedione (18.7 mg, 0.06 mmol) and NaOMe (3.4 mg, 0.06 mmol) as a pale yellow solid (20 mg, 100%). **^{1}H NMR** (400 MHz, DMSO-d_6) δ = 6.40 (s, 1 H, 1-*H*), 7.53-7.62 (m, 4 H, 5-*H*), 8.04-8.18 (m, 4 H, 4-*H*).

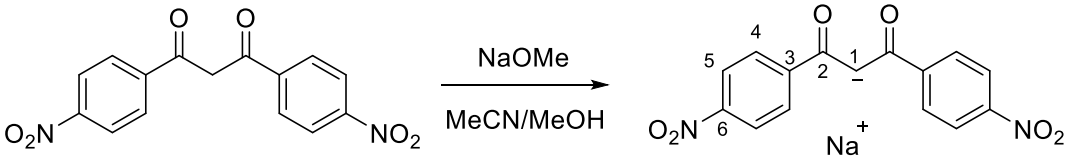

107g **144d**

Sodium 1,3-dioxo-1,3-bis(4'-nitrophenyl)propan-2-ide was obtained from 1,3-bis(4'-nitrophenyl)-1,3-propanedione (13 mg, 0.04 mmol) and NaOMe (2.3 mg, 0.04 mmol) as an orange solid. **^{1}H NMR** (400 MHz, DMSO-d_6) δ = 6.41 (s, 1 H, 1-*H*), 8.06-8.14 (m, 4 H, 5-*H*), 8.22-8.27 (m, 4 H, 4-*H*). **^{13}C NMR** (101 MHz, DMSO-d_6) δ = 92.3 (C-1), 123.2 (C-4), 127.9 (C-5), 129.6 (C-6), 147.7 (C-3), 180.2 (C-2).

8.6.3 Synthesis of potassium enolates 145a-d

General procedure: The 1,3-diphenylpropane-1,3-dione derivative (0.05-0.2 mmol, 1 equiv.) was added to a stirred solution of KO^{t}Bu, (1-1.05 equiv.) in ethanol (5-10 mL) at RT. After 10 min, the solvent was evaporated under reduced pressure and the remaining residue was triturated with Et_2O and dried under vacuum.

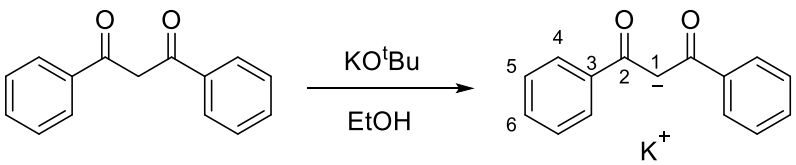

107a **145a**

Potassium 1,3-dioxo-1,3-diphenylpropan-2-ide was obtained from 1,3-diphenylpropane-1,3-dione 50 mg, 0.22 mmol) and KO^{t}Bu (25 mg, 0.22 mmol) as a colourless solid. **^{1}H NMR** (400 MHz, DMSO-d_6) δ = 6.27 (s, 1 H, 1-*H*), 7.32-7.38 (m, 6

H, 5-*H*, 6-*H*), 7.81-7.87 (m, 4 H, 4-*H*). **^{13}C NMR** (101 MHz, DMSO-d_6) δ = 90.5 (C-1), 126.6 (C-4), 127.7 (C-5), 128.6 (C-6), 144.6 (C-3), 181.2 (C-2).

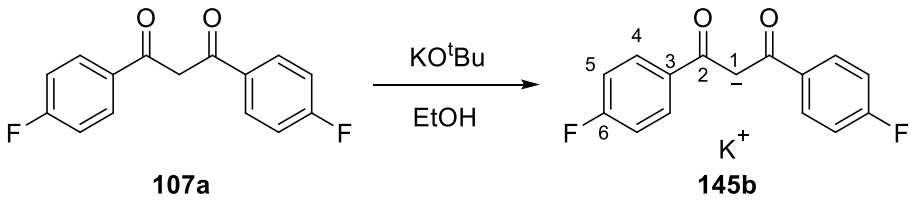

107a **145b**

Potassium 1,3-dioxo-1,3-bis(4'-fluorophenyl)propan-2-ide was obtained from 1,3-bis(4'-fluorophenyl)-1,3-propanedione (50 mg, 0.19 mmol) and KO^{t}Bu (22 mg, 0.19 mmol) as a pale yellow solid. **^{1}H NMR** (400 MHz, DMSO-d_6) δ = 6.20 (s, 1 H, 1-*H*), 7.09-7.19 (m, 4 H, 5-*H*), 7.85-7.93 (m, 4 H, 4-*H*). **^{13}C NMR** (101 MHz, DMSO-d_6) δ = 89.8 (C-1), 114.2 (d, $^2J_{CF}$ = 20.9 Hz, C-5), 128.8 (d, $^3J_{CF}$ = 8.3 Hz, C-4), 140.9 (C-3), 162.5 (d, $^1J_{CF}$ = 244.6 Hz, C-6), 179.8 (C-2). **^{19}F NMR** (376 MHz, DMSO-d_6) δ = −113.9 (s).

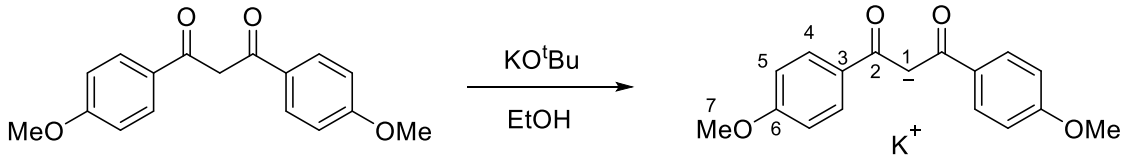

107d **145c**

Potassium 1,3-dioxo-1,3-bis(4'-methoxyphenyl)propan-2-ide was obtained from 1,3-bis(4'-methoxyphenyl)-1,3-propanedione (14.5 mg, 0.05 mmol) and KO^{t}Bu (6 mg, 0.05 mmol) as a yellow solid (11.9 mg, 72%). **^{1}H NMR** (400 MHz, DMSO-d_6) δ = 3.79 (s, 6 H, 7-*H*), 6.21 (s, 1 H, 1-*H*), 6.86-6.91 (m, 4 H, 5-*H*), 7.77-7.84 (m, 4 H, 4-*H*). **^{13}C NMR** (101 MHz, DMSO-d_6) δ = 55.1 (C-7), 89.2 (C-1), 112.8 (C-4), 128.1 (C-5), 137.3 (C-3), 159.7 (C-6), 180.3 (C-2).

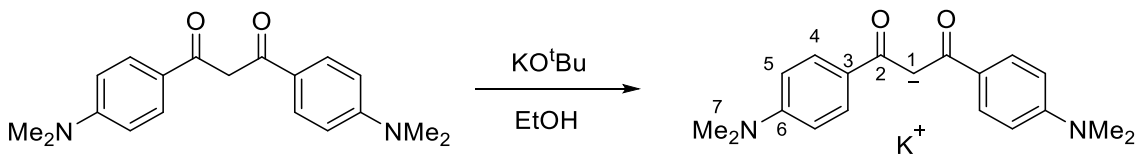

107h **145d**

Potassium 1,3-dioxo-1,3- bis(4'-(dimethylamino)phenyl)propan-2-ide was obtained from 1,3-bis[4'-(dimethylamino)phenyl]-1,3-propanedione (15 mg, 0.05 mmol) and KO^{t}Bu (5.7 mg, 0.05 mmol) as a yellow solid. **^{1}H NMR** (400 MHz, DMSO-d_6) δ = 2.93

(s, 12 H, 7-*H*), 6.13 (s, 1 H, 1-*H*), 7.63-6.68 (m, 4 H, 5-*H*), 7.67-7.71 (m, 4 H, 4-*H*). **^{13}C NMR** (101 MHz, DMSO-d_6) δ = 18.6 (C-7), 88.6 (C-1), 111.0 (C-4), 127.8 (C-5), 130.7 (C-6), 150.7 (C-3), 180.3 (C-2).

8.7 Experimental to Chapter 6:

8.7.1 Method for direct fluorination of progesterone enol acetate

Progesterone enol acetate **165** (0.18 g, 0.5 mmol) was added to a SIMAX bottle and dissolved in acetonitrile (20 mL). The reaction vessel was cooled to 0 °C, stirred rapidly and purged with nitrogen for 10 minutes then fluorine (10% *v/v* in nitrogen) was added at a prescribed flow rate (5 or 10 mL/min, 13-49 min) that was controlled by a mass flow controller. No colour change was observed. After purging with nitrogen for 20 minutes, the reaction vessel was removed and the solvent removed under vacuum to give yellow crystals, yellow oil or a mixture of both.

8.7.2 Synthesis of progesterone enol acetate

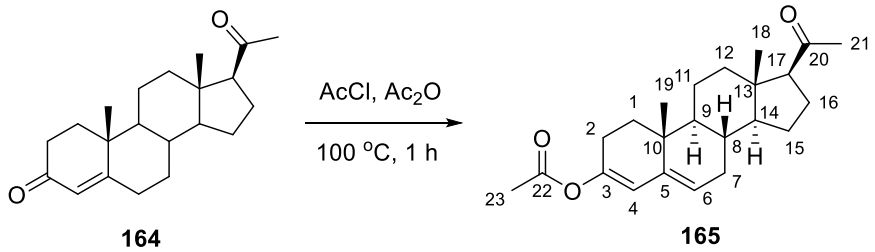

164 **165**

Progesterone (4.1 g, 13.0 mmol) was dissolved in the mixture of acetyl chloride (8.4 mL, 117.3 mmol) and acetic anhydride (6.7 mL, 70.4 mmol) and was heated to 100 °C for 1 h. After allowing the mixture to cool to room temperature, the mixture was concentrated to one third of the original volume under reduced pressure at 25 °C until a white precipitate formed. The product was filtered and washed with cold acetonitrile (10 mL) and dried under vacuum to afford progesterone enol acetate (2.8 g, 60%) as a white solid. **IR** (ATR) υ_{max}/ cm^{-1} 2939, 1749, 1703, 1670, 1365, 1219, 1202, 1188, 1119. **M.p.** 128-132 °C from MeOH (lit.[224] 130-132 °C, from MeOH). **^{1}H NMR** (400 MHz, $CDCl_3$) δ = 0.65 (3H, s, 18-H_3), 1.00 (3H, s, 19-H_3), 1.04-1.10 (1H, m, 9-*H*), 1.18-1.29 (2H, m, 14-*H*, 15-*H*), 1.30-1.38 (1H, m, 1-*H*), 1.43-1.50 (2H, m, 11-*H*, 12-*H*), 1.58-1.73 (5H, m, 11-*H*, 16-*H*, 15-*H*, 7-*H*, 8-*H*), 1.85 (1H, dd, $^{2}J_{HH}$ = 12.5 Hz, $^{3}J_{HH}$ = 5.5 Hz, 1-*H*), 2.03-2.06 (1H, m, 12-*H*), 2.12 (3H, s, 23-H_3), 2.13 (3H, s, 21-H_3), 2.14-2.22 (3H, m, 16-*H*, 2-*H*, 7-*H*), 2.41-2.47 (1H, m, 2-*H*), 2.54 (1H, t, $^{3}J_{HH}$ = 9.0 Hz, 17-*H*), 5.39 (1H, m, 4-*H*), 5.69 (1H, d, $^{4}J_{HH}$ = 1.9 Hz, 6-*H*). **^{13}C NMR** (101 MHz, $CDCl_3$) δ = 13.50 (C-

18), 19.00 (C-19), 21.24 (C-23), 21.37 (C-11), 22.99 (C-16), 24.55 (C-15), 24.93 (C-2), 31.69 (C-2), 31.87 (C-7), 31.89 (C-8), 33.93 (C-1), 35.04 (C-10), 38.96 (C-12), 44.24 (C-13), 48.02 (C-9), 57.16 (C-14), 63.83 (C-17), 117.08 (C-6), 123.81 (C-4), 139.50 (C-5), 147.18 (C-3), 169.52 (C-22), 209.64 (C-20). **ESI-MS** (ES^+, R_t 3.53) *m/z* 398 $[M+MeCN]^+$, 356 $[M]^+$, 315 $[M-Ac]^+$.

8.7.3 Synthesis of 6β-fluoroprogesterone and 6α-fluoroprogesterone

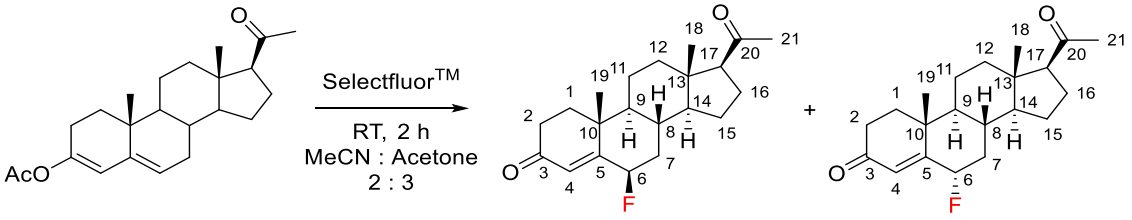

165 **166-β** **166-α**

Progesterone enol acetate (0.197 g, 0.55 mmol) was dissolved in MeCN (4 mL) and acetone (5 mL). Selectfluor™ (0.216 g, 0.606 mmol) was added and the mixture was stirred at ambient temperature for 2 hours. Solvents were evaporated and the residue dissolved in ethyl acetate (15 mL), and washed with water (3 × 15 mL). After washing with brine (15 mL) and drying over $MgSO_4$, the solvent was evaporated *in vacuo* to yield the crude product as a 2:1 mixture of β:α isomers (0.175 g, 95%). After column chromatography (hexane:ethyl acetate, 10:1 to 3:1,) 6β-fluoroprogesterone was isolated as the major product (white solid, 0.10 g, 54%). 6α-Fluoroprogesterone was isolated as the minor product.

6β-Fluoroprogesterone: **IR** (ATR) υ_{max}/ cm^{-1} 2941, 1702, 1678, 1386, 1355, 1228, 1193, 1161. **M.p.** 154-159 °C from MeOH (lit.[208] 159-161 °C, from benzene). **^{1}H NMR** (400 MHz, $CDCl_3$) δ = 0.69 (3H, s, 18-*H*$_3$), 0.99 (1H, td, $^2J_{HH}$ = 11.4 Hz, $^3J_{HH}$ = 3.9 Hz, 9-*H*), 1.10-1.27 (2H, m, 7-*H*, 14-*H*), 1.30 (3H, d, $^5J_{FH}$ = 1.3 Hz, 19-*H*$_3$), 1.30-1.34 (1H, m, 15-*H*), 1.44 (1H, td, $^2J_{HH}$ = 12.7 Hz, $^3J_{HH}$ = 3.9 Hz, 12-*H*), 1.48-1.54 (1H, m, 11-*H*), 1.62-1.77 (4H, m, 1-*H*, 11-*H*, 15-*H*, 16-*H*), 1.90-1.94 (1H, m, 8-*H*), 2.05-2.11 (2H, m, 1-*H*, 12-*H*), 2.12 (3H, s, 21-*H*$_3$), 2.17-2.24 (2H, m, 11-*H*, 7-*H*), 2.43 (1H, dt, $^2J_{HH}$ = 16.9 Hz, $^3J_{HH}$ = 3.3 Hz, 2-*H*), 2.51-2.58 (2H, m, 2-*H*, 17-*H*), 4.99 (1H, dt, $^2J_{HF}$ = 48.6 Hz, $^3J_{HH}$ = 2.5 Hz, 6-*H*), 5.87 (1H, d, $^4J_{HF}$ = 5.0 Hz, 4-*H*). **^{13}C NMR** (101 MHz, $CDCl_3$) δ = 13.45 (C-18), 18.53 (C-19), 20.98 (C-11), 22.99 (C-16), 24.37 (C-15), 30.09 (C-8), 31.59 (C-21), 34.34 (C-2), 37.04 (C-1), 37.35 (d, $^2J_{FC}$ = 23.5 Hz, C-7), 37.97 (C-10), 38.65 (C-12), 44.11 (C-13), 53.21 (C-9), 55.99 (C-14), 63.55 (C-17), 93.41 (d, $^1J_{FC}$ =

166.0 Hz, C-6), 128.57 (C-4), 161.67 (d, $^{2}J_{FC}$ = 12.6 Hz, C-5), 199.88 (C-3), 209.19 (C-20). **^{19}F NMR** (376 MHz, $CDCl_3$) δ = −166.0 (td, $^{2}J_{HF}$ = 47.8 Hz, $^{3}J_{HF}$ = 12.6 Hz).

6α-Fluoroprogesterone: **IR** (ATR) υ_{max}/ cm^{-1} 2948, 1700, 1680, 1357, 1269, 1225, 1186, 1059. **M.p.** 144-147 °C (Lit.[208] 146-148 °C, from acetone-hexane). **^{1}H NMR** (400 MHz, $CDCl_3$) δ = 0.66 (3H, s, 18-*H*$_3$), 0.99 (1H, m, 9-*H*), 1.18 (3H, m, 19-*H*$_3$), 1.23-1.33 (3H, m, 7-*H*, 14-*H*, 15-*H*), 1.39-1.46 (2H, m, 11-*H*, 12-*H*), 1.56-1.62 (1H, m, 8-*H*), 1.62-1.67 (1H, m, 11-*H*), 1.67-1.76 (2H, m, 15-*H*, 16-*H*), 1.76-1.82 (1H, m, 1-*H*), 2.03-2.10 (2H, m, 1-*H*, 12-*H*), 2.12 (3H, s, 21-*H*$_3$), 2.16-2.22 (1H, m, 16-*H*), 2.26-2.32 (1H, m, 7-*H*), 2.35-2.39 (1H, m, 2-*H*), 2.44 (1H, td, $^{2}J_{HH}$ = 14.5 Hz, $^{3}J_{HH}$ = 3.4 Hz, 2-*H*), 2.54 (1H, t, $^{3}J_{HH}$ = 8.5 Hz, 17-*H*), 5.09 (1H, ddd, $^{2}J_{FH}$ = 47.9 Hz, $^{3}J_{HH}$ = 12.3 Hz, $^{3}J_{HH}$ = 5.6 Hz, 6-*H*), 6.09 (1H, s, 4-*H*). **^{13}C NMR** (101 MHz, $CDCl_3$) δ = 13.41 (C-18), 18.20 (C-19), 21.03 (C-11), 22.96 (C-16), 24.47 (C-15), 31.60 (C-21), 33.52 (C-8), 33.83 (C-2), 36.42 (C-1), 38.48 (d, $^{2}J_{FC}$ = 17.7 Hz, C-7), 38.49 (C-12), 39.24 (C-10), 44.00 (C-13), 53.56 (C-9), 55.74 (C-14), 63.41 (C-17), 88.22 (d, $^{1}J_{FC}$ = 183.9 Hz, C-6), 119.88 (d, $^{3}J_{CF}$ = 14.8 Hz, C-4), 165.80 (d, $^{2}J_{FC}$ = 11.2 Hz, C-5), 198.79 (C-3), 209.09 (C-20). **^{19}F NMR** (376 MHz, $CDCl_3$) δ = −183.37 (ddd, $^{2}J_{FH}$ = 47.9 Hz, $^{3}J_{HH}$ = 12.3 Hz, $^{3}J_{HH}$ = 5.6 Hz, 6-*H*).

8.7.4 Synthesis of steroid derivatives 167-169 and 174-176

The following syntheses were conducted by Ben J. Murray and are included in this thesis for completeness:

Testosterone enol diacetate **167**:

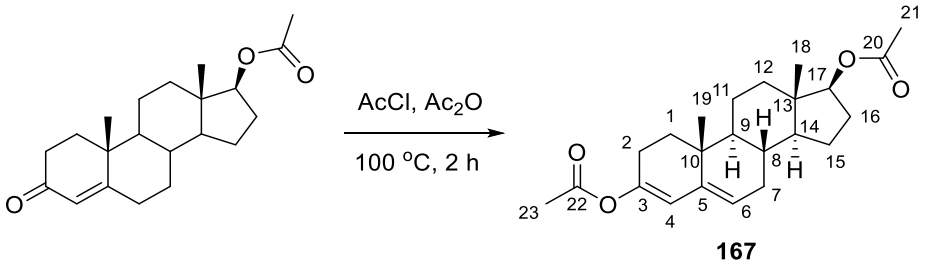

167

Testosterone (0.644 g, 2.23 mmol) was dissolved in acetyl chloride (6 mL) and acetic anhydride (4 mL) then heated to 100 °C for 2 hours before being allowed to cool to room temperature. The mixture was then concentrated *in vacuo* and the resulting solid washed with cold acetonitrile (2 × 10 mL) to give testosterone enol diacetate (0.578 g, 70%) as a white solid, m.p. 143-144 °C (lit.[250] 143-147 °C). δ_H (400 MHz; $CDCl_3$) 0.85

(3H, s, C**18**H$_3$), 1.03 (3H, s, C**19**H$_3$), 1.01-1.91 (12H, m), 2.06 (3H, s, C**17**-OAc), 2.09 (2H, m), 2.15 (3H, s, C**3**-OAc), 2.18 (2H, m), 2.44 (1H, m), 4.63 (1H, dd, $^3J_{HH}$ 9.2, $^3J_{HH}$ 7.7, C**17**H), 5.41 (1H, dd, $^3J_{HH}$ 5.3, $^4J_{HH}$ 2.3, C**6**H), 5.71 (1H, d, $^4J_{HH}$ 2.3, C**4**H). δ_C (101 MHz; $CDCl_3$) 12.19, 19.01, 20.84, 21.24, 21.33, 23.64, 24.92, 27.68, 31.54, 31.72, 33.90, 35.08, 36.86, 42.64, 48.05, 51.30, 82.86 (C**17**), 117.06 (C**6**), 123.67 (C**4**), 139.58 (C**5**), 147.20 (C**3**), 169.53 (C**3**-OAc), 171.39 (C**17**-OAc). HRMS (ESI+) *m/z* calc. for $C_{23}H_{33}O_4^+$ 373.2379; found 373.2379.

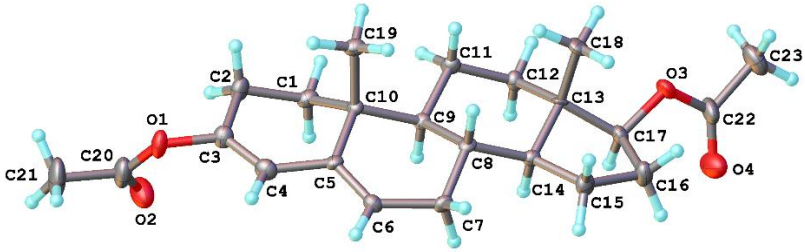

6-Fluorotestosterone acetate **174**:

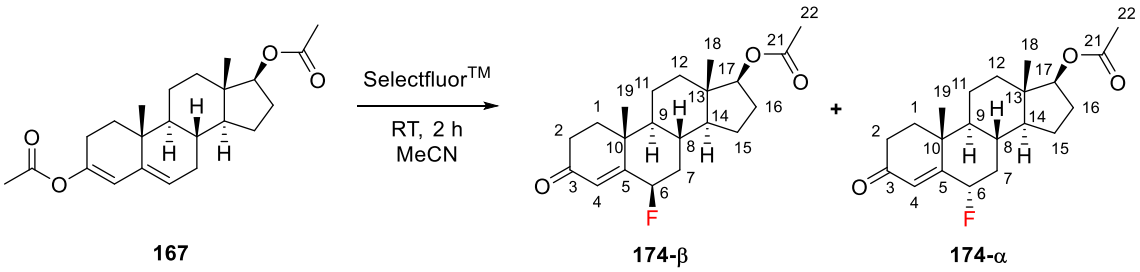

Testosterone enol diacetate (0.103 g, 0.0275 mmol) and Selectfluor™ (0.109 g, 0.0308 mmol) were dissolve in acetonitrile (10 mL) and stirred at room temperature for 2 hours. The solvent was removed *in vacuo* and the residue partitioned between ethyl acetate (20 mL) and water (20 mL). The organic layer was separated, washed with brine (20 mL), dried over $MgSO_4$ then concentrated *in vacuo* to give 6-fluorotestosterone acetate, (0.071 g, 74%), as a white solid. δ_H (400 MHz; $CDCl_3$) 0.83/0.86 (s, α/β-C**18**H$_3$), 1.19/1.30 (s, α/β-C**19**H$_3$), 2.04/2.05 (s, α/β-C**17**-OAc), 4.99 (dt, $^2J_{HF}$ 48.7, $^4J_{HH}$ 3.8, α-C**6**H), 5.07 (dddd, $^2J_{HF}$ 47.7, $^3J_{HH}$ 12.2, $^3J_{HH}$ 5.9, $^4J_{HH}$ 2.0, β-C**6**H), 5.87 (dd, $^3J_{HF}$ 3.8, $^4J_{HH}$ 1.0, β-C**4**H), 6.08 (dt, $^3J_{HF}$ 2.0, $^4J_{HH}$ 1.0, α-C**4**H). δ_F (376 MHz; $CDCl_3$) −183.41 (ddd, $^2J_{HF}$ 47.7, $^3J_{HF}$ 9.3, $^3J_{HF}$ 3.8, α-F), −165.51 (tdd, $^2J_{HF}$ 48.7, $^3J_{HF}$ 11.9, $^3J_{HF}$ 2.8, β-F). δ_C (101 MHz; $CDCl_3$) 36.48 (d, $^2J_{CF}$ 24.5, α/β-C**7**), 36.96 (d, $^2J_{CF}$ 23.5, α/β-C**7**), 82.29/82.45 (α/β-C**17**), 88.23 (d, $^1J_{CF}$ 185.2, α/β-C**6**), 93.36 (d, $^1J_{CF}$ 166.7, α/β-C**6**), 128.56/128.65 (α/β-C**4**), 161.70 (d, $^2J_{CF}$ 12.2, α/β-C**5**), 165.83 (d, $^2J_{CF}$ 11.3, α/β-C**5**),

171.21/171.31 (α/β-C**17**-OAc), 198.75/199.94 (α/β-C**3**). HRMS (ESI+) *m/z* calc. for $C_{21}H_{30}O_3F$ 349.2179; found 349.2175.

X-ray crystal structure as a mixture of both α and β isomers:

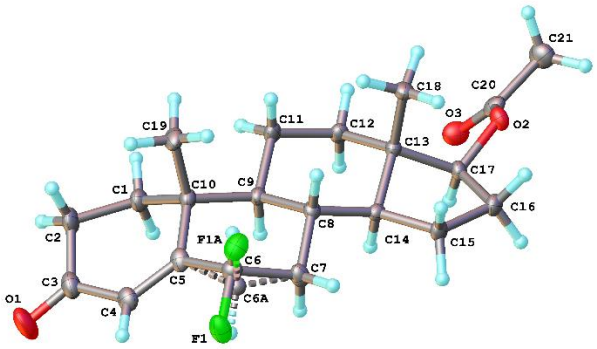

(+)-4-Cholesten-3-one enol acetate **168**:

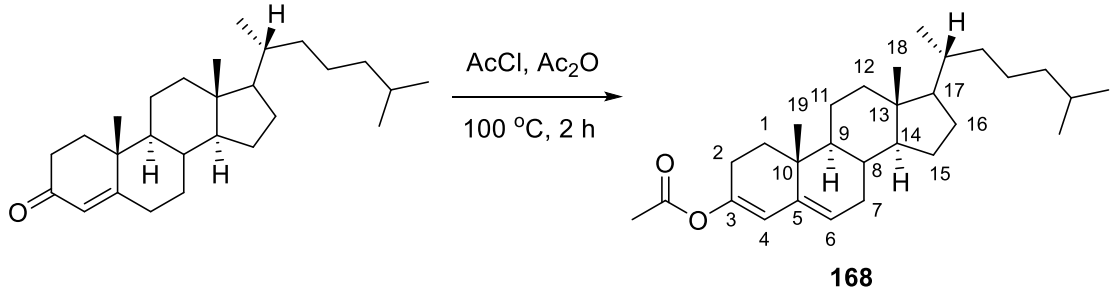

168

(+)-4-Cholesten-3-one (0.474 g, 1.23 mmol) was dissolved in acetyl chloride (6 mL) and acetic anhydride (4 mL) then heated to 100 °C for 2 hours before being allowed to cool to room temperature. The mixture was then concentrated *in vacuo* and the resulting solid washed with cold acetonitrile (2 × 10 mL) to give (+)-4-cholesten-3-one enol acetate (0.305 g, 58%) as a white solid, m.p. 81-82 °C (lit.[251] 80-81 °C). δ_H (400 MHz; $CDCl_3$) 0.70 (3H, s, C**18**H_3), 0.82-09.94 (10H, m), 1.00 (3H, s, C**19**H_3), 1.01-1.74 (15H, m), 1.85 (3H, m), 1.97-2.11 (6H, m), 2.13 (3H, s, C**3**-OAc), 2.43 (1H, m, C**17**H), 5.39 (1H, m, C**6**H), 5.68 (1H, d, $^4J_{HH}$ 2.3, C**4**H). δ_C (101 MHz; $CDCl_3$) 11.98, 18.72, 18.86, 21.12, 21.22, 22.57, 22.83, 23.83, 24.20, 24.82, 28.03, 28.25, 31.75, 31.88, 33.78, 34.90, 35.80, 36.18, 39.52, 39.75, 42.45, 47.97, 56.14, 56.85, 117.03 (s, C**6**), 124.13 (C**4**), 139.37 (C**5**), 146.97 (C**3**), 169.43 (OAc). Calc: %C 81.63, %H 10.87, %N 0; measured: %C 79.55, %H 10.61, %N -0.03.

6-Fluorocholestenone **175**:

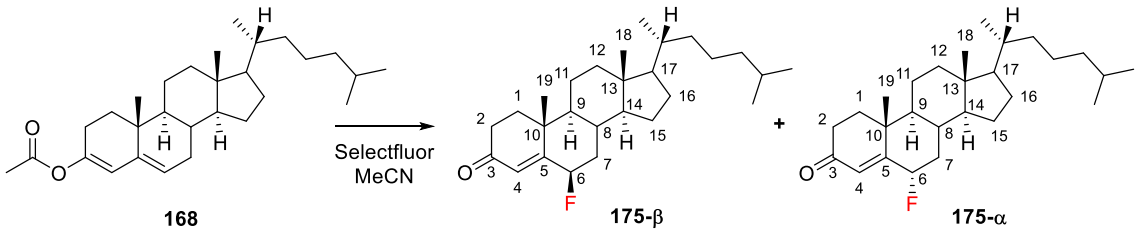

(+)-4-Cholesten-3-one enol acetate (0.279 g, 0.0652 mmol) and Selectfluor™ (0.292 g, 0.0801 mmol) were dissolve in acetonitrile (10 mL) and stirred at room temperature for 2 hours. The solvent was removed *in vacuo* and the residue partitioned between ethyl acetate (20 mL) and water (20 mL). The organic layer was separated, washed with brine (20 mL), dried over $MgSO_4$ then concentrated *in vacuo* to give (+)-6-fluoro-4-cholesten-3-one, (0.217 g, 78%), as a yellow solid. δ_H (400 MHz; $CDCl_3$) 0.70/0.73 (s, α/β-C**18**H_3), 1.19/1.27 (s, α/β-C**19**H_3), 4.97 (dt, $^2J_{HF}$ 48.2, $^3J_{HH}$ 2.8, α-C**6**H), 5.14 (dddd, $^2J_{HF}$ 48.6 $^3J_{HH}$ 12.2, $^3J_{HH}$ 5.9, $^3J_{HH}$ 2.0, β-C**6**H), 5.86 (dd, $^3J_{HF}$ 4.8, $^4J_{HH}$ 0.9, β-C**4**H), 6.07 (m, α-C**4**H). δ_F (376 MHz; $CDCl_3$) −183.06 (ddd, $^2J_{HF}$ 48.6, $^3J_{HF}$ 9.7, $^3J_{HF}$ 4.8, α-F), −165.27 (tdd, $^2J_{HF}$ 48.2, $^3J_{HF}$ 12.1, $^3J_{HF}$ 2.9, β-F). δ_C (101 MHz; $CDCl_3$) 36.12 (d, $^2J_{CF}$ 14.6, α/β-C**7**), 37.34 (d, $^2J_{CF}$ 23.4, α/β-C**7**), 88.36 (d, $^1J_{CF}$ 185.0, α/β-C**6**), 93.46 (d, $^1J_{CF}$ 166.3, α/β-C**6**), 162.19 (d, $^2J_{CF}$ 12.3, α/β-C**5**), 166.42 (d, $^2J_{CF}$ 11.1, α/β-C**5**), 198.87/200.05 (α/β-C**3**). HRMS (ESI+) *m/z* calc. for $C_{27}H_{46}FO$ 404.3454; found 405.1787.

Hydrocortisone enol tetraacetate **169**:

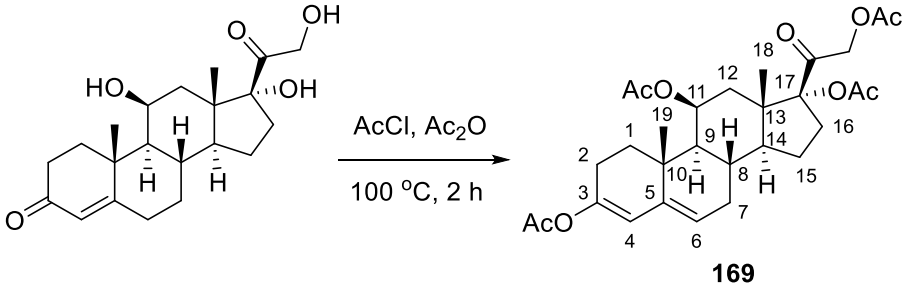

Hydrocortisone (0.811 g, 2.24 mmol) was dissolved in acetyl chloride (6.0 mL) and acetic anhydride (4.0 mL) then heated to 100 °C for 2 hours before being allowed to cool to room temperature. The mixture was then concentrated *in vacuo* and the resulting solid washed with cold acetonitrile (2 × 10 mL) to give hydrocortisone enol tetraacetate (0.670 g, 56%) as a white solid, m.p. 207-213 °C (lit.[225] 211-214 °C). δ_H (400 MHz;

$CDCl_3$) 0.86 (3H, s, C**18**H_3), 1.06 (3H, s, C**19**H_3), 1.24 (2H, t, J 7.0), 1.26-1.55 (2H, m), 1.71-2.50 (10H, m), 2.03 (3H, s, OAc), 2.09 (3H, s, OAc), 2.13 (3H, s, OAc), 2.15 (3H, s, OAc), 2.88 (1H, m), 3.72 (1H, m), 4.74 (2H, m), 5.32 (1H, m), 5.55 (1H, m, C**6**H), 5.66 (1H, d, J 2.2, C**4**H). δ_C (101 MHz; $CDCl_3$) 15.88, 20.64, 21.23, 21.35, 21.44, 22.01, 23.97, 24.62, 28.75, 30.87, 31.70, 33.54, 34.79, 36.00, 46.92, 50.14, 53.31, 67.03, 69.73, 94.69, 116.17 (C**6**), 122.54 (C**4**), 140.39 (C**5**), 147.41 (C**3**), 169.45 (OAc), 170.19 (OAc), 170.36 (OAc), 170.92 (OAc), 198.92 (C**17**). HRMS (ESI+) *m/z* calc. for $C_{29}H_{39}O_9^+$ 531.2594; found 531.2595.

6-Fluorohydrocortisone **176**:

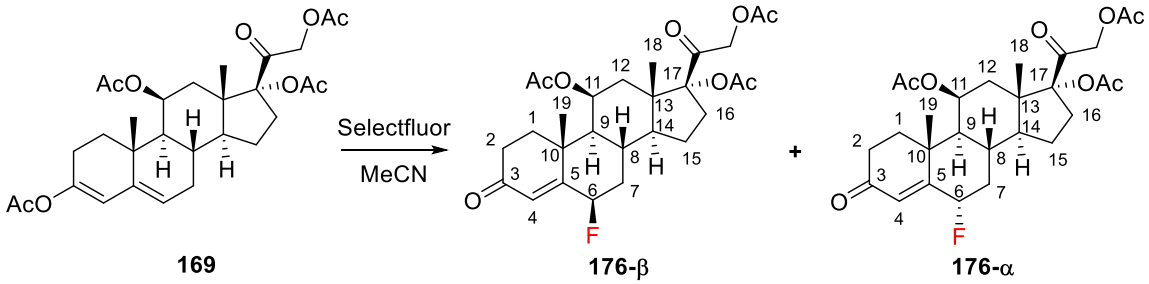

169 **176-β** **176-α**

Hydrocortisone enol tetraacetate (0.084 g, 0.157 mmol) and Selectfluor™ (0.060 g, 0.176 mmol) were dissolve in acetonitrile (10 mL) and stirred at room temperature for 2 hours. The solvent was removed *in vacuo* and the residue partitioned between ethyl acetate (20 mL) and water (20 mL). The organic layer was separated, washed with brine (20 mL), dried over $MgSO_4$ then concentrated *in vacuo* to give 6-fluoro-hydrocortisone, (0.045 g, 69%), as a white solid. δ_H (400 MHz; $CDCl_3$) 0.86/0.89 (s, α/β-C**18**H_3), 1.25/1.35 (s, α/β-C**19**H_3), 2.02/2.03 (s, α/β-OAc), 2.06/2.07 (s, α/β-OAc), 2.14 (s, OAc), 5.00 (dt, $^2J_{HF}$ 48.6, $^3J_{HH}$ 2.6, α-C**6**H), 5.16 (dddd, $^2J_{HF}$ 48.6, $^3J_{HH}$ 12.6, $^3J_{HH}$ 6.2, $^3J_{HH}$ 2.1, β-C**6**H), 5.83 (d, $^3J_{HF}$ 4.6, β-C**4**H), 6.01 (m, α-C**6**H). δ_F (376 MHz; $CDCl_3$) −184.54 (ddd, $^2J_{HF}$ 48.6, $^3J_{HF}$ 10.7, $^3J_{HF}$ 3.9, α-F), −165.83 (tdd, $^2J_{HF}$ 48.6, $^3J_{HF}$ 11.7, $^3J_{HF}$ 4.6, β-F). δ_C (101 MHz; $CDCl_3$) 37.84 (d, $^2J_{CF}$ 23.8, α/β-C**7**), 38.69 (d, $^2J_{CF}$ 18.7, α/β-C**7**), 87.38 (d, $^1J_{CF}$ 184.8, α/β-C**6**), 92.37 (d, $^1J_{CF}$ 168.3, α/β-C**6**), 161.34 (d, $^2J_{CF}$ 12.1, α/β-C**5**), 165.55 (d, $^2J_{CF}$ 11.5, α/β-C**5**), 169.71/169.93 (α/β-OAc), 170.34/170.37 (α/β-OAc), 170.75/170.78 (α/β-OAc), 198.14/198.71 (α/β-C**17**), 198.76/199.31 (α/β-C**3**). HRMS (ESI+) *m/z* calc. for $C_{27}H_{35}FO_8$ 506.2316; found 506.2230.

8.7.5 Determination of extinction coefficients

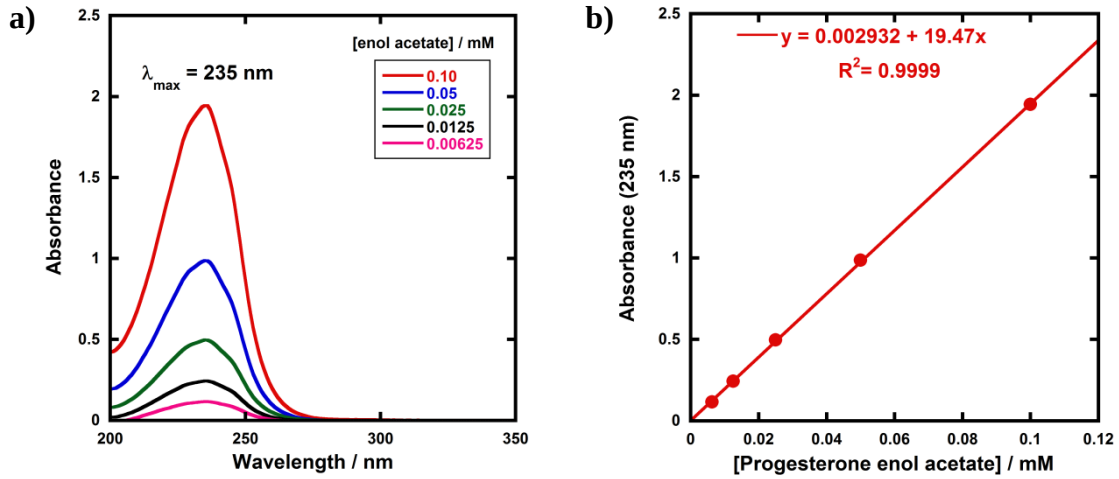

Figure 161: UV-vis spectra for progesterone enol acetate **165** at 5 concentrations.

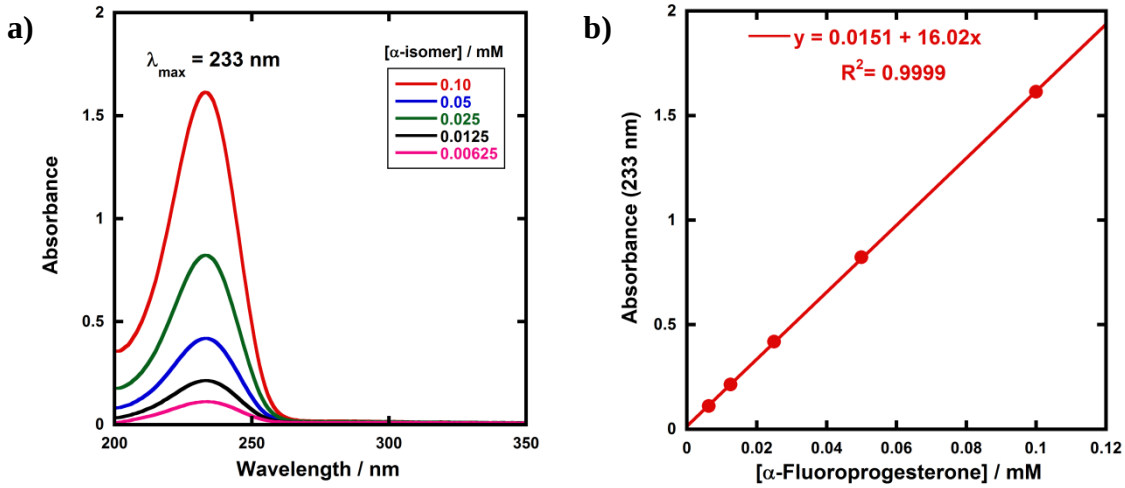

Figure 162: UV-vis spectra for 6-α-fluoroprogesterone **166-α** at 5 concentrations.

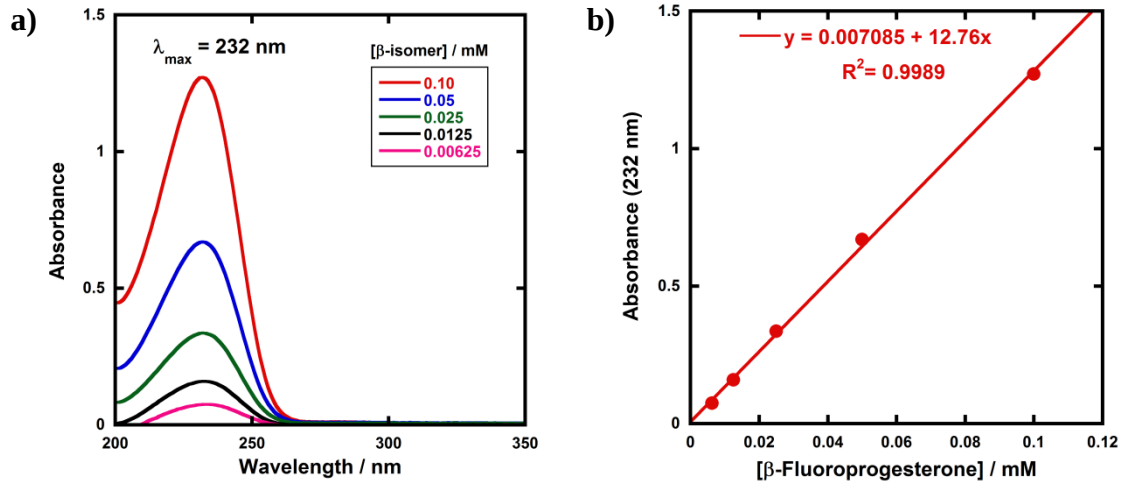

Figure 163: UV-vis spectra for 6-β-fluoroprogesterone **166-β** at 5 concentrations.

8.7.6 Kinetics data for fluorination of steroid enol acetates

Table 48: All k_{obs} values for fluorination of progesterone enol acetate **165**.

Electrophile	Solvent	Temp / °C	Ratio of F^+ : Nuc	$[F^+]$: [Nuc] / mM	$k_{obs} \times 10^3$ / s^{-1}
Selectfluor™	**100% MeCN**	25	10:1	0.50 : 0.05	1.260 ± 0.002
			20:1	1.00 : 0.05	2.370 ± 0.004
			30:1	1.50 : 0.05	3.700 ± 0.006
			40:1	2.00 : 0.05	4.740 ± 0.008
			50:1	2.50 : 0.05	5.87 ± 0.01
		30	10:1	0.50 : 0.05	1.850 ± 0.006
			20:1	1.00 : 0.05	3.67 ± 0.02
			30:1	1.50 : 0.05	5.45 ± 0.02
			40:1	2.00 : 0.05	7.15 ± 0.03
		35	10:1	0.50 : 0.05	2.545 ± 0.009
			20:1	1.00 : 0.05	5.17 ± 0.02
			30:1	1.50 : 0.05	7.63 ± 0.03
			40:1	2.00 : 0.05	9.66 ± 0.04
		40	10:1	0.50 : 0.05	3.67 ± 0.02
			20:1	1.00 : 0.05	7.01 ± 0.04
			30:1	1.50 : 0.05	10.11 ± 0.05
			40:1	2.00 : 0.05	13.39 ± 0.07
	5% H_2O in MeCN	25	10:1	0.50 : 0.05	0.757 ± 0.004
			20:1	1.00 : 0.05	1.439 ± 0.008
			30:1	1.50 : 0.05	2.165 ± 0.008
			40:1	2.00 : 0.05	2.99 ± 0.01
	10% H_2O in MeCN	25	10:1	0.50 : 0.05	0.6396±0.0008
			20:1	1.00 : 0.05	1.230 ± 0.0009
			30:1	1.50 : 0.05	1.813 ± 0.002
	20% H_2O in MeCN	25	10:1	0.50 : 0.05	0.4060±0.0008
			20:1	1.00 : 0.05	0.8040±0.0008
			30:1	1.50 : 0.05	1.230 ± 0.002
			40:1	2.00 : 0.05	1.660 ± 0.002
	30% H_2O in MeCN	25	10:1	0.50 : 0.05	0.315 ± 0.003
			20:1	1.00 : 0.05	0.601 ± 0.003
			30:1	1.50 : 0.05	0.923 ± 0.001
			40:1	2.00 : 0.05	1.230 ± 0.003

Electrophile	Solvent	Temp / °C	Ratio of F^+ : Nuc	$[F^+]$: [Nuc] / mM	$k_{obs} \times 10^3$ / s^{-1}
Selectfluor™	**10% MeOH in MeCN**	25	10:1	0.50 : 0.05	1.065 ± 0.004
			20:1	1.00 : 0.05	2.34 ± 0.02
			30:1	1.50 : 0.05	3.34 ± 0.05
			40:1	2.00 : 0.05	5.05 ± 0.09
	20% MeOH in MeCN	25	10:1	0.50 : 0.05	1.018 ± 0.007
			20:1	1.00 : 0.05	2.18 ± 0.02
			30:1	1.50 : 0.05	3.55 ± 0.06
			40:1	2.00 : 0.05	4.80 ± 0.09
	30% MeOH in MeCN	25	20:1	1.00 : 0.05	2.9 ± 0.1
			30:1	1.50 : 0.05	4.4 ± 0.2
			40:1	2.00 : 0.05	5.9 ± 0.2
			50:1	2.50 : 0.05	7.0 ± 0.1
	40% MeOH in MeCN	25	10:1	0.50 : 0.05	1.31 ± 0.05
			20:1	1.00 : 0.05	2.85 ± 0.06
			30:1	1.50 : 0.05	4.31 ± 0.09
			40:1	2.00 : 0.05	5.44 ± 0.09
	50% MeOH in MeCN	25	10:1	0.50 : 0.05	1.51 ± 0.02
			20:1	1.00 : 0.05	2.55 ± 0.02
			30:1	1.50 : 0.05	4.05 ± 0.03
			40:1	2.00 : 0.05	5.47 ± 0.03
diCl-NFPy TfO^-	**100% MeCN**	25	1:20	0.05 : 1.00	0.454 ± 0.002
			1:25	0.05 : 1.25	0.566 ± 0.001
			1:30	0.05 : 1.50	0.693 ± 0.004
			1:35	0.05 : 1.75	0.815 ± 0.002
			1:40	0.05 : 2.00	0.968 ± 0.009
			1:45	0.05 : 2.25	1.072 ± 0.004
		30	1:10	0.05 : 0.50	0.3334±0.0007
			1:20	0.05 : 1.00	0.759 ± 0.001
			1:30	0.05 : 1.50	1.025 ± 0.003
			1:40	0.05 : 2.00	1.405 ± 0.003
		35	1:10	0.05 : 0.50	0.4527±0.0006
			1:20	0.05 : 1.00	0.902 ± 0.002
			1:30	0.05 : 1.50	1.410 ± 0.003
			1:40	0.05 : 2.00	1.986 ± 0.006

Electrophile	Solvent	Temp / °C	Ratio of F^+ : Nuc	$[F^+]$: [Nuc] / mM	$k_{obs} \times 10^3$ / s^{-1}
diCl-NFPy TfO^-	**100% MeCN**	40	1:10	0.05 : 0.50	0.681 ± 0.002
			1:20	0.05 : 1.00	1.346 ± 0.006
			1:30	0.05 : 1.50	2.05 ± 0.01
			1:40	0.05 : 2.00	2.80 ± 0.03
diCl-NFPy BF_4^-	**100% MeCN**	25	1:20	0.05 : 1.00	0.527 ± 0.006
			1:25	0.05 : 1.25	0.648 ± 0.003
			1:30	0.05 : 1.50	0.733 ± 0.002
			1:35	0.05 : 1.75	0.870 ± 0.004
pentaCl-NFPy TfO^-	**100% MeCN**	25	1:4	0.05 : 0.20	25.0 ± 0.1
			1:5	0.05 : 0.25	32.1 ± 0.1
			1:6	0.05 : 0.30	39.0 ± 0.1
			1:7	0.05 : 0.35	47.4 ± 0.2
			1:8	0.05 : 0.40	52.1 ± 0.2
NFSI	**100% MeCN-d_3**	25	10:1	175.2 : 17.5	0.067 ± 0.001
			15:1	262.8 : 17.5	0.089 ± 0.002
			20:1	350.8 : 17.5	0.113 ± 0.003
			25:1	438.4 : 17.5	0.156 ± 0.004
			30:1	526.0 : 17.5	0.166 ± 0.004
triMe-NFPy TfO^-	**100% MeCN-d_3**	25	15:1	263.2 : 17.5	0.0021 ± 0.0001
			20:1	350.5 : 17.5	0.0027 ± 0.0001
			25:1	438.2 : 17.5	0.0031 ± 0.0001
			30:1	525.9 : 17.5	0.0037 ± 0.0001
			40:1	701.4 : 17.5	0.0046 ± 0.0001
NFPy TfO^-	**100% MeCN-d_3**	25	15:1	572.2 : 17.5	0.0057 ± 0.0001
			20:1	775.9 : 17.5	0.0078 ± 0.0001
			25:1	907.1 : 17.5	0.0091 ± 0.0001
			30:1	1056 : 17.5	0.0106 ± 0.001

Fluorination of progesterone enol acetate **165** with Selectfluor™:

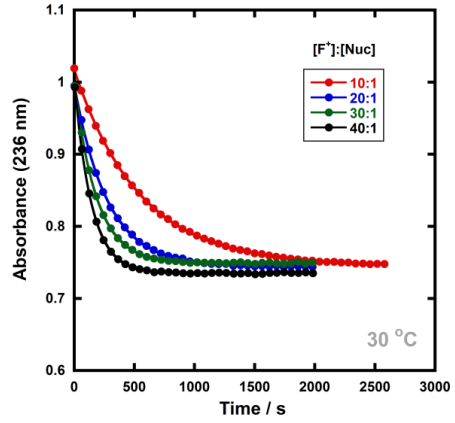

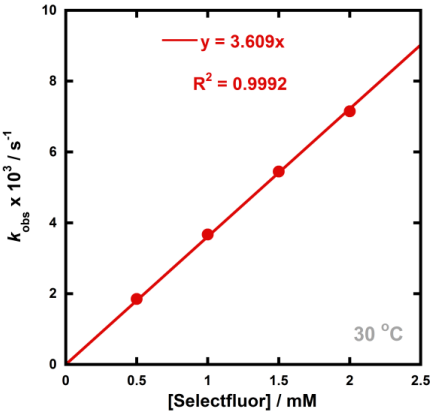

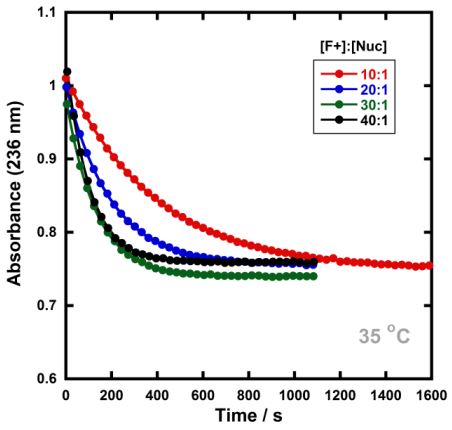

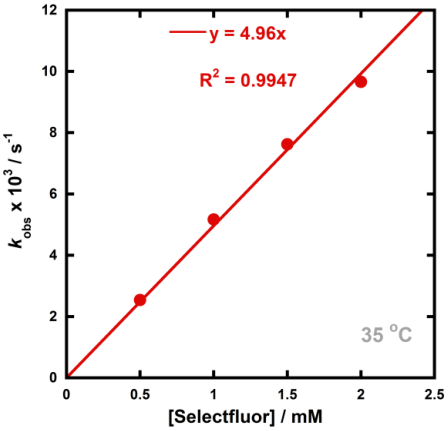

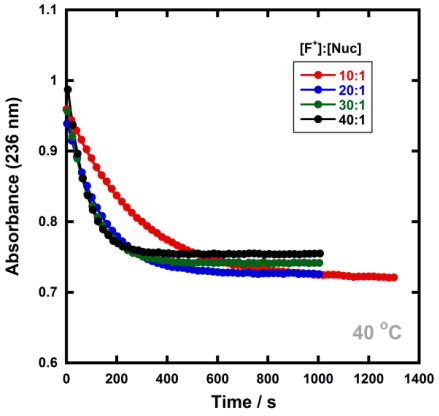

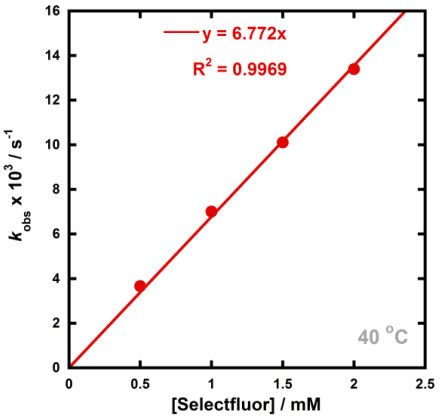

Fluorination of progesterone enol acetate **165** with Selectfluor™ in 5%, 10%, 30% water:

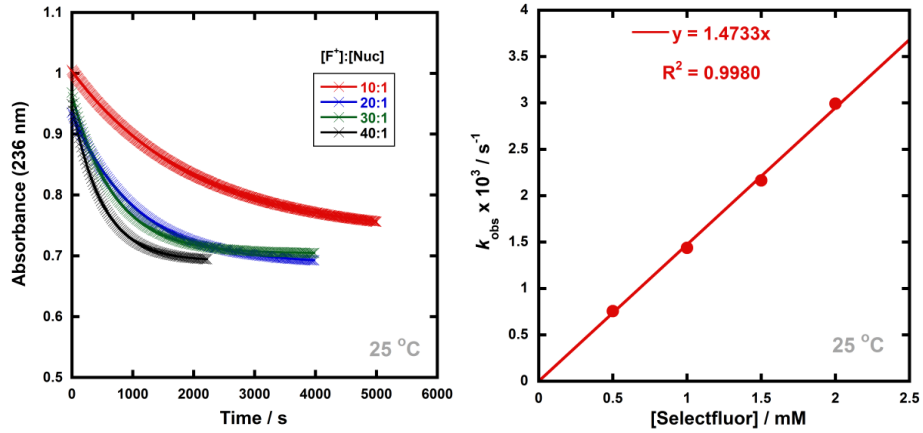

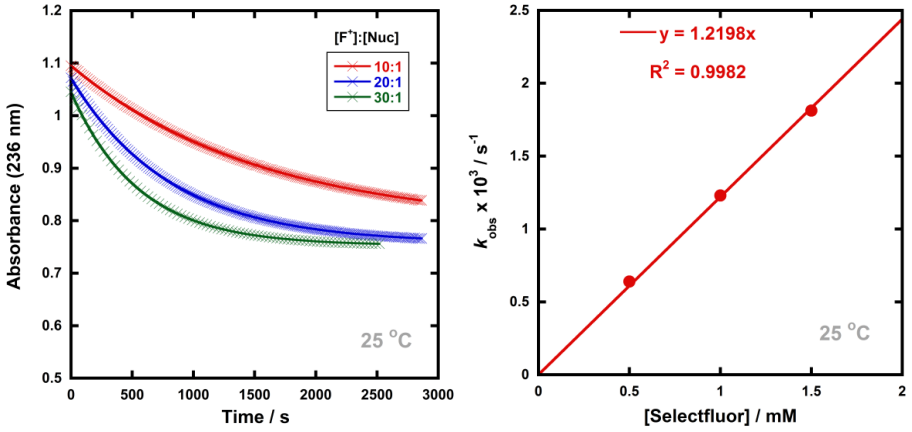

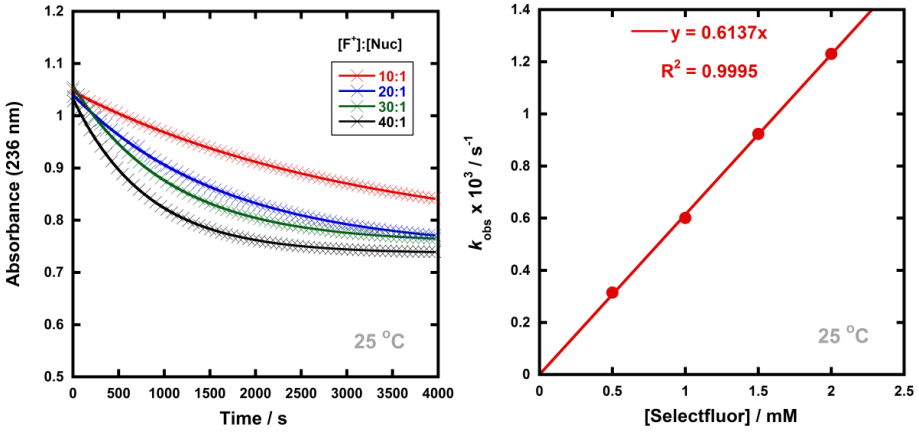

Fluorination of progesterone enol acetate **165** with Selectfluor™ in 10%, 30%, 40%, 50% methanol:

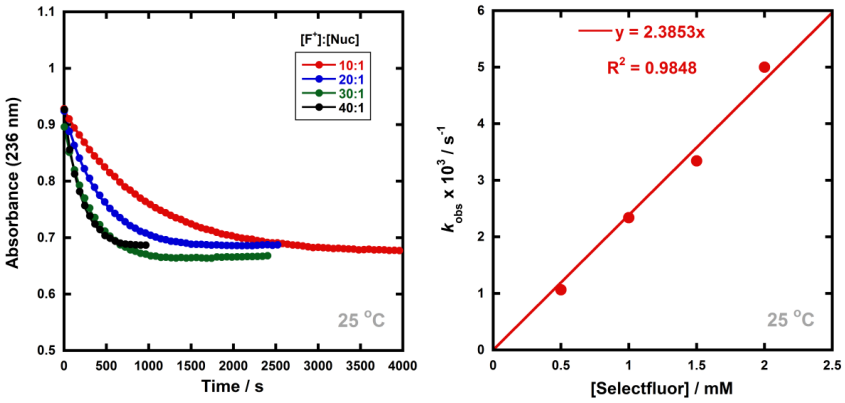

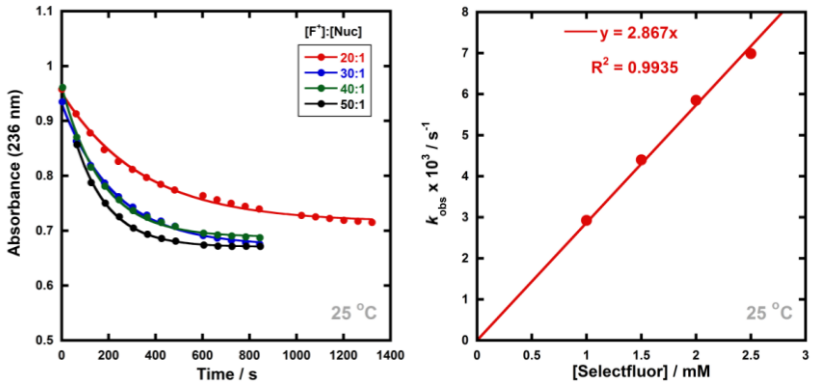

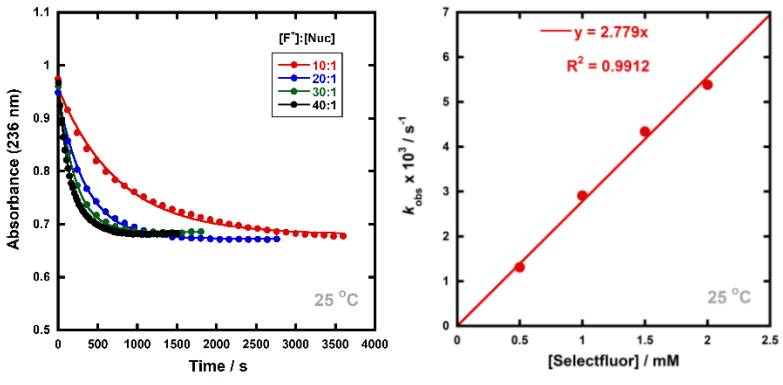

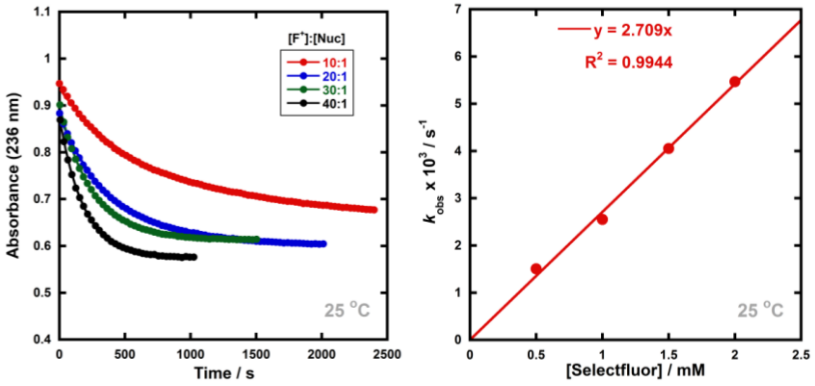

Table 49: All k_{obs} values for fluorination of steroid enol acetates **167**-**169**.

Nucleophile	**Electrophile**	**Ratio of F^+ : Nuc**	**$[F^+]$: [Nuc] / mM**	**$k_{obs} \times 10^3$ / s^{-1}**
Testosterone enol diacetate **167**	Selectfluor™	20:1	1.00 : 0.05	2.22 ± 0.01
		60:1	3.00 : 0.05	6.35 ± 0.05
		70.2:1	3.51 : 0.05	7.48 ± 0.04
		80:1	4.00 : 0.05	8.41 ± 0.06
		90.2:1	4.51 : 0.05	9.47 ± 0.05
	diCl-NFPy TfO^-	1:10	0.05 : 0.50	0.223 ± 0.001
		1:12	0.05 : 0.60	0.265 ± 0.001
		1:14	0.05 : 0.70	0.308 ± 0.001
		1:16	0.05 : 0.80	0.352 ± 0.001
	pentaCl NFPy TfO^-	1:8	0.05 : 0.40	55.73 ± 0.04
		1:10	0.05 : 0.50	71.20 ± 0.04
		1:12	0.05 : 0.60	82.90 ± 0.08
		1:14	0.05 : 0.70	98.5 ± 0.1
		1:16	0.05 : 0.80	116.3 ± 0.1
Cholestenone enol acetate **168**	Selectfluor™	20:1	1.00 : 0.05	3.154 ± 0.008
		30:1	1.50 : 0.05	4.83 ± 0.02
		40:1	2.00 : 0.05	6.04 ± 0.01
		50:1	2.50 : 0.05	8.18 ± 0.07
	pentaCl NFPy TfO^-	1:6	0.05 : 0.30	58.4 ± 0.2
		1:8	0.05 : 0.40	76.75 ± 0.07
		1:10	0.05 : 0.50	96.2 ± 0.3
		1:12	0.05 : 0.60	119.9 ± 0.3
		1:14	0.05 : 0.70	133.0 ± 0.3
Hydrocortisone enol tetraacetate **169**	Selectfluor™	10:1	0.51 : 0.05	0.559 ± 0.002
		20:1	1.00 : 0.05	1.048 ± 0.002
		30:1	1.51 : 0.05	1.533 ± 0.004
		40:1	2.00 : 0.05	2.120 ± 0.005
		50:1	2.51 : 0.05	2.688 ± 0.002
	pentaCl NFPy TfO^-	1:6.4	0.05 : 0.32	18.11 ± 0.05
		1:8.4	0.05 : 0.42	23.09 ± 0.03
		1:10.4	0.05 : 0.52	28.41 ± 0.07
		1:12.4	0.05 : 0.62	34.29 ± 0.06
		1:14.4	0.05 : 0.72	40.11 ± 0.08

Fluorination of testosterone enol diacetate **167** with Selectfluor™:

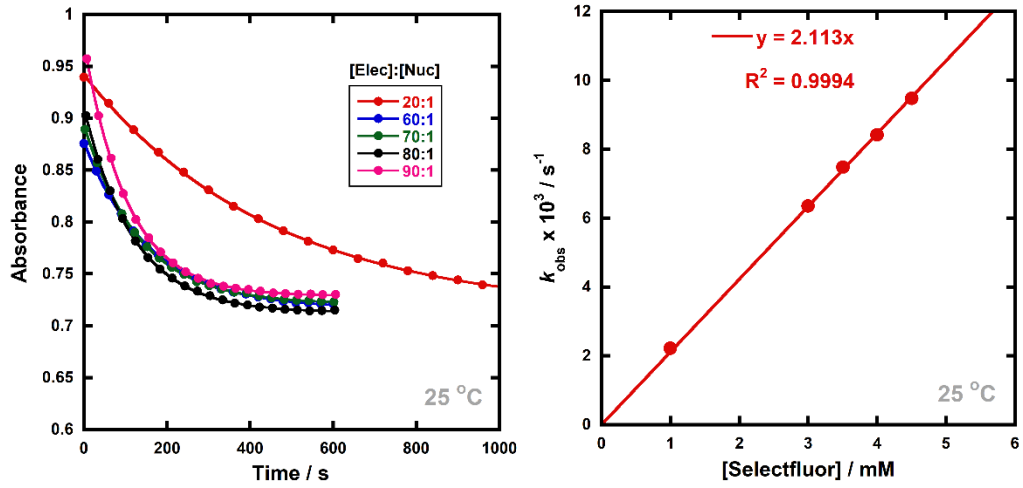

Fluorination of testosterone enol diacetate **167** with diCl-NFPy TfO⁻:

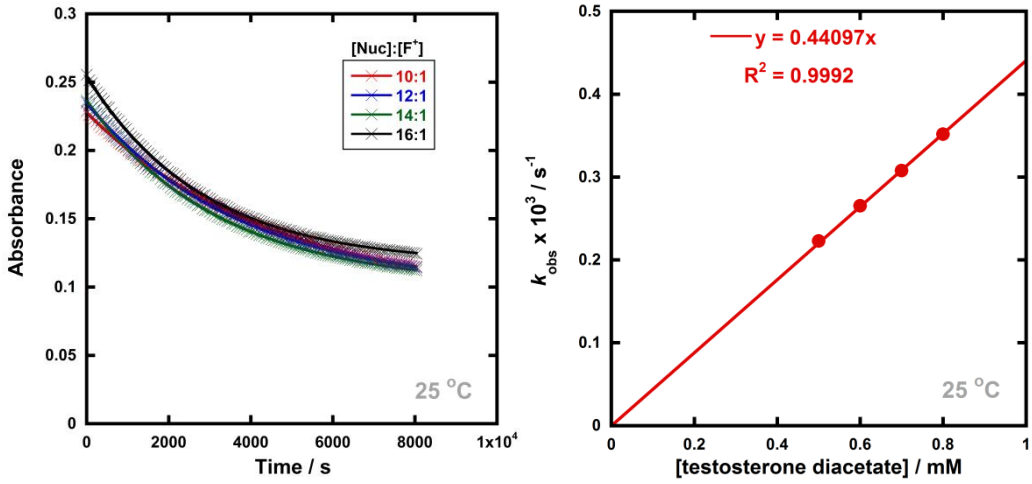

Fluorination of testosterone enol diacetate **167** with pentaCl-NFPy TfO⁻:

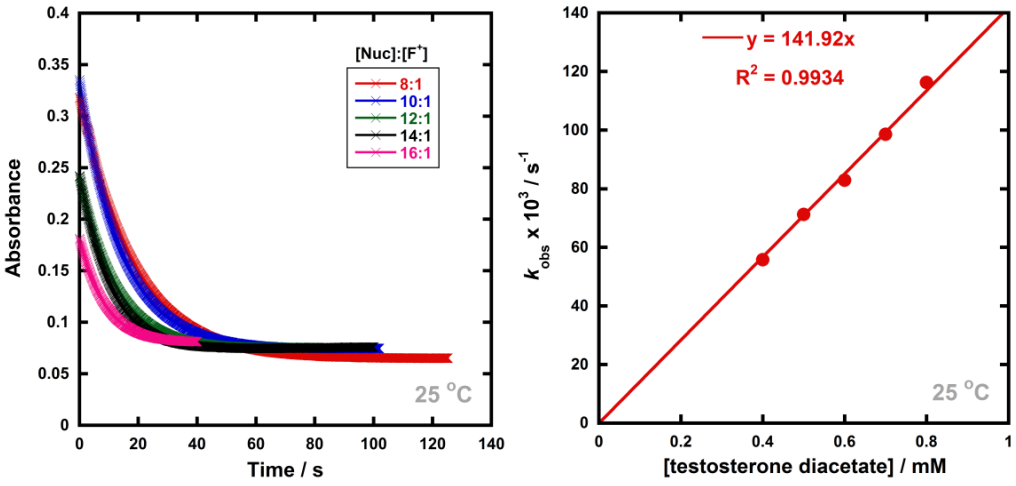

Fluorination of cholestenone enol acetate **168** with Selectfluor™:

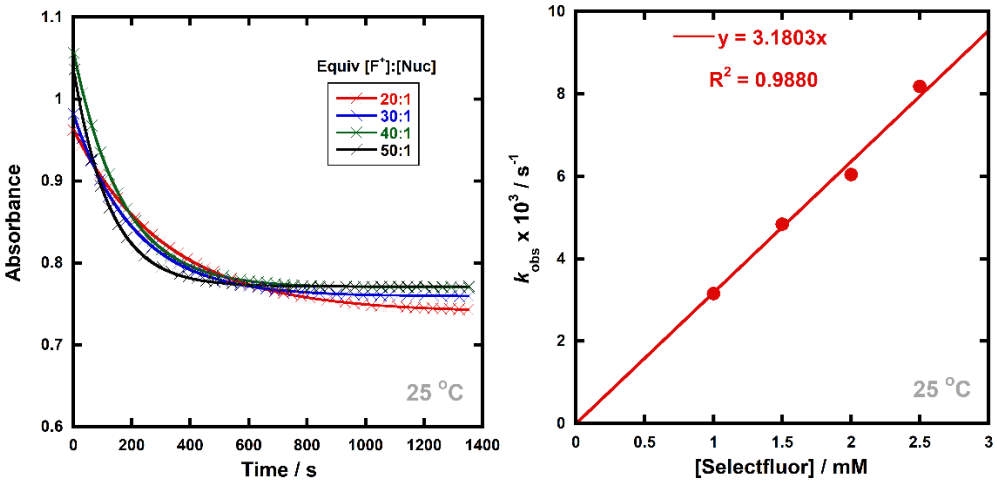

Fluorination of cholestenone enol acetate **168** with pentaCl-NFPy TfO⁻:

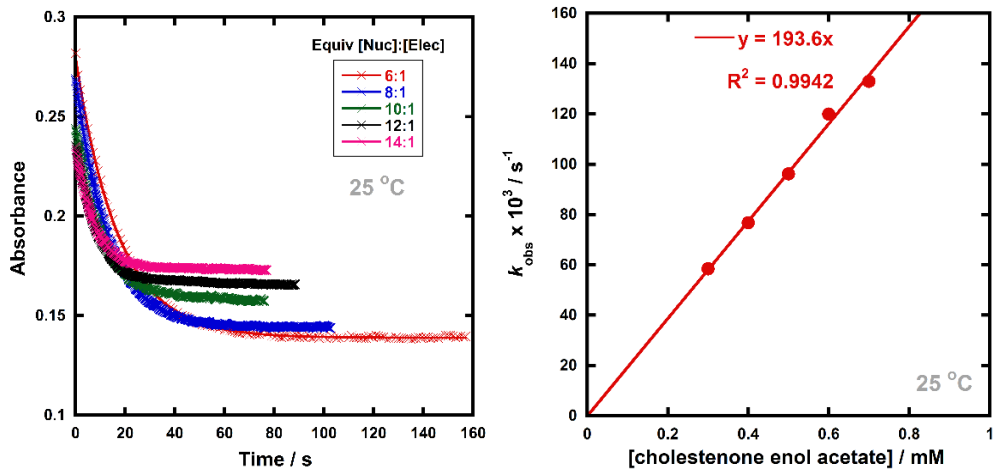

Fluorination of hydrocortisone enol tetraacetate **169** with Selectfluor™:

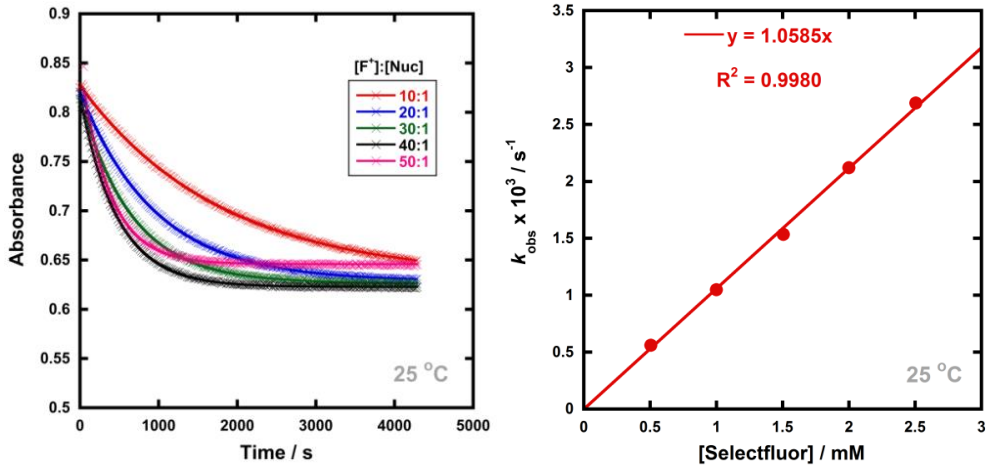

Fluorination of hydrocortisone enol tetraacetate **169** with pentaCl-NFPy TfO^-:

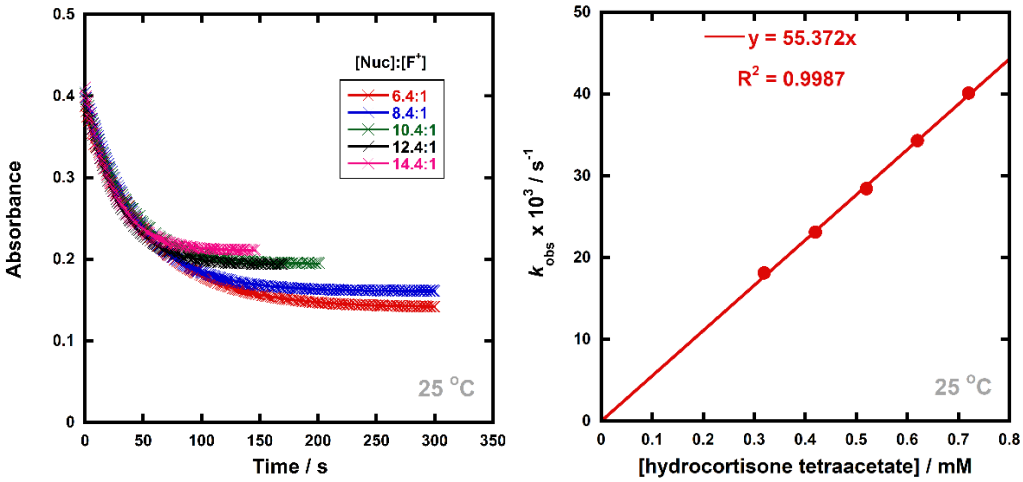

Appendices

Crystal structure data

Table 50: Crystal data and structure refinement.

	108a-keto	**108d-enol**	**108e-enol**
Empirical formula	$C_{15}H_{11}FO_2$	$C_{17}H_{15}FO_4$	$C_{15}H_9Cl_2FO_2$
Formula weight	242.24	302.29	311.12
Crystal system	monoclinic	orthorhombic	orthorhombic
Space group	I2/a	$Cmc2_1$	Pnma
a/Å	13.2572(6)	31.944(2)	6.0944(8)
b/Å	5.1221(2)	7.0229(5)	30.676(4)
c/Å	16.7741(8)	6.1827(5)	6.8810(9)
β/°	97.558(2)	90	90
Volume/$Å^3$	1129.15(9)	1387.02(18)	1286.4(3)
Z	4	4	4
$\rho_{calc}g/cm^3$	1.425	1.448	1.606
μ/mm^{-1}	0.105	0.111	0.513
F(000)	504	632.0	632.0
Reflections collected	10000	11975	20698
Independent refl., R_{int}	1359, 0.0271	1880, 0.0443	1750, 0.0444
Data/restraints/parameters	1359/132/158	1880/1/131	1750/0/113
Goodness-of-fit on F^2	1.113	1.042	1.213
Final R_1 indexes [I≥2σ(I)]	0.0342	0.0370	0.0436
Final wR_2 indexes [all data]	0.0884	0.0994	0.0971
Largest diff. peak/hole / e $Å^{-3}$	0.20/-0.22	0.37/-0.38	0.33/-0.30
Flack parameter	n/a	0.1(3)	n/a

Table 51: Crystal data and structure refinement.

	108b-keto	**108b-enol**	**108c-keto**	**108c-enol**
Empirical formula	$C_{15}H_9F_3O_2$	$C_{15}H_9F_3O_2$	$C_{17}H_{15}FO_2$	$C_{17}H_{15}FO_2$
Formula weight	278.22	278.22	270.29	270.29
Crystal system	monoclinic	monoclinic	monoclinic	monoclinic
Space group	$P2_1$	C2/c	$P2_1/c$	C2/c
a/Å	4.3647(4)	28.403(2)	8.5592(5)	11.1604(8)
b/Å	11.5018(10)	6.1029(4)	12.9739(8)	11.7655(8)
c/Å	12.3118(11)	6.9953(5)	12.3376(8)	10.8190(8)
β/°	94.065(3)	102.753(3)	102.4067(17)	114.3180(17)
Volume/Å^3	616.52(10)	1182.67(14)	1338.05(14)	1294.57(16)
Z	2	4	4	4
ρ_{calc}g/cm^3	1.499	1.563	1.342	1.387
μ/mm^{-1}	0.129	0.134	0.096	0.099
F(000)	284.0	568.0	568.0	568.0
Reflections collected	13411	12032	22309	7788
Independent refl., R_{int}	3582 0.0339	1724, 0.0345	3569, 0.0452	1646, 0.0298
Data/restraints/parameters	3582/1/217	1724/0/112	3569/0/241	1646/0/94
Goodness-of-fit on F^2	1.044	1.054	1.086	1.105
Final R_1 indexes [I≥2σ(I)]	0.0415	0.0415	0.0580	0.0721
Final wR_2 indexes [all data]	0.0981	0.1230	0.1749	0.2243
Largest diff. peak/hole / e Å^{-3}	0.22/-0.21	0.48/-0.26	0.51/-0.20	0.88/-0.54
Flack parameter	n/a	n/a	n/a	n/a

Table 52: Crystal data and structure refinement.

	Progesterone enol acetate **165**
Empirical formula	$C_{23}H_{32}O_3$
Formula weight	356.48
Temperature/K	120.0
Crystal system	monoclinic
Space group	$P2_1$
a/Å	9.3411(7)
b/Å	7.5666(5)
c/Å	13.7556(10)
α/°	90
β/°	94.038(3)
γ/°	90
Volume/Å^3	969.84(12)
Z	2
ρ_{calc}g/cm^3	1.221
μ/mm^{-1}	0.619
F(000)	388.0
Crystal size/mm^3	0.23 × 0.19 × 0.07
Radiation	CuKα (λ = 1.54178)
2Θ range for data collection/°	6.442 to 146.948
Index ranges	$-10 \leq h \leq 9$, $-9 \leq k \leq 8$, $-16 \leq l \leq 16$
Reflections collected	12155
Independent reflections	3651 [R_{int} = 0.0288, R_{sigma} = 0.0251]
Data/restraints/parameters	3651/1/363
Goodness-of-fit on F^2	1.030
Final R indexes [I>=2σ (I)]	R_1 = 0.0287, wR_2 = 0.0782
Final R indexes [all data]	R_1 = 0.0295, wR_2 = 0.0791
Largest diff. peak/hole / e Å^{-3}	0.23/-0.15
Flack parameter	-0.09(8)

Confirmation of purities of compounds 108a and 108c-e by LC-MS

All kinetic studies of keto-enol relaxation and fluorination processes were performed by monitoring the appearance or disappearance of keto and enol species by UV-vis spectrophotometry. Given that compounds **108a**, **108c-e** were prepared from **107a**, **107c-e**, we were concerned that small amounts of residual **107a**, **107c-e** in the preparations of **108a**, **108c-e** could interfere with kinetics studies. In order to confirm the spectrophotometric purities of **108a-d**, NMR analyses were supplemented by LC-MS with diode array detection. The chromatograms were viewed at or near the λ_{max} values of the enol forms of **107a**, **107c-e** and **108a**, **108c-e**. All chromatograms show only the keto and enol forms of the mono-fluorinated systems **108a**, **108c-e** and no evidence of un-fluorinated systems **107a**, **107c-e**.

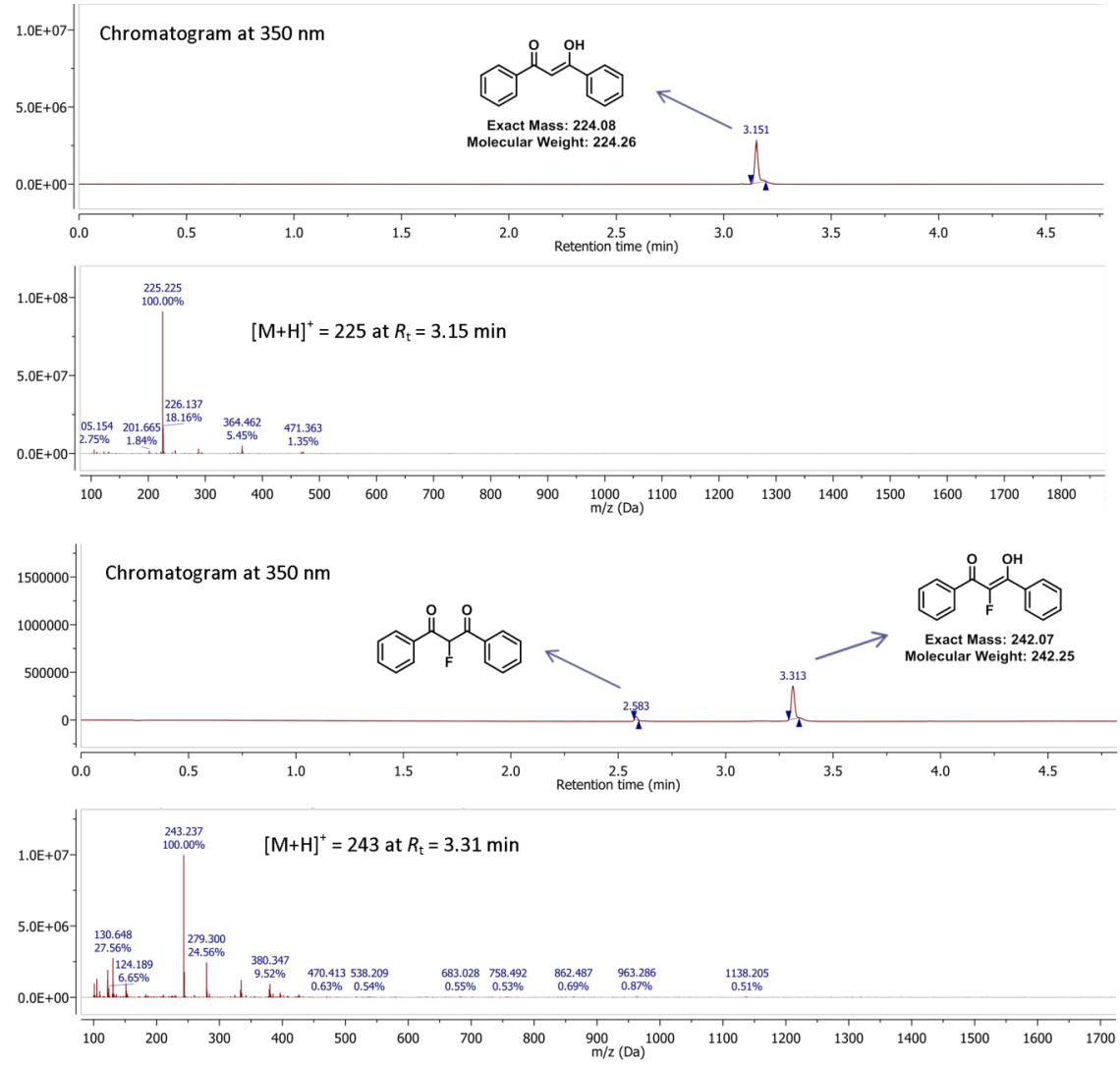

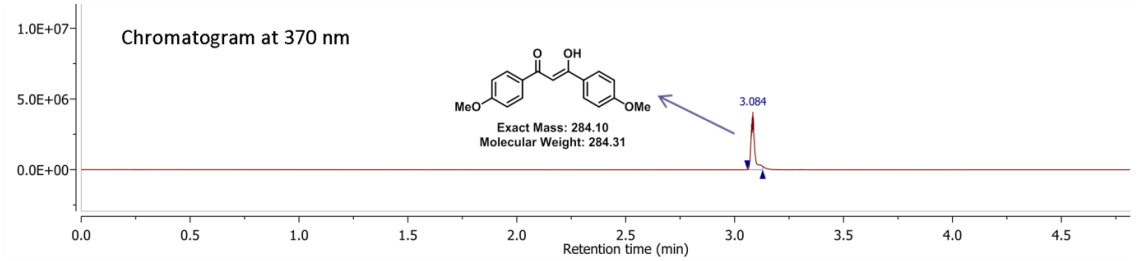
Chromatogram at 370 nm
O
OH
MeO
OMe
Exact Mass: 284.10
Molecular Weight: 284.31
3.084
1.0E+07
5.0E+06
0.0E+00
0.0
0.5
1.0
1.5
2.0
2.5
3.0
3.5
4.0
4.5
Retention time (min)

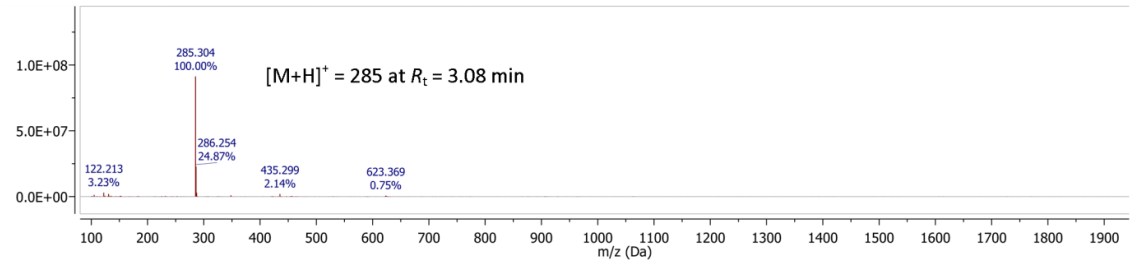
285.304
100.00%
[M+H]+ = 285 at Rt = 3.08 min
286.254
24.87%
122.213
3.23%
435.299
2.14%
623.369
0.75%
1.0E+08
5.0E+07
0.0E+00
100
200
300
400
500
600
700
800
900
1000
1100
1200
1300
1400
1500
1600
1700
1800
1900
m/z (Da)

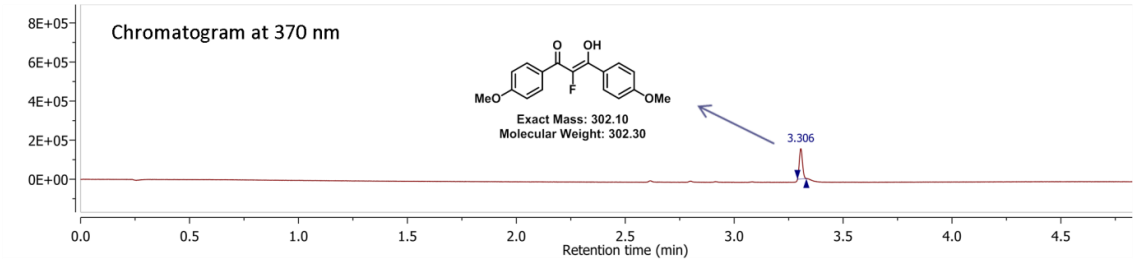
Chromatogram at 370 nm
O
OH
F
MeO
OMe
Exact Mass: 302.10
Molecular Weight: 302.30
3.306
8E+05
6E+05
4E+05
2E+05
0E+00
0.0
0.5
1.0
1.5
2.0
2.5
3.0
3.5
4.0
4.5
Retention time (min)

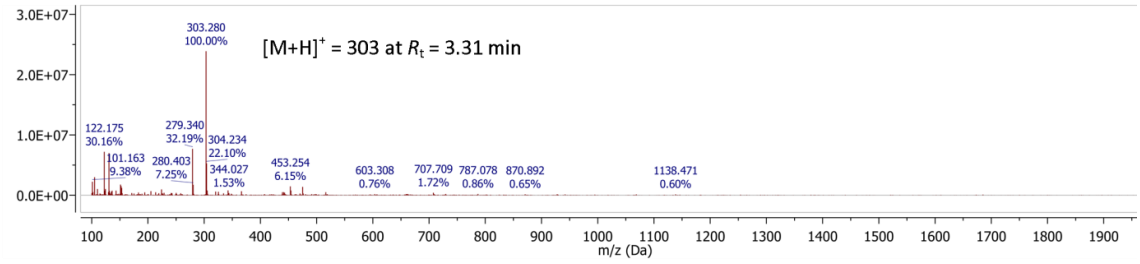
303.280
100.00%
[M+H]+ = 303 at Rt = 3.31 min
122.175
30.16%
279.340
32.19%
304.234
22.10%
101.163
9.38%
280.403
7.25%
344.027
1.53%
453.254
6.15%
603.308
0.76%
707.709
1.72%
787.078
0.86%
870.892
0.65%
1138.471
0.60%
3.0E+07
2.0E+07
1.0E+07
0.0E+00
100
200
300
400
500
600
700
800
900
1000
1100
1200
1300
1400
1500
1600
1700
1800
1900
m/z (Da)

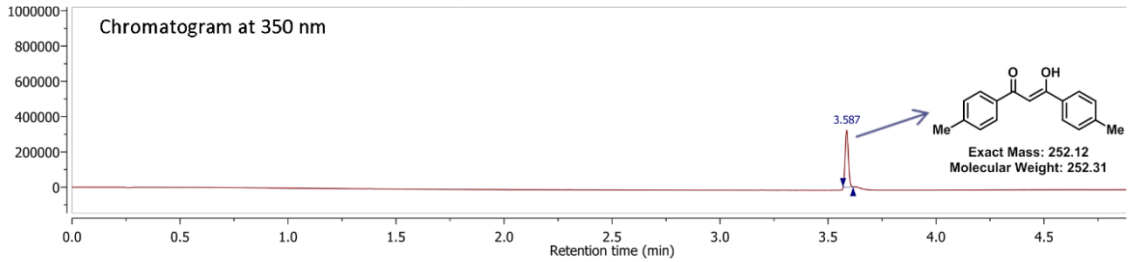
Chromatogram at 350 nm
3.587
O
OH
Me
Me
Exact Mass: 252.12
Molecular Weight: 252.31
Retention time (min)

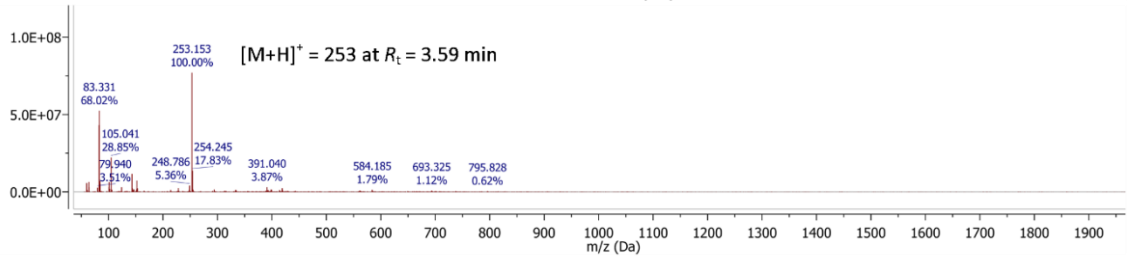
[M+H]+ = 253 at Rt = 3.59 min
253.153 100.00%
83.331 68.02%
105.041 28.85%
254.245 17.83%
248.786 5.36%
391.040 3.87%
584.185 1.79%
693.325 1.12%
795.828 0.62%
m/z (Da)

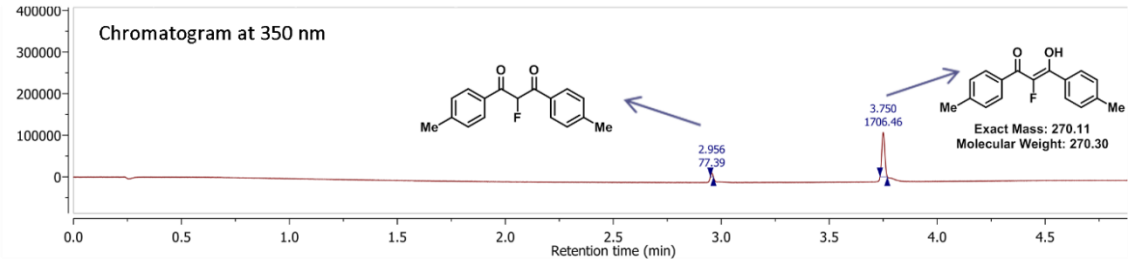
Chromatogram at 350 nm
O
O
F
Me
Me
2.956
77.39
3.750
1706.46
O
OH
Me
F
Me
Exact Mass: 270.11
Molecular Weight: 270.30
Retention time (min)

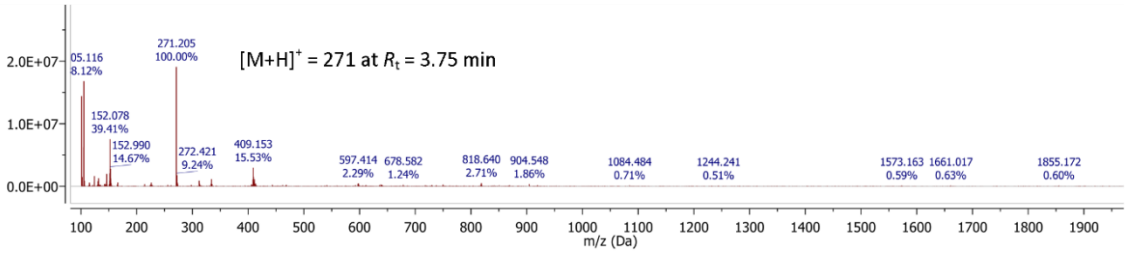
[M+H]+ = 271 at Rt = 3.75 min
271.205 100.00%
05.116 8.12%
152.078 39.41%
152.990 14.67%
272.421 9.24%
409.153 15.53%
597.414 2.29%
678.582 1.24%
818.640 2.71%
904.548 1.86%
1084.484 0.71%
1244.241 0.51%
1573.163 0.59%
1661.017 0.63%
1855.172 0.60%
m/z (Da)

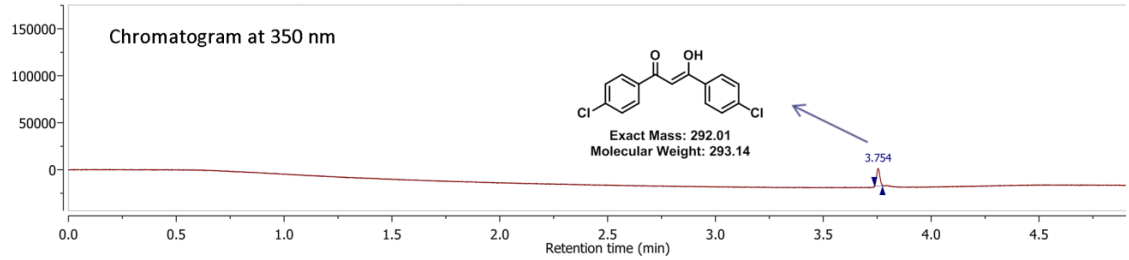
Chromatogram at 350 nm
Exact Mass: 292.01
Molecular Weight: 293.14
3.754
Retention time (min)

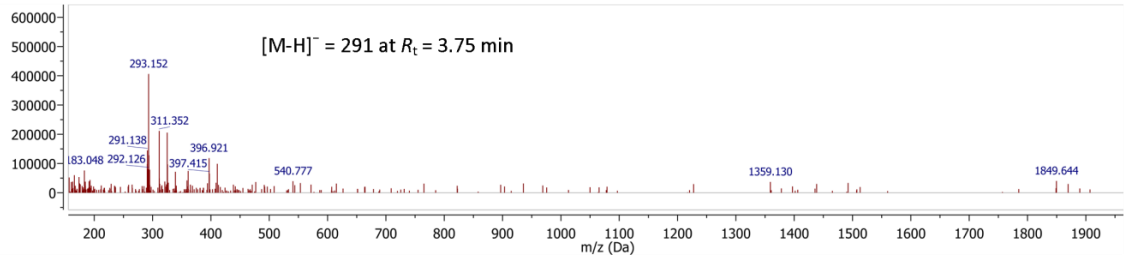
[M-H]⁻ = 291 at R_t = 3.75 min
293.152
311.352
291.138
396.921
183.048
292.126
397.415
540.777
1359.130
1849.644
m/z (Da)

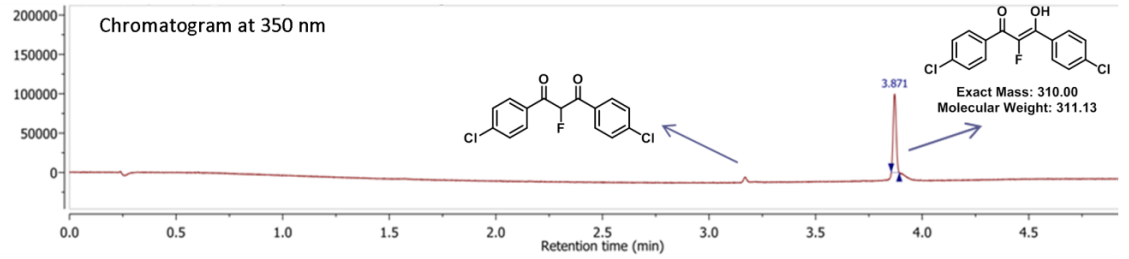
Chromatogram at 350 nm
Exact Mass: 310.00
Molecular Weight: 311.13
3.871
Retention time (min)

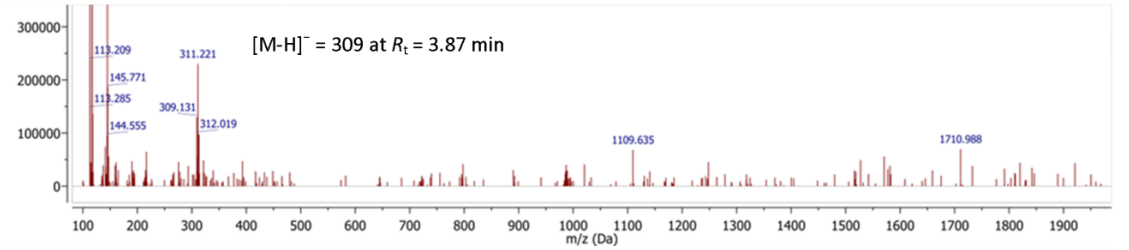
[M-H]⁻ = 309 at R_t = 3.87 min
113.209
311.221
145.771
113.285
309.131
144.555
312.019
1109.635
1710.988
m/z (Da)

References

1 K. Muller, C. Faeh and F. Diederich, *Science*, 2007, **317**, 1881–1886.
2 D. O'Hagan, *Chem. Soc. Rev.*, 2008, **37**, 308–319.
3 S. Purser, P. R. Moore, S. Swallow and V. Gouverneur, *Chem. Soc. Rev.*, 2008, **37**, 320–330.
4 T. Liang, C. N. Neumann and T. Ritter, *Angew. Chem. Int. Ed.*, 2013, **52**, 8214–8264.
5 D. O'Hagan, *J. Fluor. Chem.*, 2010, **131**, 1071–1081.
6 E. A. Ilardi, E. Vitaku and J. T. Njardarson, *J. Med. Chem.*, 2014, **57**, 2832–2842.
7 B. G. de la Torre and F. Albericio, *Molecules*, 2019, **24**, 809.
8 H. Mei, J. Han, S. Fustero, M. Medio-Simon, D. M. Sedgwick, C. Santi, R. Ruzziconi and V. A. Soloshonok, *Chem. – Eur. J.*, 2019, **25**, 11797–11819.
9 R. E. Banks, D. W. A. Sharp and J. C. Tatlow, *Fluorine the First Hundred Years (1886-1986)*, Elsevier Sequoia: New York, 1986.
10 R. E. Banks, *J. Fluor. Chem.*, 1986, **33**, 3–26.
11 L. Pauling, *The Nature of the Chemical Bond and the Structure of Molecules and Crystals: An Introduction to Modern Structural Chemistry*, Cornell University Press, 1939.
12 B. K. Park, N. R. Kitteringham and P. M. O'Neill, *Annu. Rev. Pharmacol. Toxicol.*, 2001, **41**, 443–470.
13 N. A. Meanwell, *J. Med. Chem.*, 2018, **61**, 5822–5880.
14 A. Harsanyi and G. Sandford, *Green Chem.*, 2015, **17**, 2081–2086.
15 D. O'Hagan and H. Deng, *Chem. Rev.*, 2015, **115**, 634–649.
16 J. C. S. Marais, *Onderstepoort J. Vet. Sci. Anim. Ind.*, 1944, **20**, 67.
17 C. D. Murphy, D. O'Hagan and C. Schaffrath, *Angew. Chem. Int. Ed.*, 2001, **40**, 4479.
18 S. J. Moss, C. D. Murphy, D. O'Hagan, C. Schaffrath, J. T. G. Hamilton, W. C. McRoberts and D. B. Harper, *Chem. Commun.*, 2000, 2281–2282.
19 D. O'Hagan, C. Schaffrath, S. L. Cobb, J. T. G. Hamilton and C. D. Murphy, *Nature*, 2002, **416**, 279–279.
20 J. Fried and E. F. Sabo, *J. Am. Chem. Soc.*, 1954, **76**, 1455–1456.
21 C. Isanbor and D. O'Hagan, *J. Fluor. Chem.*, 2006, **127**, 303–319.
22 "The Top 300 of 2019", ClinCalc DrugStats Database, https://clincalc.com/DrugStats/Top300Drugs.aspx, (accessed July 2019).
23 S. Haaf and H. Henrici, *Ullmann's Encyclopedia of Industrial Chemistry, "Refrigeration Technology,"* Wiley-VCH, New York, 2002.
24 B. Ameduri and B. Boutevin, *Well-Architectured Fluoropolymers: Synthesis, Properties and Applications*, Elsevier, Amsterdam, 2004.
25 Fluorite image from: https://en.wikipedia.org/wiki/Fluorite#/media/File:Fluorite-233168.jpg (Accessed August 2019).
26 K. B. Kellogg and G. H. Cady, *J. Am. Chem. Soc.*, 1948, **70**, 3986–3990.
27 M. Schlosser and G. Heinz, *Chem. Ber.*, 1969, **102**, 1944–1953.
28 S. Rozen and O. Lerman, *J. Org. Chem.*, 1980, **45**, 672–678.
29 S. Rozen, O. Lerman, M. Kol and D. Hebel, *J. Org. Chem.*, 1985, **50**, 4753–4758.
30 E. H. Appelman, L. J. Basile and R. C. Thompson, *J. Am. Chem. Soc.*, 1979, **101**, 3384–3385.
31 C. L. Chernick, H. H. Claassen, P. R. Fields, H. H. Hyman, J. G. Malm, W. M. Manning, M. S. Matheson, L. A. Quarterman, F. Schreiner, H. H. Selig, I. Sheft, S.

Siegel, E. N. Sloth, L. Stein, M. H. Studier, J. L. Weeks and M. H. Zirin, *Science*, 1962, **138**, 136–138.
32 M. J. Shaw, H. H. Hyman and R. Filler, *J. Am. Chem. Soc.*, 1969, **91**, 1563–1565.
33 G. S. Lal, G. P. Pez and R. G. Syvret, *Chem. Rev.*, 1996, **96**, 1737–1756.
34 T. Umemoto, K. Kawada and K. Tomita, *Tetrahedron Lett.*, 1986, **27**, 4465–4468.
35 T. Umemoto, K. Harasawa, G. Tomizawa, K. Kawada and K. Tomita, *Bull. Chem. Soc. Jpn.*, 1991, **64**, 1081–1092.
36 A. S. Kiselyov, *Chem. Soc. Rev.*, 2005, **34**, 1031.
37 E. Differding and H. Ofner, *Synlett*, 1991, **1991**, 187–189.
38 R. E. Banks, S. N. Mohialdin-Khaffaf, G. S. Lal, I. Sharif and R. G. Syvret, *J. Chem. Soc. Chem. Commun.*, 1992, 595–596.
39 S. Stavber, M. Zupan, A. J. Poss and G. A. Shia, *Tetrahedron Lett.*, 1995, **36**, 6769–6772.
40 H. Yasui, T. Yamamoto, T. Ishimaru, T. Fukuzumi, E. Tokunaga, K. Akikazu, M. Shiro and N. Shibata, *J. Fluor. Chem.*, 2011, **132**, 222–225.
41 C.-L. Zhu, M. Maeno, F.-G. Zhang, T. Shigehiro, T. Kagawa, K. Kawada, N. Shibata, J.-A. Ma and D. Cahard, *Eur. J. Org. Chem.*, 2013, **2013**, 6501–6505.
42 J. R. Wolstenhulme, J. Rosenqvist, O. Lozano, J. Ilupeju, N. Wurz, K. M. Engle, G. W. Pidgeon, P. R. Moore, G. Sandford and V. Gouverneur, *Angew. Chem. Int. Ed.*, 2013, **52**, 9796–9800.
43 R. Pereira, J. Wolstenhulme, G. Sandford, T. D. W. Claridge, V. Gouverneur and J. Cvengroš, *Chem. Commun.*, 2016, **52**, 1606–1609.
44 R. E. Banks and G. E. Williamson, *Chem. Ind.*, 1964, 1864–1865.
45 S. T. Purrington and W. A. Jones, *J. Org. Chem.*, 1983, **48**, 761–762.
46 W. E. Barnette, *J. Am. Chem. Soc.*, 1984, **106**, 452–454.
47 R. E. Banks, R. A. Du Boisson and E. Tsiliopoulos, *J. Fluor. Chem.*, 1986, **32**, 461–466.
48 R. E. Banks and I. Sharif, *J. Fluor. Chem.*, 1991, **55**, 207–214.
49 D. D. DesMarteau, U.S. Patent 4,697,011, 1987.
50 E. Differding and R. W. Lang, *Tetrahedron Lett.*, 1988, **29**, 6087–6090.
51 E. Differding and R. W. Lang, *Helv. Chim. Acta*, 1989, **72**, 1248–1252.
52 F. A. Davis and W. Han, *Tetrahedron Lett.*, 1991, **32**, 1631–1634.
53 R. Bohlmann, DE 4313664, 1994.
54 I. Cabrera and W. K. Appel, *Tetrahedron*, 1995, **51**, 10205–10208.
55 T. Umemoto, M. Nagayoshi, K. Adachi and G. Tomizawa, *J. Org. Chem.*, 1998, **63**, 3379–3385.
56 K. K. Laali, M. Tanaka, F. Forohar, M. Cheng and J. C. Fetzer, *J. Fluor. Chem.*, 1998, **91**, 185–190.
57 Y. Takeuchi, T. Suzuki, A. Satoh, T. Shiragami and N. Shibata, *J. Org. Chem.*, 1999, **64**, 5708–5711.
58 Z. Liu, N. Shibata and Y. Takeuchi, *J. Org. Chem.*, 2000, **65**, 7583–7587.
59 N. Shibata, E. Suzuki and Y. Takeuchi, *J. Am. Chem. Soc.*, 2000, **122**, 10728–10729.
60 D. Cahard, C. Audouard, J.-C. Plaquevent and N. Roques, *Org. Lett.*, 2000, **2**, 3699–3701.
61 H. P. Shunatona, N. Früh, Y.-M. Wang, V. Rauniyar and F. D. Toste, *Angew. Chem. Int. Ed.*, 2013, **52**, 7724–7727.
62 D. D. DesMarteau, Z. Q. Xu and M. Witz, *J. Org. Chem.*, 1992, **57**, 629–635.
63 E. Differding and G. M. Rüegg, *Tetrahedron Lett.*, 1991, **32**, 3815–3818.

64 P. T. Nyffeler, S. G. Durón, M. D. Burkart, S. P. Vincent and C.-H. Wong, *Angew. Chem. Int. Ed.*, 2005, **44**, 192–212.
65 R. E. Banks, U.S. Patent 5,086,178, 1992.
34 R. E. Banks, N. J. Lawrence and A. L. Popplewell, *J. Chem. Soc. Chem. Commun.*, 1994, 343–344.
67 R. E. Banks, M. K. Besheesh, S. N. Mohialdin-Khaffaf and I. Sharif, *J. Chem. Soc. Perkin 1*, 1996, 2069.
68 J. J. Hart and R. G. Syvret, *J. Fluor. Chem.*, 1999, **100**, 157–161.
69 Manchester REF Impact Case Study: "The Development of Selectfluor as a Commercial Electrophilic Fluorinating Agent", https://impact.ref.ac.uk/casestudies/CaseStudy.aspx?Id=28087 (accessed June 2019).
70 Y. Zhu, J. Han, J. Wang, N. Shibata, M. Sodeoka, V. A. Soloshonok, J. A. S. Coelho and F. D. Toste, *Chem. Rev.*, 2018, **118**, 3887–3964.
71 J. O. Link, J. G. Taylor, L. Xu, M. Mitchell, H. Guo, H. Liu, D. Kato, T. Kirschberg, J. Sun, N. Squires, J. Parrish, T. Keller, Z.-Y. Yang, C. Yang, M. Matles, Y. Wang, K. Wang, G. Cheng, Y. Tian, E. Mogalian, E. Mondou, M. Cornpropst, J. Perry and M. C. Desai, *J. Med. Chem.*, 2014, **57**, 2033–2046.
72 Y. Zhou, J. Wang, Z. Gu, S. Wang, W. Zhu, J. L. Aceña, V. A. Soloshonok, K. Izawa and H. Liu, *Chem. Rev.*, 2016, **116**, 422–518.
73 A. L'Heureux, F. Beaulieu, C. Bennett, D. R. Bill, S. Clayton, F. LaFlamme, M. Mirmehrabi, S. Tadayon, D. Tovell and M. Couturier, *J. Org. Chem.*, 2010, **75**, 3401–3411.
74 N. R. Curtis, S. H. Davies, M. Gray, S. G. Leach, R. A. McKie, L. E. Vernon and A. J. Walkington, *Org. Process Res. Dev.*, 2015, **19**, 865–871.
75 H. Meinert, *Z. Für Chem.*, 1965, **5**, 64.
76 M. Bedin, A. Karim, M. Reitti, A.-C. C. Carlsson, F. Topić, M. Cetina, F. Pan, V. Havel, F. Al-Ameri, V. Sindelar, K. Rissanen, J. Gräfenstein and M. Erdélyi, *Chem. Sci.*, 2015, **6**, 3746–3756.
77 T. Umemoto, *J. Fluor. Chem.*, 2014, **167**, 3–15.
78 T. Umemoto and G. Tomizawa, *J. Org. Chem.*, 1995, **60**, 6563–6570.
79 K. L. Hull, W. Q. Anani and M. S. Sanford, *J. Am. Chem. Soc.*, 2006, **128**, 7134–7135.
80 N. Shibata, T. Tarui, Y. Doi and K. L. Kirk, *Angew. Chem. Int. Ed.*, 2001, **40**, 4461.
81 D. P. Ip, C. D. Arthur, R. E. Winans and E. H. Appelman, *J. Am. Chem. Soc.*, 1981, **103**, 1964–1968.
82 J. B. Levy and D. M. Sterling, *J. Org. Chem.*, 1985, **50**, 5615–5619.
83 M. Zupan, M. Metelko and S. Stavber, *J. Chem. Soc. Perkin 1*, 1993, 2851.
84 A. G. Gilicinski, G. P. Pez, R. G. Syvret and G. S. Lal, *J. Fluor. Chem.*, 1992, **59**, 157–162.
85 E. W. Oliver and D. H. Evans, *J. Electroanal. Chem.*, 1999, **474**, 1–8.
86 Y. Zhang, X.-J. Yang, T. Xie, G.-L. Chen, W.-H. Zhu, X.-Q. Zhang, X.-Y. Yang, X.-Y. Wu, X.-P. He and H.-M. He, *Tetrahedron*, 2013, **69**, 4933–4937.
87 T. Umemoto, S. Fukami, G. Tomizawa, K. Harasawa, K. Kawada and K. Tomita, *J. Am. Chem. Soc.*, 1990, **112**, 8563–8575.
88 T. Umemoto, K. Harasawa, G. Tomizawa, K. Kawada and K. Tomita, *J. Fluor. Chem.*, 1991, **53**, 369–377.
89 P. Toullec, I. Devillers, R. Frantz and A. Togni, *Helv. Chim. Acta*, 2004, **87**, 2706–2711.

90 S. Piana, I. Devillers, A. Togni and U. Rothlisberger, *Angew. Chem. Int. Ed.*, 2002, **41**, 979–982.
91 S. Stavber, M. Jereb and M. Zupan, *J. Phys. Org. Chem.*, 2002, **15**, 56–61.
92 S. Stavber, T. S. Pečan and M. Zupan, *Tetrahedron*, 2000, **56**, 1929–1936.
93 K. O. Christe and D. A. Dixon, *J. Am. Chem. Soc.*, 1992, **114**, 2978–2985.
94 K. Sudlow and A. A. Woolf, *J. Fluor. Chem.*, 1994, **66**, 9–11.
95 X.-S. Xue, Y. Wang, M. Li and J.-P. Cheng, *J. Org. Chem.*, 2016, **81**, 4280–4289.
96 A. Harsanyi and G. Sandford, *Org. Process Res. Dev.*, 2014, **18**, 981–992.
97 M. Butters, J. Ebbs, S. P. Green, J. MacRae, M. C. Morland, C. W. Murtiashaw and A. J. Pettman, *Org. Process Res. Dev.*, 2001, **5**, 28–36.
98 T. A. Miller et al., WO2007/087129, 2007.
99 P. Kirsch, A. Hahn, R. Fröhlich and G. Haufe, *Eur. J. Org. Chem.*, 2006, **2006**, 4819–4824.
100 D. S. Reddy, N. Shibata, J. Nagai, S. Nakamura, T. Toru and S. Kanemasa, *Angew. Chem. Int. Ed.*, 2008, **47**, 164–168.
101 B. L. Shapiro and M. M. Chrysam, *J. Org. Chem.*, 1973, **38**, 880–893.
102 W. J. Middleton and E. M. Bingham, *J. Am. Chem. Soc.*, 1980, **102**, 4845–4846.
103 B. Zajc and M. Zupan, *J. Chem. Soc. Chem. Commun.*, 1980, 759.
104 B. Zajc and M. Zupan, *J. Org. Chem.*, 1982, **47**, 573–575.
105 Z.-Q. Xu, D. D. DesMarteau and Y. Gotoh, *J. Chem. Soc. Chem. Commun.*, 1991, 179.
106 O. D. Gupta and J. M. Shreeve, *Tetrahedron Lett.*, 2003, **44**, 2799–2801.
107 R. D. Chambers, M. P. Greenhall and J. Hutchinson, *J. Chem. Soc. Chem. Commun.*, 1995, 21.
108 R. D. Chambers, M. P. Greenhall and J. Hutchinson, *Tetrahedron*, 1996, **52**, 1–8.
109 R. D. Chambers and J. Hutchinson, *J. Fluor. Chem.*, 1998, **92**, 45–52.
110 R. D. Chambers, D. Holling, R. C. H. Spink and G. Sandford, *Lab. Chip*, 2001, **1**, 132.
111 R. D. Chambers, M. A. Fox and G. Sandford, *Lab. Chip*, 2005, **5**, 1132.
112 C. B. McPake and G. Sandford, *Org. Process Res. Dev.*, 2012, **16**, 844–851.
113 J.-C. Xiao and J. M. Shreeve, *J. Fluor. Chem.*, 2005, **126**, 473–476.
114 L. Hintermann and A. Togni, *Angew. Chem. Int. Ed.*, 2000, **39**, 4359–4362.
115 M. Althaus, C. Becker, A. Togni and A. Mezzetti, *Organometallics*, 2007, **26**, 5902–5911.
116 J. L. Howard, Y. Sagatov, L. Repusseau, C. Schotten and D. L. Browne, *Green Chem.*, 2017, **19**, 2798–2802.
117 J. L. Howard, Y. Sagatov and D. L. Browne, *Tetrahedron*, 2018, **74**, 3118–3123.
118 A. S. Reddy and K. K. Laali, *Tetrahedron Lett.*, 2015, **56**, 5495–5499.
119 G. Stavber, M. Zupan, M. Jereb and S. Stavber, *Org. Lett.*, 2004, **6**, 4973–4976.
120 G. Stavber and S. Stavber, *Adv. Synth. Catal.*, 2010, **352**, 2838–2846.
121 R. G. Britton, E. Horner-Glister, O. A. Pomenya, E. E. Smith, R. Denton, P. R. Jenkins, W. P. Steward, K. Brown, A. Gescher and S. Sale, *Eur. J. Med. Chem.*, 2012, **54**, 952–958.
122 K. Sato, G. Sandford, K. Shimizu, S. Akiyama, M. J. Lancashire, D. S. Yufit, A. Tarui, M. Omote, I. Kumadaki, S. Harusawa and A. Ando, *Tetrahedron*, 2016, **72**, 1690–1698.
123 A. S. Hampton, 1st Year Report, Durham University, 2017.
124 N.-Y. Yang, Z.-L. Li, L. Ye, B. Tan and X.-Y. Liu, *Chem. Commun.*, 2016, **52**, 9052–9055.
125 A. J. Cruz-Cabeza and C. R. Groom, *CrystEngComm*, 2011, **13**, 93–98.

126 T. G. Cooper, K. E. Hejczyk, W. Jones and G. M. Day, *J. Chem. Theory Comput.*, 2008, **4**, 1795–1805.
127 L. P. Hammett, *J. Am. Chem. Soc.*, 1937, **59**, 96–103.
128 H. C. Brown and Y. Okamoto, *J. Am. Chem. Soc.*, 1958, **80**, 4979–4987.
129 C. Hansch, A. Leo and R. W. Taft, *Chem. Rev.*, 1991, **91**, 165–195.
130 N. Rozatian, I. W. Ashworth, G. Sandford and D. R. W. Hodgson, *Chem. Sci.*, 2018, **9**, 8692–8702.
131 R. Linnell, *J. Org. Chem.*, 1960, **25**, 290–290.
132 D. S. Timofeeva, A. R. Ofial and H. Mayr, *J. Am. Chem. Soc.*, 2018, **140**, 11474–11486.
133 T. Ueno, H. Toda, M. Yasunami and M. Yoshifuji, *Bull. Chem. Soc. Jpn.*, 1996, **69**, 1645–1656.
134 R. S. Muthyala and R. S. H. Liu, *J. Fluor. Chem.*, 1998, **89**, 173–175.
135 F. Sakurai, T. Yukawa and T. Taniguchi, *Org. Lett.*, 2019, **21**, 7254–7257.
136 Z. Rappoport and S. Patai, *The Chemistry of Enols*, John Wiley and Sons Inc., 1990.
137 J. L. Burdett and M. T. Rogers, *J. Am. Chem. Soc.*, 1964, **86**, 2105–2109.
138 G. S. Hammond, W. G. Borduin and G. A. Guter, *J. Am. Chem. Soc.*, 1959, **81**, 4682–4686.
139 P. Markov, *Chem. Soc. Rev.*, 1984, **13**, 69–96.
140 J. Zabicky, *The Chemistry of the Carbonyl Group*, Interscience, London, 1970, vol. Volume 2.
141 M. T. Rogers and J. L. Burdett, *Can. J. Chem.*, 1965, **43**, 1516–1526.
142 R. A. Morton, A. Hassan and T. C. Calloway, *J. Chem. Soc.*, 1934, 883–901.
143 R. W. Hay and P. P. Williams, *J. Chem. Soc.*, 1964, 2270–2272.
144 J. C. Sloop, C. L. Bumgardner, G. Washington, W. D. Loehle, S. S. Sankar and A. B. Lewis, *J. Fluor. Chem.*, 2006, **127**, 780–786.
145 J. C. Sloop, P. D. Boyle, A. W. Fountain, W. F. Pearman and J. A. Swann, *Eur. J. Org. Chem.*, 2011, **2011**, 936–941.
146 D. E. Williams, *Acta Crystallogr.*, 1966, **21**, 340–349.
147 M. Moriyasu, A. Kato and Y. Hashimoto, *J. Chem. Soc. Perkin Trans. 2*, 1986, 515–520.
148 C. J. Coultous, PhD Thesis, Durham University, 1999.
149 H. Morita and H. Nakanishi, *Bull. Chem. Soc. Jpn.*, 1981, **54**, 378–386.
150 P. Gacoin, *J. Chem. Phys.*, 1972, **57**, 1418–1425.
151 G. Kittel, G. Koehler and N. Getoff, *J. Phys. Chem.*, 1979, **83**, 2174–2176.
152 P. Markov and E. Radeva, *J. Photochem.*, 1975, **4**, 179–183.
153 P. Markov and I. Petkov, *Tetrahedron*, 1977, **33**, 1013–1015.
154 D. Veierov, T. Bercovici, Y. Mazur and E. Fischer, *J. Org. Chem.*, 1978, **43**, 2006–2010.
155 D. Veierov, T. Bercovici, E. Fisher, Y. Mazur and A. Yogev, *J. Am. Chem. Soc.*, 1973, **95**, 8173–8175.
156 D. Veierov, T. Bercovici, E. Fischer, Y. Mazur and A. Yogev, *J. Am. Chem. Soc.*, 1977, **99**, 2723–2729.
157 A. Lapworth, *J. Chem. Soc. Trans.*, 1904, **85**, 30–42.
158 A. Lapworth and A. C. O. Hann, *J. Chem. Soc. Trans.*, 1902, **81**, 1499–1508.
159 A. Lapworth and A. C. O. Hann, *J. Chem. Soc. Trans.*, 1902, **81**, 1508–1519.
160 R. M. Claramunt, C. López, M. D. Santa María, D. Sanz and J. Elguero, *Prog. Nucl. Magn. Reson. Spectrosc.*, 2006, **49**, 169–206.
161 I. Andrae, A. Bringhen, F. Böhm, H. Gonzenbach, T. Hill, L. Mulroy and T. G. Truscott, *J. Photochem. Photobiol. B*, 1997, **37**, 147–150.

162 A. Cantrell and D. J. McGarvey, *J. Photochem. Photobiol. B*, 2001, **64**, 117–122.
163 J. F. Coetzee and G. R. Padmanabhan, *J. Am. Chem. Soc.*, 1965, **87**, 5005–5010.
164 B. G. Cox, *Acids and Bases: Solvent Effects on Acid-Base Strength*, Oxford University Press, 2013.
165 W. N. Olmstead and F. G. Bordwell, *J. Org. Chem.*, 1980, **45**, 3299–3305.
166 R. A. Y. Jones, *Physical and Mechanistic Organic Chemistry*, Cambridge University Press, 1979.
167 A. Kütt, I. Leito, I. Kaljurand, L. Sooväli, V. M. Vlasov, L. M. Yagupolskii and I. A. Koppel, *J. Org. Chem.*, 2006, **71**, 2829–2838.
168 W. R. Dolbier, *Guide to Fluorine NMR for Organic Chemists*, John Wiley and Sons Inc., Second Ed., 2016.
169 A. Kundu, S. Pathak, K. Debnath and A. Pramanik, *Tetrahedron Lett.*, 2014, **55**, 3960–3968.
170 S. Pathak, A. Kundu and A. Pramanik, *RSC Adv.*, 2014, **4**, 10180–10187.
171 D. E. Yerien, S. Barata-Vallejo and A. Postigo, *Chem. - Eur. J.*, 2017, **23**, 14676–14701.
172 N. A. Meanwell, *J. Med. Chem.*, 2011, **54**, 2529–2591.
173 Y. Zafrani, D. Yeffet, G. Sod-Moriah, A. Berliner, D. Amir, D. Marciano, E. Gershonov and S. Saphier, *J. Med. Chem.*, 2017, **60**, 797–804.
174 W. Peng and J. M. Shreeve, *J. Org. Chem.*, 2005, **70**, 5760–5763.
175 G. Pattison, *Eur. J. Org. Chem.*, 2018, **2018**, 3520–3540.
176 M. H. Gelb, J. P. Svaren and R. H. Abeles, *Biochemistry*, 1985, **24**, 1813–1817.
177 J. T. Welch and S. Eswarakrishnan, *Fluorine in Bioorganic Chemistry*, John Wiley and Sons: New York, 1991.
178 D. Schirlin, S. Baltzer, V. Van Dorsselaer, F. Weber, C. Weill, J. M. Altenburger, B. Neises, G. Flynn, J. M. Rémy and C. Tarnus, *Bioorg. Med. Chem. Lett.*, 1993, **3**, 253–258.
179 S. Giovani, M. Penzo, S. Brogi, M. Brindisi, S. Gemma, E. Novellino, L. Savini, M. J. Blackman, G. Campiani and S. Butini, *Bioorg. Med. Chem. Lett.*, 2014, **24**, 3582–3586.
180 J. Qian, W. Yi, X. Huang, J. P. Jasinski and W. Zhang, *Adv. Synth. Catal.*, 2016, **358**, 2811–2816.
181 R. McMullan and G. A. Jeffrey, *J. Chem. Phys.*, 1959, **31**, 1231–1234.
182 W. R. Dolbier, G. D. Purvis III, M. J. Seabury, G. E. Wicks and C. R. Burkholder, *Tetrahedron*, 1990, **46**, 7991–8004.
183 W. R. Dolbier, X. X. Rong and Y.-H. He, *Tetrahedron Lett.*, 1993, **34**, 5185–5188.
184 W. R. Dolbier and X. X. Rong, *Tetrahedron Lett.*, 1996, **37**, 5321–5324.
185 L. A. Kaplan and H. B. Pickard, *J. Chem. Soc. D*, 1969, **0**, 1500–1501.
186 Z. Zhang, Á. Puente, F. Wang, M. Rahm, Y. Mei, H. Mayr and G. K. S. Prakash, *Angew. Chem. Int. Ed.*, 2016, **55**, 12845–12849.
187 Y. Lin, W. Yi, W. Shen and G. Lu, *Org. Lett.*, 2016, **18**, 592–595.
188 D. J. Leng, C. M. Black and G. Pattison, *Org. Biomol. Chem.*, 2016, **14**, 1531–1535.
189 Z. Zhang, J. Bi, Q. Liu and G. Zhang, *J. Fluor. Chem.*, 2013, **151**, 45–49.
190 L. Tang, Z. Yang, J. Jiao, Y. Cui, G. Zou, Q. Zhou, Y. Zhou, W. Rao and X. Ma, *J. Org. Chem.*, 2019, **84**, 10449–10458.
191 C. G. Swain and C. B. Scott, *J. Am. Chem. Soc.*, 1953, **75**, 141–147.
192 C. D. Ritchie and P. O. I. Virtanen, *J. Am. Chem. Soc.*, 1972, **94**, 4966–4971.
193 T. B. Phan, M. Breugst and H. Mayr, *Angew. Chem. Int. Ed.*, 2006, **45**, 3869–3874.
194 For a comprehensive listing of N and E parameters, see https://www.cup.lmu.de/oc/mayr/reaktionsdatenbank/.

195 H. Mayr and M. Patz, *Angew. Chem. Int. Ed. Engl.*, 1994, **33**, 938–957.
196 H. Mayr, B. Kempf and A. R. Ofial, *Acc. Chem. Res.*, 2003, **36**, 66–77.
197 X.-H. Duan and H. Mayr, *Org. Lett.*, 2010, **12**, 2238–2241.
198 E. Iwasaki, Y. Matsumi, K. Takahashi, T. J. Wallington, M. D. Hurley, J. J. Orlando, E. W. Kaiser and J. G. Calvert, *Int. J. Chem. Kinet.*, 2008, **40**, 223–229.
199 S. T. Purrington, N. V. Lazaridis and C. L. Bumgardner, *Tetrahedron Lett.*, 1986, **27**, 2715–2716.
200 J. C. Torres, S. J. Garden, A. C. Pinto, F. S. Q. da Silva and N. Boechat, *Tetrahedron*, 1999, **55**, 1881–1892.
201 Y. Takeuchi, T. Tarui and N. Shibata, *Org. Lett.*, 2000, **2**, 639–642.
202 E. M. Arnett, S. G. Maroldo, S. L. Schilling and J. A. Harrelson, *J. Am. Chem. Soc.*, 1984, **106**, 6759–6767.
203 I. Kaljurand, A. Kütt, L. Sooväli, T. Rodima, V. Mäemets, I. Leito and I. A. Koppel, *J. Org. Chem.*, 2005, **70**, 1019–1028.
204 R. J. Mayer, N. Hampel, P. Mayer, A. R. Ofial and H. Mayr, *Eur. J. Org. Chem.*, 2019, **2019**, 412–421.
205 F. Corral-Bautista, R. Appel, J. S. Frickel and H. Mayr, *Chem. - Eur. J.*, 2015, **21**, 875–884.
206 Y. A. Jasem, T. Thiemann, L. Gano and M. C. Oliveira, *J. Fluor. Chem.*, 2016, **185**, 48–85.
207 J. Fried and E. F. Sabo, *J. Am. Chem. Soc.*, 1953, **75**, 2273–2274.
208 A. Bowers and H. J. Ringold, *Tetrahedron*, 1958, **3**, 14–27.
209 A. Bowers, L. Cuéllar Ibáñez and H. J. Ringold, *Tetrahedron*, 1959, **7**, 138–152.
210 A. Bowers, L. C. Ibáñez and H. J. Ringold, *Tetrahedron*, 1959, 3.
211 L. H. Knox, J. A. Zderic, J. P. Ruelas, C. Djerassi and H. J. Ringold, *J. Am. Chem. Soc.*, 1960, **82**, 1230–1235.
212 Y. Osawa and M. Neeman, *J. Org. Chem.*, 1967, **32**, 3055–3057.
213 S. J. Halkes, J. Hartog, L. Morsink and A. M. De Wachter, *J. Med. Chem.*, 1972, **15**, 1288–1292.
214 S. Rozen and Y. Menahem, *J. Fluor. Chem.*, 1980, **16**, 19–31.
215 A. J. Poss and G. A. Shia, *Tetrahedron Lett.*, 1995, **36**, 4721–4724.
216 A. J. Poss and G. A. Shia, *Tetrahedron Lett.*, 1999, **40**, 2673–2676.
217 I. Villax, Z. Mendez, WO2002100878A1, assigned to Hovione Limited, 2002.
218 S. Chernyak, M. Zarbov, D. Gutman, US Patent, US7098328B2, assigned to Taro Pharmaceuticals USA Inc., 2006.
219 S. Chernyak, M. Zarbov, D. Gutman, US Patent, US7718793B2, assigned to Taro Pharmaceuticals USA Inc., 2010.
220 V. Reydellet-Casey, D. J. Knoechel and P. M. Herrinton, *Org. Process Res. Dev.*, 1997, **1**, 217–221.
221 D. S. Negi, L. Köppling, K. Lovis, R. Abdallah, J. Geisler and U. Budde, *Org. Process Res. Dev.*, 2008, **12**, 345–348.
222 S. Wood, S. Etridge, A. Kennedy, J. Percy and D. J. Nelson, *Chem. – Eur. J.*, 2019, **25**, 5574–5585.
223 A. Harsanyi, PhD Thesis, Durham University, 2016.
224 P. N. Rao and L. R. Axelrod, *J. Org. Chem.*, 1961, **26**, 1607–1608.
225 P. Marwah, A. Marwah and H. A. Lardy, *Tetrahedron*, 2003, **59**, 2273–2287.
226 H. Mayr and A. R. Ofial, *J. Phys. Org. Chem.*, 2008, **21**, 584–595.
227 S. Minegishi, S. Kobayashi and H. Mayr, *J. Am. Chem. Soc.*, 2004, **126**, 5174–5181.
228 G. Cainelli, WO03082896A2, Farmabios S.P.A., 2003.
229 P. Macdonald, P. Rossetto, WO2004052911A1, Sicor Inc., 2004.

230 A. Harsanyi and G. Sandford, *Green Chem.*, 2015, **17**, 3000–3009.
231 S. Rozen and G. Ben-Shushan, *Tetrahedron Lett.*, 1984, **25**, 1947–1948.
232 R. D. Chambers, T. Nakano, M. Parsons, G. Sandford, A. S. Batsanov and J. A. K. Howard, *J. Fluor. Chem.*, 2008, **129**, 811–816.
233 S. Rozen and C. Gal, *J. Org. Chem.*, 1987, **52**, 4928–4933.
234 C. P. Johnston, T. H. West, R. E. Dooley, M. Reid, A. B. Jones, E. J. King, A. G. Leach and G. C. Lloyd-Jones, *J. Am. Chem. Soc.*, 2018, **140**, 11112–11124.
235 J. Zhang, J.-D. Yang, H. Zheng, X.-S. Xue, H. Mayr and J.-P. Cheng, *Angew. Chem. Int. Ed.*, 2018, **57**, 12690–12695.
236 D. Meyer, H. Jangra, F. Walther, H. Zipse and P. Renaud, *Nat. Commun.*, 2018, **9**, 4888–4897.
237 Chemistry World, News Highlight: Scale ranks reactivity of fluorinating reagents, https://www.chemistryworld.com/news/scale-ranks-reactivity-of-fluorinating-reagents/3009601.article (accessed September 2019).
238 O. V. Dolomanov, L. J. Bourhis, R. J. Gildea, J. A. K. Howard and H. Puschmann, *J. Appl. Crystallogr.*, 2009, **42**, 339–341.
239 G. M. Sheldrick, *Acta Crystallogr. A*, 2008, **64**, 112–122.
240 A. D. Becke, *J. Chem. Phys.*, 1993, **98**, 5648–5652.
241 C. Lee, W. Yang and R. G. Parr, *Phys. Rev. B*, 1988, **37**, 785–789.
242 G. A. Petersson, A. Bennett, T. G. Tensfeldt, M. A. Al-Laham, W. A. Shirley and J. Mantzaris, *J. Chem. Phys.*, 1988, **89**, 2193–2218.
243 G. A. Petersson and M. A. Al-Laham, *J. Chem. Phys.*, 1991, **94**, 6081–6090.
244 R. Martinez-Haya, L. Marzo and B. König, *Chem. Commun.*, 2018, **54**, 11602–11605.
245 J. Zawadiak and M. Mrzyczek, *Spectrochim. Acta. A. Mol. Biomol. Spectrosc.*, 2012, **96**, 815–819.
246 N. M. Shavaleev, R. Scopelliti, F. Gumy and J.-C. G. Bünzli, *Eur. J. Inorg. Chem.*, 2008, **2008**, 1523–1529.
247 B. Košmrlj and B. Šket, *Org. Lett.*, 2007, **9**, 3993–3996.
248 K. K. Laali, A. Jamalian and C. Zhao, *Tetrahedron Lett.*, 2014, **55**, 6643–6646.
249 F. Buckingham, A. K. Kirjavainen, S. Forsback, A. Krzyczmonik, T. Keller, I. M. Newington, M. Glaser, S. K. Luthra, O. Solin and V. Gouverneur, *Angew. Chem. Int. Ed.*, 2015, **54**, 13366–13369.
250 A. J. Liston and P. Toft, *J. Org. Chem.*, 1968, **33**, 3109–3113.
251 R. H. Cox and E. Y. Spencer, *Can. J. Chem.*, 1951, **29**, 398–408.